HYDRO-STRUCTURAL STUDIES ON SWATH TYPE VESSELS

by

Eko Budi Djatmiko, MSc

Thesis submitted for the Degree of Doctor of Philosophy

Department of Naval Architecture and Ocean Engineering
University of Glasgow

July, 1992

CONTAINS PULLOUTS

DECLARATION

Except where reference is made to the work of others,
this thesis is believed to be original

ACKNOWLEDGEMENTS

I am wholeheartedly grateful to Professor D. Faulkner, the Head of Department, for giving me such a chance to carry out this research as well as kindly providing supervision throughout. My understanding on ship structural design philosophy would remain feeble without his continuous guidance.

I sincerely thank Drs. P.K. Das, A.Incecik and R.C. McGregor for their useful discussions at various levels of my research. Sincere thanks are also due to Drs. H.S. Chan, H.H. Chun and Mr. Y. Pu who have allowed me to incorporate their work on SWATH motion prediction, SWATH resistance assesment and reliability analysis, respectively, into my study. Moreover, I am grateful to other fellow researchers in the Department : Messers. A.F. Miller, C. Tolikas and Mrs. L.B.Caldwell who have been so co-operative in working together within the SWATH group, Mr. R. Prince-Wright for supplying me with wave stochastics information, and Mr. M.R. Mainal for his pleasant friendship.

Gratitude is further acknowledged to all the technicians at the Hydrodynamics Laboratory for their help during the time I was carrying out the SWATH model tests. I would like also to convey my gratitude to Mrs. I.P. Faulkner who has helped me with correcting the manuscript of this thesis.

Encouragement from my colleagues at the Faculty of Marine Technology, Institute of Technology, Surabaya, is very much appreciated. I am especially grateful to Ir. Soegiono and Ir. Soeweify, MEng. for their concern with the extension of my scholarship grant. Mr. H. Choraque is thanked for his earnest companionship during my study in Glasgow.

Financial support is acknowledged to the Indonesian Government and the Marine Technology Directorate of the Science and Engineering Research Council.

Finally, I am grateful for moral support and encouragement from my mother and family at home in Indonesia. Most of all, I am forever indebted to my dearest wife Lini and son Ellinas for their endurance and patience in waiting for me to complete my study in Scotland. Appropriately this thesis is dedicated to them.

CONTENTS

CHAPTER 3 - PREDICTION OF WAVE LOADS ON SWATH SHIPS

CHAPTER 4 - PREDICTION OF SLAMMING ON SWATH SHIPS

CHAPTER 5 - PRELIMINARY SWATH STRUCTURAL DESIGN

CHAPTER 6 - FATIGUE PERFORMANCE OF SWATH SHIPS

CHAPTER 7 - CONCLUDING REMARKS

LIST OF FIGURES

CHAPTER 1

CHAPTER 2

CHAPTER 3

CHAPTER 4

CHAPTER 5

CHAPTER 6

LIST OF TABLES

CHAPTER 1

CHAPTER 2

CHAPTER 3

CHAPTER 4

CHAPTER 5

CHAPTER 6

SUMMARY

This thesis presents a study on SWATH type vessels which is directed towards the collection and use for structural design of experimental data related to motions and primary dynamic loads of such vessels. This data will be of use in the validation of a mathematical model for motion and wave load predictions recently developed at the Department. Further, experimental data on slamming will also be acquired to lay a foundation for the future development of a reliable analytical model. Design loads pertinent to SWATHs comprising the extreme primary loads, lifetime cyclic loads and local panel pressures are then built upon the former findings to be of use in structural designs, especially in the determination of initial scantlings and fatigue characterisation. Examples are given throughout on the evaluation of hypothetical SWATHs operating in the North Atlantic.

The underlying theoretical formulation of SWATH ship motions is presented together with a description of a newly developed motion prediction theory. This is followed by a clarification of the procedures for conducting seakeeping tests on SWATH models. Validation of the analytical motion model by the measured data of single and tandem strut SWATH models is then presented. Subsequently, practical applications of implementing motion predictions to the assessment of SWATH operability in real seaways are described.

Theoretical background of SWATH primary wave loads is briefly outlined. The enhancement of the motion program MARCHS to tackle the primary load on SWATHs is described. The development of experimental data on SWATH loadings by way of seakeeping techniques is presented. Correlation of this experimental data and the theoretical assessment is made to demonstrate the validity of the mathematical model so developed. Lifetime cyclic and extreme loads required in the fatigue and ultimate strength designs, respectively, are developed by applying long- and short-term wave statistics.

Slamming phenomenon attributable to SWATH operation in adverse water is being investigated by model tests. Possible formats of analytical models for slamming predictions are incorporated. Comparison of experimentally generated slamming data and the simplified predictions, as well as the pressure data from various SWATH designs, are presented.

Transforming the load effects information to preliminary SWATH structural design is the next subject addressed. Simple beam theory is adopted, instead of more

rigorous first principles approach to structural designs. Enhancement of the present design tools for more detailed design is pointed out.

Fatigue behaviour of SWATH is studied by considering the lifetime cyclic load together with the application of classical damage accumulation analysis by Miner's rule. Implementation of the simplified fatigue damage assessment, which requires the stress distribution parameter to be determined, is then used. Reliability analysis is further incorporated to assess the safety level of SWATH structure against fatigue failure. The structural inspection and maintenance strategy related to fatigue damage is established by referring to former evaluations. Finally, the need to explore fatigue of alternative lightweight construction materials, and the use of a higher level fatigue characterisation by crack propagation assessment are put forward.

CHAPTER 1

INTRODUCTION

CHAPTER 1

INTRODUCTION

The development of advanced marine vehicles today places more emphasis on better seakeeping to perform specific tasks rather than improving merchant freight storage, the area in which the present monohull/conventional ship seems to be most efficient. The SWATH vessel is one of the most recent marine vehicle concepts which offers a better seakeeping performance and less operationally imposed speed reduction when operation in severe weather.

As is mentioned by Kennell (1985) the acronym SWATH, which was chosen by the U.S. Navy in the early 1970s, refers to Small-Waterplane-Area Twin/Three-Hull Ships. Other names, as quoted by Gore (1985), for instance SSS (Semi-Submerged Ship), MODCAT (Modified Catamaran), LWP (Low Waterplane) Area Catamaran and TRISEC (Trisected) Ship have been used during the projects covering these new 'species' at the Naval Ocean System Center, at the DTNSRDC, at the Naval Ship Engineering Center and at Litton Industries, respectively. SWATH is also well recognised by other names, i.e. SSP (Semi-Submerged Platform) in the USA, and SSC (Semi-Submerged Catamaran) which is most commonly used in Japan.

1.1. HISTORY AND DEVELOPMENT OF SWATH SHIPS

The idea of the SWATH concept is to design a vessel which can sail in waves with as low a reduction in its speed as possible, without slamming and without shipping green water. The conceptual approach is that of an aerofoil slender body at the sea-air surface intersection and the majority of the buoyant volume concentrated away from wave action in a submerged torpedo-like lower hull. By attachment of an upper hull well above the sea surface, slamming and the shipping of green seas may be minimised. This single hull small waterplane area design, which is not dissimilar to the concept proposed by Boericke (1959), has insufficient transverse restoring moment. The solution to this problem lies in constructing another structure and coupling the two together with an extension of the upper hull, as is done for catamaran ships. The appearance of a SWATH ship, therefore, can be characterised by submerged hulls away from the surface and streamlined surface-piercing struts, attached to the hulls, which support a deck structure well above the waterline. The combination of these three sections is usually referred to as the hull girder (see Fig. 1.1).

In considering the SWATH concept, one may trace the history of SWATH development from two sources, i.e. multi-hulls and submerged hulls. The first multi-hulls introduced into Europe by Sir William Petty (1660) were followed by the construction of early catamarans in the 1660s. However, it is unwise not to mention the Polynesians who, some centuries ago, had sailed on multi-hull craft [Seascape (1987)]. Submerged hulls were first introduced by Lundborg (1880). McGregor (1983) considers the first SWATH can probably be credited to the design proposed by Nelson in 1905. The original design of this vessel by Nelson (1905), however, was not aimed at improved seakeeping performance, but more concerned with the storage of certain freights that may be much affected by fluctuations of the weather. Another early design leading to modern SWATHs was by Faust (1932).

Creed and Lewis first proposed their 'Mobile Seadrome', as a steady mobile landing field for aircraft operations, to the British Admiralty in 1942 and the U.S. Navy. Although an interesting idea, due to other wartime priorities this was not considered a serious contender for an aircraft carrier. According to Pieroth and Lamb (1985) neither the British Admiralty nor the U.S. Navy, therefore, attempted to develop the concept further. Nonetheless, Creed (1946) applied for and was awarded patent for the design. Two decades later Leopold (1969a, 1969b) of Litton Industries introduced a design labelled as TRISEC, which apparently resembled Creed's but with considerable development. At about the same time a moderate waterplane area twin-hull vessel *Duplus* was built in The Netherlands. The vessel had a maximum speed of 8 knots with control surfaces mounted on the hulls. By the early 70s Lang (1971) claimed his patent on SWATH, covering stabilising and canard fins in conjunction with control systems. Figure 1.2. shows SWATH patents claimed by these inventors, and for the sake of simplicity to understand the SWATH history, a diagram is given by McGregor (1983) as in Fig. 1.3.

The first SWATH ship built was a work boat for the Hawaiian Laboratory of the Naval Ocean System Center (NOSC), the 190-ton SSP *Kaimalino*. This vessel was the creation of a team led by Lang in the U.S. Naval Undersea Center (NUC), based in San Diego. The design of this SWATH started in the late 1960s, followed by the construction in the U.S. Coast Guard Shipyard in Curtis Bay in 1972. As reported by Lang et al (1971, 1973) and Lang and Higdon (1974) the ship was completed by 1973.

For a period there was an absence of SWATH ship building in the U.S.A. Then RMI, Inc., commenced the construction of a 58-ton SWATH in the early 1980s. The SD-60-SWATH, since named *Halycon*, was designed as a commercial or government service boat. Luedeke and Montague (1984) mentioned that the construction was completed and available for demonstration in March 1985. Another SWATH demonstrator, *F.G. Creed*, was produced by a US shipyard in 1987 and since has been subjected to comprehensive sea trials by Pegg et al (1990) in Canada. Two other

SWATHs have been built in the USA in the late 80s. One is a high-speed commercial leisure craft the *Navatek 1*, the design of which has been reported by Seidl (1992) at the 11th ISSC. The latest vessel is a 3500-tonne US Navy's ocean surveillance SWATH T-AGOS 19, named the *Victorious*. A number of references have been presented on this vessel, notably by Covich (1987).

Since the *Kaimalino*, SWATH efforts in the U.S., and widespread SWATH research internationally, have resulted in a number of designs as well as the construction of a demonstrator vessel, the *Suave Lino*. Concurrently, SWATH development commenced in Japan with the Mitsui Engineering & Ship Building Co., Ltd. Five vessels have been built by this company since 1977. These are the test vehicle *Marine Ace*, followed by the construction of a 343-ton ferry the *Seagull*, which was formerly named *Mesa 80*, then a 236-ton hydrographic survey vessel *Kotozaki*, the 2849-ton diver support vessel *Kaiyo* and the latest, a 19-ton leisure cruiser *Marine Wave*. Another SWATH hydrographic survey ship, the *Ohtori*, was built by Mitsubishi Heavy Industry, Ltd. which together with Mitsui, had been encouraged by the Japanese Government to foster exploitation of the SWATH concept. As indicated by Gupta and Schmidt (1986), both hydrographic vessels built in Japan are of similar size to the SSP *Kaimalino*. Some publications have lately reported further SWATHs produced by Japan in recent years.

Within the European countries, only three SWATH vessels have been built so far. The first built is a small fishing SWATH *Ali*, which was designed by MacGregor et al (1988). This vessel is currently operating in the West Coast of North Scotland. The second as reported by Milner (1990) is a high-speed ferry the *Patria*, designed and built by FBM Marine at Isle of Wight, South of England. The *Patria* is presently operated between Madeira and Porto Santo, off the Atlantic coast in North Africa. The most recent SWATH, and the largest of all existing SWATHs (Δ = 11740 tonnes), named *Radisson Diamond*, has been built at Rauma Shipyard in Finland. According to Lloyd's Ship Manager (1992) the first year of operation of this luxury cruiser will be in the Mediterranean before sailing to its final destination in the Carribean. Existing SWATH ships are listed in Table 1.1 and some are illustrated in Figs. 1.4 through 1.6. More information on SWATH ship research and developments may be found in papers by Betts (1988a) and Lang (1989).

1.2. SWATH SHIP GEOMETRY AND CHARACTERISTICS

As has been briefly outlined in the previous section, a SWATH ship is a displacement vessel in which most of the buoyancy is provided by the twin-hulls positioned sufficiently far below the water surface to be clear from the worst buffeting

of ocean waves. A twin-hull form would supply adequate beam for the necessary hydrostatic restoring moments. The slender hydrofoil struts lead to increased operational capability through greatly improved seakeeping performances in seaways, including minimising speed reduction in rough water. The arrangement of the hulls and struts in such a way presents a much smaller waterplane area to dynamic wave action than conventional monohull ships or catamarans. This concept has also been advantageously applied to the semi-submersible platform used in the offshore oil industry. The rectangular box cross structure supported by struts a considerable distance above the water make adverse wave effects, like deck bottom slamming or deck wetness, generally avoidable.

1.2.1. The SWATH Hulls

A SWATH ship incurs a penalty in greater frictional resistance due to the greater wetted surface area compared to a comparable monohull. Nevertheless, substantial improvement can be made in overall resistance by shaping the lower hulls and selecting the best length diameter ratio. This aspect of hull shaping the submerged hull had been explored by Boericke (1959) and more recently by Chapman (1977). The cross sectional area shape of the submerged hulls can be circular, elliptical or rectangular. Other alternatives include circles with flattened tops and bottoms and vertical oval sections. The circular shape of the cross sectional gives the minimum wetted surface area per unit cross-section area, so it leads to low frictional resistance. Moreover, this shape is more efficient to withstand the design pressure. As an example, circular hulls are applied for the SSP *Kaimalino*, Fig. 1.4.

The elliptical cross-section shape with the major axis horizontal, such as that constructed for the *Seagull*, provides less hydrodynamic side loads but it may increase vertical motion damping effects and added virtual mass. Furthermore, elliptical hulls can allow lower draught. Their disadvantages are increases in weight and higher manufacturing costs. Although the rectangular cross-section hull is the cheapest to construct, it may not be suitable for high speed SWATH ships since this shape tends to be heavier, gives greater drag and also provides smaller headroom. However, this shape remains suitable for stationary marine vehicles, such as semi-submersible offshore drilling rigs.

Hull shaping not only applies to the cross-section but also the longitudinal plane section, e.g. for the *Victorious* in Fig. 1.5. In this aspect efforts are primarily directed to improve the capability of arranging the machinery space in the lower hulls as well as improving resistance and seakeeping characteristics. Simple hull designs with constant cross-section along the hull length and contoured nose and tail offer ease of construction, but for a small ship may not allow sufficient space for machinery

installation. Another option is that the hull cross-section can remain constant with a local bulge to accommodate machinery. Alternatively, a simply contoured hull may be chosen, constructed with a maximum cross-section at the mid length. The addition of bulges at the nose and tail may reduce resistance at high speeds and allow even greater control over the buoyancy distribution. More details of this review are presented by MacGregor (1986).

Hull dimension is mainly characterised by the length diameter ratio, L/D, which radically influences the ship features. L/D lies between 10 and 15 for hull lengths below 60 metres. For the bigger ship, where the increase in the hull diameter with respect to the requirement of machinery installation is no longer critical, increasing the ratio to between 15 and 20 allows reduction of resistance and form drag to become possible. Nevertheless, the skin friction will increase as a result of the larger wetted surface area. Meanwhile, a higher ratio changes the water flow velocities into the propeller which in turn alters the quasi propulsive coefficient. From another viewpoint, a smaller diameter improves the ability to withstand external pressures. Deeply submerged hulls give a better sonar performance and permit easier diver and submersible operations.

1.2.2. The SWATH Struts

There are three shapes of cross-section generally constructed as the column of a floating structure, namely circular, rectangular and aerofoil or streamline shaped. Only the first two shapes are commonly used for offshore drilling rig vertical columns since the resistance is not the most prominent consideration on a stationary marine vehicle. Therefore, for a SWATH ship either aerofoil shaped or streamlined struts are the best option, as these shapes give less drag. In SWATH design, determining the number of struts per hull is one fundamental decision that must be made by the designer. The number of struts per hull affects the magnitude of side loads as well as the resistance experienced by the ship.

The tandem strut configuration should offer lower side loads, which also means lower bending moment imposed on the cross structure. With regard to maneouvring, a tandem strut SWATH theoretically gives a turning circle of approximately five times the ship length, compared to ten times for a single strut SWATH. Another attribute is that four independent struts provide a high degree of control towards LCB and LCF adjustment so that desired motion performances may be achieved.

A single strut design certainly offers some advantages compared to a tandem strut configuration. It offers more freedom in the machinery arrangement as well as easier access to the lower hull. Although control over LCB and LCF is slightly restrained,

however, as a result of higher GM_T the roll stiffness is obviously more adequate to ensure that quasi static heel angles are avoided.

The most extensive comparison between single and tandem strut per hull has been carried out experimentally on SSC *Marine Ace* by Mitsui under the sponsorship of Japan Marine Machinery Development Association (JAMDA) and is reported by Oshima et al (1979). During the test it was found that the resistance of the single strut type is lower than the tandem strut, indicating a greater miscellaneous resistance for the tandem strut due to spray drag, induced drag on fins, etc.

The strut height dictates the deck bottom clearance and draught. A relatively deeper draught allows flexibility in choosing the propeller diameter. This also ensures that the propeller submergence can be maintained in any sea state. However, deeper draught in turn influences the ship resistance and, moreover, a limitation in usable dock and harbour facilities should also be considered by a designer.

Strut dimensions are generally described by strut thickness to chord ratio, t/l, strut thickness to hull diameter ratio, t/D, or in terms of strut thickness to ship displacement$^{1/3}$ ratio, $t/\Delta^{1/3}$. A low t/l ratio offers lower wave making resistance at the expense of limitation on the machinery access into the lower hulls. Most designs have t/D ratios lying between 0.5 to 0.25. In order to improve TPI, GM_T and ease of access, the U.S. Navy recommends a $t/\Delta^{1/3}$ ratio of about 0.17; most of the existing SWATH ships have a ratio of between 0.2 and 0.1.

1.2.3. The SWATH Cross Deck Structures

The cross deck geometry of a SWATH ship is rectangular in section with an option for inner side only or inner and outer side sponsons. The bottom of the deck is the wet deck, and the distance from this deck to the waterline is defined as box clearance. When apportioning volume between struts and box, the line of demarcation is at the wet deck. Control of strut and box longitudinal separation is gained through the use of box set back. The box clearance remains an unknown parameter until an adequate clearance to avoid adverse wave effects is thoroughly investigated. Based on the SSP *Kaimalino* model investigation, Lang and Higdon (1974) reported that bottom slamming can be reduced by mounting well faired double bows on a the flat section. Another observation by Smith (1979) shows that a three hulled SWATH provides more benefit because of its smaller deck area forward, so slamming loads will be much lower.

The box depth design needs to consider the bending moment and shear force imposed by the wave loads on the deck structure through the struts. A ship with length below 30 metres should be able to have one full deck in the cross structure, whereas larger ships my need multiple decks.

1.2.4. Some Basic Design Parameters

Basic ship parameters are always the most important data required in the design process, and this is also true of SWATH ship design. The terms used here are, therefore, not different from those used for monohull ships with, of course, many more additional parameters as a consequence of the more complex SWATH geometry. In the early days of SWATH ship development researchers suffered from the lack of historical design data, so that early SWATH ships owed nothing to conventional ship design data.

The SWATH ship overall length is related to the submerged hull length and the strut length. Early SWATH ships had an overall length the same as the hull length. The hull length is mainly dictated by the displacement required, resistance characteristics, machinery, ballast, fuel arrangement and strut length arrangement.

The relationship of beam to length or displacement, i.e. L/B or $B/\Delta^{1/3}$, of a SWATH ship is different from monohull experience; this results in new challenges and even opportunities in the top side arrangement. Beam is the parameter that influences the transverse stability most, thus beam should be considered carefully. A greater value of L/B means shortening the righting arm but an excessive beam also means greater bending moment to be resisted by the cross structure.

A consequence of locating most of the SWATH ship buoyant volume well below the water surface is a much deeper draught compared to an equivalent size of a monohull ship. For large ships this deeper draught leads to some limitations due to dry docking facilities and harbour water depth. The deeper draught also brings about the increase in cross-deck bending moment, hence requires much care in structural design. However, an increase in draught allows for better underwater visual observation from dome ends or sonar properties. In addition, propeller cavitation and ventilation, which are significantly affected by the shallow submergence of the propeller, can be substantially reduced, as observed by Kennell (1985).

The summation of deeper draught, considerably high box clearance and box depth is relatively greater depth to the main deck, which also means greater freeboard. The drier deck of a SWATH ship is one of the particular benefits of greater depth and freeboard.

The SWATH basic design parameter relationships are summarised and listed in Tables 1.2 and 1.3. A comparison between a SWATH ship with an equivalent size of monohull in term of basic design parameters is given in Table 1.4.

1.3. SOME POTENTIAL APPLICATIONS OF SWATH SHIPS

Having studied the concept, some characteristics and basic design parameters of the SWATH ship, one can try to clarify advantages and disadvantages of a SWATH ship compared to a monohull, as well as some potential applications of a SWATH ship.

The primary advantage of a SWATH ship is its relatively lower magnitude of deck motions, i.e. heave, roll and pitch, in a seaway while at rest or underway, which also means lower magnitude of acceleration in the related modes. This feature directly influences the improvement of shipboard activities and safety, such as crew performance, deck equipment operability and passenger comfort. From this view point a SWATH ship is suitable to be used as an air-capable ship and as a passenger ferry.

Hightower and Seiple (1978) identified the combination of steadiness, with its station-keeping ability, makes a SWATH ship capable to carry out over-the-side work. This capability was demonstrated when the SSP *Kaimalino* successfully recovered floating equipment in a seaway after a 1000-ton monohull failed in several attempts. In addition, as a result of the high degree of directional stability such work can be conducted by a SWATH ship at any heading angle without difficulties, while a monohull is restricted to head seas. The SWATH seakeeping could possibly be enhanced as much as 50 percent by fitting active control surfaces, that is, canards forward and stabilisers aft. Considering this performance a SWATH ship offers great potential to be used as a stable support vessel.

In terms of regular transportation, reliability in maintaining the maximum speed in foul weather, in accordance with the required schedule, often can not be fulfilled by a moderate, or even large, monohull ship. A relatively small SWATH ship, however, could possibly satisfy such requirement, as its combination of slender streamlined wave-piercing struts and deeply submerged hulls with a reasonable installed power makes it amenable for operation in heavy seas. Thus a SWATH ship is considered by Wu (1985) as the merging of the speed qualities of vehicles such as hovercraft, planing boats or hydrofoil with the good seakeeping qualities of semi-submersibles. Comparative studies of SWATH and monohulls were made by the U.S. Navy in 1979. One of these was in speed performance in higher sea states, where the SWATH ship shows its superiority over the monohull, as shown in the curves of Fig. 1.7 [Mantle (1980)].

A SWATH ship is well known for having a spacious unobstructed stable deck. This certainly is of great importance for naval activities, such as V/STOL (Vertically/Short Take Off and Landing) aircraft carrier or as a missile launching base, as well as for some commercial and research operations. Due to this characteristic accommodation spaces above the main deck level can be arranged more conveniently. Odd volumes in the hull girder, especially in the struts and hulls cannot always be used which may require correct arrangement of deck houses. Existing designs have provided as much as one third of the total usable volume in deck houses.

A SWATH ship offers a high degree of survivability when damaged. This is mainly provided by the cross box which provides a huge reserve of buoyancy in case of underwater damage. The impact of a large missile on the side can possibly sink a small monohull frigate, but this would not be the case for a SWATH frigate. As the first strut that is hit resists the missile blast, the other strut may survive and the propeller on this side can still maintain its function. The situation would be more beneficial when a tandem strut per hull configuration is utilised. Nevertheless, a versatile counter flooding ballast system should still be installed due to vulnerability towards asymmetric flooding and static heeling after damage.

The deeply submerged hull is indicated by Mabuchi et al (1985) as a particular advantage for an underwater work support vessel. Sonar systems and other equipment installed in the lower hulls should work with higher accuracy, particularly when using electric power as the prime mover giving reduction in noise and vibration. The capability of underwater observation could be improved by mounting a plexiglass dome at the fore part of the hull to allow 180 degrees underwater viewing, as was done by Hightower et al (1985) on the SSP *Kaimalino*. In naval activities these features could obviously satisfy the mission carried out by a mine sweeper ship.

Although the concept of SWATH ship is relatively new, the required technology, unlike other advanced marine vehicles which require high technology considerations, is not much different from the technology of monohull ships. This means that SWATH construction can be implemented using standard shipbuilding technology with, of course, some extensions to match the unusual SWATH geometry. Nevertheless, some believe that SWATH ship owes more to the technology experiences of semi-submersibles rather than to the conventional ship.

The advantages of SWATH ships mentioned previously are not achieved without drawbacks. The first significant drawback as a result of low waterplane area of a SWATH ship is a lower tons per inch immersion (TPI). TPI indicates the sensitivity of a ship's draught to changes in weight during design or operation. As a consequence of

reduced TPI in SWATH designs, a much greater draught change would occur on a SWATH than on an equal displacement monohull for a given change in weight. This is then followed by considerable change of box clearance so that in certain cases deck bottom slamming becomes more adverse.

Secondly, a low waterplane area with short strut length brings about a reduction of moment to change trim one inch (MTI), which is a direct measure of the trim sensitivity of a ship. A ship with very low MTI, which also means low hydrostatic restoring moment, would be vulnerable towards pitch instabilities in following seas. An extra careful consideration of weight distribution including the accuracy of LCB and LCG estimation is therefore required in SWATH ship design. In addition, this would also require a sophisticated counter ballast system. Because of these deficiencies a SWATH ship certainly would not satisfy the mission of general cargo ships which require large variable payload capability.

Another problem which has arisen in association with the weight sensitivity, is exploration of new alternatives for lighter structural material than steel for SWATH construction in order to increase DWT/Δ ratio and further increase in payload. So far only alumunium is technically and economically considered as an appropriate material substitute for steel, although the use of GRP becomes more attractive lately. Existing SWATH ships to date, apart from SSC *Kaiyo* which is all steel constructed, were either constructed using all alumunium or hybrid, usually alumunium upper hull and steel struts and lower hulls. As reported in Combat Craft (1985a, 1985b), no serious problems arise from the use of all alumunium or hybrid structure except on *Suave Lino* which experienced reccurent cracking in the welding joints. The use of Dupont's explosion bonded alumunium plate Dataclad to the primary joint between alumunium and steel has been successfully adopted in the construction of SSP *Kaimalino.*

The two hull geometry of SWATH ships result in larger wetted surface area than in monohulls as shown Fig. 1.8. This creates higher total resistance in calm water operations as it is only at very high speed that the reduced wavemaking resistance of SWATH will give a lower total resistance than an equivalent monohull. Gore (1985) shows that theoretically, with the same amount of power installed, a SWATH ship will have a maximum speed approximately two knots less than an equivalent displacement monohull ship. Another consequence of increasing resistance is higher fuel consumption. Moreover, such a geometry entails more skin plating and stiffening and hence structural cost.

Small SWATH ships suffer from limitations in machinery arrangement. Small struts make machinery installation and access for maintenance very difficult. Placing the prime mover in the box brings about problems in designing the transmission system, in addition to the reduction in shaft transmission efficiency. Some transmission systems,

namely chain-drive, Z-drive, hydraulic and electrical, have been proposed to overcome the problem. As stated by Stenson (1976), the use of chain system tends to be more complex and more costly. SSP *Kaimalino* experienced a broken shaft in one of the chain-drive system early in her life. The Z-drive system is considered by Mabuchi et al (1985) to be the most suitable as this gives higher efficiency, low cost and lighter weight.

The SWATH ship's wider beam and deeper draught restrict the harbours, drydocks and channels to which it will have access. Higher freeboard makes passenger and cargo transfer onto the quayside (or smaller craft when working alongside) more difficult.

The bending moment on the cross deck structure and the motion characteristics of SWATHs with a large single strut per hull are likely to be troublesome while stationary in beam seas. Strengthening should be provided at the strut-box intersection to resist any fatigue loads as SWATHs are unbraced structures.

Some advantages in motion performance gained by the inherently high degree of directional stability are obtained at the expense of large turning circles and difficulty in turning at high speeds was indicated by Seren (1983).

The most severe hindrance to the development of the concept is concern over cost and lack of design data which have discouraged progress in development and construction of SWATH vessels.

1.4. HYDRO-STRUCTURAL STUDIES ON SWATH TYPE VESSELS

Most SWATH studies in the past have been dedicated primarily to observations of hydrodynamic performance, namely the motion and resistance characteristics. This is sound and fair because the concept behind SWATH lies in the exploitation of its seakeeping superiority over other marine craft. A vast amount of motion data has undoubtly been acquired in the past two decades and they are spread around many institutions. Despite this extensive data, Betts (1988b) indicates that explicit incorporation of this in the design programs that have evolved proves to be troublesome. This is unlike the resistance prediction that can be conveniently accommodated in most ship synthesis programs. Furthermore, realistic operability criteria still need to be developed for use in association with motion predictions. Betts (1988b) regards these motion and realistic operability criteria as being top priority for future research.

The next priority for more comprehensive investigations is accurate prediction of both the primary and secondary load effects to apply to SWATH structures. This would then be followed by the establishment of rational structural design tools incorporating reliability techniques.

The Department has undertaken the study of SWATH hydrodynamics since early in 1980s. The familiarity with such problems related to offshore structures, semi-submersible in particular, was the main experience to be transferred to SWATH vessels. The first study was conducted on a three-hull SWATH, rather than twin-hull, by Smith (1982) and followed by others, which ranges from detailed motion prediction, resistance and wave loadings, and covered both theoretical and experimental investigations, as well as the development of a SWATH synthesis design tool.

SWATH structural programme came later after the hydrodynamic problems were well formulated and the development of synthesis design tool by MacGregor (1989) was steadily in progress. Faulkner et al (1986) outlined the reliability concept by which ultimate strength and fatigue SWATH structural design can be approached. Structural design by Classification Rules is not considered as viable at present. This is due in particular to the absentee of such rules, although ABS (1990) has provisional rules but this is not comprehensive and naturally lacks support from actual experience. Recognising this concern SWATH structural synthesis must be founded upon sensible load effect modelling and a rational approach to first principles structural designs. Previous experience in rational structural design of monohull ships and offshore platforms, e.g. by Faulkner and Sadden (1978) and Lee and Faulkner (1989), are to be transformed to deal with SWATHs. The actual programme of the integrated structural design of SWATH ships was commenced in the Department by late 1990, and is funded by the SERC. The study presented within this thesis constitutes part of this integrated structural programme.

The initial aim of the present research was to generate experimental data on motions and dynamic loads from SWATH model tests. The data was used to validate a mathematical model for motion and wave load predictions recently developed at the Department. Further, experimental data on slamming will also be acquired to lay down a foundation for the development of a reliable analytical model in future. Design loads pertinent to SWATHs comprise the extreme primary loads, lifetime cyclic loads and local panel pressures. These are then built upon the former findings and their statistical treatment is an important aspect to be considered in the analysis. SWATH structural design is then exercised, primarily in the determination of initial scantlings and fatigue characteristics. A flowchart diagram of the current SWATH study as shown in Fig. 1.9 illustrates the relationships among the explored subjects. All these observations are contained in separate later Chapters of this thesis.

The underlying theoretical formulation of SWATH ship motions is firstly presented in Chapter 2. The limitation of the two-dimensional strip theory and other approaches is then indicated. This led to the need for a three-dimensional diffraction theory for predicting motion behaviours of SWATHs in regular waves. Such a program named MARCHS, which was developed by Chan (1990), is now available in the Department. The procedure for running it is to be outlined. The capability to deal more accurately and efficiently with forward speed effects on motions is the main attraction of this motion program.

In the second part of Chapter 2, emphasis is given to the procedures for conducting well planned seakeeping tests on SWATH models at the Department's Hydrodynamics Laboratory. Various instrumentation and computer softwares utilised for test data acquisitions and analysis are indicated. Validation of the analytical model by the measured data of single and tandem strut SWATH models is then presented. Following this, practical applications of implementing motion predictions to the assessment of SWATH operability in real seaways are described.

A supplementary observation on SWATH ship resistance is incorporated in this chapter. SWATH resistance characteristics are clarified by the presentation of theoretical and experimental data. An unconventional feature of SWATH resistance in waves is evidenced from the test, and suggests a further area of research that needs to be pursued.

The discussion in Chapter 3 concentrates chiefly on the topics of primary wave loadings on SWATHs. A review is given of the efforts undertaken by a number of research institutions worldwide in the development of wave loads peculiar to SWATH ships. In parallel theoretical backgrounds to this problem are briefly outlined. The enhancement to the motion program MARCHS to tackle the primary load on SWATHs is mentioned.

The development of experimental data on SWATH loadings by way of seakeeping techniques is presented. Experimental procedures, which in part refer to that presented in Chapter 2, are put forward. Further, correlation of experimental data and the theoretical assessment is made to demonstrate the validity of the mathematical model developed.

Practical design of SWATH structures calls for accurate design loads which need to be derived from a well developed understanding of the random nature of the operational environment. The frequency-domain loading data generated for regular waves by the so-called short-term analysis is used to provide an extreme response required for ultimate strength design. The long-term stochastic analysis approach is

used to establish the load distribution over the lifetime of a vessel. This latter approach is of importance in supplying the load information for fatigue design. Nevertheless, extreme loads can also be assessed based on this method by using the appropriate statistical properties.

Examples of the application of the above methods are made on three hypothetical SWATHs operating in the North Atlantic. Comparison of the design loads derived from a rigorous analysis with that from simplified formulations is another interesting aspect that is pointed out.

The slamming phenomenon attributable to SWATH operation in adverse weather is an important area that has not been sufficiently looked at in current SWATH technology developments. Chapter 4 is dedicated to explore this particular issue. Theoretical prediction to tackle SWATH slamming is barely available at present. However, an attempt will be made to elucidate possible formats for analytical models for slamming predictions.

Recognising the difficulty in deriving design pressure, an alternative investigation by way of experimental data has been programmed. Two distinct measurement technique, namely the point pressure and integrated panel force have been adopted. At the same time measurement on the relative motion is also conducted to characterise the severity of slamming impact on SWATH's deck bottom. Again, statistical distributions are used to investigate slamming behaviours of SWATH operating in actual seas.

Comparison of experimentally generated slamming data and the simplified predictions of SWATH design pressure is presented. This is augmented by the pressure data from various SWATH designs. The accumulated pressure data shows substantial scatter, but discrete trends are identified.

Having established a basic understanding of primary and secondary load effects intrinsic to SWATHs the next logical step is transferring such information to structural design. Comprehensive SWATH structural design is impossible to be accomplished in the present study because of the extensive nature of the subject, as well as the restricted time of the present research. Only a simplified design procedure which might be useful in very early design stage is, therefore, presented in Chapter 5.

A simple beam theory is adopted in the present design. The analysis can only accommodate a limited variations in structural configurations, but it does allow a few alternative structural materials to be explored. Improvement of the present computation tool, to include the wet deck scantlings and lower hull design routines, is indicated.

Another aspect of practical structural design that is addressed within this study is on the fatigue characteristics of SWATHs, as presented in Chapter 6. The well established design technology from monohull ships is transferred for SWATH analysis. Lifetime cyclic loads developed in Chapter 3 are used. Classical damage accumulation analysis by Miner's rule is then applied. Simplified fatigue damage is then assessed with derived stress distributions. Applying this approach allows for sensitivity evaluations of aspects affecting fatigue performance of SWATHs to be carried out rapidly, with an acceptable accuracy.

Reliability analysis is incorporated to assess the safety level of SWATH structure against fatigue failure. The general advanced first order second moment (AFOSM) approach is utilised with Wirsching's fatigue reliability format. Rational structural design is demonstrated by this safety evaluation.

A related subject to be discussed in this chapter focuses on the structural inspection and maintenance strategy for fatigue damage. Finally, the need to explore fatigue of alternative lightweight construction materials, and the use of a higher level fatigue approach for crack propagation is considered.

General conclusions to the current study are presented in Chapter 7 by referring to the findings drawn for the preceding chapters. At this point suggestions for future research are put forward. For this purpose some preliminary observations on the relevant subjects , mainly in the form of state of art review, are supplemented in the appendices.

Table 1.1. SWATH vessels existing worldwide until June 1992

Vessel Name(s)	Year Completion	Country	Design Role	Length O.A. (metres)	Beam O.A. (metres)	Draught (metres)	Displacemet (tonnes)	Speed (knots) Service/Max
Twin Drill (Duplus)	1969	Netherlands	Seabed Operations	47.00	17.06	5.50	1200.00	6 - 7/8
Trisec 1	1971	USA	Experimental	6.10	2.44	0.61	1.18	~/8.0
Kaimalino	1973	USA	Naval Workboat	27.10	14.17	4.66	193/224	~/18.0
Marine Ace I	1977	Japan	Experimental	12.35	6.50	1.55	18.40	~/17.3
Marine Ace II	1978	Japan	Experimental	12.35	6.50	1.55	22.20	~/15.4
Seagull	1979	Japan	Fast Ferry	35.90	17.10	3.15	343.00	23.0/27.1
Ohtori	1980	Japan	Hydrographic Survey	27.00	12.50	3.40	239.00	20.6/~
Kotozaki	1980	Japan	Hydrographic Survey	27.00	12.50	3.20	236.00	19.0/20.5
Betsy (Suave Lino)	1981	Japan	Sport Fishing	19.20	9.10	1.90~2.13	39~49	18.0/~
Charwin	1983	USA	Scallop Fishing	~	~	~	100.00	~
Kaiyo	1984	Japan	Diving Support	61.50	28.00	6.30	3500.00	13.25/14.1
Halcyon	1985	USA	Demonstration	18.29	9.14	2.13	43~47	18.0/22.4
Marine Wave	1985	Japan	Saloon luxury boat	15.10	6.20	1.60	25.40	16.0/18.2
Chubasco	1987	USA	Yacht	21.95	9.45	2.13	56~79	17.0/20.0
Sun Marina	1987	Japan	Cabin luxury boat	15.05	6.40	1.60	25.40	~/20.5
Samhach	1988	UK	Test Bed	6.60	2.83	0.84	3.50	~/5.0
Frederick G. Creed	1989	USA	Ocean Survey	20.40	9.75	2.60	80.00	25.0/29.0
Bay Queen	1989	Japan	Multi-purpose boat	18.60	6.80	1.60	~	~/20.0
Victorious/T-AGOS 19	1989	USA	Sonar Support (SSV)	70.70	28.65	7.54	3556.00	9.6/~
Patria	1989	UK	Fast Ferry	37.00	13.00	2.70	180.00	30.0/32.0
Navatek 1	1989	USA	Day/Dinner Excursion	43.00	16.00	2.40~4.27	365.00	15.0/18.0
Seagull 2	1989	Japan	Fast Ferry	39.30	~	3.25	567.00	~/30.0
Ali	1990	UK	Creel Fishing/Trial	12.00	5.00	1.60	20.00	8.0/~
Diana	1990	Japan	Day Trip/Party	20.80	6.80	1.60	~	15.0/19.20
Hibiki	1990	Japan	SSV	67.00	29.90	7.50	3700.00	11.0/~
Theodore Von Karman	1991	USA	Experimental	31.70	10.05	~	~	10.0/18.0
?	1991	Poland	Experimental	6.09	~	0.57	1.88	15.54
Radisson Diamond	1992	Finland	Cruise liner	131.00	32.20	8.00	11740.00	13.0/14.0
Abel/T-AGOS 20	Now Building	USA	SSV	70.70	28.65	7.54	3556	9.61/~

Table 1.2. The SWATH Ship Basic Design Parameters [Gore (1985)]

Volume of displacement :		
∇	:	65 ~ 90% contained in the hulls (average 80%)
	:	15 ~ 20% contained in the struts
Hull :		
L/D	:	14 ~ 22 (average 15 ~ 17) (>L/D for Δ ≥ 15,000 tons)
Hull Prismatic Coefficient :		
Cp	:	0.45 ~ 0.93 (average 0.7 ~ 0.9)
Strut thickness :		
t/D	:	30 ~ 60%
l/t	:	5 ~ 15 for tandem strut per hull
	:	20 ~ 40 for single strut per hull (for Δ ≥ 15,000 tons average l/t : 30 ~ 40)
Strut Waterplane :		
Area Coefficient	:	0.7 ~ 0.8
Deck :		
L/B	:	2.0 ~ 5.0 (>L/B for ships ≥ 15,000 tons)
Vol. of Deck Houses	:	1/3 of total vol. of hull girder (average 20 ~ 25%)
Vol. of struts and hulls	:	30 ~ 50% of total internal vol. (average 35 ~ 40%)
SWATH ship density	:	15 ~ 20 lbs/cuft

Table 1.3. Basic Design Parameter Relationships [MacGregor (1986)]

Volume of hull	:	$V_{hull}/\nabla = 0.8$
Length overall	:	$L = 5.4\,\Delta^{1/3}$
		$L = 6.2\,\Delta^{1/3}\left(\frac{V}{V+2}\right)^2$
Breadth overall	:	$B = 2.39\,\Delta^{1/3}$
		$B = 0.46\,L$
Design draught	:	$T = 0.57\,\Delta^{1/3}$
Depth	:	$D_{Wet\ Deck} = 1.56T$
		$D_{Main\ Deck} = 2.08T$
Hull dimensions	:	L/D = 10 ~ 15 (L < 60m)
		L/D = 15 ~ 20 (L > 60m) for circular hulls
		$D = 0.336\,\Delta^{1/3}$
		D = 0.6T
Hull submergence	:	S = 0.32—1/3
		S/D = 1.00 (D < 4)
		S/D = 1.25 (D > 4)
		S/T = 0.70
Strut thickness	:	$t/\Delta^{1/3} = 0.1 \sim 0.2$
		t/D = 0.25 ~ 0.5
Structural Weight	:	$SW/\Delta = 0.43$
Payload	:	$Payload/\Delta = 0.13$
Endurance	:	$\mathrm{Log}_{10}(\text{endurance}) = 2.092 - 2.9\log_{10}\left(\frac{V}{\sqrt{g\Delta^{1/3}}}\right)$

Table 1.4. Comparison Between SWATH and Monohull Ship [Gore (1985)]

Total internal volume :	SWATH 20 ~ 30% > monohull
Length :	SWATH 30 ~ 40% < monohull
Beam :	SWATH 60 ~ 70% > monohull
Draught :	SWATH 60 ~ 70% > monohull
Wetted surface area :	SWATH ± 60% > monohull
Depth to main deck :	SWATH ± 75% > monohull
	SWATH ± 50% > monohull (for larger ships)
Freeboard :	SWATH ± 25% > monohull

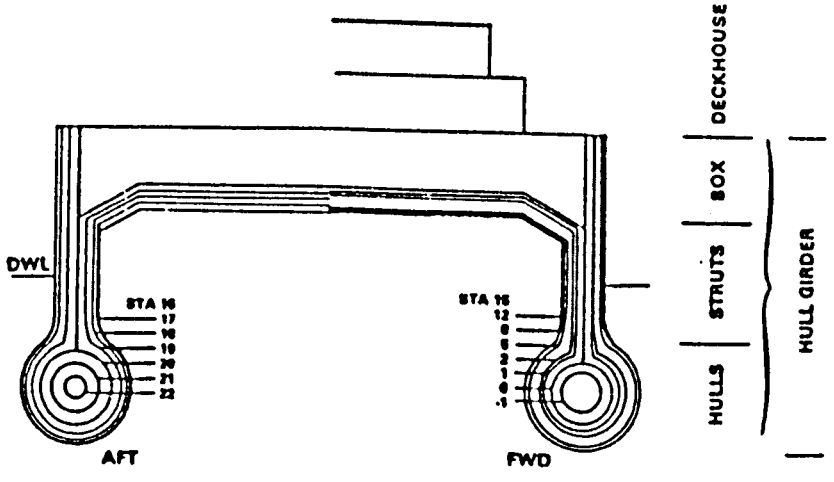

Figure 1.1. SWATH ship geometry [Kennell (1985)]

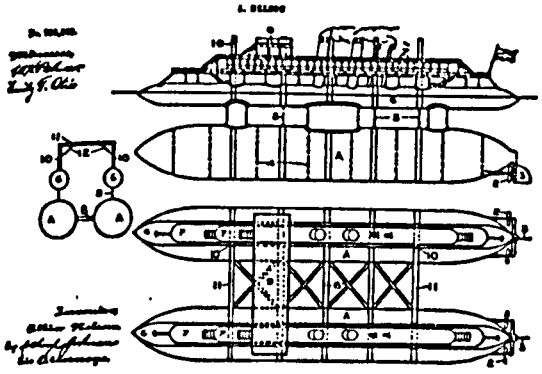

NELSON - 1905

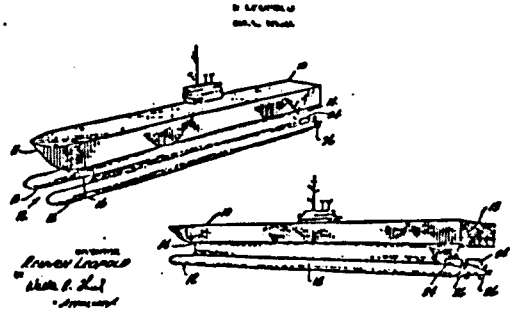

LEOPOLD - 1967

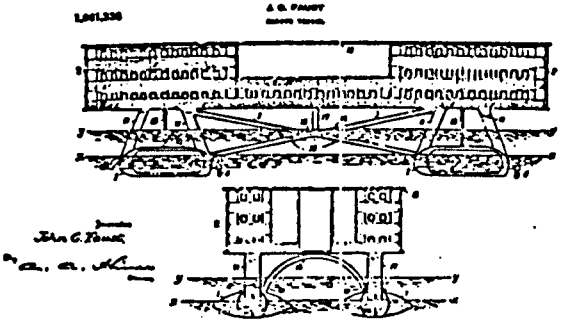

FAUST - 1932

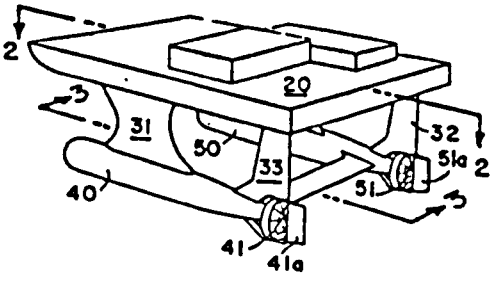

LANG - 1971

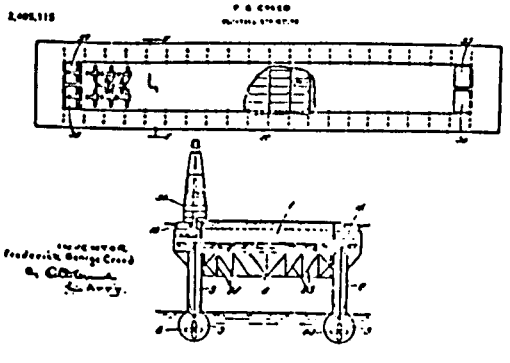

CREED - 1946

Figure 1.2. SWATH Patents

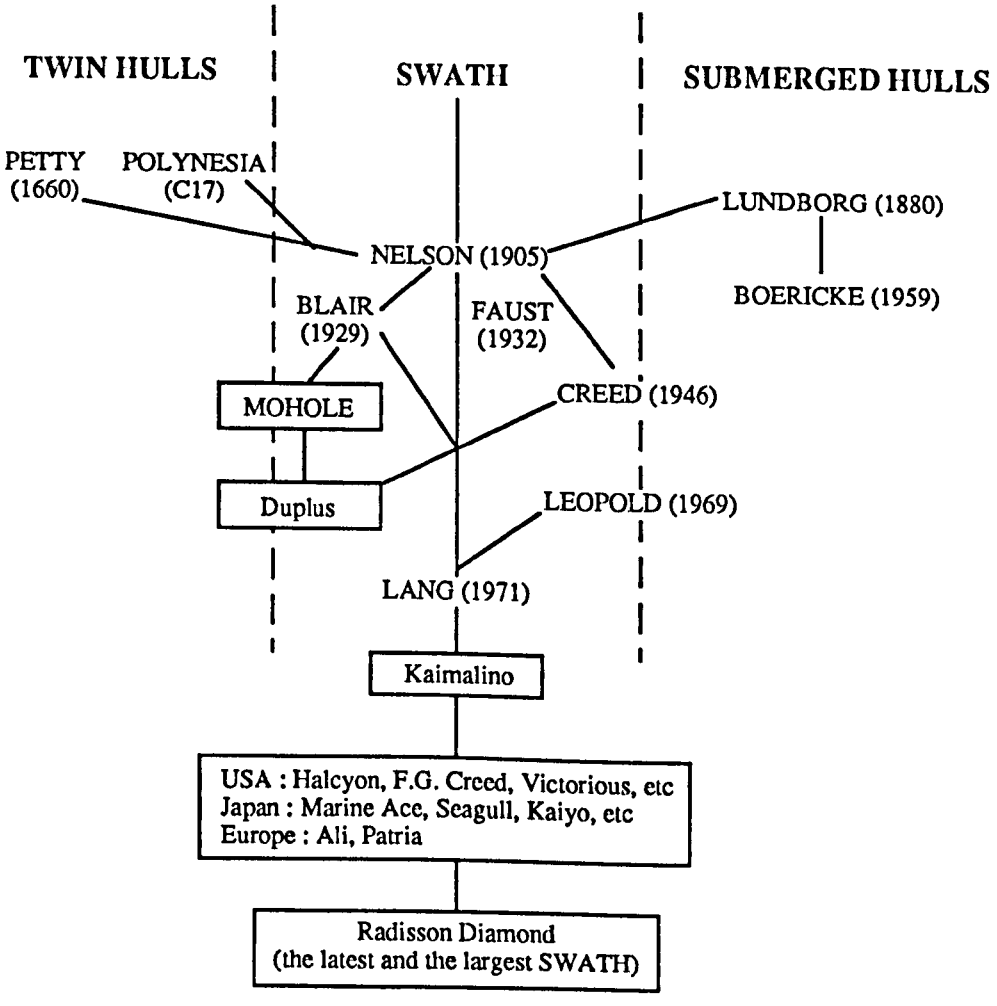

Figure 1.3. A schematic history of SWATH [McGregor (1983)]

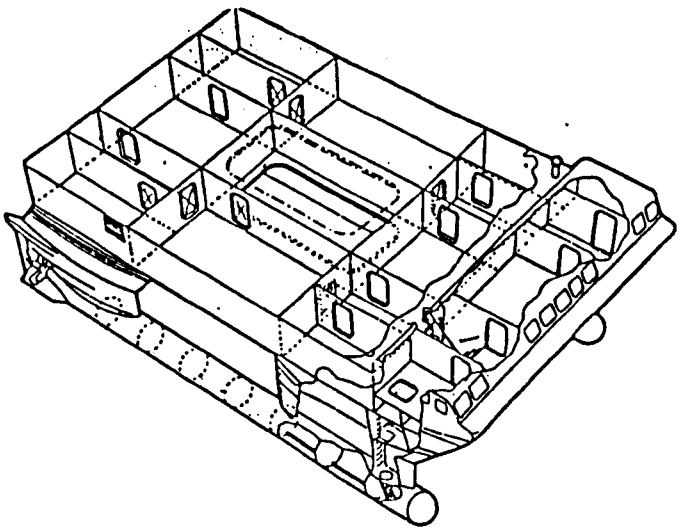

Cutaway showing basic hull configuration of SSP *Kaimalino*

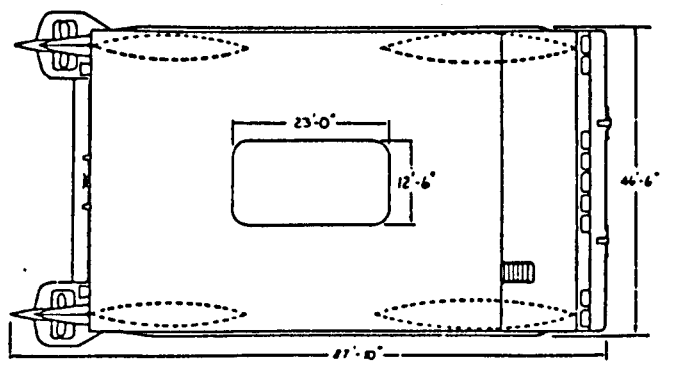

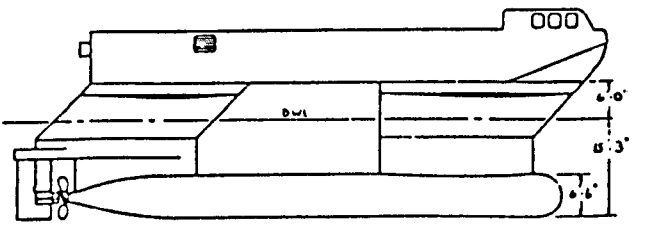

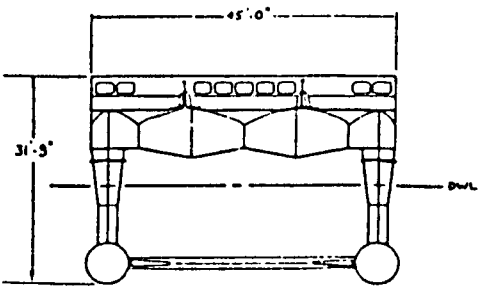

General arrangement of SSP *Kaimalino*

Figure 1.4. General arrangement plan for the SSP *Kaimalino*

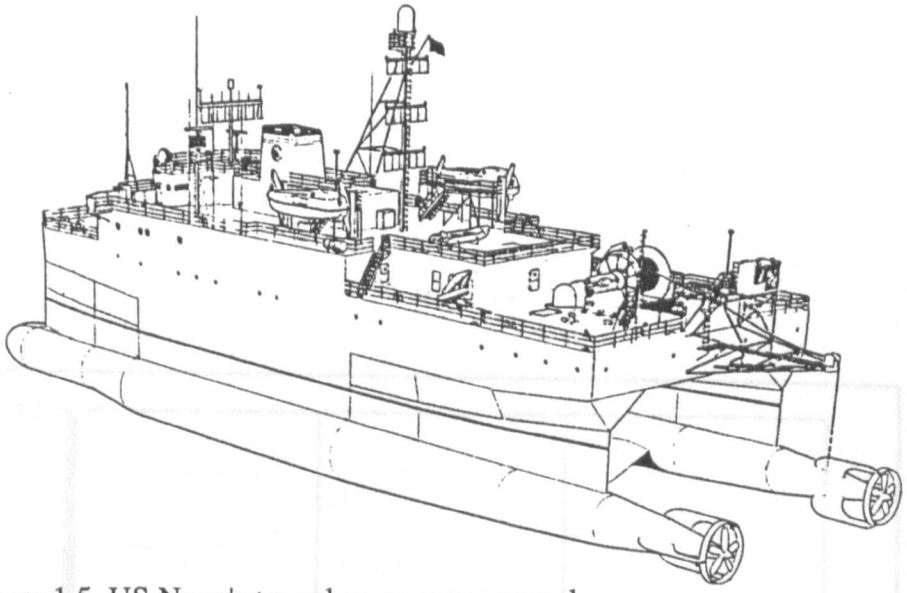

Figure 1.5. US Navy's towed-array sonar vessel the *Victorious* (T-AGOS 19)

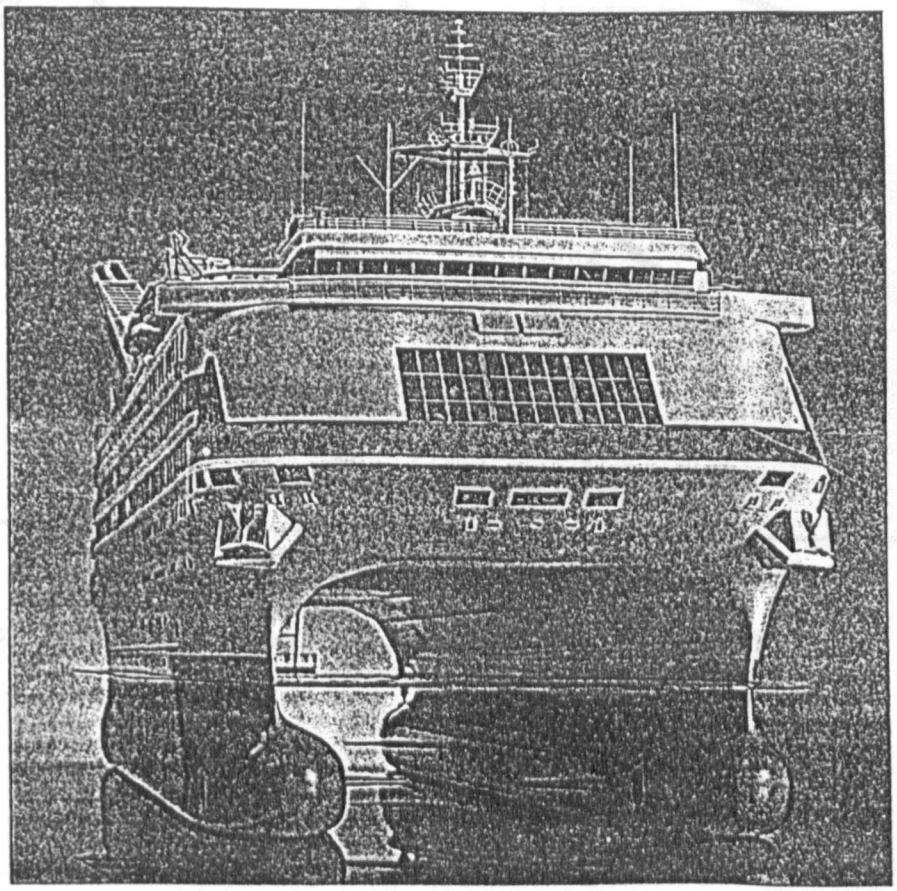

Figure 1.6. The world largest SWATH vessel *Radisson Diamond*

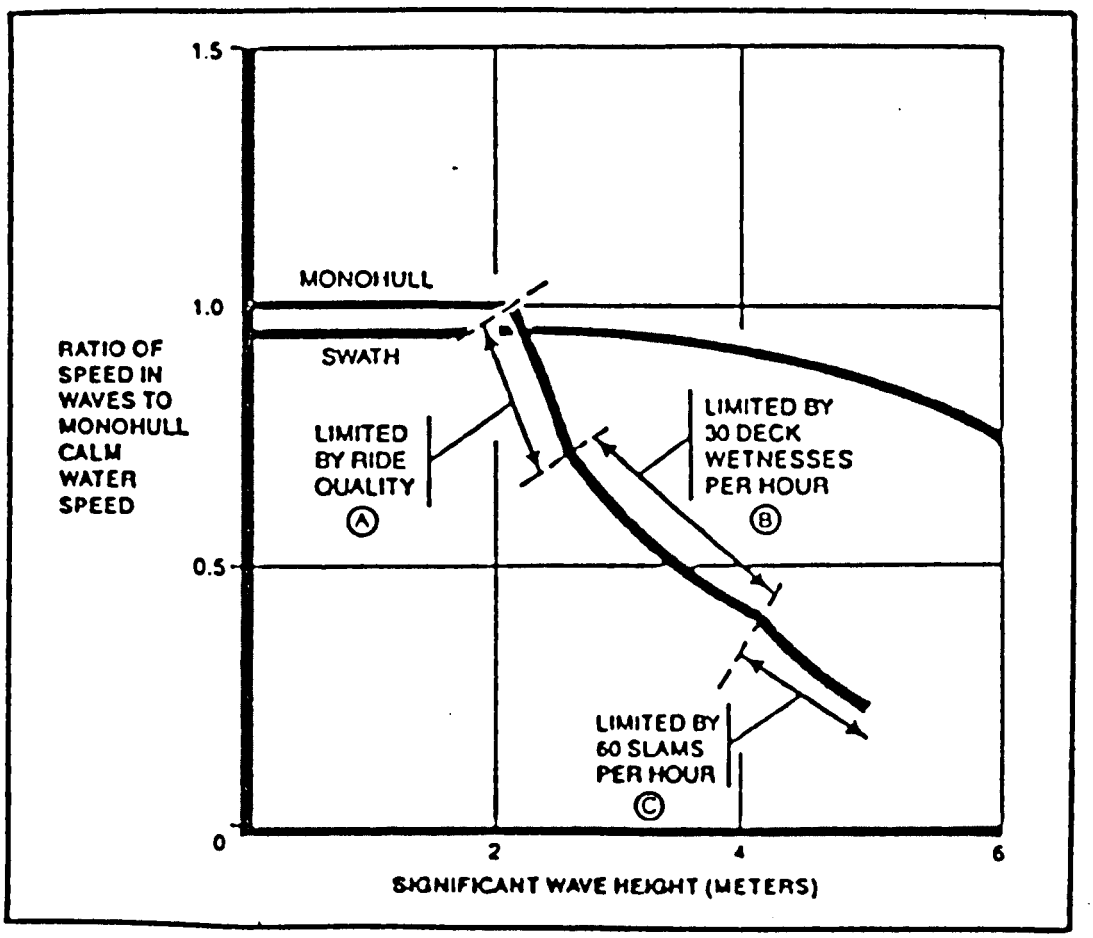

Figure 1.7. SWATH and Monohull Speeds in Rough Seas [Mantle (1980)]

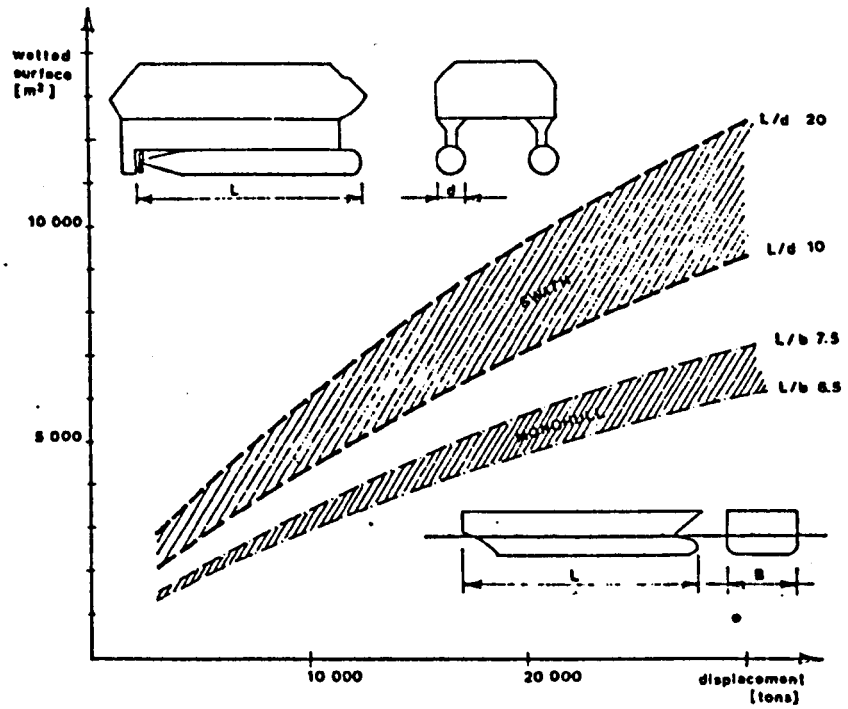

Figure 1.8. SWATH and Monohull Wetted Surface Area [Routa (1985)]

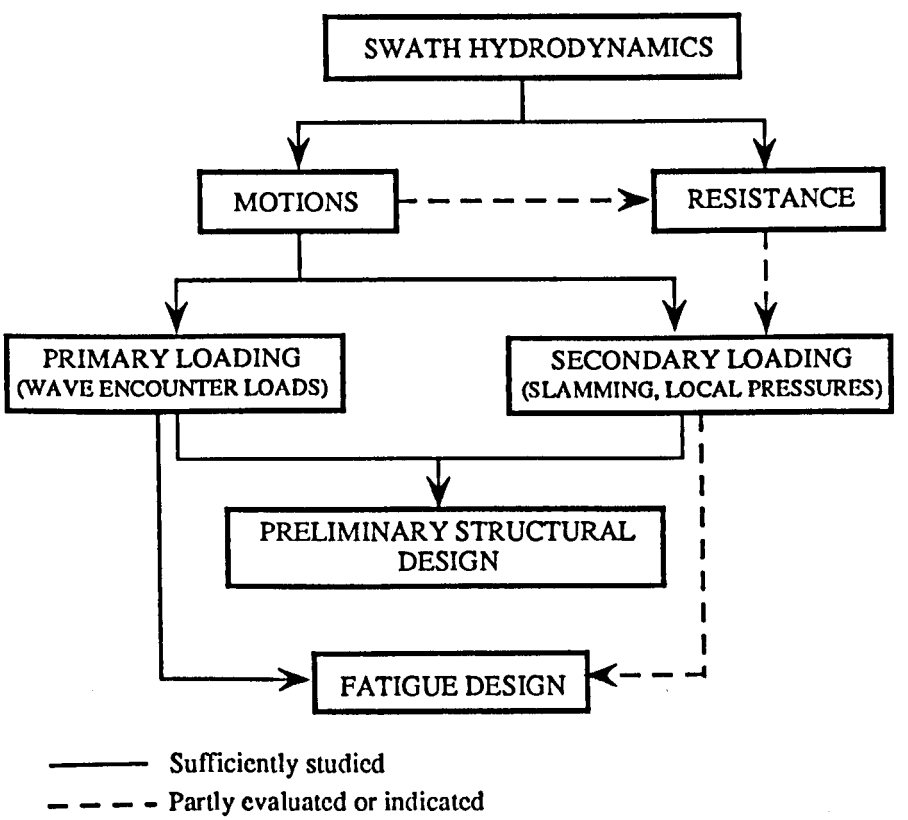

Figure 1.9. Schematic diagram of hydro-structural study on SWATHs

CHAPTER 2

HYDRODYNAMIC FEATURE OF SWATH SHIPS

CHAPTER 2

HYDRODYNAMIC FEATURES OF SWATH SHIPS

2.1. INTRODUCTION

For many centuries speed performance had traditionally been regarded as the most important factor, while seakeeping performance had not held the same importance in ship design. Many advanced marine vehicles, such as surface effect ships, hydrofoil crafts and planing hull type vessels were conceived and established to overcome the speed limitation of conventional displacement vessels.

Nevertheless, stable platforms with good mobility even in adverse waters achieved a new significance in recent years, since many activities of ocean technology development have looked to exploit and ensure the natural resources in the ocean. Hosada et al (1983) suggest that seakeeping performance is now increasingly recognised as important not only in the field of ocean development but also in the fields of marine transportation and naval activities. The reason is obvious, because better seakeeping qualities lead to a higher operational rate, improve the operability (less down time) hence ensuring regularity in services, and better passenger comfort which results in successful operation of the ferries as well as better crew performances on board and more accurate data acquisition which affects the mission effectiveness. A novel concept of SWATH type vessels has evolved within the past two decades to meet the requirement for better seakeeping operations.

This chapter studies motion characteristics of SWATH vessels. Much emphasis is given to the motion data acquisition carried out experimentally at the Hydrodynamics Laboratory. Comparison is then made between experimental and theoretical results for validation purposes. For this particular reason a background review of the theoretical concept and the development of prediction tools will be first outlined. Operational performance of SWATHs in real seaways based on the appropriate seakeeping criteria is further studied by applying a sea spectral prediction method. To supplement this observation on hydrodynamic performance of SWATHs a brief observation on their resistance aspects is put forward. An investigation of SWATH motion and resistance behaviour at high speed operations is another area necessary to be pursued in the future. Design implications due to hydrodynamic performances of SWATH type vessels are discussed.

2.2. THE NATURE OF SWATH SHIP MOTIONS

SWATH ships have been proved to have much lower motion than monohull ships in any mode of oscillation. This lower motion is obtained from the combination of deeply submerged hulls and the small waterplane area of the struts. The deeply submerged hulls, which provide the buoyancy, will experience low wave exciting forces, whereas the small waterplane area of a SWATH ensures the natural frequency will be much lower than an equivalent conventional vessel. The relationship between the natural frequency and the waterplane area in the heave mode of motion is :

$$\omega_z = \sqrt{\frac{\rho g A_w}{M + AVM_z}} \tag{2.1}$$

This expression shows that a decrease in A_w (waterplane area) brings about lower natural frequency ω_z. The other expressions of natural frequency for roll and pitch modes of motion are :

$$\omega_\phi = \sqrt{\frac{\rho g \nabla GM_T}{I_\phi + I_{A\phi}}} \tag{2.2}$$

and

$$\omega_\theta = \sqrt{\frac{\rho g \nabla GM_L}{I_\theta + I_{A\theta}}} \tag{2.3}$$

Again, compared with monohull ships the roll and pitch natural frequencies of SWATH ships will be much lower. The lower natural frequencies in heave, pitch and roll motions also means that longer natural periods are gained. Long natural periods prevent the resonance with most sea waves, thus degradation of SWATH operability will be avoided. The most striking comparison of ship motions resulted from the joint U.S. Navy and Coast Guard sea trials conducted off Hawaii in 1978, as reported by Woolaver and Peters (1980) and Holcomb and Allen (1983). The ship deployed during the comparative trials was a 3100-ton high endurance Coast Guard cutter, USCGC *Mellon*, a 220-ton U.S. Navy SWATH, SSP *Kaimalino* and a 110-ton USCG patrol boat *Cape Corwin*. The SWATH experienced slightly less pitch and heave, and much less roll. The curves in Fig. 2.1 show the superior seakeeping of a small SWATH ship compared to a monohull ship which is 15 times larger. It should also be noted the 200-ton SWATH has half the roll motion of the 3100-ton monohull.

2.3. CONCEPT OF FLUID FORCES ON A CYLINDER IN WAVES

As outlined by Comstock (1977) the basic understanding of ship motion can easily be studied by considering the case of a freely floating cylinder in a train of regular harmonic (sinusoidal) waves which are long with respect to the cylinder.

When surface waves pass through a floating body the ambient fluid will exert hydrodynamic forces and moments on the body. These consist of two components, i.e. the unsteady exciting components, known as the first order forces, lead to the body oscillations and these components are linearly proportional to the wave height. On the other hand, second order forces are attributable to the non-linear effects and these components are generally small and proportional to the square of the wave height.

Figure 2.2 from Atlar et al (1987) shows the diagram of the division of the fluid forces and moments exerted by the surrounding fluid on the floating body subjected to the surface waves. The following clarification is concerned with the division of forces (or moments).

The first order oscillatory forces can be divided into two main components, namely, viscous force and pressure force. The viscous force, F_V, is brought about by the fluid viscosity and deals with the fluid flow velocities relative to the body. The flow velocities are generated by the body motion and by waves. The former, i.e. flow velocities generated by the body motion, create damping force on the body, known as damping force due to viscosity. The latter in certain cases, such as rolling cylinders in fluid where the pressure force is very small, the fluid force will be dominated by viscosity force.

The pressure force consists of the hydrostatic restoring force and the hydrodynamic force. The hydrostatic force, F_C, is the force caused by the fluid displaced when the floating body changes its submerged volume. This force usually corresponds linearly to the motion displacement and acts against it. Therefore, F_C can be written as :

$$F_C = -Cs \tag{2.4}$$

where C = restoring force coefficient, and
s = motion displacement

The hydrodynamic inertial force, F_A, which is created by the hydrodynamic added mass A corresponds with the acceleration, $\ddot{s}$, and opposes the motion, and is written as :

$$F_A = -A\ddot{s} \tag{2.5}$$

where A = hydrodynamic added mass (or mass moment of inertia)

The hydrodynamic velocity force, F_B, is proportional to the velocity, $\dot{s}$, and acts against it. This force is a result of energy losses of the body due to radiated surface waves :

$$F_B = -B\dot{s} \tag{2.6}$$

where B = hydrodynamic damping per unit velocity.

The wave induced force, F_w, is the summing of the incident wave force, F_I, and the diffracted wave force, F_D. This force is also known as the wave exciting force and, since its magnitude varies with time, it is included as follows :

$$F_W = \left(F_I + F_D\right) e^{-i\omega t} \tag{2.7}$$

where i = $\sqrt{-1}$
ω = radian frequency of the incident waves, and
t = time

According to Newton's second law, the sum of the above fluid forces will be balanced by the inertial forces (or moments). F_M is equal to the body mass (or mass of moment inertia) multiplied by the acceleration of the body motion as :

$$F_M = M\ddot{s} = F_W - F_A - F_B - F_C \tag{2.8}$$

where M = total body mass (or mass moment inertia)

By substituting equations (2.4) and (2.6) into equation (2.8), the force (or moment) equation becomes :

$$\begin{aligned} M\ddot{s} &= F_W - A\ddot{s} - B\dot{s} - Cs \text{ or} \\ (M + A)\ddot{s} + B\dot{s} + Cs &= F_W \end{aligned} \tag{2.9}$$

2.4. MOTION EQUATION OF A SWATH SHIP

The theoretical background to solve the problem of six-degree of freedom coupled motions of a SWATH ship in regular quartering seas addressed in this section is extracted from the reports by Lee and Curphey (1977), Seren and Atlar (1984a), and Atlar (1986).

2.4.1. Definition of a Co-ordinate System

The co-ordinate system applied in the analysis is a right handed rectangular co-ordinate system, as shown in Fig. 2.3. This co-ordinate system can be described as follows :

a. Earth fixed axes ($O\text{-}X_0Y_0Z_0$) are fixed with respect to earth. Their origin is located arbitrarily but usually at the calm-water surface.
b. Body fixed axes (G-xyz) have their origin at the centre of gravity of the body and are coincident with the intersections of the principal planes of inertia.
c. Space-fixed or mean body axes (O-XYZ) originate at the main position of the body centre of gravity and are used to describe the body oscillations. The system is parallel to the earth-fixed ($O\text{-}X_0Y_0Z_0$) system but translates with the advancing ship speed U.

2.4.2. Formulation of Equations of Motion

There are some assumptions that should be stated in this analysis so that the solution performed could be justified. These assumptions are :

a. the exciting forces and moments are assumed to be solely contributed by free surface waves
b. the wave amplitudes or the wave slopes are assumed to be small
c. the vessel is operated in an infinitely deep ocean, therefore, no appreciable currents or winds would cancel the linear response assumption, and
d. the submerged parts of the vessel are assumed to be reasonably slender.

Considering these assumptions, the six-degree of freedom linear coupled equation of motion for a floating body subject to sinusoidal wave excitation of frequency w may be expressed in the following form :

$$\sum_{k=1}^{6}\left(M_{jk}+A_{jk}\right)\ddot{s}_k + B_{jk}\dot{s}_k + C_{jk}s_k = F_j \qquad (2.10)$$

where k = mode of motion takes 1,2,3,4,5 and 6 for the surge, sway, heave, roll, pitch and yaw, respectively

j = mode of excitation and takes the values similar to k for the corresponding modes

M_{jk} = mass matrix containing the mass, mass moment of inertia and products of inertia of the body

A_{jk} = added mass matrix containing added mass and added moment of inertia per unit acceleration, which are frequency dependent

B_{jk} = damping matrix containing damping force and moment of inertia per unit velocity

C_{jk} = restoring matrix containing restoring force and moment matrix per unit displacement

s_k = complex motion displacement vector per unit wave amplitude, and

F_j = complex wave exciting force and moment vector per unit wave amplitude.

In some references M_{jk} and s_k that are presented by the index notation, as given in equation (2.10), can also be identified according to the initial definition and the correspond axes defined in Fig. 2.3, as follows :

$M_{11}=M_{22}=M_{33}=M$; i.e. the mass of the ship

$M_{44},M_{55},M_{66}=I_4,I_5,I_6$; i.e. mass moment of inertia in the roll, pitch, and yaw mode, respectively

$s_1,s_2,s_3,s_4,s_5,s_6 = x,y,z,\phi,\theta,\psi$; i.e. motion displacement in the surge, sway, heave, roll, pitch, and yaw, respectively.

As the wave exciting force and moment vector on the right hand side of equation (2.10) is a complex function, so it can be expressed as :

$$F_j = \mathrm{Re}\left(\bar{F}_j e^{-i\omega t}\right) \qquad (2.11)$$

where F_j is the complex force amplitude which can be written in terms of the real (R) and imaginary (I) part as :

$$\bar{F}_j = F_{jR} + iF_{jI} \qquad (2.12)$$

By substituting eq. (2.11) into eq. (2.12), it can be found that :

$$F_j = \left\{\left(F_{jR} + iF_{jI}\right) e^{-i\omega t}\right\} \text{ or}$$
$$F_j = F_{jR} \cos \omega t + iF_{jI} \sin \omega t \qquad (2.13)$$

and eq. (2.13) can be written as :

$$F_j = \left|F_j\right| \cos\left(\varepsilon_j - \omega t\right) \qquad (2.14)$$

where $$\left|F_j\right| = \sqrt{\left(F_{jR}^2 + F_{jI}^2\right)} \qquad (2.15)$$

= maximum of the wave exciting force, and

$$\varepsilon_j = \arctan\left(F_{jR}/F_{jI}\right) \qquad (2.16)$$

= the phase shift of the maximum of the wave exciting force from the incident wave at the origin of the wave co-ordinate system [see p.4 of the report by Seren and Atlar (1984a)].

To be compatible with the complex expression of F_j, the motion displacement s_k is also assumed to be a complex function given by :

$$s_k = \text{Re}\left(\bar{s}_k\, e^{-i\omega t}\right) \qquad (2.17)$$

Furthermore, the velocity and the acceleration components can be expressed as :

$$\dot{s}_k = -i\omega\, \bar{s}_k\, e^{-i\omega t} \qquad (2.18)$$
$$\ddot{s}_k = -i\omega^2\, \bar{s}_k\, e^{-i\omega t} \qquad (2.19)$$

Following the above sequence from eq. (2.11) to (2.16) the motion displacement can also be written as follows :

$$\bar{s}_k = s_{kR} + is_{kI} \qquad (2.20)$$
$$s_k = s_{kR} \cos \omega t + s_{kI} \sin \omega t \qquad (2.21)$$
$$\left|s_k\right| = \sqrt{\left(s_{kR}^2 + s_{kI}^2\right)} \qquad (2.22)$$
$$s_k = \left|s_k\right| \cos\left(\alpha_k - \omega t\right) \qquad (2.23)$$
$$\alpha_k = \arctan\left(s_{kI}/s_{kR}\right) \qquad (2.24)$$

where : $|s_k|$ = the maximum of the motion displacement, and

α_k = the phase shift of the maximum of the motion displacement from the maximum of the incident wave at the origin of the wave co-ordinate system.

2.4.3. Solution of the Motion Equation

The surge mode is assumed to be decoupled from the other modes. Moreover, the added mass, damping and diffracted wave force in the x-direction are assumed to be small and negligible. The equation of surge motion, therefore, can be expressed by :

$$M_{11}\ddot{s}_1 = F_1 \tag{2.25}$$

or by using the coordinate system as a reference, eq. (2.25) becomes :

$$M\ddot{x} = F_1 \tag{2.26}$$

The symmetry of the hull with respect to the longitudinal centre plane leads to the decoupling of the vertical plane (heave and pitch) from the horizontal plane (sway, roll and yaw) modes. Consequently the equation of motion can be divided into two groups.

By expanding eq. (2.10) for heave and pitch modes, i.e. j,k = 3 and 5, this can be written as :

$$\begin{aligned}
\left(M_{33} + A_{33}\right)\ddot{s}_3 + B_{33}\dot{s}_3 + C_{33}s_3 + A_{35}\ddot{s}_5 + B_{35}\dot{s}_5 + C_{35}s_5 &= F_3 \\
\left(M_{55} + A_{55}\right)\ddot{s}_5 + B_{55}\dot{s}_5 + C_{55}s_5 + A_{53}\ddot{s}_3 + B_{53}\dot{s}_3 + C_{53}s_3 &= F_5
\end{aligned} \tag{2.27}$$

or, by using the corresponding co-ordinate system, eqs.(2.27), becomes :

$$\begin{aligned}
\left(M_{33} + A_{33}\right)\ddot{z} + B_{33}\dot{z} + C_{33}z + A_{35}\ddot{\theta} + B_{35}\dot{\theta} + C_{35}\theta &= F_3 \\
\left(M_{55} + A_{55}\right)\ddot{\theta} + B_{55}\dot{\theta} + C_{55}\theta + A_{53}\ddot{z} + B_{53}\dot{z} + C_{53}z &= F_5
\end{aligned} \tag{2.28}$$

Substituting eqs. (2.18) and (2.19) into eq. (2.27) for j,k = 3 and 5 the following equations are derived :

$$\left\{\left(M_{33}+A_{33}\right)\left(-\omega^2\right)+B_{33}(-i\omega)+C_{33}\right\}\bar{s}_3+\left\{A_{35}\left(-\omega^2\right)+B_{35}(-i\omega)+C_{35}\right\}\bar{s}_5=\bar{F}_3$$
$$\left\{\left(M_{55}+A_{55}\right)\left(-\omega^2\right)+B_{55}(-i\omega)+C_{55}\right\}\bar{s}_5+\left\{A_{53}\left(-\omega^2\right)+B_{53}(-i\omega)+C_{53}\right\}\bar{s}_3=\bar{F}_5 \quad (2.29)$$

By substituting eqs. (2.12) and (2.20) into eq. (2.29) for k,j = 3 and 5 and arranging the right and left hand-side of the above equation in terms of the real and imaginary part, the following matrix form of the resulting equation is obtained :

$$\begin{bmatrix} -\omega^2(M_{33}+A_{33})+C_{33} & -\omega^2A_{35}+C_{35} & \omega B_{33} & \omega B_{35} \\ -\omega^2A_{35}+C_{35} & -\omega^2(M_{55}+A_{55})+C_{55} & \omega B_{53} & \omega B_{55} \\ -\omega B_{33} & -\omega B_{35} & -\omega^2(M_{33}+A_{33})+C_{33} & -\omega^2A_{35}+C_{35} \\ -\omega B_{53} & -\omega B_{55} & -\omega^2A_{53}+C_{53} & -\omega^2(M_{55}+A_{55})+C_{55} \end{bmatrix} \times \begin{bmatrix} s_{3R} \\ s_{5R} \\ s_{3I} \\ s_{5I} \end{bmatrix} = \begin{bmatrix} F_{3R} \\ F_{5R} \\ F_{3I} \\ F_{5I} \end{bmatrix}$$
....(2.30)

or by using the index notation corresponding to the co-ordinate system eq. (2.30) can be written as :

$$\begin{bmatrix} -\omega^2(M_{33}+A_{33})+C_{33} & -\omega^2A_{35}+C_{35} & \omega B_{33} & \omega B_{35} \\ -\omega^2A_{35}+C_{35} & -\omega^2(I_5+A_{55})+C_{55} & \omega B_{53} & \omega B_{55} \\ -\omega B_{33} & -\omega B_{35} & -\omega^2(M_{33}+A_{33})+C_{33} & -\omega^2A_{35}+C_{35} \\ -\omega B_{53} & -\omega B_{55} & -\omega^2A_{53}+C_{53} & -\omega^2(I_5+A_{55})+C_{55} \end{bmatrix} \times \begin{bmatrix} z_R \\ \theta_R \\ z_I \\ \theta_I \end{bmatrix} = \begin{bmatrix} F_{3R} \\ F_{5R} \\ F_{3I} \\ F_{5I} \end{bmatrix}$$
....(2.31)

By expanding eq. (2.10) for sway, roll and yaw modes, i.e. j,k = 2,4 and 6, this can be written as :

$$\begin{aligned} &\left(M_{22}+A_{22}\right)\ddot{s}_2+B_{22}\dot{s}_2+A_{24}\ddot{s}_4+B_{24}\dot{s}_4+A_{26}\ddot{s}_6+B_{26}\dot{s}_6=F_2 \\ &\left(M_{44}+A_{44}\right)\ddot{s}_4+B_{44}\dot{s}_4+C_{44}s_4+A_{42}\ddot{s}_2+B_{42}\dot{s}_2+A_{46}\ddot{s}_6+B_{46}\dot{s}_6=F_4 \\ &\left(M_{66}+A_{66}\right)\ddot{s}_6+B_{66}\dot{s}_6+A_{62}\ddot{s}_2+B_{62}\dot{s}_2+A_{64}\ddot{s}_4+B_{64}\dot{s}_4=F_6 \end{aligned} \quad (2.32)$$

Applying the corresponding co-ordinate system, motion equation (2.29) becomes :

$$
\begin{aligned}
&\left(M_{22}+A_{22}\right)\ddot{y}+B_{22}\dot{y}+A_{24}\ddot{\phi}+B_{24}\dot{\phi}+A_{26}\ddot{\psi}+B_{26}\dot{\psi}=F_2\\
&\left(M_{44}+A_{44}\right)\ddot{\phi}+B_{44}\dot{\phi}+C_{44}\phi+A_{42}\ddot{y}+B_{42}\dot{y}+A_{46}\ddot{\psi}+B_{46}\dot{\psi}=F_4\\
&\left(M_{66}+A_{66}\right)\ddot{\psi}+B_{66}\dot{\psi}+A_{62}\ddot{y}+B_{62}\dot{y}+A_{64}\ddot{\phi}+B_{64}\dot{\phi}=F_6
\end{aligned}
\qquad (2.33)
$$

A similar procedure, as in the coupled heave and pitch, is implemented for the sway, roll and yaw, i.e. k,j = 2,4 and 6, which yields the following matrix form of eq. (2.32) as :

$$
\begin{bmatrix}
-\omega^2(M_{22}+A_{22}) & -\omega^2A_{24} & -\omega^2A_{26} & \omega B_{22} & \omega B_{24} & \omega B_{26}\\
-\omega^2A_{24} & -\omega^2(M_{44}+A_{44})+C_{44} & -\omega^2A_{46} & \omega B_{24} & \omega B_{44} & \omega B_{46}\\
-\omega^2A_{62} & -\omega^2A_{44} & -\omega^2(M_{66}+A_{66})+C_{66} & \omega B_{62} & \omega B_{64} & \omega B_{66}\\
-\omega B_{22} & -\omega B_{24} & -\omega B_{26} & -\omega^2(M_{22}+A_{22}) & -\omega^2A_{24} & -\omega^2A_{26}\\
-\omega B_{24} & -\omega B_{44} & -\omega B_{46} & -\omega^2A_{24} & -\omega^2(M_{44}+A_{44})+C_{44} & -\omega^2A_{26}\\
-\omega B_{62} & -\omega B_{64} & -\omega B_{66} & -\omega^2A_{62} & -\omega^2A_{44} & -\omega^2(M_{66}+A_{66})+C_{66}
\end{bmatrix}
\times
\begin{bmatrix} s_{2R}\\ s_{4R}\\ s_{6R}\\ s_{2I}\\ s_{4I}\\ s_{6I}\end{bmatrix}
=
\begin{bmatrix} F_{2R}\\ F_{4R}\\ F_{6R}\\ F_{2I}\\ F_{4I}\\ F_{6I}\end{bmatrix}
$$

....(2.34)

or by using the index notation in conjunction with the coordinate system equation above can be written as :

$$
\begin{bmatrix}
-\omega^2(M_{22}+A_{22}) & -\omega^2A_{24} & -\omega^2A_{26} & \omega B_{22} & \omega B_{24} & \omega B_{26}\\
-\omega^2A_{24} & -\omega^2(I_4+A_{44})+C_{44} & -\omega^2A_{46} & \omega B_{24} & \omega B_{44} & \omega B_{46}\\
-\omega^2A_{62} & -\omega^2A_{44} & -\omega^2(I_6+A_{66})+C_{66} & \omega B_{62} & \omega B_{64} & \omega B_{66}\\
-\omega B_{22} & -\omega B_{24} & -\omega B_{26} & -\omega^2(M_{22}+A_{22}) & -\omega^2A_{24} & -\omega^2A_{26}\\
-\omega B_{24} & -\omega B_{44} & -\omega B_{46} & -\omega^2A_{24} & -\omega^2(I_4+A_{44})+C_{44} & -\omega^2A_{26}\\
-\omega B_{62} & -\omega B_{64} & -\omega B_{66} & -\omega^2A_{62} & -\omega^2A_{44} & -\omega^2(I_6+A_{66})+C_{66}
\end{bmatrix}
\times
\begin{bmatrix} y_R\\ \phi_R\\ \Psi_R\\ y_I\\ \phi_I\\ \Psi_I\end{bmatrix}
=
\begin{bmatrix} F_{2R}\\ F_{2R}\\ F_{6R}\\ F_{2I}\\ F_{4I}\\ F_{6I}\end{bmatrix}
$$

....(2.35)

2.4.4. Hydrodynamic Forces

The first order, external oscillatory fluid forces acting on a ship can be divided into two linearly superimposable components, that is, wave-induced (or excitation)

forces and motion-induced (or reaction) forces, as shown by Seren et al (1985). The first force consists of the incident wave force calculated on the assumption that the presence of the body does not distort the wave which can be derived from the Froude-Krylov theory, and the diffracted wave force, which accounts for the scattering of the incident wave by the presence of the body.

The reaction force, as has been described in the foregoing section, is considered to be a property of the structure and consists of three components which directly relate to the three components of hydrodynamic excitation. The three components are : a quasi-static (or buoyancy) restoration in heave, roll and pitch modes and a body-generated hydrodynamic force which is subdivided into an inertial (added mass) force and damping force as a result of the circumfusion of energy from the body in radiating surface waves, which are linearly proportional to the body acceleration and velocity respectively. This force is calculated with the assumption that the body undergoes the same motion in calm water as in waves. This is called a radiation problem.

It should be borne in mind that the excitation and reaction forces possess viscous components caused by the wave-induced viscous fluid damping and the body-induced viscous fluid motion, respectively. Both components are combined into a single viscous force resulting from the relative velocity of body and fluid.

2.4.4.1. Problem Formulation with Forward Speed. The body fixed axis (G-xyz) which coincides with the space-fixed co-ordinate system (O-XYZ) at time t=0, moves along the X-axis with a steady forward speed U. The relationship between the fixed and translating co-ordinate system as used by Seren et al (1985) can be written as follows :

$$X = x + Ut;\ Y = y;\ Z = z \tag{2.36}$$

whereas the relationship between the wave frequency and the frequency of encounter, ω_e, is given by :

$$\omega_e = \omega_0 + Uk_0 \cos \mu \tag{2.37}$$

where ω_0 = the incident wave frequency at zero speed
μ = the wave heading angle, which is defined so that μ=0 indicates following or overtaking seas directly from astern
k_0 = the wave number = ω_0^2/g, and
g = the acceleration due to gravity.

In a reference frame (G-xyz) moving with steady forward motion the incident wave potential which generates the wave is expressed as :

$$\phi_I(x,y,z;k_0,\mu,t) = \phi_I(y,z;k_0,\mu)\, e^{i(k_0 \cos\mu - \omega t)} \tag{2.38}$$

with

$$\phi_I(y,z;k_0,\mu) = -\frac{i g \zeta_A}{\omega_0}\, e^{(k_0 z)}\, e^{(ik_0 \sin\mu)} \tag{2.39}$$

where ζ_A = wave amplitude.

If the influence of the phase shift, due to the longitudinal location of the strip section relative to the crest of the incident wave through the body axis, is omitted until the final calculation for the force on the body, then the expression of the incident wave velocity potential given in eq. (2.39) can be written in its odd (o) and even (e) parts as follows :

$$\begin{aligned} \phi_I^{(o)}(y,z,k_0,\mu) &= \mathrm{Re}\left[\phi_I(y,z,k_0,\mu)\right] = \frac{g\zeta_A}{\omega_0} e^{k_0 z} \sin(k_0 y \sin\mu) \\ \phi_I^{(e)}(y,z,k_0,\mu) &= \mathrm{Im}\left[\phi_I(y,z,k_0,\mu)\right] = \frac{g\zeta_A}{\omega_0} e^{k_0 z} \cos(k_0 y \sin\mu) \end{aligned} \tag{2.40}$$

2.4.4.2. The Froude-Krylov Component. When the body fixed axis, G-xyz, moves with a steady forward motion, the incident wave potential is identical to that at zero-speed, except for the change in frequency of encounter.

In matrix notation, the Froude-Krylov sectional forces per unit wave amplitude, $f^K_{(m)}$, in the in-plane modes of motion as given by Seren and Atlar (1984b), are (omitting the time factor) :

$$\begin{bmatrix} f^K_{(2)}(x) \\ f^K_{(3)}(x) \\ f^K_{(4)}(x) \end{bmatrix} = \rho g \int_{S(x)} e^{k_0 z} \begin{bmatrix} \sin \\ \cos \\ \sin \end{bmatrix} \left(k_0\, y \sin\mu\right) \begin{bmatrix} -dz \\ dy \\ ydy + (z - z_0)dz \end{bmatrix} \tag{2.41}$$

where $\int_{S(x)}$ = the contourwise integral at station x

ρ = density, and

subscript (m) = denotes the dependence on the mode of motion

Integrating the foregoing sectional forces along the ship length, taking into account the phase angle, yields the resultant Froude-Krylov forces and moments per unit wave amplitude, $F^K_{(m)}$:

$$\begin{bmatrix} F^K_{(2)} \\ F^K_{(3)} \\ F^K_{(4)} \\ F^K_{(5)} \\ F^K_{(6)} \end{bmatrix} = \int_L e^{ik_0 x \cos\mu} \begin{bmatrix} if^K_{(2)}(x) \\ if^K_{(3)}(x) \\ if^K_{(4)}(x) \\ if^K_{(5)}(x) \\ if^K_{(6)}(x) \end{bmatrix} \begin{bmatrix} dx \\ dx \\ dx \\ -dx \\ xdx \end{bmatrix} \tag{2.42}$$

where $\int_L$ = the lengthwise integral for the component.

Whenever a product with the imaginary unit i is involved, only the real part of the product will be recognised.

2.4.4.3. The Diffraction Component. The sectional sway, heave and roll-exciting forces and moments due to diffraction, $f^D_{(m)}$, are given by :

$$\begin{bmatrix} f^D_{(2)}(x) \\ f^D_{(3)}(x) \\ f^D_{(4)}(x) \end{bmatrix} = i\rho\omega \int_{S(x)} \begin{bmatrix} \phi^{(0)}_D(y,z,k,\mu) \\ \phi^{(e)}_D(y,z,k,\mu) \\ \phi^{(0)}_D(y,z,k,\mu) \end{bmatrix} \begin{bmatrix} -dz \\ dy \\ ydy+(z-z_0)dz \end{bmatrix} \tag{2.43}$$

where $\phi_D{}^{(o)}$ = the odd complex diffraction velocity potential which corresponds to $\phi_I{}^{(o)}$, and

$\phi_D{}^{(e)}$ = the even complex diffraction velocity potential which corresponds to $\phi_I{}^{(e)}$.

The diffraction velocity potential ϕ_D can be expressed as a function of Green's theorem and the complex source strength. By taking the normal derivative of the function as :

$$\frac{\partial}{\partial n}\phi^{(m)}_D = \left[\sum_{j=1}^{N} Q^{(m)}_j I^{(m)}_{ij} + \sum_{j=1}^{N} Q^{(m)}_{N+j} J^{(m)}_{ij}\right] + i\left[\sum_{j=1}^{N} Q^{(m)}_j J^{(m)}_{ij} - \sum_{j=1}^{N} Q^{(m)}_{N+j} I^{(m)}_{ij}\right] \tag{2.44}$$

where Q_j = the Green's function at any segment j

I_{ij}, J_{ij} = termed as the 'influence coefficients' [Seren et al (1985)].

By separating the right hand side of eq. (2.44) into its real and imaginary part, the odd function can be written as :

$$\sum_{j=1}^{N} Q_j^{(m)} I_{ij}^{(m)} + \sum_{j=1}^{N} Q_{N+j}^{(m)} J_{ij}^{(m)}$$

and the even function as :

$$\sum_{j=1}^{N} Q_j^{(m)} J_{ij}^{(m)} + \sum_{j=1}^{N} Q_{N+j}^{(m)} I_{ij}^{(m)}$$

The even functions for both the incident and the diffraction produce wave exciting forces in heave, while the odd functions produce sway and roll forces.

Taking into account the phase angle, the resultant diffraction forces and moments per unit wave amplitude, $F^D_{(m)}$:

$$\begin{bmatrix} F^D_{(2)} \\ F^D_{(3)} \\ F^D_{(4)} \\ F^D_{(5)} \\ F^D_{(6)} \end{bmatrix} = \begin{bmatrix} F^D_{(2)}(k) \\ F^D_{(3)}(k) \\ F^D_{(4)}(k) \\ F^D_{(5)}(k) \\ F^D_{(6)}(k) \end{bmatrix} + \begin{bmatrix} 0 \\ 0 \\ 0 \\ \frac{U}{i\omega} F^D_{(3)}(k) \\ -\frac{U}{i\omega} F^D_{(3)}(k) \end{bmatrix} + \Gamma \begin{bmatrix} f^D_{(2)}(x) \\ f^D_{(3)}(x) \\ f^D_{(4)}(x) \\ -f^D_{(3)}(x) \\ -f^D_{(2)}(x) \end{bmatrix} \qquad (2.45)$$

with

$$\Gamma = \frac{U}{i\omega} e^{ik_0 x \cos\mu}$$

The elements of the first matrix in the right hand side of eq. (2.45), $F^D_{(m)}(k)$, are independent of speed, but depend on encounter frequency. The elements of the second matrix are the so-called speed dependent terms which influence only the pitch and yaw modes. The terms in the third matrix are the end terms. x refers to the longitudinal distance from the origin of the co-ordinate system and :

$\Big|_L$ indicates $\Big|_{l_a}^{l_f}$

with l_f and l_a, respectively, the distance of the forwardmost and aftermost sections from the origin of the co-ordinate system used in the calculation.

The resultant wave exciting force per unit wave amplitude acting on the SWATH-type ship proceeding in regular oblique seas is obtained by adding the Froude-Krylov force, eq. (2.42), and the diffraction force, eq. (2.45).

Lee and Curphey (1977) introduced the phase relationship by taking a cosine and a sine component (in phase with the acceleration and velocity, respectively) of all the quantities involved in the calculation.

2.4.5. Hydrodynamic Coefficients

The three-dimensional added mass/inertia and wave damping coefficients, A_{ij} and B_{ij} respectively, as given in Table 2.1, are expressed in terms of the corresponding sectional coefficients which are assumed frequency dependent, a_{ij}, b_{ij}, with $\int_L$ the lengthwise integral for the component.

When the areas of the end-sections are zero, the end terms vanish. The remaining terms, if any, in a certain mode mode of motion are the speed dependent terms which are characterised by U. The subscripts of the coefficients denote a coefficient in i^{th} force or moment equation due to motion in j^{th} mode. The superscript '0' denotes terms evaluated at zero speed. The expressions in Table 2.1 are only the potential part of the motion coefficients of an unappended SWATH ship. To obtain reasonable predictions of SWATH ship motions alternative formulations, which include both the hull viscous effects and the hydrodynamic effects due to the fins contribution, ought to be applied. Such formulations can be found in the reference by Lee and Curphey (1977).

2.4.6. Hydrostatic Restoring Forces

Based on the hydrostatic considerations, the restoring forces in the equation of motions are given in Table 2.2. Where GM_T and GM_L are the transverse and longitudinal metacentric height, respectively, M_{AW} is the moment of the waterplane area about the y-axis, and ∇ is the volume of displacement.

2.5. SOME METHODS OF SWATH SHIP MOTION ASSESSMENT

As for conventional monohull ships and offshore structures, there are three main methods which can be applied to estimate the wave induced loads and motions on a SWATH ship. These methods are well known as :

a. Morison's Formula
b. Strip Theory
c. Three-dimensional Sink-source Technique.

The application of Morison's formula is justified when three assumptions relating to the submerged body can be satisfied. Firstly, the diameter of the SWATH hulls should be small compared to the wave length. When the hulls are subdivided into several small cylinders, the ratio of the hull diameter to the wave length should be less than 0.2. Furthermore, Morison's formula requires the potential damping attributed by waves to be ignored. Secondly, the hulls are assumed to be deeply submerged and, thus, unbounded ambient fluid can be used for added mass and damping. The third assumption is the hulls are not closely spaced. This implies that the hull spacing should be large with respect to the cross-sectional element dimensions so that the hydrodynamic interference between the elements may be neglected. These assumptions lead to restrictions in the application of Morison's formula particularly for SWATH ships. Therefore, this method is considered to be inappropriate.

By using the strip theory, the solutions are found basically in the same way as for Morison's formula, that is, the submerged hulls are sliced into several elements. Each element is considered individually, thus, the hydrodynamic interference between the elements can be neglected and the forces on each element calculated utilising the two-dimensional Close-fit technique developed by Frank (1976). There is an assumption in the application of strip theory, i.e. the submerged hulls should satisfy the longitudinal slenderness. In this theory the SWATH vertical struts are considered as surface-piercing extensions of the hulls and included in the two-dimensional beamwise strip sections. The hydrodynamic interference between the hulls and the struts is treated separately. This theoretical approach has been successfully applied for SWATH ship designs by Nordenstrom et al (1971), Kim and Chou (1973), Lee (1976), and Seren and Atlar (1984a).

For some types of large twin-hull semi-submersibles, such as pipelaying barges, with relatively short columns and cross-sectional dimensions which are similar to the hull separation, Morison's formula and the strip theory approach are no longer suitable. Therefore, calculation of wave loads should be determined by the three-dimensional

sink-source technique. This approach is considered by Paulling and Hong (1977) and Zheng (1988) as an accurate method since the scattering of the incident waves by the columns is taken into account. However, there is disadvantage in this method which takes a large amount of computer time and computational effort, consequently it is much more costly.

Comparison of the above methods has been made by Mathisen and Carlsen (1980) and Atlar et al (1985) and it was concluded that in operational draughts there is a good agreement between strip theory and Morison's formula. Furthermore, it was also found that the strip theory had good agreement in transit draughts with the three-dimensional sink-source technique. Nevertheless, consideration of the cost and time required by the three-dimensional sink-source technique and the restrictions of Morison's formula in application make the strip theory the most attractive method to be developed and used in predicting wave loads and motions of a SWATH ship.

2.6. EXISTING COMPUTER PROGRAMS FOR SWATH MOTIONS AND DYNAMIC STRUCTURAL LOADINGS ASSESSMENT

Three different computer programs to assess the SWATH ship motions and dynamic structural loadings have been written in the Department. The first program is based on the strip theory method, the second on the three-dimensional sink-source technique, and the third on the three-dimensional pulsating-translating source.

2.6.1. Computer Program Based on the Strip Theory

This program, SWATHL, was written for and run on the VAX 11/730 computer system and was evolved at the Hydrodynamics Laboratory by Seren and Atlar (1984b), Seren and Leitch (1982), Seren and Miller (1982), Seren et al (1983a,1983b), and Drysdale (1986a). The program was originally written to predict the motions and loadings of twin-hulled semi-submersibles. Nevertheless, the versatility and sophistication of the technique used has led to a wider range of its application. This program, therefore, is also applicable for other configurations of twin-hulled semi-submersible vehicles such as SWATH ships and even for monohull conventional vessels. The computer program has since been enhanced to meet the demand of control surfaces for SWATH. The earliest study on aft fins for the computer program has been compared with the experimental data and can be found in the papers by Wu (1984, 1985a, 1985b) and Wu and McGregor (1986) and the more comprehensive improvement in the reports by Drysdale (1986a, 1986b). The routine of SWATHL has recently been enhanced by Drysdale (1987) to assess SWATH structural responses. In this section, review is mainly concerned with running of the program SWATHL.

Some input data required to run the program and this can be classified as processed input data and pure input data, as described by Drysdale (1986a). The processed input data is the geometry data from, e.g. SW11.DAT and the mass data from SW11MAS.DAT, where SW stands for SWATH, and 11 stands for SWATH1 model with geometry configuration 1. By running the program SWATHL and inputing SW11.DAT the hydrostatic data of the model can be obtained, whereas inputing SW11MAS.DAT results in mass distribution data of the model.

The pure input data required is wave frequency, model characteristic length and draught, model speed, water density and the model heading angle towards wave trains. Additional input data, i.e. the mass of the deck and the deck beam are required to obtain dynamic structural loads. The number of wave frequencies in radians/second input into the running program varies from 1 to 30 and this input influences the running time. Variation of the model position with respect to wave propagations is between 0^{o} and 180^{o}.

The output data obtained from running the main program is motion induced coefficients, wave exciting force/moment and phases, motion amplitudes and phases and bending moments and shear forces at the midpoint of crossdeck and phases.

2.6.2. Computer Program Based on the Three-dimensional Sink-Source Technique

The computer program to assess the motions and dynamic loadings of SWATH ships based on the three-dimensional sink-source technique is called SHIPM1.0, and was written to run on the VAX Cluster computer system at the University. This computer program was developed from a basic understanding of ship hydrodynamics by Zheng (1985,1986,1988) and then gradually improved to solve the problem of six-degree of freedom of ship motion and dynamic loads.

The SHIPM1.0 computer program comprises three routines, namely, SHIPM1A, SHIPM2A and HFORCE. The SHIPM1A routine calculates the hydrodynamic forces imposed on a floating body without the effect of free surface. Whereas the SHIPM2A routine takes into account the free surface effect or viscosity which are frequency dependent, and consequently to run this computer program more time is consumed than for running SHIPM1A. The HFORCE computes the hydrodynamic forces, motions and wave loads, and creates graphs of motion and structural responses.

Two types of input data, that is, geometry data and variable data, are required to run the SHIPM1A computer program. The geometry data is a large data set specially generated and permanently stored. To create a geometry data of a ship, half of the hull geometry is needed and the whole ship geometry data is obtained by applying a symmetrical hull body principle.

The variable data comprises of five parts which are :

a. frequency of wave : the number of frequencies and values of frequencies
b. forward speed : the number of speeds and their values
c. wave heading angle : the number of headings and the values of the heading angles in degrees
d. Inertia and restoring coefficients : ship main dimensions and hydrostatic data (i.e. L, B, D, A_W, GM_T, and GM_L) and the mass and mass moment of inertia data (i.e. m, I_{44}, I_{55}, I_{66}, and I_{46}), and
e. control data : the program asks wether or not output data is required to be printed immediately. 1 or 0 corresponding to yes or no should be entered in response.

There are four kinds of output data which can be generated by the program, that is, pressure distributions (this is a large data and hardly required), motion responses with or without viscous effect, structural responses (i.e. vertical and horizontal shear forces, bending moment and torsional moment), and graphs of motion and structural responses, etc.

The computer program capable of assessing motion and structural responses of monohull and SWATH ships. As reported by Zheng and McGregor (1987) the versatility of the program has also been successfully examined to predict the motion and loading behaviour of a semi-submersible type crane barge. The barge, has four large circular columns on each hull with the two hulls relatively close to each other. Such a structure is very difficult to analyse using two-dimensional theory since this approach assumes that the column should be a slender body and the interference effects between the two hulls are negligible.

2.6.3. Computer Program Based on the Three-dimensional Translating Pulsating Source Technique

The latest ship motion program MARCHS was developed by Chan (1990a) at the NA&OE Department. A translating pulsating source technique was adapted to enhance the accuracy of motion prediction for ships advancing in waves. This is the case since the pulsating sink source approach considers only two-dimensional waves which are

unaffected by the forward motion, thus some restrictions must apply to forward speeds. In order to place no restrictions on the frequency of oscillation and the forward speed of the ship, the three-dimensional unsteady forward motion problem ought to be first solved by some mathematical order, as described by Chan (1989). In spite of the accuracy offered when the translating pulsating source is implemented, the amount of computational time and processing memory is substantially large. The program is therefore also furnished with a correction formula on forward speeds (similar to that explained in section 2.4.4.1) to be associated with the pulsating source only, so that computational costs may be reduced.

The MARCHS program was initially developed to cater for the motion problems of monohull ships. However, the versatility of the approach adapted makes it possible to tackle the problems of twin-hull ships. Chan (1991) has reported this latest modification on the MARCHS program. Some other features that can be analysed using this program include the second-order drift force, added resistance and structural loads on both mono- and twin-hull ships.

The program itself was written on the IBM/3090 main frame at the University of Glasgow's Computer Centre. The input data required and output data produced by the program is similar to that for SHIPM1.0. To generate the hull mesh of a certain SWATH hull configuration, the STATION program written on the VAX Cluster is to be incorporated. The resulting mesh data is then transferred to the IBM to be formatted by HULSURF routine for the computation using MARCHS. The characteristic hull parameter of the designed vessel is to be generated by the HULDAT routine. The output data which comprises the response amplitude of the six-degree of ship motion, hull pressure distribution, wave forces, and so on, are transferred automatically to the file storage.

To obtain the wave load values of SWATHs a separate program called the WVLOAD is to be used. Pressure data generated by the motion program is above is used in the execution of WVLOAD. For further details on running the program see reference by Chan (1990b). The required CPU time to run the MARCHS program for a single wave heading and considering the pulsating source only is around 20 hours for the input data containing approximately 25 regular wave frequencies. The total CPU time for running is also dependent on the number of panels of the hull facets. The MARCHS program is used in the present study to generate theoretical predictions of SWATH motions and wave loads to be compared with experimental findings.

2.7. EXPERIMENTAL INVESTIGATION OF SWATH SHIP MOTIONS

The need for model testings to observe motion behaviour of a vessel is evident. Particular reasons for this are, firstly, observation of ship motions by way of full scale trials to obtain a realistic seakeeping information is extremely expensive. In addition, such a full scale trial is exceptionally difficult for the experimenter to control, especially sea states and directional wave spectrum that occur naturally during measurements. Moreover, as scrutinised by Lloyd (1989) and Hutchison (1990), the results of full scale tests on a given ship are not practically useful for predicting the behaviour of a newly proposed design.

An analytical model to predict motion behaviour of a vessel is the most favoured design tool since its deployment is not at all expensive on top of the design flexibility that is offered. Nonetheless, development of a sophisticated analytical model requires a vast amount of effort and time and substantially large budgets. The argument follows that the level of accuracy which can be expected from a newly developed analytical model remains apprehensive due to the incompetence of the assumptions imposed as well as some restrictions, hence, uncertainties in the mathematical formulations. Secondly, model tests will be a useful approach to provide data for the validation of analytical models. The importance of analytical model validation is even more important with novel concept, such as SWATH, where past experience is limited or non-existent, is dealt with. Even then, in the presence of a reliable analytical model which sometimes has been well calibrated by operational experiences, the need of model test data in practical designs is imperative. Classification societies and ship owner surveyors usually specify the requirement of model test data in contract designs.

In recognition of the above considerations, experimental programmes on SWATH vessels have been comprehensively planned worldwide since early in the 1970s. The most notable effort was in the USA, e.g. by Kallio and Ricci (1976) and McPherson and Voight (1983). Seakeeping experimental programmes in Japan, the worlds largest SWATH operator to date, have been reported by Oshima et al (1979) and Mabuchi et al (1985). In these papers they also clarified the necessity of performing model tests in actual SWATH designs. Another example of a model test, as required in actual design of the largest SWATH ever built *Radisson Diamond* (11740-tonne), is contained in Marine Report (1990).

The motion experiment programme on SWATH models were started as early as the development of analytical studies in the NA&OE Department. The earliest version of the family of SWATH models procured at the Hydrodynamic Laboratory was a three- hulled configuration, rather than twin-hulled, which has been subjected to extensive investigations by Smith (1982,1983). The next generation of SWATH

models available in the Laboratory are tandem-strut type models SWATH-1 and SWATH-2. The former is of circular hull configuration, which has been seakeeping tested in various headings and forward speeds by Djatmiko (1987) and with the effects of stabilising fins by Wu (1985). The SWATH-2 model has rectangular hulls and was made available in particular for resistance observations by Chun (1988), besides some seakeeping evaluations by Djatmiko (1987). Later the SWATH-1 model was converted to become the SWATH-3 model, which is a single-strut type model. SWATH-3, together with the latest Fishing SWATH model (SWATH-FV), are studied in the present research.

In the following sections several important points in experimental procedures and test data analysis will be clarified. Some instrumentation used in the model test are indicated. For a more detailed explanation of the seakeeping experiment on SWATH models see Djatmiko (1987).

2.7.1. Measurement of SWATH Model Motions at Zero Speed

All the seakeeping tests described herein were carried out in the 76m x 4.6m x 2.5m towing tank at the Department's Hydrodynamics Laboratory. There is practically no limitation to the wave heading that can be generated in the towing tank as far as the motion test at zero speed is concerned. However, due to cost and time considerations a programmed test would be restricted to wave headings which is counted to be most important. Normally five wave headings, namely, head, bow quartering, beam, stern quartering and following seas, are selected to represent the 180 degree range of wave headings. The general instrumentation set up and running of the test is explained as follows.

2.7.1.1. Measurement Devices. The model is first equipped in the workshop with any necessary devices. Principal instruments for the measurement of model motions could be either linear variable displacement transformers (LVDTs) or selspots, or may be a combination of both, as is used in the present study. The use of LVDTs is suitable for measuring the motions of the model in vertical modes (heave, roll, and pitch) whereas, for the horizontal modes (surge, sway, and yaw), selspots are probably more appropriate. Djatmiko (1987) observed that the SWATH model horizontal motions are much restricted by the presence of string wires which connect between the model and the LVDTs, therefore using selspots this problem could be overcome. The positions of these instruments are as illustrated in the test arrangement sketch of Fig. 2.4.

As shown in Fig. 2.4, which is the general test set up in oblique waves, four LVDTs were mounted on the model. A combination of these, i.e. summation and substraction of the electronic signals generated, would give the heave, pitch and roll amplitudes as appropriate. Two selspot systems, each comprising a camera detector and one or more light emitting diodes (LEDs), were used for measuring horizontal motions. A combination of signals from LED1 and LED2 would provide amplitudes of sway and yaw. Whereas LED3, which was associated with camera detector 2 (C/D2), measured the surge oscillations. As shown, the model is moored to the tank side to maintain its, intended heading to the wave propagation. If the model is tested in head or beam seas only two LVDTs are needed for measuring the vertical motions, that is, heave and pitch or heave and roll, respectively. Horizontal mode in these cases is, respectively, surge or sway, which may be measured by a single selspot system.

The wave elevations generated by the parabolic wavemaker at the top end of the tank were measured by wave probes. A wave probe generates electronic signals based on the submergence of the capacitor metal bar in the water. Three wave probes were positioned on the bridge across the tank well away from the model upstream from the wavemaker. The spreading of the wave probes was made, i.e. at B/2, B/3 and B/4 from the tank side wall where B is the tank width, so that any changing in the wave patterns across the tank could easily be identified. Another wave probe was situated in the vicinity of, and parallel to, the bowline of the model. This arrangement made it possible to observe the phase difference between the wave excitation and the model motion.

2.7.1.2. Amplifier and Data Acquisition Devices. The amplifier is used to convert the signals from measuring instruments into codes readable by data acquisition devices. In the amplifier signals from various sources each will be treated differently according to the nature of the signals. For instance, the amplifier decodes the signals sent by the LVDT so that they can be read by the recorder. The signals sent by the strain gauges in the case of the wave load test, which are mostly very small and therefore unreadable to the recorder, need to be amplified and decoded. Each of the measuring instruments is connected to an allocated channel in the recorder devices as illustrated in a diagrammatic arrangement in Fig. 2.5.

There were two types of recording (data acquisition) devices used during the test, that is, a pen recorder and a computer terminal Macintosh IIICi which accommodates a software package named LabView. Although a pen recorder is a reliable device its capability is limited by the number of channels that can be connected to it. The use of a computer is more flexible even when a relatively large number of electronic channels is required. Moreover, the use of a computer is more convenient when a complicated data

analysis is to be carried out. Computer data analysis is much less time consuming than the analysis which should be done manually when data acquisition is performed using pen recorders. The benefit of computer data analysis is most appreciated when tackling the problem of hydrodynamic observations in random waves. The amplifier and data acquisition devices are shown in the photographs of Fig. 2.6.

2.7.1.3. Running the Test. Before the first run of the day was commenced, calibrations were conducted to eliminate any changes in signal levels caused mainly by atmospheric state surrounding the devices, i.e. temperature, humidity, static current, etc. The calibration factor generated is automatically stored in the computer to convert the electronic signals from any measuring devices. This gives the resulting quantity of the measured motion or wave elevations as the actual magnitude corresponding to the appropriate units (cms or degrees).

In general, the model test was conducted in the wave frequency range from 0.3 up to 1.6 Hz with intervals of 0.05 Hz. In the vicinity of the heave, roll and pitch natural frequencies the interval was decreased. This allows the motion behaviour of the model to be well investigated in the critical frequency region. In order to anticipate the range of wave frequencies needed to be run during the test it is necessary to observe the natural frequencies of the model in the three purely oscillatory motions, i.e. heave, roll and pitch. Djatmiko (1987) shows in detail the procedure of measuring these natural frequencies on SWATH models.

A recording of motions and wave patterns in each test was taken after the established wave train had passed the model and when the model had drifted from its original position to a new mean position about which it was oscillating steadily. Besides the variation to the frequency, the amplitude of wave elevations were in some cases also altered. Normally two different wave heights were generated during the test, namely, 5 cms and 10 cms, but the former is more frequently used. By generating two different wave heights for the same frequency it is then possible to observe the non-linear effect on the motion that has been caused, if any.

2.7.2. Measurement of SWATH Model Motion with Forward Speeds

Because the restrictions of the towing tank dimensions only head and following sea tests could be made on the model which underway with forward speeds. For this type of experiment the model was located under the mobile main carriage, as shown in Fig. 2.7. Two LVDTs for measuring heave and pitch oscillations of the model were mounted on the gantry. These LVDTs were used to measure the rate of sinkage and

static trim of the model, which is important in studying the model resistance characteristics. The only connecting line used had two functions, first to drag the model along the tank and second to connect the model with the dynamometer where the surge oscillations and the resistance of the model were recorded. Four guide rods, two on each side of the model, were installed to maintain the model in the right course, so that there was no yaw, roll or sway.

Each of the models studied was tested at four speeds, i.e. 0.5m/s, 1.0m/s, 1.5m/s and 2.0m/s which correspond, respectively, to the Froude numbers on average of 0.13, 0.26, 0.39 and 0.52. These characteristic speeds conducted in the experiment are associated with a medium speed SWATH. The model was run in a given speed which was controlled by an operator from the control desk at the mobile carriage. The data acquisition was taken on a pen recorder, computer terminal, and the dynamometer. Calibration procedure and other measurements are as orchestrated for the stationary tests. Photographs of a SWATH model underway in progressing waves are seen in Figs. 2.8 and 2.9.

2.7.3. Test Data Analysis

Most of the test data analysis was carried out on the VAX Cluster computer system therefore the recorded data needed to be transferred from the Macintosh IICi to the main frame by KERMIT software. A data analysis program was available for the analysis in the VAX cluster. The program was generally used to process the digital data to obtain, for instance, the average amplitudes of any mode of the model motion.

As mentioned earlier, most of the data has been converted in the amplifier to the appropriate units for any mode of motion by sum and difference process, as well as by taking into account the calibration factor. For example, the heaving motion at the centre deck of the model is determined by the oscillation of the four LVDTs. Let x_1, x_2, x_3, and x_4 be the elevations, and c_1, c_2, c_3, and c_4, the calibration factors of LVDT1, LVDT2, LVDT3 and LVDT4, respectively. Thus the heaving amplitude is calculated in the program in a loop as :

$$\text{Heave elevation} = \frac{(c_1x_1 + c_2x_2 + c_3x_3 + c_4x_4)}{4} \text{ (cms)}$$

and so on for other modes of motion. Figure 2.10 shows the sum and difference unit in the amplifier.

The analysis program was written to plot the test data by identifying the file labelling as appropriate to the channel number allocated to an individual record. Typical plots of motion and wave elevations as functions of elapsing time are as shown in Fig. 2.11.

Overall, ten sets of results for an oblique sea case can be derived from the test data analysis at any single wave frequency run. These are amplitudes of six-degree of freedom of the model motion and four different wave amplitudes. To compare the test results with other theoretical predictions it is more convenient to present the motion data in the normalised form. Two different parameters are used for normalising the motion data, namely, wave amplitude and wave number, for translational (surge, sway, and heave) and rotational (roll, pitch, and yaw) modes, as follows :

$$\zeta'_{ti} = \frac{\zeta_{ti}}{\zeta_w} \tag{2.46}$$

and

$$\zeta'_{rj} = \frac{\zeta_{rj}}{\zeta_w \, \omega^2 / g} \tag{2.47}$$

where ζ'_{ti} = non-dimensional translational response in i^{th} mode
ζ'_{rj} = non-dimensional rotational response in j^{th} mode
i = 1, 2, and 3 for surge, sway, and heave, respectively
j = 4, 5, and 6 for roll, pitch, and yaw, respectively
ζ_{ti} = translational amplitude in i^{th} mode (m)
ζ_{rj} = rotational amplitude in j^{th} mode (rad)
ζ_w = wave amplitude (m)
ω = wave frequency (rad/sec), and
g = acceleration due to gravity (=9.81 m/s^2).

The motion responses are plotted against the wave (encounter) frequency, which is normalised as :

$$\omega' = \frac{\omega}{\sqrt{g/L}} \quad \text{or} \quad \omega_e' = \frac{\omega_e}{\sqrt{g/L}} \tag{2.48}$$

where ω' (ω_e') = non-dimensional wave (encounter) frequency, and
L = characteristic length of the model (m).

2.8. COMPARISON OF EXPERIMENTAL RESULTS AND THEORETICAL PREDICTIONS

In this section correlation between experimental and theoretical predictions on SWATH model motions is observed. As mentioned earlier, during the period of the present study two SWATH models of single strut per hull configuration, namely, SWATH-FV and SWATH-3, have been extensively tested. Nevertheless, for the sake of completeness, experimental data for tandem strut SWATH model (SWATH-1) provided by Djatmiko (1987) are also considered in validating the predictions from MARCHS. The main particulars of these SWATH models are listed in Table 2.3, and the underwater hull forms are presented in Figs. 2.12a,b and c.

2.8.1. Head Seas

Comparison of theoretical assessment and test data in stationary condition is presented in Figs. 2.13 through 2.17. The motion characteristics of SWATH-FV in head seas (180 deg), as shown in Fig. 2.13, can be described in the following manner. The theoretical prediction agrees well with measured data for surge mode of motion in the supercritical region (frequencies higher than the resonance), but underestimate the response values at the resonance and subcritical frequencies. Chan (1990a) suggests that this is due to the effect of water depth. Investigations on monohull ships operating in restricted water depth indicate the same pattern of surge response as on SWATH model, that is, the rise of the response curve to infinity at low frequency zone.

In the resonance frequency, in particular, the surge response is influenced strongly by the pitch motion. As shown in the Figure pitch response is also smaller than the measured one when the viscous effect is taken into account. Reducing the viscous damping may lead to a better correlation for pitch, but not so with the surge. The quality of measured data for the subcritical region of surge and pitch might not be too convincing. However, much better correlation of surge and pitch responses for other models (SWATH-1 and SWATH-3) is evident, as presented in Appendix A, together with the rest of the motion data.

The correlation of heave responses from the two sources is excellent. The discrepancy of predictions based on the potential wave damping and with the inclusion of viscous damping is apparent at the critical frequency. The former also demonstrates clearly the coupling effects among the three modes of motion. This account is accepted due to the fact that the small waterplane are the deeply submerged main hulls of SWATHs contribute much smaller wave damping than those for conventional monohulls. The viscous damping effects were taken into account for the present prediction by a semi-empirical iterative method, as given by Thwaites (1960). As can

be seen, the viscous damping is more dominant than the wave damping at the resonance frequency vicinity. The viscous damping effects in subcritical, and similarly in the supercritical regions, however, is not so significant.

2.8.2. Beam Seas

In beam seas (90 deg), as shown in Fig. 2.14, the theory predicts good heave motions as in head seas. A satisfactory correlation is also found for the surge and roll responses. The highly tuned roll response in the resonance frequency (ω'=1.15) may be reduced by introducing higher viscous damping. However, this leads to the penalty of reducing the pitch response even further. The coupling effect of rolling on the sway motion is also clearly indicated at the first resonance peak. The second peak of the sway response at ω'=3.1~4.0 is considered by Zheng (1988) to bring about the presence of standing waves in the hollow space between the SWATH struts. This phenomenon is also observed for SWATH-1 and SWATH-3 models (see Appendix A).

2.8.3. Quartering Seas

Theoretical predictions and measured data for three SWATH model motions in bow-quartering seas (135 deg) are plotted in Figs. 2.15 to 2.17. Confirmation of the results are fairly good in most cases. The correlation of surge responses is best for SWATH-1 (Fig. 2.17), even though the theoretical prediction does not show the high tuned response at the resonance frequency (ω'≈1.25). The theoretically predicted sway motion is most closely related for SWATH-3 (Fig. 2.16). The SWATH-1 measured data for this mode is lower than the predicted. This may be due to the restrictive motion induced by the mooring line since the model was tested by LVDT for measuring the horizontal motions. The effect of viscous damping varies for different models especially for pitch and roll motions, although the same damping coefficient was taken for the three models. The heave motion predictions agree well with the measured data. For all three models, as expected the yaw responses are dominantly influenced by the sway. The trend is similar for different model configurations.

2.8.4. Head Seas with Forward Speeds

Examples of the correlation between theoretical predictions and measured data of SWATH model motions in head seas with forward speeds are as plotted in Figs. 2.18 and 2.19 for SWATH-1, respectively, at the Froude numbers ($Fn = V / \sqrt{gL}$, where V is model speed in m/s and L is the model length) of 0.39 and 0.52. In both Figures the

theoretical curves trace the measured data quite closely. The scatter of surge data in the subcritical region may be attributed to inadequacy in controlling the test, which might also be due to the model contouring the wave surface at low frequencies. The dominance of heave coupling on other mode of motions is also apparent. The non-linearity of the motions due to different wave heights (measured 1 and measured 2 correspond respectively to the wave heights of approximately 5 and 10 cms) is not clearly indicated in those cases. The same phenomenon applies also to SWATH-1 model motions in stationary conditions. Other data in head seas with forward speeds can be found in Appendix A, where correlations are mostly found to be satisfactory.

2.8.5. Following Seas with Forward Speeds

Only SWATH-FV among those models has so far been tested in following seas. The experimental results of the model tested at Fn of 0.13 up to 0.26 are presented, together with the theoretical curves, in Figs. 2.20 to 2.23. In these Figures good agreement is found for heave motion. On the pitch motion, discrepancies become larger at lower frequencies, i.e. below ω of approximately 3.0 rad/sec. Lee and Curphey (1977) observed a similar behaviour for a SWATH 6A model tested at the DTRC, which was explained as being caused by the uncontrolled constant speed of the model when running at low frequencies. With the increase of forward speeds (Fn=0.39 and 0.52) theoretical predictions on surge motions become uncertain. A new pattern of heave and pitch motions at these speeds arises with magnified peak responses in certain frequencies, i.e. approximately at ω=6.5 rad/sec and 5.0 rad/sec for Fn=0.39 and 0.52, respectively. These incoming wave frequencies correspond to the encountering frequencies approaching zero. Hong (1986) suggests that in such a frequency the predicted hydrodynamic coefficients decrease substantially, hence the motions are magnified. Overall, the scattering of experimental data presented herein shows a similar tendency to those found in the papers by Hong (1986) and Fang (1988).

Considering the satisfactory correlation between the theory and experiment data of SWATH motions in head and following seas, it might also be interesting to observe the trend of forward speed motions at different wave headings. Bow quartering seas may represent these other headings, as shown for SWATH-FV in Fig. 2.24. As expected, the peak responses shift from higher incident wave frequencies to the lower regimes due to the encountering phenomenon. The peak values of heave and pitch response tend to enlarge with the increase of the speeds. The heave coupling effects on pitch motion, and hence on the surge, fortify in parallel to the speed increase. Thus, as shown, the peak of pitch and surge responses occur at the resonance frequency of the heave motion. Despite the strong influence of heave motion on the surge, a gradual decrease in the response magnitude over most of the frequency range is evident. This account similarly applies to the sway mode of motions. A rapid fall off in response magnitude is

even more pronounced in the case of rolling. The attenuation of roll response in higher speeds was also recognised by Lee and Curphey (1977), which was mainly due to the increase in effectiveness of viscous damping. The attenuation of yaw responses at lower frequencies (ω=3.0 rad/sec or less) is eventually affected by the roll mode. However, a new peak at ω=5.0 rad/sec for Fn=0.52 which simultaneously appears on surge and yaw response is noted. This cannot be explained and requires further investigation.

In general, the theoretical predictions correspond very well with the measured data as seen in the above comparisons. The discrepancies in following seas is simply explained due to the limitation of the theory which is, as mentioned by Chan (1991), based on the assumption of high frequency oscillation. This implies that predictions at very low frequency (approaching zero), such as in following seas at high speeds, would not be justified. Viscous damping plays an important role in generating the correct response magnitude of heave, roll and pitch mode of motions for SWATH ships. The evaluation presented here has basically validated the motion assessment tool so developed.

Comparisons of experimental data for SWATH-1, SWATH-3 and SWATH-FV with the earlier predictions generated using the program by Zheng (1988) can be found, respectively, in papers by McGregor et al (1988), Chun et al (1990) and Djatmiko et al (1990). Whereas comparisons of experimental data with the predictions by the two-dimensional theory was presented by Atlar et al (1987).

2.9. SWATH PERFORMANCE IN SEAWAYS

Failure to maintain effectiveness in carrying out a mission of ships in adverse seas is probably the main concern in seakeeping studies. Hoffman (1976) has earnestly addressed the seakeeping impact on ship operations with main emphasis on the associated economic merits. In that paper is cited the first level by which the ship operational cost has been substantially increased due to the prevalent speed reductions, hence operational delays, that were caused by severe weather. In the second level, seakeeping quality affects the lifetime cost by virtue of additional requirements of repairs on structural damages brought about by excessive environmental loads. Moreover, safety of onboard items, such as cargo and equipment, as well as passengers and personnel, should be accounted for as endangered by the degradation of seakeeping effectiveness.

Because of this, one of the ultimate targets in seakeeping studies is, the ability of the designer to predict the behaviour of ships when severe seas ought to be

encountered. Further, the outcome of such evaluation is documented as part of the ship operational guidances.

The seakeeping effectiveness of a vessel, or widely known as the seaworthiness, may be measured by the rate of operability that can be attained when operation is made in a prescribed sea environment. Systematic procedures of ship operability evaluations have been introduced by many, e.g. McCreight (1987) and Graham (1990). The common way to assess the ship operability is by integrating the motion responses, as described in the previous sections, into a real sea system. This is followed by the introduction of operational constraints designated as the seakeeping criteria. In this respect operability is acquired when the limit criteria is not violated by any individual element involved in the characterisation of ship response to the seaway. On the other hand, the conditions where any one or more constraints set up within the criteria is infringed would fall into the category of mission failure or down time.

The characterisation of ship responses to the real sea environment was first introduced to the naval architect community by Pierson and St. Denis (1953). Order statistics were used to describe the random nature of seaways. Accordingly, the ship response to seaways should be represented in stochastic manners. If the randomness of sea waves is defined by the sea energy spectral density function $S(\omega)$, then, adopting a linear superposition relationship, the variance of ship motion of a particular mode is obtained by :

$$E = \int_0^\infty \left[\frac{|\zeta_i|}{\zeta_w}\right]^2 S(\omega)\, d\omega = m_0 \tag{2.49}$$

where $[|\zeta_i|/\zeta_w]^2$ is the response amplitude operator (RAO). The variances for velocity and acceleration of the i^{th} mode of motion can also be obtained by :

$$E_v = \int_0^\infty \omega^2 \left[\frac{|\zeta_i|}{\zeta_w}\right]^2 S(\omega)\, d\omega = m_2 \tag{2.50}$$

and

$$E_a = \int_0^\infty \omega^4 \left[\frac{|\zeta_i|}{\zeta_w}\right]^2 S(\omega)\, d\omega = m_4 \tag{2.51}$$

Since the sea energy spectra density function of waves and ship motions are assumed narrow banded, the distribution may then be described by a Rayleigh probability density function. Under this assumption, the statistical averages of ship

responses can be expressed in the form :

$$\text{'Average' amplitude} = C_a\sqrt{(E)} \tag{2.52}$$

Here $\sqrt{(E)}$ is referred to as the Root Mean Square (RMS) of a particular motion amplitude and C_a is the constant of the average value; C_a=1.25 gives the average; C_a=2.0 gives the one-third highest average or significant value; C_a=2.55 gives the one-tenth highest average.

Considering a ship in transit at speed U and at a heading angle μ to the dominant direction of the waves, then it will 'encounter' the waves at a frequency different from that which it would meet if it were at rest. The encounter frequency is then written as in eq. (2.37). The energy of the wave remains the same whether it is expressed in terms of ω or ω_e , so that :

$$E_w[\zeta^2] = \int_0^\infty S(\omega)\, d\omega = \int_0^\infty S(\omega_e)\, d\omega_e \tag{2.53}$$

where

$$S(\omega_e) = \frac{S(\omega)}{|\, d\omega_e / d\omega \,|} \tag{2.54}$$

Finally the wave encounter spectrum is rewritten as :

$$S(\omega_e) = \frac{S(\omega)}{\left|\, 1 - \frac{2U\omega}{g} \cos\mu \,\right|} \tag{2.55}$$

There are a number of mathematical formulations for sea spectra which have been developed from the analysis of extensive wave data. The wave spectra most commonly used include the deep water (fully aroused and fetch unlimited) and the fetch limited spectra. The spectral forms developed by Bretschneider (1959) and Pierson and Moskowitz (1964) are examples of deep water spectra. In coastal waters, where the fetch may be limited, the JONSWAP (Joint North Sea Wave Project) spectrum provided by Hasselman et al (1973) is recommended.

For the present study, seakeeping evaluation is made on SWATH ships operating in the North Atlantic. The aforementioned spectral forms are basically amenable for the present analysis. Nevertheless, there is now available sea spectra established specifically for the North Atlantic region. The six-parameter wave spectra, as it is known, was developed by Ochi and Huble (1976). The formulation was developed to

cover the shape of spectra which varies considerably depending on the growth-decay stage of storms and existence of swell. From a statistical analysis of the parameters, a family of 11 members has been established for a given sea severity. Of these 11 spectra, one is the 'most probable spectrum' for a given significant wave height, and the remaining 10 spectra are those expected to occur with 95 percent confidence. More on the six-parameter spectra is presented in Chapter 3.

Ideally, seakeeping analysis should be performed by prescribing the intended ship route within a particular sea environment. In addition, the expected operational speeds ought to be defined. It will then be possible for the designer to assess the probability level of speeds and wave headings in which the ship is to operate. In the present evaluation combinations of four wave headings (head, bow-quartering, beam and following seas) and five different speeds corresponding to the Froude number of 0.0, 0.13, 0.26, 0.39 and 0.52 are assumed to be equally likely to be encountered by the ships. Three 2500-tonne SWATHs (main particulars as listed in Table 2.4) scaled up from the models are investigated. The main objective is to compare the seaworthiness of these SWATHs operating in the same seaways with the long term wave probability distribution, as shown in Table 2.5.

The seakeeping criteria for oceangoing ships are now widely available. The developed criteria generally is based on the considerations of personnel workability (safety), structural safety and specific functions, such as aircraft take off and landing. The selected SWATH naval vessel criteria as proposed by Olson (1978) is adopted for the three vessels operating in the North Atlantic, as given in Table 2.6. The criteria is not appropriate for passenger vessels where the requirements of passenger comfort is stringent, as discussed by Dallinga (1992).

Computations on the motion characteristics of the three SWATHs have been performed for all combinations of wave headings and ship speeds. Any single response value derived from the spectral analysis was compared with the appropriate criteria. Matrices as shown in Tables 2.7a and 2.7b, corresponding with the general, and general and helicopter criteria, respectively, were then composed. The numbers printed in the first matrix of each table represent the criteria which was first exceeded by the motion value. The second matrix lists maximum significant wave heights where operations can be safely executed. The third matrix shows the level of probability where operation can be properly performed. The probability of operation was weighted by the probability of ship heading, operational speed, sea spectrum and occurrence of a particular significant wave height as printed in the second matrix.

The operability of those SWATHs are found to be the summation of the probability values as listed in the third matrix of Table 2.7a and 2.7b. The results of the

operability analysis is given in Table 2.8. Regarding the same criteria imposed on those vessels, SWATH-1 seems to override the other two SWATHs in terms of their operability rates (OR). If only the general criteria (1-4) is considered, the ORs of SWATH-1, SWATH-3, and SWATH-FV are expected to be, respectively, 0.896, 0.843 and 0.817. Considering the general and helicopter criteria (1-7) the ORs are mostly reduced by some 24~25% from the former to 0.671, 0.632, and 0.618, respectively.

The down time of these vessels mostly occurs due to the limiting 3 degree single amplitude average pitch motion (criteria 2) for the first case, and the limiting 2.55 metres double amplitude significant vertical displacement at the flight deck (criteria 6). The OR is in general lower at Fn=0.0 and 0.52, but steadily better at Fn between 0.13 and 0.39. With respect to the wave headings, those vessels are mostly debased in following or head seas, due to larger pitch motions associated with criteria 2. The SWATHs perform very well, however, in beam seas even at the highest speed. The down time distributions as the function of forward speeds for SWATH-FV are presented in Figs. 2.25a-b. Generally those SWATHs could be expected to perform well up to sea state 6.

Comparison of the seakeeping quality of those vessels with other SWATHs of similar size would be interesting. Nevertheless, such information derived by a similar criteria and wave data as adopted here is not yet available. Chilò and Santos (1983) have investigated the operability of 2500-tonne SWATHs for operation in the North Atlantic. Their finding is that OR of the SWATH could attain as high as 0.978 or 0.995. These figures seems to be very optimistic, which is, however, believed to be due to the different wave data selected. Chilò and Sartori (1979) provide the wave data for the North Atlantic, as shown in Table 2.9. Comparing this to the wave data used in the present study (see Table 2.5), then it is clear that the difference of cumulative probability of wave occurrence is quite large. For the wave height up to three metres alone, Chilò and Sartori (1979) give the cumulative probability as high as 86%, compared to 58% in Table 2.5. Any other differences could possibly be brought about by the spectral forms which have been selected for the evaluation.

2.10. SWATH SHIP RESISTANCE

In this section resistance data of the SWATH-FV model collected in conjunction with the motion tests in head seas with forward speeds is presented. The measurement of SWATH model resistance was made by using a dynamometer available on the main carriage (see Fig. 2.7). The total resistances were measured for a wide range of Froude numbers both in calm water and in waves at a certain frequency corresponding to the

wave length/model length ratio equal to unity (λ/L=1.0). A comparison was further made between the measured data and the theoretical assessment.

The estimation of SWATH total calm water resistance is calculated as the sum of four resistance components, namely, wave-making, frictional, appendage and additional resistance. The SWATH resistance program available in the NA&OE Department was developed by Chun (1988). In the resistance formulation a plane source distribution method is adopted to assess the magnitude of the wave-making drag of SWATH ships. By using the plane source distribution, the wave-making resistance of a non-circular cross-sectional body can be accurately calculated.

The skin frictional resistance is calculated using the ITTC'57 formulation where the Reynolds Number is calculated based on the individual lengths of the components of a SWATH ship. The additional resistances, which are contributed by several drag components, i.e. form effect, eddy, viscous pressure, wave-breaking and spray drags, are calculated based on an empirical formula which was derived from the extensive resistance tests on various SWATH configurations, as provided by Chapman (1972) and Salvensen et al (1985).

The wave making resistance coefficient and components of the SWATH-FV model are shown against Froude number in Fig. 2.26, together with the measured residuary resistance coefficient. The large measurement of resistance at high speeds was due to the excessive bow trim, resulting in green water on the deck. This green water effect is well reflected at the last speed, showing an abrupt increase in the measured resistance. The calculated and measured total resistance of the SWATH-FV model are shown in Fig. 2.27. In general, the agreement between the measurement and the prediction is good apart from at high speeds.

Added resistance was measured in waves of a frequency corresponding to λ/L=1.0 and presented in Fig. 2.28, together with the total calm water resistance. It can be seen from the Figure that the resistance of the model decreases in waves compared to calm water resistance at the region of Fn between 3.0 and 4.0. This unusual result was previously observed for other SWATH models by Chun (1988). As reported by Suhrbier et al (1990), a similar finding on negative added resistance in the primary hump region was also acquired at MARIN, even though the magnitude of resistance reductions were not as great as that reported by Chun (1988) and Chun et al (1989). Therefore, the present result further enhances the previous findings that added resistance of SWATH ships has a tendency to become negative over some speed range. Chun and McGregor (1989) suggest that several hydrodynamic interferences have led to this phenomenon. The variation of sinkage and trim in waves relative to those in calm water increased apparent speed of the models due to oncoming waves, changed the speed of water particles near the model due to the increase surge motion with the

increase of wave height, and the interference effects between the struts combined with some motion aspects of the model are those that need to be examined to develop the understanding on negative added resistance.

2.11. DISCUSSION

Several important aspects of SWATH hydrodynamics have been thoroughly addressed. Excellent seakeeping characteristics of SWATHs compared to monohull vessels are obtained from the concept of deeply submerged hull and slender surface piercing struts. As reflected in many proposed seakeeping criteria, vertical motions (heave, roll and pitch) are of utmost importance in the hydrodynamic design of seagoing vessels. Attention should therefore be prominently given to these modes of motions if a better seakeeping performance is to be achieved.

In the early design stage, the first action needed to be taken regarding the motion of SWATHs is to aptly determine correct natural frequencies for those vertical motions. Lamb (1988) describes an approach to this problem by considering a typical SWATH response curve, as shown in Fig. 2.29. Lets tuning factor be defined as the ratio of the frequency of encountering waves to the SWATH's natural frequency. The largest motion response would then be expected to occur when the value of the tuning factor becomes unity. As the tuning factor decreases, the motion responses become smaller. In this designated supercritical region the ship is expected to run at a platforming mode. In the subcritical region where the tuning factor is larger than unity the ship movements will be in phase with the oncoming waves (contouring behaviour), thus the heave amplitude, for instance, will have a magnitude of relatively the same as the wave amplitude. An attempt therefore has to be made to avoid the natural frequency of the ship coinciding with the predominant modal frequency of the sea waves where the ship is to be operated. The best design is envisaged if the ship could operate most of the time in the supercritical region.

It is best to design the natural frequency of ships as low as possible so as not to resonate with the wind generated waves, which is known largely to oscillate at relatively high frequency. There are two possible ways to depress the heave natural frequency ω_z without changing the ship displacement, that is, referring to eq. (2.1), by increasing the heave added mass A_{33} or by reducing the waterplane area. The former may be accomplished by designing the hull sections so as the horizontal diameter of the hull is larger than the vertical diameter. Options to this are elliptical hulls, or alternatively, rectangular hulls. Another solution is by introducing canard and/or stabilising fins. The governing factors where reducing waterplane area should be

limited are the roll static stability requirements as well as the structural strength and access to the lower hulls considerations.

The pitch natural frequency can be decreased by either increasing the longitudinal mass inertia I_{55} or reducing longitudinal metacentric height GM_L (see eq. 2.3). The I_{55} could be increased by distributing the ship mass near the fore or aft ends of the SWATH. As presented in Table 2.3, due to this mass distribution effect, I_{55} for the tandem strut model SWATH-1 is appropriately larger than the single strut SWATH-3. The increase of GM_L contributes to reducing pitch motion because of the increased restoring moment. In general a shorter strut and longer hull combination provides a longer pitch period (lower pitch frequency) with the help of the decreased GM_L. In the same way as for heave, fins would provide a favourable effect in increasing pitch period.

In general, a wider hull spacing results in a greater roll inertia I_{44} and hence provide a lower roll natural frequency. A smaller GM_T gives a lower natural frequency (see eq. 2.2) but this is penalised by larger roll response owing to the reduced restoring moment as shown in Table 2.2. MacGregor (1989) has compiled a number of algorithms related to SWATH motions which would be useful in initial seakeeping design.

SWATH ships with an improved seakeeping characteristic is obviously favourable for high speed operations, especially when adverse sea is concerned. The finding on negative added resistance is promising in view of the high speed aspects. Nevertheless, the observation is merely based on model scale, which to some extent must be proved by actual experience. A particular issue of most concern to SWATH designers is the tendency of such a vessel to suffer from larger static trim at high speeds. The munk moment effect, as it is known, is inherent to SWATHs due to the smallness of the waterplane area, hence lower hydrostatic restoring capability. The problem is identical to that on a slender aircraft, as was discussed by Munk (1924). As mentioned earlier, applying canard fins forward is one solution to this problem. Another remedy for static trim is by designing the so called slashed bow, where the fore part of the lower hull bottom is flattened. An example of such a design was presented by Chun et al (1988).

A versatile tool for predicting the motions of SWATH type vessels is now available in the NA&OE Department. Some additional experimental data might need to be collected to assure the validity; especially experiments in oblique waves with forward speed. The theoretical prediction so developed can actually deal with other hull configurations, that is elliptical and rectangular hulls. However, for the former, experimental data is not yet available. Experimental data on rectangular hull SWATHs

has been provided by Djatmiko (1987), but the existing hull mesh generator remains to be enhanced.

Various parametric studies regarding SWATH motions should be studied further in future. Aspects of different hull configurations should be thoroughly investigated in an attempt to generate a data base for design optimisation. The so called seakeeping indices approach is generally used to study this particular aspect. Lloyd (1991) and Sariöz et al (1992) have recently exemplified the seakeeping evaluation by such a method. The main hindrance in accumulating too large a data base is the requirement of storage memory needed in the computing process. The management of this data base, and its acquisition in design, is probably best orchestrated by an expert system.

2.12. CONCLUSIONS

Extensive experimental data on SWATH motions has been presented. The data was derived from the seakeeping tests of three SWATH models conducted at the Department's Hydrodynamics Laboratory. One model has a tandem strut per hull configuration, while the other two are of single strut configuration. Some problems associated with experimental arrangement, which in turn affect on the quality of the measured data, are indicated. Alternative arrangement, with the use of different measurement devices, to overcome such problems are described.

Efficiency in conducting seakeeping tests is the primary concern in both saving the tank time and experiment cost. Well planned model tests should be capable of simultaneously collecting the data for several type of measurements. This are now possible with the availability of more sophisticated data acquisition system using computers. Subsequently, test data analysis can be performed much more rapidly, and accurately, than reading from record papers as was done in the past.

Comparison of experimental data with theoretical predictions from MARCHS computer program was then performed. Test data measured at several important wave headings, which includes head, beam, bow quartering and following seas, has been collected. For the former three headings, at stationary conditions, the theory predicted motion values excellently close to the measured data. This good correlation is also found for model motion in head seas with forward speeds. In the following seas at low speeds the theory gives a reasonably good agreement with experimental data, but discrepancies, notably in surge and pitch, become apparent at higher speeds. Nevertheless, such discrepancies are acceptable with regard to the limitation of the theory which was built upon the assumption of short period waves. Regardless these slight discrepancies correlation between the two results is generally excellent, hence

validation is adequately achieved. The tool developed is reliable for a wider range motion study which needs to be pursued in future.

A further seakeeping performance analysis was made on three 2500-tonne SWATHs scaled up from the three models. The results of motion predictions were integrated into a spectral analysis to assess the motion characteristics of the vessels operating in the North Atlantic. A seakeeping criteria was incorporated to weigh the operability rate of such vessels and rates between 82% and 89% are achievable by the present design. Another SWATH with about the same displacement designed elsewhere shows a higher operability rate (some 98%) for operation in the same sea region. Nonetheless, this higher operability rate is due to the different wave data, and might as well the spectral formulation, that has been adopted. The rate of operability can be substantially improved when the SWATHs are appendaged with stabilising fins. This particular aspect has been comprehensively investigated by Wu (1985).

In addition, SWATH resistance data derived from the test on a Fishing SWATH model is also presented. Comparison with analytical prediction has been made. An interesting observation especially is on the finding of negative added resistance that arises when a certain frequency of wave is encountered. This finding confirms the earlier observations made on the other models. However, further investigation is required, preferably from actual experience, before the issue can be considered to be conclusive.

Table 2.1. Motion induced coefficients (potential)

$$A_{22} = \int_L a_{22}dx + \frac{U}{\omega^2} b_{22}(x)\Big|_L$$

$$B_{22} = \int_L b_{22}dx - Ua_{22}(x)\Big|_L$$

$$A_{24} = \int_L a_{24}dx + \frac{U}{\omega^2} b_{24}(x)\Big|_L$$

$$B_{24} = \int_L b_{24}dx - Ua_{24}(x)\Big|_L$$

$$A_{26} = \int_L a_{22}xdx - \frac{U}{\omega^2} B_{22}^0 + \frac{U}{\omega^2} xb_{22}(x)\Big|_L$$

$$B_{26} = \int_L b_{22}xdx - UA_{22}^0 - Uxa_{22}(x)\Big|_L$$

$$A_{33} = \int_L a_{33}dx + \frac{U}{\omega^2} b_{33}(x)\Big|_L$$

$$B_{33} = \int_L b_{33}dx - Ua_{33}(x)\Big|_L$$

$$A_{35} = \int_L a_{33}xdx - \frac{U}{\omega^2} B_{33}^0 + \frac{U}{\omega^2} xb_{33}(x)\Big|_L$$

$$B_{35} = \int_L b_{33}xdx - UA_{33}^0 - Uxa_{33}(x)\Big|_L$$

$$A_{55} = \int_L a_{33}x^2dx + \frac{U^2}{\omega^2} A_{33}^0 - \frac{U^2}{\omega^2} xa_{33}(x)\Big|_L + \frac{U}{\omega^2} x^2 b_{33}(x)\Big|_L$$

$$B_{55} = \int_L b_{33}x^2dx + \frac{U^2}{\omega^2} B_{33}^0 - Ux^2 a_{33}(x)\Big|_L - \frac{U^2}{\omega^2} xb_{33}(x)\Big|_L$$

$$A_{53} = A_{35}^0 - \frac{U}{\omega^2} B_{33}^0 + \frac{U^2}{\omega^2} a_{33}(x)\Big|_L - \frac{U}{\omega^2} xb_{33}(x)\Big|_L$$

$$B_{53} = B_{53}^0 - UA_{33}^0 + Uxa_{33}(x)\Big|_L + \frac{U^2}{\omega^2} b_{33}(x)\Big|_L$$

$$A_{44} = \int_L a_{22}dx - \frac{U}{\omega^2} b_{44}(x)\Big|_L$$

$$B_{44} = \int_L b_{44}dx - Ua_{44}(x)\Big|_L$$

$$A_{42} = A_{24}$$

$$B_{42} = B_{24}$$

$$A_{46} = \int_L a_{24}xdx - \frac{U}{\omega^2} B_{42}^0 + \frac{U}{\omega^2} xb_{24}(x)\Big|_L$$

$$B_{46} = \int_L b_{24}xdx - UA_{42}^0 - Uxa_{24}(x)\Big|_L$$

$$A_{66} = \int_L a_{22}x^2dx + \frac{U^2}{\omega^2} A_{22}^0 - \frac{U^2}{\omega^2} xa_{22}(x)\Big|_L + \frac{U}{\omega^2} x^2 b_{22}(x)\Big|_L$$

$$B_{66} = \int_L b_{22}x^2dx + \frac{U^2}{\omega^2} B_{22}^0 - Ux^2 a_{22}(x)\Big|_L - \frac{U^2}{\omega^2} xb_{22}(x)\Big|_L$$

$$A_{62} = A_{26}^0 - \frac{U}{\omega^2} B_{22}^0 + \frac{U}{\omega^2} xb_{22}(x)\Big|_L - \frac{U^2}{\omega^2} a_{22}(x)\Big|_L$$

$$B_{62} = B_{26}^0 - UA_{22}^0 - Uxa_{22}(x)\Big|_L - \frac{U^2}{\omega^2} b_{22}(x)\Big|_L$$

$$A_{64} = A_{46}^0 + \frac{U}{\omega^2} B_{42}^0 - \frac{U^2}{\omega^2} a_{22}(x)\Big|_L + \frac{U}{\omega^2} xb_{24}(x)\Big|_L$$

$$B_{64} = B_{46}^0 - UA_{42}^0 - Uxa_{24}(x)\Big|_L - \frac{U^2}{\omega^2} a_{24}(x)\Big|_L$$

Table 2.2. Hydrosatic restoring forces

$$C_{33} = \rho g A_W$$
$$C_{35} = C_{35} = -\rho g M_{AW}$$
$$C_{44} = \rho g \nabla (GM_T)$$
$$C_{44} = \rho g \nabla (GM_L)$$

Table 2.3. Main particulars of SWATH models for motion studies

	SWATH-1	SWATH-3	SWATH-FV
Length of hull, L_h (mm)	1510.00	1510.00	1491.00
Diameter of hull, d_h (mm)	89.20	89.20	140.00
Length of strut, L_s (mm)	2 x 400.00	1155.00	1249.00
Max. strut thickness, t_s (mm)	50.00	50.00	84.00
Draught, T (mm)	178.40	178.40	224.00
Hull centreline spacing, B_O (mm)	720.00	720.00	560.00
C_p of hull	0.900	0.900	0.918
C_p of strut	0.665	0.665	0.920
Wetted area, S (m^2)	1.0252	1.1078	1.5138
Displaced volume, ∇ (m^3)	0.0218	0.0261	0.0559
LCG from nose (mm)	732.50	732.50	715.00
KG (mm)	175.30	197.00	240.50
KB (mm)	64.00	75.70	103.00
GM_T (mm)	204.00	386.00	135.90
GM_L (mm)	229.00	207.00	252.10
I_{44} in air ($kg.m^2$)	3.5231	3.3137	5.0400
I_{55} in air ($kg.m^2$)	3.9574	2.991	6.6669
I_{66} in air ($kg.m^2$)	6.2889	5.4520	10.3253
Heave natural period, T_z (secs)	1.701	1.230	1.390
Roll natural period, T_ϕ (secs)	2.340	1.512	2.060
Pitch natural period, T_θ (secs)	2.234	1.967	1.717

Table 2.4. Main particulars of notional SWATHs

	SWATH-1	SWATH-3	SWATH-FV
Length overall, LOA (m)	75.00	70.00	54.65
Length of hull, L_h (m)	72.00	67.95	52.20
Length of strut, L_s (m)	2 x 19.20	51.50	43.70
Diameter of hull, d_h (m)	4.28	4.01	4.90
Centrehulls spacing, B_O (m)	34.56	32.40	19.60
Draught, T (m)	8.56	8.03	7.85
Waterplane area, A_{wp} (m^2)	124.42	206.55	235.69
Displacement, Δ (tonnes)	2486.00	2452.00	2467.00

Table 2.5. Long-term distribution of wave occurrence in the North Atlantic [Ochi (1978)]

Significant Wave Height (m)	Frequency of Occurrence	Significant Wave Height (m)	Frequency of Occurrence
<1	0.05030	9 - 10	0.00790
1 - 2	0.26650	10 - 11	0.00540
2 - 3	0.26030	11 - 12	0.00290
3 - 4	0.17570	12 - 13	0.00160
4 - 5	0.10140	13 - 14	0.00074
5 - 6	0.05890	14 - 15	0.00045
6 - 7	0.03460	15 - 16	0.00020
7 - 8	0.02090	16 - 17	0.00012
8 - 9	0.01200	17<	0.00009

Table 2.6. Selected seakeeping criteria and categories for SWATHs [Olson (1978)]

General Criteria

(1) 12^{o} single amplitude average roll
(2) 3^{o} single amplitude average pitch
(3) Significant heave acceleration $\leq 0.4g$ (no people working on deck)
(4) Significant heave acceleration $\leq 0.2g$ (people working on deck)

General Criteria

(5) 12.8^{o} double amplitude significant roll
(6) 2.55m double amplitude significant vertical displacement at the flight deck due to pitch
(7) 2.13m/s significant vertical velocity at the flight deck

Table 2.7. ASSESSMENT OF SWATH OPERABILITY

(a) Vessel : SWATH - FV
Criteria : 1 - 4 (General)

Fn	Following 0 deg	Beam 90 deg	Bow-Quart. 135 deg	Head 180 deg
0.00	2	1	2	2
0.13	2	4	2,4	2
0.26	2	4	2	2
0.39	2	4	2	2
0.52	2	4	2	2

ACCEPTABLE SIGNIFICANT WAVE HEIGHT, Hs (m)

Fn	Following 0 deg	Beam 90 deg	Bow-Quart. 135 deg	Head 180 deg
0.00	3.00	6.00	5.00	3.00
0.13	4.00	8.00	8.00	6.00
0.26	5.00	8.00	6.00	5.00
0.39	5.00	9.00	4.00	4.00
0.52	3.00	9.00	4.00	3.00

RATE OF OPERABILITY

Fn	Following 0 deg	Beam 90 deg	Bow-Quart. 135 deg	Head 180 deg	
0.00	0.0289	0.0457	0.0427	0.0289	0.1461
0.13	0.0376	0.0484	0.0484	0.0457	0.1802
0.26	0.0427	0.0484	0.0457	0.0427	0.1795
0.39	0.0427	0.0490	0.0376	0.0376	0.1670
0.52	0.0289	0.0490	0.0376	0.0289	0.1444
Total =	0.1808	0.2406	0.2121	0.1837	**0.8172**

(b) Vessel : SWATH - FV
Criteria : 1 - 7 (General & Helicopter)

Fn	Following 0 deg	Beam 90 deg	Bow-Quart. 135 deg	Head 180 deg
0.00	6	5,6	6	6
0.13	2,6	5,6	6	6
0.26	2	6	6	6,7
0.39	2,6	6	6	6
0.52	2	6	6	6

ACCEPTABLE SIGNIFICANT WAVE HEIGHT, Hs (m)

Fn	Following 0 deg	Beam 90 deg	Bow-Quart. 135 deg	Head 180 deg
0.00	2.00	4.00	3.00	3.00
0.13	3.00	5.00	4.00	2.00
0.26	5.00	4.00	4.00	4.00
0.39	4.00	3.00	3.00	3.00
0.52	2.00	3.00	3.00	3.00

RATE OF OPERABILITY

Fn	Following 0 deg	Beam 90 deg	Bow-Quart. 135 deg	Head 180 deg	
0.00	0.0158	0.0376	0.0289	0.0289	0.1112
0.13	0.0289	0.0427	0.0376	0.0158	0.1250
0.26	0.0427	0.0376	0.0376	0.0376	0.1556
0.39	0.0376	0.0289	0.0289	0.0289	0.1242
0.52	0.0158	0.0289	0.0289	0.0289	0.1024
Total =	0.1409	0.1757	0.1618	0.1400	**0.6185**

Table 2.8. Operability of SWATHs in the North Atlantic

	SWATH - 1	SWATH - 3	SWATH - FV
General Criteria (1-4)	0.896	0.843	0.817
Gen. & Heli. Criteria (1-7)	0.671	0.632	0.618

Table 2.9. Wave data for the North Atlantic [Chilò & Sartori (1979)]

Table 3
NORTH ATLANTIC

wave height (m)	observed wave period (T_p) (sec.)										
	2.5	6.5	8.5	10.5	12.5	14.5	16.5	18.5	20.5	over 21	totals
0 - 1	18.6846	4.5036	1.0144	0.3511	0.1381	0.0512	0.0341	0.0179	0.0976	0.5336	25.4262
1 - 2	14.4152	17.6097	6.4484	1.7936	0.5534	0.1852	0.0721	0.0218	0.0213	0.0913	41.2120
2 - 3	1.5051	6.9322	6.7253	2.9229	0.9292	0.2935	0.0825	0.0230	0.0064	0.0074	19.4275
3 - 4	0.2466	1.5878	2.7234	1.9934	0.9298	0.3039	0.0945	0.0299	0.0039	0.0032	7.9164
4 - 5	0.0666	0.4775	1.0347	0.9763	0.5518	0.2304	0.0907	0.0290	0.0058	0.0037	3.4665
5 - 6	0.0197	0.0868	0.2222	0.2434	0.1522	0.0701	0.0237	0.0048	0.0019	0.0019	0.8266
6 - 7	0.0191	0.0903	0.2038	0.2534	0.1622	0.0723	0.0271	0.0064	0.0017	0.0017	0.8380
7 - 8	0.0045	0.0384	0.0996	0.1212	0.0873	0.0425	0.0189	0.0037	0.0009	0.0017	0.4187
8 - 9	0.0023	0.0172	0.0450	0.0671	0.0570	0.0304	0.0155	0.0026	0.0014	0.0024	0.2409
9 - 10	0.0018	0.0110	0.0353	0.0602	0.0495	0.0315	0.0163	0.0080	0.0043	0.0024	0.2203
10 - 11	-	0.0003	0.0005	0.0010	0.0014	0.0005	-	0.0002	-	-	0.0039
11 +	-	0.0003	0.0003	0.0008	0.0018	0.0001	-	-	0.0001	-	0.0034
Totals	34.9655	31.3551	18.5529	8.7844	3.6137	1.3116	0.4754	0.1473	0.1453	0.6492	100.0004

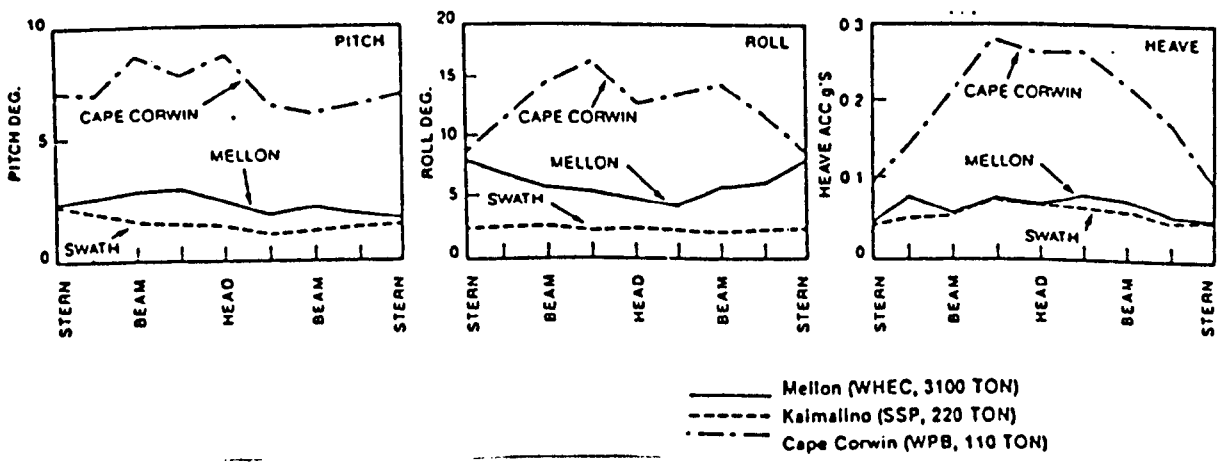

Figure 2.1. US Navy/Coast Guard Seakeeping Trials Motions Comparisons [Woolaver & Peters (1980)]

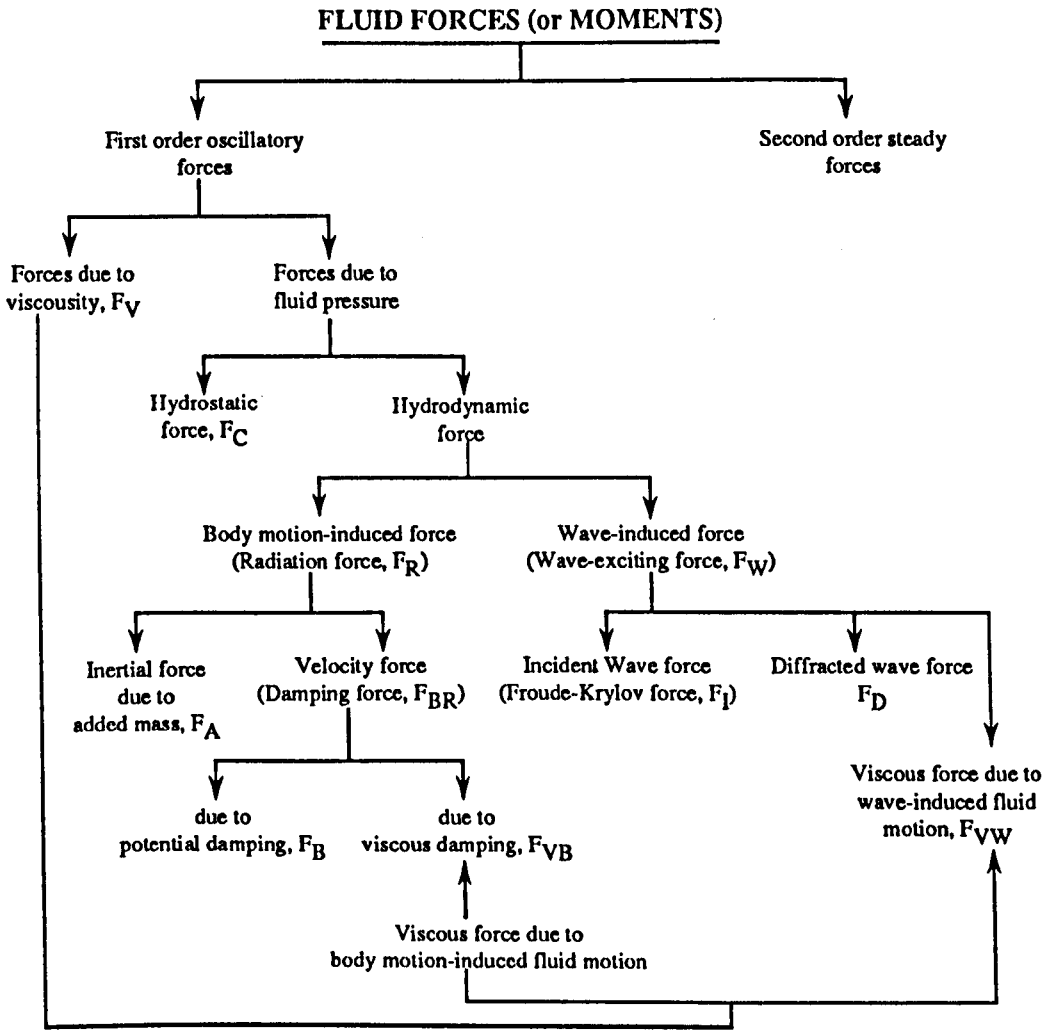

Figure 2.2. Fluid forces and moments diagram [Atlar et al (1987)]

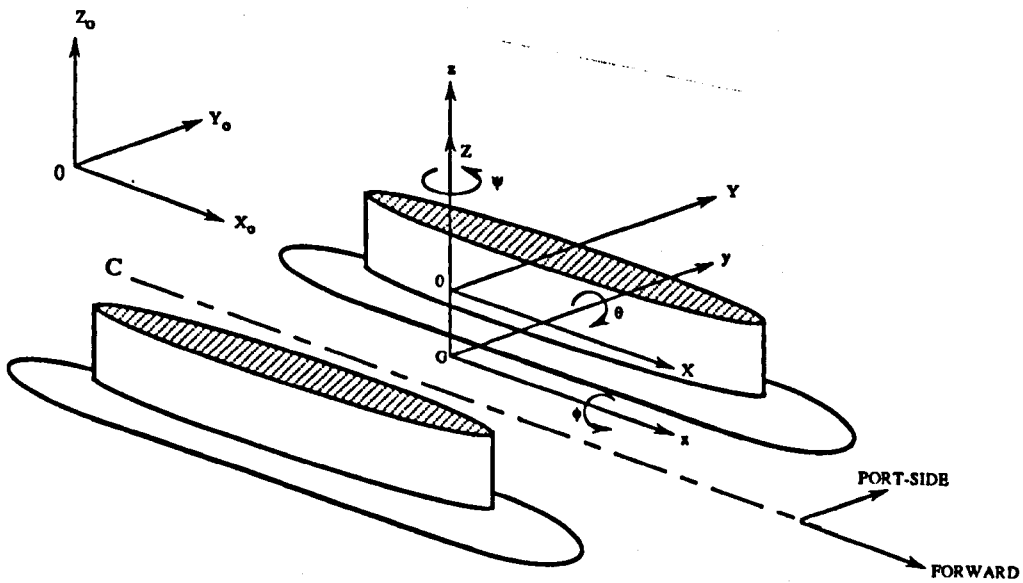

Figure 2.3. Co-ordinate system

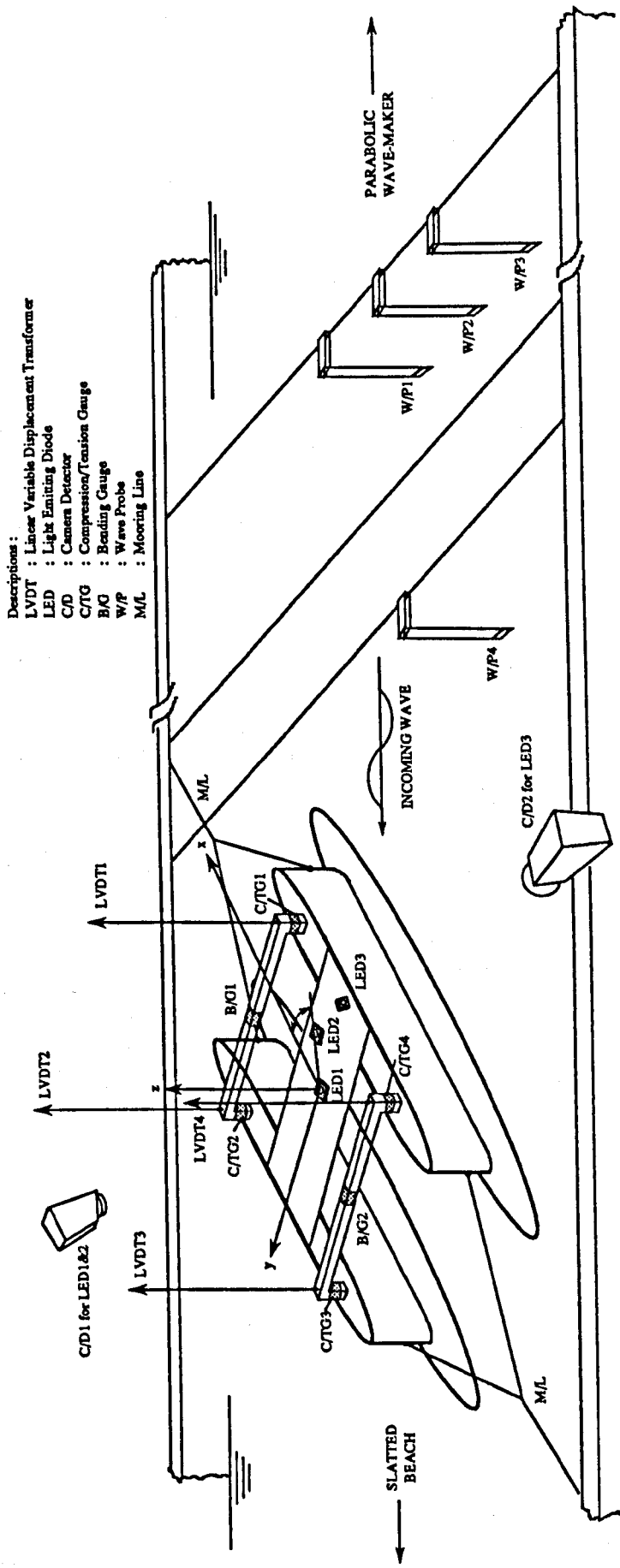

Figure 2.4. Model test arrangement at zero Froude number

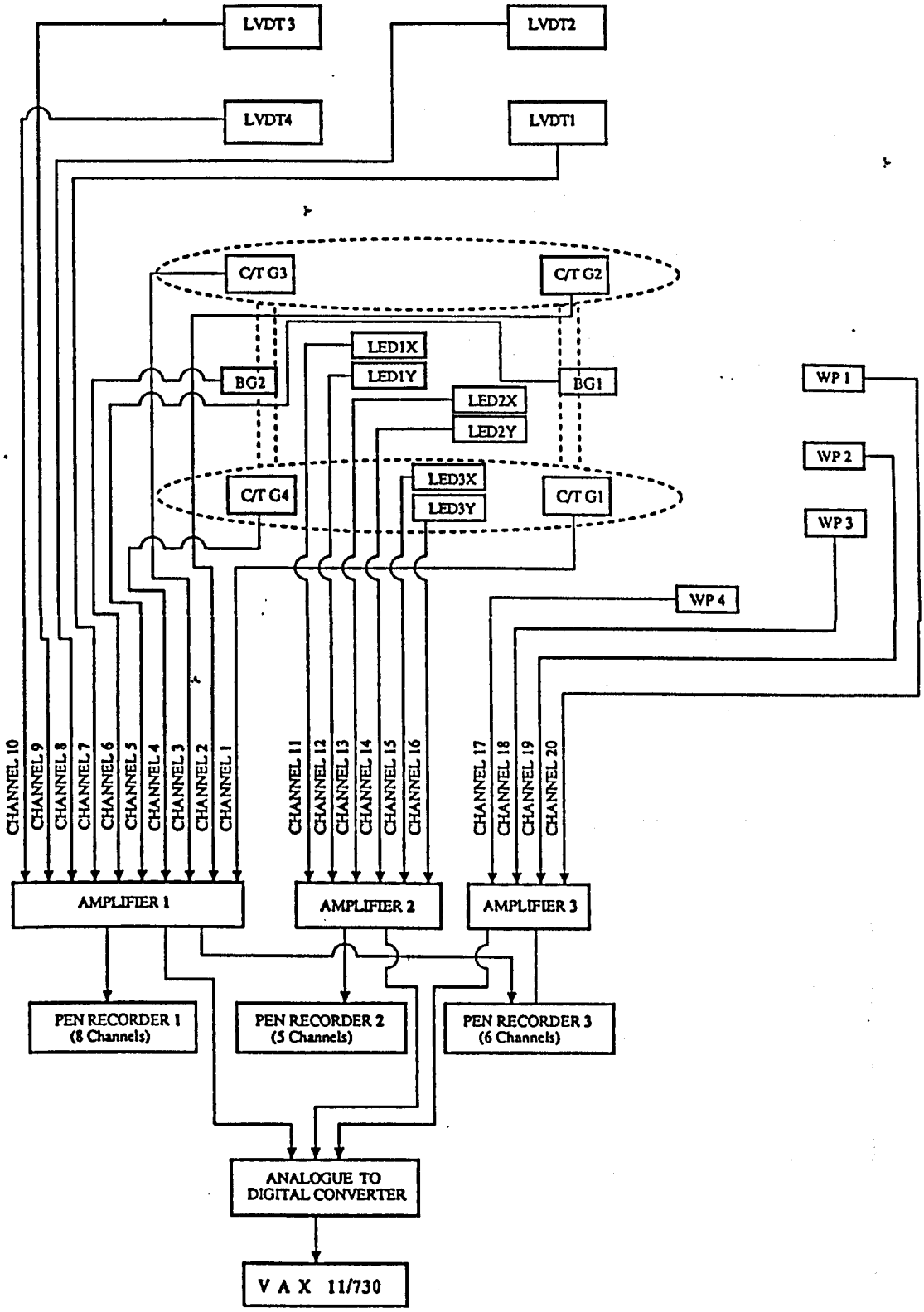

Figure 2.5. Diagrammatic arrangement of instrument connections for SWATH model motion and wave load tests

Figure 2.6. Photograph of the amplifier and recording devices for SWATH model tests

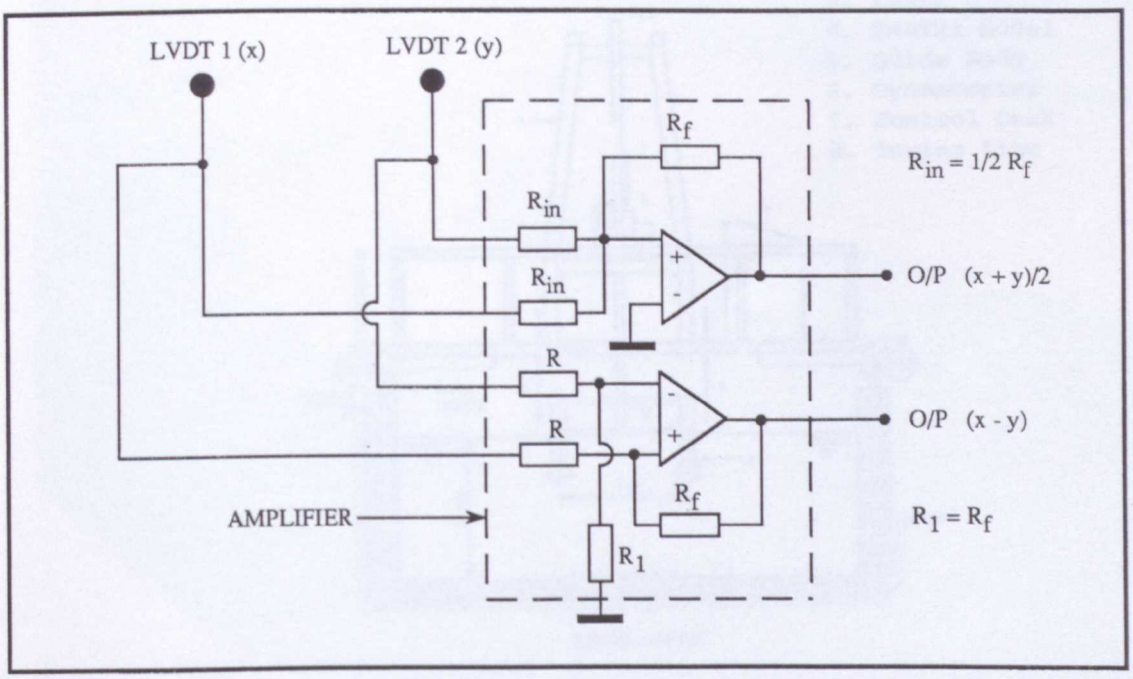

Figure 2.10. Sum and difference unit in the amplifier

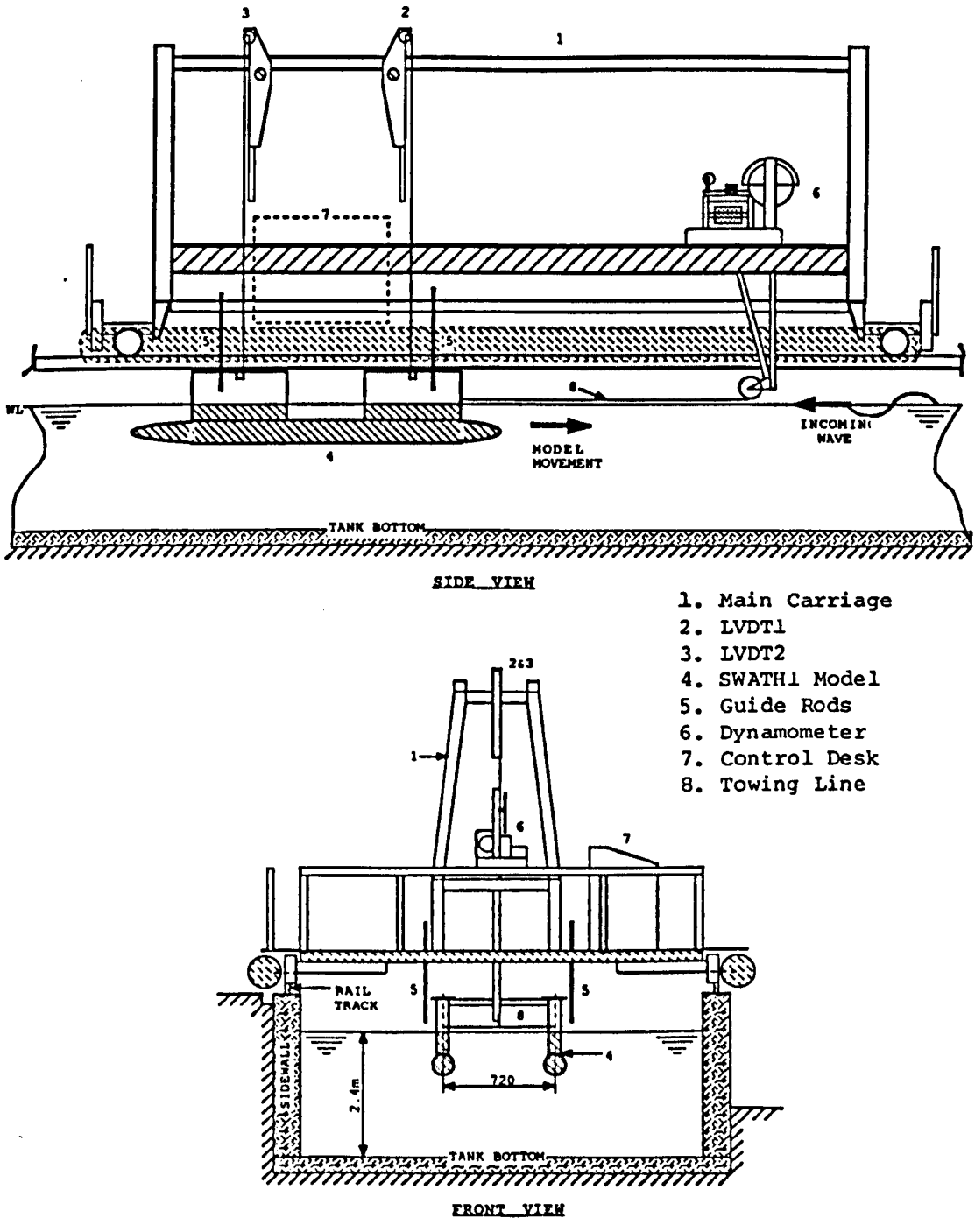

Figure 2.7. SWATH model mounted on the towing carriage

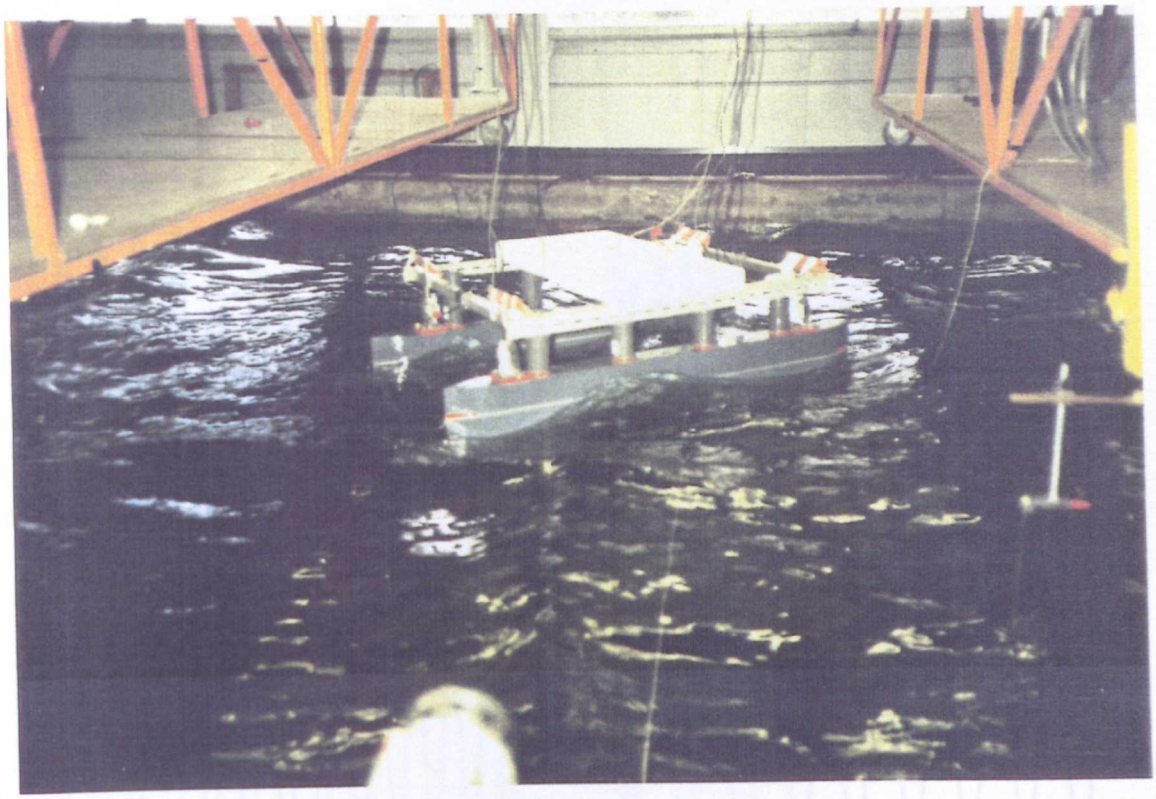

Figure 2.8. Photograph SWATH model in stationary test

Figure 2.9. Photograph SWATH model underway in a head wave

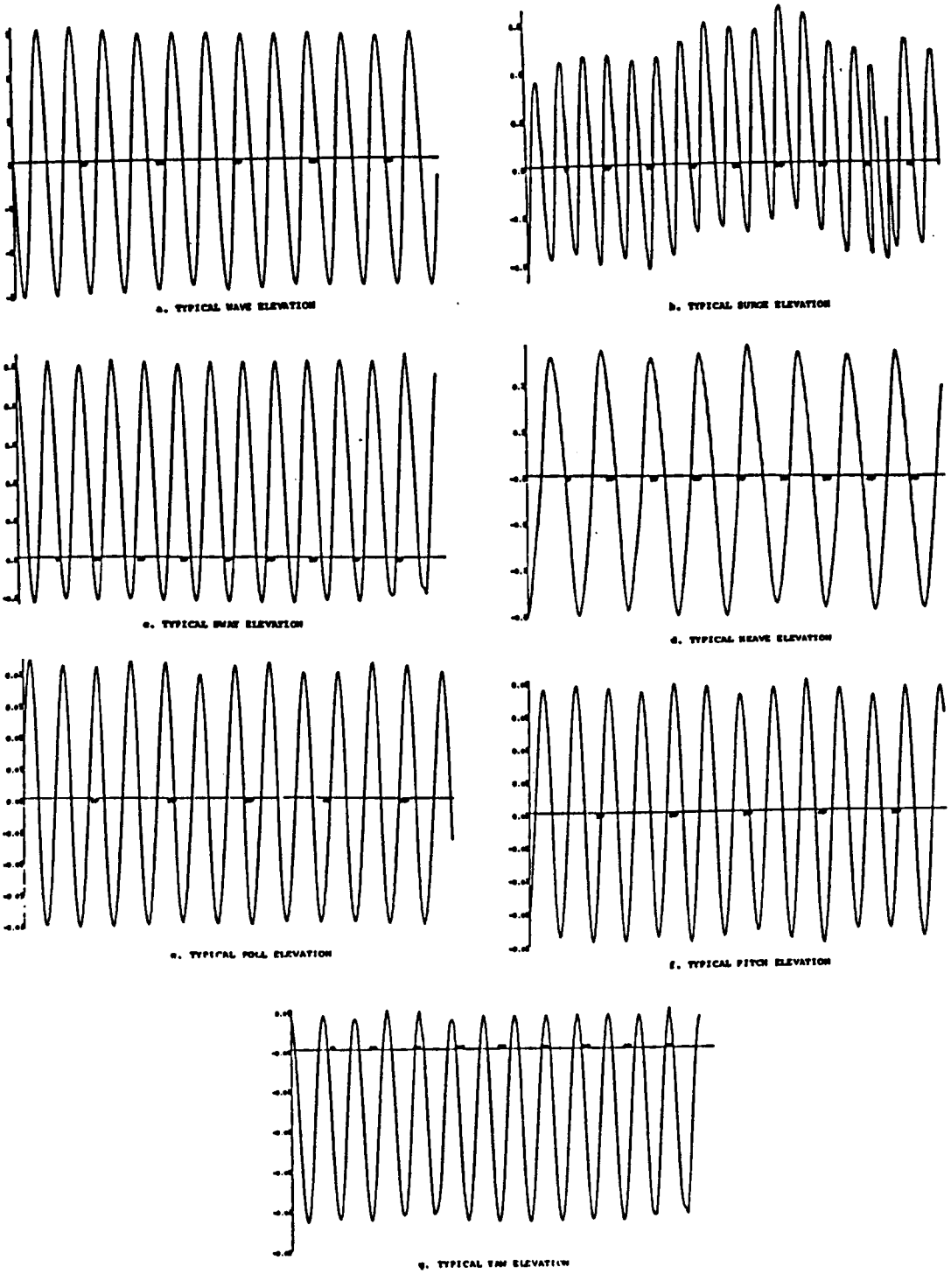

Figure 2.11. Typical wave and motion elevations from data analysis program

Model	SWATH-1	SWATH-3	SWATH-FV
Length of hull, L_h (mm)	1500.0	1500.0	1491.0
Hull diameter, d_h (mm)	89.2	89.2	140.0
Length of strut, L_s (mm)	400.0	1155.0	1249.0
Max. strut thickness, t_s (mm)	50.0	50.0	84.0
Draught, T (mm)	178.4178	178.4	224.0
Natural Periods			
Heave, T_z (sec)	1.701	1.230	1.390
Roll, T_ϕ (sec)	2.340	1.512	2.060
Pitch, T_θ (sec)	2.234	1.967	1.717
Number of panels	544	496	408

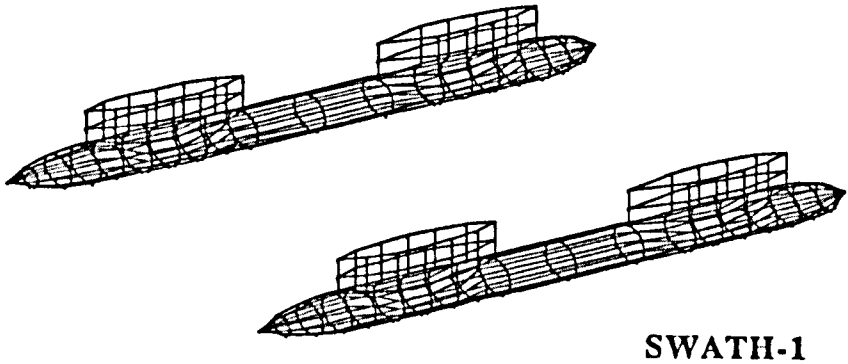

SWATH-1

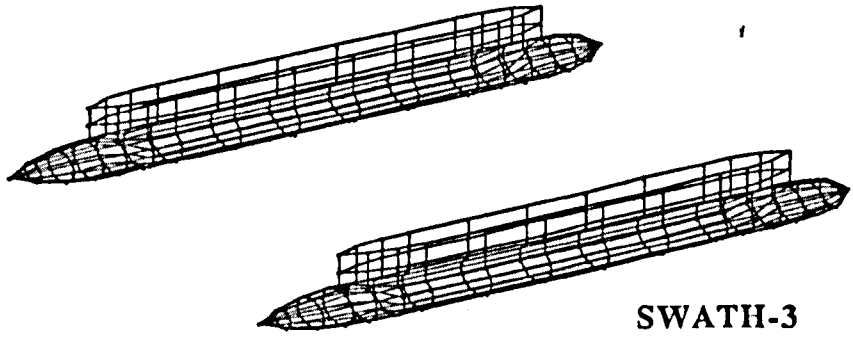

SWATH-3

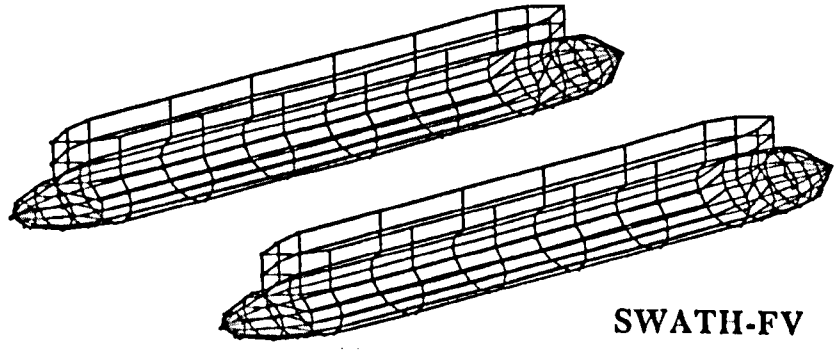

SWATH-FV

Figure 2.12. Discretisation of SWATH models

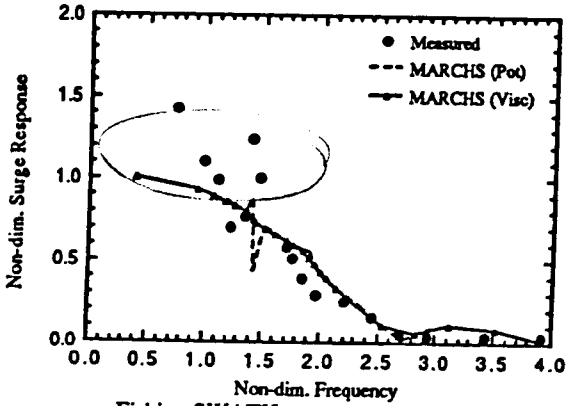

Fishing SWATH model Surge responses in head seas (Fn=0.00)

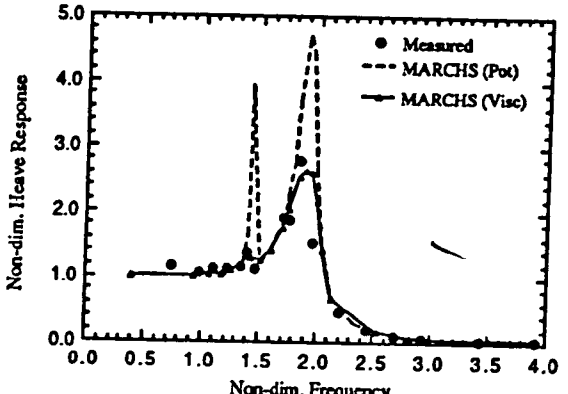

Fishing SWATH model Heave responses in head seas (Fn=0.00)

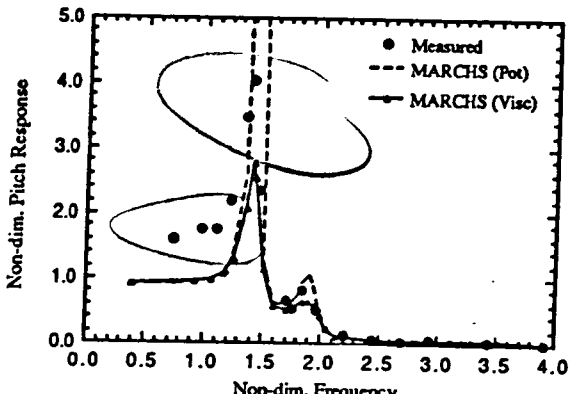

Fishing SWATH model Pitch responses in head seas (Fn=0.00)

Figure 2.13. SWATH-FV model motions in head seas (Fn=0.00)

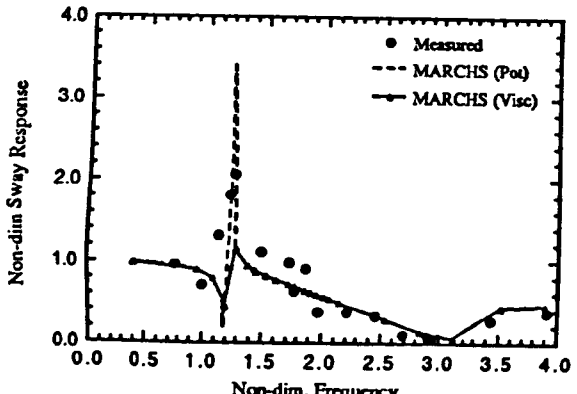

Fishing SWATH model Sway responses in beam seas (Fn=0.00)

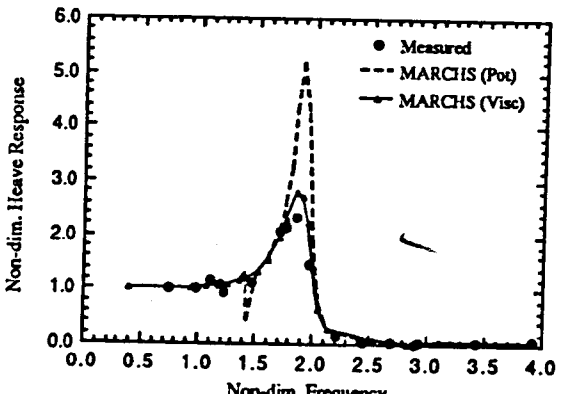

Fishing SWATH model Heave responses in beam seas (Fn=0.00)

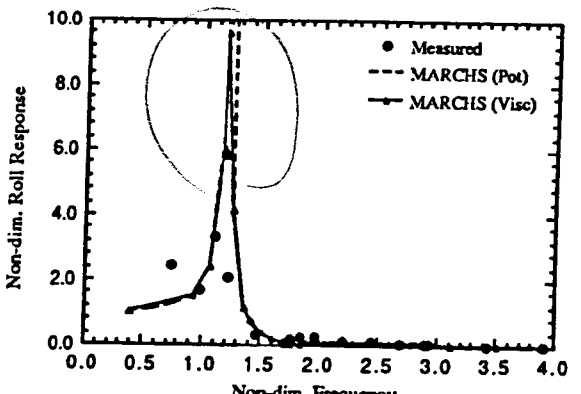

Fishing SWATH model Roll responses in beam seas (Fn=0.00)

Figure 2.14. SWATH-FV model motions in beam seas (Fn=0.00)

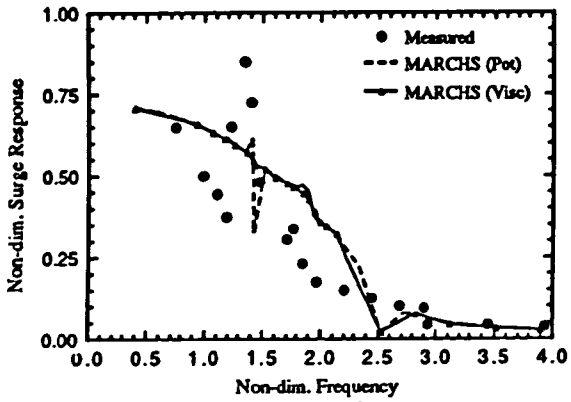

Fishing SWATH model Surge responses in quartering seas (Fn=0.00)

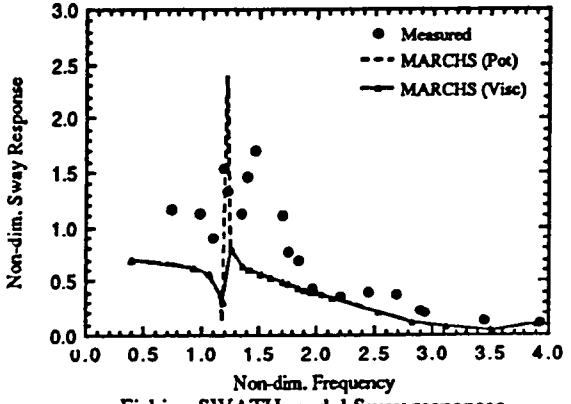

Fishing SWATH model Sway responses in quartering seas (Fn=0.00)

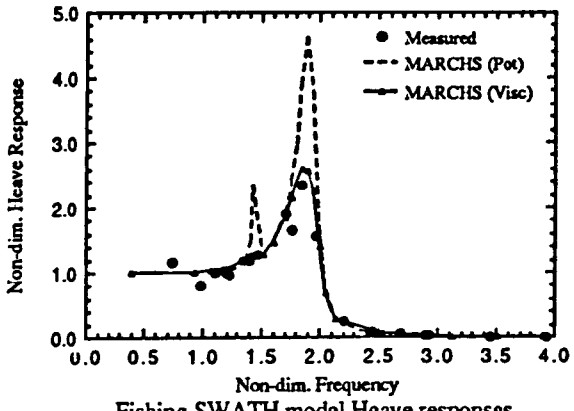

Fishing SWATH model Heave responses in quartering seas (Fn=0.00)

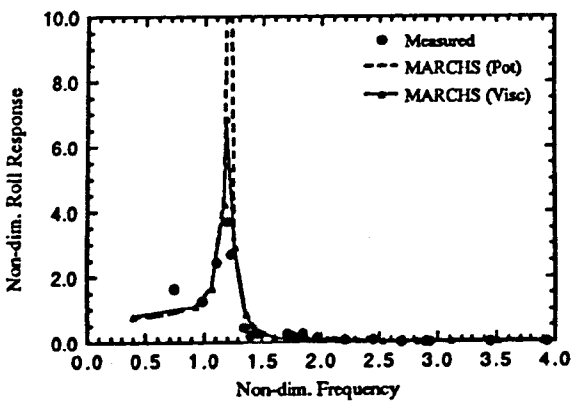

Fishing SWATH model Roll responses in quartering seas (Fn=0.00)

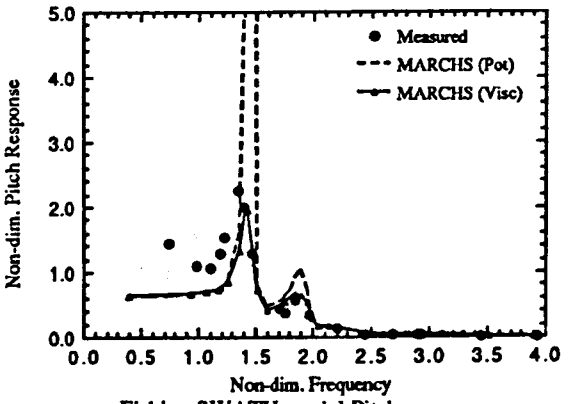

Fishing SWATH model Pitch responses in quartering seas (Fn=0.00)

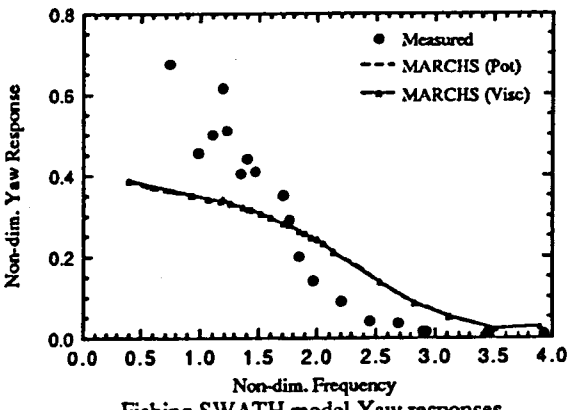

Fishing SWATH model Yaw responses in quartering seas (Fn=0.00)

Figure 2.15. SWATH-FV model motions in bow-quartering seas (Fn=0.00)

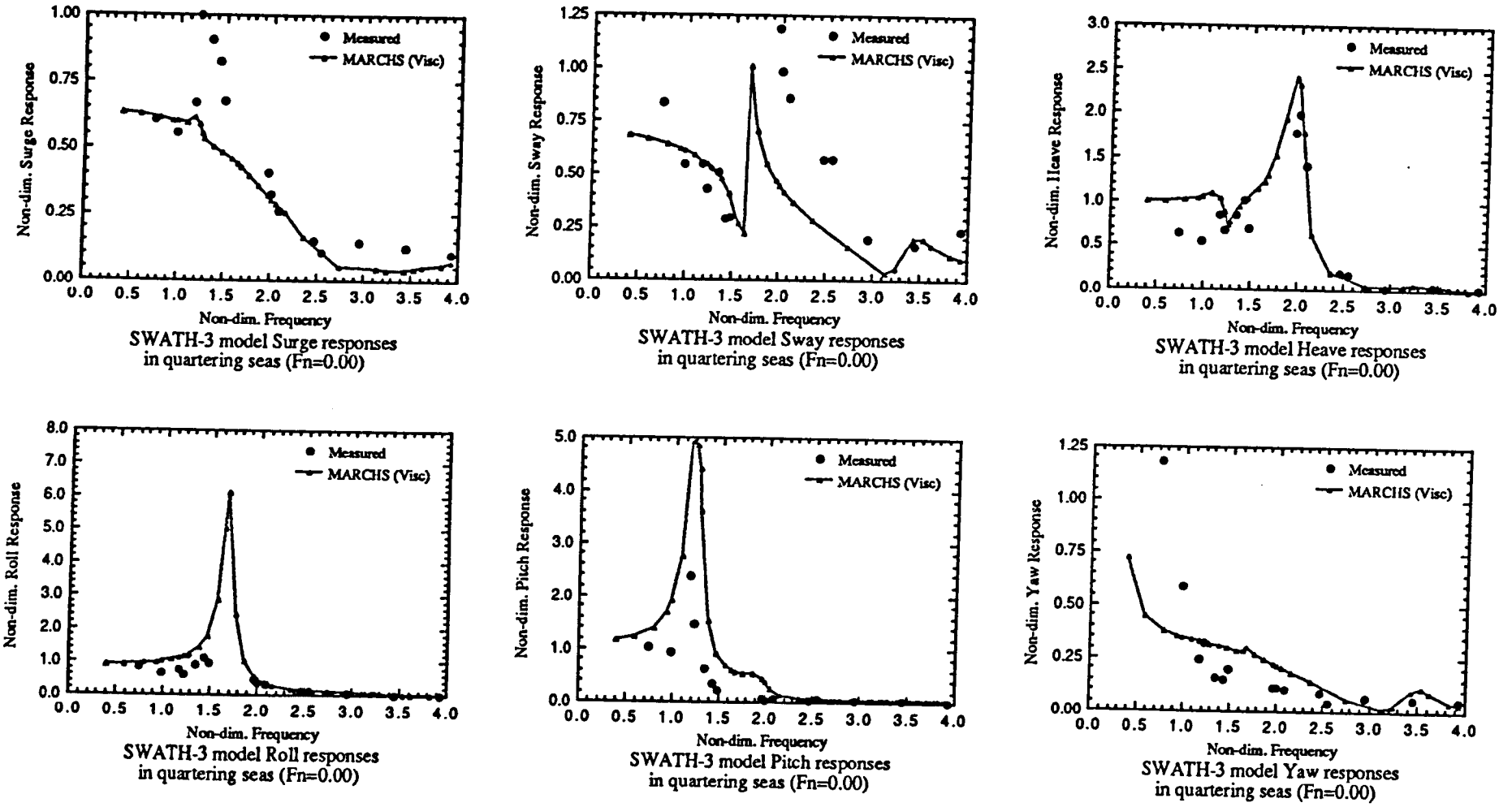

Figure 2.16. SWATH-3 model motions in bow-quartering seas (Fn=0.00)

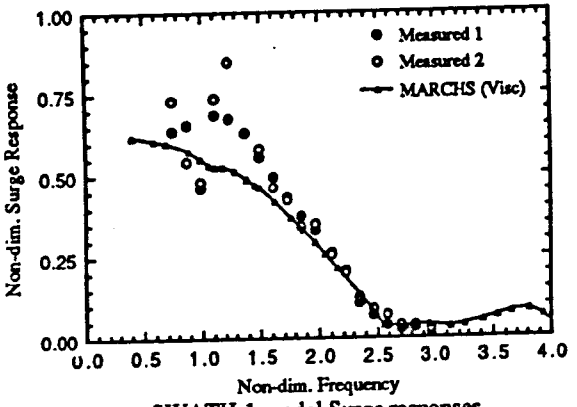

SWATH-1 model Surge responses
in quartering seas (Fn=0.00)

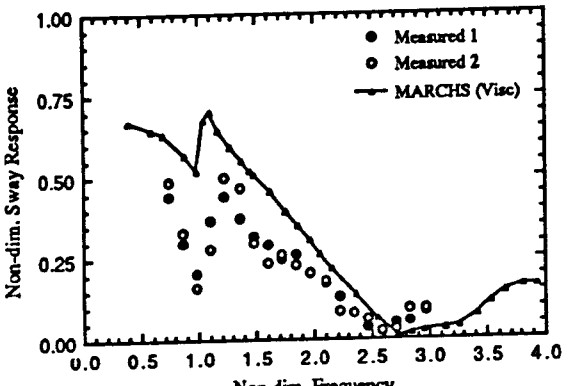

SWATH-1 model Sway responses
in quartering seas (Fn=0.00)

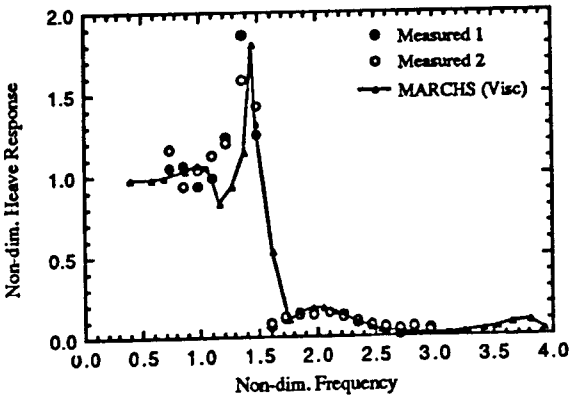

SWATH-1 model Heave responses
in quartering seas (Fn=0.00)

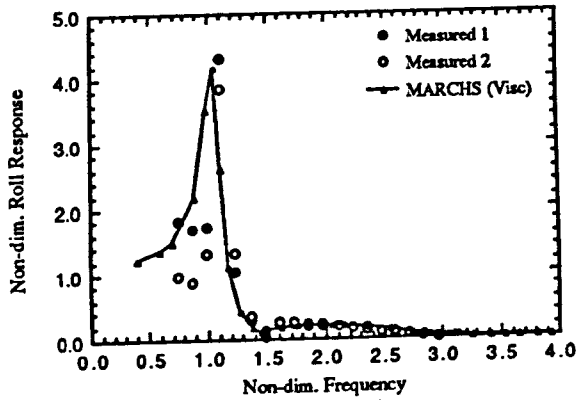

SWATH-1 model Roll responses
in quartering seas (Fn=0.00)

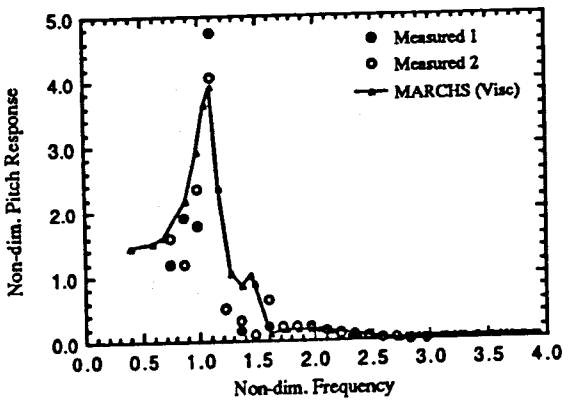

SWATH-1 model Pitch responses
in quartering seas (Fn=0.00)

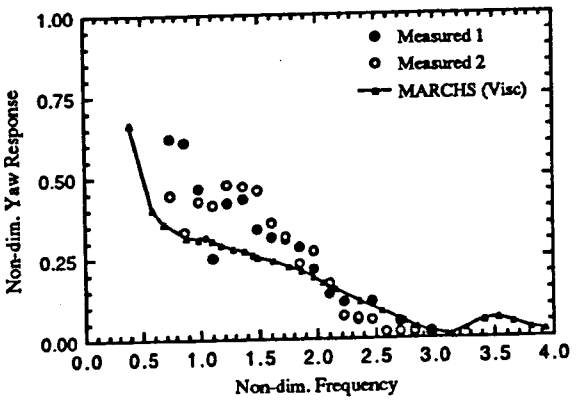

SWATH-1 model Yaw responses
in quartering seas (Fn=0.00)

Figure 2.17. SWATH-1 model motions in bow-quartering seas (Fn=0.00)
(tandem strut per hull configuration)

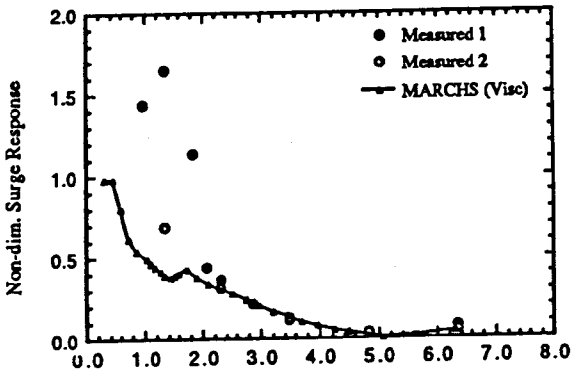

SWATH-1 model Surge responses in head seas (Fn=0.39)

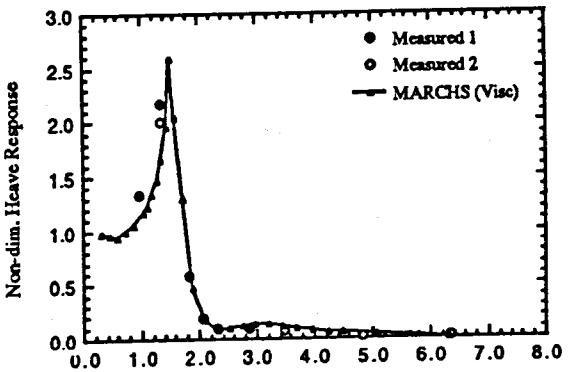

SWATH-1 model Heave responses in head seas (Fn=0.39)

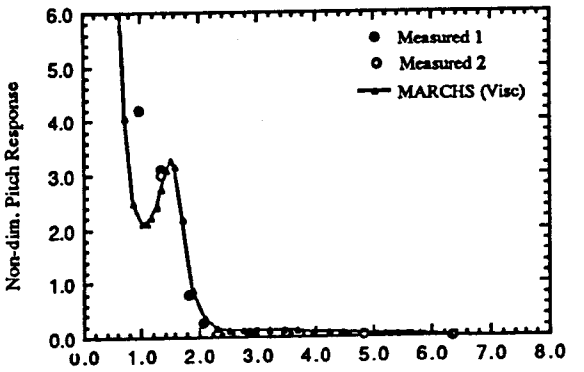

SWATH-1 model Pitch responses in head seas (Fn=0.39)

Figure 2.18. SWATH-1 model motions in head seas (Fn=0.39)

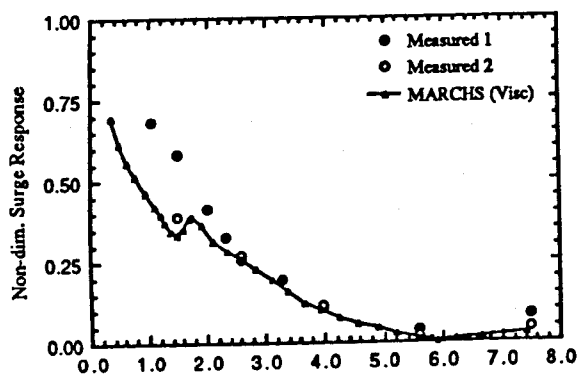

SWATH-1 model Surge responses in head seas (Fn=0.52)

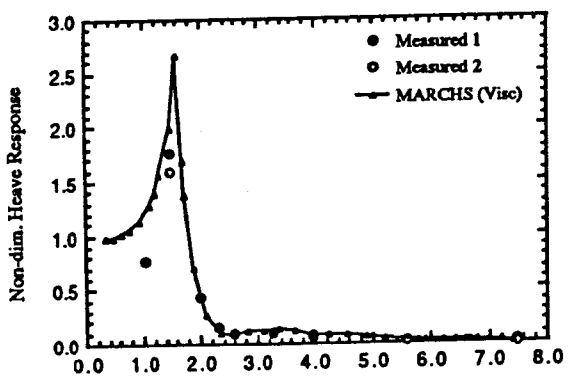

SWATH-1 model Heave responses in head seas (Fn=0.52)

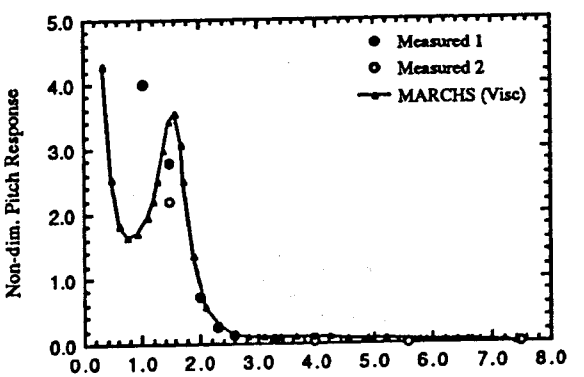

SWATH-1 model Pitch responses in head seas (Fn=0.52)

Figure 2.19. SWATH-1 model motions in head seas (Fn=0.52)

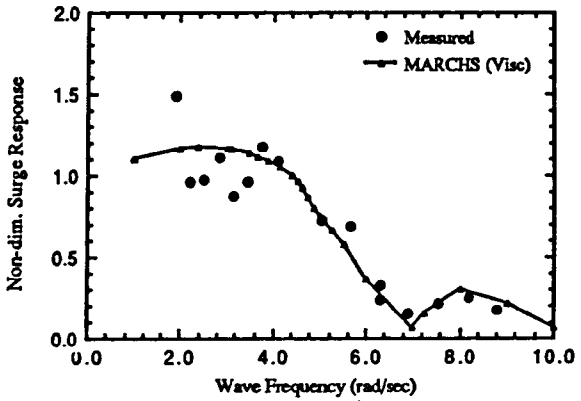

Fishing SWATH model Surge responses in following seas (Fn=0.13)

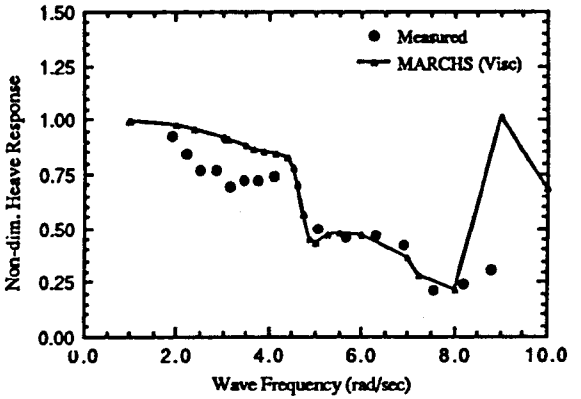

Fishing SWATH model Heave responses in following seas (Fn=0.13)

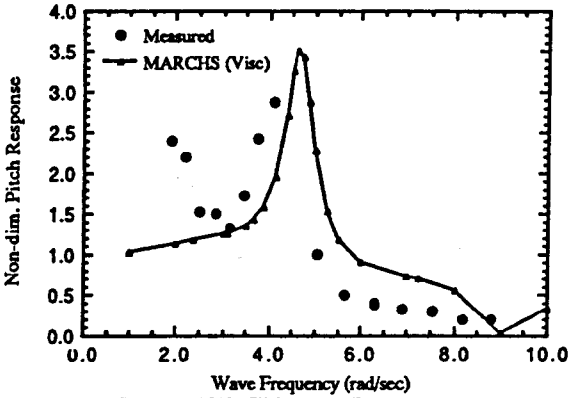

Fishing SWATH model Pitch responses in following seas (Fn=0.13)

Figure 2.20. SWATH-FV model motions in following seas (Fn=0.13)

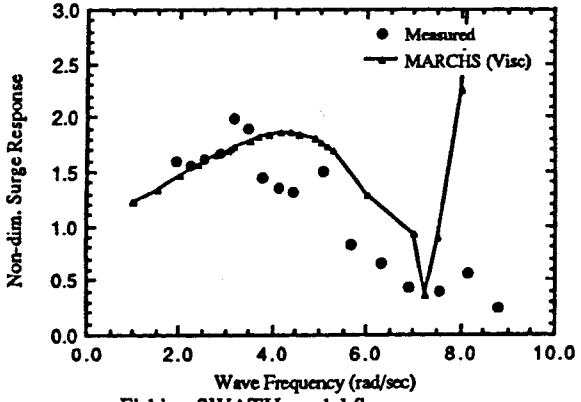

Fishing SWATH model Surge responses in following seas (Fn=0.26)

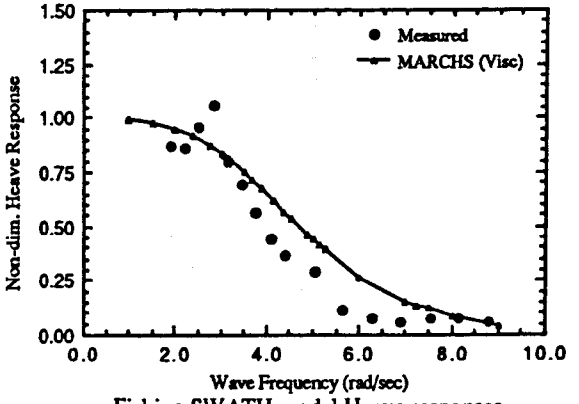

Fishing SWATH model Heave responses in following seas (Fn=0.26)

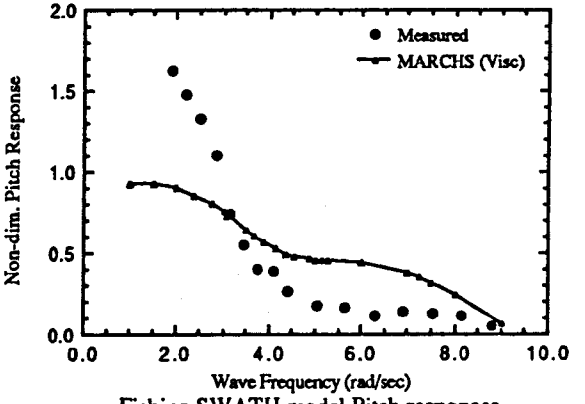

Fishing SWATH model Pitch responses in following seas (Fn=0.26)

Figure 2.21. SWATH-FV model motions in following seas (Fn=0.26)

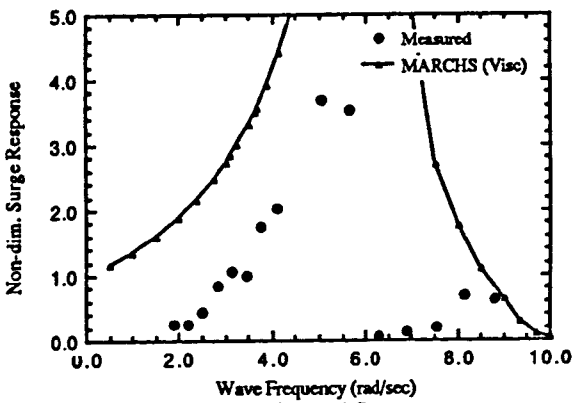

Fishing SWATH model Surge responses in following seas (Fn=0.39)

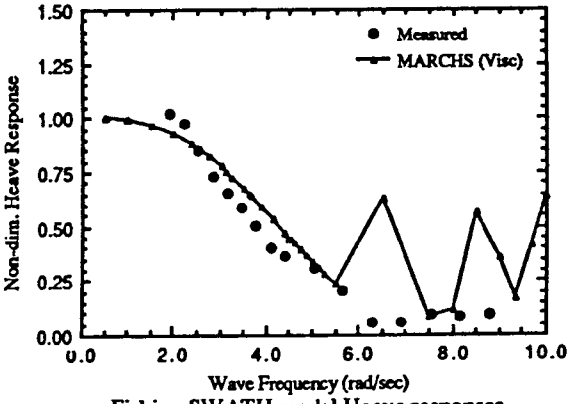

Fishing SWATH model Heave responses in following seas (Fn=0.39)

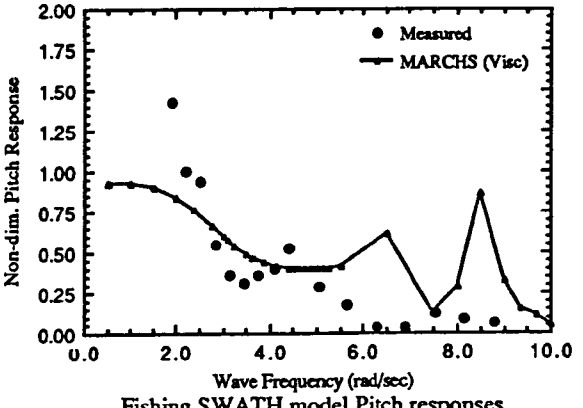

Fishing SWATH model Pitch responses in following seas (Fn=0.39)

Figure 2.22. SWATH-FV model motions in following seas (Fn=0.39)

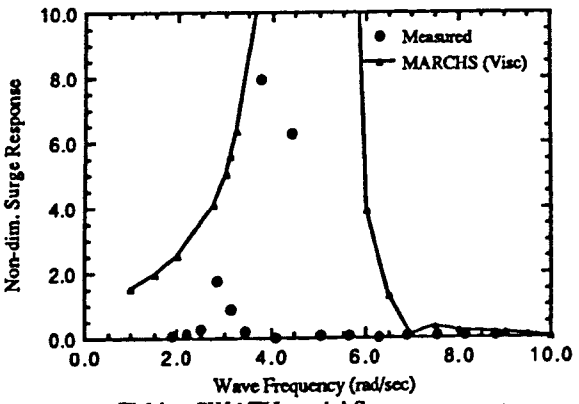

Fishing SWATH model Surge responses in following seas (Fn=0.52)

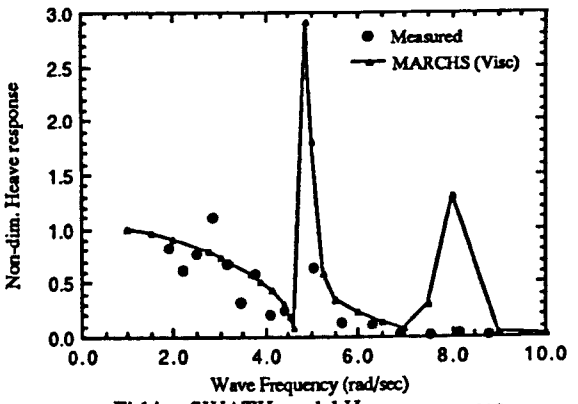

Fishing SWATH model Heave responses in following seas (Fn=0.52)

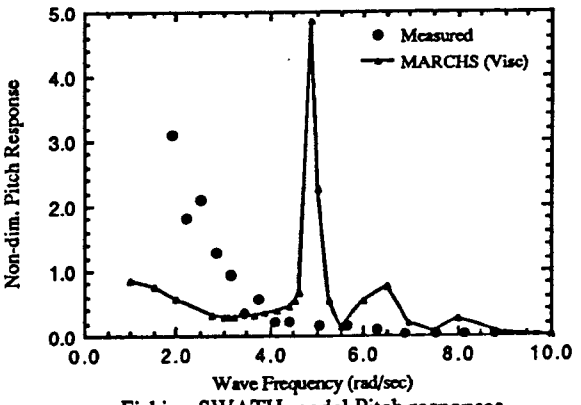

Fishing SWATH model Pitch responses in following seas (Fn=0.52)

Figure 2.23. SWATH-FV model motions in following seas (Fn=0.52)

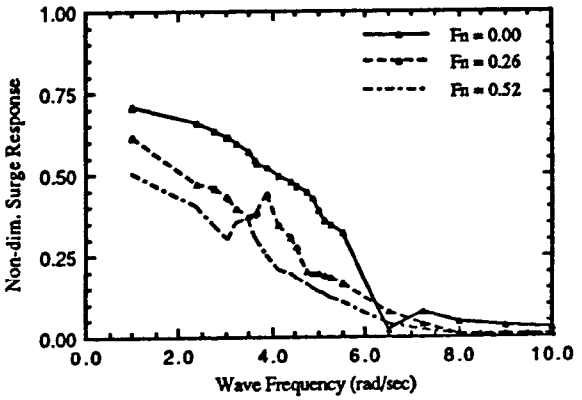

Fishing SWATH model Surge responses in quartering seas

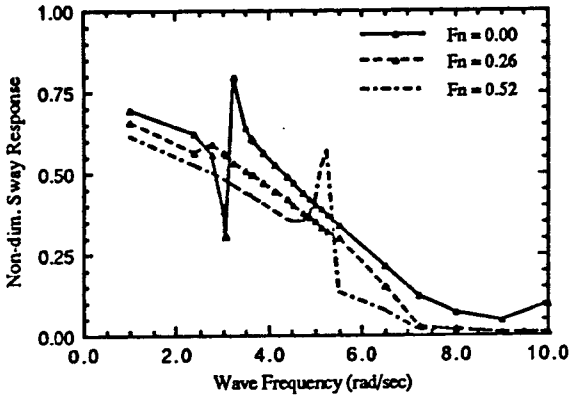

Fishing SWATH model Sway responses in quartering seas

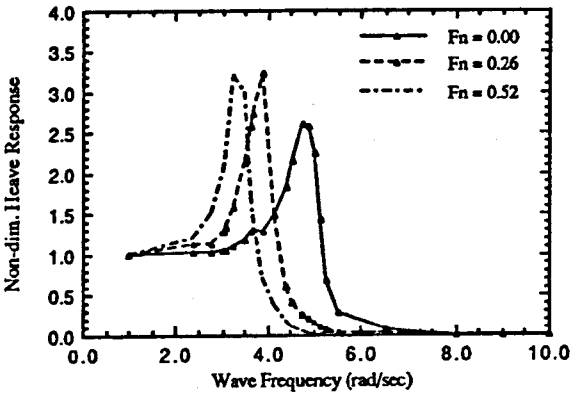

Fishing SWATH model Heave responses in quartering seas

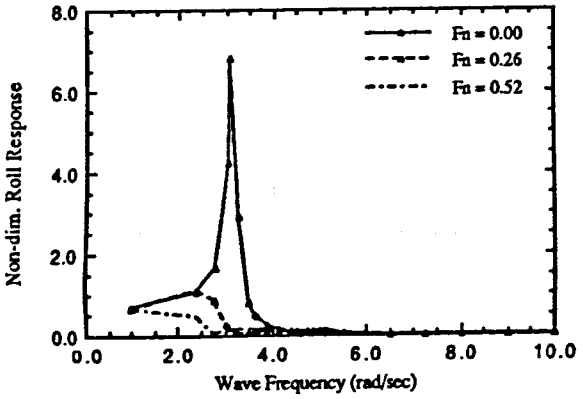

Fishing SWATH model Roll responses in quartering seas

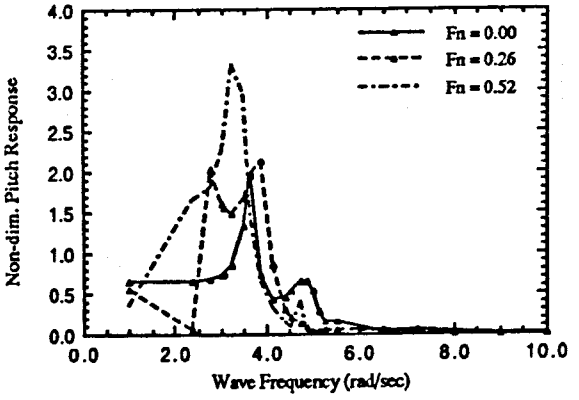

Fishing SWATH model Pitch responses in quartering seas

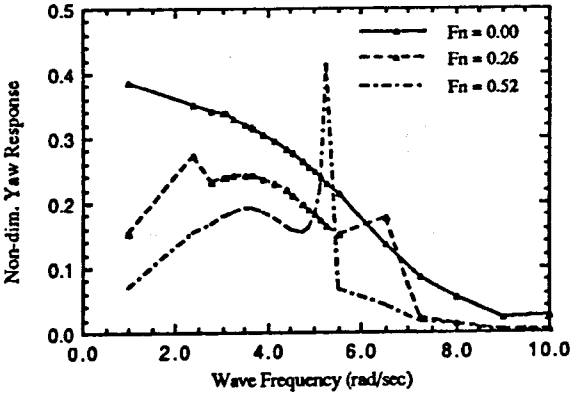

Fishing SWATH model Yaw responses in quartering seas

Figure 2.24. SWATH-FV model motions in bow-quartering seas at various Froude numbers

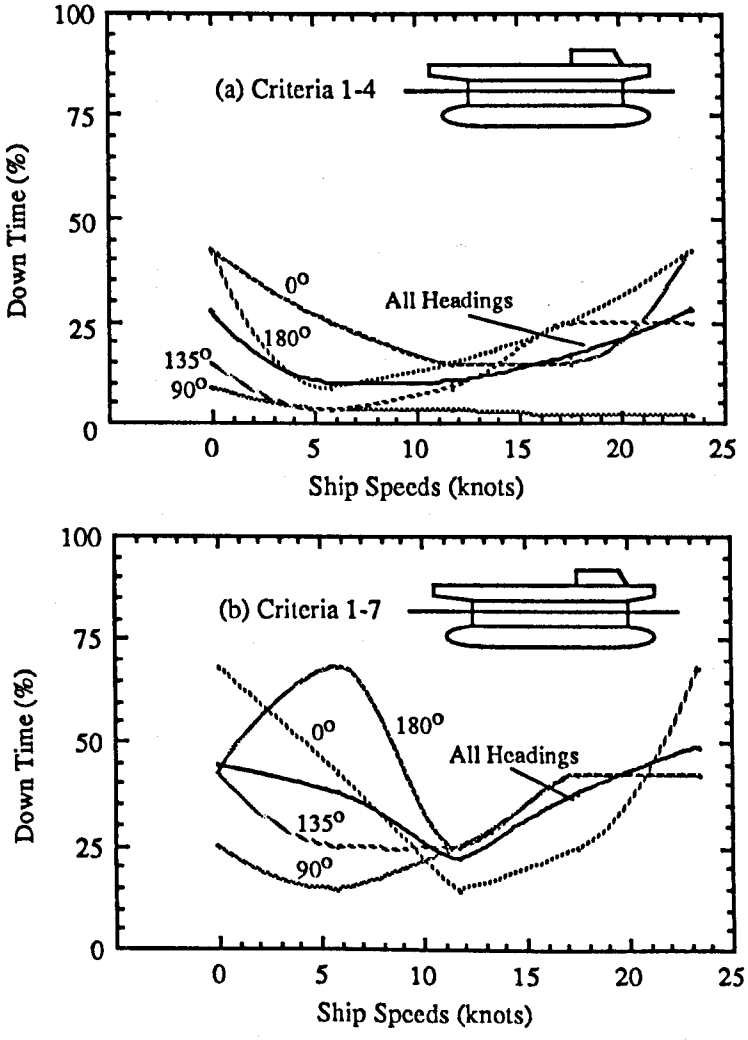

Figure 2.25. Distribution of the down time for SWATH-FV operating in the North-Atlantic

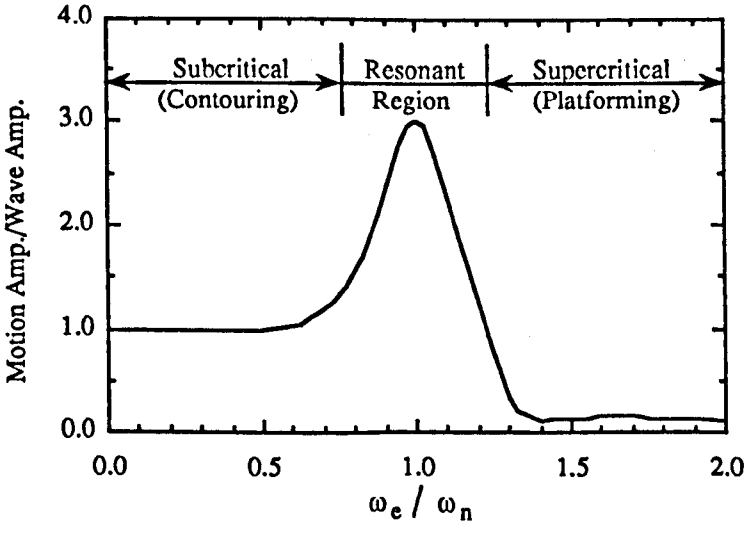

Figure 2.29. Typical variations of SWATH vertical motion responses (heave, roll, pitch) vs tuning factor [Lamb (1988)]

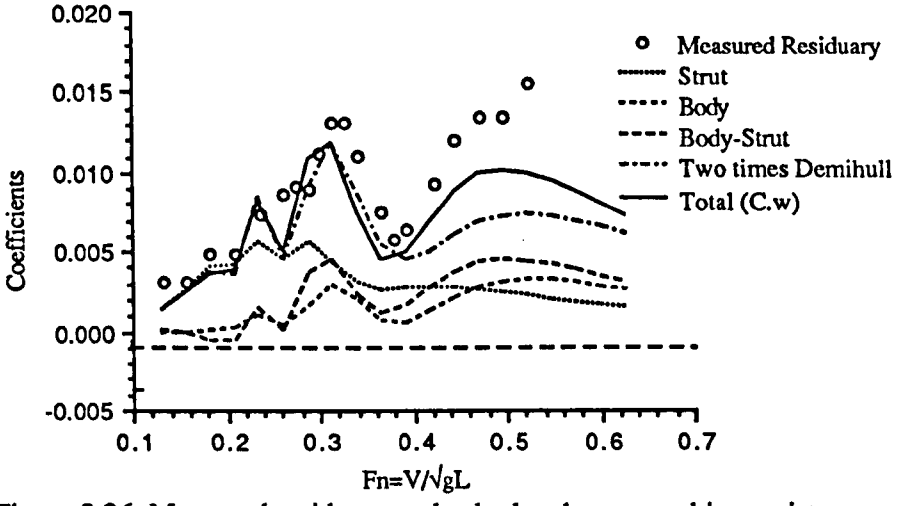

Figure 2.26. Measured residuary and calculated wave-making resistance coeff. for SWATH-FV model and its component contribution vs Froude Number

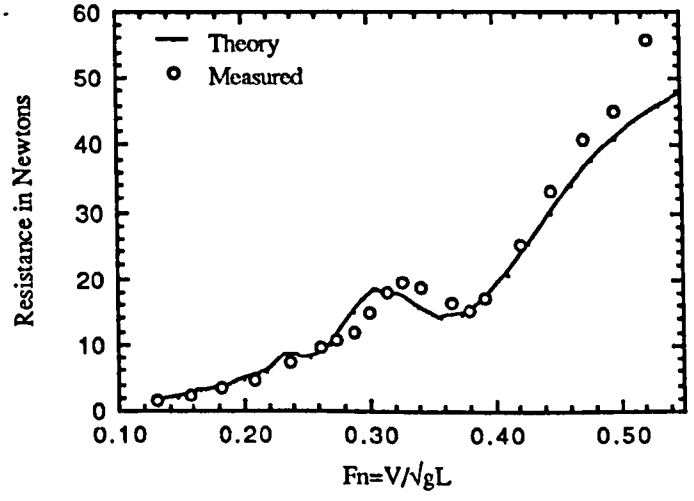

Figure 2.27. Total resistance of SWATH-FV model in calm water vs Froude Number

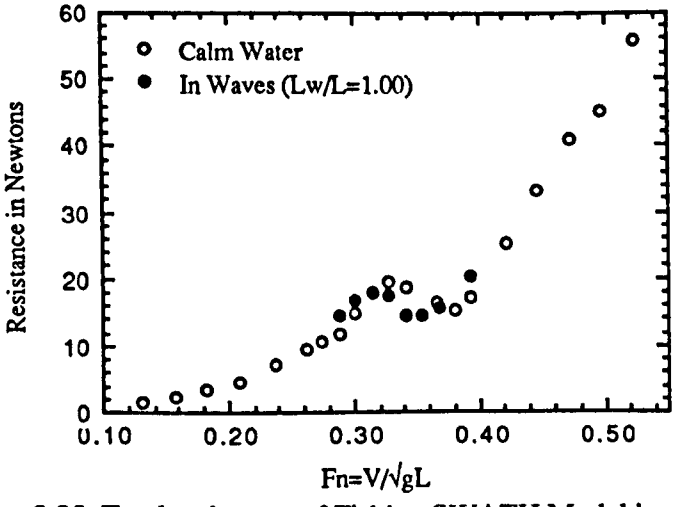

Figure 2.28. Total resistance of Fishing SWATH Model in calm water and in waves vs Froude Number

CHAPTER 3

PREDICTION OF WAVE LOADS ON SWATH SHIPS

CHAPTER 3

PREDICTION OF WAVE LOADS ON SWATH SHIPS

3.1. INTRODUCTION

A rigorous investigation by Burke (1981) indicates the many possible causes that has led to serious damage on ship structures. Ranked at the top of the most frequent causes of structural damage was contact with other structures and collisions between vessels in operation. Damage due to extreme waves or heavy weather ranked fifth. An interesting cause of damage as recorded, however, is the design fault. It was reported that, even though design fault did not rank at the top, it has the largest average repair cost index compared to the others. Accordingly, the repair time consumed due to design faults is found to be the longest of all. One may therefore suspect that crucial structural damage due to design faults and extreme sea loads is interrelated.

The nature of design fault cannot be easily characterised, but some are due to applying new, insufficiently tested technology, some due to compromises made with construction methods, and some may be identified purely due to errors. It is therefore quite fair at this point to mention that the designer should first of all be concerned with the basic source of such problems, namely, the appropriateness in determining the design loads. The above quotations are appropriate to new concepts such as SWATH, which is dealt with here.

Like many other floating structures, it is obvious that wave is the main contributor to the external load acting on SWATHs. Hence, this primary load might solely represent the maximum load to be considered in the structural design of SWATH ships. Because of this, hydrodynamicists have been studying this subject for long time, and various methods to approach the prediction have been developed.

Various investigations on physical model and full scale SWATH ships, as reported by Meyerhoff et al (1988), show that the most critical wave loads were experienced when the ship is operating in beam seas with zero speed. This critical structural load is found in the form of vertical bending moment at the mid point of cross structure. The main contributor on such a load is the side force excited by the beamwise wave actions. This type of wave load is worse on SWATHs compared with catamarans, as the former usually requires greater box clearance to avoid slamming impact on the bottom of the deck. As suggested by Lee and Curphey (1977) and

Dallinga (1981), the increase in vertical bending moment is also induced by increasing of the vertical moment arm, inherited from the fact that the main hulls should be sufficiently deeply submerged, for the horizontal hydrodynamics forces acting on the struts and the demihulls. Further, wave loads might be even more critical when concerning the stress level that is created on the strut to cross deck transition (haunch area).

Another type of structural response which could possibly cause failure on the cross structure is the twisting moment resulting from the wave force in oblique seas. The situation would definitely worsen when a combination of the vertical bending and twisting moment is superimposed with the occurrence of other secondary loads, such as wave slap on the side structure and/or deck bottom slamming. It is well known that many designers have failed to attain an optimum design because they were ignorant of the necessity of applying more precise load information. Concerning the requirement of the accurate primary (wave) load prediction, firstly, validity on the hydrodynamic modellings should be regularly monitored. If necessary (and this apparently becomes more demanding lately), reliability techniques should also be included in the hydrodynamic aspects. Secondly, the modelling of environmental conditions and adequacy of environmental data should be carefully observed. It is obvious that an observation to at least identify the characteristics of wave load on SWATH is urgently required. Overall, there are six components of wave loads acting on the cross deck structure of a SWATH ship due to wave excitation, as follows :

a. vertical bending moment, i.e. the moment which tends to roll the hulls relative to each other
b. vertical shear force, i.e. the force which tends to heave the two hulls opposes each other
c. horizontal shear force, i.e. the force which tends to differentially translate the hulls athwartships
d. torsion moment, i.e. the moment which tends to pitch the hulls with respect to each other
e. yawing moment, i.e. the moment which tends to create differential yawing on the hulls, and
f. longitudinal force, i.e. the force which tends to surge the hulls differentially.

The first sections of this chapter review the works undertaken by a few research institutions to develop the prediction of wave load acting on SWATH ships. In approaching the solution, both analytical and experimental methods have been adopted. The development of an analytical model is necessary, in view of the flexibility it may then offer to accomplish a rational ship design procedure. An experimental approach is important chiefly to clarify the newly developed analytical model, especially in the

absence of full scale experience. The first and second parts of this chapter summarise these aspects.

In practice the aforementioned wave load prediction methods will be used to generate information necessary in the detailed design stage of SWATHs. In the interest of the load prediction at the concept design stage several rough estimation formulae on the maximum design load will be put forward. In the very early stage of design process, that is, at the feasibility study stage, for example, designers will be more interested to know the approximate value of maximum wave load. In this respect rough estimation of maximum wave load is usually associated with the displacement parameter of the vessel, as suggested by Betts (1988b) and Luedeke and Montague (1984). In the later date, following the SWATH loading data which became more available, an enhanced algorithm to estimate maximum wave load for SWATH has been developed by Sikora et al (1983). The derivation of simple algorithms of design loads useful for practical approximation in the preliminary SWATH design stage, based on the analytical and experimental results, will be discussed later.

Stirling et al (1988) aptly cited the phenomenon related to design load of SWATH vessels. It is stated that the prediction of wave induced loads is evolving and is not an exact science even for monohull where an extensive database of wave loads exist. The design loads must be sufficiently high to have a small probability of exceedance but must not be so high that the structure is uneconomic. This latter consideration is of most concern in SWATH ship design as the structural configuration of SWATH is inherent from the weight critical penalty. It is not surprising therefore if, in the field of SWATH structural design, effort is mainly directed to reducing structural weight, as reported in the papers, e.g. by Sikora (1988a) and Loscombe (1987, 1988).

In order to cope with the uncertainties in predicting the design loads, especially because of the random nature of ocean waves, a stochastic approach should be applied. The so called long- and short-term statistical analysis of wave spectra are used in deriving the likely extreme load responses which are to be considered in the fatigue and ultimate strength designs of SWATH ships. Further, the results from this rigorous analysis are compared with the value generated from simple algorithms to gain a perspective of the appropriateness of such simplified predictions.

3.2. ANALYTICAL METHODS ON WAVE LOAD PREDICTION

The use of analytical models in assessing wave load responses is very convenient in many ways. For instance, as is cited in the Introduction, in the final fabrication of a SWATH vessel parts of the main structure sometimes need to be slightly modified to meet the producibility requirement. Such a modification could affect the loading

performances which obviously have to be re-examined. Utilising an analytical model the procedure of re-examination can be done fairly quickly both in preparing the input data and running the computer program.

The work on the prediction of wave loads for SWATH ships was pioneered by Lee and Curphey (1977). In their prediction a method based on the two-dimensional strip theory, originally developed for catamaran vessels as presented by Curphey and Lee (1974), was adopted and modified to tackle the problem inherent in SWATH ship configuration. The vast development of digital computers in the 80s, as well as the extensive numerical solution of more complex mathematical problems, has since led to the establishment of various analytical approaches using the three-dimensional theory, e.g. as forwarded by Papanikolaou et al (1990). More advanced three-dimensional approaches incorporating the aspect of hydroelasticity on structural responses [Price et al (1985)] and another which accounting for the translating-pulsating sources [Chan (1990a)] have also evolved lately. The latter method is believed to be a powerful tool in dealing with structural response on a vessel underway with forward speeds whereas most of the existing theoretical predictions of forward speed effects are worked out semi-empirically.

The existing theoretical predictions of wave loads on SWATH vessels are mostly developed in conjunction with the prediction of motions, since these two problems are closely related as follows.

3.2.1. DTNSRDC

The study of wave load on SWATH type vessels, which is based on the analytical method developed for catamarans, was pioneered at the David Taylor Naval Ship Research and Development Center (DTNSRDC) [Lee and Curphey (1977), Lee et al (1973), Curphey and Lee (1974)] and has since been significantly evolved. In their method a two-dimensional strip theory is adopted to calculate the wave pressure distribution and the total wave load is derived by integrating the pressure along the submerged parts of the vessel.

The following theoretical approach describes those developed by Curphey and Lee (1974, 1977), i.e. the two-dimensional strip theory. To simplify the problem so that two-dimensional strip theory can be applied, some assumptions have been proposed and are briefly described as follows :

a. the hulls are assumed to be symmetrical about the vertical centre plane and possess longitudinal symmetry, therefore, only the sway, heave and roll modes of motions are excited by the incident beam waves
b. without pitching or yawing motion the three-dimensional loading problem has been simplified into loadings on an equivalent two-dimensional body
c. the ship is approximated by uniform twin cylinders having cross sectional shape equal to a representative section (usually midship section) of the ship analysed, and
d. the prediction is limited to the loads exerted in the transverse cross section plane. Thus, only the vertical bending moments, horizontal shear forces and vertical shear forces are considered.

Referring to the assumptions above and Fig. 1 various loading per unit length on the cross section of a SWATH ship requires the motion of the body and pressure distribution of the hull which can be expressed as :

-. horizontal shear force

$$V_2^{(0)} = -\frac{1}{2}\int_{R+L} pN_2(\pm y)dl \tag{3.1}$$

-. vertical shear force

$$V_3^{(0)} = \frac{1}{2}my_0\ddot{\zeta}_4 - \frac{1}{2}\int_{R+L} pN_3(\pm y)dl \tag{3.2}$$

-. vertical bending moment

$$M_3^{(0)} = \frac{1}{2}my_0\ddot{\zeta}_3 - \frac{1}{2}\int_{R+L} p\{N_3|y| + N_2(h_0 - z)(\pm y)\}dl \tag{3.3}$$

where $\int_{R+L} dl$ = integral over the submerged contour of the cross section on the right and the left demihulls at the mean position

p = the hydrodynamic pressure

m = mass of the cross section (per unit length)

N = (N_2, N_3) the unit normal vector pointing into the body

y_0 = the y-coordinate of the centre of gravity of the right half portion of the hull cross section

$+y$ = the y variable on the right half side

$-y$ = the y variable on the left half side

$\ddot{\zeta}_3$ = heave acceleration, and

$\ddot{\zeta}_4$ = roll angular acceleration.

The hydrodynamic pressure on any segment on the hull section can be determined by applying Bernoulli's equation for the time varying velocity potential, plus additional terms representing the change in the static pressure head as the hull experiences heave and roll motion :

$$p(y,z,t) = \frac{\partial}{\partial t}\bar{\phi}(y,z,t) - \rho g(\zeta_3 + y\zeta_4) \tag{3.4}$$

and the velocity potential is expressed as :

$$\bar{\phi}(y,z,t) = \phi(y,z)e^{-i\omega_0 t} = (\phi_I + \phi_D + \sum_{j=2}^{4}\phi_j\zeta_{j0})e^{-i\omega_0 t} \tag{3.5}$$

where ζ_{j0} = complex amplitude of ζ_j

ζ_j = ζ_2, ζ_3 and ζ_4 denote sway, heave and roll displacement, respectively

ϕ_I = complex velocity potential which represents incoming wave

ϕ_D = wave diffraction potential and represents scattering of incident wave by body, and

ϕ_j = fluid disturbance caused by oscillatory body motion in j^{th} mode.

It clearly suggests, from eqs. (3.1) to (3.5), that there are five components of wave load which must be first solved to proceed with the prediction of structural responses. These components are (a) body mass or inertia forces, e.g. the first term at the right hand side of eq. (3.3), (b) incident wave or Froude-Krylov force, (c) diffracted wave force, (d) hydrodynamic force due to body motions and (e) hydrostatic restoring force due to vertical displacement.

The analytical prediction by Lee and Curphey (1977) has been compared with a large number of experimental data and several full scale test results. From the correlation study it is found that the experimental data of SWATH dynamic loads confirms the basic validity of the developed analytical approach.

3.2.2. American Bureau of Shipping (ABS)

ABS has developed an analytical tool to compute wave loads on SWATH ships based on a method similar to the one applied at DTNSRDC, as reported by Reilly et al (1988), Shin et al (1988), and Reilly et al (1990). The analytical model was initially established to solve the problem of linear response of SWATH ships to wave excitation

in the five-degree of freedom only. The hydrodynamic coefficients and wave exciting forces on the twin hull are computed using the procedures of strip theory for slender ships and the resulting hydrodynamic forces due to wave and body motions are computed by applying the Frank close-fit source distribution method. The motion prediction has been enhanced by considering the hydrodynamic interaction effect between the two submerged hulls. The computer program was then modified to account for all six-degree of freedom ship motions and was further extended to compute the wave loads on the structure.

The way that ABS accounts for the motion effects in the computation of wave loads is slightly different from Lee and Curphey (1977). In the former not only sway, heave and roll are considered, but also pitch and yaw are dealt with. This procedure, therefore, allows calculation to be made on the five major type of wave loads at the cross structure, i.e vertical shear force, horizontal shear forces, prying (vertical bending) moment, yaw splitting moment, and pitch torsional moment. The prediction on vertical shear force, horizontal shear force, and prying moment given by the developed analytical model correlates well with experimental data of the SWATH model in beam and quarter seas. The two remaining loads, nevertheless, have not been validated by experimental data (at least in the published literature), and the explanation has not yet been released for this.

3.2.3. Mitsui Engineering & Shipbuilding (MES)

Again, similar to those three research organisations, MES developed the analytical prediction on wave loads in correlation with motion prediction using the strip theory. Oshima et al (1979) reported that the prediction has been well evaluated and correlation with test data from a small physical model and full scale SWATHs shows fairly good agreement. Even though, there has been no further detailed information in the open literature concerning the status of the analytical prediction of wave loads at MES despite the fact that most SWATH ships in operation nowadays were built by MES.

3.2.4. Hyundai Heavy Industries (HHI)

Hyundai Heavy Industries in co-operation with the Korean Institute of Machinery and Metals has developed a wave load prediction based on the SWATH motion program. Strip theory approach was adopted in this case as reported by Lee et al (1988). The correlation of theoretical prediction and experimental data on high-speed coastal ferries was found satisfactory. Hence a wider range of studies on SWATH wave load can be made by this analytical tool.

3.2.5. Brunel University

Research into wave loads on SWATH type vessels at Brunel University has adopted an almost completely different approach to those discussed in the foregoing sections. At Brunel the theoretical approach based on a general linear hydroelasticity theory has been used to analyse the structural response (ie. displacement, distortions, bending moments, shearing forces, torsional moments and stresses) of an idealised flexible SWATH travelling in regular waves [Price et al (1985), Bishop et al (1986), Price et al (1987), Keane et al (1988)].

The hydroelasticity theory, as described by Clayton and Bishop (1982), proposes that a marine vehicle seldom performs an absolutely steady motion since some other parasitic motions, such as structural distortion, will certainly occur following the external (wave) excitation. From this idea, in analysing a flexible SWATH it therefore requires the detailed information of the mass, damping and stiffness properties of the structure in the dry or in vacuo mode. So that the dry structural properties can be generated rapidly, especially when a three dimensional structure is to be analysed, it is preferable during the process to use a suitable finite element model. For this particular requirement an FEM package called PAFEC 75 is utilised by Price et al (1985) at Brunel. Having defined the SWATH dry structural properties, the dynamic characteristics of the structure in the absence of external forces can be determined.

For further analysis, i.e with respect to the assessment of SWATH structural responses under wave excitation, the above in vacuo properties are included in the calculation of steady motion. This process is called the wet analysis. For this purpose the generalised fluid loads experienced by the SWATH in waves are evaluated by adopting a three-dimensional singularity distribution panel method which considers the influence of forward speed. Later the analytical prediction was extensively improved by Price and Wu (1987) to account for the non-linear fluid forces effect, and extended to assess the response behaviour in time domain.

The analytical method developed at Brunel University is one of the most sophisticated and could be expected to produce fairly accurate wave load predictions. Price and Wu (1987) consider the only hindrance to using the hydroelasticity theory for SWATH structural response analysis is because considerable computational effort is needed in development of the program. Moreover, a skilful operator is required for data preparation and even to run the program

3.2.6. NTU Athens

The National Technical University, Athens (NTUA), in collaboration with Germanischer Lloyd, has in the past few years studied various aspects of SWATH design. One part of their study concentrates on the development of a mathematical tool to predict structural loads associated with SWATH motion assessment. Papanikolaou et al (1990) describe the prediction method of SWATH wave loads based on a 3-dimensional theory of ship motion. Schellin and Papanikolaou (1991) have further reported comparisons of analytical predictions and measured data.

3.2.7. NTH Trondheim

The development of a wave load prediction tool for twin-hull vessels at NTH, Norway, was presented by Faltinsen et al (1992). The numerical prediction which was initially evolved to cater for the primary load problem on high speed catamarans has been further enhanced by Faltinsen and Svensen (1992) to study the loading behaviour of SES. It is believed that the tool can be modified further to tackle the problem on SWATH primary loads. It was particularly mentioned that comparison has been made with the data presented by Kobayashi et al (1990), which is probably on SWATHs.

3.2.8. University of Glasgow

There are three different computer programs for predicting wave loads on SWATH vessels developed at the Department of Naval Architecture and Ocean Engineering, University of Glasgow. As is mentioned earlier in Chapter 2, all three programs are associated with the modelling of SWATH ship motions. The first prediction, which was based on the two-dimensional strip theory, computes the hydrodynamic loads on the beamwise strip of a SWATH's submerged body. For this purpose the SWATH ship is split into a number of equally distributed vertical load sections from aft to forward so that the number of stations should be specified by users. Further, the calculation of added mass, damping/inertia and wave exciting force is based on the two-dimensional Frank close-fit technique, as provided by Atlar (1986). The improvement of the designated SWATHL program with respect to the assessment of structural responses has been made by Drysdale (1987). SWATHL is not considered as a 'user friendly' program owing to the incomprehensiveness of the documentation during its development.

The second prediction was developed on the basis of the three-dimensional sink-source theory. This wave load modelling is contained in a program package called SHIPM written by Zheng (1988) and the package consists of two versions, namely,

SHIPM 1.0 and SHIPM 2.0 which is used to predict the motion and wave load responses for twin-hull and monohull vessels, respectively. A procedure to run these program is fully described by Zheng (1989).

One idea on the necessity of developing a three-dimensional wave load prediction is because the generic restrictions of most two-dimensional theory when it is applied in wave directions other than beam sea. It is clear in the strip theory, for instance, that the loading on the cross deck of a SWATH is calculated under the equivalent two-dimensional hull form assumption thus, only the beam sea case can be dealt with, whereas the pitch and yaw motion effect is neglected. The most prominent enhancement of the 3D method is the ability to solve the problem of torsional loads. From the standpoint of torsional loads twin hull ship configuration experienced the worst condition in quartering seas which, as is mentioned before, would be inaccurate to be predicted by 2D methods.

The most recent wave load prediction was augmented at the Department by Chan (1990a). A more versatile approach, namely, the pulsating translating source method, was adopted to accurately account, not only for the effect of three-dimensionality, but also the effect of advancing speeds. The underlying analytical solutions on SWATH global load responses is briefly described in the following.

The wave load responses on SWATH structure are basically calculated from the integration of several pressure components applied to the oscillating body. These components comprise the motion-induced radiation pressure, the quasi-hydrostatic pressure, the Froude-Krylov and diffraction pressures. These pressure components are derived from the velocity potential, as shown in eq. (3.5). In spite of only three motion components being taken into account in that equation, all the six-degree of motion amplitudes and radiation velocity potentials are now considered. In addition, the translating source is added, hence a general form of potential equation may be rewritten as :

$$\phi(\vec{x},t) = -Ux + \overline{\phi}(\vec{x}) + \tilde{\phi}(\vec{x};t) \tag{3.6}$$

where U is mean forward speed of the body, $\overline{\phi}(\vec{x})$ is the steady perturbation potential due to forward motion, and $\tilde{\phi}(\vec{x};t)$ is the first-order velocity potential of the unsteady wave system due to incident waves, diffraction and radiation waves given by :

$$\tilde{\phi}(\vec{x};t) = \left[\zeta_w(\phi_I + \phi_D) + \sum_{j=1}^{6} \zeta_j \phi_j\right] e^{-i\omega t} \tag{3.7}$$

Chan (1991) shows that using the perturbation analysis and Taylor series expansion, the fluid pressure p can be expressed by the mean wetted surface S_o in the form :

$$p(x;t) = \rho\left\{\tfrac{1}{2}(\vec{W}\bullet\vec{W} - U^2) + (gz + g\vec{\alpha}\bullet\vec{k}) + \tilde{\phi}_t + \vec{W}\bullet\nabla\tilde{\phi} + \tfrac{1}{2}\vec{\alpha}\bullet\nabla(\vec{W}\bullet\vec{W})\right\} \tag{3.8}$$

where the local displacement vector $\vec{\alpha}$ of a point $\vec{r}$ on the body surface S_w due to translational motion $\vec{\zeta}$ and rotational motion $\vec{\Omega}$ with respect to S_o can be expressed as :

$$\vec{\alpha} = \vec{\zeta} + \vec{\Omega}\times\vec{r} \tag{3.9}$$

The 'lateral' (the term is adopted to distinguish from the 'longitudinal' loads as applied to monohulls) loads on the centreline of the cross-structure of a SWATH ship are shown in Fig. 2. The defined V_1, V_2, V_3, M_4, M_5, and M_6 are, respectively, the longitudinal shear, side force, vertical shear force, prying moment, pitch torsional moment, and the yaw splitting moment. These load responses can be determined by considering the two portions of the body to be free on both sides of the cut through the centreline. Taking into account the quasi-hydrostatic and hydrodynamic pressures applied to the port and starboard sides of the body, F_{jP} and F_{jS}, the following load equations are derived :

$$V_1 = -\tfrac{1}{2}\left(M\bar{y}_G\ddot{\zeta}_6 + F_{1P} - F_{1S}\right) \tag{3.10}$$

$$V_2 = -\tfrac{1}{2}\left(F_{2P} - F_{2S}\right) \tag{3.11}$$

$$V_3 = -\tfrac{1}{2}M\bar{y}_G\ddot{\zeta}_4 - \tfrac{1}{2}\left(F_{3P} - F_{3S}\right) \tag{3.12}$$

$$M_4 = \tfrac{1}{2}M\bar{y}_G\ddot{\zeta}_3 + i_{45}\ddot{\zeta}_5 - \tfrac{1}{2}\left(F_{4P} - F_{4S}\right) \tag{3.13}$$

$$M_5 = i_{54}\ddot{\zeta}_4 + i_{56}\ddot{\zeta}_6 - \tfrac{1}{2}\left(F_{5P} - F_{5S}\right) \tag{3.14}$$

$$M_6 = -\tfrac{1}{2}M\bar{y}_G\ddot{\zeta}_1 + i_{65}\ddot{\zeta}_5 - \tfrac{1}{2}\left(F_{6P} - F_{6S}\right) \tag{3.15}$$

where M is the ship's mass; $\bar{y}_G$ is the transverse distance of the centre of gravity of one hull to the ship's centreline; $i_{45} = i_{54}$ the product moment of inertia of one hull about the longitudinal and vertical ship centrelines; $i_{56} = i_{65}$ the product moment of inertia of one hull about the vertical ship centreline and the neutral axis of the cross-deck. $\ddot{\zeta}_j$ is the acceleration of body motion with frequency of oscillation ω in j^{th} mode such that j = 1, 2, 3, 4, 5, 6 refer to surge, sway, heave, roll, pitch and yaw modes of motion,

respectively. The correlation of F_{jP} and F_{jS} in the foregoing equations is defined as follows :

$$F_{1P} - F_{1S} = \rho \iint \mathrm{sig}(y)\,(\tilde{\phi}_t - U\tilde{\phi}_x)\,n_1\,ds \tag{3.16}$$

$$F_{2P} - F_{2S} = \rho \iint \mathrm{sig}(y)\,(\tilde{\phi}_t - U\tilde{\phi}_x)\,n_2\,ds - \tfrac{1}{2}\rho \int \mathrm{sig}(y)dx\left(U^2 a_l \alpha_2(x) + \frac{8}{3\pi} C_D\, v_2(x)\|v_2(x)\| \right) dx \tag{3.17}$$

$$F_{3P} - F_{3S} = \rho \iint \mathrm{sig}(y)\,(\tilde{\phi}_t - U\tilde{\phi}_x)\,n_3\,ds - \rho g \zeta_4 \int \mathrm{sig}(y)\,y\,dA_w - \tfrac{1}{2}\rho \int \mathrm{sig}(y)\,B_m(x) \left(U^2 a_l \alpha_3(x) + \frac{8}{3\pi} C_D\, v_3(x)\|v_3(x)\| \right) dx \tag{3.18}$$

$$F_{4P} - F_{4S} = \rho \iint \mathrm{sig}(y)\,(\tilde{\phi}_t - U\tilde{\phi}_x)\,n_4 ds - \rho g \iint \mathrm{sig}(y)(y\zeta_3 - xy\zeta_5)dA_w + h_o(F_{2P} - F_{2S}) - \tfrac{1}{2}\rho \int \mathrm{sig}(y)d(x)d_2(x)\left(U^2 a_l \alpha_2(x) + \frac{8}{3\pi} C_D\, v_2(x)\|v_2(x)\| \right) dx - \tfrac{1}{2}\rho \int \mathrm{sig}(y)B_m(x)b(x)\left(U^2 a_l \alpha_3(x) + \frac{8}{3\pi} C_D\, v_3(x)\|v_3(x)\| \right) dx \tag{3.19}$$

$$F_{5P} - F_{5S} = \rho \iint \mathrm{sig}(y)\,(\tilde{\phi}_t - U\tilde{\phi}_x)\,(n_5 - h_o n_1)ds + \rho g \zeta_4 \int \mathrm{sig}(y)\,xy\,dA_w - \tfrac{1}{2}\rho \int \mathrm{sig}(y)\,xB_m(x) \left(U^2 a_l \alpha_3(x) + \frac{8}{3\pi} C_D\, v_3(x)\|v_3(x)\| \right) dx \tag{3.20}$$

$$F_{5P} - F_{5S} = \rho \iint \mathrm{sig}(y)\,(\tilde{\phi}_t - U\tilde{\phi}_x)\,n_6\,ds - \tfrac{1}{2}\rho \int \mathrm{sig}(y)\,x\,d(x) \left(U^2 a_l \alpha_2(x) + \frac{8}{3\pi} C_D\, v_2(x)\|v_2(x)\| \right) dx \tag{3.21}$$

where h_o is the vertical distance of the neutral axis of the cross section about the mean free surface; sig (y) sign function that sig (y)=0, 1 and -1, respectively if y=0, >0 and <0; a_l the lift coefficient; α_j angle of attack to uniform form in j^{th} direction; C_D drag coefficient of cross-flow; U advancing speed, and A_w waterplane area.

The numerical computation to the above load response formulations is accommodated in the MARCHS computer program run on the IBM/3090. Some of the essential procedures for running this program are clarified in Chapter 2, and for more detailed explanation refer to Chan (1990b)

3.3. EXPERIMENTAL APPROACH

Regardless of the convenience rendered from using analytical methods, one may realise that the initial work to develop the programs will be laborious and take a vast

amount of time. In most cases an analytical prediction is not yet available, since people tend to be rather reluctant to work deeply on a novel concept. For SWATH from its earliest days, experimental investigations were generally used. Thus, it is accepted that experiments on small scale models are primarily carried out to generate data which will be useful to anticipate the trends of a particular parameter or performance in such a new design. A summary follows on the experimental programmes that have been carried out by several research organisations to evaluate wave loads on SWATH ships.

The most extensive programme on the derivation of wave loads based on the experimental approach has been conducted by DTNSRDC, as indicated, by experimental data of several SWATH models in the papers by Kallio and Ricci (1976) and Lee and Curphey (1977). It is reported that at least ten SWATH models, consisting of a single and tandem strut per hull configuration, have been built and tested. Sikora et al (1983) suggest that those models represent several SWATHs designed for various missions, i.e. from a 3000 tonnes auxiliary ship up to a 100,000 tonnes aircraft carrier. The test results have been systematically documented and this is believed to be one of the most comprehensive wave load data bases existing at present. Undoubtedly the data base is kept updated from time to time with additional test data either accumulated in the Center or from exchange of technical information with other organisations, such as Mitsui.

Another research organisation which has also spent a substantial effort in the SWATH wave load model testing is the Canada-Netherlands SWATH Ship Project, i.e. a join research co-operation between DREA (Canada) and MARIN (the Netherlands). The test data of about ten SWATH designs has been accumulated and analysed to obtain an estimation of design load for a single strut SWATH configuration. This estimation, which was then included in a computer aided SWATH design suite named SWACEM (SWATH Concept Exploration Model) by Nethercote and Schmitke (1982) and Koops and Nethercote (1988), is believed to be reliable in not producing a conservative design side load. Nevertheless, the information on this applied side load algorithm remains unrevealed for the wider community to evaluate.

Pattison et al (1988) mention that the experimental programme on the load measurements at the Admiralty Research Establishment (ARE) at Haslar has only been started early in 1988. The first test was conducted on a model of the SWATH Surveillance Vessel (SSV) designed under assistance from the MoD. The three metre long SSV model is of a single strut configuration with the contoured elliptical section hulls. The measured results have been compared with analytical predictions from ARE, Dunfermline. Stirling et al (1988) indicate a slight discrepancy found in the correlation study and claim to have been caused by only a minor factor which can easily be refined.

MES is one of the most competent sources of information when dealing with measured data on SWATH wave loads. This is recognised as many models have been tested within this company prior to the building of several of the earliest SWATH ships. As suggested by Oshima et al 1979) and Mabuchi et al (1985), it has become a common procedure at MES to conduct a model test even on the initial design stage. The databank has ever since been enriched with the prototype and full scale measurements.

The NA&OE Department at the University of Glasgow commenced its experimental oriented programme to study wave loads on SWATH ships in 1986. The first model which was tested by Djatmiko (1987) at the Hydrodynamics Laboratory is a tandem strut SWATH configuration designated as SWATH-1. In the initial stage, experimental techniques similar to those used in the measurement of wave loads on semi-submersibles by Incecik (1982), was adopted for SWATH-1 model testing. Observation was conducted on the measurement of vertical bending moment at mid point of the cross deck, as well as on the side and vertical shear forces on the strut when the model restrained in beam and bow quartering seas. The side load was not measured due to the difficulty in the instrumentation arrangement. Following SWATH-1 two other models of single strut per hull configuration, that is, SWATH-3 (modification of SWATH1) and the Fishing SWATH (SWATH-FV) models, have been subjected to wave load tests.

3.3.1. Procedures of Wave Load Tests Carried Out at UoG

Similar to the analytical model, experimental work on wave loads was carried out in conjunction with the motion test, and the seakeeping technique of model test was adopted in this case. As shown in Fig. 2.4 of the seakeeping test arrangement, a SWATH model was equipped with load measurement devices. These comprise the bending gauges mounted at the centre of the two aluminium cross bars for measuring the bending moment supposedly at the centreline of the cross-structure. The vertical shear force on the model was measured by the combination of four sets of strain gauges attached to the vertical aluminium bars. The set up of these strain gauges was made in such a way that only the intended load responses were measured. Detailed strain gauges set up can be found in several references, e.g. Dally and Riley (1978).

From various investigations it was found that the vertical force applied to SWATH models is very much lower than the side force experienced. During the earlier test on SWATH-1 model it was observed that the dominance of side force was proven. It was found that those gauges on the vertical bars recorded the side force signals rather than the intended vertical force. It was decided to replace the strain gauges with load cells when the test was conducted on the SWATH-FV model. The use of load cells was

believed to be more reliable in measuring the correct vertical force signals. Due to the fact that vertical force signals were substantially low, a proper amplifier was also used to provide a more readable record.

The loading test on each model was carried out in regular waves at frequencies ranging from 0.3 Hz up to 1.6 Hz. As suggested by Lee and Curphey (1977), the maximum transverse bending and side load responses on SWATHs are expected to occur at wave frequencies which correspond to wave-length/centre hull separation ratio (λ/B_o) around 3.0 and 4.0. But it very much depends on the configuration of the model. Some SWATH models may experience peak bending at lower values of λ/B_o. Several additional tests were made at around the peak frequencies to generate a smoother data. The peak value of vertical force commonly occurs at around the roll resonant frequency, thus a smaller frequency increment was carried out. The calibration procedures and test data analysis are similar to that for motion tests, as explained in Chapter 2.

The presentations of structural loadings on SWATH are in the form of non-dimensional loads (forces or moments) against wave-length/characteristic beam ratio, as above. The axial forces are non-dimensionalised as :

$$V_i' = \frac{V_i L}{g \Delta \zeta_w} \tag{3.22}$$

and the moment responses as :

$$M_j' = \frac{M_j}{g \Delta \zeta_w} \tag{3.23}$$

where V_i = force responses at i^{th} mode (N)
i = 1, 2, 3 for, respectively, longitudinal shear, side force and vertical shear
M_j = moment responses at j^{th} mode (Nm)
j = 4, 5, 6 for prying, pitch torsional, and yaw splitting moments, respectively
L = characteristic length of the model (m)
Δ = displacement of the model (kgs), and
g = acceleration due to gravity.(= 9.81 m/s^2).

From the wave frequency generated in the experiment, the wave-length in metres can be calculated as follows :

$$\lambda = \frac{g}{2\pi f} \tag{3.24}$$

where f is frequency in Hz.

3.3.2. Comparison of Experimental and Theoretical Predictions on SWATH Primary Loads

Although the usefulness of experimental data is important when the analytical approach is not yet available, nevertheless, the essence of carrying out model tests would not diminish afterwards. With respect to a newly developed analytical prediction the next procedure commonly to be accomplished is calibration on the predicted results. The calibration is primarily intended to evaluate the validity of the analytical approach. Moreover, as quoted by Bhattacharyya (1980), it has been proven in many cases that the improvement of theoretical methods has been made by referring to an extensive experimental data. It is noteworthy that a model test is often conducted, even after a final design on a vessel is concluded, due to certain requirements by the designers, classification societies, and sometimes shipyards.

Comparisons of the theoretical predictions using MARCHS with the measured data is presented in Figs. 3.3 to 3.7. The correlation of side forces on the SWATH-3 model measured in beam and bow quartering seas (Fig. 3.3) is satisfactory. The prediction shows that the non-dimensional peak value in quartering seas is about one half (10.0) of that in beam seas (20.0). Similarly, the correlation of vertical shear forces on SWATH-FV, as in Fig. 3.4, is excellent. The peak value of vertical shear forces of around 1.5 and 1.0 (non-dimensional) for beam and bow-quartering sea cases, respectively, are found to occur at the λ/B_0 region of around 11.5. Converting this λ/B_0 value we find the corresponding incoming wave frequency of some 3.0 rad/sec. This frequency is approximately at the roll resonant peak, thus it is clear that the vertical shear force is closely related to roll motion of the model, as shown also in eq. (3.12) and Fig. 2.24. Comparing the side and vertical shear responses it is clear that the former is much more dominant, i.e. some 15 times larger than the latter. It is not surprising, therefore, if the sensitivity of the measuring instrument for vertical force is poor than the side force would possibly distort the recorded signals, as mentioned in the earlier section.

The correlation of measured and predicted prying moments at the cross-deck of SWATH-1, SWATH-3 and SWATH-FV models is subsequently presented in Figs. 3.5, 3.6 and 3.7. Generally the correlation of these data is fairly good. A slight discrepancy is found only on the SWATH-3 model, that is, for the peak value in bow-

quartering seas. Explanation has not been found for this, but it is suspected that the instrument did not function very well during the test. An interesting account, when comparing the peak responses in beam and quartering seas of SWATH-1 model, is shown in Fig. 3.5. In beam seas the peak is found at λ/B_0 of about 2.5, whereas in bow quartering seas this is identified at 1.2, i.e. one half of the former one. This phenomenon was explained by Zheng (1988) as occurring because of the dominance of the second standing waves at the space between the port and starboard side struts. The second peaks are also detected on the other models, although not as high as on SWATH-1.

As noted from those Figures, the shape of the prying moment curve resembles that for the side force. This suggests that the prying moment is mainly contributed to the side force times an equivalent arm from the cross structure. The effect of vertical force to the prying moment is fairly mild, as shown also in those Figures at higher λ/B_0 ranges. Lee and Curphey (1977) suggest that normal SWATHs usually have the peak prying moment magnitudes of around 2.0 and 3.0. Figures 3.8 and 3.9 are presented to further illustrate the effects of different headings to the magnitude of side forces. As shown, the response is largest in beam seas. The prediction and measured prying moments in head seas on SWATH-FV was also augmented, and can be found in Appendix B together with the rest of the wave load data.

As described in Section 3.2.8, other load responses which can be predicted by the current analytical model include the longitudinal shear force, pitch torsional moment and yaw splitting moment. Nevertheless, at present no measured data on such responses is available for comparison. The theoretically derived load response on these modes, however, is demonstrated in Fig. 3.10. In bow-quartering seas the peak longitudinal shear is approximately as high as the vertical shear, although these remain in the lower order compared to the side force. In this wave condition, the yaw splitting moment is apparently found to be greatest among other moment responses. If this is correct, then the designer must be aware of this occurrence, especially when the in-phase combination with the prying moment should arise. Apart from these types of loads, another aspect that has not been able to be compared is the forward speed effects on SWATH structural response. Again this is due primarily to the scarcity of such data.

The capability of the present theory to deal with the forward speeds is as shown in Fig. 3.11. The forward speed apparently does not have a significant effect to the side force in beam seas, but it does have in bow-quartering seas. Even though, Kobayashi and Shimada (1990) suggest that the side force in beam waves should decrease with the increasing of speeds. The vertical shear in beam seas, on the other hand, is predicted by the present model to attenuate as the speed becomes higher.

Regardless of the limited data available, the correlation presented above demonstrates the basic validity of the developed theoretical model. In addition, the MARCHS program prediction has also been compared with experimental data for a 3000-tonne SWATH made available at ABS by Reilly et al (1988,1990). The correlation of the two predictions is very good, as reported by Chan et al (1992).

3.4. DETERMINATION OF SWATH WAVE LOADS AT THE PRELIMINARY DESIGN STAGE

The ship designer is in favour of simple empirical formulae being available and while there is a need to roughly estimate the wave load at the early design stage. Such a simple formulae for conventional ships, based on principal dimensions and form coefficients, is widely found in the Classification Society Rules. On the subject of deriving an empirical formulae, a sufficiently large number of load data, which can be either from the wave load theory or from past experience, should be made available. This procedure has been adopted by Sikora et al (1983) in producing a simple algorithm to estimate the single maximum lifetime amplitude side force on SWATH ships at the DTNSRDC.

In all, wave load data of some thirteen models and full scale SWATHs have been collected and included in the analysis. Further, a parametric study of wave loads on a notional 3000 tonne SWATH was undertaken using the theoretical prediction described by Lee and Curphey (1977). Six basic parameters, namely, the hull and strut lengths, hull separation, draught, metacentric height, waterplane area and displacement, were considered in the study. The first four parameters were varied ± 20% one at a time, and the others were kept constant. Later it was found that there is a systematic effect in varying the length, draught and hull separation variables. There is no such substantial effect of the metacentric height variation upon the side load. Combining the wave load data from measurement and parametric study, Sikora et al (1983) then derived a maximum lifetime side force algorithm as a function of the non-dimensional draught parameter (T), displacement parameter (D) and length parameter (L). The formulation is given in the following equation :

$$\frac{F_{max}}{\Delta} = TDL \tag{3.25}$$

where $T = 0.5319\, t$

$t = 3.271 \times d / \nabla^{1/3}$

$D = 1.55 - 0.75 \tanh(\Delta / 11000)$

$L = 0.725 + 2.989 \tanh(L_e / 24)$

$$L_e = LS + \tfrac{1}{2}(LH - LS)\frac{HD}{t}\left(1 - \frac{0.1\,G}{HD}\right)$$

$$LH = 3.271 \times L_h / \nabla^{1/3}$$

$$LS = 3.271 \times L_s / \nabla^{1/3}$$

$$HD = 3.271 \times d_h / \nabla^{1/3}$$

$$G = 3.271 \times g_s / \nabla^{1/3}$$

Δ = displacement
∇ = volume displacement
d = draught of the ship
L_e = effective length
L_h = length of the lower hull (ft)
L_s = length of struts at the design waterline (ft)
d_h = lower hull diameter (ft)
g_s = length of gap between tandem struts (ft)

Re-evaluation of the algorithm has been made to correlate with measured data of the thirteen models scaled at 3000, 10000 and 100000 tonnes. Average standard deviation of 11% was acquired and this demonstrates fairly good agreement when considering the natural scatter of experimental data from different models, towing basins and data acquisition systems. Chalmers (1989) considers that this algorithm is appropriate in the concept design after the principal dimensions have been determined. ABS (1990) has recently adopted the above algorithm in its 'Preliminary SWATH Rules'. Besides the side load, ABS (1990) also provides simplified empirical formulations to determine the transverse bending moment, longitudinal bending moment, vertical shear force and wave impact to be applied in the design.

Sikora and Dinsenbacher (1990) has further adjusted the above length parameter to a much simpler form as :

$$L = 0.75 + 0.35 \tanh(0.5L_s - 6.0) \qquad (3.26)$$

There is no clear explanation as to what consideration has been ratified to impose this adjustment.

In some cases, at the feasibility study, a SWATH designer should be able to guess the design load when only the displacement of the vessel is known. In this respect Betts (1988b) of UCL provides a rough estimate of side load based on the regression analysis of the published data, that is :

$$F = K \times \Delta^{0.77} \tag{3.27}$$

where K=7.94 for single struts and 4.26 for tandem struts.

In the very early development of the SWATH concept Aronne et al (1974) estimated a design side load of between 0.4 and 0.6 would be adequate for SWATH ship displacements ranging from 3000 up to 22000 tonnes. The study conducted by Luedeke et al (1984,1985) at RMI Ltd. during the design of the *Halcyon*, a 60 tonne SWATH demonstrator, has estimated the maximum side force on a vessel of this size to be about 0.95 to 1.0 times the vessel's gross weight. Inducing a safety factor of 20% the final side load of 1.2 times the gross weight was selected in the structural design. Observation of a 3000 tonne SWATH by Sikora et al (1983) using a fatigue load spectrum combined with the algorithm in eq.(3.25) yields a maximum life time side load of around 0.94 times the ship displacement.

Other information regarding the design side load for SWATHs is provided by Kerr et al (1978). A study was conducted on several SWATHs of 4000 tonnes in displacement from Froude scaled up test data. The examination of these data showed that the dominant sea induced load increased with wave height in lower sea states and approached maximum in higher operational seas, as shown in Fig. 3.12. The steady side force in higher sea state, as seen from this Figure, ranges between 0.5 up to 1.1 times the ship displacement. A similar presentation is given by Allen and Holcomb (1982), as shown in Fig. 3.13. This later side load information is intended for small SWATHs, probably 200-tonne or less. Loscombe (1987) has compiled a large number of side force data from various sources. The side force, non-dimensionalised by the projected side area, is presented against the wave frequency. Upper bound curve was drawn for the data. Design side load is calculated using this default by applying the two-parameter spectra with nine family members. Although the data was collected by Loscombe (1987) for small SWATHs of less than 500-tonne, it is appropriate also for larger ships.

Other loads that can be derived from the primary side force are torsional load and vertical shear force. Chalmers (1989) quoted from unpublished US sources that the torque on the hull can be given as :

$$M_5 = 0.13\, F_{max}\, L_s \tag{3.28}$$

which is suggested to be worst for seas between 15° and 45° off beam. The shear force which is most critical on the box structure is estimated by :

$$V_3 = 0.25\, F_{max} + 1.25\, g\, M_{b/2} \tag{3.29}$$

where g is acceleration due to gravity, and $M_{b/2}$ is half of the box mass.

In addition to those empirical formulations, Miller (1991) suggests another method to predict the design load for SWATH. This approach adopts the hydrodynamic coefficients as those commonly applied in designing semi-submersible offshore vessels. The comparison of the design load generated by this method has been made for the *Victorious* (T-AGOS 19) and the *Patria*, which show good correlation with other methods.

3.5. ASSESSMENT OF THE LONG-TERM PRIMARY LOAD FOR SWATH SHIPS

As stated in the Introduction, rational structural design should be based on comprehensive knowledge of two design criteria, firstly, the vessel is subjected to extreme load and, secondly, the vessel is subjected to cyclic load. The former is dealt with in the structure ultimate strength analysis, whereas the latter is associated with fatigue performance of the structure. This section presents the development of the lifetime primary load assessment to be associated with the analysis of fatigue lives for SWATH structures. The subject is approached by first of all defining the so called operational mode and thereafter a long-term prediction method based on the sea spectral analysis is adopted. A computer program to aid the whole computational procedures was written. The corresponding results in the form of graphs are given with particular examples on notional 2500 tonne SWATHs operating in the North Atlantic.

3.5.1. The Determination of Cyclic Lifetime Load

As has been briefly mentioned, one of the most important factors in the interest of achieving an optimum structural design is the capability of the designer to identify the fatigue performance of the vessels. This is of particular concern in SWATH design, which is regarded as a weight critical structure. Faulkner (1981) has stressed that even in the case of monohulls the argument remains strong that taking advantage of weight saving would in principle largely affect the degradation of the fatigue performance of the primary structure rather than, say, on its ultimate strength efficiency. The matter could be worse when it is associated with SWATHs where primary wave load is mostly exerted against the main structural components, which are generally much slender in size than monohulls. These structural components, for instance, at the strut and cross deck intersection, will undoubtly suffer an unconventionally high stress concentration which is in itself vulnerable to fatigue failure. It is clear, therefore, that to

produce an appreciable weight saving a SWATH designer should be able to compromise between optimising the size of the structure and maintaining a sufficient level of fatigue resistance on the structure.

To deal with the problem of fatigue on SWATH structures one should first conceive to the phenomenon in which fatigue is initiated. Fatigue on a structural component is a dynamic phenomenon which is brought about by a large number of repetition on the applied loads. The repetition (cyclic action) of the external load will in turn create a stress fluctuation on the structure which up to a certain level could generate a fatigue damage in the form of a microscopic crack, usually located at the concentrated stress. On marine structures the main source of cyclic load comes from the environmental waves. It is obviously impossible to entirely eliminate the cyclic load excitation on marine structures due to the natural oscillating behaviour of ocean waves. The only way to prevent the structure from fatigue damage is by minimising the cyclic wave loads. Hence, it is of importance first of all to explore how the cyclic wave load excitation is developed.

Ocean waves on which a marine structure operates are characterised by the random fluctuation of the water surface. Accordingly, the resulting wave excitation on the structure will also behave randomly. In such a case the solution can be made statistically by applying a probabilistic approach, as forwarded by Newland (1986). As shown by Sikora and Dinsenbacher (1988, 1990), the predicted load response amplitude operator (RAO) which is derived by the assumption of regular waves needs to be converted into an irregular measure by using a spectral analysis (see Fig. 3.14). Further, the load distribution (histogram) is established by selecting an appropriate probability density function in accordance with the wave spectral formulation. In this extent a histogram contains information on the number of cycles of every single load interval pertinent to a prescribed operational mode. This general procedure, known as the design sea load method, is most widely applied in assessing the design values of the wave induced load on marine structures. In the following section a step by step procedure of generating the lifetime cyclic load, with a particular case on SWATHs, will be thoroughly explained.

3.5.1.1. Wave Load Responses. With regard to the case study presented in this section, wave load data extracted from the tests carried out on small SWATH models is adopted, e.g. transverse bending moment responses in Figs. 3.5 to 3.7. Applying the Froude scaling law the corresponding wave load responses on a full scale notional 2500 tonne SWATH-FV, for instance, is derived, as shown in Fig. 3.15. This latter data is an example which will be used throughout this study. The main particulars of the three 2500 tonne SWATHs is given in Table 2.4 of Chapter 2.

3.5.1.2. Operational Modes. As designers know load responses on the structural parts of a vessel underway in waves will be governed by speed, the heading relative to the waves, and the height of encountering waves. Further, as the random nature of the wave scatter then the spectrum of any particular wave (fully developed, fetch limited or others) will also have an effect on the load magnitude. A combination of these four conditions which have a direct influence on the response magnitude is defined as the operational mode. Sikora et al (1983) clarify the definition of this operational mode, as is seen in Fig. 3.16. The Figure shows that the whole operational condition of a vessel can explained as a box consisting a large number of smaller cubes which relate to a particular set of wave height, heading and speed. For instance, a particular set comprises the range of speed between 10 and 15 knots, heading between -15^{0} and $+15^{0}$ and wave height between 3 and 4 metres. In addition, this particular set should be related to a certain spectral condition. Furthermore, in actual designs where the ship is to be operated in different sea regions, any particular sea area is to be defined as an individual operating block. Such account has been exemplified by Faulkner (1981) on a tanker operating between North America and the Far East.

The whole lifetime response of a structure is then compiled by adding up every single operational mode, from the lowest order to the highest one, by accounting for its probability of occurrence. The probability of operating in a particular mode is given by multiplying the probability occurrence of each component of the operational mode. An example of probability occurrence of wave heights in the North Sea is given by Ochi (1978), see Table 2.5. Owing to the limited information on SWATHs in operation it is assumed that all headings are equally probable, whereas the speed probability for SWATHs can be approximated from the data of monohull ships, as proposed by Sikora et al (1983) and listed in Table 3.1. The probability occurrence of wave spectra will be given in the next section, together with an explanation on the selection of spectral formulation.

A recent development in offshore technology has pointed out that another parameter needs to be introduced to define the operational mode. This parameter is termed by Faulkner (1991a) as the joint probability occurrence of wave, wind and current. The necessity to include this parameter is obvious for offshore structures as in stationary position the combined effects of those three environmental loadings will be significant. For oceangoing vessels, on the other hand, the two latter load components might not be significant, especially when considering that the ship operators have more freedom to change the vessel's course when a severe sea condition is encountered. Only in special cases, such as a SWATH research vessel (low motion characteristic of SWATH makes it attractive for research vessel purposes) which spends most of its operation in station keeping, then the joint probability should be seriously considered.

3.5.1.3. Selection of Sea Spectra. In designing marine vessels the selection of a proper sea spectrum is as important as determining the highest wave height to be expected in the lifetime of the vessels. Various spectral formulations which cover almost any sea condition are available for designers to use. These spectral formulations have been observed by Ochi and Bales (1977). As a conclusion the responses (consisting of motions and wave loads) which were computed for the same significant wave height appear to be scattering quite substantially. It is therefore clear, as cited by Faulkner (1991b), if a SWATH design is to be an efficient structure, it must not be over-designed. Then the right scenario of sea environment in which the vessel is to be operated should be extensively evaluated. This is of particular concern since there are several spectral formulations derived for a similar sea condition. However, the adopted wave data could vary depending on the sea region where the waves were measured. As a result, the parameters applied in those formulations would differ quite significantly and, accordingly, the responses obtained.

For the present study, the 2500 tonne SWATHs are assumed to operate in the North Atlantic region. The spectra which best explains the sea conditions at this region is the one developed by Ochi and Wang (1976), designated as the six-parameter wave spectra. The formulation of this spectra is as written below :

$$S_6(\omega) = \frac{1}{4} \sum_j \frac{\left(\frac{4\lambda_j + 1}{4} \omega_{mj}\right)^{\lambda_j}}{\Gamma(\lambda_j)} \times \frac{H_{sj}^2}{\omega^{4\lambda_j + 1}} \times e^{\left\{ -\frac{(4\lambda_j+1)/4}{(\omega_{mj}/\omega)^4} \right\}} \qquad (3.30)$$

where H_s is the significant wave height, ω_m is the modal frequency, λ is the shape parameter and j=1,2 represent the lower and higher frequency components, respectively. The latter two components are applied with respect to the contribution of the underlying swell and the locally generated waves in composing a spectrum.

Combination of the two components and the other three parameters result in six governing parameters to a single spectrum. Moreover, another aspect of sea conditions was considered in developing the six-parameter spectra. From observations at many wave stations in the North Atlantic it was experienced that the shape of spectra varies considerably even though the significant wave heights are the same. Eventually the difference in the spectrum shape brought about the divergence of the wind duration, growth and decay-stage of storm and existence of swell. In order to cover a variety of stages of the sea a series of wave spectra was introduced. There are 11 variations of spectra corresponding to any single significant wave height where one of those spectra acquires 50% probability of occurrence (most probable) and the rest possesses 5% probability each. One set of this spectra corresponding to one particular wave height is

described as the family spectra. The values of the six parameters for the family consisting of 11 members are presented as functions of significant wave height H_S and are given in Table 3.2.

A computer program (SIXPAR) was written to of compute the sea spectra as well as other calculations to generate lifetime load described within this section. Figure 3.17 shows a sample plot of the family spectra resulting from the program for significant wave height H_S=3.0 metres. The solid line curve indicates the most probable spectrum and the others are those with 95% confidence. From any single spectrum curve can be clearly traced the two distinct peaks at lower and higher frequency zones as expected which represent the effect of swell and locally generated wave.

The next step of the procedure in determining the lifetime load of a vessel is to generate the response spectra. As shown in Fig. 3.14, the response spectra is calculated by multiplying the load RAO (eg. square of the response values in Fig. 3.15) and the wave spectra. Since there are 17 increments of significant wave heights (see Table 2.5) to be evaluated, 187 response spectra corresponding to a single set of heading angle and forward speed will be generated. A sample plot of the response spectra correlating with a significant wave height H_S=3.0 metres is presented in Fig. 3.18. These figures explain even better the effect of different sea spectra on the resulting responses. From Fig. 3.17 it can be seen that the leftmost curve is one of the spectra with largest peaks. However, the corresponding response spectrum (in Fig. 3.18) shows a lower curve (containing less energy).

Hence, it can be said that the wave is expected to amplify the response when the two peaks of wave spectrum and RAO closely coincide in a given encounter frequency. Therefore, thorough experience in selecting the most suitable spectral formulation for such a case is absolutely necessary. Otherwise arbitrary selection of spectral might lead to an over-estimation of the wave load predicted which in turn could lead to a high redundancy of the structure. On the other hand under-estimating the maximum load will increase the risk of the structure inherent to the increase in high probability of failure.

3.5.1.4. Lifetime Load Distribution. Having obtained the response spectra of any operational mode embodied in the analysis, a further stage to determine the number of load cycles experienced by the ship can then be performed. The following equation defines the average number of responses per unit time (n) using the information given from the response spectrum :

$$n = \frac{1}{2\pi}\sqrt{\frac{m_0}{m_2}} \tag{3.31}$$

where m_0 is the area under response spectrum and m_2 is the second moment of response spectrum. The total number of responses to be experienced by the ship during its lifetime is calculated by summing up all responses and weighted by the probabilities at any single operational mode as :

$$N = \left(\sum_i \sum_j \sum_k \sum_l n \times p_i p_j p_k p_l \right) \times T \qquad (3.32)$$

where T = lifetime at sea (secs)
p_i = ship heading probability
p_i = ship speed probability
p_i = wave height probability
p_i = wave spectral probability

Previous evaluation of the three SWATH vessels, as presented in Chapter 2, indicates that the vessels' operability in the North Atlantic could reach between 82% ~ 89% of all year. The evaluation of the vessel's operability was checked against the seakeeping criteria of naval vessels from Olson (1978). Considering this information the lifetime operation of the 2500 tonne SWATH is assumed to be 20 years based on 270 days per year at sea ($T=4.665 \times 10^8$ secs).

In order to develop the lifetime load histogram, i.e. the final step as shown in Fig. 3.14, a suitable probability distribution pertinent to the applied wave spectra should then be selected. Milgram (1976) suggests that the probability density distribution of the wave height, and hence the load response, is commonly regarded to follow the Rayleigh probability law. The assumption of adopting the Rayleigh distribution is valid as the random sea can be considered as a steady state Gaussian (normal) process, the wave spectrum is narrow banded and the response to waves satisfy the principle condition of linearity. The Rayleigh probability density function of response magnitude corresponding to a given response spectrum can be written as :

$$p(x) = \frac{x}{m_0} e^{-x^2/2m_0} \qquad (3.33)$$

where x is response magnitude and m_0 is the varians of the response time history and equal to the area under the response spectrum. An example of the probability distribution function of the load response is shown in Fig. 3.19. This response probability curve, which corresponds to the significant wave height H_s=3.0 metres, presents the summing up of the contributions from all variations in the response family spectra that were weighed by their probability of occurrences.

The load histogram which correlates to any particular response spectrum is obtained by applying the actual number of response cycles for this operational mode onto the corresponding probability distribution function. In turn, the lifetime load histogram is obtained by adding up all the components of load histogram from each sub-block in the operational mode.

3.5.2. Description of the Result on Long-Term Analysis

Figure 3.20a presents the lifetime load histogram for a 20 year SWATH operation in the North Atlantic resulting from the present analysis. Since the number of cyclic responses for higher load magnitude is not readable another histogram with a logarithmic y-axis is then provided, as shown in Fig. 3.20b. The histogram is divided in the bin interval of 10 MNm. From the computation the total number of cycles to be experienced by the vessel in its lifetime will be in excess of 8.0×10^7. Munse et al (1982) suggest that for fatigue design the number of wave cycles costumarily is taken as about 10^8 for a 20 year lifetime of a ship.

From the evaluation of the results it is found that the bending moment magnitude to be expected to occur once in a lifetime is 490 MNm, 385 MNm, and 365 MNm for SWATH-1, SWATH-3, and SWATH-FV, respectively. The largest number of load cycles however is observed between the zero load magnitude up to 100 MNm. In this range the portion of load cycle are in excess of 90% of the total number of cycles to be experienced in 20 years. SWATH-3 experiences the largest load cycle in this range, that is, some 95~96% of the total. At this stage the criteria to define the significance of the lifetime load with respect to the number of cycles is rather vague. Nevertheless, it is obvious that the contribution of the response load in the lower side is extremely important for consideration in fatigue design. More on this aspect will be presented in Chapter 6.

To be compatible with most of the existing structural fatigue data the load histogram needs to be transformed into the load exceedance curve. Using a cumulative distribution process values of any given response being equalled or exceeded can be obtained. Figure 3.21 depicts the load exceedance for the SWATH-3 derived from the corresponding load histogram. In this Figure is also shown the component of load cycles computed for head, beam, bow-quartering, and following seas, and the total exceedance added up from these components. It is interesting also to observe the difference between the number of load cycles derived by accounting for various sea headings and by only considering the beam sea, as presented in Fig. 3.22. As is seen,

the difference of the load exceedances at the upper and lower tails is not significant. Even so, along the middle part an appreciably large difference is observed. The number of exceedance in beam sea for a given load response gradually increases from 2 up to 4 times larger than the all heading weighted. This fact implies that cyclic load for fatigue design would not be correct if solely determined from the beam sea load response. In other words, such consideration will be misleading for fatigue design. However, this would not be the case when the derivation of extreme response for ultimate design is concerned, as will be seen in the next section.

3.6. SHORT-TERM ANALYSIS OF SWATH STRUCTURAL RESPONSE TO ENVIRONMENTAL LOADS

This section presents an evaluation on the structural responses of SWATHs subjected to environmental loadings based on the short-term stochastic waves. The prediction methodology to be applied throughout the analysis is adopted from Ochi and Hubble (1976). The importance of such an analysis is obvious in the interest of generating approximate extreme loads useful for ultimate strength design analysis of such vessels. Computational procedures are outlined, and an example is given on the analysis of a hypothetical SWATH vessel. Comparison of the predicted extreme loads is made against the values derived from the long-term response assessment.

Needless to say, the extreme value for design has to be determined by taking into account all sea severities, all varieties of wave spectral shapes, speeds (in the case of a ship), headings to waves, and so on, expected in the ship's lifetime weighted by the frequency of occurrence of each factor. This gives the impression that the extreme value should be evaluated only through the long-term prediction approach. However, as is shown later, the results of computations to evaluate extreme values through both short- and long-term prediction clearly indicate that the short-term prediction in severe seas is much to be desired for estimation of extreme values. The estimation procedure, as well as the accuracy of the computation for the short-term, appears to be much superior to that for the long term prediction. This subject is discussed in detail in connection with the application of wave statistics for the long-term prediction to design.

In using the six-parameter family spectra for the short-term response prediction for each sea severity, one of the family members yields the largest response, while another yields the smallest response with confidence level of 0.95. Hence, by connecting the points obtained in each sea severity, the upper and lower bound responses can be established.

3.6.1. Factors Affecting the Extreme Value of Responses

For estimating the extreme values of the responses, various factors such as operation (or exposure) time, risk parameter, frequency of encounter with seas, and speed, all of which affect the magnitude of the extreme values, have to be considered for each sea severity. A more detailed discussion on each of these subjects is given in the following.

3.6.1.1. Operation Time. The extreme values of responses are a function of the number of encounters with waves, and hence the persistence of each sea state has to be considered in the estimation. This implies that for a ship the estimation of extreme responses is made assuming that the ship maintains a certain speed in a given sea as long as the sea condition is unchanged.

Figure 3.23 taken from a paper by Ochi and Motter (1974) shows the longest persistence every 1.52 m interval of significant wave height estimated from analysis of data given by Moskowitz et al (1965). For example, significant wave heights between 6 m and 7.5 m can be expected to persist for a maximum of 40 hours. For seas of significant wave height of 4 m or less, a 45 hour (h) duration is used by extending the curve in the Figure. It is noted that the extreme values increase significantly during the first several hours and thereafter increase very slowly with time. Hence the extension of the curve given would not cause any significant error in predicting the extreme values for mild sea states.

3.6.1.2. Risk Parameter. Estimation of extreme response such as wave-induced bending moment, etc., for design consideration is made using the concept of a risk parameter as proposed by Ochi (1973). The risk parameter, denoted by α, represents the probability that the extreme response in a given sea will exceed the estimated design load. This implies that if α is chosen as 0.01, then the response of one ship in 100 sister ships operating in the same environment may exceed the estimated extreme value.

It is noted that the ship may encounter seas of the same severity k-times in her lifetime. Thus, for each sea state it is necessary to divide the risk parameter α by k for evaluating the design response so that the value which is unlikely to exceed with $(1-\alpha)$ percent assurance can be estimated for all sea states. Although the value of a risk parameter can be chosen at the designer's discretion, the results of computations made on various types of marine vehicles have indicated that $\alpha = 0.01$ appear to be appropriate in practice.

3.6.1.3. Frequency of Encounter with Seas. As mentioned in the discussion on risk parameter, information concerning the frequency of encounter for a marine system with each sea severity in her lifetime is necessary in order to evaluate the design extreme response. For this, information on the frequency of occurrence of each sea state is necessary. Since the frequency of occurrence differs depending on the geographical location, information on the frequency in the service area(s) of the SWATH should be considered. A method to obtain the frequency of occurrence of various sea severities, including the estimation of the severest sea condition can be found in a paper by Ochi (1978).

3.6.1.4. Ship Speed in a Seaway. For evaluating the extreme SWATH responses in a seaway, the speed in each sea severity has to be estimated since the number of encounters with waves depends on ship speed. Two different types of speed reduction in a seaway should be considered, i.e. one due to added resistance and reduced propulsive efficiency associated with waves and ship motions, and the other due to voluntary slowdown by the ship's master by virtue of severe ship motions. The methods to evaluate the former speed reduction are well addressed, e.g. by Maruo (1957), Joosen (1966), Geritsma and Beukelman (1972), Strom-Tejsen et al (1973), while the method to estimate the latter is presented in the paper by Ochi and Motter (1974). For a quick evaluation of ship speed loss in a seaway at the design stage, a formula given by Aertssen (1969, 1975) derived from full-scale trials is recommended.

3.6.2. Extreme Value of Responses

To estimate the maximum response of a structure operated in a given seaway the stochastic theory of extreme values is adopted.

By taking into consideration these various factors which affect the magnitude of extreme responses, the probable and the design extreme values for a sea of specified severity can be evaluated by the following formula :

Probable extreme value (amplitude) :

$$\bar{y}_n = \sqrt{2 \ln \left\{ \frac{(60)^2 T}{2\pi} \sqrt{\frac{m_2}{m_0}} \right\}} \sqrt{m_0} \qquad (3.34)$$

Design extreme value (amplitude) :

$$\hat{y}_n(\alpha) = \sqrt{2 \ln \left\{ \frac{(60)^2 T}{2\pi(\alpha / k)} \sqrt{\frac{m_2}{m_0}} \right\}} \sqrt{m_0} \qquad (3.35)$$

where : T = longest duration of specified sea in hours
α = risk parameter, and
k = number of encounters with a specified sea in ships' lifetime.

Using the probabilistic theorem and order mathematics, it is found that the probability of occurrence of the most probable load response determined by eq. (3.34) is 63.2% (i.e. $1\text{-}e^{-1}$). Ochi (1973) noted that the extreme values given in eqs. (3.34) and (3.35) include the effect of the bandwidth of the response spectrum on extreme values.

In the present study, analysis of SWATH structural responses using the short-term prediction method has been accomplished by using the SIXPAR computer code which was enhanced to incorporate the above formulation. The computational results of the extreme responses and the comparison against the maximum value generated by the long-term assessment is given in the following.

3.6.3. Comparison of SWATH Structural Responses by the Short- and Long-Term Analysis

The primary advantage of short-term prediction is the minimum of computation required, since the calculation can be made straight forward into the evaluation of the most vulnerable condition associated to a given vessel. In the case of SWATH, for instance, such a condition is expected to occur when the vessel is encountering beam waves at zero speed. In contrast, the computational process in the long-term prediction could be lengthy, because the evaluation must account for any condition of heading angle, as discussed in Section 3.5

The computational results of the structural responses on hypothetical 2500-tonne SWATHs (scaled up from the model) are as shown in Figs. 3.24a-f. Figures 3.24a-c show, respectively, the significant, the most probable extreme, and the extreme values of transverse bending moments associated with the most probable spectrum of the six-parameter family. Whereas Figs. 3.24d-f show the items which are associated to the particular spectrum which gives the largest response. In addition, Figs. 3.25a and 3.25b are presented to illustrate the range of the most probable and extreme response values, respectively, from all the members of the six-parameter spectra family. As is seen, for each value of significant wave height, H_s, there are 11 variations of response

values, which are essentially incorporated into the spectral family defined by Ochi and Hubble (1976). The 11-variation comprises one value, the most probable spectrum (with a 50% level of confidence), and other 10 spectra having a probability of occurrence of 5%.

On the most probable extreme transverse bending responses the most probable spectrum (for H_s=17 m) as shown in Fig. 3.24b gives approximately 400 MNm, 310 MNm and 290 MNm respectively for SWATH-1, SWATH-3, and SWATH-FV. Whereas the maximum spectrum shown in Fig. 3.24e gives, for the corresponding sequence, 490 MNm, 375 MNm and 360 MNm. The most probable spectrum (50% confidence) yields the extreme values of transverse moments for those SWATHs of 510 MNm, 395 MNm, and 380 MNm, respectively, as shown in Fig. 3.24c. Still for the same sequential, the maximum spectrum as shown in Fig. 3.24f gives the extreme values of 630 MNm, 495 MNm and 470 MNm for SWATH-1, SWATH-3 and SWATH-FV. These latter values are supposedly to be the design loads for these SWATHs. The above values are all calculated by considering a 3.3 hour storm duration at H_s=17 m. If the storm duration should increase by about twice (6.5 hour), the response value might increase on average of some 2~3 %, which is appreciably small.

In Section 3.5 the computation by long-term approach has been demonstrated in obtaining the load response value to be experienced by the SWATHs in 20 years operation. To compare the extreme response, as derived from short-term approach, an additional analysis should be made on the long-term. This is basically similar with the short-term analysis to determine the extreme value, that is, by adopting the risk parameter. Ochi (1978) has shown the approximate method by which the extreme responses can be evaluated from a large number of data n, i.e. as computed in Section 3.5. Suppose that the cumulative distribution function can be expressed asymptotically in the following form :

$$F(x) = 1 - e^{-q(x)} \tag{3.36}$$

On the other hand, the probability density function of the extreme value in n-observations, denoted by $g(y_n)$, is given by :

$$g(y_n) = n\left[f(x)(F(x))^{n-1} \right]_{x=y_n} \tag{3.37}$$

Thus, the probable extreme value, denoted by $\bar{y}_n$, is obtained by letting the derivative of $g(y_n)$ with respect to y_n be zero. It can be derived with the aid of eq. (3.36) that the probable extreme value for large n satisfies the condition below :

$$e^{q(\bar{y}_n)} = n \tag{3.38}$$

Hence, from eqs. (3.36) and (3.38) it gives the probability of exceeding x in n-observations as :

$$1 - F(\bar{y}_n) = \frac{1}{n} \tag{3.39}$$

By selecting a certain risk parameter α , the extreme value for design consideration, $\hat{y}_n$, can be obtained from :

$$1 - F(\hat{y}_n) = \frac{\alpha}{n} \tag{3.40}$$

Application of the above approach in design may be explained by referring to Figs. 3.26a and 3.26b. In these Figures, the response magnitudes are plotted against the logarithmic value of the load reversals. This load reversal can be determined in a frequent time interval, i.e. hours, days, months or years. Then the logarithmic value of the load reversal and the response magnitude exceeded once in each observation is plotted. The extreme value for design is derived by extending the plotted data up to a given logarithmic value corresponding to the n/α observations. The difference between Fig. 3.26a and b is on the curve fit for extending the observed data. In the former the data is extended by the linear curve fit, whilst the latter is extended by the third order polynomial fit. Both conditions of all heading and beam sea dominated operations are again considered.

Using the third order polynomial fit, the extreme values are found to be 420 MNm and 440 MNm for, respectively, the all heading weighed and the beam sea dominated. Whereas, for linear fit these values are some 459 MNm and 489 MNm. The extreme value for SWATH-FV from the short-term analysis was obtained previously as 470 MNm, which is closer to 459 MNm. The extreme value for SWATH-3 has also been computed by the long-term approach, which is found to be about 485 MNm for all heading with linear fit. This figure is also close to 495 MNm as derived from short-term analysis. Thus both short and long-term analysis would provide a close approximation on the design value. The preference for short-term analysis is obvious owing to the simplicity of the computation.

3.7. COMPARISON OF DESIGN VALUES FROM RIGOROUS ANALYSIS WITH SIMPLIFIED APPROACHES

For comparison purposes the design side loads for three SWATHs have been calculated by adopting several simplified formulations, as described in Section 3.4.

Other computations using the short- and long-term probability approaches have also been made. All the results are listed in Table 3.3. The various results derived from rigorous analysis are given, namely, the lifetime, most probable, and the extreme values. In addition, for the short-term analysis, variations are made to account for the most frequent spectrum, maximum spectrum, and the mean values derived by considering the all member of spectrum.

From the simplified approach it may be explained as follows. The ABS formulation, which adopts the earlier algorithm by Sikora et al (1983), yields design loads of about 19150 kN, 27795 kN, and 19759 kN for SWATH-1, SWATH-3, and SWATH-FV, respectively. It should be noted that SWATH-1 is a tandem strut vessel, whereas the others are of single strut configuration. The new algorithm by Sikora et al (1990) gives these values of 16548 kN, 28994 kN and 17946 kN, in which only the side load for SWATH-3 is higher than the former algorithm. UCL's formulation derives 17278 kN for SWATH-1, and 32204 kN for both SWATH-3 and SWATH-FV (as expected for both vessels the values are the same as the algorithm in terms of displacement and a single coefficient for single strut SWATHs). The RMI and Aronne (1974) estimate the design values for the three SWATHs, respectively, 29430 kN and 14715 kN.

Regarding the design value for SWATH-1, the short- and long-term analysis yields some 30837 kN and 28500 kN, which are closest to RMI's estimate. SWATH-3 and SWATH-FV, however, are predicted to have design values in excess of 40000 kN, which is extremely high. This is a matter for concern because the rigorous evaluation has been carried out by considering the operation of the vessel in a maximum significant wave height of 17 metres. Lloyd (1989) regards such significant wave height, which is correlated to sea state 9, as a phenomenal wave. Allowing those three SWATHs to operate in a milder environment, such as that for the 2500-tonne Yarrow's SSV design by Smith et al (1987), then sea state 6 can be considered. This is apparently also suggested from the operability analysis in Chapter 2.The design side loads with a 99% confidence for SWATH-1, SWATH-3 and SWATH-FV in this sea state by the short-term analysis are 18945 kN, 32532 kN and 27771 kN, respectively. The difference of the design loads from Sikora et al (1983) are, respectively, in the order of -1.0%, +17%, and +40%. Whereas with the values from UCL are +9%, +1%, and -13%, respectively.

It remains uncertain as to which value ought to be selected when considering ship operation in sea state 9 (H_s=17 m). The extreme design values derived from rigorous analysis are substantially high for this case. Nevertheless, in a lower sea state, which is more reasonable for the operation of those notional SWATHs, the generated design values are in favour of those derived empirically.

3.8. DISCUSSION

The development of wave load predictions for SWATH type vessels by some research organisations has been reviewed. Hydroelasticity theory seems to be the most sophisticated method in loading analysis, as this considers the flexibility behaviour of SWATH structure. Even though the development of such computation tools is extremely complex. A reasonably accurate estimation could be attained by most of the two-dimensional strip theory. Enhancement by adopting the three-dimensional theory is mainly intended when dealing with the structural responses in oblique seas, in addition to coping with the problem of longitudinal shear, pitch torsional moment, and yaw splitting moment responses on SWATH structure. A three-dimensional method based on the translating pulsating source recently developed in the NA&OE Department to tackle SWATH wave load problems has been addressed. Various algorithms to obtain a rough estimation of maximum wave load useful in the preliminary design stage has also been clarified.

Experimental investigations on SWATH wave loadings have been carried out by many institutions worldwide covering an ample geometry of SWATH models, e.g. as reported by Kallio and Ricci (1976), Oshima et al (1979), and Pattison et al (1988). Some may say that experimental work to a certain extent is rather expensive, but the following reasons might not justify this claim. If a model test is sufficiently well arranged then it will be possible to measure various performance parameters simultaneously in effect will be less costly and save a considerable amount of time. Further, versatile data acquisition softwares, not to mention a large number of comprehensive electronic instrumentations, are now widely available to be used by experimenters to ease their work. The experimental process, including analysis, becomes faster and less laborious with the use of very powerful computers. Furthermore, the data accumulated is much more reliable. It is not too exaggerated to conclude, therefore, that experimental methods still play an important role in various aspects of future development in SWATH technology.

SWATH model testing to generate wave load data is highly recommended to validate the developed analytical model as well as to give an assurance as part of the final design process. This has been exercised in the present study where experimental data has been extensively used in calibrating the newly developed analytical model. The accumulated data has proved to be useful to identify the pattern of SWATH structural response, even though it is still considered insufficient to be implemented in the derivation of design load algorithm. The programme continues with emphasis on observation in different sea headings and possibly at forward speeds, with some more SWATH models, including the one with rectangular hull configuration which is available at the Laboratory. Technical problems concerning the measurement of side

loads appears to have been solved and a new arrangement will be used in future model tests.

A better understanding on the random sea phenomenon has led to an improvement in the prediction design load. Long-term and short-term statistical methods are now widely accepted in most design. Rational design process can now be accomplished with an improved code of safety. A study on the assessment of lifetime primary load for SWATHs has been presented within this chapter. A computer program was especially written to carry out lifetime load analysis. Examples of computational results with the main aim to generate information on cyclic load distribution was made for the case of hypothetical 2500 tonne SWATHs operating in the North Atlantic.

From the analysis, the largest portion of cyclic response, reaching 90% of the total in 20 year life of the 2500 tonne SWATHs, is found to be at the load interval of zero up to 100 MNm. Considering this type of load distribution it implies that, contrary to the ultimate strength, fatigue life of SWATHs will be governed primarily by the contributions of wave load with the lower magnitude since the occurrence of these loads happen to be much more frequent than the larger wave loads. The once in life exceeded values of the response calculated by the long-term prediction are approximately 490 MNm, 385 MNm and 365 MNm for, respectively SWATH-1, SWATH-3, and SWATH-FV.

A procedure for predicting SWATH structural responses based on the short-term stochastic wave is outlined in this Chapter. Computational results, in the form of extreme load values, generated from the enhanced program were then presented. Comparison is further made between the predicted responses analysed by the short- and long-term methods. The two approaches seem to correlate with each other very well. A sequel analysis was also made on the design side load by both methods to be compared with the values derived by simplified formulations.

The present study has not looked into the possibility of magnification due to the superposition of primary loads. This phenomenon is likely to occur when a SWATH is operated especially in oblique waves where certain phase differences between prying moment and torsional moments may amplify the structural response magnitude. In addition, the superposition with secondary load contributor ought to be observed. For instance, the possibility of slamming occurrence which coincides with the maximum combined primary loads have to be sufficiently understood. Lewis and Zubaly (1981) and Mansour (1981) address such superposition procedures, which may be adopted for SWATHs in future. Further, no single reference reported herein has ever mentioned the implication of maneouvring in waves towards the possibility of increasing side force. Even so, Lang and Higdon (1974) consider that the high speed turn in itself could be

one of the primary sources of side load and a safety factor of 2.0 is suggested by Meyerhoff et al (1988) for the structural design to cover this eventuality.

In addition to the above, the present analysis approach needs to be enhanced to allow for spatial energy spreading to be taken into account. Faulkner e al (1989) have shown that analysis on offshore platforms by considering this effect could be expected to give rise to appreciable attenuation of extreme loads and especially to fatigue loading from more moderate seas. Lewis and Zubaly (1981) stated that most Classification Societies also recognise the significance of this energy spreading, hence load analysis on newly designed monohulls is now required to incorporate such an aspect. This certainly is an important area that needs to be pursued in future SWATH studies.

3.9. CONCLUSIONS

The basic aspects of dynamic loads acting on SWATH structure have been thoroughly studied. A review has been made to the latest development in SWATH loading research by various institutions worldwide. This is followed by a description of a newly developed analytical model for SWATH wave load assessment in which forward speed is explicitly included. Some existing simplified design load formulations were put forward, and these show considerable scatter.

A procedure for generating wave load data by a seakeeping experimental technique on SWATH models was fully described. Devices and instrumentation set up specifically applied to measure structural responses were identified. Measuring the bending moment and side force will be adequate when using strain gauges, because the relatively large electronic signals imposed by these loads on the model, and hence on the gauges. High sensitivity instrument such as load cells, however, are needed when low signals are to be accurately registered. Vertical force induced signals are among those which are generally low in magnitude. Thus, when strain gauges are used to measure vertical shear force it is then likely that the registered signals will be that induced by the side force, which is more dominant in nature.

The measured data from three SWATH models, comprising side force, vertical force and prying moment on the bridging structure of the models, are further compared with predictions from analytical model. Very good correlation between the two is observed, hence, validation of the developed analytical model is basically attained. Further validation requires measured data of other load responses, namely, longitudinal shear, pitch torsional and yaw splitting moment. In addition, experimental data of load response for SWATH with advancing speeds should also be pursued.

Evaluation of design loads for SWATHs was conducted by applying the short- and long-term stochastic wave approaches. The generated design values from the two approaches were found to be in good agreement. For instance, the transverse moment with 99% confidence for SWATH-FV of 459 MNm was obtained from the long-term analysis compared to 470 MNm from the short term analysis. When only beam sea heading is considered in the long-term analysis then a value of 495 MNm is derived, which is some 4% larger than that predicted by the short-term analysis.

Comparison of design side loads by rigorous analysis was also compared with those values predicted by simple algorithms. The former generally overpredict the design load by as much as 50%, and sometimes even larger. These large values were derived by imposing a design significant wave height of 17 metres (corresponds to a sea state 9), which is cited by Lloyd (1989) as 'hypothetical' in its occurrence. A reasonable agreement is obtained, however, by restricting the evaluated SWATHs to operate in sea state 6.

Table 3.1. SWATH speed probabilities [Sikora et al (1983)]

	Displacement (Δ): ≤ 10,000 ton			> 10,000 ton		
Wave Height (m):	0 - 5	6 - 10	> 10	0 - 5	6 - 10	> 10
Ship Speed (kts)						
0 - 10	0.25	0.10	0.60	0.05	0.05	0.40
10 - 20	0.60	0.80	0.40	0.65	0.85	0.60
> 20	0.15	0.10	0.00	0.30	0.10	0.00

Table 3.2. Values of six parameter spectra as function of significant wave height, H_s (m) [Ochi (19780]

	H_{s1}	H_{s2}	ω_{m1}	ω_{m2}	λ_1	λ_2
Most Probable Spectrum	$0.84H_s$	$0.54H_s$	$0.70e^{-0.046H_s}$	$1.15e^{-0.039H_s}$	3.00	$1.54e^{-0.062H_s}$
	$0.95H_s$	$0.31H_s$	$0.70e^{-0.046H_s}$	$1.50e^{-0.046H_s}$	1.35	$2.48e^{-0.102H_s}$
	$0.65H_s$	$0.76H_s$	$0.61e^{-0.039H_s}$	$0.94e^{-0.036H_s}$	4.95	$2.48e^{-0.102H_s}$
	$0.84H_s$	$0.54H_s$	$0.93e^{-0.056H_s}$	$1.50e^{-0.046H_s}$	3.00	$2.77e^{-0.112H_s}$
	$0.84H_s$	$0.54H_s$	$0.41e^{-0.016H_s}$	$0.88e^{-0.026H_s}$	2.55	$1.82e^{-0.089H_s}$
0.95 Confidence	$0.90H_s$	$0.44H_s$	$0.81e^{-0.052H_s}$	$1.60e^{-0.033H_s}$	1.80	$2.95e^{-0.105H_s}$
Spectra	$0.77H_s$	$0.64H_s$	$0.54e^{-0.039H_s}$	0.61	4.50	$1.95e^{-0.082H_s}$
	$0.73H_s$	$0.68H_s$	$0.70e^{-0.046H_s}$	$0.99e^{-0.039H_s}$	6.40	$1.78e^{-0.069H_s}$
	$0.92H_s$	$0.39H_s$	$0.70e^{-0.046H_s}$	$1.37e^{-0.039H_s}$	0.70	$1.78e^{-0.069H_s}$
	$0.84H_s$	$0.54H_s$	$0.74e^{-0.052H_s}$	$1.30e^{-0.039H_s}$	2.65	$3.90e^{-0.085H_s}$
	$0.84H_s$	$0.54H_s$	$0.62e^{-0.039H_s}$	$1.03e^{-0.030H_s}$	2.60	$0.53e^{-0.069H_s}$

Table 3.3. Design side loads (in kN) by various methods

	SWATH : Δ = 2500 tonnes		
	SWATH-1	SWATH-3	SWATH-FV
MPEV-ST (50% conf. spectrum)	19451.0	31539.0	27947.0
MPEV-ST (Max. spectrum)	24252.0	39217.0	34734.0
MPEV-ST (Mean)	19942.0	32019.0	28436.0
EV-ST (50% conf. spectrum)	24745.0	40203.0	35587.0
EV-ST (Max. spectrum)	30837.0	49985.0	44222.0
EV-ST (Mean)	25357.0	40808.0	36202.0
Lifetime-LT	23000.0	36600.0	33000.0
EV-LT	28500.0	46250.0	41650.0
UCL	17278.0	32204.0	32204.0
ABS (Sikora et al 1983)	19150.0	27795.0	19759.0
Sikora 1990	16548.0	28994.0	17946.0
RMI (1.2Δ)	29430.0	29430.0	29430.0
Aronne (0.6Δ)	14715.0	14715.0	14715.0

Notes :
MPEV : Most probable extreme value (63.2% probability of occurrence)
EV : Extreme value (1% probability of occurrence)
Lifetime : Exceeded once in lifetime of the structure (20 years)
ST : Short-term analysis
LT : Long-term analysis
The mean extreme values have a COV of averagely 16%~17%

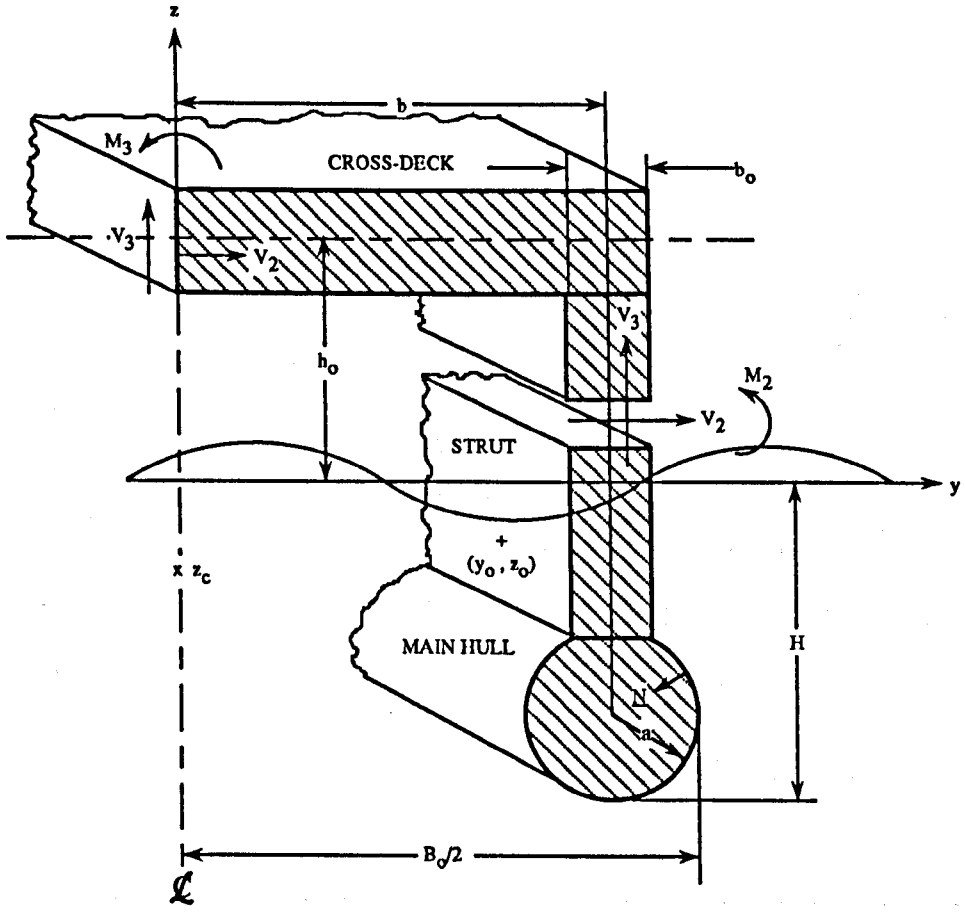

Figure 3.1. Definition sketch of SWATH cross-section
[Lee & Curphey (1977)]

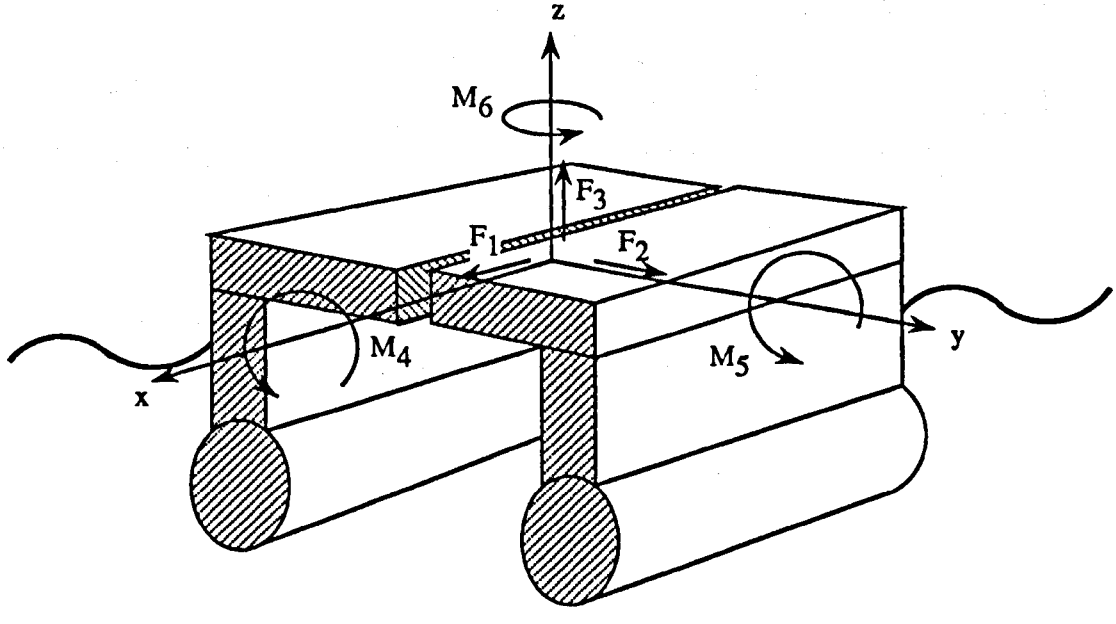

Figure 3.2. Definition of global wave loads [Chan (1991)]

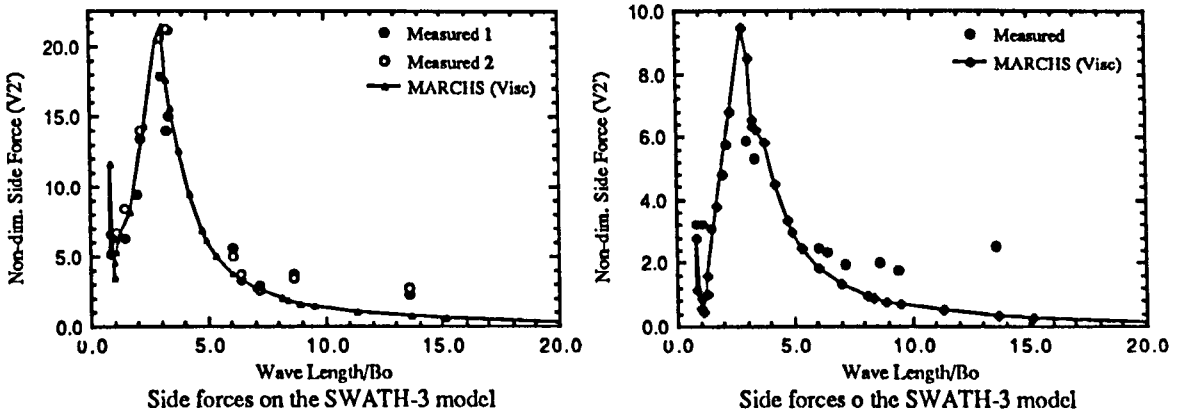

Side forces on the SWATH-3 model in beam seas (Fn=0.00)

Side forces o the SWATH-3 model in quartering seas (Fn=0.00)

Figure 3.3. Side forces (V2) on SWATH-3 model in beam and bow-quartering seas

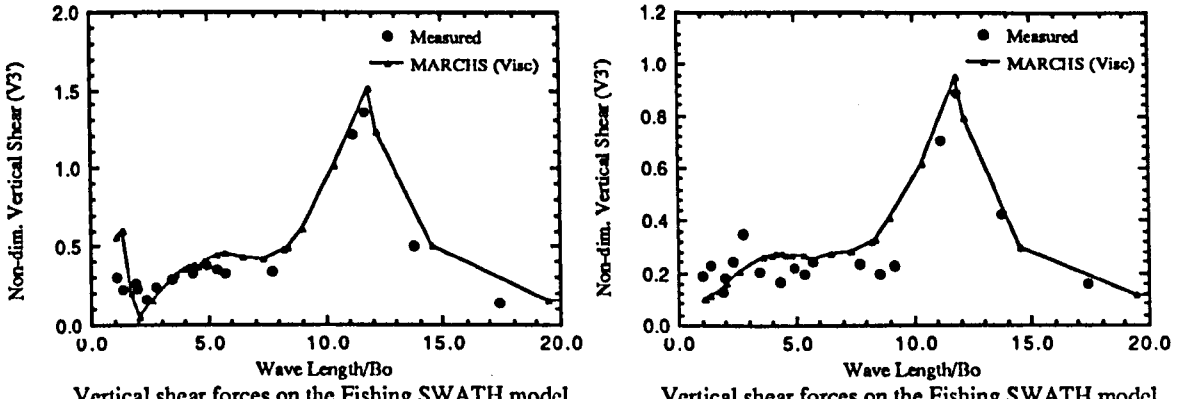

Vertical shear forces on the Fishing SWATH model in beam seas (Fn=0.00)

Vertical shear forces on the Fishing SWATH model in quartering seas (Fn=0.00)

Figure 3.4. Vertical shear forces (V3) on SWATH-FV model in beam and bow-quartering seas

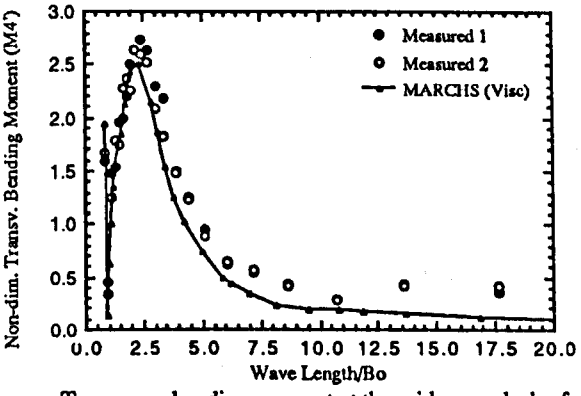

Transverse bending moment at the mid cross-deck of the SWATH-1 model in beam seas (Fn=0.00)

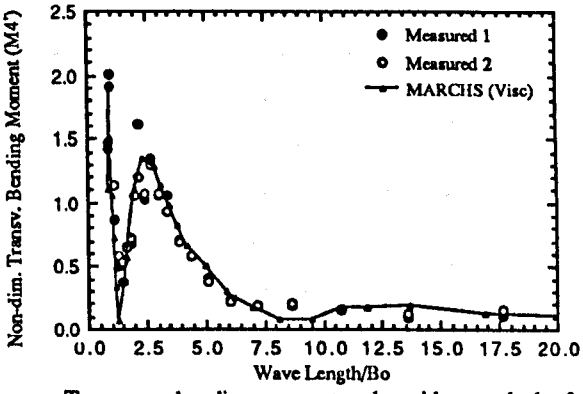

Transverse bending moment at the mid cross-deck of the SWATH-1 model in quartering seas (Fn=0.00)

Figure 3.5. Transverse bending moments (M4) on SWATH-1 model in beam and bow-quartering seas

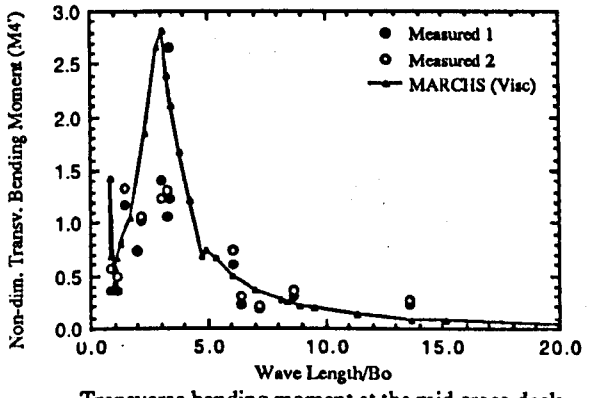

Transverse bending moment at the mid cross-deck of the SWATH-3 model in beam seas (Fn=0.00)

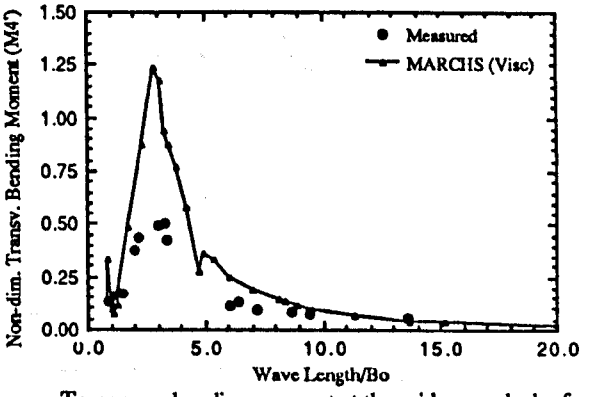

Transverse bending moment at the mid cross-deck of the SWATH-3 model in quartering seas (Fn=0.00)

Figure 3.6. Transverse bending moments (M4) on SWATH-3 model in beam and bow-quartering seas

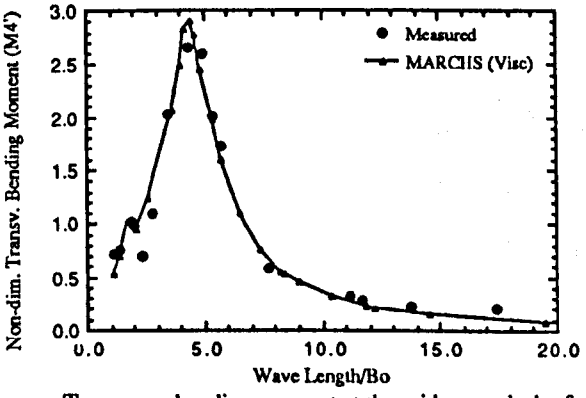

Transverse bending moment at the mid cross-deck of the Fishing SWATH model in beam seas (Fn=0.00)

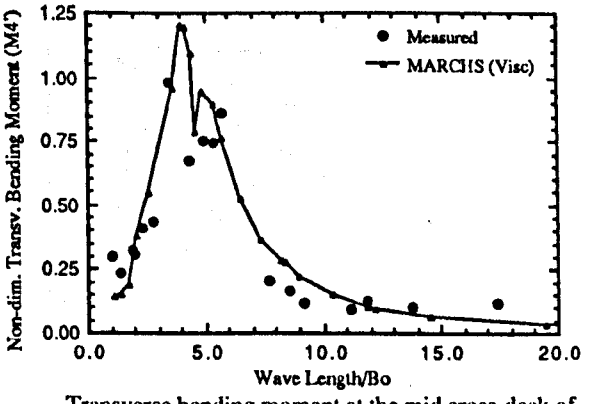

Transverse bending moment at the mid cross-deck of the fishing SWATH model in quartering seas (Fn=0.00)

Figure 3.7. Transverse bending moments (M4) on SWATH-FV model in beam and bow-quartering seas

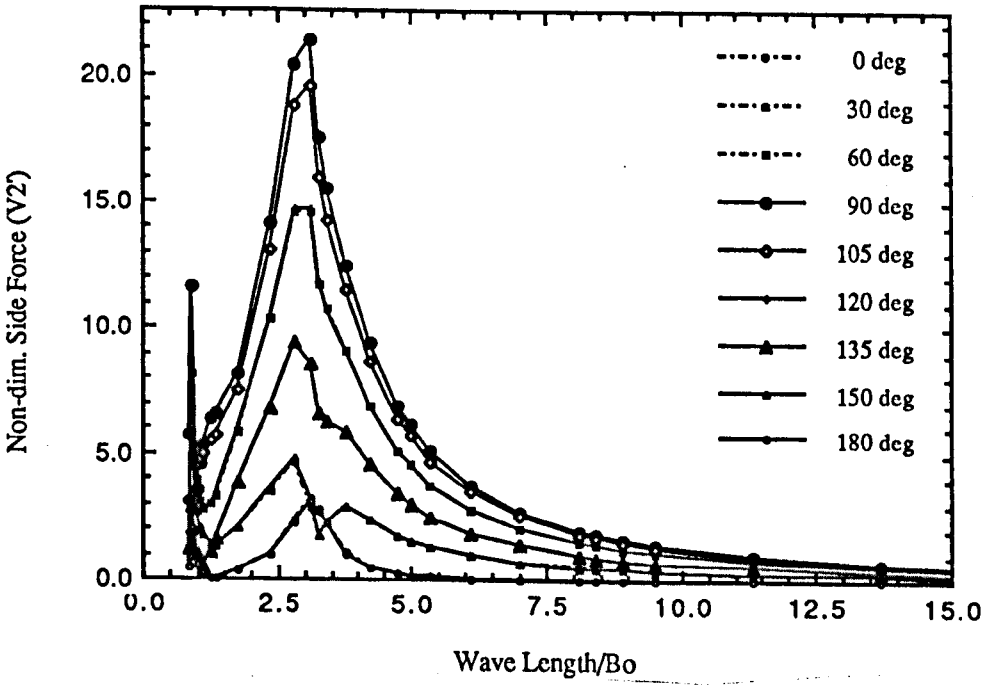

Figure 3.8. Side forces (V2) on SWATH-3 model in various wave headings (Fn=0.00)

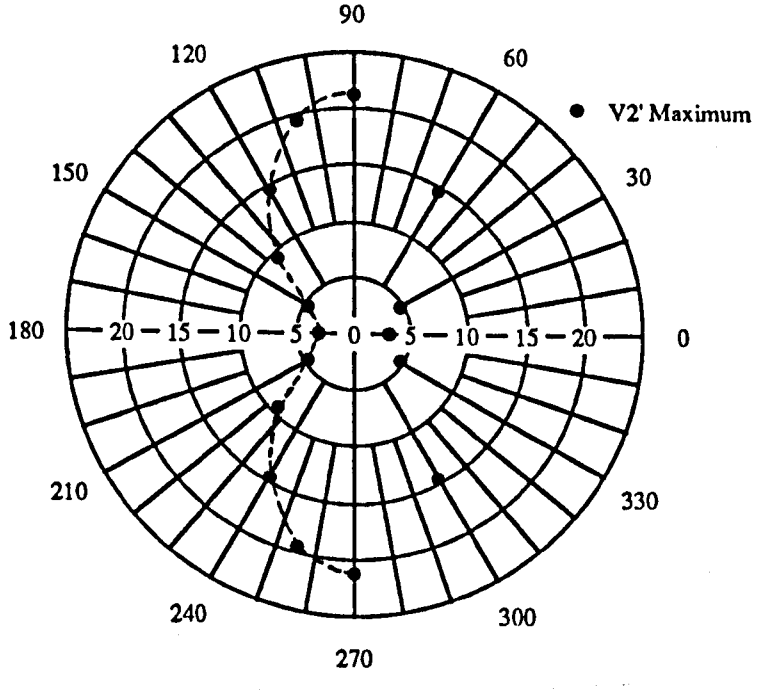

Figure 3.9. Peak values of side forces (V2') on SWATH-3 in various wave headings (Fn=0.00)

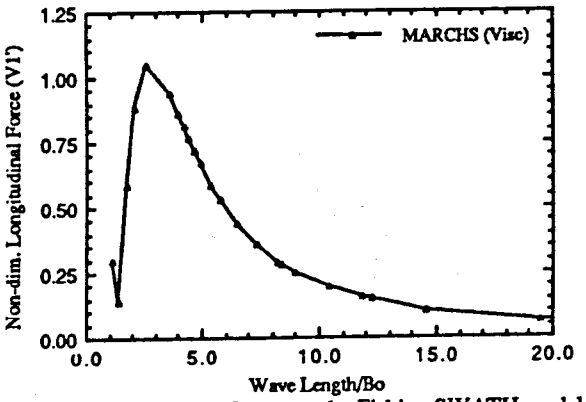

Longitudinal shear forces on the Fishing SWATH model in quartering seas (Fn=0.00)

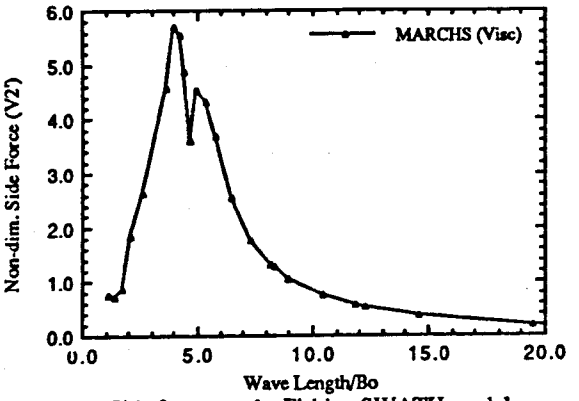

Side forces on the Fishing SWATH model in quartering seas (Fn=0.00)

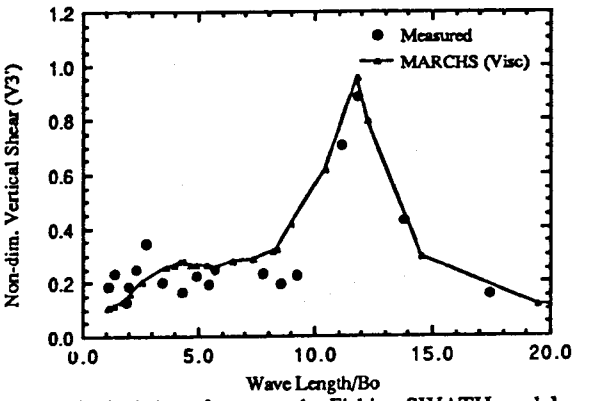

Vertical shear forces on the Fishing SWATH model in quartering seas (Fn=0.00)

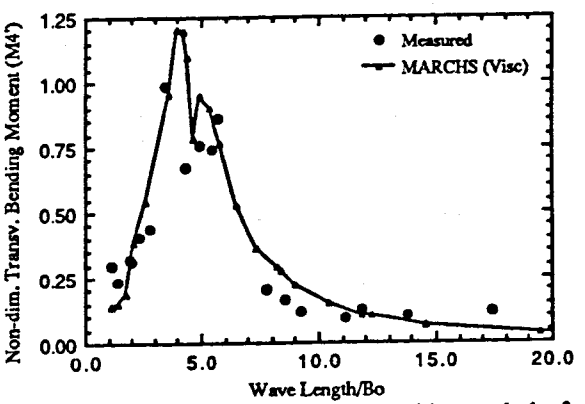

Transverse bending moment at the mid cross-deck of the fishing SWATH model in quartering seas (Fn=0.00)

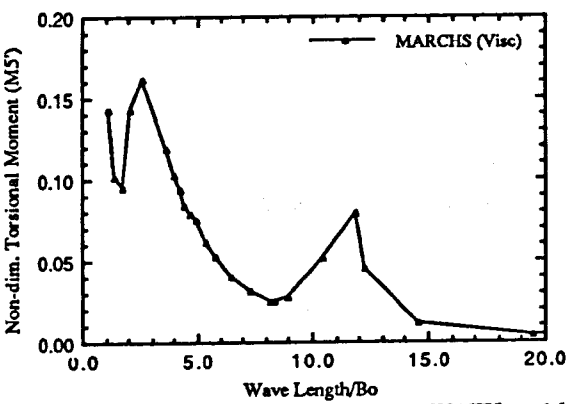

Pitch torsional moment on the Fishing SWATH model in quartering seas (Fn=0.00)

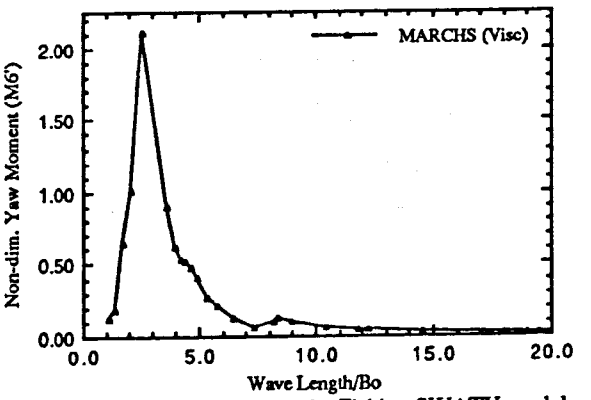

Yaw splitting moment on the Fishing SWATH model in quartering seas (Fn=0.00)

Figure 3.10. Wave load responses of SWATH-FV model in bow-quartering seas (Fn=0.00)

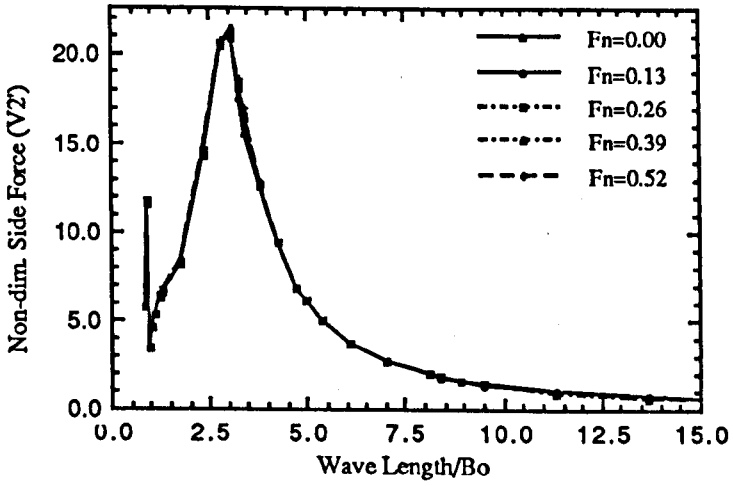

a). Side forces (V2) on SWATH3 in beam seas for various Fn

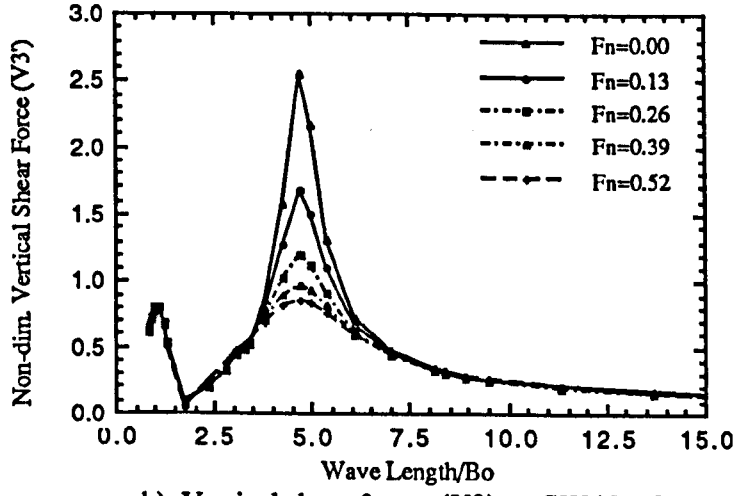

b). Vertical shear forces (V3) on SWATH3 in beam seas for various Fn

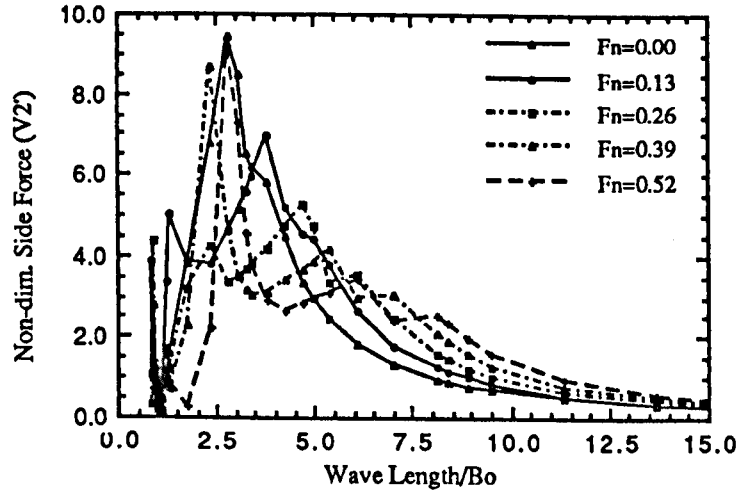

c). Side forces (V2) on SWATH-3 in quartering seas for various Fn

Figure 3.11. Forward speed effects on load responses

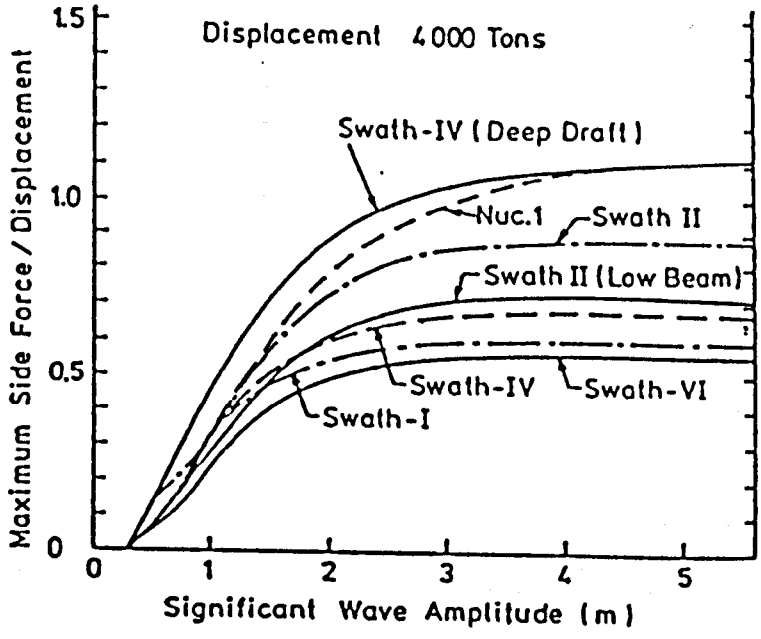

Figure 3.12. SWATH side force from model tests [Kerr et al (1978)]

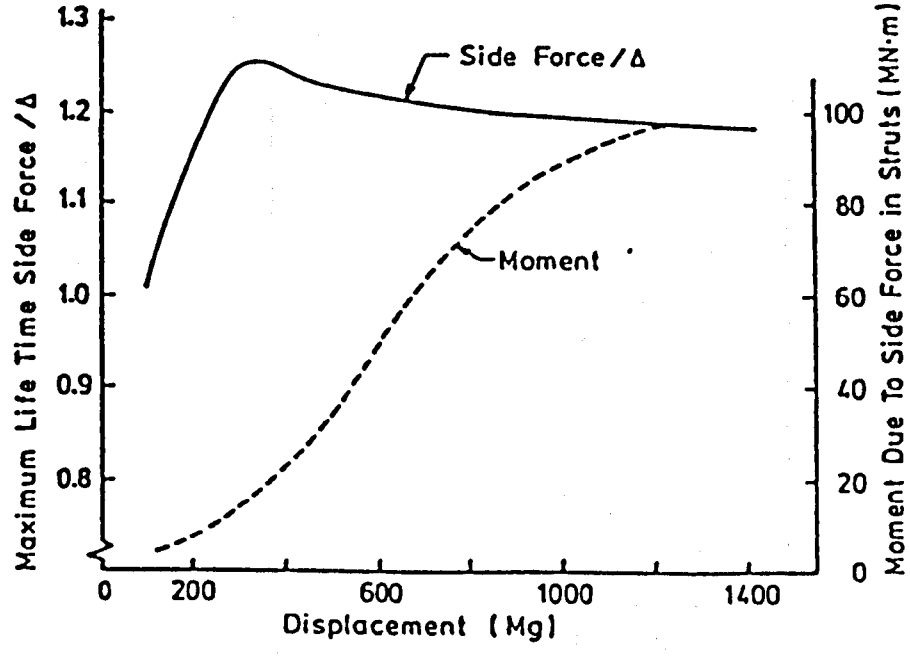

Figure 3.13. Maximum lifetime side force and moment in struts for small SWATHs [Allen & Holcomb (1982)]

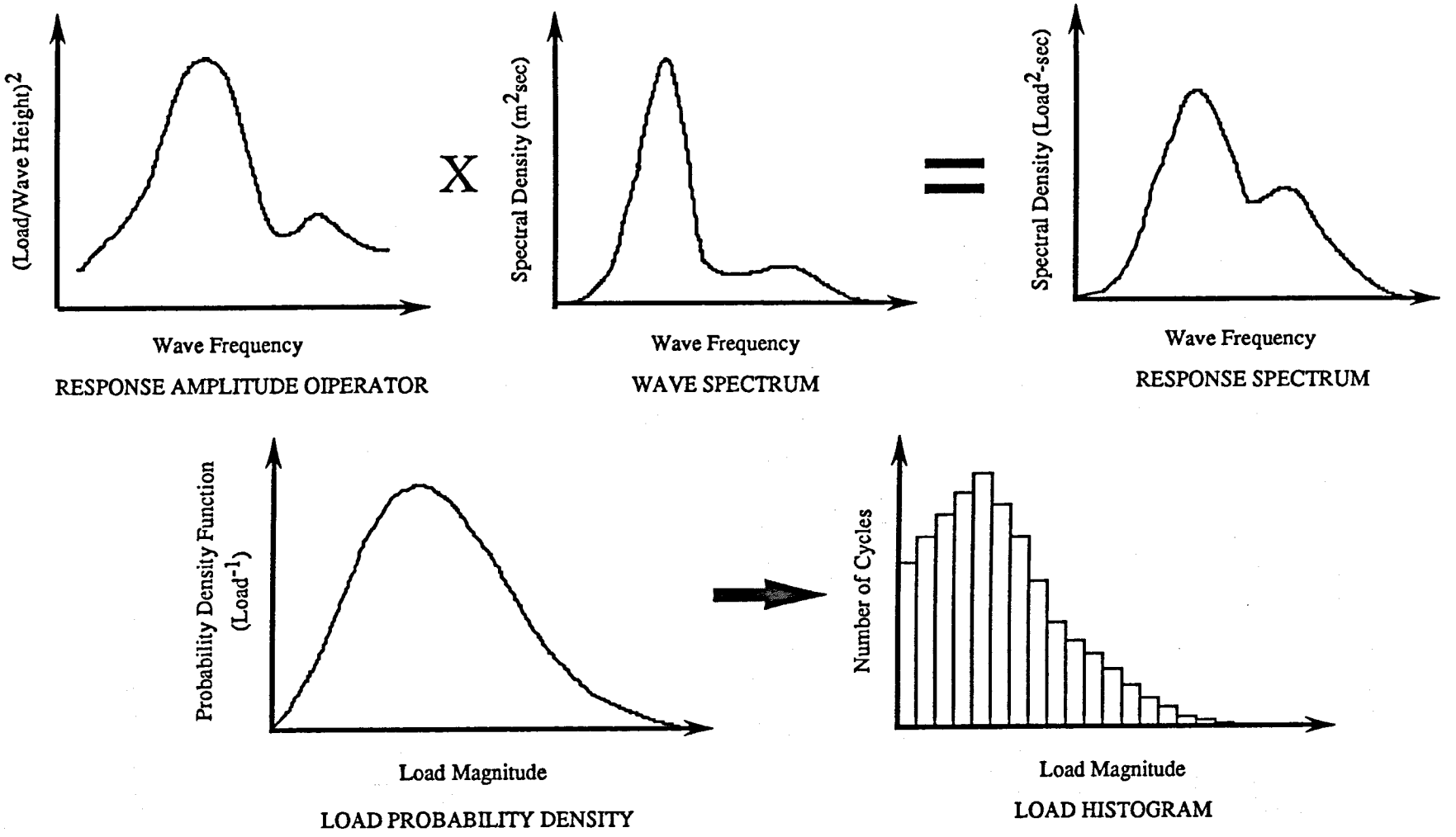

Figure 3.14. Procedure of the computation on wave load diostribution
[Sikora (1988)]

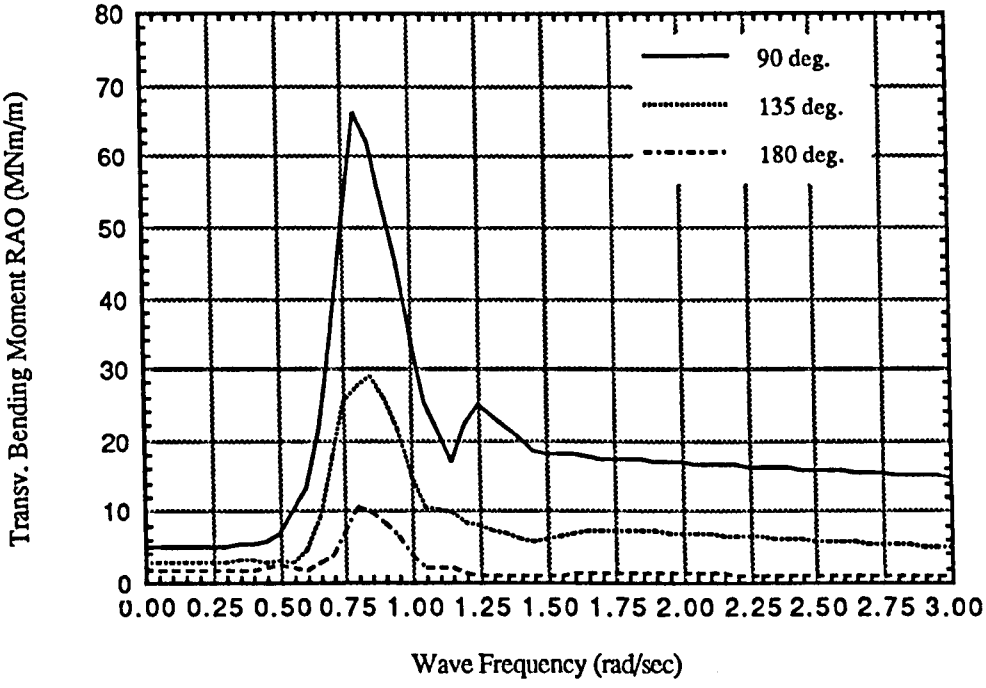

Figure 3.15. Transverse bending moments on the cross-deck of the 2500-tonne SWATH-FV in regular waves

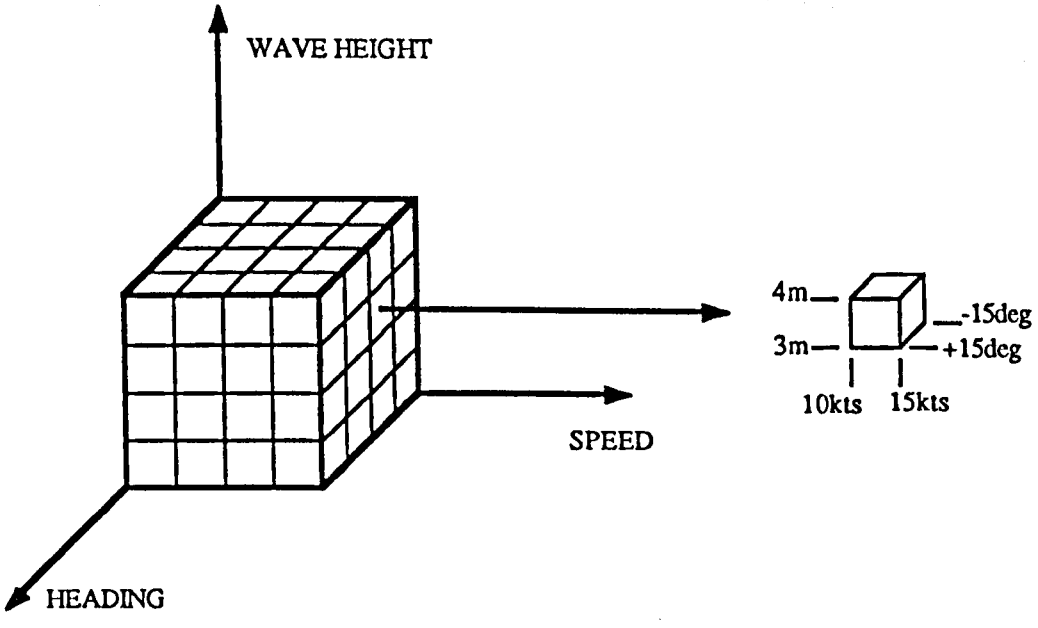

Figure 3.16. Schematic of operating mode [Sikora et al (1983)]

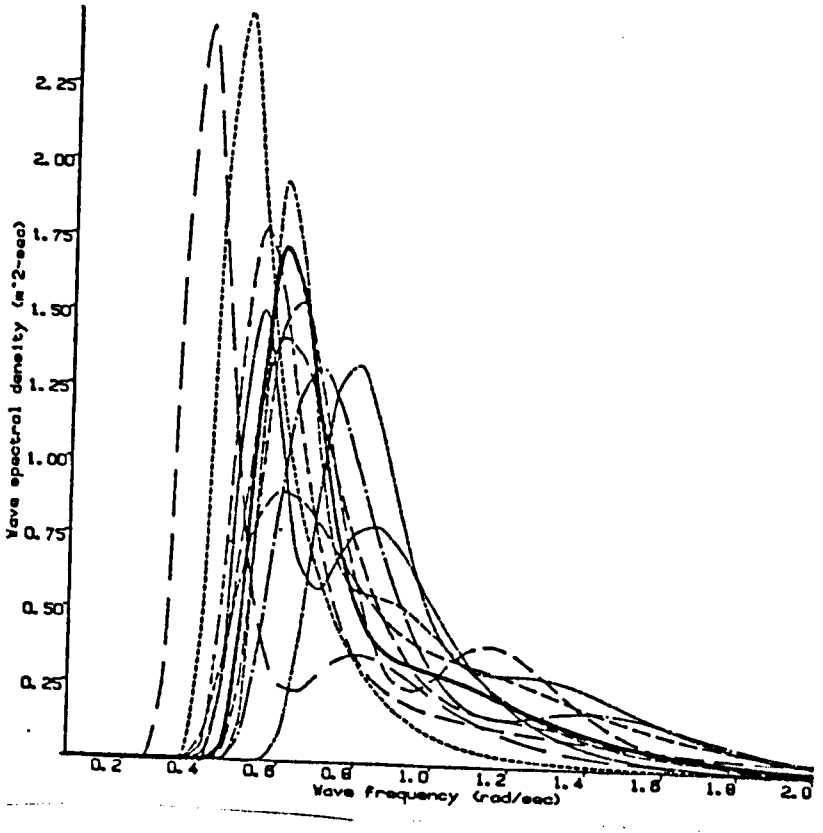

Figure 3.17. Family of six-parameter wave spectra (H_s = 3.0 m)

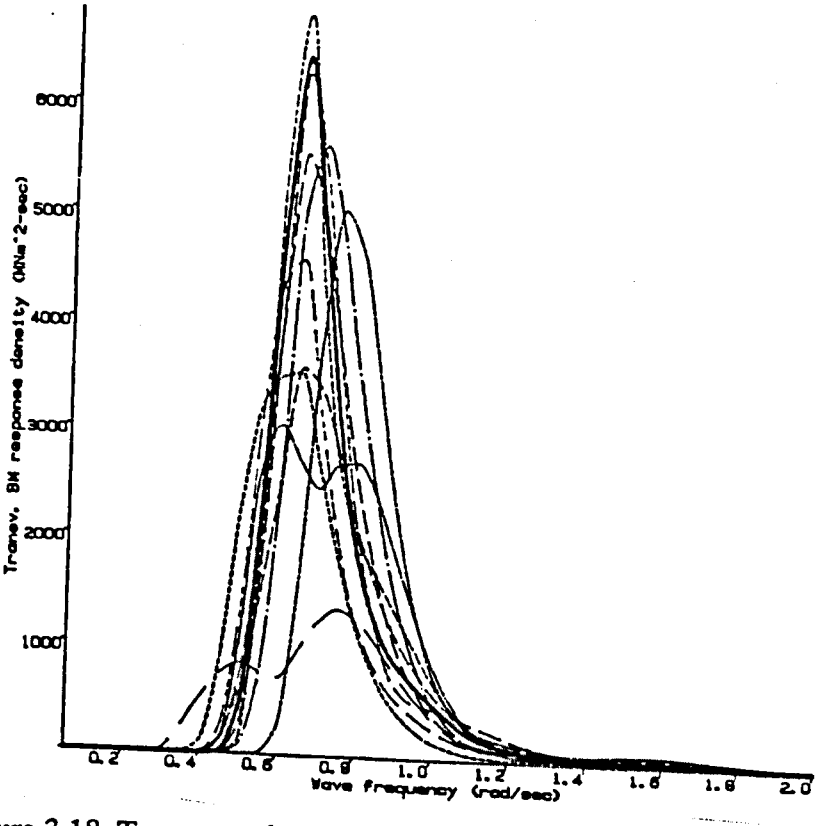

Figure 3.18. Transverse bending moment response spectra for the 2500-tonne SWATH-FV in beam seas (H_s = 3.0 m)

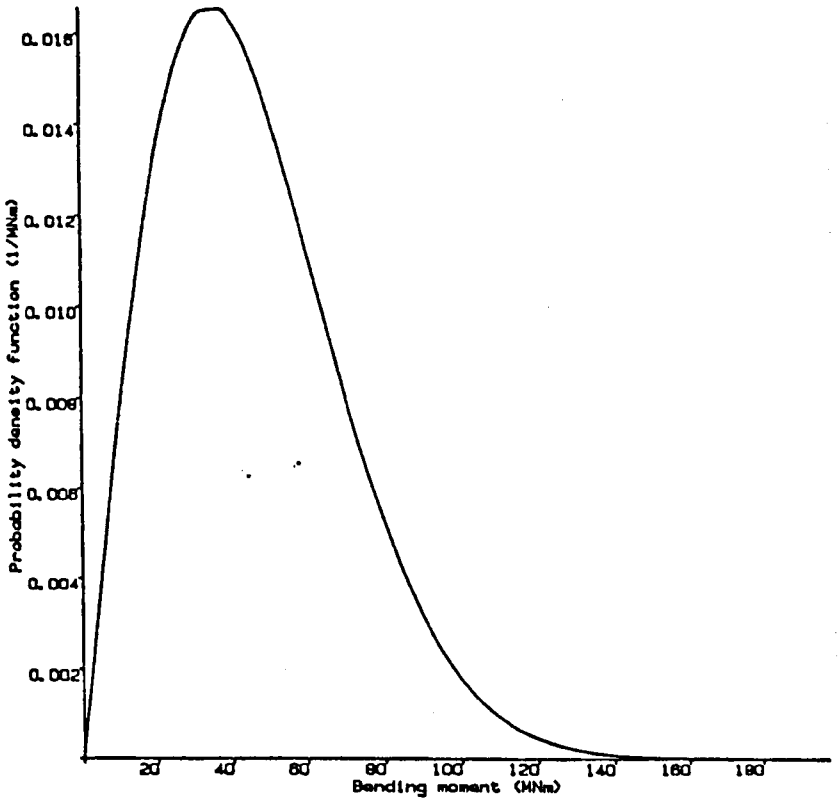

Figure 3.19. Probability density function of transverse bending moment for the 2500-tonne SWATH-FV in beam seas (H_s = 3.0 m)

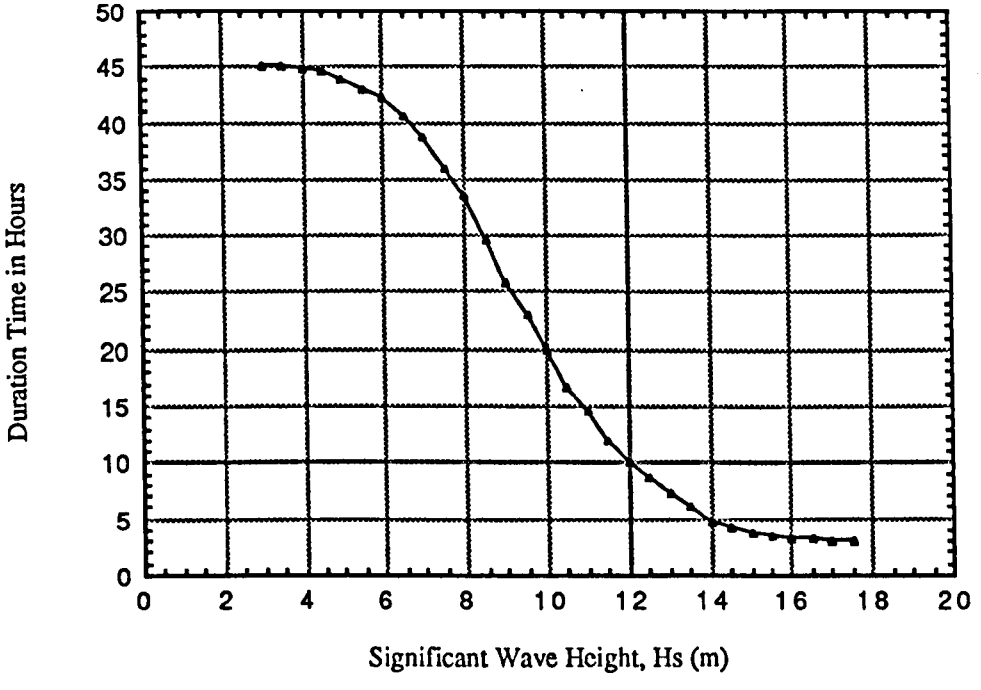

Figure 3.23. Significant wave height and its persistence in the North Atlantic every 1.52-m interval [Ochi and Motter (1974)]

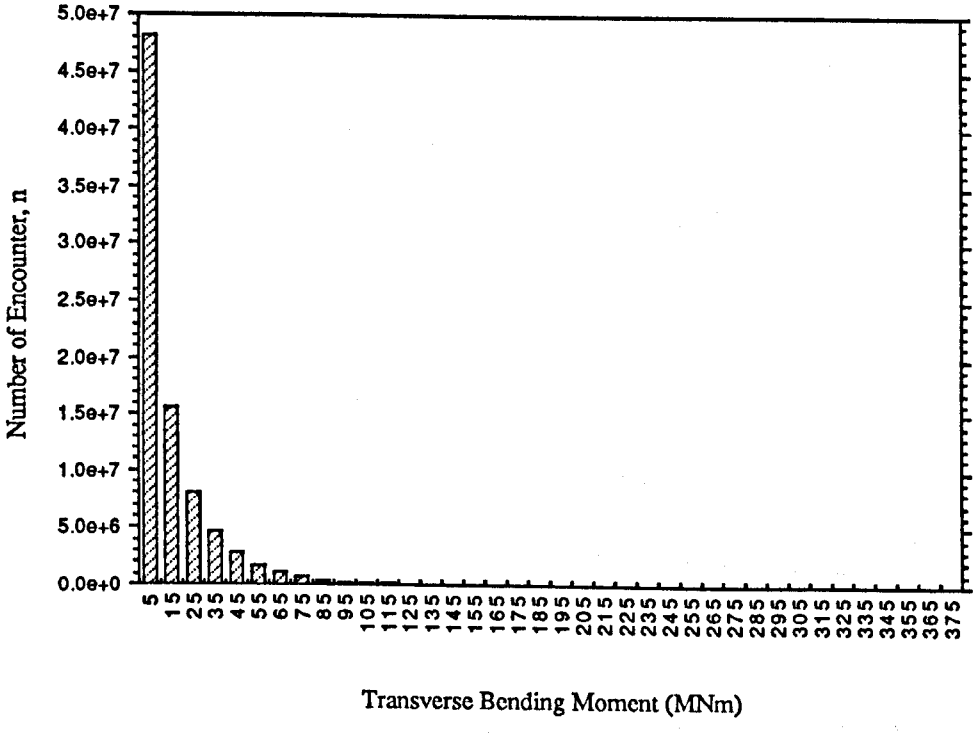

(a)

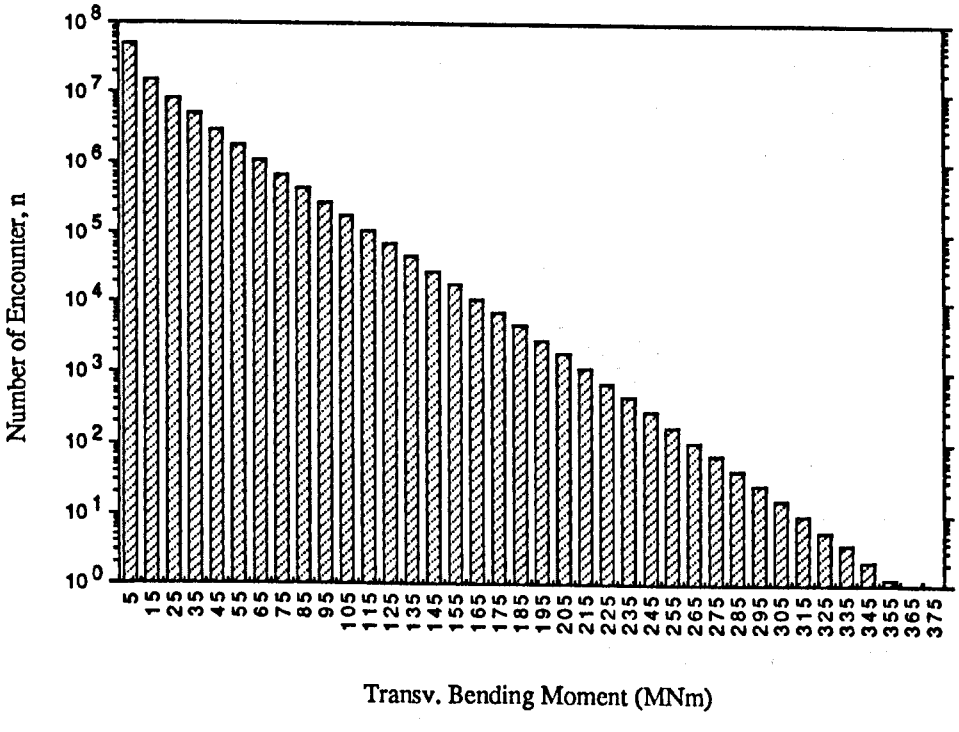

(b)

Figure 3.20. Transverse bending moment histogram of the 2500-tonne SWATH-FV operating in the North Atlantic
(a. linear vertical axis ; b. logarithmic vertical axis)

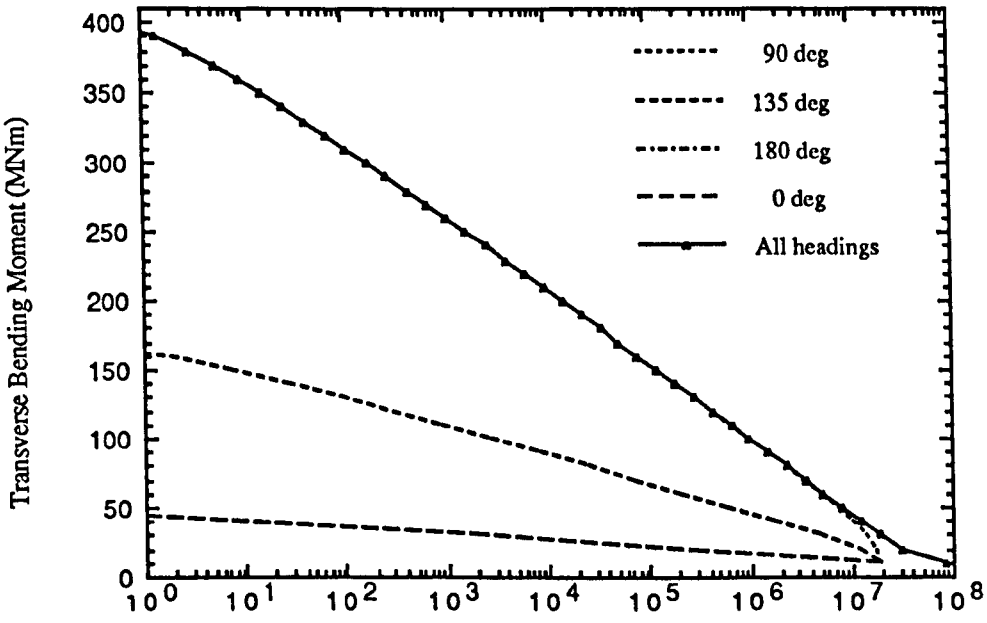

Figure 3.21. Lifetime transv. bending moment for the 2500-tonne SWATH-3 in the North Atlantic

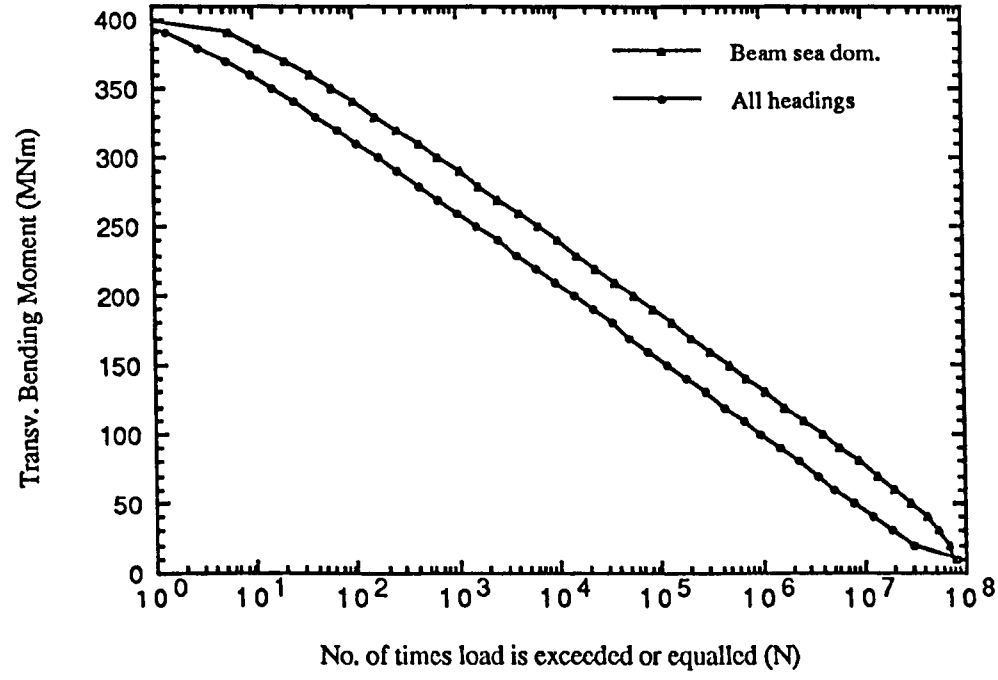

Figure 3.22. Beam sea dominated vs all headings lifetime transv. bending moment for the 2500-tonne SWATH-3 in the North Atlanctic

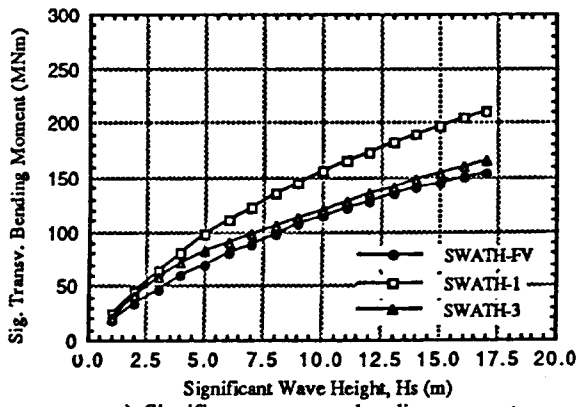

a). Significant transverse bending moment related to the most probable spectrum

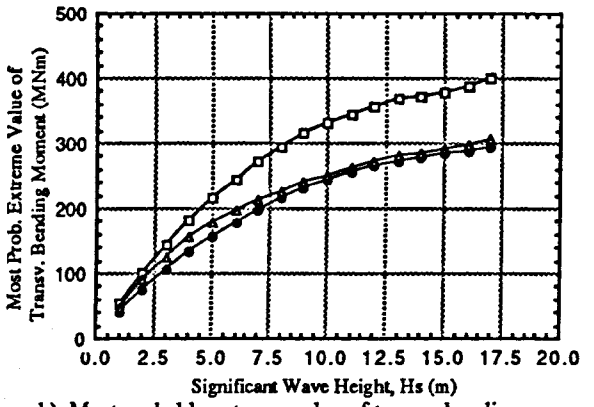

b). Most probable extreme value of transv. bending moment related to the most probable spectrum

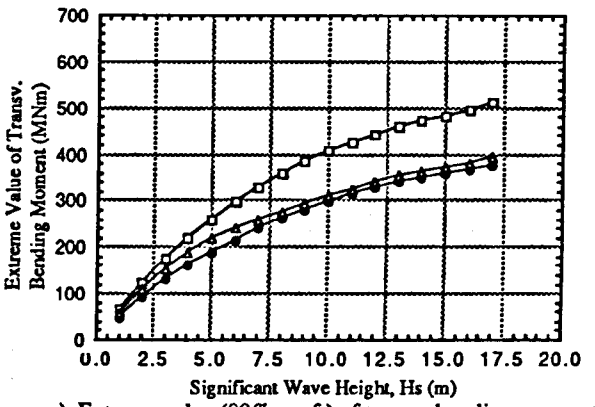

c). Extreme value (99% conf.) of transv. bending moment related to the most probable spectrum

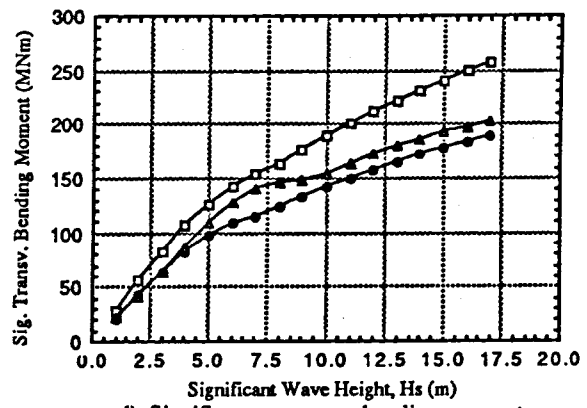

d). Significant transverse bending moment related to the maximum spectrum

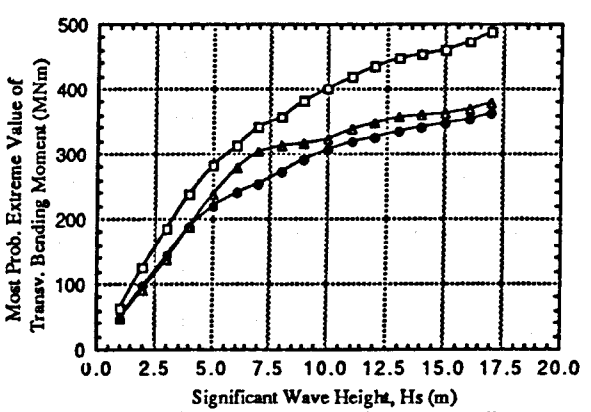

e). Most probable extreme value of transv. bending moment related to the maximum spectrum

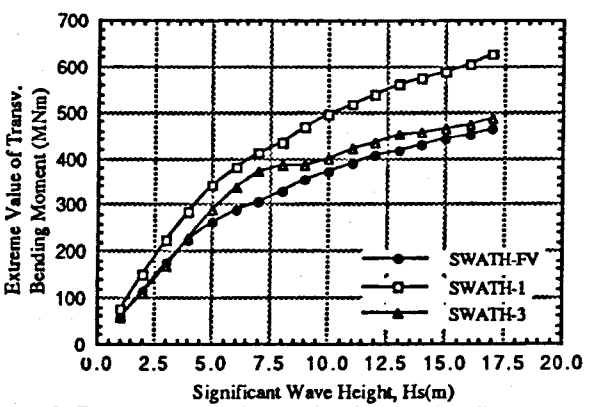

f). Extreme value (99% conf.) of transv. bending moment related to the maximum spectrum

Figure 3.24. Statistical values of transverse bending moments for SWATHs by the short-term analysis

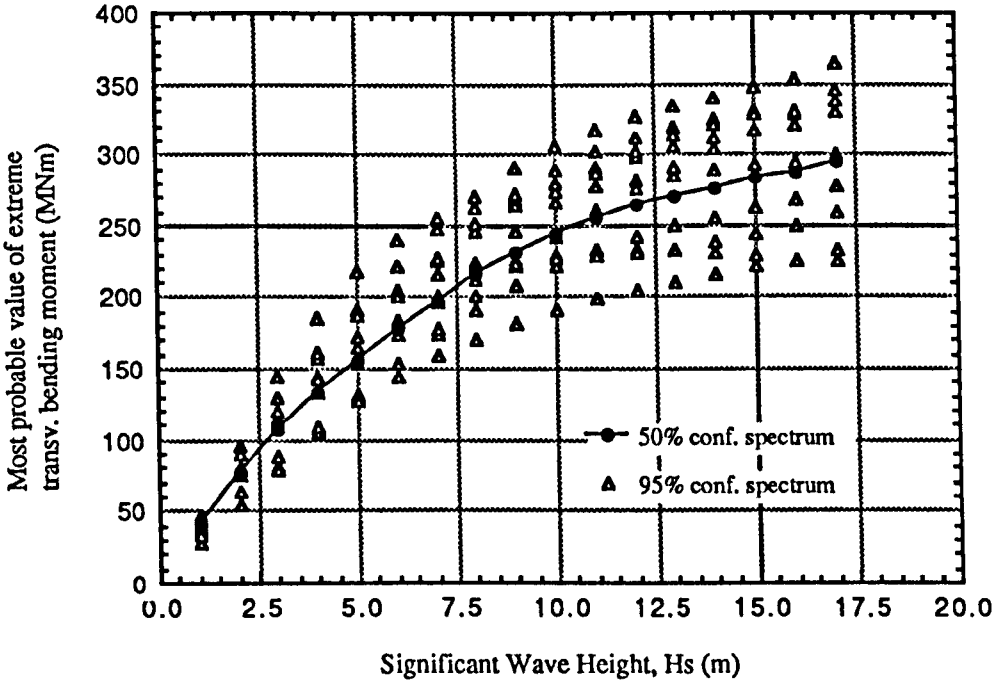

Figure 3.25a. Most probable extreme transv. bending moment on the 2500-tonne SWATH-FV

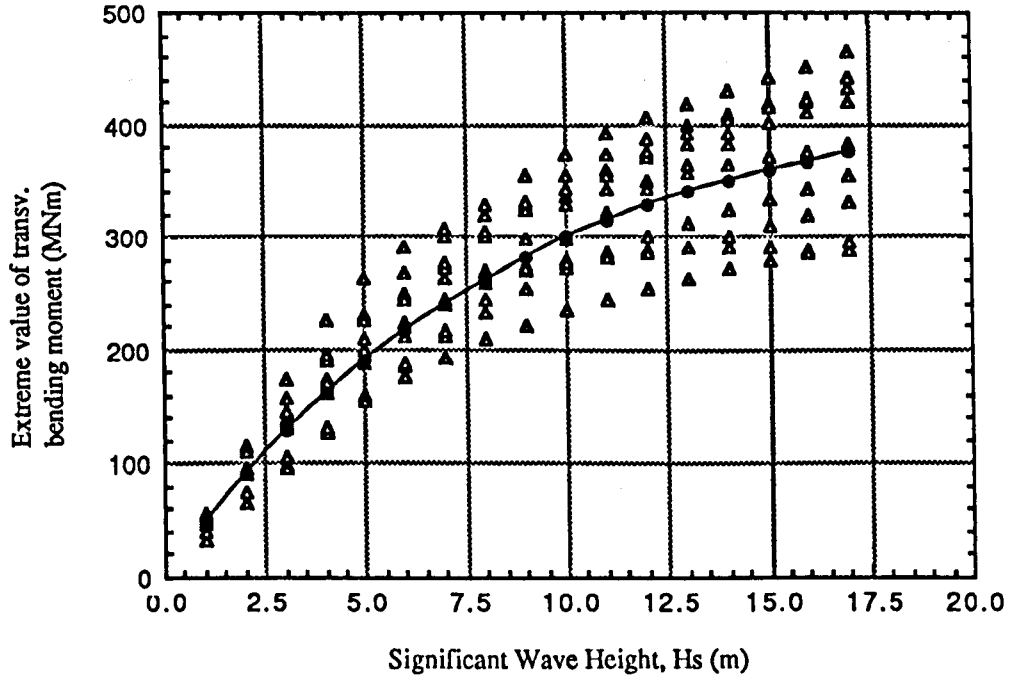

Figure 3.25b. Extreme transverse bending moment with 99% confidence on the 2500-tonne SWATH-FV

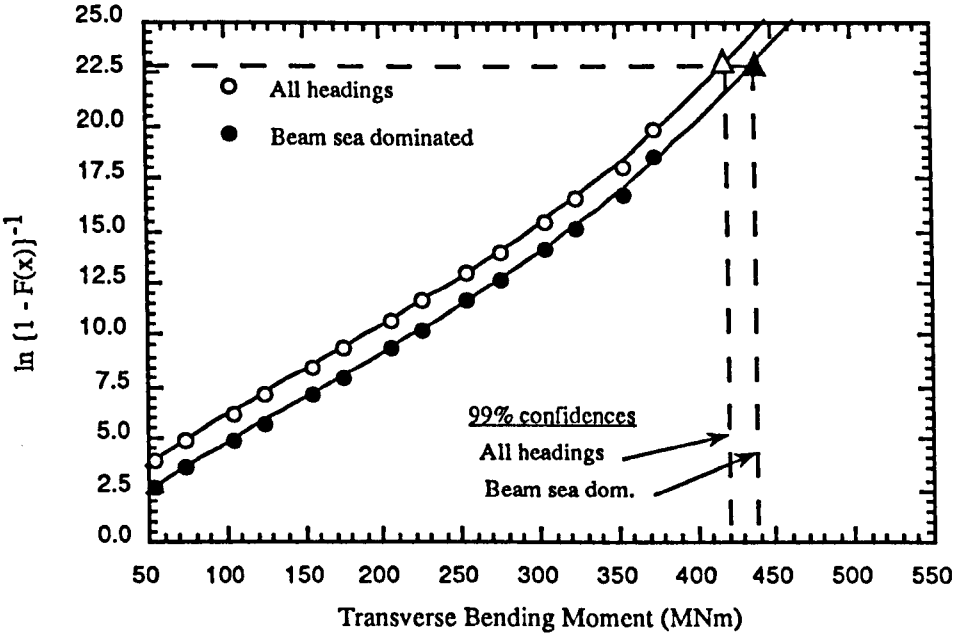

(a)

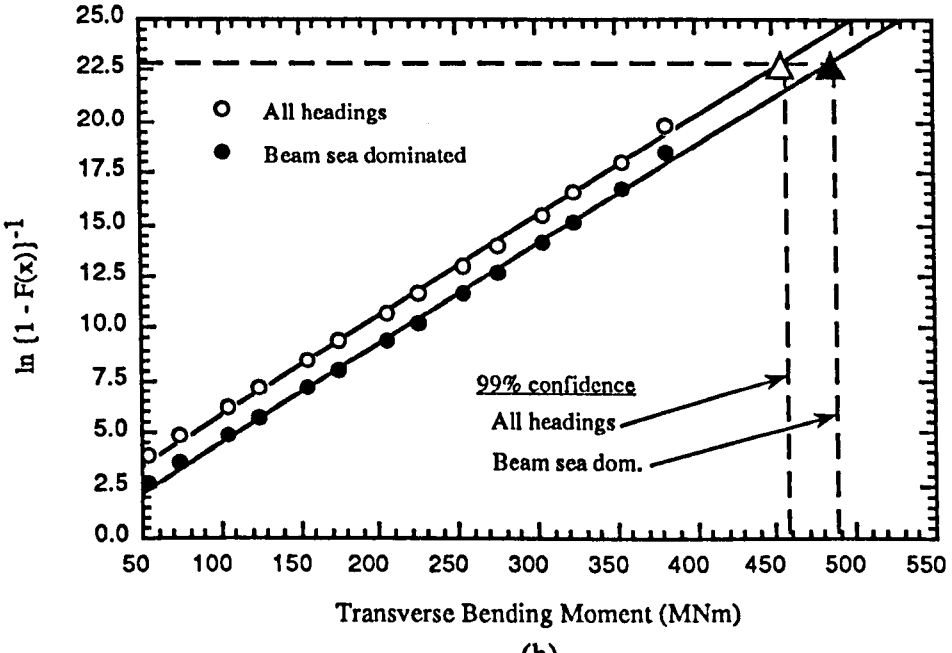

(b)

Figure 3.26. Extreme values of transverse bending moment on the 2500-tonne SWATH-FV by Long-Term analysis
a) third order polynomial fit ; b) linear fit

CHAPTER 4

PREDICTION OF SLAMMING ON SWATH SHIPS

CHAPTER 4

PREDICTION OF SLAMMING ON SWATH SHIPS

4.1. INTRODUCTION

The structural loading on SWATH, like on any other type of marine craft, can be classified into two categories, namely, primary and secondary loads. The former may comprise side load, bending moment and torsional moment which are considered as critical for the main structure mainly at the crossdeck and deck-strut intersection. Betts (1988b) suggests that the understanding of SWATH primary loading probably has been quite well established at present although further enhancement is still required. Secondary loads are those which are mainly considered to be imposed on local structure, namely, wave slap, slam-induced impacts, and deck loads due to shipping green sea. Whilst these secondary loads are wave-induced and associated with the hydrodynamics form of a vessel, other secondary loads on SWATHs as suggested by Faulkner (1992) include the live loads, berthing impacts, docking, ice loads and collisions. Despite the advance in SWATH research, these latter load considerations have not yet been given the attention they deserve. This latter area is therefore suggested for the next stage of SWATH research activity.

Kerr et al (1978) imply that the most significant secondary contributor considered in the derivation of maximum lifetime design loads of SWATHs are those due to slamming impacts. The phenomenon results when there is contact between the cross deck structure and the water surface at small or moderate impact angles. The initial impact force due to slamming pressure on the wet deck of SWATHs can be high enough to induce local damage to the cross-structure bottom plating and also other significant effects in the overall hull girder vibration. The vibratory motion following a slam is called whipping which by itself is a special area which needs to be studied separately from the usual structural behaviour problems.

In another set of circumstances, it may be that the initial impact force is not high enough to cause local damage on the wet deck of a SWATH. However, as the pressure is imposed on a relatively large flat bottom area when the body is immersed further, the resulting slamming force could be much more severe than at first thought. This occurrence is in nature quite similar to the phenomenon of bow flare slamming on aircraft carriers and other specialist monohull ships with large overhangs. Moreover, as observed by Nagai and Chuang (1977), the duration of this type of force is generally

longer than the bottom slamming force which is considered as significant on ordinary monohull ships. It is obvious, therefore, that it might not be appropriate to predict slamming on SWATH type vessels by conventional methods which have been well developed largely on the monohull bottom slamming. It is apparent that box clearance is an important dimension in determining slamming occurrence and further, the magnitude of impact pressure on the bottom of the cross-structure of SWATH ships is affected by the relative vertical velocity, the local section shape (flat or flared) and the ramp angle [Lee et al (1973), Giannotti (1975), Kaplan (1987)].

Slamming is expected to be most critical in head seas, and for a monohull the superposition of the resulting whipping stress and the basic wave-induced longitudinal bending stress will increase the total stress significantly, e.g. as observed by Nagai and Chuang (1977) and Ochi (1958). For SWATHs, on the other hand, where the maximum wave induced bending stress occurs in beam seas, such a superposition is unlikely to occur. However, Stirling et al (1988) suggest that in bow quartering seas, although the transverse bending load is generally lower than in beam seas; when this occurs simultaneously with slamming loads at speeds then the resulting loads could be more severe than those predicted in beam seas. As in the case of reducing vertical motions, slamming can be reduced by employing motion control fins. To reduce slamming by increasing the wet deck clearance should be considered with great care since this at the same time increases the bending loads in the cross-deck.

Generally slamming loads on SWATH are much lower than primary loads, but locally they can severely damage the structure, such as at the haunch, strut or the wetdeck. Experience on the SSP *Kaimalino* (220-tonne) shows that in the early days of its operation substantial damage was discovered by personnel of the DTRC. According to Hightower et al (1985) the damage on the framing at the port prow, which can be observed from inside the cross structure, was caused by slamming in rough weather. Another structural part which was also damaged, although only by a small deformation, was observed in the wet deck under the diesel generator compartment. This is thought to have been caused by large wave slamming, but other causes, like welding distortion, could also be possible. From such experiences, therefore, Loscombe (1989) claims that slamming loads should be treated as important as primary loads, especially for small SWATHs.

To date, knowledge of slamming phenomenon on SWATHs is limited, therefore one may not be certain as to how to deal with the practical problems of predicting slamming, or reducing slamming. This is not as simple as merely increasing the wetdeck clearance for the reason given earlier.

SWATH slamming investigation can, to some extent, be built upon past experience of other advanced marine vehicles, or even conventional monohull vessels, that is, by developing theoretical or semi-empirical predictions and/or by experimental methods. The former can be gained by modification of the existing motion prediction, i.e. to generate the prediction of relative vertical motion combined with slamming pressure data from the open literature. The experimental methods which are expected, by Meyerhoff et al (1988), to dominate SWATH slamming research in the near future, can be carried out in three different ways, namely, drop tests on 2-D models, drop tests on 3-D models and seakeeping tests.

The seakeeping model tests on SWATH slamming can be divided into two categories, that is, one dealing with measurement of relative motion and the other with the measurement of slamming impact pressure. The former describes slamming behaviour of a marine craft in probabilistic terms. The latter, which some may consider to be more important, is aimed at generating the data on the magnitude of impact pressure. The two findings will later be combined to derive the so called lifetime slamming load for design by way of spectral analysis.

This chapter will first present a review on different analytical methods of prediction of slamming for advanced marine vehicles. This is followed by selection of the appropriate method to be considered in the future development of a time-domain motion program to predict slamming on SWATHs. In the first approach the problem is restricted to head seas. Further developments in assessing post slamming behaviour which should take into account the buoyancy force due to the cross deck immersion, are outlined. Advantages of adopting a time-domain approach in preference to a frequency-domain approach will be mentioned. Further, the measured data from slamming tests on a small SWATH model carried out at the Hydrodynamics Laboratory will be presented. Some simplified formulations for predicting design pressure due to slamming on advanced marine vehicles are put forward. These are then evaluated with the principal aim of finding an alternative approach to estimate slamming pressure for SWATHs, at least in the early design stage.

4.2. ANALYTICAL APPROACHES FOR SLAMMING PREDICTION

For structural design purposes, the governing parameter required in determining the local (deck bottom) scantlings is the maximum impact pressure arising from slamming. This peak slamming pressure can be written in the general form of the pressure-velocity relation as :

$$p_s = \gamma \rho V_R^2 \tag{4.1}$$

where γ is the peak pressure coefficient, ρ the mass density of the fluid and V_R the relative velocity of the desired point at the fore portion of wet deck normal to the wave surface. It is clear from eq. (4.1) that the solution to the problem relies on finding the relative vertical velocity and in obtaining the peak pressure coefficient.

4.2.1. Frequency-Domain Analysis

In determining the relative velocity, and hence the slamming pressure, Graham (1988) follows the procedure developed by Stavovy and Chuang (1976). This approach is similar to the method described by Giannotti (1975) in which the slamming pressure on the bottom is assumed to be assembled from two different components of pressures, namely, the impact pressure (p_i) and the planing pressure (p_p). These pressures are, respectively, due to the normal and tangential components (V_n and V_t) to the wave surface of the relative velocities between the impact surface and the wave. Those two pressure components are written as follows :

$$p_i = \frac{1}{2} \rho \, k(\xi) \, V_n^2 \tag{4.2}$$

and

$$p_p = \frac{1}{2} \rho \, V_t^2 \tag{4.3}$$

where $k(\xi)$ denotes the form factor as a function of impact angle ξ, that is, the angle between wave and hull surfaces at the point of impact as given by Stavovy and Chuang (1976). It is obvious that the instantaneous impact angle can not be included in a frequency-domain approach, thus a time-domain method should be applied. However, for a given relative velocity calculated in the frequency domain, extreme slamming pressure can be assessed by selecting a constant impact angle, usually the worst possible case. Obviously severe slamming will occur at a small impact angle, that is when V_n is fairly near to the relative velocity normal to the hull surface, V_{ns}. The extreme impact pressure for a given relative velocity can be calculated using the equation below :

$$p_{i(ext)} = \frac{1}{2} \rho \, k_{max} \, V_{ns}^2 \tag{4.4}$$

where k_{max} is the maximum over the range of ξ, or $k(\xi)$. It is further assumed that V_{ns} can be evaluated in the direction normal to the mean position of the box. The impact angle, as shown in Fig. 4.1 at the point of impact R, can be found from the correlation between the wave slope at the instant of impact (θ_w) and the local box profile angle (α).

By neglecting surge, the velocity vector of the SWATH, V_s, can be written as :

$$\vec{V}_s = U\hat{x} + V_{sz}\hat{z} \tag{4.5}$$

where U is the forward speed and V_{sz} is the velocity component of the SWATH perpendicular to the calm water surface. The wave profile, ζ, and the orbital velocity of water particles on the surface, V_0, are written as :

$$\zeta = \zeta_0 \cos(Kx + \omega t) \tag{4.6}$$

and

$$\vec{V}_0 = -\omega\zeta_0 \cos(Kx + \omega t)\hat{x} - \omega\zeta_0 \sin(Kx + \omega t)\hat{z} \tag{4.7}$$

If $\hat{n}_R$ denotes the unit outward normal to the hull at point R, then V_{ns} can be found as :

$$V_{ns} = (\vec{V}_s - \vec{V}_0).\hat{n}_R \quad \text{or}$$

$$V_{ns} = \left[\omega\zeta_0 \cos(Kx + \omega t) + U\right]\sin\alpha - \left[\omega\zeta_0 \sin(Kx + \omega t) + V_{sz}\right]\cos\alpha \tag{4.8}$$

To take into account the moving co-ordinate system with origin at the mean position of the centre gravity of the SWATH, eq. (4.8) becomes :

$$V_{ns} = \left[\omega\zeta_0 \cos(Kx + \omega_e t) + U\right]\sin\alpha - \left[\omega\zeta_0 \sin(Kx + \omega_e t) + V_{sz}\right]\cos\alpha \tag{4.9}$$

where ω_e is the frequency of encounter. For the horizontally flat portion of the wet deck, i.e. α=0, eq. (4.9) reduces to :

$$V_{ns} = -\omega\zeta_0 \sin(Kx + \omega_e t) - V_{sz} \tag{4.10}$$

The tangential velocity component required to calculate the planing pressure is obtained simply by taking into account the forward speed U as :

$$V_t = U\cos\alpha \tag{4.11}$$

Another slamming prediction in the frequency-domain by Kaplan (1987) is described subsequently. This method was originally developed for SES type crafts, however, the sophistication of the method makes it possible to be applied in the prediction of slamming on SWATH ships. The termed effective vertical velocity at any point on the bow ramp impact surface relative to the wave surface is obtained by involving the heave and pitch motion velocities as follows :

$$V_R = U\tan(\alpha+\zeta_5)+w_r \tag{4.12}$$

with

$$w_r = \dot{\zeta}_3 - x\dot{\zeta}_5 + U\zeta_5 + \frac{D\zeta}{Dt} \tag{4.13}$$

where U is the forward speed, α the ramp angle, ζ_5 the pitch angle (as shown in Fig. 4.2), $\dot{\zeta}_3$ and $\dot{\zeta}_5$ are, respectively, the heave and pitch velocities and the operator $\frac{D\zeta}{Dt} = \frac{\partial\zeta}{\partial t} - U\frac{\partial\zeta}{\partial x}$ where ζ denotes the wave elevation. On the flat part of the wet deck eq. (4.12) is reduced to :

$$V_R = U\tan\zeta_5 + w_r \tag{4.14}$$

4.2.2. Time-Domain Analysis

A computer program to predict motions of SWATH ships using a time-domain technique has been developed in the Department, although it still needs to be improved further. The program was first developed by Arthur (1988) to solve only the heave and pitch coupled motion problem in head seas, and since then has been extended to deal with the general five-degree of freedom motions problem at arbitrary heading angles, as reported by Jones et al (1990) and McGregor et al (1990). The development of this time domain program was, of course, not intended to replace the existing 2D and 3D frequency domain programs [Seren et al (1985), Zheng (1988), Chan (1990a)] in predicting SWATH motions. It is, however, intended to tackle matters which are not possible to be solved with a frequency domain method. Such a problem is the cross structure slamming which is a non-linear dynamic phenomenon that must be modelled in the time domain.

4.2.2.1. Prediction of Slam Occurrence. The first task in creating a slamming prediction program is to be able to establish when and where a slam occurs. Let Z_{cx} be the deck clearance above the calm water of a point on the deck bottom at the distance x from the longitudinal centre of gravity, then a slam in that particular point is expected to occur when Z_{cx} is exceeded by the absolute value of relative displacement (Z_{drel}) between the wet deck and the wave surface [Lee et al (1973), Giannotti (1975)] which is written as :

$$\left|Z_{drel}\right| > Z_{cx} \tag{4.15}$$

The maximum relative vertical displacement of the point from the wave surface can be obtained by :

$$Z_{drel}(x) = Z_{dabs}(x) - \zeta(x) \tag{4.16}$$

where ζ denotes the wave elevation from the calm water and Z_{dabs} is the absolute vertical motion of the point which is caused by a train of regular head waves as :

$$Z_{dabs}(x) = \zeta_3(t) - x\zeta_5(t) \tag{4.17}$$

4.2.2.2. Instantaneous Relative Vertical Velocity. Once it has been established that an impact had occurred it is necessary to compute the relative vertical velocity at the impact point when slamming occurs. The formulation of relative vertical velocity on the wet deck surface of SWATHs that has been applied, is a combination of both procedures given by Graham (1988) and Kaplan (1987). In the present computation, eq. (4.9) is modified to take into account the pitch angle at each time step as follows :

$$\begin{aligned} V_{ns}(t) = &\left[\omega\zeta_0 \cos(Kx + \omega_e t) + U\right]\sin\left\{\alpha - \zeta_5(t)\right\} \\ &-\left[\omega\zeta_0 \sin(Kx + \omega_e t) + V_{sz}(t)\right]\cos\left\{\alpha - \zeta_5(t)\right\} \end{aligned} \tag{4.18}$$

with the vertical velocity component of SWATH, V_{sz}, taken as :

$$V_{sz}(t) = \dot{\zeta}_3(t) - x\dot{\zeta}_5(t) + U\zeta_5(t) \tag{4.19}$$

where the minus sign of the pitch angle is attributed to the definition of pitch being positive when the bow is down.

The planing velocity given in eq. (4.11) is then modified into the form of :

$$V_t(t) = U\cos\left\{\alpha - \zeta_5(t)\right\} \tag{4.20}$$

Accordingly, the calculation of impact angle should also include the pitch angle, as illustrated in Fig. 4.3, and is given as :

$$\xi(t) = \theta_w(t) - \{\alpha - \zeta_5(t)\} \tag{4.21}$$

where α is the ramp angle and $\theta_w(t)$ is the instantaneous wave slope, which takes the form :

$$\theta_w(t) = -\zeta_0 K \sin(Kx + \omega_e t) \tag{4.22}$$

4.2.2.3. Evaluation of Impact Pressure. Having obtained the relative vertical velocity during the slam then the peak impact pressure can be calculated using the formulation given in eq. (4.2). The concern is then how to select a suitable value of peak pressure factor (k) to be applied on SWATHs when there is no available data specifically derived for these types of vessels. As the wet deck structure of most SWATH ships is a simple flat shape then most published theoretical methods and experimental data on geometrical shapes commonly used for marine vehicles can be aptly applied. A number of investigators have proposed different theoretical approaches to work out the phenomenon of hydrodynamic impact based on the knowledge of fluid dynamics, e.g. Verhagen (1967), Chuang (1969), Koehler and Kettleborough (1977), Geers (1982), Gallagher (1985), Watanabe (1987).

Experimental measurement of impact pressure in laboratories can be categorised into two major groups, namely, drop test and seakeeping model test. The so called drop test technique, such as described by Chuang (1966), Lewison and Maclean (1968), Sellars (1976) or Ando (1989), seems to be the simplest way, and is considered as reliable, although sometimes rather conservative, to derive the peak slamming coefficient. At this stage the peak pressure coefficient given by Stavovy and Chuang (1976) is selected, which can be used for most general shapes of wet deck structure, to be included in the time domain program to calculate maximum impact pressure. The selected data proves to be reliable [ISSC's Committe II.3 (1979)] as this has been validated with test results from catamaran models by Stavovy and Chuang (1976) and from a full scale catamaran by Chuang (1974) with underdeck configuration quite similar to SWATHs. The peak pressure factor in terms of normal impact velocity, k, can be calculated from the peak pressure factor in terms of vertical impact velocity, k_1, which is found from drop tests, as :

$$k = k_1 / \cos^4 \xi \tag{4.23}$$

The value of k_1 to be used herein is obtained from the averaged value of the test data by means of a three dimensional analysis, and is given by Stavovy and Chuang (1976) in the following equation as a function of impact angle, ξ :

1. For $0 \leq \xi < 2.2$ deg :

$$k_1 = 0.37\xi / 2.2 + 0.5$$

2. For $2.2 \leq \xi < 11$ deg :

$$k_1 = 2.1820894 - 0.9451815\xi + 0.2037541\xi^2 - 0.0233896\xi^3 + 0.0013578\xi^4 - 0.00003132\xi^5$$

3. For $11 \leq \xi < 20$ deg : (4.24)

$$k_1 = 4.748742 - 1.3450284\xi + 0.1576516\xi^2 - 0.0092976\xi^3 + 0.0002735\xi^4 - 0.00000319864\xi^5$$

4. For $20 \text{ deg} \leq \xi$:

$$k_1 = (1 + 2.4674 / \tan^2 \xi)\ 0.76856471 / 288$$

4.2.2.4. Post Impact Behaviour. After a slam (impact occurs) a period of time elapses in which part of the cross deck structure becomes immersed before the vessel rises out of the waves. This post impact, buoyancy effect, results in a pressure loading on the cross deck structure. Although the effect is likely to be small in magnitude, relative to the impact pressure, and may not affect the local strength of the cross deck, it will influence the overall loading on the cross deck, and must be included in a thorough investigation of slamming effects. The buoyancy force can be evaluated by calculating the instantaneous submerged volume of the cross deck, ∇_{CD}, for the duration of immersion, and is given as follows :

$$F_B = \rho g \nabla_{CD}(t) \tag{4.25}$$

where g is acceleration due to gravity.

The pressure loading can be assumed to be evenly distributed over the wetted surface, A_{CD}, and so the average pressure due to the effect is given as :

$$P_B = F_B / A_{CD} \tag{4.26}$$

4.2.2.5. Structure of Program SLAMTIME. A computer program, SLAMTIME, say, to simulate the occurrence of a slam, and evaluate the impact pressure and buoyancy force on the wet deck of SWATH ships using the aforementioned theory, is now proposed for development. The structure of the program is outlined in the flowchart diagrams, as shown in Figs. 4.4a-d. Fig. 4.4a shows the main time solver program.

Input Section The strut and hull dimensions, hydrostatic values and wave details, such as amplitude, frequency and heading angle are input. A geometry file is created giving a definition of the submerged hull form. If slamming is to be considered a cross deck file is created defining the geometry of the cross deck structure and box clearance.

Database The restoring coefficients are calculated from the hydrostatics and hydrodynamics coefficients can be evaluated using a 3D source-sink distribution method as presented in by Zheng (1988) or Chan (1990a).

Time Solver Values of heave and pitch amplitudes and velocities, s_3, $\dot{s}_3$, s_5 and $\dot{s}_5$ are set to zero to represent the initial conditions of the simulation. For the forward speed case, a speed is selected and corrections to the added mass and damping coefficients are applied. These values are inserted into the coupled motion equations.

Harmonic time functions of wave encounter frequency are then applied to the wave exciting forces and moments. Ramp functions are applied to the wave exciting forces and moments if necessary.

Solutions obtained for the first time step represent initial conditions for the next, and are fed into the reconditioning routine and are used to calculate the instantaneous parameters to be input at the next time step. In the case of regular waves the same procedure is repeated for subsequent solution steps until constant amplitude, steady solutions for heave and pitch are obtained.

Reconditioning Routine The solutions obtained for the last time step are fed back into the time solver to form the initial conditions for the next. Routine SLAM is called. Fig. 4.4b shows routine SLAM which determines whether or not a slam has occurred and instigates the calculation of either impact pressure, if it is a first impact, or buoyancy force, if it is a post impact submergence of the cross deck.

4.2.2.6. Routine SLAM. To predict when and where a slam occurs, the condition given by eq. (4.15), i.e. the box clearance exceeded by the absolute value of relative displacement of a point on the cross deck bottom, must be tested for, along the length of the cross deck structure. Therefore a loop is set up testing for this condition and incrementing over closely spaced cross deck sections (defined at the beginning, B(I) to B(N)) from the extreme forward end of the cross deck structure and working aft.

Once it is established that contact has occurred, at this position, the question is posed - *Did contact occur here at the last time step?* If NO contact occurred at this

position, at time t - 1, then this must be the point of first impact and routine PIMPACT is called.

4.2.2.7. Routine PIMPACT. Figure 4.4c shows routine PIMPACT which calculates the peak impact pressure on first impact of each wave on the cross deck structure. The cross deck ramp angle is input, if it exists. The vertical velocity component is calculated, using the motion velocities and forward speed as in eq. (4.19) and fed in to calculate the relative vertical velocity, i.e. eq. (4.18). The instantaneous wave slope and impact angle are calculated using eqs. (4.22) and (4.21), respectively. Using eq. (4.24) the value of k_1 is evaluated; from which the form factor in terms of normal impact velocity, k, can be found by using eq. (4.23). An option to apply the form factor from other references is reserved in the program. Finally the peak impact pressure (P_i) is solved by eq. (4.2).

4.2.2.8. Routine POSTSLAM. If contact has occurred at this position, at time t - 1, then this is the starting point of the post impact submergence (see Fig. 4.4d). The routine then enters a second loop, testing whether or not contact has occurred to determine the extent of the submergence, and the depths of submergence, of the cross deck at each point.

Once these have been established the projected area of submergence and resultant buoyancy force can be calculated. The resulting impact force and post impact buoyancy can be output to the time solver to give a slamming force time history over the duration of a run.

Output Data The expected output data from the time-domain motion/slamming program is listed below :

1. Heave elevation (ζ_3)
2. Pitch elevation (ζ_5)
3. Wave elevation (ζ_w)
4. Absolute motion elevation of any given point at the bow wet deck (ζ_{dabs})
5. Relative motion elevation of any given point at the bow wet deck (ζ_{drel})
6. Slam motion elevation of any given point at the bow wet deck ($\zeta_{drel} - Z_c$)
7. Relative velocity elevation of any given point at the bow wet deck (ζ_{vrel}),
8. Impact angle (ξ), and
9. Slamming pressure elevation of any given point at the bow wet deck (ζ_{sp})

4.2.3. Probabilistic Approach

The probabilistic approach is to some extent quite convenient for predicting slamming behaviour if only motion predictions in the frequency domain are available. In this context, slamming behaviour of SWATHs refers to the three different, but interrelated, measures of slamming qualities, namely, the frequency of occurrence of slamming impact, the expected number of impacts per unit time and the largest magnitude of impact (extreme value) expected to occur on the cross deck bottom during a specified ship operation time. Development of the present widely used probability analysis on ship slamming was pioneered by Ochi (1964, 1973) and Ochi and Motter (1969, 1971, 1973). As the method was initially derived for monohull ships, the dominant factor which determines the probability occurrence of slamming, besides the relative vertical motion, is the ship draught at the desired position where slamming is observed. In the case of SWATHs, as well as for catamarans, the dominance of the draught factor, as has been discussed in the previous section, is replaced by the wet deck clearance above the water level. Taking the two factors above and eq. (4.15) into consideration, the probability of impact taking place along the wet deck of a SWATH ship operated in a particular sea region can be calculated using the formula :

$$P_r\{\text{slam impact}\} = \exp\left\{-\frac{Z_{cx}^2}{2E_d}\right\} \tag{4.27}$$

where E_d is the variance of relative vertical displacement, which can be determined by taking the relative motion response amplitude operator into account and applying an appropriate sea spectrum, $S(\omega)$, for a particular sea environment as :

$$E_d = \int_0^\infty (Z_{drel} / \zeta_w)^2 \, S(\omega) \, d\omega \tag{4.28}$$

where ζ_w is the wave amplitude.

The probability given in eq. (4.27) may be more meaningful if it is expressed in terms of the number of impacts which may occur in a period of time. The formulation below is given to determine the number of impacts expected per unit time :

$$n_s = \frac{1}{2\pi}\sqrt{\frac{E_v}{E_d}}\exp\left\{-\frac{Z_{cx}^2}{2E_d}\right\} \tag{4.29}$$

where E_v is the variance of relative vertical velocity which can be obtained simply by

substituting the wave frequency factor into eq. (4.28) as follows :

$$E_v = \int_0^\infty (\omega Z_{drel} / \zeta_w)^2 \, S(\omega) \, d\omega \qquad (4.30)$$

The expression in eq. (4.29) can then be expanded to assess the expected number of impacts sustained by the wet deck at a particular position in T hours of wave persistence as :

$$N_s = \frac{3600T}{2\pi} \sqrt{\frac{E_v}{E_d}} \exp\left\{-\frac{Z_{cx}^2}{2E_d}\right\} \qquad (4.31)$$

Referring back to eq. (4.27), that expression is an ideal situation, where every contact between wet deck and the wave surface is thought as 'slamming'. Even though, this set of circumstances is not completely true as not all the surface contacts create a significant effect on the cross deck structure that can be categorised as an actual slam. Defining the actual slamming obviously is a subjective matter in which different people will have different considerations. Aertssen (1972) gives a generally accepted definition of slamming, that is, a severe impact which may cause the captain to substantially reduce the speed in seaways. Nonetheless, such a definition is still uncertain and may differ from one ship to another, and it is suggested by Ochi and Motter (1973) that this matter should be confirmed experimentally.

Discussion on the 'actual slamming' has led to the concept of threshold (relative vertical) velocity, V_{Th}, that is, the magnitude of velocity required to incite a slamming impact. For monohulls of about 160m LBP, Ochi and Motter (1973) suggest the value of 12 fps (3.65 m/s) for the threshold velocity, whereas Aertssen (1972) for ships of that size suggests a value of 18 fps.(5.48 m/s). There has been no available data of threshold velocity in the open literature for SWATH ships. Even so, a threshold velocity value of 10.8 fps (3.3 m/s), which was used for a full scale catamaran by Hadler et al (1974), is worth considering for SWATHs. It is reported that this relative velocity or greater was required to induce a pressure of approximately 30 psi on the wet deck of USNS *Hayes* can result in slowdown or changing of course of the catamaran. In another source, an approximation formula to calculate threshold velocity is given by Sellars (1976). Here, threshold velocity is considered as the speed of a body's approach for which the free surface cannot move out of the way fast enough to avoid impact. Thus, when the scale of the water wave disturbance is defined to be the local beam, b, at the slamming point, an analytical expression for V_{Th} is found by equating wave phase speed and body relative velocity.

For an impulse wave, the phase speed C_w is :

$$C_w^2 = \frac{\sqrt{2}}{\pi} g \frac{b}{2} \tag{4.32}$$

The resultant speed of the approaching body is :

$$V_R^2 = V_n^2 + V_t^2 \tag{4.33}$$

where V_n and V_t are the relative velocity components, respectively, normal and tangential to the impact surface. When the resultant body speed, V_R, is equated to wave phase speed, the threshold velocity becomes :

$$V_{Th} = \sqrt{\frac{gb}{\sqrt{2}\pi} - V_t^2} \tag{4.34}$$

Considering the threshold velocity, the probability occurrence of 'actual slamming' can then be calculated by inserting the velocity term into eq. (4.27) as :

$$P_r\{\text{slam impact}\} = \exp\left\{-\frac{Z_{cx}^2}{2E_d} - \frac{V_{Th}^2}{2E_v}\right\} \tag{4.35}$$

From a design practice point of view it is very important to evaluate the largest (extreme value of) impact pressure a ship may encounter in a certain operating time and region. It is, therefore, suggested that this extreme value is applied as a design criteria, instead of the average or significant values, as in its operation a ship must be capable of withstanding such high impact loads which may induce failure on the bottom structure. The magnitude of extreme slamming pressure, with a probability of exceedance α throughout N_s slamming observation in a certain operation time T, can be predicted by the following equation from Ochi and Motter (1969,1973) :

$$\hat{p}_s(\alpha) = p_0 - \rho k E_v \ln\left\{1-(1-\alpha)^{1/N_s}\right\} \tag{4.36}$$

where p_0 is the threshold pressure given by :

$$p_0 = \tfrac{1}{2} \rho k V_{Th}^2 \tag{4.37}$$

To apply eq. (4.36) the designer must first define the small probability of

exceedance, α. For instance, if α is set to be 0.01 then the estimated extreme value has a 99 percent assurance of not being exceeded in that particular operating time. So the smaller the value of α the greater safety assurance for the ship.

4.3. SLAMMING EXPERIMENTS ON A SMALL SWATH MODEL

It has been pointed out by many researchers, e.g. Nagai and Chuang (1977), Ochi (1958) and Sellars (1976), that the experimental approach is extremely important, as well as the development of mathematical models, when studying slamming on seagoing vessels. The importance of the approach is highlighted for novel concepts of marine vehicles, such as SWATH, where specific information on the matter is very limited [Graham (1988), Meyerhoff et al (1988)]. Experimental investigation of slamming may cover the measurement of impact pressure in relation to the relative vertical velocity and/or the measurement of hull girder response to slamming. Only the former measurement is considered in more detail herein.

Experimental methods to measure impact pressure in a hydrodynamics laboratory can be classified into three different techniques. These are, drop tests on the two-dimensional models, which could be either blunt rigid bodies or stiffened plate structures, drop tests on the three-dimensional ship models in calm water and seakeeping tests on the three-dimensional models in waves. These three methods show the level of accuracy of the data obtained that can be expected to be applied on the real ship design. Sellars (1976) and Ochi and Motter (1973) concluded that the data drawn from a two-dimensional drop test in general gives relatively too high a magnitude of impact pressure compared with the data from a seakeeping test. This matter is possibly attributed to the velocity of airflow released from beneath the impact surface which is not aptly modelled in a two-dimensional drop test. From various observations it is well recognised that the entrapped air which accompanies slamming impact provides a cushioning effect on the impact surface, thus reducing the magnitude of pressure. For practical purposes a correction factor to the reduction of impact intensity should be introduced when using the drop test results suggested by Lewison and Maclean (1968) and Whitman and Pancione (1973). The cushioning effect induced by the entrapped air could be even higher for SWATH ship's wet deck slamming compared with their monohull counterparts, as the side struts on SWATHs might act as the side walls to increase the resistance to transverse airflow. It is necessary, therefore, to generate slamming impact data specifically for SWATH ships if the design load is to be properly estimated.

A model experiment to investigate slamming characteristics of SWATH ships was performed in parallel with development of the slamming simulation program and was conducted on a physical model of a SWATH vessel. A full description, including the

main particulars of the PVC constructed fishing SWATH model (see technical drawing in Fig. 4.5), which has been subjected to an extensive test programme on motions, resistance and wave loadings, can be found in Chapters 2 and 3. The model is not scaled for structural response, that is, the material of the model was not scaled to vibrate and resonate as the full scale ship does. At this stage, therefore, the experiment emphasis the investigation of pressure-velocity relationship in accordance with the slamming impacts on the underdeck structure.

4.3.1 Measurement of Relative Motions

The measurement of relative motions was conducted on a fishing SWATH model using seakeeping test techniques, as discussed in Chapter 2. Detailed procedures and instrumentations peculiar to the measurement of relative motions only will be mentioned in this section.

The relative motions of the SWATH model were measured at four different positions, designated as P(point)1, P2, P3 and P4, at the forward part of the model at the wet deck, as shown in Fig. 4.6. Selection of those locations was based on monohull experiences and on logical expectation that severe slamming on a marine vehicle will occur at the bow. The relative motion elevations were detected by means of capacitance wave probes located at those points. The wave probes which were fixed on the model followed the vertical motion of the model and detected the changing of submergence in water levels. Relative motion of each single location can then simply be derived by substracting these water elevations from the local deck clearance. Ideally the wave probes should be arranged in such a way that the relative motion elevation recorded represents the situation of perpendicular to both wave and cross-deck surfaces. Nevertheless, such an arrangement was very difficult because it should consider the angular movement of the model and the progressing movement of the water surface, which change with the elapsed time. To minimise the error arising from the relative elevation of the wave surface and the wet deck the wave probes, thought to be the best arrangement, were then mounted perpendicular to the underdeck plane.

The model was tested in head seas at four different forward speeds, that is, 0.5, 1.0, 1.5 and 2.0 m/s which correspond to the Froude number of some 0.13, 0.26, 0.39 and 0.52, respectively. Over 20 frequencies of regular waves in the range of 0.3Hz up to 1.4Hz with increments of 0.5Hz were generated for each forward speed. Shorter wave frequency intervals were generated at the critical (resonance) frequency region as visually observed. The undisturbed wave elevations were detected by using three wave probes mounted on the bridge at the far end of the towing tank close to the wave maker.

During the experiment data acquisition was received using a software package named LabView run on an Apple IIICi terminal which was mounted on the mobile carriage. The electronic signals from the instrumentation were collected through an amplifier convertor and then stored in a 40MByte built up hard disc in the form of ASCII code data file.

4.3.2 Measurement of Slamming Pressures

Two ways could be used to observe slamming impact on the wet deck of a SWATH model, namely, the point pressure measurement and panel pressure measurement. As the terms imply, the former is mainly directed towards the measurement of impact pressure at a discrete location (point) along the wet deck, whereas the latter is arranged to measure the integrated pressure over a larger portion area of the wet deck, described as follows.

4.3.2.1. Point Pressure Approach. As for relative vertical motion, the measurement of slamming pressure on the SWATH model was performed at four positions at the bow where more frequent large slamming was anticipated. A compact type of pressure transducer system consisting of an inner core where the pressure instrument is accommodated and an outer cylinder protector was mounted on each location by drilling a hole on the underdeck plate. The electronic signals picked up by the transducers were transferred to the storage via an amplifier in a similar manner as that described in Section 4.3.1.

From experience during the measurement of relative motion it was learned that slamming on the wet deck is likely to develop when the model is underway in the resonance frequency region. The regular waves used for this test were, therefore, concentrated in the resonance frequency region of the vertical motion of the SWATH model. To accumulate as much data as possible the test was then conducted in a manner to generate four or five different wave heights for every single wave frequency selected which would allow the increment of slamming pressure with respect to the relative velocity to be observed.

The increment of wave height in each prescribed frequency has to be selected accurately. In the earlier stage of the test when the model was run at a 0.55Hz and 3-volt wave (in excess of 10cms in amplitude) extreme slamming occurred and much green water overflowed onto the deck which caused damage on the aftermost transducer (transducer number 4). Because of this, and the shortage of supply on pressure transducers at the laboratory, the transducer for point 1 was used to replace the damaged one. Such a decision had been made as no substantial slamming could be

recorded, so far, at the foremost transducer. It was observed that to induce slamming on point 1 quite large pitching is required, which in some points is rather difficult to produce at the resonance region, as will be described later in the analysis of relative vertical motion. Comparatively small waves, on the other hand, simply could not produce significant slamming on the deck bottom as intended.

4.3.2.2. Panel Pressure Approach. While conducting the slamming tests by this latter approach, experiences from the previous tests had been gained. In this slamming impact measurement the pressure transducers located at the slope and flat portion of the wet deck were replaced by PVC panels size 70 x 100mm, as shown in Fig. 4.7. Further, each panel was equipped with a load cell, hence the measured impact quantity would be the integrated pressure over the panel area (i.e. impact force). The measurement of relative vertical velocities corresponding to impact forces imposed on the panel was performed using three wave probes attached on the deck bottom along the side of each panel, approximately at the centre and both edges of the panel. This made it possible to identify the maximum impact velocity on the panel which could be anywhere along its length, that is, by tracing the peak velocities from each wave probe.

The tests were done, having learned from the previous investigation, that is, on which particular wave frequencies the impact pressures were expected to persist. Similarly, different wave heights were generated to induce some level of impact severities on the panels. Figure 4.8a-b shows the SWATH-FV model subjected to a severe slamming impact in a regular head wave typical during the slamming tests.

4.3.3 Test Data Analysis and Results

During the experiment data acquisition was received using a software package named LabView run on an Apple IIICi terminal which was mounted on the mobile carriage. The electronic signals from the instrumentation were collected through an amplifier convertor and then stored in a 40MByte built up hard disc in the form of ASCII code data file. Such storage allows the data to be released to another computer network, such as VAX 11/730, for further test data analysis.

The data collected during the test has been automatically converted into the corresponding unit of any mode measured. This was made possible by inputing the calibration factors into the data acquisition software prior to the test. Hence, for further test data analysis, the magnitude of the response can be read directly from the record. Figure 4.9 shows a typical record data of relative vertical motions for all corresponding positions along the fore wet deck, whereas Fig. 4.10 presents a typical measured

impact pressure, together with the relative motion elevation recorded at the same local point.

The magnitude of relative vertical motion response is measured in relation to the amplitude (height) of the incident wave. In this analysis the average relative motion and wave amplitude were computed, and the response found to be the ratio of the two values. The results of the analysis are grouped, depending on the Froude number, for every local point in the form of non-dimensional relative vertical motion against non-dimensional wave encounter frequency, as shown in Figs. 4.11a-4.14d. The solid lines plotted on the graphs represent the interpolation fit of the scattered data points.

The trend of relative motion response is quite clear, as can be seen in those Figures, with two distinguished peaks over the lower frequency region. The exception is Fn=0.26 where only one peak appears. The first peak, which is mostly in the order of lower than 1.0, corresponds to the resonance of the pitch mode, while the second peak, which is more significant, i.e. in the order between 3.0 and 5.0, might be associated with the heave resonance (see motion responses presented in Chapter 2 or Appendix A). It is quite obvious that the magnitude of relative vertical motion is highly governed by the heave mode of motion which becomes dominant with increase of the forward speed.

The continuation of the curve beyond the non-dimensional frequency of 0.8 is uncertain. The response of relative motions in short waves (high frequencies) is almost approaching singular, which is due to the very small vertical motion of the model, hence only wave elevation contributes to the magnitude of relative motion. This is one reason why it may not be practical to carry out the measurement of slamming pressure in short waves. Even if very large amplitudes are generated, this may only result in the wave slapping on the wetdeck and not actually creating slamming as such.

No theoretical predictions of the relative vertical motion was available for comparison at the time of writing this thesis. Nevertheless, the program to predict SWATH motion exists in the Department, which should be enhanced to compute relative motions in future.

As a step in the analysis of slamming pressure it was the initial intention of this experimental study is to be able to provide a classical pressure-velocity correlation, as developed by Ochi and Motter (1973), pertinent to SWATH sectional forms in term of the correlation of slamming pressure and velocity as given in eq. (4.4). From this experiment the magnitude of impact pressure can be directly read from the record (see Fig. 4.10), while the impact velocity needs to be derived from the time history of the corresponding relative motion elevation. It is always very interesting to observe the phenomenon of slamming pressure from the record. As shown in Fig. 4.15, slamming

pressure rises abruptly, after the initial impact, from steady level to a maximum and then reduces steeply in a very short period, i.e. in a matter of milliseconds. Nevertheless, argument always arises about the significance of this high pressure in a very short period and in a very small location in determining the pressure load over a larger area applied to the design of bottom plating.

Relative velocity during slamming impact might be developed in the following manner, as described by Lloyd (1989). Assuming the relative motion elevation in the short period is to be approximated by a sinusoidal wave, see Fig. 4.16, in which its equation can be written as :

$$\zeta_r = \zeta_{r0} \sin\left(\omega_r t + \delta_r\right) \quad \text{(m)} \tag{4.38}$$

The relative motion at impact can then be calculated by :

$$-D_{ri} = \zeta_{r0} \sin \delta_r \quad \text{(m)} \tag{4.39}$$

so that

$$\delta_r = \sin^{-1}\left(\frac{-D_{ri}}{\zeta_{r0}}\right) \quad \text{(rads)} \tag{4.40}$$

The relative velocity can be obtained by differentiating eq. (4.38) as :

$$\dot{\zeta}_r = \omega_r \zeta_{r0} \cos\left(\omega_r t + \delta_r\right) \quad \text{(m/s)} \tag{4.41}$$

and the relative velocity at impact is given by setting t=0 as :

$$\dot{\zeta}_{ri} = \omega_r \zeta_{r0} \cos \delta_r = \omega_r \sqrt{\left(\zeta_{r0}^2 - D_{ri}^2\right)} \quad \text{(m/s)} \tag{4.42}$$

The results of the analysis on the measured data correlation between pressure and velocity can then be plotted, as shown in Figs. 4.17a-4.19c. Only data from three local points of observation is presented since the pressure transducer at local point 1 has been transferred to local point 4, as stated earlier. For convenience of comparison, the pressure-velocity data is given in both Imperial and SI units. The form factor (k) which is required in eq. (4.4) is obtained by plotting the pressure magnitudes against the squared relative velocity. Although the data scattering is quite large, the trend of increase in pressure with respect to the increasing of velocity is obvious. In fact the scattering of the present data is not as large as that produced by Graham (1988), which was also derived from a SWATH model test. It was claimed that the large scattering of pressure data in the latter case has brought about the uncertainty in measuring the

impact velocity, which adopts a different method from the one used in the present study. The measurement of slamming in irregular waves as conducted by Graham (1988) may add to such uncertainties, as opposed to the measurement in regular waves carried out in the present study.

The maximum k values in each local point, as given in Figs. 4.17c, 4.18c and 4.19c, are approximated from the average of one-tenth largest data points. This of course is only the first approximation which may need to be evaluated further by possibly taking the least square fit from all the scattering data. The largest k value is yielded at local point 2, i.e. about 32.0, and less for the two other positions, that is, 26.0 and 9.0 for local points 3 and 4 respectively. The maximum k of 32.0 is significantly lower than that suggested by Graham (1988), which is approximately 70.0. This is almost certainly due to scaling problems arising from the size of the pressure transducer.

The results of measurement by using load-cell equipped panels is now described. First of all, considering the time history of slamming impact as shown in Fig. 4.20, the panel measurement yields a typically longer period of time. This type of persistence is similar to the slamming force on the bow flare of monohull ships, e.g. as reported by Yamamoto et al (1985). It is believed that such an integrated pressure applied to a larger area of the bottom plating would induce a more serious damage than a much larger pressure applied only in a much smaller area.

The average impact pressure over each panel was further derived by dividing the measured maximum force with the area of the panel. The results of the test data analysis are given in Figs. 4.21 and 4.22, for panel A and panel B, respectively. As is seen, the scatter of the impact pressure data is not as large as the point pressure measurements, which can be explained as follows. In the point pressure measurement it is possible that the maximum registered value was not the actual peak pressure. This is so because the instrument has only a small surface area, hence it is quite likely that the peak pressure may occur at a small distance from the location of transducer, but the fluctuation of pressure was still detected by the transducer. For the panel measurement, on the other hand, any maximum registered pressure was almost definitely the peak value because the panel covered a sufficiently large amount of area of the deck bottom. The peak pressure which occurred anywhere along the length of the panel would be detected.

4.4. SOME METHODS FOR ESTIMATING DESIGN SLAMMING PRESSURES

In this section some methods are presented to assess maximum (design) pressure due to slamming available in the open literature. Some of these methods, which were not necessarily developed specifically for SWATH ships, are explored with the particular aim of obtaining an alternative approach which may be applicable for

SWATHs. Existing slamming pressure data are also included to provide a reference for the evaluation.

4.4.1 Existing Design Slamming Pressure Data

Despite the importance of slamming pressure as a secondary load for designing the wetdeck scantling of SWATH ships, such information is not widely known. This is due to the limited slamming tests which have been done previously, as well as the lack of measurement of full scale slamming impact carried out on the small number of SWATHs which are now in operation. Only four sources of information are available to date, as described below.

For the design of the wetdeck scantlings for the SSP *Kaimalino* ($\Delta \approx 220$ tonnes) a gross loading of 14 psi (97 kPa) was selected by Hightower et al (1985). Later on this value was found to be inadequate to resist a severe slam when the vessel was operated in a relatively rough sea condition, which resulted in damage to the framing at the port prow. It is claimed that if the deck clearance was increased to be larger than the initial 4 feet such a severe slam could be safely avoided.

Sikora and Dinsenbacher (1988, 1990) reported that the lifetime slamming pressures p_S which is used in designing the wetdeck plating of the T-AGOS ($\Delta \approx 3500$ tonnes) are 55 psi (380 kPa), 49 psi (338 kPa), 63 psi (434 kPa) and 20 psi (138 kPa) for the flat panel at the forward slope, forward flat, midship and at the stern, respectively. These slamming pressures are measured on the flat panel size of 2x4 feet (0.6x1.2-m approximately, and $Ap=0.72m^2$). It is also shown by Sikora and Dinsenbacher (1988) that slamming pressure of 30 to 90 psi (207 to 620 kPa) on a plate panel size of 8x20 feet would be typical for 2000 to 6000-tonne SWATH ships.

The design slamming loads selected for the RMI's SWATH demonstrator *Halcyon* ($\Delta \approx 60$tonnes) p_S are 20 psi (138 kPa) and 5 psi (35 kPa) and were used in the design of wet deck plating at the forward and aft of the knuckle, respectively [Luedeke and Montague (1984), Luedeke et al (1985)].

The only full scale measurement of slamming pressure which can be found in the open literature has been conducted during the trials of a 75-tonne SWATH *Frederick G. Creed* which was built by SWATH Oceans System. The trials of this SWATH vessel were organised by collaboration of the Defence Research Establishment Atlantic (DREA), Institute of Marine Dynamics (IMD) and the Canadian Department of Fisheries and Ocean. All of the trials took place in the North Atlantic off the coast of Nova Scotia during a 10-day period. In addition to the measurement of slamming load,

motion, and structural response towards wave load at various ship headings and speed, have also been made by Pegg et al (1990).

From the trial data analysis the maximum slamming pressure of 206 kPa (30 psi) recorded on the haunch region near the bow was measured when the vessel was underway in a bow oblique wave. On the wet deck portion, maximum impact pressure of 102 kPa (15 psi) was measured slightly aft of amidship at the centre line. Only as high as 21 kPa (3 psi) slamming pressure has been recorded at the bow portion of the wet deck. This low impact on the bow region was apparently brought about by a fairly large trim by stern. An interesting feature of the *Creed* is the configuration of anti slamming strakes at the intersection of lower struts and the haunches. The strakes are undoubtedly very effective in preventing severe impact occurring on the wet deck. It is claimed that slamming pressure in excess of 210 kPa (30.5 psi) have been experienced on the strakes.

4.4.2 Empirical Formula for Design Slamming Pressures

4.4.2.1 Sellars Method. A rigorous analysis on the existing impact load data from various model tests was done by Sellars (1976) which resulted in a single equation of pressure load. The solution of impact pressure was based on consideration of the impact of a liquid-gas mixture on a flat elastic structure. The inclusion of liquid-gas mixture parameters allows effects of entrapped air in, probably, reducing the maximum pressure. The pressure equation is :

$$p_2 = \frac{p_1}{2}\left[\left(1+C\frac{V_0}{V_1}-\frac{C}{\delta_v}\right)+\sqrt{\left(1+C\frac{V_0}{V_1}-\frac{C}{\delta_v}\right)^2+\frac{4C}{\delta_v}}\right] \quad \text{(psi)} \qquad (4.43)$$

where : p_2 = absolute impact pressure
p_1 = absolute ambient pressure
V_0 = relative velocity at impact
V_1 = $p_1/\rho_0 C_0$
ρ_0 = mass density for pure liquid
C_0 = speed of sound for pure liquid
C = structure impedance ratio
δ_v = liquid-air mixture volumetric impedance ratio (=0.0236).

In the absence of information on relative impact velocity, the value of V_0 can be approximated by considering the maximum vertical (heave) velocity ($\dot{Z}_T$) of the craft at the location in question and the design significant wave height (H_s) by using the relationship below :

$$V_0 = \dot{Z}_T + \omega_0 \frac{H_s}{2} \quad \text{(fps)} \tag{4.44}$$

where : ω_0 = average frequency in rad/sec

The structural impedance ratio C is defined as the ratio of the structural impedance to the fluid impedance, and can be calculated by taking into account the deflecting wave speed C_1. The factor C_1 is obtained by :

$$\frac{C_1}{C_L} = \frac{1}{\sqrt{12\,\varepsilon}}\left[1 + \frac{1}{A^2}\right] \quad \text{(fps)} \tag{4.45}$$

where : A = panel aspect ratio (l/b)
l = panel length
b = panel width
C_L = speed of sound in solid (fps)
ε = panel parameter ($b/\pi h$)
h = plate thickness.

Hence the structural impedance ratio is found as :

$$C = \left(\frac{C_1}{C_L}\right)\left(\frac{\rho_1\, C_L}{\rho_0\, C_0}\right)\frac{1}{\alpha} \tag{4.46}$$

where impact area parameter α=1.0 might be taken for conservative estimate of the peak pressure. The rest of the parameters and coefficients applied in deriving the impact load using the above formulation are fully given by Sellars (1976).

Having determined the pressure ratio, the peak impact pressure was applied to the plate panels as quasi static load using the following formulation :

$$p_s = 14.7\left(\frac{p_2}{p_1} - 1\right) \quad \text{(psi)} \tag{4.47}$$

4.4.2.2 Allen and Jones Method. The study on slamming pressure load by Allen and Jones (1978) is based on a theoretical approach combined with experimental data. This has resulted in a simple formulation which allows structural design-limit pressure values and distributions to be predicted on a number of advanced marine craft. It is further claimed that the method can be applied even when no extensive knowledge of vehicle motion is to hand, thus it can be conveniently used in the early design stage.

The design limit pressure for SES, ACV wet deck and SWATH flat cross structure can be determined by first calculating the average pressure over the impact reference area as :

$$\bar{p} = \frac{2240\, N_Z\, \Delta}{A_R} = \frac{N_Z\, W_L}{A_R} \quad \text{(psi)} \tag{4.48}$$

where : N_Z = impact load factor or maximum amplitude vertical acceleration
Δ = full load displacement (long tons)
W_L = gross weight of the vehicle (lbs)
A_R = impact reference area (in^2) which can be determined by :

$$A_R = \frac{12.6\, W_L^{2/3}}{\left(1 + r_x^2\right)^{2/3}} \quad \text{(in2)} \tag{4.49}$$

where r_x is the ratio of the distance from the LCG to the foremost point of impact and the pitch radius of gyration.

Next, the maximum pressure over the impact pressure area (p_m) can be calculated by considering the ratio of maximum pressure and the design pressure (p_s) as follows :

$$p_m = \frac{\bar{p}}{p_s / p_m \text{ at } A_d / A_R = 1.0} \quad \text{(psi)} \tag{4.50}$$

which is found to be :

$$p_m = \frac{\bar{p}}{0.09} \quad \text{(psi) for unprotected structure, or}$$

$$p_m = \frac{\bar{p}}{0.18} \quad \text{(psi) for structure behind seals.}$$

The structural design-limit pressure (p_s), that is, equivalent uniform static design pressure, is then determined by substituting eq. (4.49) into eq. (4.50) and including

pressure correction factors as :

$$p_s = C\,F\,K_D\,N_Z\,W_L^{1/3}\,(1+r_X^2)^{2/3} \quad \text{(psi)} \tag{4.51}$$

where : C = 0.88 for unprotected structures
= 0.44 for structure behind seals
F = longitudinal pressure distribution factor
K_D = pressure reduction coefficient.

Allen and Jones (1978) also provide a simpler approximation of A_R, such that the estimation of design pressure can be made without considering the radius gyration value. The equation for A_R takes the form :

$$A_R = 4\%\ A_U \quad \text{(in 2)} \tag{4.52}$$

where : A_U = underbody area (in^2)
= $L_U x B_U$
L_U = length of underbody structure or cross structure for SWATH (in)
B_U = breadth of underbody structure (in)

4.4.2.3 Det norske Veritas (DnV). The design slamming pressure on flat cross structure is suggested by Det norske Veritas (1991) to be taken as the greater of :

$$p_s = 2.6\,k_t \left(\frac{\Delta}{A}\right)^{0.3} a_{cg} \left(1 - \frac{H_C}{0.07L}\right) \quad \text{(kPa)} \tag{4.53}$$

and

$$p_s = 125 + \frac{L}{2.6} \quad \text{(kPa)} \tag{4.54}$$

where : k_t = longitudinal pressure distribution factor
Δ = fully loaded displacement (tonnes)
A = design load area for element considered (m^2)
= 2.5 s^2 (for plating) and not to be less than $0.002\Delta/T$
s = load factor
T = service draught (m)
a_{cg} = design vertical acceleration at craft's centre of gravity
= varies between $0.2Vg_o/\sqrt{L}$ up to $0.8Vg_o/\sqrt{L}$ depending on craft type

H_c= vertical distance from waterline to load point (m)
L = ship length (m)
g_o = acceleration of gravity ($9.81 m/s^2$)

4.4.2.4 Lloyd's Register (LR). The formulations to estimate the design slamming pressure on the underside of the cross-deck structure of catamaran type vessels as given by Lloyd's Register (1990) are as follows :

For $0.25L_s \geq x_b > 0$

$$p_s = 11(\Psi - 2x_b / L_s)\sqrt{L_s} \quad \text{(kPa)} \tag{4.55}$$

For $0.5L_s \geq x_b > 0.25L_s$

$$p_s = 11(2\Psi - 1)(1 - 2x_b / L_s)\sqrt{L_s} \quad \text{(kPa)} \tag{4.56}$$

Aft of midship

$$p_s = 0 \tag{4.57}$$

where : L_s = scantling length (m)
x_b = the distance aft from the forward end of the deepest static load waterline to the point considered, measured on the waterline in (m); if the point considered is forward of the forward end of the deepest static load waterline, x_b is to be taken as 0
$H_{1/3}$ = design significant wave height (m)
Ψ = 2 where $G_A \leq H_{1/3}$
= 1 where $G_A \geq 1.75H_{1/3}$
= $e^{1.6-0.9\varepsilon}$ where $H_{1/3} < G_A < 1.75H_{1/3}$
ε = $H_{1/3}/G_A$
G_A = air gap at the point considered (m)

4.4.2.5 American Bureau of Shipping (ABS). The prediction of maximum wave impact load on the wet deck of SWATH proposed by the American Bureau of Shipping (1990) adopts the formulation developed by Allen and Jones (1978). The formulation applied is :

$$p_{max} = \frac{N_Z \times 2240 \times \Delta}{0.09 \times A_R} \quad \text{(psi)} \tag{4.58}$$

where : N_Z = acceleration due to impact or impact load factor
Δ = limiting displacement for strength (long tons)

A_R = reference area (in^2)
= 0.06 x L_{cr} x B
L_{cr} = length of cross structure (in)
B = total ship breadth, from shell to shell (in).

ABS gives the reference area formulation as a modification of eq. (4.52) by applying a safety factor of 1.5. The design pressure due to slamming for deck bottom plating design is then obtained by applying correction factors to eq. (4.58) as :

$$p_s = F_L \; K_D \; p_{max} \quad \text{(psi)} \tag{4.59}$$

where : F_L = longitudinal pressure distribution factor
K_D = pressure reduction coefficient.

The omission of factor C in eq. (4.59), compared to eq. (4.51), is questionable. Probably it is intended to be rather conservative, i.e. to increase the correction factor from C=0.88 to C=1.0.

4.4.2.6 Loscombe's Algorithm. A simple algorithm to predict the underdeck design pressure at the early design stage of SWATHs has been developed by Loscombe (1990) based on a parametric study using the methods by Sellars (1976) and Allen and Jones (1978). The algorithm takes the form :

$$p_s = C \, K(\alpha) \, K_A \, \Delta^a \left(\frac{H_s}{\nabla^{1/3}} \right)^b \quad \text{(kPa)} \tag{4.60}$$

where : C = constant as function of SWATH form parameter and speed
= 70 or 190 for zero speed or 20 knots, respectively
$K(\alpha)$ = the risk factor term
= 1.0 or 1.5 for the risk factor (α) 1.0 or 0.01, respectively
K_A = load correction factor for panels area other than $0.375 m^2$

$$K_A = \frac{2.03 + \log(\nabla^{2/3}) - \log(A_D)}{2.45 + \log(\nabla^{2/3})} \tag{4.61}$$

A_D = area of panel being designed (m^2)
Δ (∇) = displacement in tonnes (m^3)
H_s = the design significant wave height (m)
a = 0.3
b = 1.07

4.4.2.7 Graham's Approach. In determining the magnitude of impact load on the cross-deck bottom of SWATHs Graham (1988) adopts the pressure-velocity formulation as given in eq. (4.4). A maximum form factor value (k) of 70, which might be found to be a conservative estimate, has been suggested for SWATH type vessels. The form factor given was derived from an experiment on a 5.5 metre long radio-controlled SWATH model which took place at Bedford Basin in Canada.

For design purposes, a statistical approach can be used to obtain the extreme value of design slamming pressure as :

$$p_{ext} = \rho\, k_{max}\, m_2 \ln\left[\frac{3600\, T \exp(-Z_c^2 / 2m_0)}{2\pi\alpha}\sqrt{\frac{m_2}{m_0}}\right] \quad \text{(kPa)} \qquad (4.62)$$

where : T = ship operation time (hours)
Z_c = local deck clearance (m)
m_0 = RMS of local relative motion (m^2)
m_2 = RMS of local relative velocity (m^2/s^2)
α = risk factor
= 1.0 for the most probable occurrence
= 0.01 for the probability of exceedance of 0.99.

4.5. SLAMMING CHARACTERISTICS OF A NOTIONAL SWATH - A CASE STUDY

Use of experimental data to evaluate the slamming characteristics of a full scale SWATH is demonstrated. The evaluation is made on a notional 2500-tonne SWATH-FV which is scaled up from the model. The main particulars of this 2500-tonne SWATH-FV are as listed in Table 2.4.

Slamming characteristics, comprising probability of slamming occurrence and the extreme slamming pressure in a typical 20-hours operation, are investigated by adopting the short-term spectral analysis method. Operational area to be selected, which is arbitrary and subject to the availability of the wave data, is around Orkney Island in the North of Scotland. The wave data for this area, as given in Tables 4.1a-b, has been collected at the designated Stations JS01 and JS02 located at (59.92°N, 2.29°W) and (59.92°N, 0.91°W), respectively are presented by Chen and Mavrakis (1988). Two wave spectral formulations are used for this purpose, namely, Bretschneider two-parameter spectra and JONSWAP formulation. A simple computer program SPECTRA

has been written on the VAX Cluster to accommodate the analysis using both formulations.

The Bretschneider two-parameter spectra takes the following form :

$$S(\omega) = 487.3 \frac{H_s^2}{T_m^4 \omega^5} \exp\left(\frac{-1949}{T_m^4 \omega^4}\right) \quad \text{(m2-s)} \tag{4.63}$$

where : $S(\omega)$= spectral density (m^2-sec)
H_s = significant wave height (m)
T_m = modal period (sec)
= $1.296T_a = 1.41\ T_z$
T_a = average period (sec)
T_z = mean zero up crossing period (sec)
ω = wave frequency (rad/sec).

The JONSWAP spectral formulation is a modification of the two-parameter spectra above specifically for the North Sea region, by including the peakedness correction parameter. The modified spectral form is written as :

$$S(\omega) = 0.658\ C\left\{ 487.3 \frac{H_s^2}{T_m^4 \omega^5} \exp\left(\frac{-1949}{T_m^4 \omega^4}\right)\right\} \quad \text{(m2-s)} \tag{4.64}$$

where :

$$C = 3.3^{\exp\left[\frac{-1}{2\gamma^2}\left(\frac{\omega T_m}{2\pi} - 1\right)^2\right]} \tag{4.65}$$

γ = 0.07 for $\omega < 2\pi/T_m$
γ = 0.09 for $\omega > 2\pi/T_m$

4.5.1 Probability of Slamming Occurrence

To estimate the probability of slamming occurrence in a given period of operation, information on the relative vertical motion, that is, the response amplitude operator, is required. Information on the deck clearance (Z_c) for a given location along the wet deck and the threshold velocity (V_{th}), if it is available, is then used to predict slamming characteristic of a SWATH statistically using the formulation developed by Ochi (1964) as described in Section 4.2.3.

There is no data available, however, which considers the threshold velocity for SWATH. Nevertheless, for a first approximation V_{th} of about 10.8 fps (3.3m/s) obtained from a full scale measurement on a catamaran research vessel USNS *Hayes* by Hadler et al (1974) might be adopted. To be conservative, then the second term in eq. (4.35) may be omitted leaving the deck clearance term to determine the probability of slamming. Having determined the probability of slamming, the amount of slamming to be expected in a particular period of observation, T, can be calculated by eq. (4.31).

In this study computation was conducted to yield the slamming occurrence which might be experienced by the 2500T SWATH during operations in the area of stations JS01 and JS02 as mentioned above. Evaluation was made at the local point 2 of the wetdeck where the deck clearance is about 5.5m, and at the largest forward speed (Fn=0.52) in which slamming is expected to be most severe. The threshold velocity of 3.0m/s is considered, rather than 3.3m/s as for the USNS catamaran *Hayes*. The selected V_{th} would accordingly give a threshold impact pressure of some 80 kPa if the form factor k of 9.0 from panel pressure measurement corresponding to the observed local point 2 is applied. There is no firm justification whether such a pressure value is acceptable from a structural point of view or not. Nevertheless, a pressure value of 80 kPa can be considered as acceptably mild when compared to the threshold pressure of around 174 kPa as applied by Conolly (1974) for the evaluation of monohull ships. Further, effects of the static change on the deck clearance due to sinkage and static trim inherent at high speed to be considered. Two different slamming criteria are then applied in observing the down time operation attributable to slamming severity. The first criteria, as suggested by Aertssen (1968) and Olson (1978), limits the slamming acceptability as 4 (four) slams per 100 pitch oscillations of the vessel. The second criteria, as applied by Conolly (1974), reveals an acceptance of one slam per minute of operation.

From the analysis, the slamming occurrence rates (number of slamming per second) for SWATH-FV operation in region JS01 are found, e.g. as listed in Table 4.2. Both spectral analysis using the Bretschneider and JONSWAP formulations were performed, and the frequency response function (RAO) of relative motion from the experiment at Fn=0.52 is utilised. The static trim and sinkage corrections are taken from the previous resistance test, as shown in Fig. 4.23a-b. Using these corrections, the considered effective deck clearance is reduced from the initially 5.5m down to 3.7m. Using the first criterion, and referring to the joint probability of significant wave height and modal period, the down time operation of the SWATH-FV in region JS01 could be expected to be as much as five percent (5%), as shown in Fig. 4.24a. It is also interesting to observe the down time rate for conditions other than that given in this Figure.

As shown in Figs. 4.24b-e, different effects of parameters may be evaluated as follows. For the first condition (see Fig. 4.24b), evaluation was made without considering the threshold velocity, hence the probability of slamming is derived by taking into account the corrected deck clearance term only. In this circumstance the down time rate has increased significantly to about 20.5%, either analysed on the basis of JONSWAP or Bretschneider spectrum. In the second circumstance, as shown in Fig. 4.24c, initial (uncorrected) deck clearance is considered, and gives a down time of some 5%. Nevertheless, this evaluation is unrealistic, as static trim and sinkage are always present at high speeds. A similar account was found on monohulls, as forwarded by van Sluijs (1974). Using the second criterion (see Fig. 4.24d) for the first condition, the down time is found to differ quite significantly when analysed by the Bretschneider and JONSWAP spectra, that is some 19.9% compared to 5.15%, respectively. The operation of SWATH-FV in the region JS02 (Fig. 4.24e), for the first condition and the first criteria, is expected to experience a down time of some 14%.

It is clear from the above comparison that the modal period significantly affects the rate of slamming occurrence. In some cases spectral formulations could give quite a large difference in the result, hence suggest the spectral formulation to be properly selected. The difference is significant when only the deck clearance is considered and if the threshold velocity is taken into account. The rate of operability in different operational areas differs solely due to the joint probability of wave occurrence, apart from those aspects as stated previously.

4.5.2 Extreme Slamming Pressure

The extreme slamming pressures are computed for local points 2, 3 and 4 at the wet deck of the 2500T SWATH by using eq. (4.62). The form factors derived from experimental data of point pressure measurements are used for the corresponding locations. The two extreme pressures based on the risk parameter α=1 (most probable extreme value) and α=0.01 (extreme value with confidence of 99%) are derived similarly for the operational areas of JS01 and JS02. The computational results are presented in Figs. 4.25a-4.26c. These results are calculated at the largest value of significant wave height for each group of modal period (see Table 4.1a-b) using both spectral formulations.

As observed from those Figures, the prediction based on the two-parameter spectra generally provides higher extreme values than predicted by the JONSWAP formulation. At location JS01 the highest slamming pressure (α=0.01) happens to be at local point 2, which is on the ramp, and approaches 4500 kPa. Further, this highest

pressure is predicted when the significant wave height of approximately 13.0 metres is imposed, whereas in larger significant wave height the pressure attenuates. The same argument is given, that is, the extreme value is largely related to the magnitude of modal period. At location JS02 the largest pressure predicted is even more severe than at JS01, i.e. approaching 10,000 kPa at a significant wave height H_s=11.6m. The calculation has also been carried out in the case of the most probable wave at the two locations. At station JS01 the most probable wave is H_s=3.05m and T_m=9.87 with the joint probability of occurrence close to 17.5%. For this condition the extreme slamming pressure based on risk parameter α=1.0 calculated by two-parameter and JONSWAP spectral forms is about 387 kPa and 168 kPa, respectively. For station JS02 where the most probable wave (17% of occurrence) is H_s=3.05m and T_m=9.07, the extreme slamming pressure is accordingly found to be about 572 kPa and 270 kPa. These values are somewhat more reasonable for design pressure load, for example, when compared to the design pressure for T-AGOS (3500T).

Referring to the slamming characteristics of the 2500-tonne SWATH-FV it can be concluded that the predicted slamming occurrence, as well as the extreme slamming pressure which might be experienced by the vessel during its operation, depend almost entirely (not to mention the seakeeping quality of the vessel) on the environmental condition and the spectral formulation to be applied. It is, therefore, necessary for SWATH designers to select the appropriate wave data and spectral formulation for the analysis so that a correct prediction can be achieved.

4.6. COMPARISON OF ESTIMATED DESIGN SLAMMING PRESSURES

Calculation of design slamming pressure has been made on the *Halcyon* (60 tonnes) and the notional 2500-tonne SWATH-FV using several formulations, as described in Section 4.4, in order to evaluate the applicability of these methods for SWATHs. The observation of these methods for only two vessels may be disputed. Nevertheless limited information on any other SWATHs has restricted wider evaluation to be conducted at present. It is expected, however, that evaluation on both vessels could represent the trend of design slamming pressure for small and large SWATHs. The results of the calculations carried out on these vessels are as presented in Table 4.3 and Fig. 4.27. Slamming pressure data from other sources are also included in the table and graph so that the validity of the comparison might be attained.

For small SWATHs (the *Halcyon*), with one exception the formulations from the three classification societies give reasonably close answers with the data provided by the designer. Loscombe's algorithm, as can be seen, gives a substantially larger

prediction, in the order of 2 or 3 times, than the other. On the 2500T SWATH-FV, a design slamming pressure of some 1800 kPa is obtained when referring to the operation in the JS01 region and the computation based on the JONSWAP spectrum using the risk factor α=1.0. Such a value is as large as that given by Graham (1988) for a 5000-tonne SWATH. Nevertheless, these design pressures are derived by accounting for slamming form factors measured at a discrete location (point pressure). Using the largest form factor developed from the panel pressure measurement, the design pressure value for the SWATH-FV is found to reduce to only 518 kPa. This amount is more reasonable to be adopted in design consideration.

The methods by Allen and Jones (1978) and ABS (1990), as expected, do not have substantial discrepancy, and both are much lower than the previous result developed using the point pressure form factor, but relatively close to that obtained using the panel form parameter. The results from DnV (1991) and LR (1990) are even lower, and only slightly higher than the prediction on the *Halcyon*. This might be because the formulations by DnV and LR are intended for the design pressure of fast vessels which, in general, are smaller craft. The highest value overall is the one predicted using Sellars (1976) method, i.e. in the order of higher than 6000 kPa.

Comparison of design pressure for a number of SWATHs, as shown in Fig. 4.27, may be evaluated as follows. The compiled data shows a substantial scatter, hence could not be easily identified as to the trend of the increase in design value in relation to the increase in ship displacement. This is particularly demonstrated by the design of a series of Patrol Vessels from the US Coast Guard as presented by Holcomb and Allen (1983). In their study, patrol vessels with sizes ranging from 125 tonnes up to 1270 tonnes were investigated. Interestingly, the same value of design slamming pressure amounts of 414 kPa was adopted for those vessels. Secondly, SWATH designs by Aronne et al (1974) also show the use of a fixed design pressure of 690 kPa (100 psi) for three different ships, i.e. Ship A, Ship B and Ship C with displacements of, respectively, 4000, 4500 and 5250 tonnes. These examples suggest that design pressure might not necessarily change with respect to the variation of displacements.

Based on the limited pressure data that has been accumulated so far, a crude correlation was made by a statistical regression analysis. A three step analysis was performed to those data, that is, by considering all the data available then omitting the value developed from Sellars formulation, and finally omitting all unreasonable pressure magnitudes. The pressure-displacement correlation for these three conditions can then be expressed in the equations belows :

$$p_{s1} = 258 + 0.21\Delta \quad (4.66a)$$

$$p_{s2} = 175 + 0.15\Delta \quad (4.66b)$$

$$p_{s3} = 166 + 0.10\Delta \quad (4.66c)$$

The last expression is probably the most reasonable for obtaining the pressure design value for SWATHs, and hence might be used in the early design stage. To be consistent with the pressure data available, nevertheless, the use of this equation should be limited for vessel displacement up to 6000 tonnes. Beyond this size the design pressure value is rather uncertain by virtue of the lack of information. There is a possibility that lower pressure magnitudes are acceptable for larger SWATHs. For instance, as forwarded by Pieroth and Lamb (1983) a design pressure of some 350 kPa may be adopted for a SWATH of approximately 15000 tonnes. Arguments can be advanced which suggest that for larger vessels slamming pressure should reduce with increasing displacement. The equation also ignore forward speed which is surely important.

4.7. DISCUSSION

A preliminary study of SWATH slamming characteristics has been addressed in the previous sections. The study develops gradually from the review of existing publications related to ship slamming in general, and converges to the slamming problems on SWATH vessels. Analytical solution to the problem was further forwarded, in which time-domain simulation format is preferred for the accuracy of the slamming prediction. Experimental investigation was then conducted to characterise SWATH slamming in terms of relative motion and impact pressure measurements. The experimental data obtained was finally used in the evaluation of slamming behaviour of a notional full scale SWATH.

Further experimental study related to SWATH slamming may be directed to the observation of surface wave swelling up which takes place before initial impact. Such a phenomenon is known to give rise in the severity of slamming impact, hence limiting the operational capability of monohull ships. This account might apply also to SWATH ships and ought to be accounted for in the analytical assessment. Other issues which need to be pursued in future are on the aspects of slamming in structural design and further slamming investigation by way of drop test technique, as shown as follows.

4.7.1. Slamming Aspects of SWATH Structural Design

A consideration of slamming impact pressures in structural design may be divided into two categories, namely, the hull girder response and the local structural response to

slamming. The former is due to the fact that when a ship encounters rough seas and slamming occurs, the accompanying impact exerted on the hull bottom may excite a vibration on the hull girder. Such a vibration is known as whipping, and the vibratory stress created is called whipping stress. At the design stage, it is very important to evaluate the combined effect of wave induced (hull bending) and whipping stresses.

A particular interest of this aspect is to analyse the magnitude of whipping stress that is superimposed on the peak value of wave induced stress. To estimate the contribution of the impact to overall hull loadings the total impact force needs first to be calculated based on time histories of the impact pressure distribution. The study of this combined effect has been well established for monohull ships as reported by Nagai and Chuang (1977), Ochi and Motter (1973), Mansour and d'Oliveira (1975) and Evans (1982). On the other hand, as stated by Meyerhoff et al (1988), there has been no available method in the open literature to predict such a combined effect on SWATH ships. Nevertheless, a procedure to estimate slamming force as reported by Giannotti (1975) could be used as a preliminary study. An alternative approach, based on the momentum exchange as developed by Kaplan (1987) for SES, could be considered for application to SWATHs.

On local structural response; the initial slamming at a certain level generates a large pressures which can severely damage local structures. Such a structure in SWATHs is the deck bottom, mainly at the forward portion. To design the deck bottom structure it is first necessary to define the design pressure, that is, a representative value of uniform pressure which will result in approximately the same deformation and same maximum stress as produced by the actual peak loading on the structure.

A method of deriving this representative average (design) pressure from the peak slamming pressure calculated in the mathematical model is fully explained, e.g. by Giannotti (1975). The derived design pressure can then be applied as a uniform quasi-static load on the deck bottom structure. This reasoning is also found from the stress analysis by Nagai and Chuang (1977) and Ochi and Motter (1973), that is, because of the hydroelastic interaction between the impact surface and the fluid during slamming. This shows that the problem is usually quasi-static in nature in which the dynamic load factor is within the range of, or slightly beyond, unity. Accordingly, in most cases the dynamic slamming load can be considered as a load having the same dynamic peak load in magnitude applied quasi-statically to the deck bottom.

Having calculated the design pressure, the deck plating and stringer geometry can be determined as a panel bounded by adjacent frames and longitudinal stringers. For panels whose length is greater than two or three times the width, the end supports at the frames are of little influence. As a consequence, plate thickness is determined by investigating a thin strip of skin of unit width between the longitudinal stringers and

considering this to be a fixed ended beam [Drummond et al (1976)]. By assuming a safety factor of 1.5, based on the tensile yield strength σ_y of the material, plate thickness, t_p, can be determined from the bending moment and section modulus relationship as :

$$t_p = b\sqrt{\frac{1.5\, p_d}{2\,\sigma_y}} \tag{4.67}$$

where b is the stringer spacing, and p_d is the equivalent uniform design pressure.

The stringer is designed by assuming the ends are fixed at each frame and the distributed load is equal to the impact pressure acting over the panel area. Stringer bending moment, M_s, and required section modulus for a factor of safety of 1.5 are determined as :

$$M_s = \frac{p_d\, S_F^2\, b}{12} \tag{4.68}$$

and

$$Z = \frac{1.5\, M_s}{\sigma_y} \tag{4.69}$$

where S_F is the frame spacing. Faulkner (1975a) introduced a correction to the b parameter in eq. (4.68) for grillages under uniform pressure, hence the bending moment equation is rewritten as :

$$M_s = \frac{p_d\, S_F^2\, b\left\{1 - b/2S_F\right\}}{12} \tag{4.70}$$

The plate is assumed to effectively contribute to the bending and longitudinal strength of the section by means of an effective breadth and width, b_e, as given by MacGregor (1989) and Drummond et al (1976), respectively can be written as :

$$b_e = b\left\{0.333\,(S_F / b)^{0.6667}\right\} \tag{4.71}$$

or

$$b_e = 1.7\, t_p\sqrt{\frac{1.5\, E}{\sigma_y}} \tag{4.72}$$

Eventhough Faulkner (1975b) shows some different expressions to these effective breadth and width for grillage designs, and should be considered for comparisons.

A study of SWATH T-AGOS 19 by Covich (1986, 1987) yielded the following proportions for wet deck 'angle' web height (h_w) and thickness (t_w), and flange breadth (b_F) and thickness (t_F) for steel :

$$t_w = h_w/14$$
$$b_F = h_w/1.75$$
$$t_F = b_F/8$$

Whereas the study on hydrofoil ships by Drummond et al (1976) yielded the proportions of the steel bottom panels as follows :

$$t_w = h_w/20$$
$$b_F = h_w/1.5$$
$$t_F = b_F/11$$

4.7.2. Further SWATH Slamming Investigations - Drop Tests

Within the Integrated SWATH Structural Programme, the Department has planned a further study on SWATH slamming by way of drop test model. The main consideration in conducting a drop test is to clarify the nature of the slamming impact which it has not been possible to be investigated by seakeeping tests. Such observations will involve identification of impact pressure distribution and the effects of impact angle on the severity of slamming pressure. In addition, the study is also intended to identify certain structural responses induced by slamming impact. For this purpose a literature survey has been carried out and the design of the drop test model was subsequently performed, as reported in Appendices C and D, respectively.

The model was designed so that a wide range of impact angles can be tested. A number of pressure transducers are mounted on the model at various locations over the bottom plating. The structural responses are measured by using strain gauges attached to the bottom stiffener inside the model. One model will be equipped with haunches to simulate the fluid flows underneath the SWATH's wet deck during slamming. The fabrication of the steel model has been accomplished, and a preliminary drop test was recently performed. The test was unsuccessful, because of initial instrumentation fault. They are being checked and further tests have been scheduled in the near future.

4.8. CONCLUSIONS

A review on the theoretical and experimental methods to predict slamming on marine vehicles has been reported in order to study this phenomenon on SWATH type ships. An analytical approach was then formulated which suggests the preference for time-domain simulation in view of its greater accuracy in slamming prediction. The

detailed study of SWATH slamming by the seakeeping technique was further advanced.

A small SWATH model was used in the present study. SWATH slamming characteristics were investigated by measurement of relative motions and impact pressures. The measurement of impact pressure was first made by using pressure transducers located at discrete locations over the fore part of the wet deck. Further measurement was made by a load cell equipped panel attached on the wet deck. Slamming form factors, which correlate the amount of slamming pressure and relative impact velocity, were then extracted from the accumulated data. A large difference of form factor value was obtained from the point pressure and from panel pressure measurements, that is in the order of about 4 : 1. This is of course will vary with panel size, which should be chosen to represent plate panels.

Slamming characteristics were also evaluated for a hypothetical SWATH using the measured relative motion and slamming pressure data. SWATH operability related to slamming occurrence and weighted by certain criteria was identified by a probabilistic analysis. Using the form factors developed from the test, design slamming pressure of this particular SWATH was then derived. A design pressure value of some 1800 kPa was obtained, when the form factor from point pressure data is adopted, compared to 518 kPa from the panel pressure measurement. The latter seems to be a reasonable value as compared to the design values derived using other simplified formulations available in the open literature. In addition, such a design value is within the range of 200 to 620 kPa as that suggested by Sikora and Dinsenbacher (1988) for typical 2000 to 6000 tonne SWATHs.

Comparative evaluation was then performed on the existing design pressure data accumulated so far. The trend in the increase of design slamming pressure with the increase in SWATH displacement is uncertain due to the substantial scatter of the data. Nevertheless, a regression analysis has been made and yields a simple pressure-displacement correlation pertinent to SWATHs. The expression developed is acceptable for first estimation of design pressure for SWATH ship displacements up to 6000 tonnes.

The results of the present study will be useful in the development of a further study on SWATH ship slamming. Areas which need to be pursued in future are first of all, the development of a mathematical model for SWATH slamming assessment, preferably a time-domain simulation. Secondly, the development of structural design procedure for SWATH deck bottom scantlings based on slamming impact. The accumulation of slamming data from model tests remains necessary to validate any analytical prediction that may be available in the future.

Table 4.1a. Joint probability of significant wave height and period at grid point JS01 59.92°N, 2.29°W [Chen & Mavrakis (1988)]

Hs (m)	Modal Period, Tm (sec)									
	4.23	7.05	9.87	12.69	15.51	18.33	21.15	23.97	26.79	Marginal
0.61	0.95	10.15	10.13	2.85	0.99	0.21	0.05	0.02	0.02	25.38
1.83	-	13.70	11.25	2.99	0.76	0.16	0.04	-	-	28.91
3.05	-	0.22	17.47	2.58	0.49	0.07	-	-	-	20.84
4.27	-	-	7.80	3.91	0.30	0.04	0.01	-	-	12.06
5.49	-	-	0.21	6.24	0.28	0.03	0.01	-	-	6.77
6.71	-	-	-	3.10	0.35	0.01	0.01	-	-	3.46
7.92	-	-	-	0.70	0.89	0.01	-	-	-	1.60
9.14	-	-	-	-	0.56	0.02	-	-	-	0.58
10.36	-	-	-	-	0.27	0.02	-	-	-	0.29
11.58	-	-	-	-	0.05	0.01	-	-	-	0.06
12.80	-	-	-	-	0.01	0.01	-	-	-	0.02
14.63	-	-	-	-	-	0.01	-	-	-	0.01
Marginal	0.95	24.08	46.88	22.38	4.95	0.60	0.12	0.02	0.02	100.00

Table 4.1b. Joint probability of significant wave height and period at grid point JS02 59.92°N, 0.91°W [Chen & Mavrakis (1988)]

Hs (m)	Modal Period, Tm (sec)									
	3.89	6.48	9.07	11.66	14.62	16.85	19.44	22.03	24.62	Marginal
0.61	2.50	14.21	10.21	4.62	1.42	0.41	0.08	0.01	0.01	33.48
1.83	-	17.60	12.07	2.61	0.74	0.21	0.04	-	-	33.28
3.05	-	0.08	16.90	1.92	0.39	0.06	-	-	-	19.35
4.27	-	-	3.93	4.46	0.18	0.04	0.02	-	-	8.63
5.49	-	-	0.01	3.05	0.28	0.02	-	-	-	3.36
6.71	-	-	-	0.67	0.63	-	-	-	-	1.30
7.92	-	-	-	0.01	0.36	0.01	-	-	-	0.38
9.14	-	-	-	0.01	0.13	0.01	-	-	-	0.15
10.36	-	-	-	0.01	0.03	0.02	-	-	-	0.06
11.58	-	-	-	0.01	-	-	-	-	-	0.01
Marginal	2.50	31.90	43.13	17.37	4.16	0.78	0.14	0.01	0.01	100.00

Table 4.2. Slamming rates of SWATH-FV operating in JS01 region

Fn = 0.52 ; Vth = 3.0 m/s ; Location 2 NUMBER OF SLAM/SECOND

Zc = 3.7 m (static trim and sinkage are taken into account)

Wave Data : JS01

Spectral Form : Bretschneider Tm (sec)

Hs (m)	4.33	7.05	9.87	12.69	15.51	18.33	21.15	23.97	26.79
0.61	0.000000	0.000000	0.000000	0.000000	0.000000	0.000000	0.000000	0.000000	0.000000
1.83	-	0.000004	0.000000	0.000000	0.000000	0.000000	0.000000	-	-
3.05	-	0.003447	0.000152	0.000001	0.000000	0.000000	-	-	-
4.27	-	-	0.004438	0.000231	0.000002	0.000000	0.000000	-	-
5.49	-	-	0.017781	0.002839	0.000132	0.000001	0.000000	-	-
6.71	-	-	-	0.010098	0.001263	0.000046	0.000000	-	-
7.92	-	-	-	0.020855	0.004588	0.000419	-	-	-
9.14	-	-	-	-	0.010392	0.001700	-	-	-
10.36	-	-	-	-	0.017940	0.004334	-	-	-
11.58	-	-	-	-	0.026306	0.008351	-	-	-
12.80	-	-	-	-	0.034759	0.013461	-	-	-
14.63	-	-	-	-	-	0.022302	-	-	-

Spectral Form : JONSWAP Tm (sec)

Hs (m)	4.33	7.05	9.87	12.69	15.51	18.33	21.15	23.97	26.79
0.61	0.000000	0.000000	0.000000	0.000000	0.000000	0.000000	0.000000	0.000000	0.000000
1.83	-	0.000012	0.000000	0.000000	0.000000	0.000000	0.000000	-	-
3.05	-	0.005175	0.000012	0.000000	0.000000	0.000000	-	-	-
4.27	-	-	0.001185	0.000050	0.000000	0.000000	0.000000	-	-
5.49	-	-	0.007882	0.001082	0.000007	0.000000	0.000000	-	-
6.71	-	-	-	0.005147	0.000170	0.000001	0.000000	-	-
7.92	-	-	-	0.012550	0.001079	0.000032	-	-	-
9.14	-	-	-	-	0.003478	0.000245	-	-	-
10.36	-	-	-	-	0.007602	0.000952	-	-	-
11.58	-	-	-	-	0.013150	0.002467	-	-	-
12.80	-	-	-	-	0.019597	0.004935	-	-	-
14.63	-	-	-	-	-	0.010273	-	-	-

Table 4.3. Comparison of design slamming pressure (in kPa) calculated by various methods

Ships	Δ (tonnes)	Designer -	Trial -	Sellars Eq. (4.43)	Allen&Jones Eq. (4.51)	DnV1 Eq. (4.53)	DnV2 Eq. (4.54)	LR Eq. (4.55)	ABS Eq. (4.59)	Loscombe Eq. (4.60)	Graham Eq. (4.62)	Point Press. Eq. (4.62)	Panel Press. Eq. (4.62)
Halcyon	60.0	138.00	-	-	168.00	109.00	132.00	84.00	121.00	312.00	-	-	-
Korean Ferry	70.0	54.00	-	-	-	-	-	-	-	-	-	-	-
F.G. Creed	75.0	-	102.00	-	-	-	-	-	-	-	-	-	-
EODC	75.0	110.00	-	-	-	-	-	-	-	-	-	-	-
Notional	125.0	-	-	650.00	495.00	-	-	-	-	-	-	-	-
Notional	125.0	82.00	-	-	-	-	-	-	-	-	-	-	-
USCG OPV	125.0	414.00	-	-	235.00	-	-	-	-	-	-	-	-
Notional	180.0	-	-	-	-	-	-	-	-	531.00	-	-	-
Kaimalino	220.0	97.00	-	-	284.00	-	-	-	-	-	-	-	-
USCG OPV	254.0	414.00	-	-	308.00	-	-	-	-	-	-	-	-
USCG OPV	765.0	414.00	-	-	444.00	-	-	-	-	-	-	-	-
Bazan OPV	914.0	627.00	-	-	483.00	-	-	-	-	-	-	-	-
USCG OPV	1270.0	414.00	-	-	497.00	-	-	-	-	-	-	-	-
YSL-SSV	2500.0	432.00	-	-	-	-	-	-	-	-	-	-	-
SWATH-FV	2500.0	-	-	6214.00	238.00	95.00	145.00	143.00	394.00	887.00	-	1842.00	518.00
Kaiyo	3500.0	690.00	-	-	-	-	-	-	-	-	-	-	-
Victorious	3500.0	380.00	-	-	455.00	-	-	-	-	-	-	-	-
Ship A	4000.0	690.00	-	-	440.00	-	-	-	-	-	-	-	-
Ship B	4500.0	690.00	-	-	400.00	-	-	-	-	-	-	-	-
DREA SWATH	5000.0	-	-	-	-	-	-	-	-	-	1800.00	-	-
Ship C	5250.0	690.00	-	-	433.00	-	-	-	-	-	-	-	-
UCL ASW	5500.0	-	-	-	417.00	-	-	-	-	-	-	-	-
AMCM	5869.0	283.00	-	-	395.00	-	-	-	-	-	-	-	-

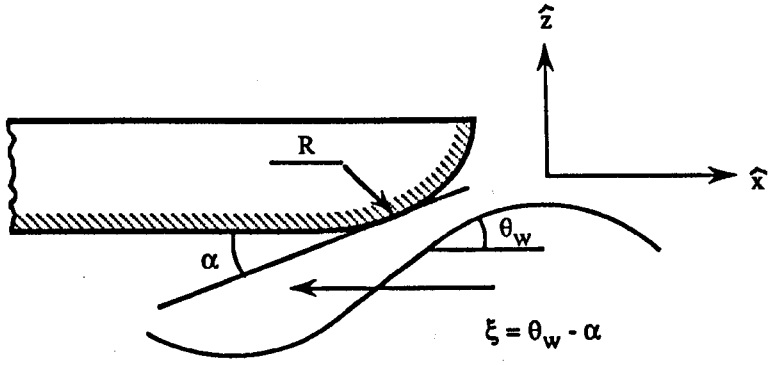

Figure 4.1. Impact angle [Graham (1988)]

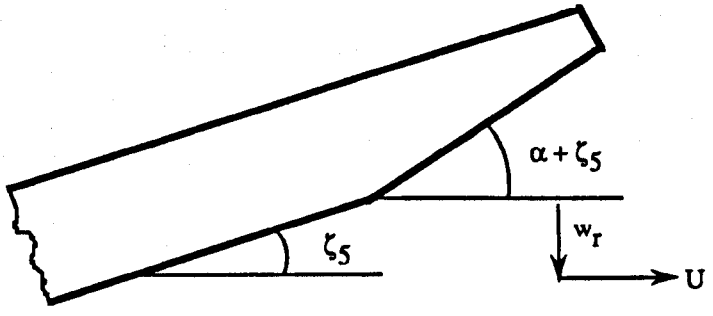

Figure 4.2. Relations between variables in bow ramp during slam impact [Kaplan (1987)]

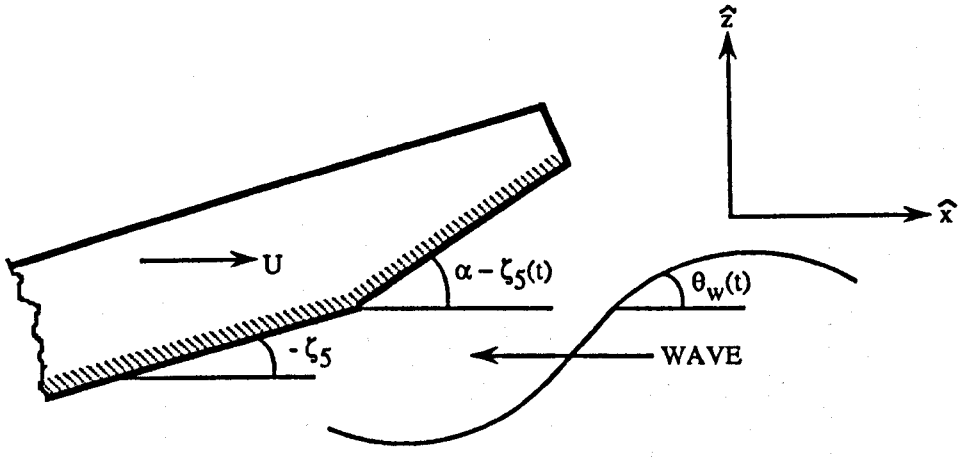

Figure 4.3. Impact angle relations on the wet deck of SWATH

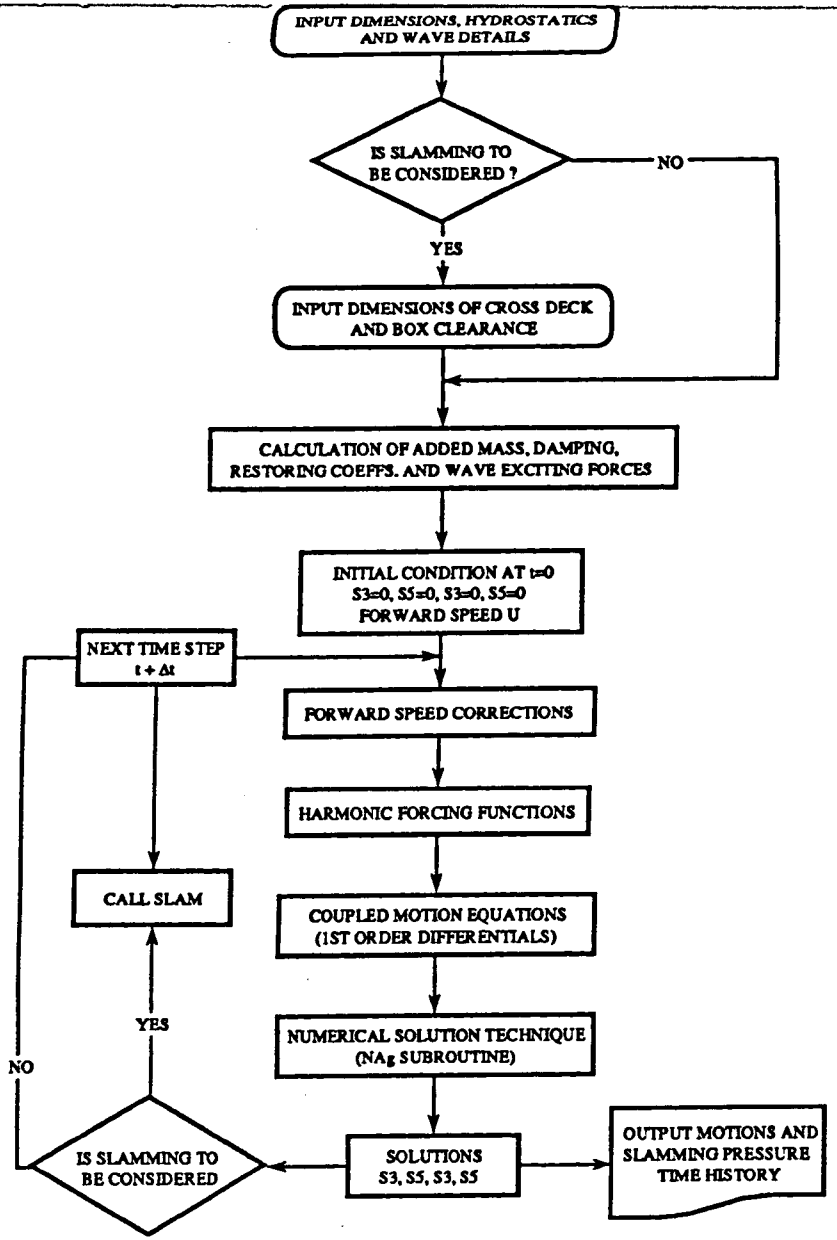

Figure 4.4a. Proposed slamming program SLAMTIME

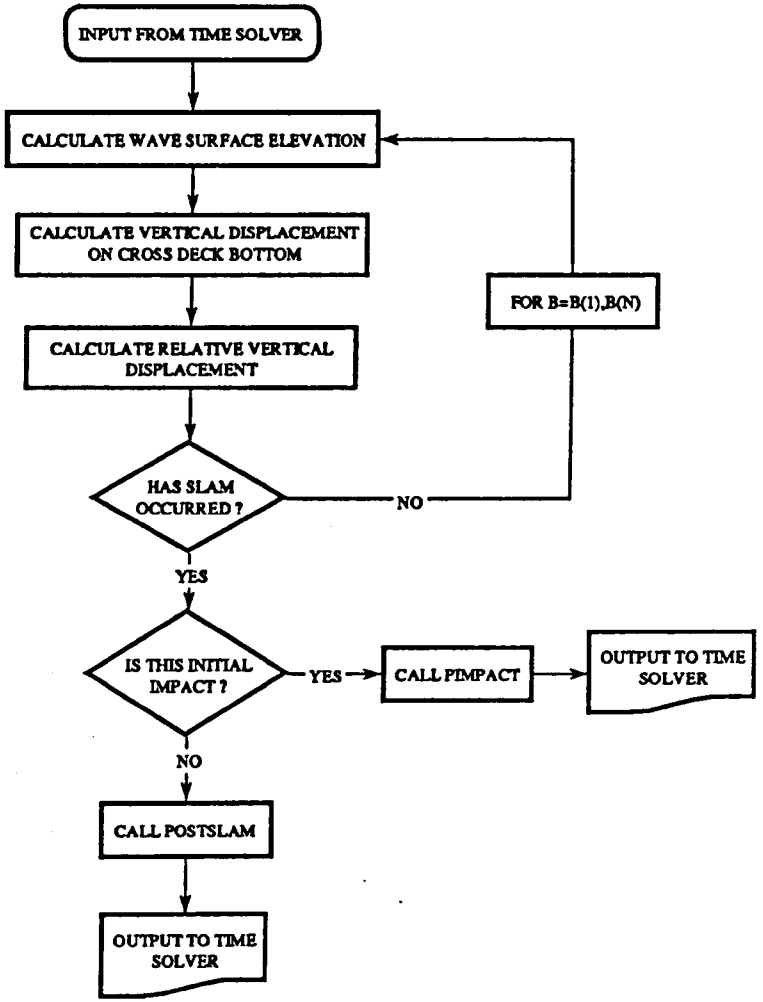

Figure 4.4b. Routine SLAM

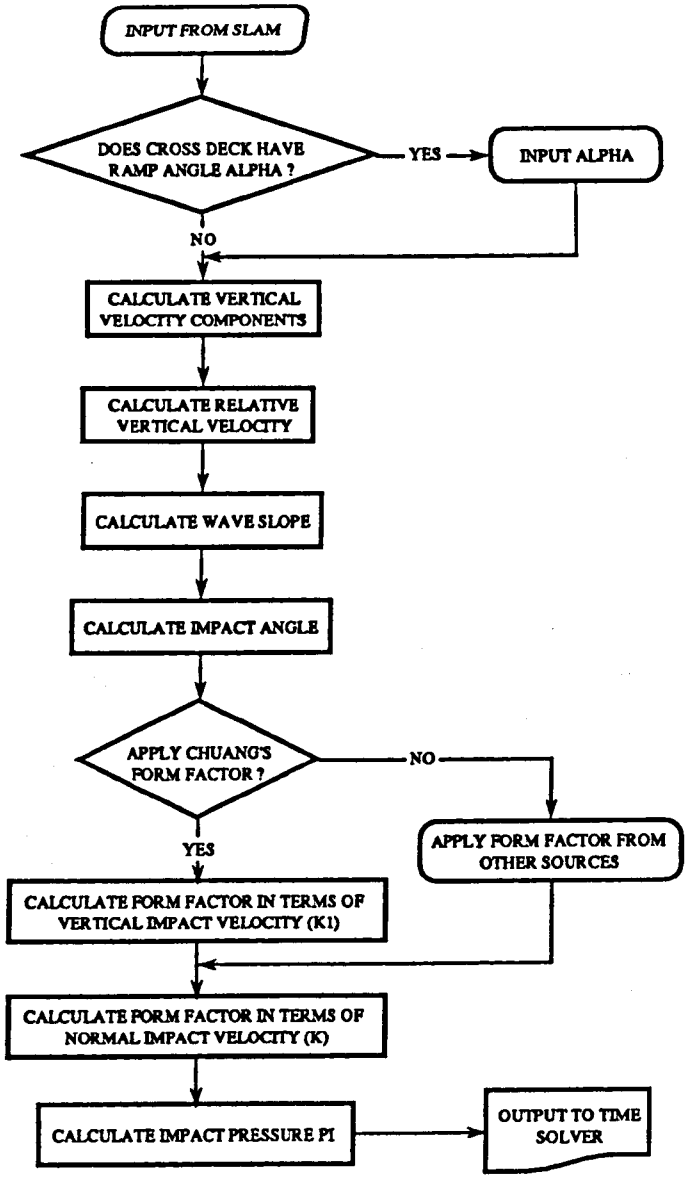

Figure 4.4c. Routine PIMPACT

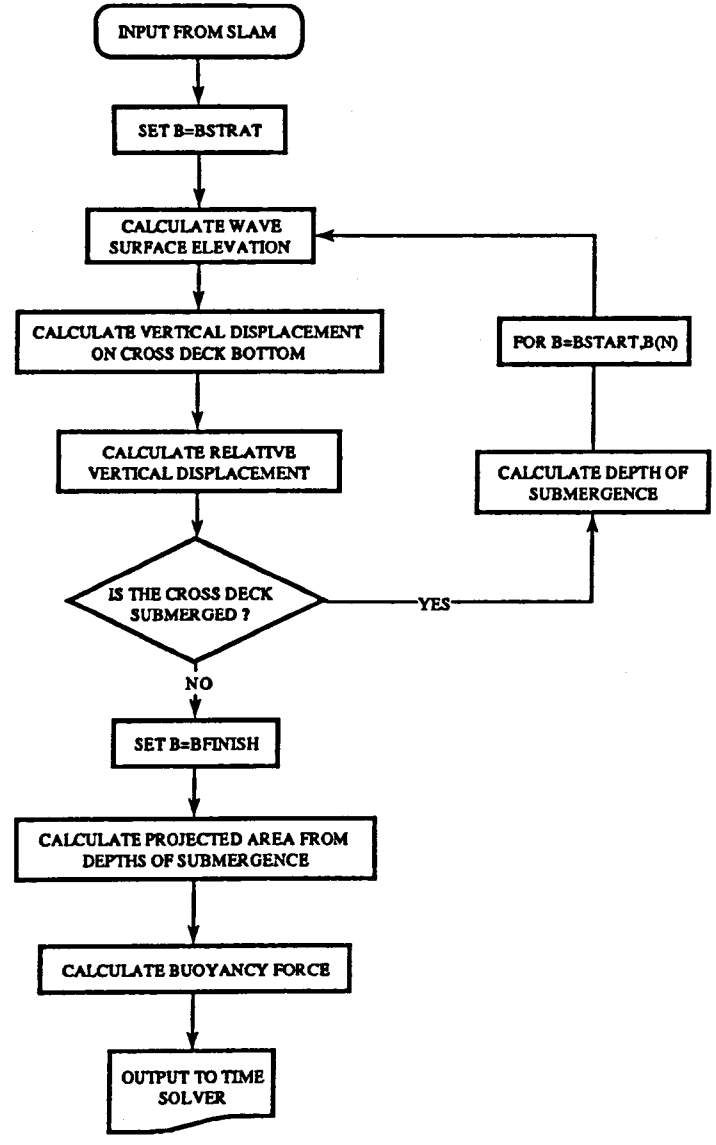

Figure 4.4d. Routine POSTSLAM

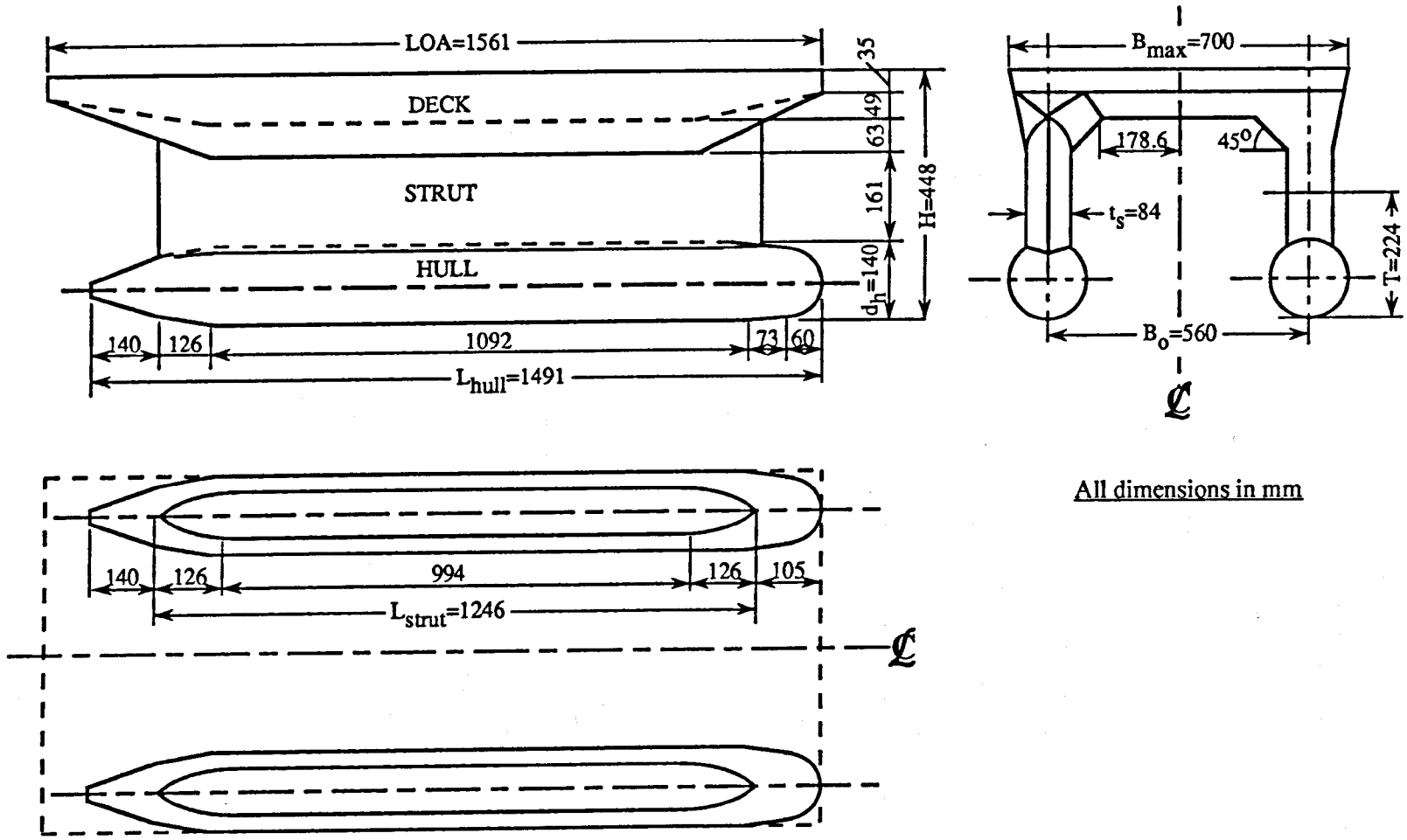

Figure 4.5. Technical drawing of the Fishing SWATH model

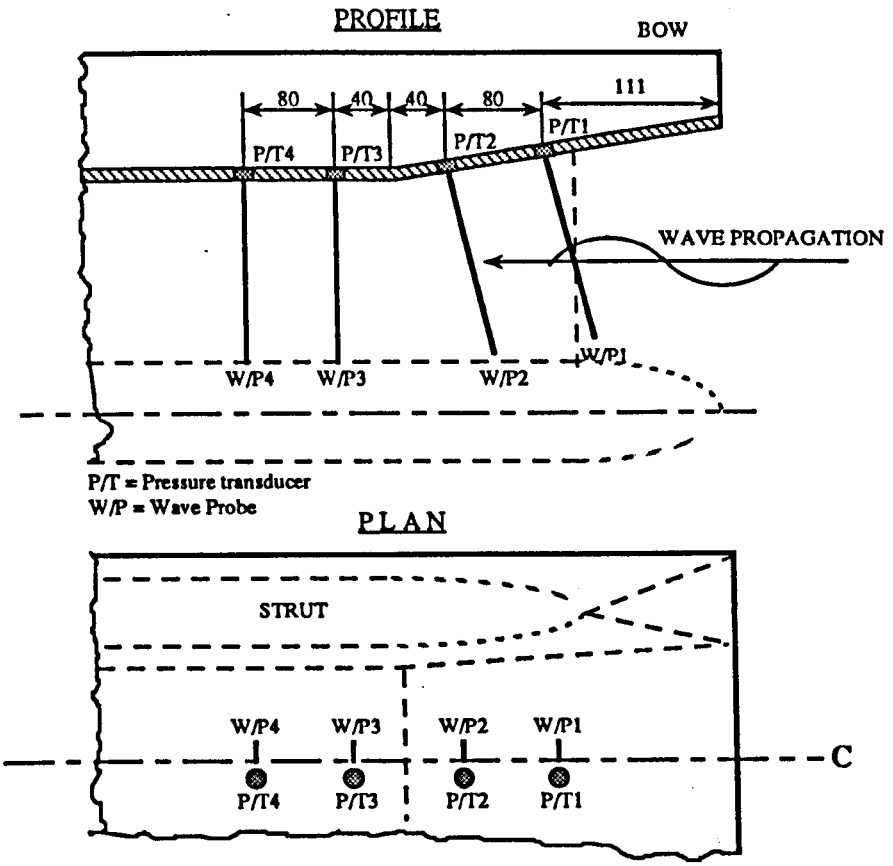

Figure 4.6. Instrumentation arrangement for SWATH slamming test

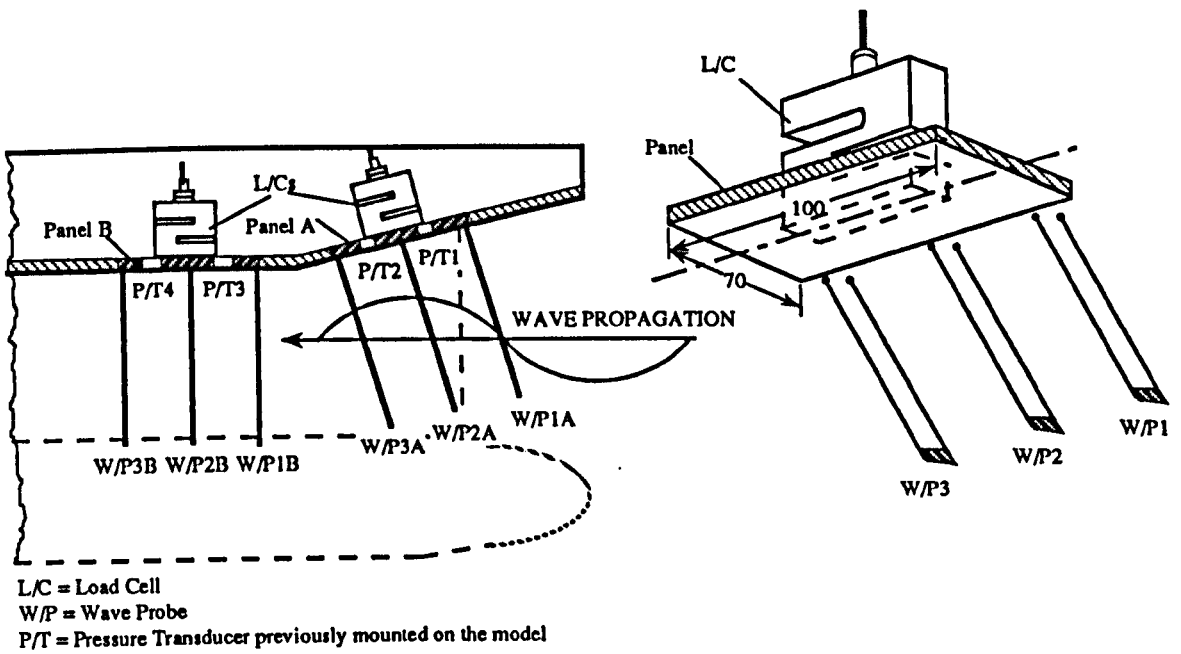

Figure 4.7. Instrumentation set up for the panel slamming test

a)

b)

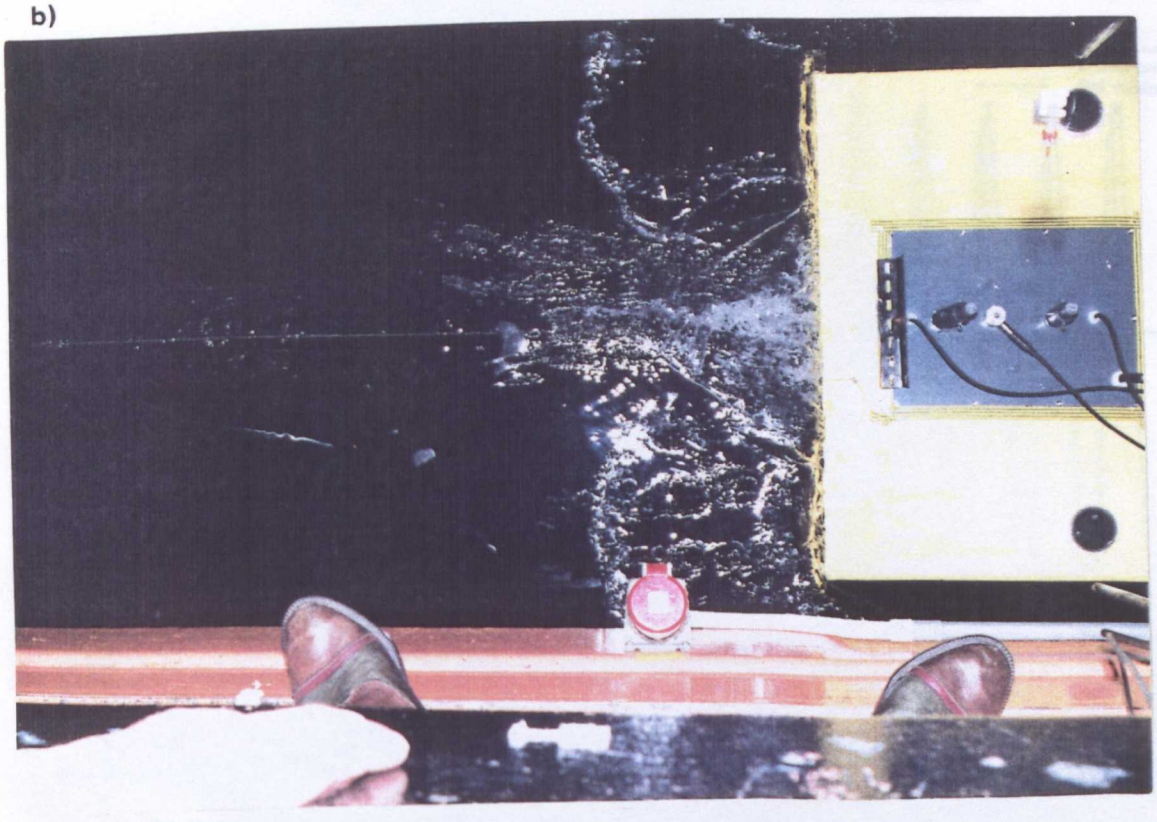

Figure 4.8. Photographs of SWATH-FV model subjected to severe slamming
(a. front view ; b. plan view)

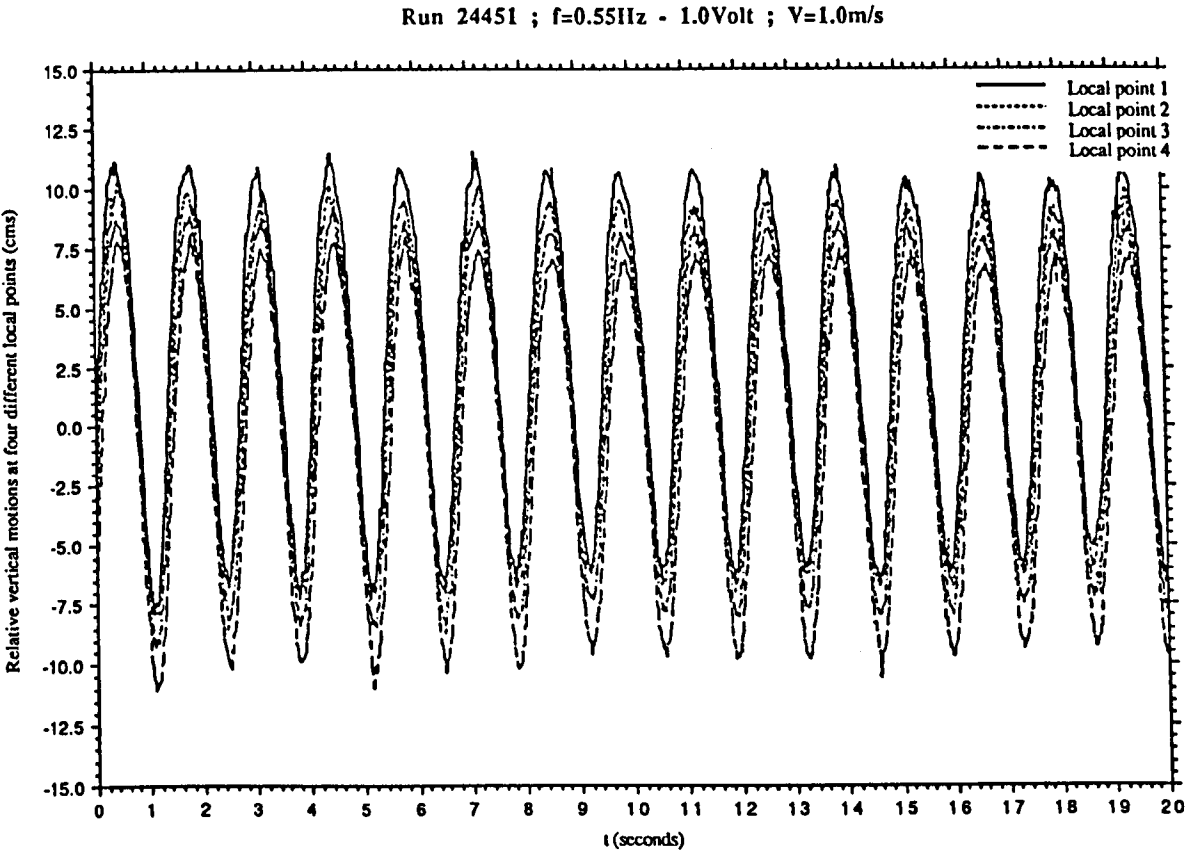

Figure 4.9. Typical record of relative motions at four local points

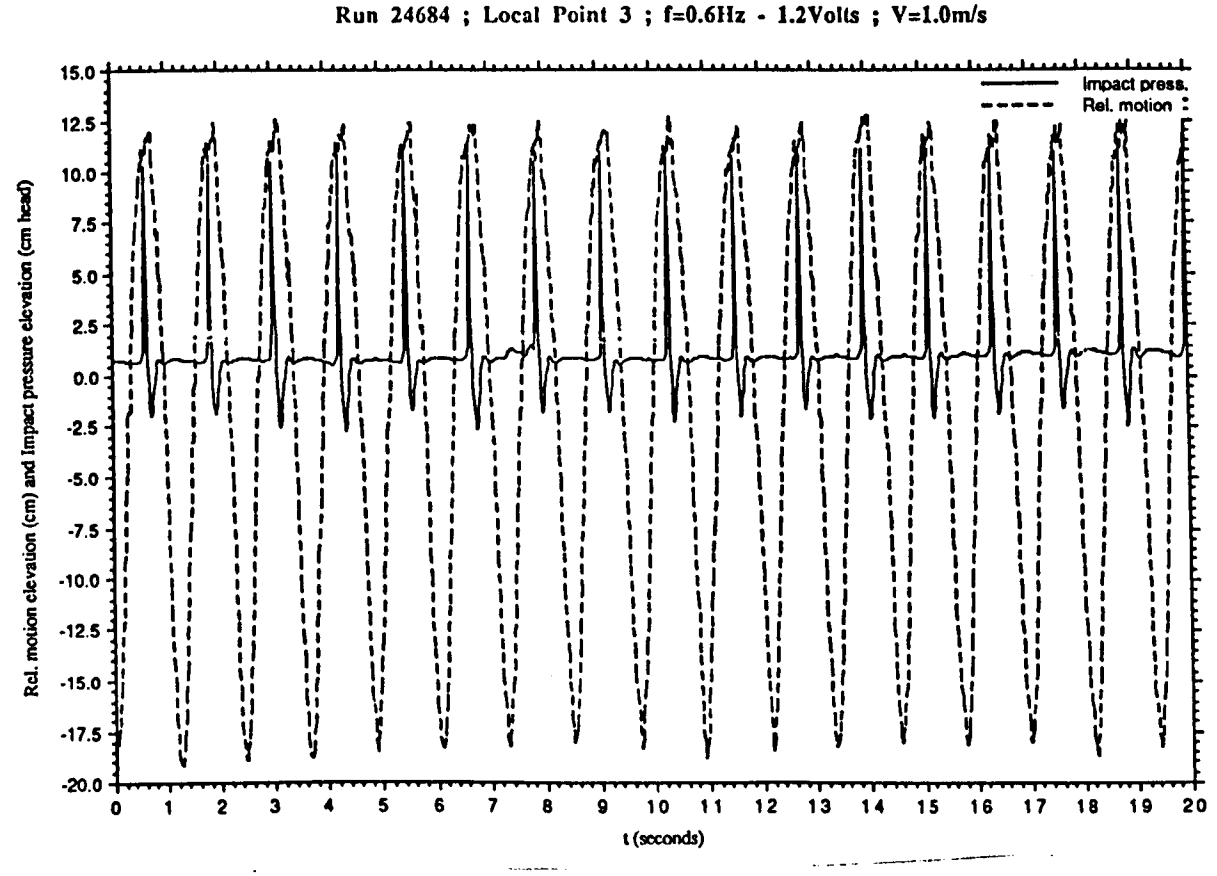

Figure 4.10. Typical record of slamming pressure and the corresponding relative motion

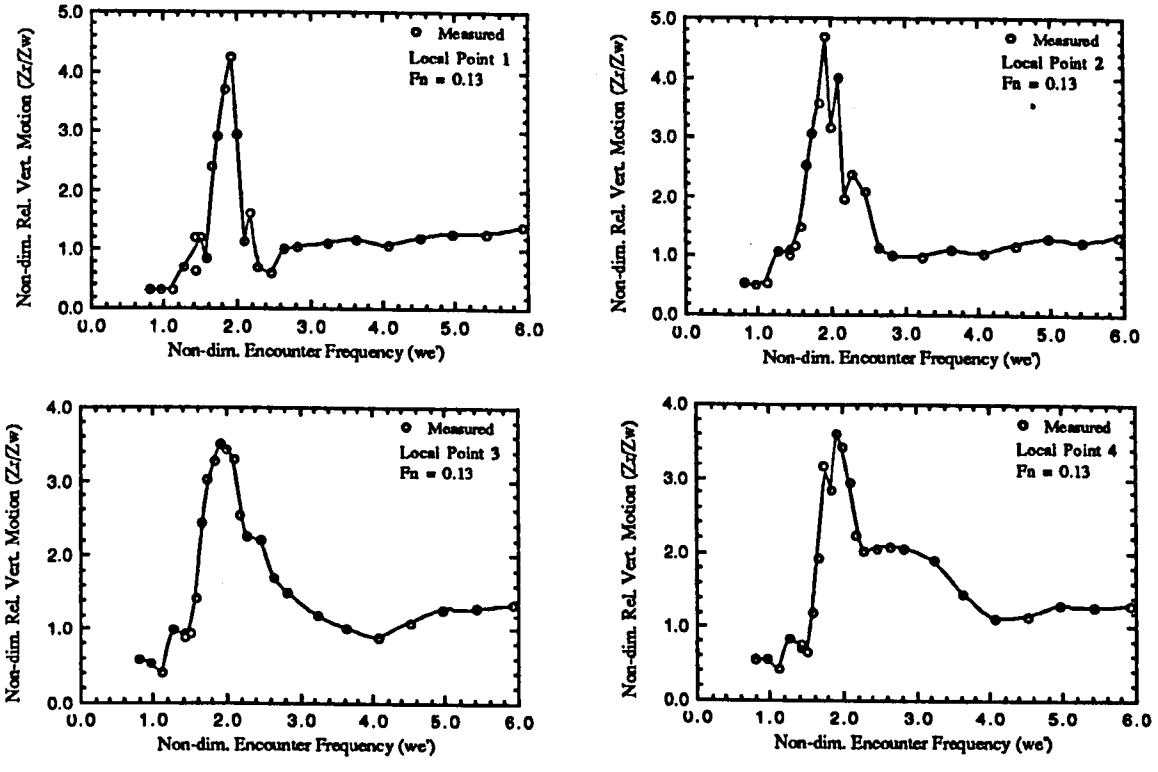

Figure 4.11. Relative vertical motion at four local points of SWATH-FV (Fn=0.13)
(a. Point 1 ; b. Point 2 ; c. Point 3 ; d. Point 4)

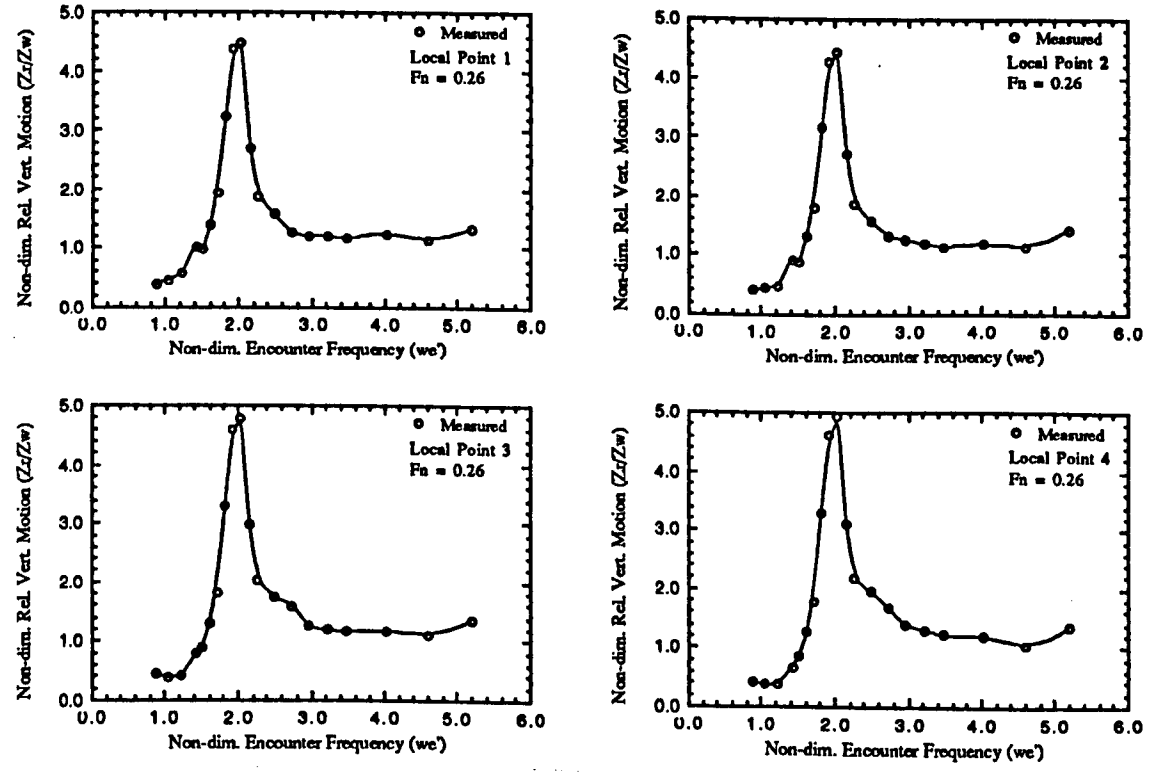

Figure 4.12. Relative vertical motion at four local points of SWATH-FV (Fn=0.26)
(a. Point 1 ; b. Point 2 ; c. Point 3 ; d. Point 4)

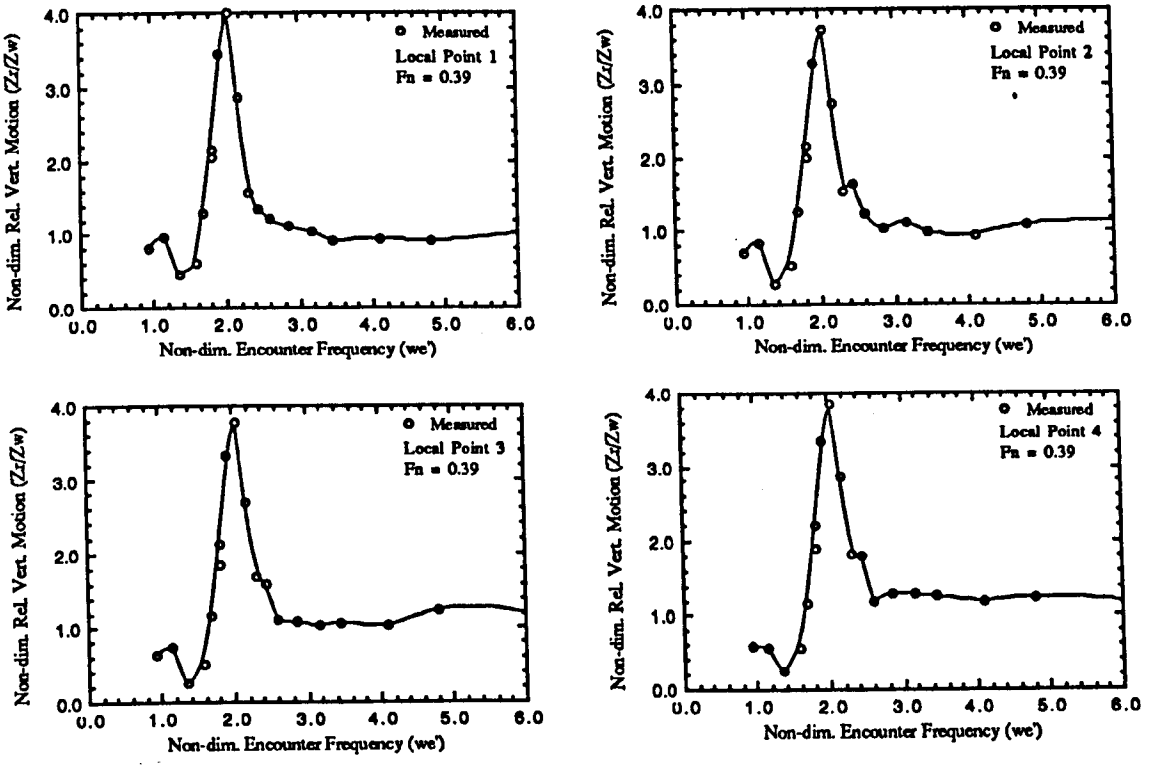

Figure 4.13. Relative vertical motion at four local points of SWATH-FV (Fn=0.39)
(a. Point 1 ; b. Point 2 ; c. Point 3 ; d. Point 4)

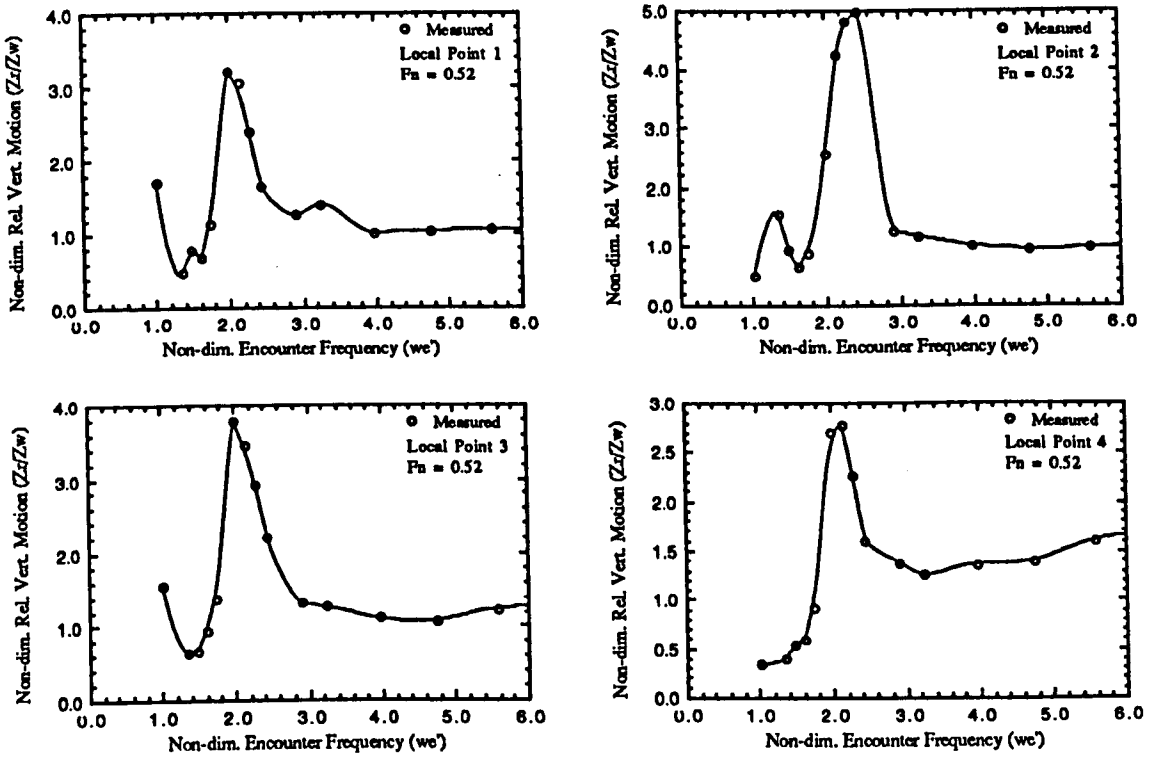

Figure 4.14. Relative vertical motion at four local points of SWATH-FV (Fn=0.52)
(a. Point 1 ; b. Point 2 ; c. Point 3 ; d. Point 4)

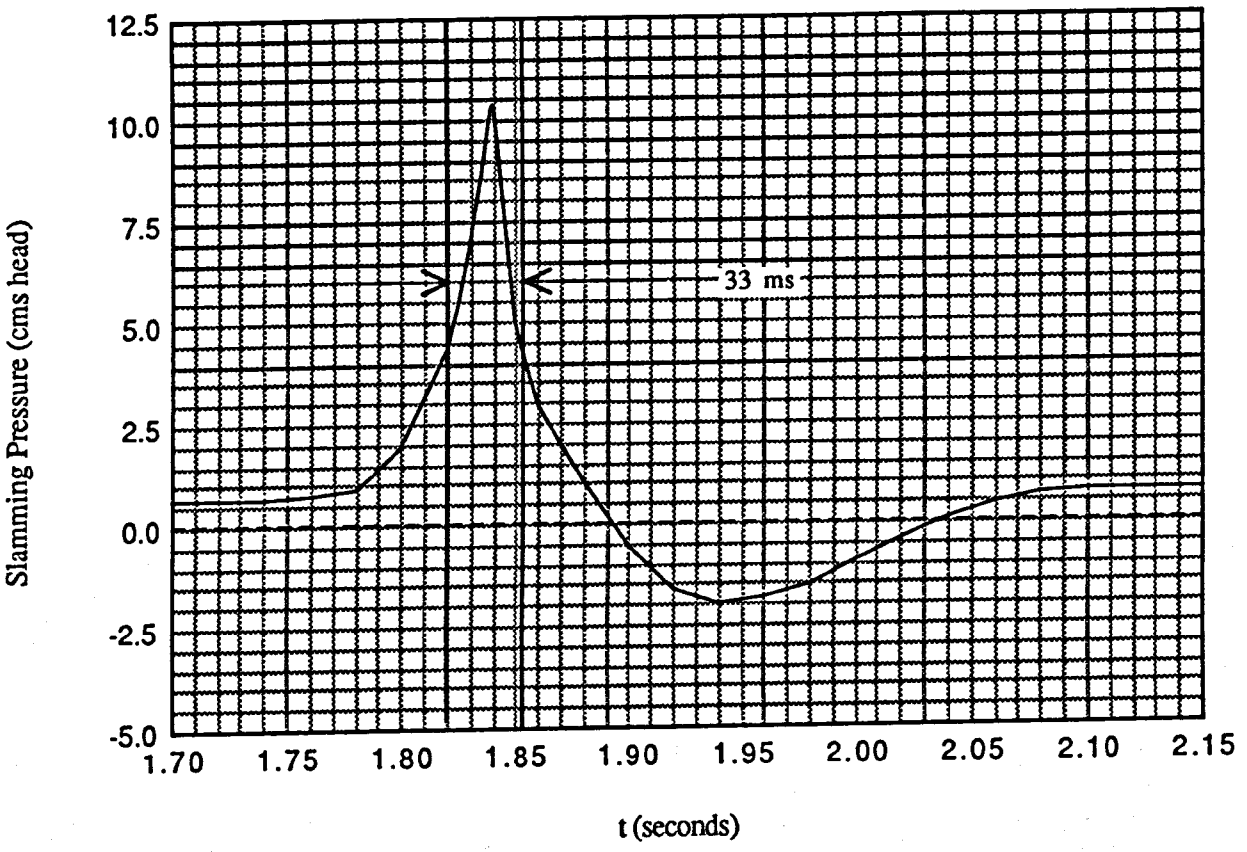

Figure 4.15. Slamming pressure time history (point pressure impact)

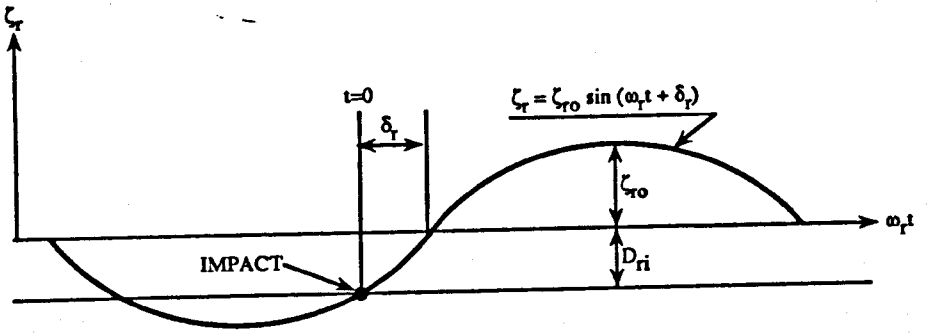

Figure 4.16. Relative motion time history [Lloyd (1990)]

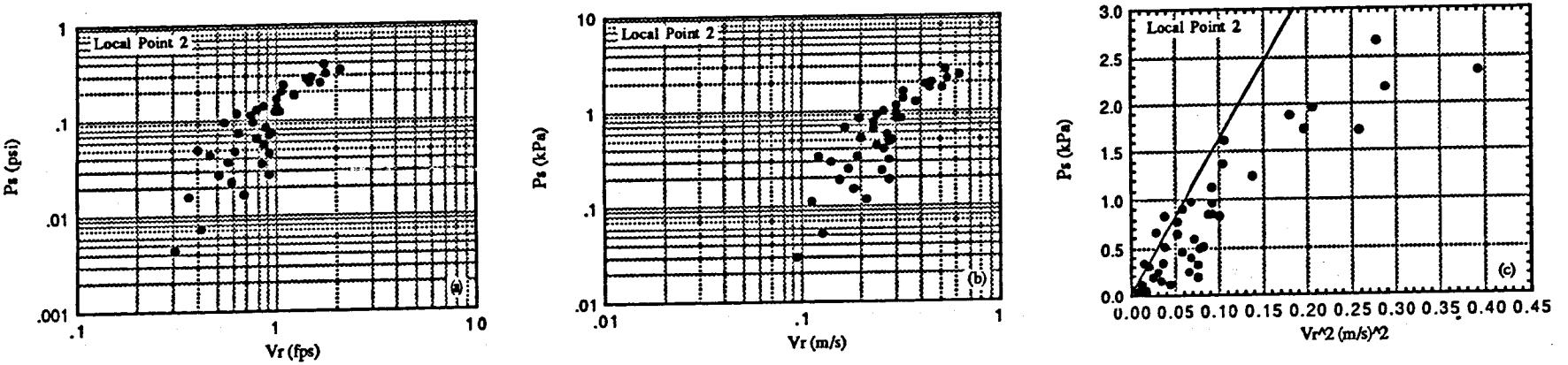

Figure 4.17. Slamming pressure Ps vs squared relative velocity V_r^2 measured at Position 2 of the wet deck of SWATH-FV model (k=32)

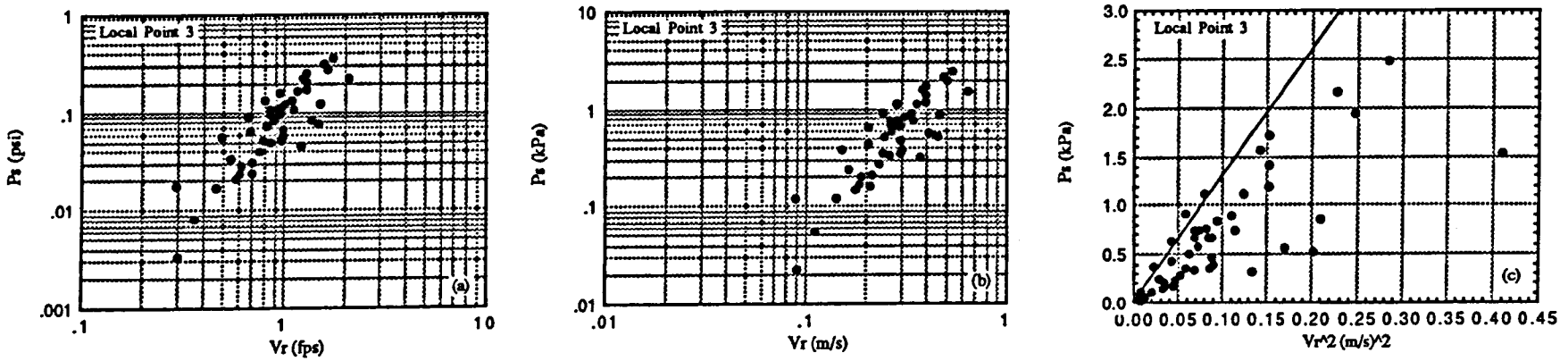

Figure 4.18. Slamming pressure Ps vs squared relative velocity V_r^2 measured at Position 3 of the wet deck of SWATH-FV model (k=26)

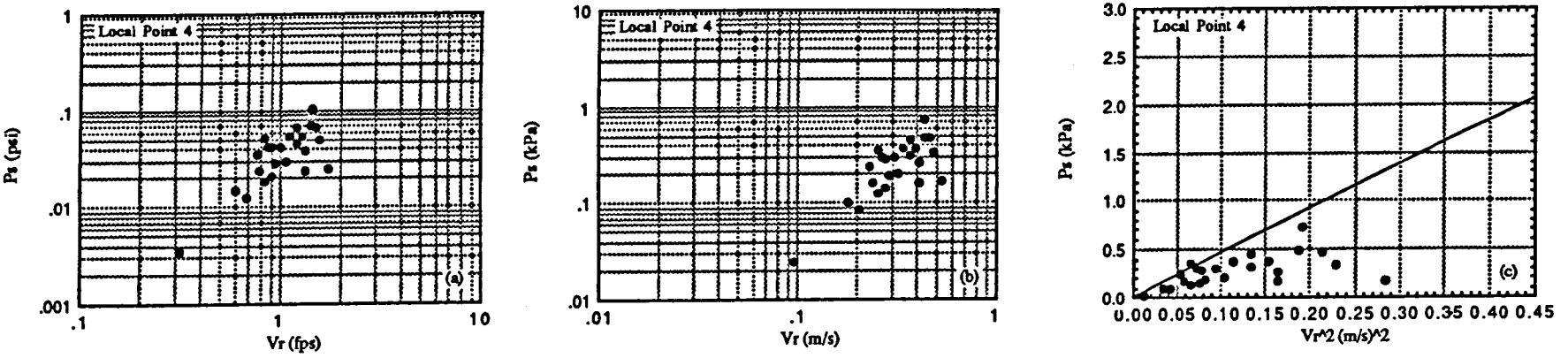

Figure 4.19. Slamming pressure Ps vs squared relative velocity V_r^2 measured at Position 4 of the wet deck of SWATH-FV model (k=9)

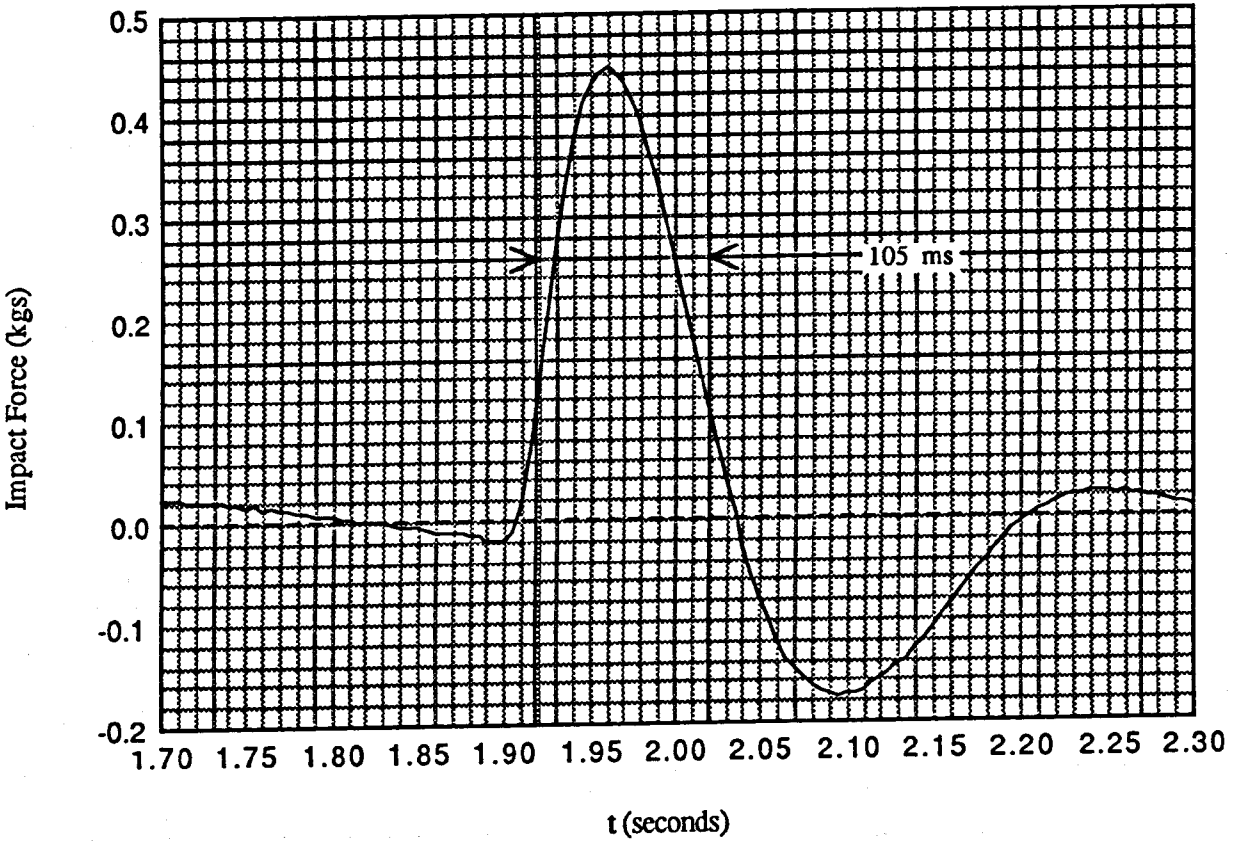

Figure 4.20. Typical time history of slamming force on Panel A

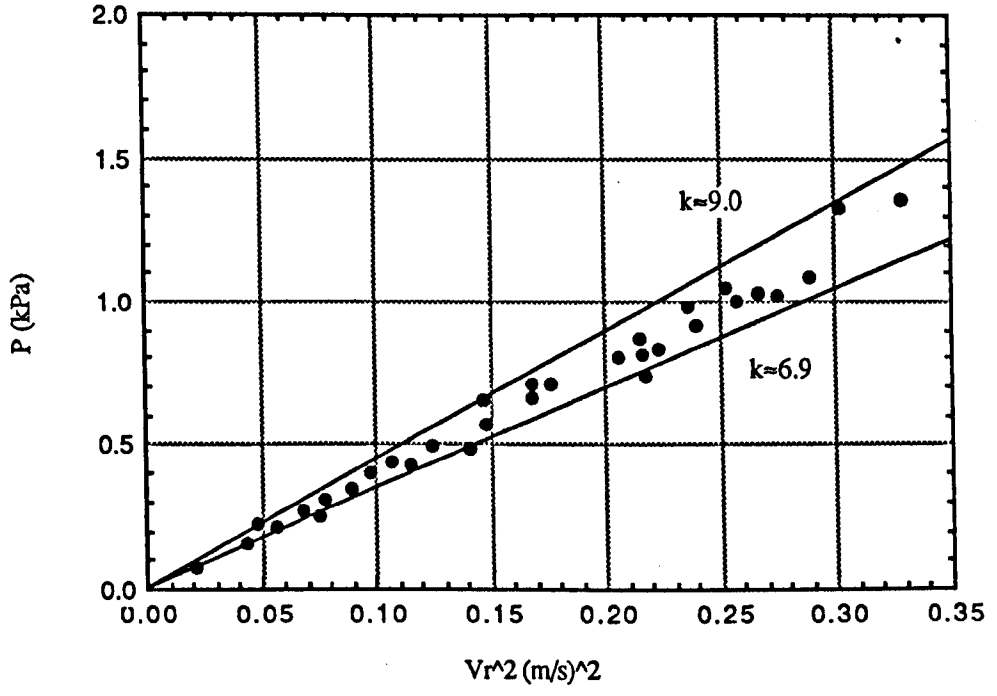

Figure 4.21. Average slamming pressure vs Vr^2 measured at Panel A on the underdeck of the Fishing SWATH model

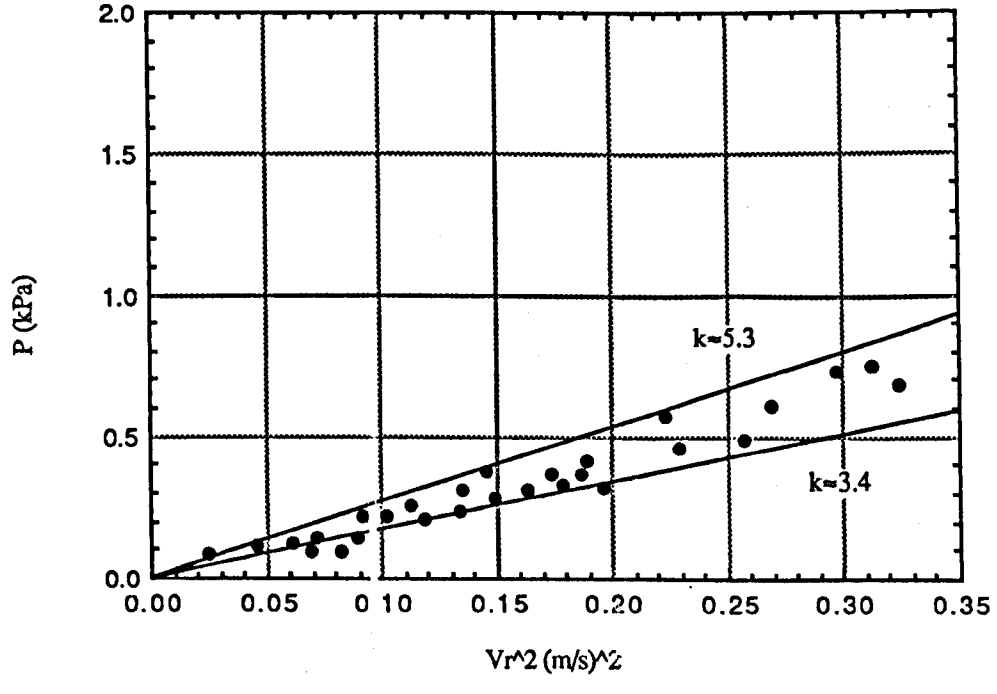

Figure 4.22. Average slamming pressure vs Vr^2 measured on Panel B on the underdeck of the Fishing SWATH model

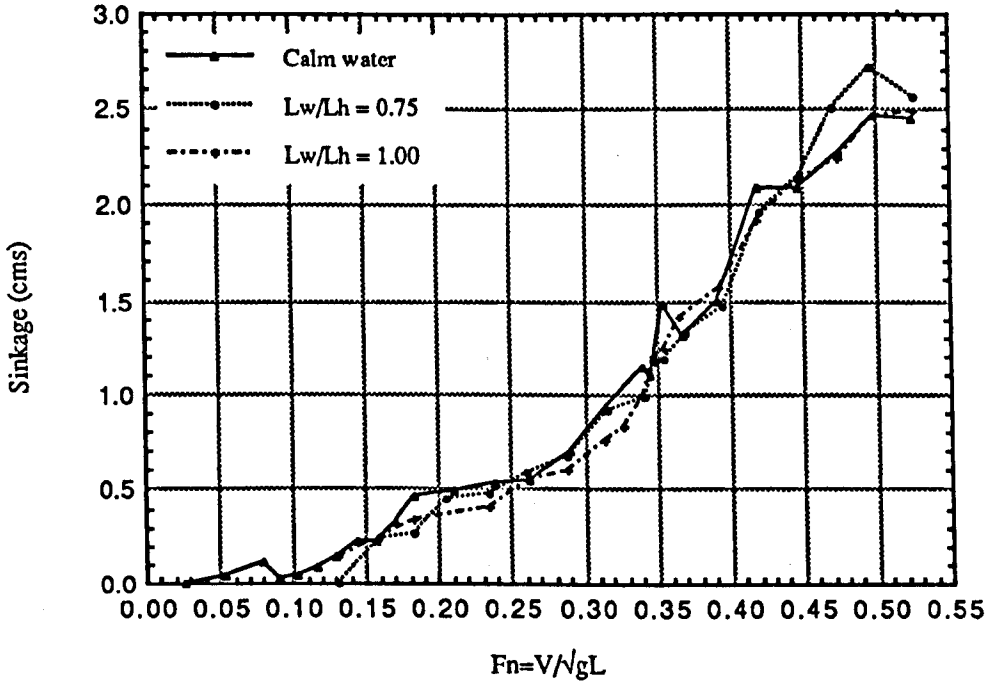

Figure 4.23a. Sinkage of SWATH-FV model in calm water and in waves at forward speeds

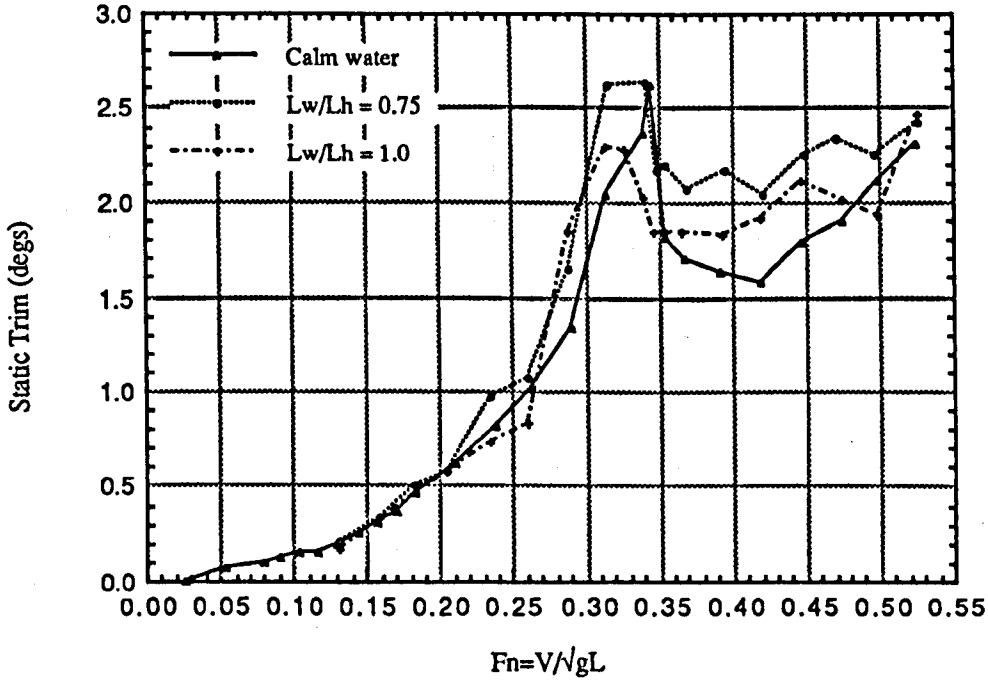

Figure 4.23b. Static trim of SWATH-FV model in calm water and in waves at forward speeds

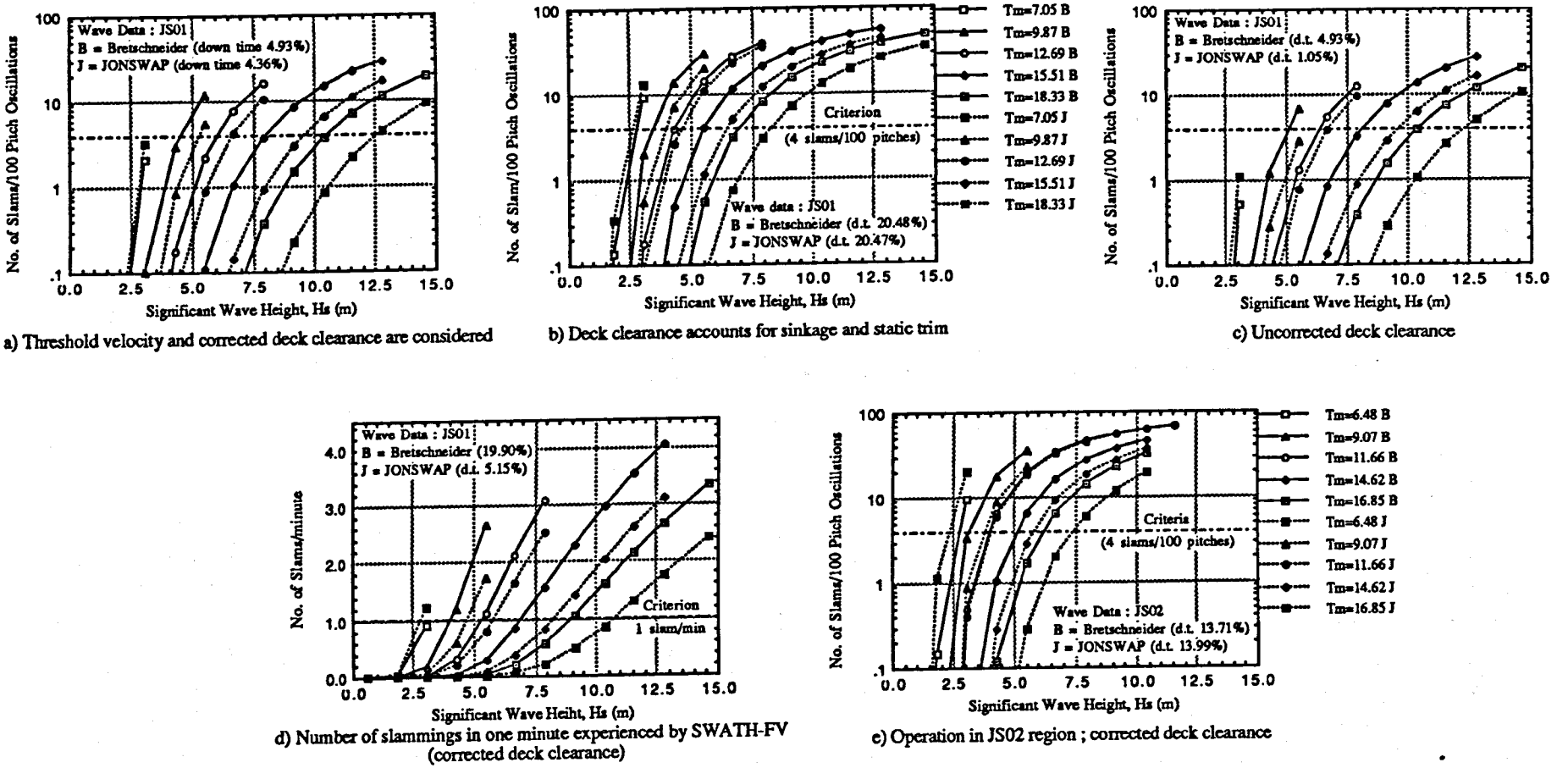

a) Threshold velocity and corrected deck clearance are considered

b) Deck clearance accounts for sinkage and static trim

c) Uncorrected deck clearance

d) Number of slammings in one minute experienced by SWATH-FV (corrected deck clearance)

e) Operation in JS02 region ; corrected deck clearance

Figure 4.24. Slamming occurrences of SWATH-FV for different conditions

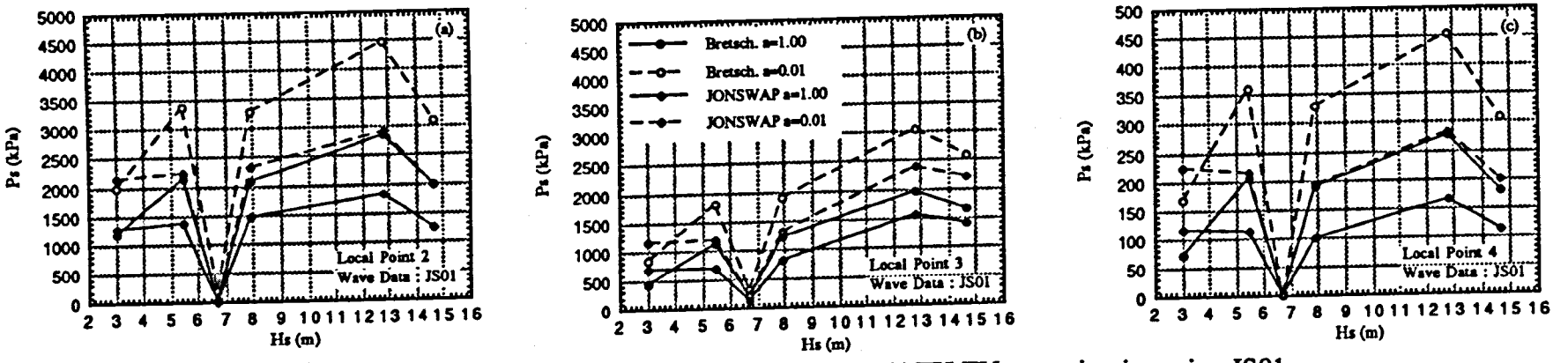

Figure 4.25. Extreme slamming pressures on SWATH-FV operating in region JS01
(a. Position 2 ; b. Position 3 ; c. Position 4)

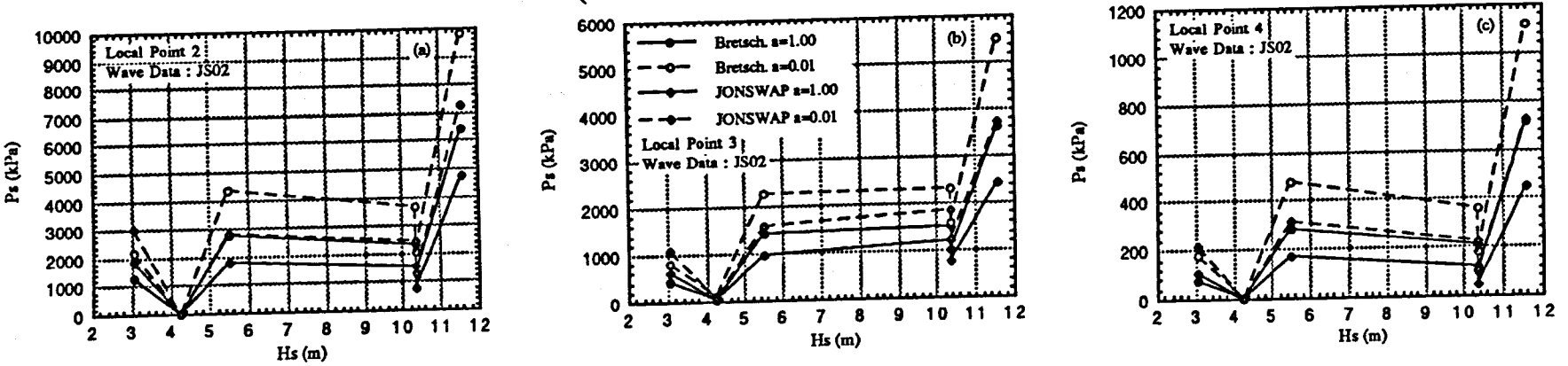

Figure 4.26. Extreme slamming pressures on SWATH-FV operating in region JS02
(a. Position 2 ; b. Position 3 ; c. Position 4)

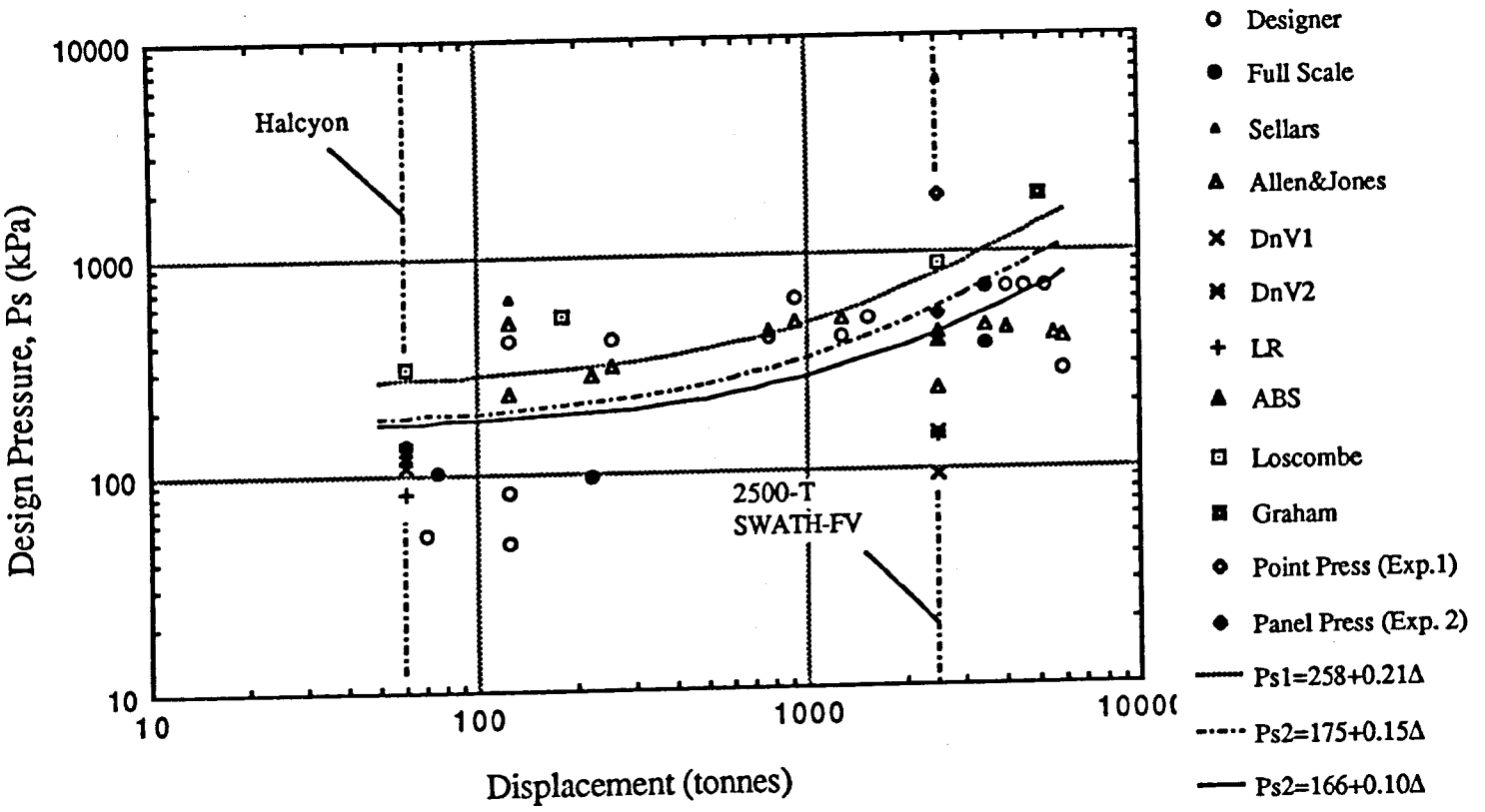

Figure 4.27. Comparison of design slamming pressure for SWATHs by various methods

CHAPTER 5

PRELIMINARY SWATH STRUCTURAL DESIGN

CHAPTER 5

PRELIMINARY STAGE IN SWATH STRUCTURAL DESIGN

5.1. INTRODUCTION

The relatively limited demand on SWATHs by commercial operators as well as by governments (the Navy) is widely recognised due to the comparably higher capital expenditure required for construction. Betts (1988b) suggests that the higher construction (structural) cost of a SWATH is due to the larger size of the ship (approximately 20 to 30%) compared to a monohull with an equivalent capability in carrying out a certain mission. The criterion applied in the scoring of equivalent mission is, in this case, governed by the capability of the vessel to carry an amount of payload, i.e. main cargo and/or operational equipment. Whilst the structural weight of a SWATH ship is approximately 40% of its full load displacement, thus the amount of payload which can be transported by a SWATH is less than that by a monohull.

There is practically no other way to put an appreciable increase in payload without attempting to reduce the structural weight. A report by Sikora and Dinsenbacher (1990) on the design study of a notional 9000 tonne SWATH suggests that a 10% structural weight reduction could be the expected result in a 16% increase in range, or a 24% increase in payload. Realising this, various efforts were then undertaken by SWATH researchers worldwide to solve the problem of effective structural design by examining all possible alternatives on the general and detailed structures.

Several attempts suggested as viable to reduce SWATH production cost and/or structural weight are extracted as follows. Improving the producibility of structural components which in general may be acquired by slightly modifying the initial structural arrangement into a much simpler configuration, as shown by Covich (1986) or DeVries (1991). For this special case the involvement of production engineers in the earliest design process is therefore necessary if a further reduction in the production cost per tonne structural weight is to be achieved.

The selection of longitudinal framing, which tends to be avoided by conservative designers, is also a potential arrangement which could provide weight saving compared to the commonly used transverse framing in SWATH ships. A thorough design study on a 500 tonne SWATH by Gupta and Schmidt (1986) reveals that longitudinal framing configuration could be 3 to 12% lighter than a transverse one. Sikora (1988) points out

another concept for weight saving that is, firstly investigating the proper arrangement of transverse bulkhead spacing and the use of partial bulkheads in high shear areas. Secondly, evaluating the use of high strength steels designed to elasto-plastic criteria for wetted shell plating and, thirdly, adopting lightweight lower hull configurations.

Even though the above weight saving concepts are feasible to apply in the design of larger SWATHs, further considerations still need to be explored for smaller vessels. Structural weight fraction of small SWATHs tends to be higher than for larger ones [Betts (1988b)]. Fortunately, research on lighter construction materials nowadays is well advanced and has offered many alternatives for marine structure applications. Light weight material has a substantial impact on the operational cost, although it usually imposes higher initial production cost. Lighter structure means higher payload which might be carried by a vessel. Thus, even if the freight rate is brought to a relatively lower value, the rate of return could still be expected to be acceptably high.

It is not surprising, therefore, that most small SWATHs which are presently in operation were constructed using aluminium alloys, hybrid (steel-aluminium combination) and even glass reinforced plastics (GRP), as shown in Fig. 5.1. A fuller investigation on alternative materials to be adopted for SWATH construction is reported by Loscombe (1987, 1988, 1989). Besides aluminium alloy or GRP, high tensile strength steel is also popular in the construction of larger SWATH. Aronne et al (1974) indicate HTS will lead to some 10% weight reduction on SWATH structure.

In general the structural design method applied to SWATHs will follow that traditionally practised in monohull ships. This may involve the extrapolation from previous successful designs or may commence from scratch and evolve gradually. Even if a designer is able to find a parent ship for comparison, modification to achieve an optimum structure in line with the ship missions is mandatory. The next step of design will then consist of a stepwise process in which the designer performs an analysis of the structure in order to evaluate its performance. If necessary, scantlings are revised until the design criteria is met. The resulting configuration is then modified in a way that is expected to lead to an improvement in performance or cost. Figure 5.2 illustrates the ship structural design process where, on the left hand side is shown the key steps of the design and the right hand side is the criteria. A detailed explanation of the design philosophy can be found in a report by Moan et al (1991).

5.2. SWATH STRUCTURAL DESIGN CRITERIA

From structural perspective, the overall hull geometry of a SWATH ship requires that the two widely separated displacement hull/struts be rigidly tied to a central semi-monocoque deck structure. Critical hull loading response is in the transverse bending mode where the transverse main deck and wet deck plating is subject to in-plane forces

resulting from bending loads induced through lateral components of hull/strut hydrodynamic forces. High transverse load suggests a system of transverse framing to take the bending loads. Transverse framing, however, must also be spaced in a way to reduce production fit-up and cost. The wet deck, in addition to participating in transverse bending, must also be able to sustain high local impact loads. Regional normal panel loads are expected to be especially severe near the bow where slamming pressure may be quite high. This in turn drives main deck plating thicknesses upward to maintain a balanced section to resist transverse pressure loads.

Owing to the critical side force on SWATHs transverse bulkheads, together with main and wet decks are the primary structures which act in resisting the bending so resulted. Additionally, transverse bulkheads represent the primary component that sustain shear stresses which present simultaneously under bending loads. Unfortunately the small of SWATHs gives rise to considerable shear lag effects and local stress concentration that do not behave conventionally. Shear lag effect is well recognised to reduce the effectiveness of plate strip that sustain the loadings. Chalmers (1989) suggests the amount of effective side shell (b_e) of about 50 times plate thickness is expected to act with the bulkheads in resisting bending. Sikora (1988) shows that effective width of the plating varies over the decks and strut sides. In some cases the effective width may be approximated by :

$$b_e = at\sqrt{E/\sigma_y} \tag{5.1}$$

where a is a constant and t is the plate thickness. Faulkner (1992) gives a factor of 1.9 for a, whilst Aronne et al (1974) suggest a factor of 2.0.

To ease these prevalent peak and shear stresses in the bulkhead one can fit partial transverse bulkheads midway between the existing bulkheads. Investigated by Sikora and Dinsenbacher (1990), show that inserting partial bulkheads could be expected to reduce the peak stresses at the critical haunch-wetdeck intersection by 20% and the shear stress in the upper corner of the transverse bulkhead by 40% (because of the added shear area). The use of partial bulkheads also results in more uniform stress distribution in the hull plating due to less critical shear lag effects.

Another problem which the designer should pay attention to is that SWATHs are potentially vulnerable to failure in the region of strut/sponson to cross structure attachment. The attachment must be thoroughly designed to eliminate stress concentrations. Clearly, this is an area of opportunity for future design development. The cross structure/sponson structure is composed of a series of closed cells which are expected to have a high degree of torsional rigidity. This rigidity is essential. Longitudinally varying hull/strut loads will induce a torsional moment along the cross

structure/sponson structure. Accordingly, large penetrations in the main deck above the sponson must be thoroughly analysed during later design, particularly for corner stress concentrations in way of the engine box cutouts.

Longitudinal hull girder bending is not typically a significant factor in SWATH design. In this respect, panel stiffener strength characteristics normally reflect only local panel pressure loads. Scantlings designed to these loads are normally sufficient to resist any longitudinal bending and the two maximum conditions of longitudinal and transverse bending are assumed not to occur simultaneously. Also, since the hulls are cylindrical, substantial reduction in plate thickness may be obtained, and the combined plate and stiffener scantlings can be comparatively light. The strut acts like a large stiffener attached to the lower hull. The overall effect permits use of relatively light scantlings. Although strength requirements may permit a light structure, consideration of deflection and vibration may call for higher plate and shape inertias.

Basic design criteria requires material properties and construction standards which meet current monohull design practice. This objective suggests the use of classification society standards (or other practices, e.g. the Royal Navy or US Navy criteria) to guide overall structural design assumptions. However, given the ship's unusual form, conventional monohull design techniques cannot be applied blindly, and hence some judgement is necessary in their application. The designer may sometimes have to be more conservative to acquire a safe design. Malakhoff et al (1991) for instance presents an analysis on SWATH ultimate strength which exceeds the maximum lifetime load by a factor of 2.5. This compares with a factor of 1.5 for monohulls, but such conservatism is justified because of the lack of service experience of SWATHs. Further, it might as well of interest in the following to look at the difference between the Royal Navy (RN) and US Navy (USN) criteria in SWATH structural design as described by Stirling et al (1988).

Essentially the difference between the two criteria is that USN approach is developed on the basis of the working stress design (WSD), whilst the RN apply the ultimate limit state design (ULS). However, the determination of initial design load for both criteria is actually adopting the same algorithm which was provided by Sikora et al (1983). This algorithm gives a side load magnitude for SWATHs which thence to be transformed into the design extreme expected lifetime transverse bending moment on the cross structure in order to be compatible with the criteria. For the USN criteria this design bending moment $\overline{M}_{dc}$ is factored down by 0.67 to correspond to the 'characteristic' load of monohull which is derived from static balance on wave height equal to $1.1\sqrt{L}$ (ft). Adopting this condition the corresponding hull girder stress should not be higher than 40 % of the yield stress of the material ($0.4\sigma_y$). Lets M_y denotes the

bending moment that incite the material yield stress, hence the WSD criteria may be written as :

$$\overline{M}_{dc} \leq M_y \tag{5.2}$$

To meet the ULS criteria, the same value of $\overline{M}_{de}$ as above is factored up statistically by approximately 1.6 to attain an extreme bending moment value with a 99% confidence (1% probability of exceedance). Such a load factor was derived from considerations of possible errors which might arise from :

-. the determination of design load algorithm
-. differences in ship life and operability
-. experimental procedures
-. the statistics of the sea and mission profile.

The uncertainties of the above possible errors has been determined by Stirling et al (1988) which gives a total standard deviation of some 0.255 at 0.99 total mean of the variables. Further, the 1% probability of exceedance value corresponds to 2.33 standard deviations above the mean value, and may be written as

$$M_{dc(\alpha=0.01)} = 0.99 + (2.33 \times 0.255)\overline{M}_{dc}$$
$$= 1.584\,\overline{M}_{dc}$$

Similar to the reasoning as forwarded by Malakhoff et al (1991) where lack of experience owing to the novelty of SWATH concept thus additional margin of safety should be given. The RN suggest a 10% safety margin above the design extreme value will be appropriate. The actual design load confined by the ULS criteria is then given by :

$$1.74\,\overline{M}_{dc} \leq M_u \tag{5.3}$$

where M_u is the ultimate bending moment which corresponds to the ultimate strength of the structure. A brief remarks to the ultimate strength concept may be described by referring to Rutherford and Caldwell (1990) as belows.

It is believed that the concept of ship girder ultimate strength has been brought into the attention of naval architect community by Caldwell (1965). The cogitation behind this concept is to replace the conventional longitudinal strength calculation which relies solely on the elastic response of the hull girder to a prescribed condition of wave loading. In this manner the primary measure of hull girder strength is thus embodied by the section modulus of the structure. Nonetheless, the elastic modulus by itself might not always be the correct criterion of strength, because structural stability is also characterised by the resistance to buckling of the compressed members which highly possible to differ from one structure to another. Therefore, the maximum resistance of ship structure to applied bending moments should be established on the

basis of ultimate strength of the structure in order to obtain the true 'margin of safety' of a given structure.

The description of ultimate strength on a ship structure may be idealised by the box girder under longitudinal sagging moment as illustrated in Fig. 5.3. In the course of the gradual increase in bending moment due to the persistence of , say, progressing wave, three important stages of structural behaviour will develop. Firstly, when the magnitude of bending moment reaches a certain yielding will then occur at the deck and bottom of the structure. In this circumstance the stress distribution at the midship section will be as shown in Fig. 5.3b. A further increase in bending will lead to the gradual spread out of yield stress on the side members of the structure. The corresponding stress distribution, in this designated elasto-plastic zone, will be as displayed in Fig. 5.3c. Should the load increases even further, subsequently yielding takes place all over the structure (see the stress distribution in Fig. 5.3d). At this stage the structure incurs a plastic failure which leads to a total collapse. It should be noted here that the neutral axis of the cross section similarly changes it positions in conjunction with the changing of structural characteristics starting from the yield stage. The three stages can also be presented in a curve of moment M against structural deflection φ as shown in Fig. 5.3e.

In actual condition the behaviour of the structure under bending moment will not be as described above. The major difference in this case is that the compressed part of the structure will experience buckling. In sagging condition the buckled parts of the box girder will be across the deck structure. The stress distribution at the structural part above the 'plastic neutral axis' will behave differently, and is characterised by an irregular distribution of stress as exhibited in Fig. 5.4a. To a certain extent this irregular stress distribution can be represented by an average uniformly distributed stress as shown in Fig. 5.4b. In doing so a designated 'knockdown' factor should be introduced to transform the yield stress into the uniform stress magnitude that represent the irregular stress distribution. Lets ϕ_D and ϕ_S denote the knockdown factors for the uniform stresses on the upper deck and the side structures, respectively, then the ultimate bending moment of the structure may be expressed as

$$M_u = \sigma_y A D (\phi_D \alpha_D + \phi_S \alpha_S) \qquad (5.4)$$

where A = total area of the cross section
D = depth of the hull girder
α_D = ratio of deck sectional area (A_D) and total sectional area
$= A_D/A$
α_S = ratio of side structure sectional area (A_S) and total sectional area
$= A_S/A$

The knockdown factors of T stiffened plate grillages with various slenderness parameter under longitudinal compression have been forwarded by Faulkner (1965). Later on Faulkner (1975a) has provided much more information on the compression strength of plate grillages which can be selected for most practical application in ship structures.

Further, the resulting ultimate failure of hull girders in the presence of grillage buckling will be different from that in pure plastic collapse as shown in Fig. 5.3e. It is as well explained by Rutherford and Caldwell (1990) the ultimate bending moment M_u will be different in sagging and hogging conditions. The possible moment-curvature relationships of ultimate failures on ship hull girders can be illustrated as in Fig. 5.4c. As indicated in that figure, various types of hull girder response are possible as the curvature is increased, and the maximum moment of resistance can vary correspondingly between quite wide limits.

The development of analytical study on ultimate strength of ships has rapidly evolved since the 60s. In the UK development is notably at DRA (formerly ARE) Dunfermline, e.g. by Smith (1977), Dow et al (1982), and Chalmers and Smith (1992). The remarkable development of ultimate strength approach in recent years has been made possible by the wide availability of versatile FEM packages. The incorporation of reliability method in ultimate strength design has been proposed by Mansour and Faulkner (1973). The use of reliability method has now become a common practice in ultimate strength design of ship structures, e.g. as presented by Lee (1992) and Beghin (1992).

5.3. SWATH STRUCTURAL DESIGN PROGRAMS

Most of the SWATH structural design programs available are claimed to be useful only in the early stage of design. In this respect those programs are developed primarily to synthesise the initial scantlings. In the actual preliminary design these initial scantlings need to be evaluated further by a more sophisticated design approach, such as finite element analysis. In addition to those programs, initial scantlings may also be developed from past experience of a similar craft. Appendix D of this thesis contains a number of SWATH structural arrangements which may provide useful information to those who intend to design a SWATH ship when initial design programs are not available.

5.3.1. DTNSRDC *ASSET/SWATH* Program

As described by Mulligan and Edkins (1985) ASSET/SWATH is a ship synthesis computer program developed for SWATH ships. The development of this program was sponsored by the Naval Seas System Command (NAVSEA) under the aegis of the existing U.S. Navy program called ASSET (Advanced Surface Ship Evaluation) which is described by Sheridan et al (1984). This synthesis program sufficiently accommodates most of the important steps as normally explained in the design spiral.

The Hull Structure Module (HSM) as a component of the synthesis program was developed to embody the design of initial structural scantlings. The first-principle approach is employed in this module for the design analysis. Input data required by HSM is automatically transferred from the preceding module (Hull Geometry Module) together with data interactively supplied by the designer. This latter data comprises the material types, loading conditions, and structural design factors, which are determined by setting the appropriate indicators. A typical SWATH configuration and different applied loads recognised by the HSM is shown in Fig. 5.5. Transverse bending moments caused by the side force in beam seas is the only primary load which is currently considered. Other primary loads, that is, the longitudinal bending and torsional moments have not been accounted for. This is because such load data is lacking and is presumed to be less severe.

Three main components of SWATH structure are analysed in the HSM, namely, the cross deck (box), the struts, and the lower hulls. The box is characterised by six distinct plating areas which are sized individually. These are : main deck, wet deck, internal deck, fore and aft external transverse bulkheads, and internal longitudinal bulkheads. Nine options of structural material are provided by default, with a tenth option should the user have his own choice. Seven parameters of the structural material have to be assigned if the tenth option is prompted.

The applied side load could be either from the default, i.e. calculated by Sikora's algorithm [Sikora et al (1983)], or supplied by the user interactively. These are given in terms of the side load-full displacement ratio, or a certain side load magnitude in tonnes. The side load, which is assumed to act at the mid draft of the SWATH, beside being responsible for the transverse hog and sag bending moments also induces in-plane axial stresses in the structure. When these effects are added up the weight-induced sag moment, then the primary stresses in the box, are given by :

$$\sigma_1 = \frac{M_B C}{I_B} \pm \frac{P_B}{A_B} \qquad (5.5)$$

where M_B is the primary bending moment in the box, C is distance from box neutral-axis to outermost fibre, I_B is box moment of inertia, P_B is axial force in the box caused by the side load, F, and A_B is box cross sectional area. The above essentially ignores shear lag in the box decks.

In addition to this the box carries vertical shear stresses, which may be approximated by :

$$\tau = \frac{R_B}{A_{SB}} \tag{5.6}$$

where R_B is box shear force, and A_{SB} is box shear area.

One of the special features of the program is that two types of stresses, namely the nominal and peak stresses, can both be assessed. The former simply ignores stress concentrations at some distinct locations of the box, while the latter accounts for these consequences. Algorithms to correct such effects are developed by Sikora and Swanek (1982). Their drawback is that the scantling sizes tend to be heavier, because the entire box is treated as a uniform plate thickness. In the ASSET/SWATH program scantling sizes are characterised by a smeared thickness T_s. In this concept the in-plane stress is calculated for a thickened plate rather than the actual plate and stiffener(s). The smear ratio is defined as the ratio of the stiffener cross-sectional area to the parent plate. Then correlation between T_s and the nominal plate thickness T_p is :

$$T_s = (1 + \text{smear ratio})\, T_p \tag{5.7}$$

To arrive at a final smeared plate thickness iterative computation is performed where necessary so that the acceptable design stress is not exceeded. Following this the section properties of the stiffened plate are determined by imposing a default condition on the stiffener proportions.

The logic adopted in the box scantling design procedure is also applied to the strut and hull. Freedom to select different materials from the box is available for the struts, even though stiffener spacing is kept the same to ensure structural continuity. The primary and secondary loads, as depicted in Fig. 5.5, are accounted for in determining the stress level at the hull-strut intersection. Other loads induced in the hulls are hydrostatic pressure and docking forces. The weight for the superstructure is developed from past experience, and can be adequately assessed by specifying only the material type and the corresponding volumetric density.

5.3.2. US Navy Structural Synthesis Design Program (*SSDP*)

The structural synthesis design program (SSDP) which was initially developed for monohull combatants, e.g. as described by Wiernicki et al (1983), has been adapted by Aronne et al (1974) to provide rapid estimates of primary structure weight of SWATHs. The principal design tool incorporated within the SSDP is a design computer program developed at NSRDC to optimise the weight of midship section structures according to accepted US Navy criteria. The program, designated as the MIDSHIP, employs an iterative procedure and selects spacings for supported structure, panel sizes, and all scantlings suitable for the applied loads. For SWATH design purposes, the program was modified to generate an arrangement of transverse section and a longitudinal section through the bridging structure. Use of the program allowed assessment of many more design approaches and structural concepts than would have been possible through manual methods.

Parametric studies have been carried out using the MIDSHIP program on three different SWATHs, namely, SWATH A, B, and C. Several design factors governing SWATH structural weight were investigated at various levels, as described by Aronne et al (1974). The initial evaluation on the SWATH-A (4000 tonnes) was directed toward gaining an understanding of the effect on 'basic' structural weight of varying transverse web frame spacing and of changing the primary construction material (steel grades). The study resulted in a 2 ft frame spacing and the use of HTS being the lightest structure, as summarised in Table 5.1.

Referring to the findings from SWATH A the frame spacing for SWATH B (4500 tonnes) was fixed at 2 ft spacing and HTS structural material was selected. Parametric evaluations were then performed by varying the slamming pressure, external hydrostatic head, distance between strut centres, and transverse bending moment to attain the least basic weight. The use of hybrid and aluminium as structural materials for the box component was also examined. Following this a study was made on SWATH C (5250 tonnes), which was aimed at comparing the structural weight obtained by different design approaches from other agencies. Detailed observations and results can be found in a paper by Aronne et al (1974).

Apart from the capability of evaluating the influence of several applied loads and construction materials, as indicated above, the MIDSHIP program was also organised to tackle other design aspects as follows. The program allows for variation of geometric configuration, such as the number of decks and bulkheads, deck heights, strut thicknesses, and so on. The analysis of tandem strut configuration is also available. Design of structural segments can be accomplished either with or without stiffeners taken into account. The program allows for modifications such as the incorporation of grillage inner bottom design.

Another design study using the SSDP was performed by Stevens (1972) on a 4300-tonne SWATH. The versatility of the SSDP and ASSET/SWATH has attracted other agencies, e.g. in the UK where, according to Pattison et al (1988), these two programs are currently under evaluation for use within the MoD.

5.3.3. DREA CEM Program for SWATH Ships

A design suite program designated as the Concept Exploration Model for SWATH ships (SWACEM) was developed by Nethercote and Schmitke (1982) at the Defence Research and Establishment Atlantic (DREA) in Canada. The earlier version of CEM has been successfully utilised in this institution for the design of small warships, as described by Eames and Drummond (1977). SWACEM is a simplified form of ship synthesis model which addresses the earliest phase of ship selection process. The model takes as input a set of primary SWATH ship discriptors and simple operational requirements and calculates from this, ship geometry, stability, performance and other capabilities. The basic computational blocks are hull definition and stability analysis, resistance and propulsion, weight estimation and performance analysis. Algorithms are mostly used in the computational process. The latest refinement of the SWACEM was reported by Koops and Nethercote (1988).

The structural evaluation contained within SWACEM is limited to the determination of structural weight. A structural density approach is adopted for the box, strut and lower hull portions of the SWATH. The algorithms for computing the structural densities have developed from calculations of the weights of plating, bulkheads, decks, stiffeners and other structural members for a number of SWATH designs using the US Navy's SSDP. For the box, the structural weight is due to the outer shell, longitudinal bulkheads, intermediate decks and transverse bulkheads. For each of these categories an empirical expression has been derived from weight data. Summation of these individual densities yields the total box structural density. A similar procedure is followed in the derivation of the lower hull structural density.

Strut structural weight is due to the shell, transverse bulkheads and internal platforms. An empirical expression gives basic strut structural density as a function of strut geometry and the number of platforms. Stresses in the strut due to compressive and side loads are calculated and are used to decide if the prescribed minimum shell and transverse bulkhead thicknesses (3/8 in and 3/16 in, respectively) need to be increased.

The full expression of structural weight (in tons) for steel structure is written as :

$$W_h = (1 + w_{sm})(V_{BT}d_B + V_{ST}d_S + V_H d_H) / 2240 \qquad (5.8)$$

where w_{sm} is structural weight margin (an optional input). V_{BT}, V_{ST} and V_H are total box, strut and lower hull volumes. d_{BT}, d_{ST} and d_H are box, strut and hull structural densities.

5.3.4. UCL SWATH Structural Design Program

A preliminary structural design program adopting a similar approach as utilised in ASSET/SWATH has been developed by Walker (1984) at University College London (UCL). Smeared thicknesses and weight of major structural elements are outputs of the system. Only primary wave load is taken into account in the computation, so scantling sizes, which call for secondary loads, cannot be generated. It is, therefore, the effect of different framing systems, as well as frame spacings, on structural weight cannot be examined. Nonetheless, the program facilitates alternative examination of construction materials for users to select, in addition to the approximation of structural cost which is determined by using the Carreyette (1977) method.

To allow for realistic stresses at various SWATH critical regions to be properly predicted, correction algorithms developed by Sikora and Swanek (1982) are employed. The correction algorithms to obtain the actual peak stresses account for the effects of shear lag between bulkheads, stress concentrations due to haunch geometry, and the combination of shear stress developed locally in the transverse bulkheads. The peak stress is related to the nominal stress by considering the stress magnification factor which is written in general form as :

$$\sigma = \sigma_{nom} A(mx^C + B) \tag{5.9}$$

where coefficients A, B, C, x and m are functions of locations on a SWATH cross section, as shown in Fig. 5.6, and their expressions are given in Table 5.2.

5.3.5. USCG Small SWATH Structural Design

Holcomb and Allen (1983) adopted the predominantly local pressure loads in their design of small, lightweight structure SWATH OPVs. A computer program was developed to cater for initial scantling design based on the panel area 'densities' approach for plating under uniformly pressure loads, as shown by Hadler et al (1978). The initial scantlings were then checked by applying transverse bending loads and, if stresses proved excessive, extra material was added at extremities.

5.3.6. Loscombe's Small SWATH Structural Design

Loscombe (1987, 1988, 1989) has focused his work at Southampton on small SWATH crafts, i.e. 250 tonnes or less. Specific interest in this study is primarily in the exploration of alternative construction materials other than steel. Aluminium alloy and GRP are light weight materials which are thought to be the most suitable for small SWATHs in terms of both economics and structural strength.

A set of three computer programs was developed by Loscombe (1987) to integrate the load calculations, structural design and economic merit evaluations for small SWATHs. A convenient feature of this is that it can be used on a personal computer. Rather than using a single maximum lifetime side force for small SWATHs, as suggested by Allen and Holcomb (1982), a side force RAO default is used. A single design (maximum) global load is then calculated by using the design sea method based on a two-parameter Bretschneider spectrum. The secondary (slamming) load for determining the wet deck and haunch scantlings is derived using the method given by Allen and Jones (1978) or by Sellars (1976). In addition, hydrostatic pressures are incorporated to determine the scantlings of other structural parts.

The design of SWATH plate thicknesses is treated by small deflection theory which may be modified by use of a 'large deflection' stress reduction coefficient. This is then followed by the scantling design in which the required section modulus of plate-stiffener combinations (PSC) is calculated by treating the component as a built in beam, subject to a uniformly distributed load. The effective width of the plate flange is obtained from Faulkner (1975b) as :

$$\frac{b_e}{b} = \frac{1.1 \times 0.85}{1 + 2(b \times 0.85 / 0.583L)^2} \tag{5.10}$$

where b is the stiffener spacing and L is the stiffener span.

The stress on the primary structures (box, haunch and strut) under a given global loading is determined, as in eq. (5.5). Should the obtained primary stress exceed a prescribed design value then the structural dimension(s) is increased. The scantling sizes are then scrutinised for their secondary and tertiary stresses. The secondary (stiffener) stress is calculated as :

$$\sigma_{ST} = \sigma_2 \left[\frac{\sigma'_{cr}}{\sigma'_{cr} - \sigma_1} \right] + \sigma_1 \tag{5.11}$$

and tertiary (panel) stress as :

$$\sigma_{PL} = \sigma_3 \left[\frac{\sigma''_{cr}}{\sigma''_{cr} - \sigma_1} \right] + \sigma_1 \qquad (5.12)$$

where σ_1 = primary stress as calculated by eq. (5.5)
σ_2 (σ_3) = bending stress under design head on stiffener (plate)
σ'_{cr} (σ''_{cr}) = elastic buckling stress of stiffener (plate).

The allowable secondary and tertiary stress is defined as the limit stress (yield, proof or ultimate) divided by safety factor (set at 1.1 for metal and 3 for GRP). If again the maximum stresses exceed that allowed, plate or stiffener scantlings are incremented and the calculation repeated.

As inmost SWATH structural design programs, the option for structural geometry (arrangement) is restricted. Loscombe (1987) has allotted standard arrangements as seen in Figs. 5.7a and 5.7b, respectively for small SWATHs made from, steel or aluminium and GRP. The structural arrangement for steel or aluminium shown in Fig. 5.7a is typical for small SWATHs (see *Halcyon*'s design described by Luedeke et al (1985)). Longitudinal framing of the lower hulls and struts is adopted for ease of construction. Transverse framing of the box is adopted chiefly to sustain the predominantly transverse nature of primary loads. A non-integrated haunch-box connection is adopted to facilitate hybrid construction. Single skin construction for the GRP box was selected due to the uncertainty of assessing the skin-core bond in what was the critical region of the ship. Elsewhere, sandwich construction was adopted to give the lightest structural weight.

The third (evaluation) program accommodates computations of components of light weight (structural, machinery, etc) and costings. From some design evaluations Loscombe (1990) found that structural design of small SWATHs is governed more by the secondary slamming load rather than the global loads, which is in agreement with Holcomb and Allen (1983). Encouraged by this aspect, Loscombe (1990) has developed a simple algorithm for SWATH design slamming pressure. In general, the algorithm is suitable to approximate design pressure for small SWATH, even though to some extent it also gives a reasonable prediction for larger SWATHs, as examined in Chapter 4.

5.3.7. Rule-Based SWATH Structural Design

Classification rules are undoubtedly the most important guidelines for designers to consider in their vessel designs. Two aspects in particular are important in structural design. Firstly, any commercial vessel must have approval from a classification society before it can operate. Therefore, referring to the classification rules in the vessels design assures approval is given. Secondly, as a guideline these rules normally contain information required in the design, such as loadings, scantlings, criteria, etc. Most of this information is given in simple algorithms, thus computation can be carried out rapidly. The introduction of these algorithms, which have to a certain extent been extensively examined through sophisticated model analysis as well as from real experience, would obviously ease the design process.

In spite of the convenience offered, one may not always find classification rules which are intended for a specific design. This is especially so when a novel concept, such as SWATH ships, is to be dealt with. In these circumstance either rules are not available or they are incomplete. Faulkner (1992) notes that this situation is primarily brought about the classification societies do not always keep up with new developments.

Despite the fact that 20 years have elapsed from the time when the concept was first introduced, there is only one classification rule on SWATHs available now. Even so, this rule from ABS (1990) is only a provisional one and is still not extensive for designers to apply in practical designs. The ABS SWATH-rules will be best if used together with the 'first principle' structural design procedures such as those described in the previous sections. These rules indicate loading requirements, adapted from algorithms developed elsewhere. For example, the primary load derivation is based on Sikora's algorithm, while the secondary load is derived from the well known Allen and Jones (1978) method.

Formulation of some structural scantlings is also given, but designers should be aware of the definitions incorporated. For determining the bulkhead plating, for instance, a variable is defined as 'distance from the lower edge of the plate to the bulkhead deck at centre'. For a monohull ship this definition is clear enough. For SWATH, on the other hand, 'lower edge' of the bulkhead could be from the bottom of the lower hull, but it may also be from the flat wetdeck or from the bottom of the strut. Likewise the 'bulkhead deck at centre' is not very clear as to whether this is at the centreline of the vessel or at the centre line of the lower hulls or struts.

The application of other classification rules are viable provided some restriction is recognised. Small SWATHs to some extent may be designed using either DnV (1991) rules for high-speed and light craft or LR (1990) provisional rules for high-speed

catamarans. The susceptibility of small SWATHs' to slamming impact can be considered as similar to other high-speed small craft. This could be because smaller SWATHs are normally operated within a limited route of relatively less severe seas, hence the prevalent side load might not be so crucial as to affect the global strength of the structure. Therefore scantling requirements as set by those rules might not differ for SWATHs. Design checks against global loading, however, are strongly recommended. It is worth noting that most existing small SWATHs now in operation have been designed, at least by referring to the high-speed craft rules.

5.4. INITIAL SCANTLING DESIGN FOR SWATH SHIPS

5.4.1. Computer Program for Initial Scantling Design

In this section structural design study is put forward emphasising the determination of the initial scantlings of SWATHs. A case study given shows the structural analysis of a 2500-tonne SWATH operating in the North Atlantic. A computer code was written for the purpose of the design study based on the work by Walker (1984). An iterative process is used in the program to allow repetitive computations on SWATH scantlings to meet the prescribed criteria. An additional feature of the program is the capability to examine both analysis based on stress concentration corrections from Sikora and Swanek (1982) and effective width approaches. A flowchart of the developed program is shown in Fig.5.8.

In the present computation a SWATH structure is divided into six main regions, as shown in Fig. 5.6. The structural breakdown is imposed to separately evaluate the effect of stress distribution over the individual member of the transverse section of the SWATH. The stress magnification factors are then applied, depending on the structural locations, so that the strength criteria is met. The magnification factors are applied to compensate the effectiveness of the wet deck and main deck platings. In this way calculation of the sectional properties can then be made by accounting for the actual dimension of the structure. A design check was also made by considering only a certain amount of plate strips of the decks and side shells which effectively contribute to resist transverse bending and shear loads. For this latter approach magnification factors are not accounted for.

Further assumptions in the present design are as follows. The superstructure is considered non-effective in sustaining the primary loads. Hence the superstructure scantlings are designed based on the local load criteria. The box is idealised as a simply supported beam. Two longitudinal bulkheads are assumed to be positioned over the

strut haunch/box intersection. The number of strut bulkheads equals that in the box plus an extra bulkhead forward and aft for damage stability reasons. All box bulkheads are positioned directly over the strut bulkheads. Fore and aft flares are not calculated, together with the mid structure, even though 10% extra is given to the final weight due to these structural members. The haunch angle is taken to be 45 degrees throughout. Secondary load due to slamming is not taken into account in the present program.

The input data required to run the program comprises the main dimensions of the vessel. Selection of structural material is facilitated for different regions of the structure. The primary load considered in the analysis may be either interactively given by the user, or optionally calculated using the algorithm by Sikora et al (1983). The primary stress calculation is then made by the formulation as shown in eq. (5.5). Variables are taken as appropriately for the box deck or the struts. Further options are given to the user once computation is completed. These allow the user to carry out further analyses for different structural configurations, structural materials, wave load values or combinations of these. A sample of output data is given in Table 5.3.

5.4.2. Sensitivity Evaluation of Structural Weight

Using the design load derived by Sikora's algorithm, together with the magnification factors on member stress, yields an overall structural weight of about 954 tonnes for the 2500-tonne SWATH-FV. Whereas computation by imposing the effective width of deck and side platings results in a substantially higher structural weight of approximately 1120 tonnes, which some 17% higher than the former. As mentioned earlier, even though the first approach accounts for stress magnification factors, the actual scantling dimensions are included in the calculation of sectional properties. Nonetheless, the structural weight derived by considering the effective width correlate better with another SWATH of similar size. For the design of a 2500-tonne Sonar Support Vessel by Smith et al (1987) was found the structural weight was found to be 1055 tonnes. The structural weight fraction (ratio of structural weight to full displacement) for the 2500 SWATH-FV is about 0.45 compared to 0.42 for the SSV. As observed by MacGregor (1989) these values are within the range typical to SWATH vessels, i.e. between 0.41 to 0.52. Parametric study by Stirling et al (1988) in structural design on RN SWATH a using three different programs apparently support this account.

The corresponding value of 0.38 was obtained when the magnification factor approach is applied. Figure 5.9 illustrates the comparison of structural weight by the two approaches for various load magnitudes. The relationship is quite linear for both cases. A change of primary load by ±30% results in an average of only 12.5% change in structural weight.

The effect of different construction materials on the structural weight has also been examined. The combinations of construction material studied is as listed in Table 5.4. Figure 5.10 presents the computational results in which the percentage of the weight variation is plotted against the primary load. The reference weight in this case is taken to be the one obtained by imposing the side load using Sikora's algorithm for material combination 1 in Table 5.4. As is shown, structural weight decreases only about 2% when the superstructure is constructed from GRP while retaining B quality steel for the rest of the structural members. The corresponding structural cost for this combination (2), as shown in Fig. 5.11, increases by some 12%. Structural combination 3, for which high stress regions are fabricated out of HY80 steel, only reduce the structural weight of by around 5%. Unfortunately, the structural cost in this case increases by around 200%. A significant weight reduction of 37% can be attained by combination 4 where aluminium is used in the regions 1, 2 and 3A. The additional cost required for this combination 4 is in excess of 60%. Retaining aluminium for the construction of those regions, and combining with HY80 steel for high stress members, may result in a 39% weight reduction. However, this is only 2% less than the former one while structural cost becomes 120% higher than the reference cost. These comparisons suggest structural combination 4 should be the best choice for designers.

Another interesting comparison is seen from the effects on structural weight by modifying the vessel particulars. It is not the intention here to suggest any modification of ship's main parameter to achieve an acceptable weight saving, rather it is to emphasise that such action is prohibitive. The reason is obvious that modification in ship's parameter could likely jeopardise its hydrodynamic performances and possibly other main features without much benefits, as demonstrated in the following.

The two parameters to be altered are the maximum beam of the vessel and the deck clearance. For the first case, the computational output has been plotted, as shown in Fig. 5.12. It is seen from this figure that altering the maximum breadth of the vessel is quite beneficial. To acquire some 8% reduction in structural weight the designer would need to reduce the maximum breadth by approximately 5 metres. This means around 540 m^2 of useful deck area (about 21% of the initial area) has to be sacrificed. The corresponding useful deck volume loss in this case is about 710 m^3, and can be up to 983 m^3 if the volume under the double bottom is considered. The gain in minimising structural cost is equally unpromising. Cost saving attained by 8% weight reduction may not be higher than 10%.

Similar results unfortunately apply when box clearance alteration is attempted, as can be seen in Fig. 5.13. An approximately one metre deck clearance reduction (22% from original) gives only 9% less weight, with cost saving gained is about 11%. On

top of that, reducing deck clearance would increase the susceptibility of the SWATH to slamming loads. There is then a trade off in increase of wet deck scantlings. From a further evaluation, the same amount of weight saving (8-9%) is shown to be achievable by the addition of transverse bulkhead, as shown in Fig. 5.14. Moreoyer, such additional bulkhead will improve shear lag characteristic of the structure. Hence this method is favourable for the designer.

5.5. DISCUSSION

The study presented in the foregoing could only be expected to be useful in the very early design process. Many more improvements still need to be pursued in future. The present code is only developed to tackle the design of SWATHs with single strut per hull configuration, hence modification to account for tandem strut forms is necessary. A further improvement ought to be made by including the secondary slamming loads for the determination of wet deck scantlings. The pressure design can be obtained by empirical methods, as given in Chapter 4. The pressure data is then to be associated with various plate strength criteria, e.g. as introduced by Clarkson (1956). The plate and stiffener sizings are finalised to satisfy the corresponding criteria in relation to modes of plate panel collapse. Many high speed craft designs have adopted such an approach, as well as by referring to the society rules. Examples of bottom structure design by the first principle can be found in papers by Heller and Jasper (1961), Spencer (1975), Drummond et al (1976), and Henrickson and Spencer (1982).

The lower hull design calls for a more reliable tool if a realistic solution is to be gained. Some approaches practised for semi-submersible offshore structures generally are in favour with the scantling design of SWATH lower hulls. Some design methods, as developed by Bose (1982) or Penney and Riiser (1984), may be considered in commencing a more rigorous SWATH design. The cost analysis incorporated in the present program is also limited to the data for 1984. More updated information is therefore necessary if accurate structural cost estimation is to be achieved. Recent cost data for steel structure, as provided by Buxton (1987), may be considered to revise those presently adopted. Loscombe (1988) has made cost data available for other structural materials. The development of cost analysis for the latter is based on the work by Smith and Monks (1982).

As important as those rigorous approaches is information in the form of simplified algorithms which may be applied in the early stage of structural design. MacGregor (1989) has diligently gathered SWATH structural data and analysed this to derive simple expressions of various parameter correlations for SWATH structure.

These expressions include, among others, structural densities, stiffened area densities for wet decks, and simplified lower hull weight formulation. Also found in that reference are the compartment lengths, transverse frame spacings, wet deck scantling proportion etc, which are normally applied to SWATH designs.

One of the best examples that ought to be targeted within SWATH research is an integrated hydro-structural design tool as was established at JAMSTEC/Mitsui. Takeuchi et al (1985) present this design program, which eventually incorporate various sophisticated analysis. The package program pertinently contains sub programs for determining the global-structural loads by a 3-dimensional theory, a finite element package for stress analysis, and a versatile program for the evaluation of ultimate strength. In addition to this, a sub-program to generate the secondary slamming load is also embodied in the design suite. The determination of relative vertical velocities and the corresponding impact pressures are synthesised in a ship motion program which includes also algorithms of pressure loads from various sources.

5.6. CONCLUSIONS

A SWATH structural design study has been presented in this chapter by first of all indicating generic attributes of this type of vessel. Design procedures for such vessels should not differ from those traditionally practised for monohull ships. Some design criteria may also be adapted from monohull, but further evaluation is necessary. A review of SWATH design methodology evolved at some institutions was made to in developing the study.

A computer program was subsequently written to facilitate structural calculation which is iterative in nature. Some of the early findings have been presented. The primary comparison was to identify the differences between the magnification factor and effective width approaches on the resulting design values. A relatively large difference in structural weight (around 17%) is found from the two computations. Nevertheless, the effective width approach yields a comparatively better estimate of structural weight fraction when referring to another design of SWATH. A value of 0.45 is obtained in the present design on the SWATH-FV compared to a 0.42 for the SSV. Note that both vessels are 2500 tonne in displacement. The corresponding value derived by the magnification factor approach is of the order 0.38.

A parametric study has been conducted in which the primary load is altered by ±30% from a given standard maximum value. In this way an average change of 12.5% in structural weight results. The discrepancy is quite large if compared to the observation by Aronne et al (1974). From their study it was found that altering the primary bending moment by ±50% only resulted in approximately 5% change of

structural weight. This is obviously an area which needs to be pursued further. The parametric study follows with an investigation of the use of lightweight materials in SWATH construction. Aluminium-steel hybrid structure seems to be the best choice for the designer. By adopting such a combination some 37% weight saving is achievable, while the increase in structural cost is acceptable. An attempt to attain a respectable weight saving by the conversion of the primary configuration (maximum breadth or deck clearance) would not be beneficial. Additional transverse bulkheads would gain some weight reduction, in parallel to the improved shear lag characteristics.

Table 5.1a. Summary of 'Basic' weights and densities for Ship A, HY100 and different frame spacings

Nominal Transverse Frame Spacing (feet)	Weight in Tons (Steel-HY100)				Density (lbs/cu ft)			
	Bridge Structure	Struts	Lower Hulls	Total	Bridge Structure	Struts	Lower Hulls	Total
16.20	1128.00	664.00	634.00	2426.00	6.61	9.46	11.81	8.24
5.00	1121.00	536.00	319.00	1976.00	6.56	7.65	5.95	6.71
4.00	1001.00	483.00	303.00	1787.00	5.86	6.89	5.65	6.07
3.00	982.00	444.00	298.00	1725.00	5.75	6.33	5.56	5.86
2.00	1032.00	405.00	301.00	1738.00	6.05	5.78	5.60	5.90

Table 5.1b. Summary of 'Basic' weights and densities for Ship A, 3-foot transverse frame spacing and different materials

Type of Material	Weight in Tons				Density (lbs/cu ft)			
	Bridge Structure	Struts	Lower Hulls	Total	Bridge Structure	Struts	Lower Hulls	Total
MS	870.00	533.00	379.00	1782.00	5.09	7.60	7.06	6.05
HTS	843.00	470.00	326.00	1639.00	4.94	6.70	6.08	5.56
HTS (2 ft)	811.00	420.00	299.00	1530.00	4.75	6.00	5.55	5.19
HY80	878.00	451.00	308.00	1637.00	5.14	6.43	5.73	5.56
HY100	982.00	444.00	298.00	1725.00	5.75	6.33	5.56	5.86

Table 5.4. Combinations of structural material for structural weight observation

Combinations	1	2	3	4	5
Region 1	M1	M2	M1	M3	M3
Region 2	M1	M1	M4	M3	M3
Region 3A	M1	M1	M4	M3	M3
Region 3B	M1	M1	M4	M1	M4
Region 4	M1	M1	M4	M1	M4
Region 5	M1	M1	M1	M1	M1
Region 6	M1	M1	M1	M1	M1

M1 : B Quality Steel
M2 : GRP
M3 : Aluminium NP8N
M4 : HY80 Steel

Table 5.2. Magnification factors to the nominal stress for several critical locations on SWATH cross structure [Sikora and Dinsenbacher (1990)]

Point A - Centreline longitudinal bulkhead-transverse bulkhead-main deck .

Factor = $A(mx^C + b)R$

where x = 0 at centreline, y = 0 at transverse bulkhead (spacing TBS)

A = 0.831 + 2.803 (TBS/BHC) where BHC is hull centreline spacing

$m = 0.41 - 0.625\sqrt{y}$

$b = 0.579 - 0.194y$

$R = 0.99 - 0.14y^2$

C = 2

Factor A = 0.573 (0.831 + 2.803 TBS/BHC)

Point B - Transverse bulkhead-main deck (inboard of outboard longitudinal bulkhead)

Factor = $A(mx^C + b)R$

x = 0.8, y = 0, C = 2, m = 0.41, b = 0.579, R = 0.9004

Factor B = 0.757 (0.831 + 2.803 TBS/BHC)

Point C - Outboard longitudinal bulkhead-transverse bulkhead-main deck

Factor = APR_0

this factor allows for the effect of an insert plate where

t = thickness of insert plate, t_0 = thickness of parent plate, and $t/t_0 = 1.5$ is assumed

$P = 1.96 - 0.96\ Vt/t_0$

$R_0 = 0.85$

A = 1.831 + 2.803 (TBS/BHC)

Factor C = 0.667 (0.831 + 2.803 TBS/BHC)

Point D - Outboard longitudinal bulkhead-transverse bulkhead-wet deck

Factor = $A(mx^C + b)R$

A = 1.829 + 6.114 (TBS/BHC)

x = 0, y = 0, C = 2

m = 0.716, b = 0.276, R = 1.15

Factor D = 0.317 (1.829 + 6.114 TBS/BHC)

Point E - Transverse bulkhead-wet deck (inboard of outboard longitudinal bulkhead)

Factor = $A(mx^C + b)R$

A = 1.829 + 6.114 (TBS/BHC)

x = 0.8, y = 0, C = 2

m = 0.716, b = 0.276, R = 0.958

Factor E = 0.703 (1.829 + 6.114 TBS/BHC)

Table 5.2 Contd.

Point F - Outboard longitudinal bulkhead - transverse bulkhead-wet deck
Factor = APR_0
A = 1.829 + 6.114 (TBS/BHC)
t = thickness of insert plate, t_0 = thickness of parent plate, and $t/t_0 = 1.5$ is assumed
P = 0.784, R_0 = 0.91
A = 1.831 + 2.803 (TBS/BHC)
Factor F = 0.714 (1.829 + 6.114 TBS/BHC)

Point G - Outer haunch/strut knuckle - strut platform deck - transverse bulkhead
Factor = APR_0
A = 1.198 + 1.784 {TBS/(T+BC+DB-DH)}
t = thickness of insert plate, t_0 = thickness of parent plate, and $t/t_0 = 1.5$ is assumed
P = 0.784, R_0 = 1.14 - 0.09 (r/TS)
r/TS = 0.5 where r is the radius of the strut inner shell
A = 1.831 + 2.803 (TBS/BHC)
Factor G = 0.858 {1.198 + 1.784 TBS/(T+BC+DB-DH)}

Point H - Outer strut sideshell - transverse bulkhead (below strut platform deck)
Factor = $A(mx^C + b)R$
A = 1.198 + 1.784 {TBS/(T+BC+DB-DH)}
x = 0.8, y = 0, C = 1, b = 0, m = 0.923, R = 1.149
Factor H = 0.848 {1.198 + 1.784 TBS/(T+BC+DB-DH)}

Point K - Inner haunch/strut knuckle - strut platform deck - transverse bulkhead
Factor = APR_0
A = 4.212 - 0.182 {TBS/(Strut Depth)}
t = thickness of insert plate, t_0 = thickness of parent plate, and $t/t_0 = 1.5$ is assumed
P = 0.784, R_0 = 1.17
Factor K = 0.917 {4.212 - 0.182 TBS/(Strut Depth)}

Point L - Inner haunch/strut knuckle - transverse bulkhead (below platform deck)
Factor = $A(mx^C + b)R$
A = 4.212 - 0.182 {TBS/(Strut Depth)}
x = 0.8, y = 0, C = 1, b = 0, m = 0.996, R = 1.19
Factor L = 0.951 {4.212 - 0.182 TBS/(Strut Depth)}

Table 5.3. Sample of output data from initial scantling design program

```
** INITIAL STRUCTURAL DESIGN FOR SWATH **

NAME OF THE VESSEL : SWATH - FV
M I S S I O N      : OCEANO RESEARCH
OPERATIONAL AREA   : NORTH ATLANTIC

***** SWATH CONFIGURATION NO :  1 ******

SWATH PARTICULARS -
DISPLACEMENT    =     2467.00 tonnes
OVERALL LENGTH =       57.20 m
MAXIMUM BEAM    =      25.60 m
DRAUGHT         =       8.20 m
BOX DEPTH       =       3.60 m
BOX CLEARANCE   =       5.10 m
STRUCTURAL WEIGHT FRACTION =   0.40
SUPERSTRUCTURE LENGTH  =  20.00 m
SUPERSTRUCTURE BREADTH =  18.00 m
NUMBER OF A/C HANGERS  =  1
NO. OF DECKS IN BOX    =  1
NO. OF TRANSV. BKHDs is 7 at  9.53 m spacing (INCLUDING ENDS)
NO. OF LONGT. BKHDs IN BOX =   3
LENGTH STRUT NOSE   =   4.60 m
LENGTH STRUT CENTRE =  36.40 m
STRUT THICKNESS     =   3.00 m
LENGTH STRUT TAIL   =   4.60 m
NO. DECKS IN STRUT  =    3
NO. TRANSV. BKHDs STRUT =   7
LENTICULAR STRUT NOSE
DIAMETER OF HULL = 5.10 m
LENGTH OF HULL    =  54.65 m

MATERIALS SELECTED
>>>>>>>>>>>>>>>>>>
REGION 1 (SUPERSTRUCTURE)                                  BQUALITY STEEL
REGION 2 (BOX UPPER DECK AND INTERNAL STRUCT)              BQUALITY STEEL
REGION 3A (LOW STRESS REGION OF BOX WET DECK)              BQUALITY STEEL
REGION 3B (HIGH STRESS REGION OF BOX WET DECK)             BQUALITY STEEL
REGION 4 (HIGH STRESS REGION OF STRUT AND HAUNCH)          BQUALITY STEEL
REGION 5 (LOWER STRUT)                                     BQUALITY STEEL
REGION 6 (HULL)                                            BQUALITY STEEL

  !! WARNING-MATERIAL SELECTED MAY RESULT IN STRUCTURAL WEIGHT
                FRACTION EXCEEDED IN BUILD !!
```

Table 5.3 Contd.

RESULT OF THE INITIAL DESIGN ANALYSIS :
>>

DESIGN SIDE FORCE F = 15.09 MN
TRANS. B.M. OCCURS IN SAG CONDITION AT BOX CENTRE = 186.11 MNm
TOTAL STRUCTURAL WEIGHT = 953.82 tonnes

SUMMARY OF SMEARED THICKNESSES AND STRESSES

REGION	TSM (mm)	STRESS	MAX. PRIMARY (MPa)	ALLOW. WORKING
2	7.00	-117.20	147.00	262.00
3A	23.00	46.17	147.00	262.00
3B	23.00	143.23	147.00	262.00
4	18.00	125.08	147.00	262.00

OTHER SCANTLINGS :

BOX TRANS BULKHEADS = 5.0 mm
STRUT TRANS. BULKHEADS = 6.0 mm
BOX LONGITUDINAL BULKHEADS = 8.0 mm
BOW, TRANSOM, SIDES = 10.0 mm
BOX AND STRUT DECKS = 6.0 mm
LOWER STRUT SHELL = 10.0 mm
HULL PLATING = 10.0 mm

WEIGHT OF STRUCTURAL ELEMENTS :

SUPERSTRUCTURE =	32.8 tonnes	COST =	0.7 Mil. Pds.
B O X =	412.5 tonnes	COST =	5.4 Mil. Pds.
S T R U T S =	420.1 tonnes	COST =	3.1 Mil. Pds.
H U L L S =	88.4 tonnes	COST =	1.1 Mil. Pds.

BREAKDOWN OF STRUCTURAL WEIGHT :
PRIMARY = 848.9 (86. %)
SECONDARY = 104.9 (11. %)
MINOR = 33.0 (3. %)

APPROXIMATE COST OF STRUCTURE = 10.3 Million Pounds

N.B. Based on procurement and labour costs - Including margins. Cost results should only be used as a basis for comparison between structural and material options during parametric study.

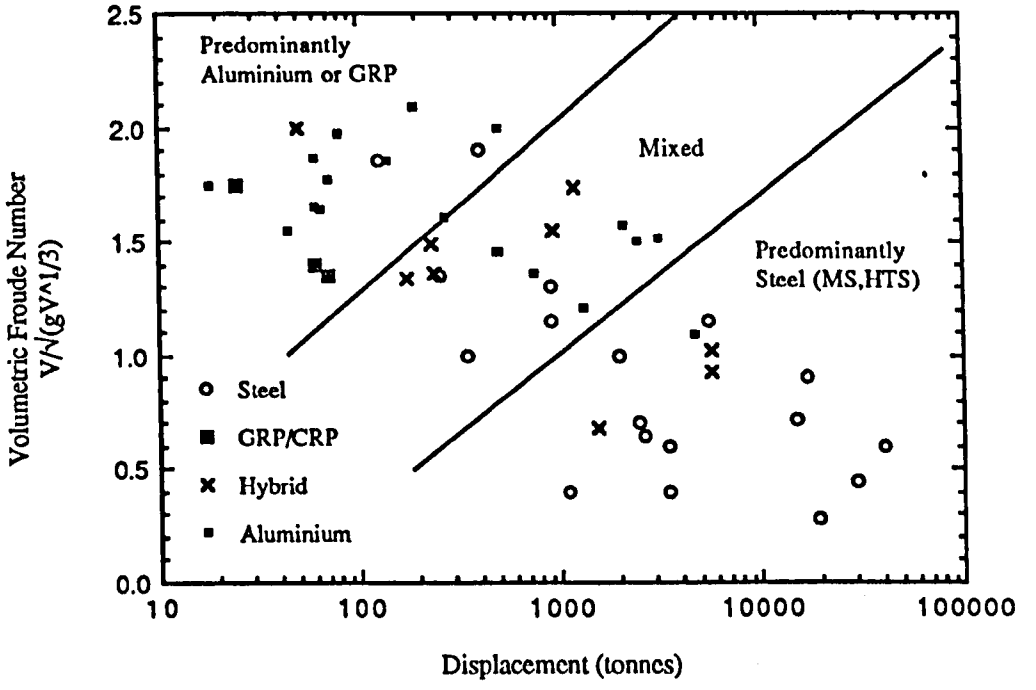

Figure 5.1. Structural materials used in SWATH vessels
[MacGregor (1989)]

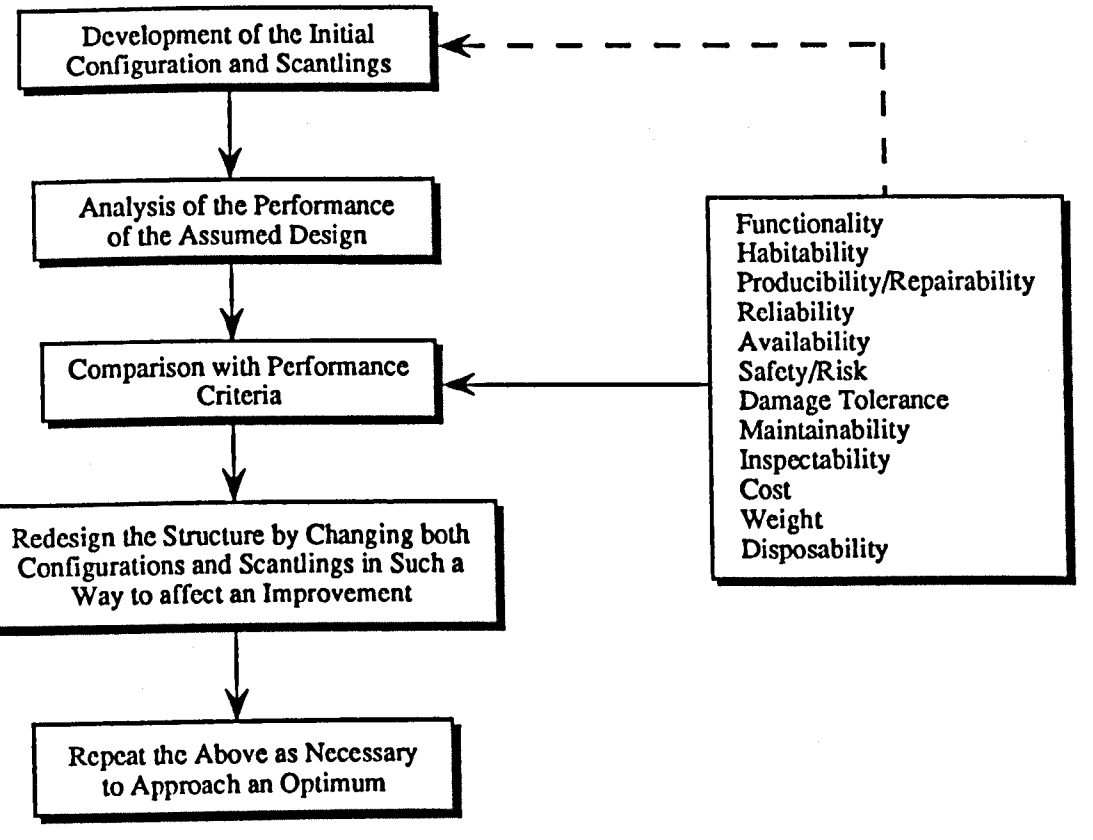

Figure 5.2. Ship structural design process

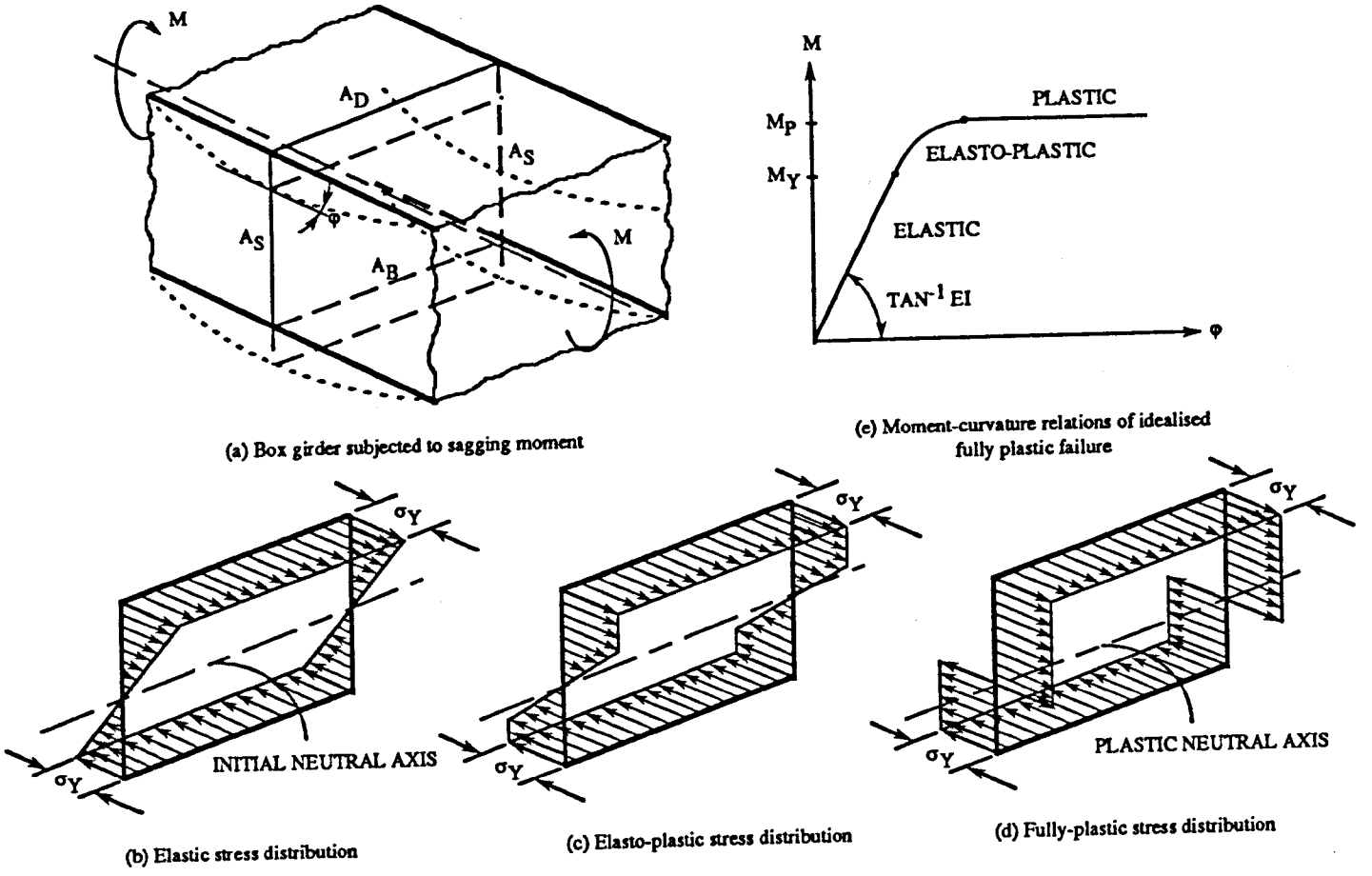

Figure 5.3. Box girder under sagging moment
[Caldwell (1965)]

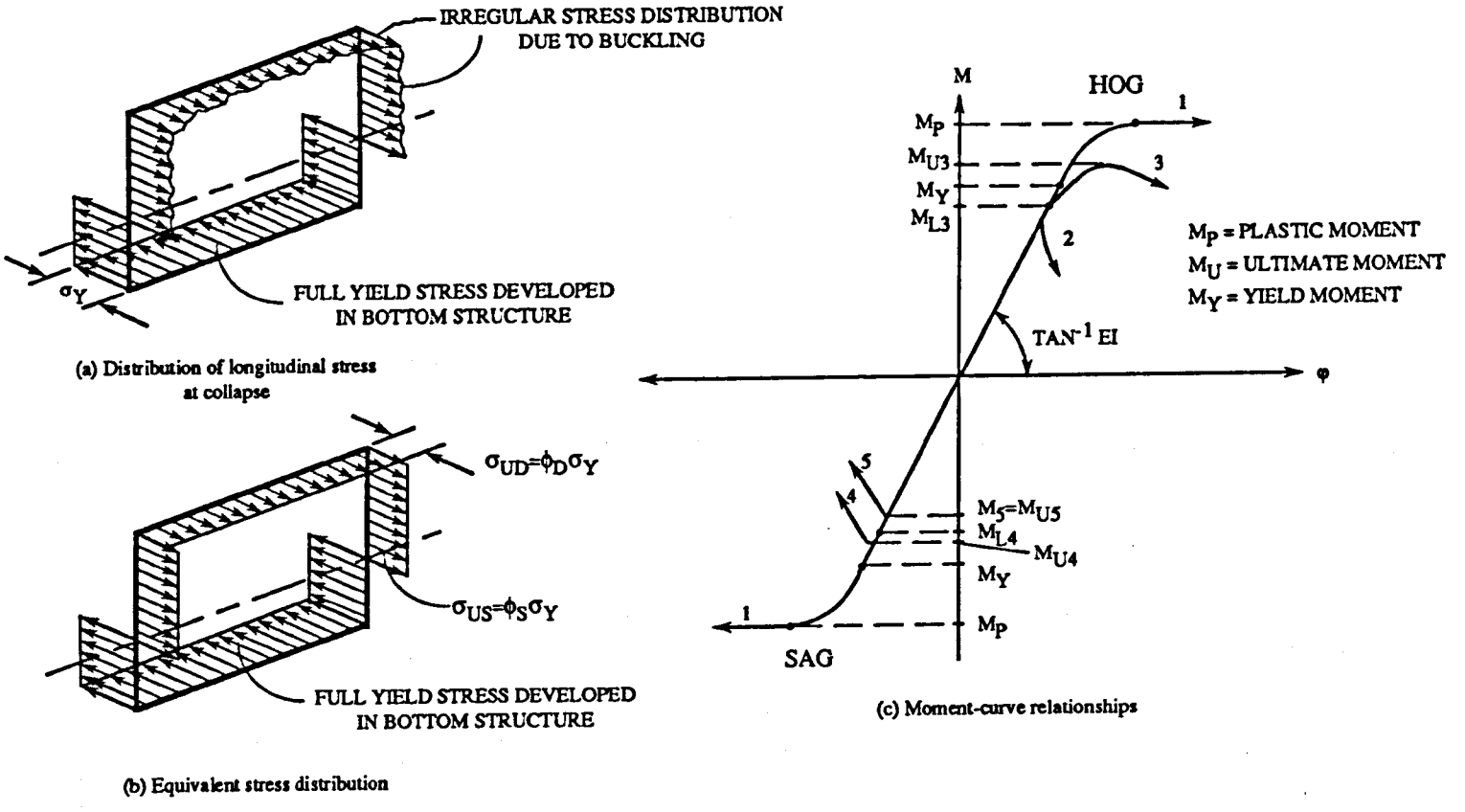

Figure 5.4. Ultimate stress distribution taking into account of buckling
[Caldwell (1965), Rutherford and Caldwell (1990)]

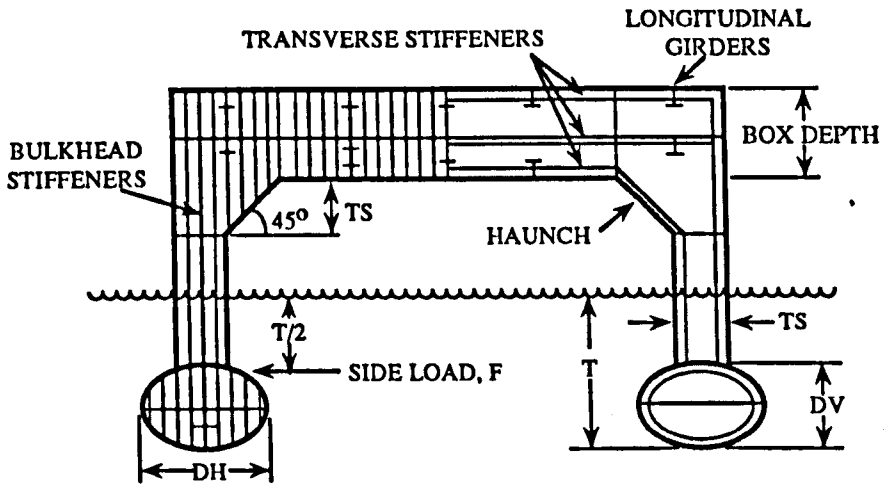

(a) STRUCTURAL CONFIGURATION

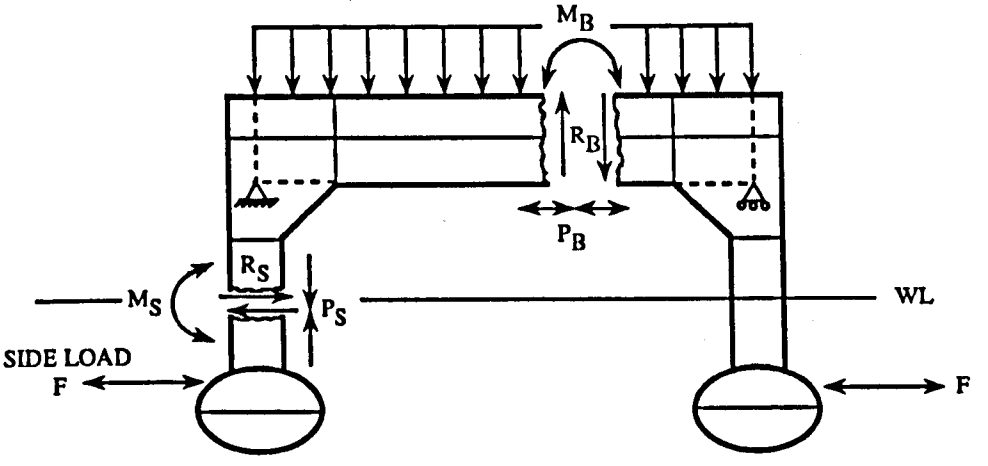

(b) PRIMARY LOADS AND FORCES

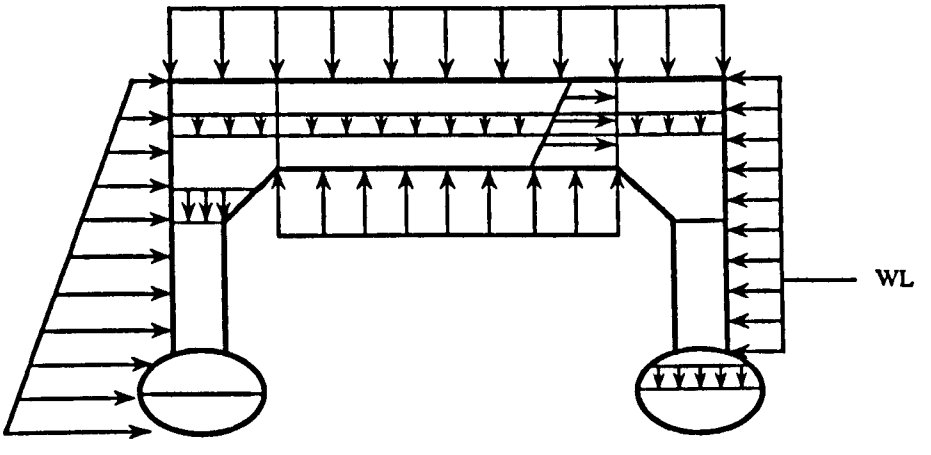

(c) SECONDARY LOADS

Figure 5.5. SWATH structural configuration and loading conditions [Mulligan and Edkins (1985)]

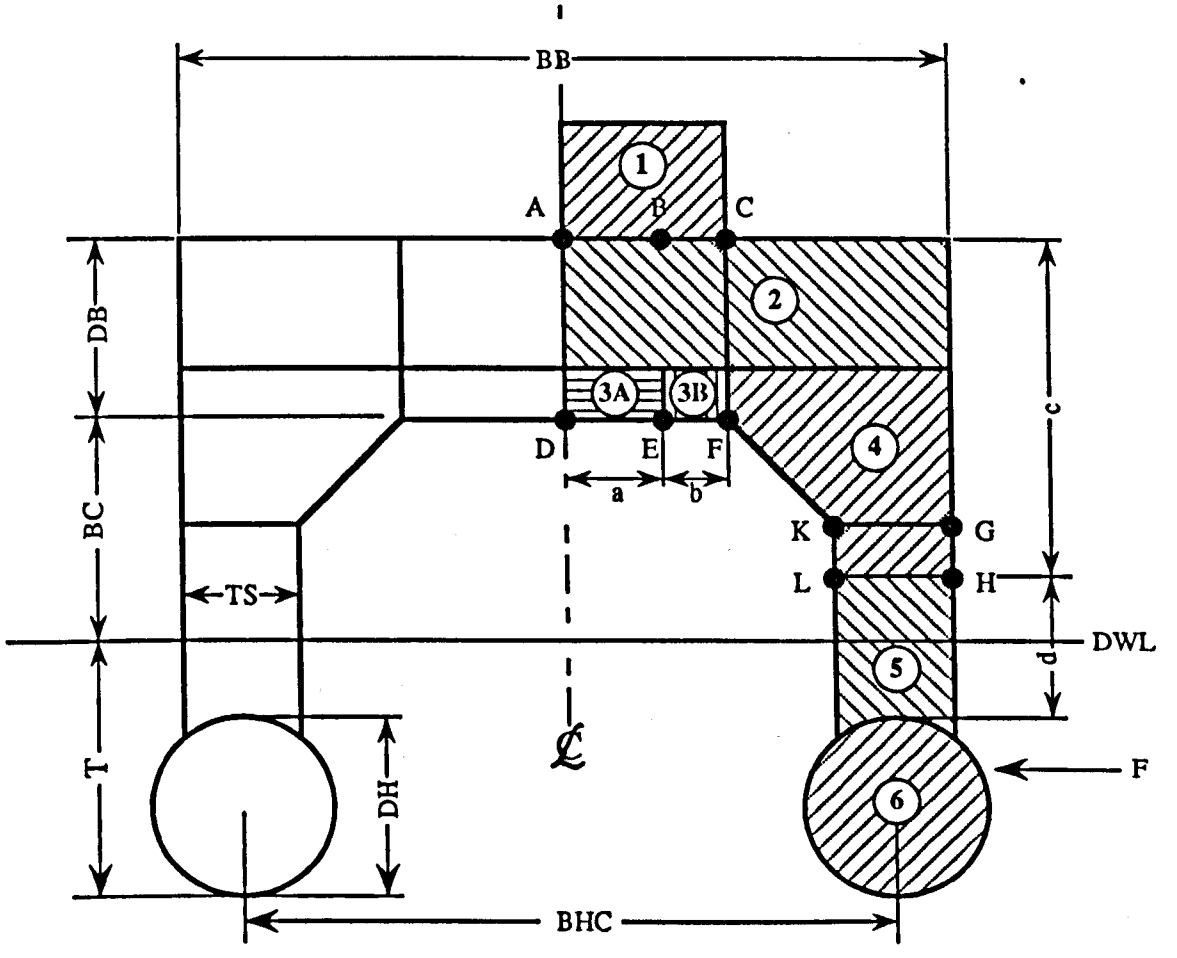

Definitions :

1. Superstructure
2. Box weatherdeck andinternal structure

3A. Low stress region of box wet deck

3B. High stress region of box wet deck

4. High stress region of upper strut and haunch
5. Lower strut
6. Lower hull

a = {BB-0.2(BB+11TS)}/2

b = {0.1(BB+11TS)-1.5TS}/2

c = 0.2(BC+T-DH)+0.8TS

d = 0.7DH-0.2T+0.8(BC-TS)

Figure 5.6. Definition of structural regions and location in cross structure of points of stress calculation [Walker (1984), Sikora and Dinsenbacher (1990)]

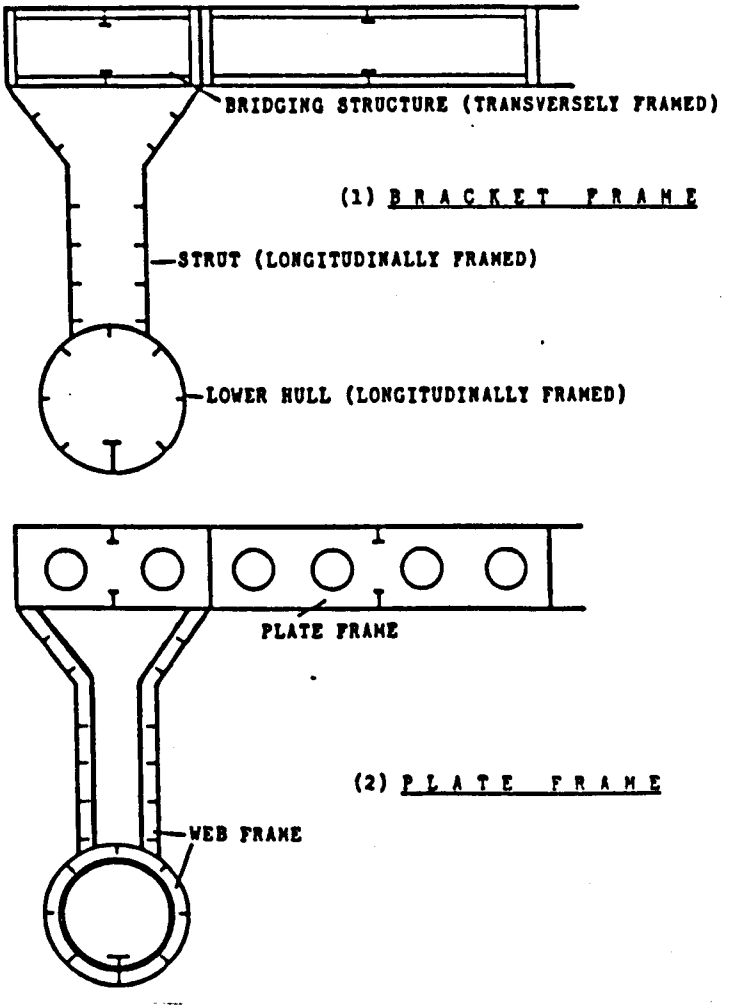

Figure 5.7a. Standard arrangement for small SWATHs constructed out of steel or aluminium [Loscombe (1987)]

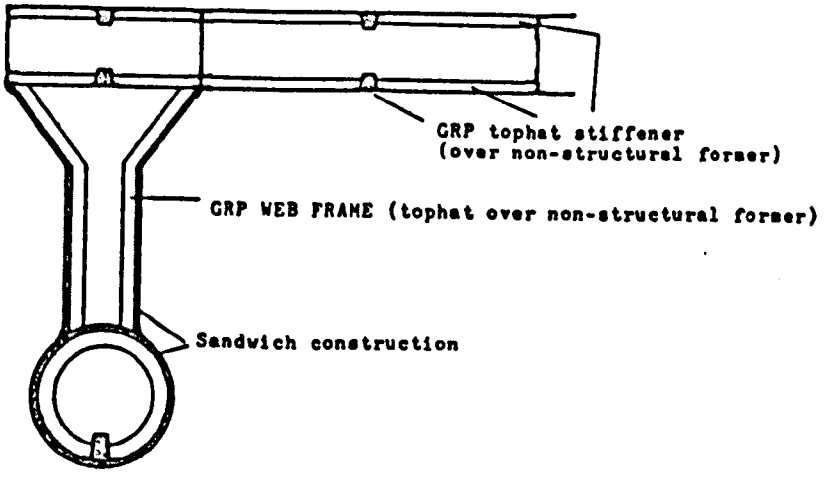

Figure 5.7b. Standard arrangement for small SWATHs constructed out of GRP [Loscombe (1987)]

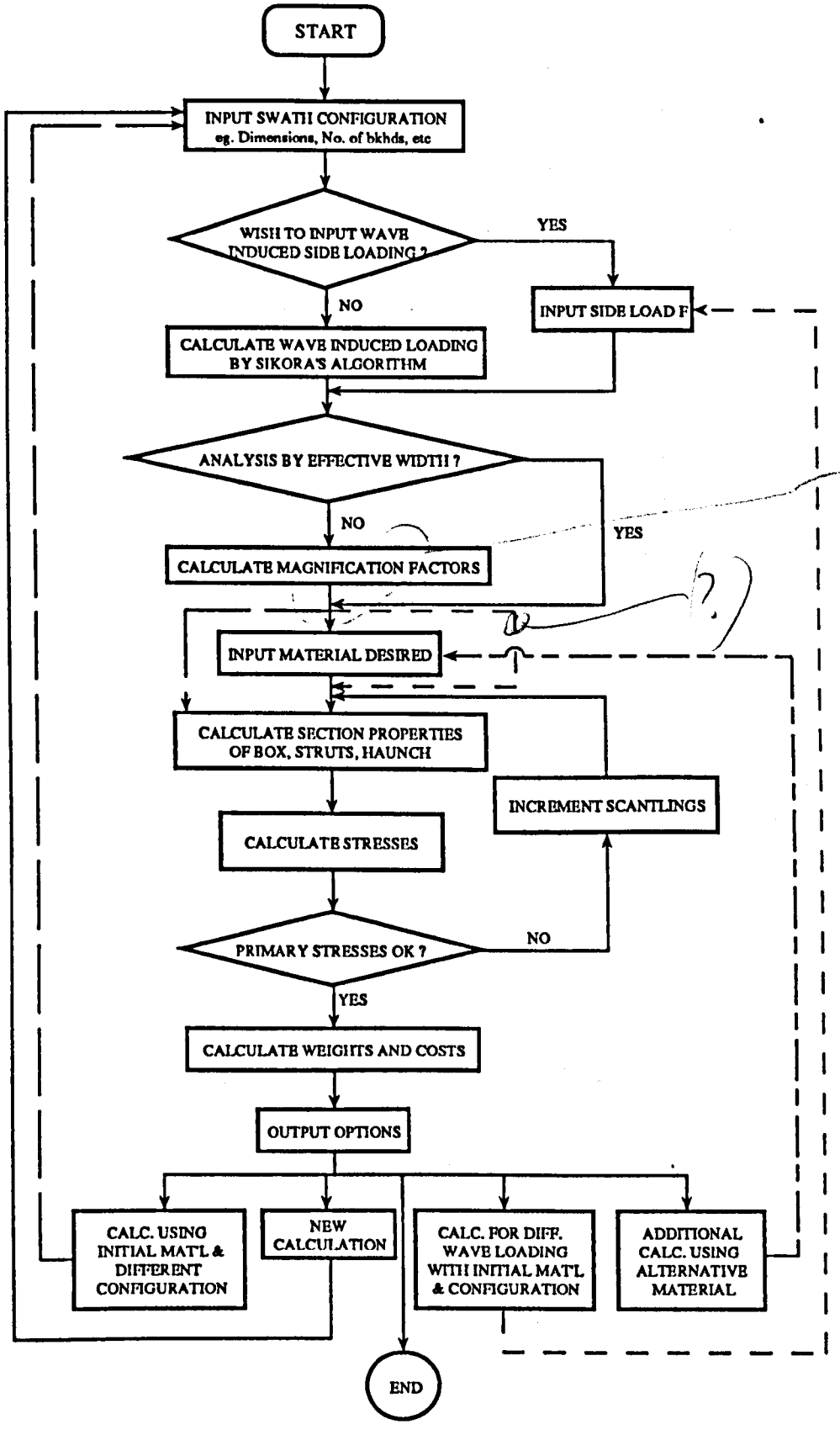

Figure 5.8. Flowchart diagram of the program to determine initial scantlings of SWATH vessels

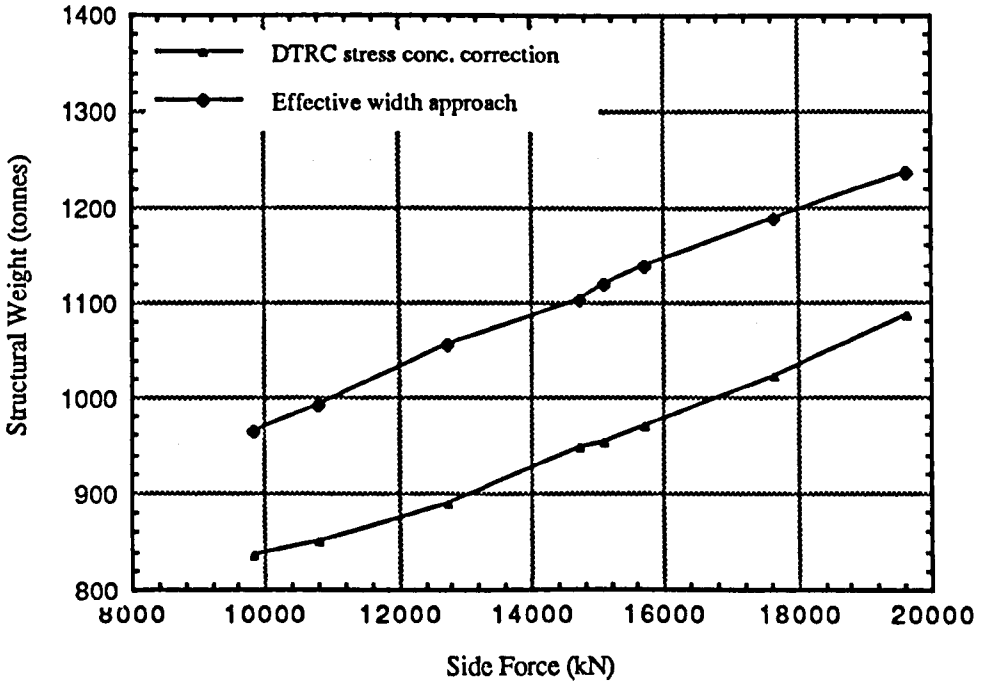

Figure 5.9. Comparison of structural weights from stress concentration and effective width approaches

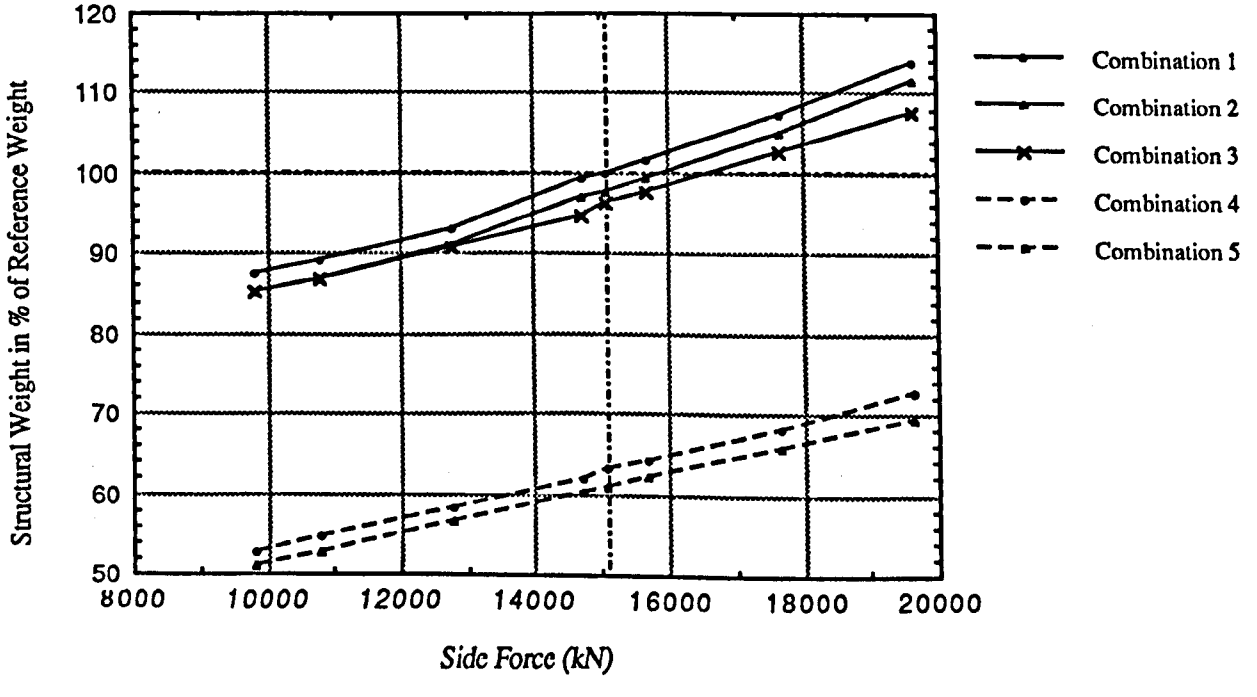

Figure 5.10. Effect of construction material combinations on the structural weights

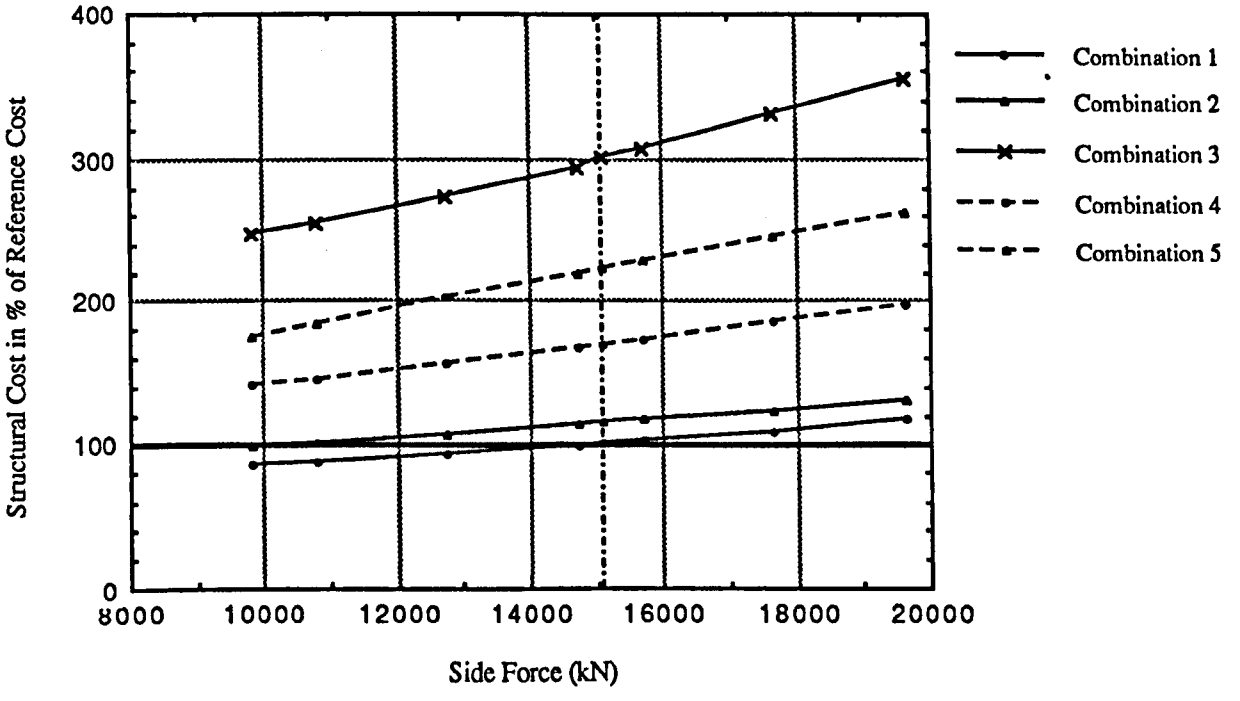

Figure 5.11. Effect of construction material combinations on the structural costs

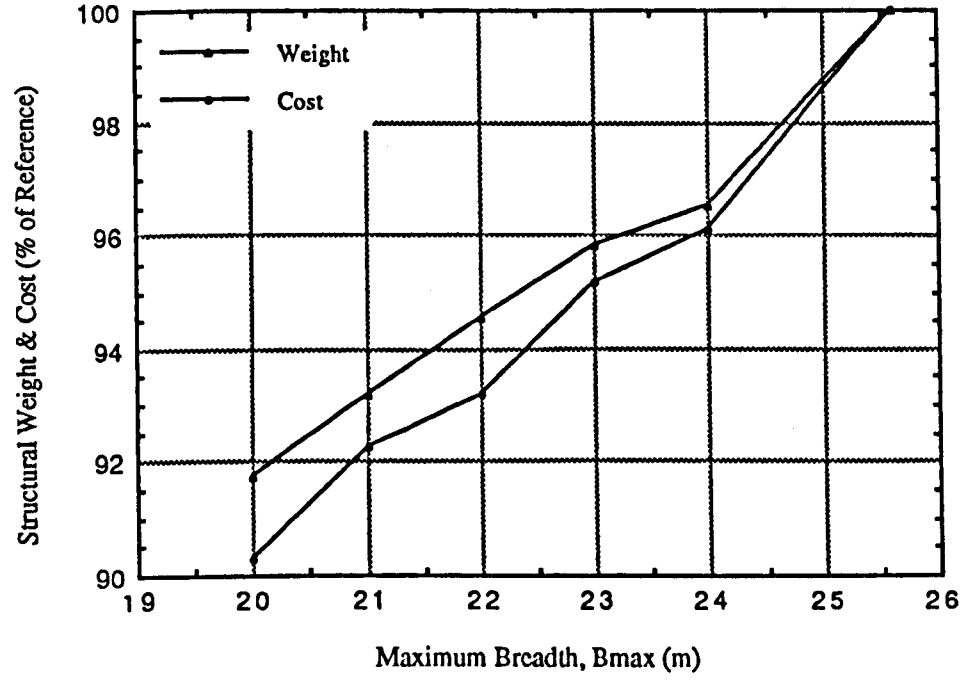

Figure 5.12. Effect of change in maximum breadth to structural weight and cost

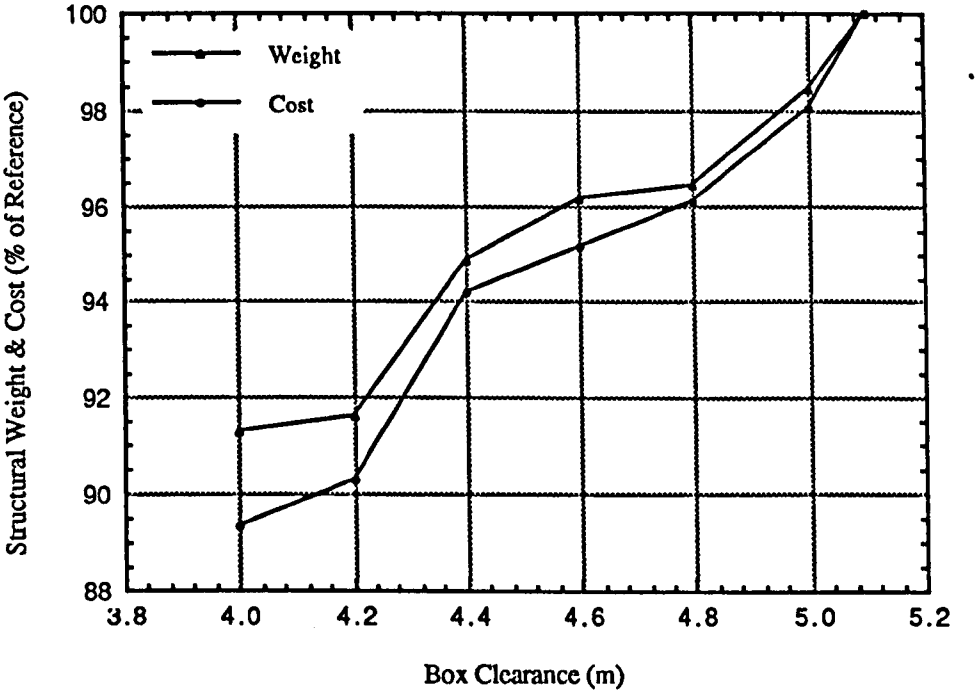

Figure 5.13. Effect of change in box clearance to structural weight and cost

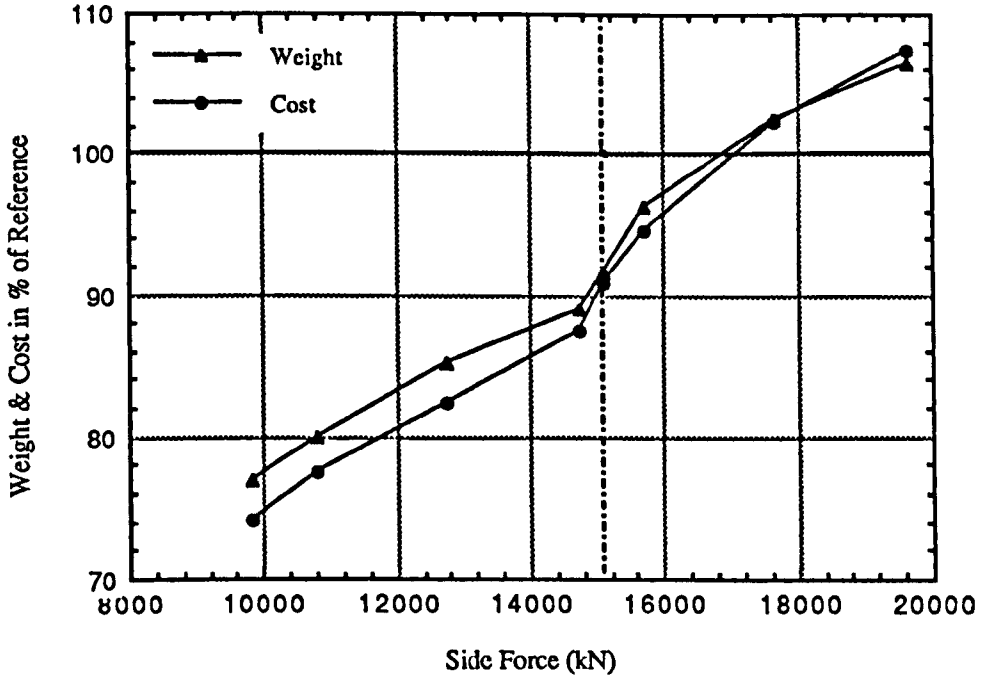

Figure 5.14. Effect of additional one transverse bulkhead to structural weight and cost

CHAPTER 6

FATIGUE PERFORMANCE OF SWATH SHIPS

CHAPTER 6

FATIGUE PERFORMANCE OF SWATH SHIPS

6.1. INTRODUCTION

Fatigue performance of a structure generally is measured by its capability to sustain predominantly cyclic loads. Under such loads, many engineering structures will fracture after a sufficient number of cycles even though the alternating stress amplitude is much less than the static yield stress of the structural material. Marine vehicles are highly susceptible to this type of loads because of the nature of the sea waves which are substantially cyclical. Besides that other operational factors would to a certain degree incite additional cyclic loads, which in some cases can be profoundly critical. Munse (1983) indicates four main categories of cyclic loads involve in characterising the fatigue performance of a marine vehicle, namely

a. the low frequency cyclic load (quasi-static), which is primarily due to repeated of wave action to the structure. The number of cycles experienced during a lifetime of ship (normally around 20 years) is some 10^7 up to 10^8. Some factors affecting the intensity of wave load are as described in Chapter 3,

b. the high frequency (dynamic) cyclic loads, which can further be classified according to the nature of their excitations into the transient and steady state loads. The former is identified due to slamming, i.e. water impact on the bottom of a vessel, which manifests its effect into a vibrational response on the structure, and is known as the hull whipping. The steady state dynamic loads are those generated by the ship's machinery or propeller. The response of the structure to this type of load is usually referred to as hull springing.A ship in its operational life could experience as much as 10^6 cycles of this dynamic loads,

c. still water incites cyclic loads to a floating vessel in virtue of fluctuating in the ship weight and buoyancy, as well as the self-generating waves. The fluctuating weight and buoyancy is mainly in effect of the decrease in fuel and provision consumed, as well as the fluctuation of the loaded and unloaded cargoes. In addition to this the wave generated by a vessel in high speed operation has a quite significant load impact to the hull structure. The number of load cycles in this category is, however, quite small, that is only in the order of 340, and

d. the fourth cyclic load is that caused by the irregular thermal gradient on the ship structure. This is primarily brought about the everchanging of environmental weather, the sea-air temperature differential, and exposure to the sun. In addition to these environmental consequences, temperature fluctuation is also experienced by

vessels carrying certain cargoes that requires specific air conditionings (e.g. reefer ships). The level of load cycle incited by the thermal gradient is approximately 7000.

The degree of the marine vehicle's proneness againsts cyclic loads is globally depending on its overall form or configuration, hence its behaviour in response to the loads especially that due to the waves. The hull configuration of a conventional ship, for instance, is closely resembled by a long slender beam. In head waves with a characteristic length comparable to the ship length a ship may be modelled by a simply supported beam at both ends (sagging) or on its centre (hogging). In those circumstances a beam is of in most critical condition since maximum bending apply on to its centre point. The accumulation of such load reversals on ship hulls, even though they are not excessive in magnitude, would gradually deteriorate its structural strengths. It is not surprising, therefore, if many fatigue defects on the structural members are found in the midship part and its vicinity. Petershagen (1982) reported most fatigue damages on midship of tankers are in forms of cracks at brackets, bulkheads and notches. Thus it is clear that primary wave loadings instigate fatigue failures on structural members of a floating structure depending on the predominant mode of structural response inherent to the configuration of the structure.

With the growing interest on advanced marine vehicles (AMVs) worldwide designers are now exposed to unconventional problems on their structural designs, unexceptionally to fatigue. A short cut approach to resolve such problems is by adopting past experiences from monohull vessels on top of identifying peculiar structural characteristics of the newly designed AMVs. This approach should apply also to the design of SWATH ships. As it is obvious that wave loads on a SWATH are largest in beam seas (see Chapter 3) then the primary structural members designed to resist these are subjected to fatigue damages. The vulnerability of SWATHs to fatigue failures is rather uncertain. Gore (1985), for instance, suggests that fatigue is not expected to be a problem for SWATH ships constructed of ordinary ship building material. In practice, however, the use of ordinary shipbuilding material might not be appropriate in the interest of reducing structural weight.

The drawback of SWATHs owing to the larger structural weight is well recognised to be one of the obstacles for SWATHs to become commercially competitive. This drawback has a two fold generic effects, namely lower sum of payload and higher construction cost. If it is considered that increasing the payload is more important in expense of, probably, a little increase in construction cost, then lighter shipbuilding material should be used. Alternatively, employing lighter material and different structural configuration (longitudinal framing) as proposed by Gupta and Schmidt (1986) might satisfy both requirements. Nevertheless, these two solutions probably not the best solution from the fatigue point of view. Regarding the first type

of solution light weight materials that can be selected for SWATH structure are Aluminium-Alloy, Glass Reinforced Plastic (GRP) and High Tensile Steel (HTS).

The first two alternative materials need much more care as far as fatigue is concerned, simply due to the inadequacy of their strength to this mode of excitation. HTS undoubtly appears to be the best alternative, because it has a comparably formidable strength especially in the persistence of longitudinal stresses. Even though, Skaar et al (1987) hinted that the use of HTS to carry a higher dynamic design stresses might not be in favour with fatigue considerations. The second solution of adopting longitudinal framing with a carefully arranged web frames and transverse bulkheads is quite promising. The matter is how to assure the stress concentrations on the reduced transverse members would not exceed a certain level which could jeopardize their fatigue resistances. In view of these considerations fatigue problem on SWATHs ought to be promptly explored.

Further importance of performing fatigue analysis to SWATH structures is clearly expressed by some maritime authorities. Malakhoff et al (1991) suggests that the US Navy would impose a fatigue criteria on their newly designed naval SWATHs. It is clarified that in the vessel's design the load spectrum is used in conjunction with S-N fatigue curves for a typical structural detail, assuming linear cumulative damage to determine the design allowable stress through an iterative process. For this analysis, mean life minus one standard deviation was used for the S-N curve, providing 16% probability of crack initiation in 30 years. American Bureau of Shipping (1990) has indicated that fatigue analysis should be included as one of primary requirements upon the submission of the document of SWATH structural design. Despite these strong requirements by outstanding maritime institutions only a limited number of research has been done on this subject.

The study on the assessment of SWATH fatigue lives was pioneered by Sikora et al (1983 & 1986) where the weighted sea method (spectral analysis) is applied. The minimum input data required include a response amplitude operator for side load in beam seas, and operating speed and heading probabilities for the ship in consideration. The output data includes a listing of response (side load) magnitudes and number of cycles exceeding each of these magnitudes. Lifetime stress exceedance curves were developed for several nominal design stresses. This information was used with linear cumulative damage theory to predict expected fatigue life as a function of design stress. Existing small specimen data for HTS, HY-80, and HY-100 were used as a basis for fatigue life calculations.

That study by Sikora et al probably is the only extensive reference on SWATH fatigue so far. Other studies on SWATH fatigue notably at ABS are presented by Liu (1989). The study addressed within this chapter attempts to contribute further

information related to fatigue design on SWATHs. The adopted design methodology is discussed, and a case study associated to SWATH ships operating in the North Atlantic is put forward.

6.2. PREDICTIONS OF SHIP FATIGUE LIFE

6.2.1. Full Spectral Analysis

For the case of welded structures , the most widely used method for performing fatigue checks at the design stage is to refer to S-N curves for the relevant weld details, and this is also the basis of fatigue design rules [Maddox (1991)]. The slope of S-N curve, e.g. Fig. 6.1 from Gurney (1976), in the high cycle range is commonly plotted in log-log coordinates and is approximated by the following function :

$$N S^m = A \tag{6.1}$$

where A is a function of the material, joint geometry and type of weld from appropriate data sources (mostly developed from fatigue tests). m, which is the inverse negative slope of the log-log S-N curve, is usually derived with A by regression analysis of log S vs log N plots from acceptable test data or, m may chosen from theoretical fracture mechanics considerations and only A established by test data regression.

In certain circumstances where the S-N data of an intended structural detail is not available, one may then use the data of a similar geometry and weld joint by imposing a certain correction factor. The UK DEn Guidance Notes suggest a modification of fatigue strength based on predictions with a reference structure of different thickness given by :

$$S / S_{ref} = (t / t_{ref})^{-0.25} \tag{6.2}$$

The application of S-N test data to a ship's hull girder requires a relationship between the characteristic value of wave induced random stress and the constant amplitude stress of the S-N curves. The analysis necessitates to call upon a method to which these two information to be combined, hence to work out the state associated with fatigue failures.

There are several methods of fatigue live estimations developed mainly in the field of mechanical engineering which can be adopted to marine vehicles. One classical method, but still is irreplaceable todate, is that which was developed by Miner (1945) known as the cumulative damage approach. By the Miner hypothesis, it is assumed that

one cycle of the randomly varying stress, having an amplitude S_i, causes an amount of fatigue in the following proportion :

$$\partial D_i = \frac{1}{N_i} \tag{6.3}$$

Here, N_i is the number of cycles of a sinusoidally varying stress of amplitude S_i required to cause failure.

The cumulative damage due to fatigue during exposure to the random stress environment will then be given by :

$$D = \sum_{i=1}^{b} \frac{n_i}{N_i} \tag{6.4}$$

where n_i is the number of cycles of stress of level S_i during the period of exposure and the summation is taken over all level of stress experienced, i.e. over the total blocks b, during the period of time in question. Failure of the structure is then presumed to take place when the length of exposure is sufficient for this sum to equal to unity. According to this criterion failure is defined by the initiation of crack on the member or weld. The effect of different plate thickness to the fatigue life of a detail can be evaluated by substituting eqs (6.1) and (6.2) into eq. (6.4). The increase of plate thickness by a factor of α, say, will reduce fatigue damage D by a factor of $\alpha^{-0.75m}$.

For the purpose of evaluating the fatigue life of a vessel, the number of cycles n_i corresponding to a given stress block S_i can be derived by applying the long-term spectral analysis as demonstrated in Chapter 3. To commence such an analysis the stress transfer function (stress RAO) on the structure need first to be developed. Liu (1989) suggests that stress RAOs connected to at least eight wave headings (head, bow quartering from port and starboard, stern quartering from port and starboard, beam from port and starboard, as well as following seas) are required by ABS.

Using stress RAOs and a selected wave energy spectra, the mean square value of the fatigue stress process for each seastate is observed. The mean square value is then used to define the distribution of fatigue stresses (commonly assumed to be Rayleigh distributed) such that the number of cycles in each stress block is obtained. The lifetime distribution of fatigue stress is then developed by accounting for the combination of the probability of occurrences of sea-sate, wave spectrum, forward speed and wave headings. A worked example for this can be found in Chapter 3. A diagramatical full spectral fatigue analysis is as shown in Fig. 6.2.

6.2.2. Simplified Approach in Fatigue Analysis

Instead of evaluating the fatigue performance of a structure rigorously as above one may apply a simplified approach. This method is now well accepted within the maritime community, e.g. as addressed by Almar-Næss (1985), Chen (1989) and Faulkner (1991). In this way the spectral representation of the seaway and, thus, the stress environment involved, the fatigue damage summation may be expressed in a more compact form. Let p(S) be the probability density function for the stress, which is defined so that the quantity, $p(S_1)\,dS$ equals the fraction of all the oscillatory stress peaks whose values lie within the the interval dS centered on the mean value S_1. Further, taking that the average frequency of the randomly varying stress and that the total time of exposure are f and T, respectively. The incremental damage caused by all of the stress oscillations of amplitude S_1 occurring during interval T is then given by :

$$dD = \frac{T f\, p(S_1)\, dS}{N(S_1)} \tag{6.5}$$

Here $N(S_1)$ is the number of cycles to failure at stress S_1 as obtained from the S-N curve for the material or the structural component.

The expected value of the total damage during time period T is then given by the integral of eq. (6.3) as follows :

$$E(D) = Tf \int_0^\infty \frac{p(S)\, dS}{N(S)} \tag{6.6}$$

or by using the total number of cycle n_o, that is the multiplication of frequency and period, and replacing N(S) by A and S^m as in eq. (1) the above expression becomes :

$$E(D) = \frac{n_o}{A} \int_0^\infty S^m \frac{p(S)\, dS}{N(S)} \tag{6.6a}$$

From various observations it is found that the long term distribution of sea-state can be represented by the two-parameter Weibull distribution. Accordingly the structural stresses induced by sealoads on a vessel can be approximated by the same distribution. The Weibull probability density function for stress p(S) may be written as :

$$p(S) = \frac{\xi}{\lambda}\left(\frac{S}{\lambda}\right)^{\xi-1} \exp\left[-\left(\frac{S}{\lambda}\right)^{\xi}\right] \tag{6.7}$$

where λ is the scale parameter and ξ is the shape parameter which is a function of the type of the structure and the sea region. If S_e is the expected extreme stress occurring once in a lifetime of n_o wave encounters the scale parameter can then be given by :

$$\lambda = S_e \, (\ln n_o)^{-1/\xi} \tag{6.8}$$

Substituting eq. (6.7) into eq. (6.6a) we find the expected value of damage E(D), or simply the damage ratio D as :

$$D = \frac{n_o}{A}\int_0^{\infty} S^m \frac{\xi}{\lambda}\left(\frac{S}{\lambda}\right)^{\xi-1} \exp\left[-\left(\frac{S}{\lambda}\right)^{\xi}\right] dS \tag{6.9}$$

This integral expression is further simplified by employing the gamma function $\Gamma(x)$ and substituting eq. (6.8) to become :

$$D = \frac{n_o}{A} \frac{S_e^m}{(\ln n_o)^{m/\xi}} \Gamma\left(\frac{m}{\xi} + 1\right) \tag{6.10}$$

6.3. EVALUATION OF SWATH FATIGUE BEHAVIOUR

6.3.1. Identification of SWATH's Fatigue Susceptible Regions

As is implied in Section 6.1 structural optimisation on SWATHs should look extensively at the problem of fatigue in order to achieve a reasonable competitive expenditure. For this reason SWATH designers are obliged to identify various areas in which their designs should be carefully checked so that the risk of fatigue failures could be minimised without imposing much redundancy to the structure. Several factors which are generally considered in the identification of fatigue susceptible areas on marine structures would be applicable to SWATHs. The identification of fatigue susceptibility on a structure may be classified into those induced by the design constraints and by fabrication factors. These two aspects are basically interrelated, which to some extent need to be jointly resolved. Fatigue susceptibility due to design constrains are mostly introduced by specific requirements of the structure configuration.

A semisubmersible's configuration, for example, necessitates the designer to arrange some additional bracings in order to sustain extreme environmental loads. To the structure as a whole these bracings would provide a sufficient additional strength against ultimate load say. Individual bracing especially at the joint to the main structure, however, will suffer from a concentrated stress flow. This is made worse when fabrication procedures on it are not carefully performed. Although this has sometimes performed well but because of the awkward location of the member make it difficult for welder to work on it. That is to say bad accessibility to the location may result in poor workmanship. Other structural areas where fatigue failure would persevere are at transition of different structural members (or change in geometry), cut outs for equipments, port holes, attachments for equipment and so on.

In most cases if fatigue criterion on a structure are not satisfied Almar-Næss (1985) suggest the following actions. Firstly, changing the layout (geometry) to reduce concentration of the stress flow. Secondly, increase plate thickness in areas of high local stress, or introduce stiffeners whichever is thought more effective. Combined this with, thirdly, smoothing local geometry (brackets, fully penetrated welds than fillet welds, grinding butt welds and the tows of fillet welds. Overall these imply the need of a better understanding between structural designer and production engineer. Early in the design designers should have take a full consideration on the geometrical tolerances during fabrication, e.g. the possibility of misalignments from the distortions due to welding, etc.

Under the consideration of the main factor affecting fatigue performance, that is structural components where stress concentrations persist, a SWATH might be divided into several fatigue regions. As shown by Sikora (1988) the haunch-deck and strut-haunch intersections, as well as the deck-outer shell intersection are the primary regions where high stress concentrations, so as the position of the hotspots, are found (see Fig. 6.3). At this locations discontinuity of transverse frames is unavoidable, thus require special cautions. Other structural regions that is viewed to suffer from a stress concentration would be along centreline of the mid-cross deck structure, when it is subjected to a beam waves. Torsional stress due to a differential pitching of the side structures (hulls) when a bow wave is encountered could further increase the stress range in this particular region. Fabrication factor may affect significantly to the haunch area, especially on small SWATHs, mainly due to the poor accessibility in the strut space. Such a poor accessibility is also a major obstacle to requisite inspections. Fatigue problem on the superstructure connection onto the main deck of SWATHs probably is quite similar to monohull ships. A number of references, e.g. Petershagen (1986), Hugill and Sumpter (1990), Clarke (1991), address this aspect quite extensively, thus recommended to SWATH designers.

Cyclic loading excited by the primary wave actions may not severely influence the wet deck at the bow. Nevertheless, exposure to frequent slamming loads on this structural part would possibly incite local fatigue damages. Strut to lower hull intersection is a major geometrical changing on SWATHs, however, it is unlikely that this part will introduce any fatigue failure as the primary cyclic loads due to waves are not directly apply on it. Only in special cases where a local source of repeating loads presents within the vicinity, e.g. vibrations due to the machinery located in the lower hull, then fatigue damage may persist. Care should be taken in such cases because, even though the magnitude of the load excitation is relatively low but much higher frequency may critically affect the local structure.

Having observed several areas where fatigue damage is expected to arise on SWATHs the remaining task is to propose a solution(s) to this problem. The first alternative is by using insert plate on the haunch-deck and haunch-strut intersections. Increasing plate thickness at the haunch should not be allowed since this is contradictory to the idea of reducing the structural weight. Another way to ease stress concentration in this part is by designing a shallower haunch angle at the wet-deck. As observed by Sikora (1988) introducing rounded knuckle might not be effective if it is only in a fraction of a meter, but larger than that would be beneficial. The optimum from stress concentration viewpoint would be to replace the entire haunch with one large arc of a circle which is tangent to both strut and wet deck. Chalmers (1989) advises to pay a full attention in designing details and structural discontinuity at the haunch. Transverse framing with additional partial bulkheads in the corner region remains the best configuration for SWATHs to sustain cyclic stress due to predominant transverse loads.

6.3.2. Determination of SWATH Ship Structural Stress

Early in the design stage nominal stress on SWATH may be approached by the beam theory as was established by Mulligan and Edkins (1985). The method idealises the cross-deck structure as a simply supported beam, and the struts as cantilever rigidly fixed to the cross-deck. Bending moments on the cross-deck and struts result from side load which is assumed to act perpendicular to the centreline at mid draft. Peak stresses at critical locations can be obtained by applying correction coefficients to the nominal stress, even though the result tends to be conservative. Recognising this fact it may not be appropriate to assess structural stress on modern sophisticated ships, such as SWATHs, by a simple calculation model.

A more versatile approach, such as the well known finite element analysis, therefore, has to be employed. Even though, the accuracy of the results predicted by the

application of FEM still depends very much on the adequacy of the structural mesh arrangement. This is the case especially in way of structural details which embodies a dominant influence on the fatigue strength of the structure. The stress analysis for fatigue assessment requires much more effort and is even more costly than say for the ultimate strength prediction.

The matter is clear as indicated in Section 6.2.1 that stress transfer functions have to be established for a number of sea headings at various wave frequency, not to mention the amount of structural details that ought to be investigated. In order to reduce the cost and time spent on the analysis a global analysis using a three-dimensional coarse mesh FEM is necessary. Using a 3-D FEM one would then be able to pin point approximate locations of the stress concentration on a SWATH, which can further be used for a reference in the detailed analysis. Quite a number of 3-D FEM package now available, in which MAESTRO-FEM being the one widely employed within the SWATH community. The Department's SWATH Research Group has recently exercised the package for the analysis of the *Patria* as reported by Tolikas et al (1992).

As a sequel to the use of a 3-D FEM the stress analysis on any structural detail may now be commenced utilising a two-dimensional fine mesh model. This is preferred because such modelling generally provides more accurate prediction especially regarding the peak stress. Liu (1989) has suggested a way in which this time consuming analysis can be relaxed. Instead of obtaining all stresses for any wave frequency increment at a certain wave heading a single reference value of stress on the transfer function is determined. It is recommended to determine the magnitude of stress related to the value of wave load at vicinity of modal (peak) period. Using the reference stress thus calculated, the entire transfer function may then be assembled following the pattern of the load transfer function. A few more stress values may be determined if it is felt that a single value is not too convincing.

6.3.3. Fatigue Performance of SWATH Ships - A Case Study

Within the limited information on SWATH fatigue performance it is attempted to identify certain important factors related to this aspect by a hypothetical study. Two notional SWATH vessels are selected for evaluation, namely SWATH-FV and SWATH-3, both of which are approximately 2500-tonne in displacement. Analysis was first made by employing the Miner's linear cumulative damage rule, which was then followed by the application of the simplified assessment as is clarified in the following.

6.3.3.1. Assessment of SWATH Fatigue Life. In order to calculate the cumulative damage ratio the number of cycle n_i pertinent to a given stress range S_i is taken from the long-term load response analysis as in Chapter 3. The stress range value corresponding to each block (i) is determined by assuming that : a) the structural behaviour is essentially within the limit of elasticity, and hence b) the stress magnitude can be considered to correlate proportionally to the structural response (i.e. bending moment or side load). In this particular study the Class-D weld joint S-N data provided by Gurney (1976) is selected.

The selection of class-D weld joints for the example in this evaluation merely is based on the consideration that most structural connections in a ship are the typically of butt joints or fillet welds. Especially the former, moderate workmanship would be expected to produce weld joints for the structure that can be categorised to have the quality of this class. The damage initiation equation of this Class-D weld joint for two standard deviation with a 97.7% probability level of survival is given in metric unit as :

$$N S^3 = 1.5136 \times 10^{12} \qquad (6.11)$$

The calculation may be carried out by first setting up a given lifetime (expected extreme) stress range, say 200 N/mm^2, and the stress distribution of which can be derived linearly from the loading information, as exemplified in Table 6.1 for SWATH-FV. The fatigue life of this SWATH corresponding to each lifetime stress range is then derived by multiplying the expected life of the vessel to the fraction of the cumulative damage ratio so obtained. The same procedure has been performed to evaluate the fatigue life of another hypothetical vessel (SWATH-3), for comparison. The computed results are further presented in Fig. 6.4, in which the fatigue life is plotted against the lifetime stress (single amplitude). As shown in this Figure, the difference of the fatigue life between the SWATH-FV and SWATH-3 is insignificant. Nonetheless, it should be recognised that such a small difference is merely due to the same maximum stress range imposed, which will only be the case when the structural section of one SWATH is different from the other. If, however, it is accepted that any level of load response on the two SWATHs should correspond to a certain stress magnitude (i.e. the cross structure having an equal section modulus say) then the difference in fatigue life is apparent (see Fig. 6.5).

It is clear from Fig. 6.5 that for a given stress level SWATH-FV would maintain a longer lifetime than SWATH-3, or, in other words, the load carrying capacity of SWATH-FV from the fatigue point of view is greater than SWATH-3. It is worthwhile to mention an interesting point here that SWATH-FV has in fact experienced a larger number of cyclic load than SWATH-3 (in the order of 8.40×10^7 compare to 8.24×10^7), yet the former has a better fatigue characteristic. Such a phenomenon is highly possible

if one consider that there exists a dominant effect of wave period over the responses of different structures (see Chapters 2-4). Moreover, fatigue life is also substantially governed by the stress distribution during the lifetime of the structure as is discussed below.

To some extent the simplified approach in predicting fatigue life of a vessel is the most convenient method that should be applied by a structural designer. By applying such a method predictions can be made rapidly (even manually), which is of importance requirement when a wider range of sensitivity study ought to be performed. A crucial problem, nonetheless, has to be well understood before an analysis could be proceeded. As is indicated in eq. (6.10) the damage ratio is governed by the total number of cyclic load n_0, characteristic values of the selected S-N data (A and m), extreme stress range (S_e), and the Weibull-shape parameter ξ. It is the latter which proves to be the most difficult to determine, especially for those dealing with a new type of vessel as past experience is very limited (if non-existent). Even for conventional ships this parameter could not be easily chosen from other vessel of a similar size without carefully evaluating various factors pertinent to the vessel so designed. One of the most apparent factors which strongly instigates the Weibull parameter is the sea region, i.e. the severity of the seawaves, and others such as the prevalent wave headings and operational speeds.

In the early design stage a rule of thumb is given by Munse et al (1983), where shape parameters of roughly 0.7 up to 1.0 and 1.0 up to 1.3 are typical to, respectively, larger ships (eg Tankers, Bulk Carriers) and smaller ships (eg General Cargo vessels). A similar finding by Nordenström (1973) reveals that long-term distributions of waves and wave-induced structural response can be closely approximated by Weibull distributions with shape parameters close to unity (ξ ±1.0), that is approximately exponential distribution. It is suggested by Almar-Næss (1985) to be cautious with the approach of selecting the Weibull parameter ξ if it is not supported by significant quantitative experience of similar ships.

In the almost non-existent information it is quite interesting to explore such Weibull parameters peculiar to SWATH vessels by the following procedure. Using an available lifetime load (stress) data a damage ratio D corresponding to a given extreme stress range can be calculated by Miner's rule as above. An iterative computation is then performed on the simplified damage equation (eq. 6.10) by first setting an initial value of ξ and further imposing an increment value of $\Delta\xi$ to finally obtaining the damage ratio which is equal to the one obtained from Miner's rule. The ξ which correlates to this damage ratio D is selected as the value that will closely represent the stress lifetime distribution. Table 6.2 presents the results of the iterative computation on ξ for the notional SWATH-FV. Similarly, computation has been performed for SWATH-3 studied herein. Weibull shape parameters ξ of 0.94 and 0.945 are obtained from the

calculation represent the lifetime response distributions of SWATH-FV and SWATH-3, respectively. Once such a nearly exact value of ξ is derived various sensitivity study, especially the extreme stress range effects on the fatigue life can be made.

For the sake of comparison the same procedure as above has been employed to investigate an idealistic condition where those SWATHs are operated in dominant beam sea waves. The computation of the fatigue damage of Class-D weld joints using the Miner's rule by assuming a lifetime mean stress range of 200 N/mm^2 in beam sea dominated condition for SWATH-FV and SWATH-3 has been made. The corresponding iterative calculation in obtaining the Weibull-shape parameters ξ is also exercised. The parameters derived are in the order of 1.226 and 1.265, respectively, for SWATH-FV and SWATH-3. Fig. 6.6 provides the plot of lifetime stress histories of the two SWATHs which show their dependence on Weibull-shape parameters.

6.3.3.2. Sensitivity Evaluation. A convenient feature from the explicit expression for D once the ξ is obtained is that early in the design stage the maximum allowable extreme stress range for any likely critical structural detail can be assessed as suggested by Munse (1981) as :

$$S_{ca} = \left[\frac{A\delta}{n_0 \Gamma(m/\xi + 1)}\right]^{1/m} (\ln n_0)^{1/\xi} \qquad (6.12)$$

Where for any acceptable damage ratio, or preferably referred to as the damage index, δ the allowable stress range S_{ca} is found as a function of the detail S-N variables, the expected lifetime stress cycles n_0, and the Weibull shape parameter ξ. Assuming a damage index δ = 1.0 and based on the lifetime stress cycles for SWATH-FV and SWATH-3, it is found that the allowable extreme stress range in a 20-year period for the Class-D weld joints of the two vessels are 292 N/mm^2 and 291 N/mm^2, respectively. These stress magnitudes are slightly higher than that put forward by Sikora et al (1983). From fatigue analysis of several SWATH designs it was observed design stresses of 9 tsi (140 N/mm^2) to 18 tsi (280 N/mm^2), depending upon material and conditions, result in acceptable expected fatigue lives.

An evaluation of allowable stress range for a 30 years lifetime by imposing a damage index δ = 0.67 has also been made, and gives an S_{ca} value of about 255 N/mm^2 (37 ksi). Sikora and Dinsenbacher (1990) presents a relatively lower amount of allowable stress range for the T-AGOS (3500-tonne) than those two SWATHs, i.e. about 28 ksi (193 N/mm^2). It is deceptive to take a full account on the previous value for SWATH-FV or SWATH-3, which is some 30% larger than for the T-AGOS,

because other factors of safety, e.g. due to stress concentration, fabrication tolerances etc, have not been taken into account.

The plate thickness correction should not crucially affect fatigue performance of a given structural joints as long as the designed material has a thickness less than that of the material tested to derive the applied S-N curve. Berge (1984) has clearly mention this account, with the reasoning that should two structures with different thicknesses experience an equal stress gradient then the thicker plate would tend to fail more rapidly under fatigue persistence. The expression in eq. (6.2) shows this phenomenon. In this respect the currently evaluated SWATHs are believed not to have plate thicknesses thicker than that used in the fatigue test by Gurney (1976), which is typically some 22 mm in thickness or more.

In an actual design it is hardly found that δ is taken to be 1.0. Sometimes a damage index value of even much less than 1.0 (as low as 0.3) should be taken, especially if the fatigue failure of the designed member will lead to a catastrophic collapse of the system. Nevertheless, when a member failure is not significantly affects the whole structure (or any major structural segment) then the value of δ may be relaxed. In defining this factor other aspects related to the fatigue quality of a member has to be accounted for. These are, for instance, fabrication difficulties including accessibility, exposures to sea water, level of difficulty for inspection, redundancy and so on.

Clearly, setting up δ to be less than 1.0 is aimed at allowing a sufficient survival before fatigue fracture on any detail could be detected in a regular inspection. In other words it is intended to render an adequate residual strength against load reversals in damage condition. This sort of precaution is recommended although it is a common sense to believe that total failure is quite unlikely to occur due to only local damages.

Another format to assure margin of safety for fatigue for fatigue not to be exceeded one may also adopt the concept of partial coefficient. This concept is similar to that usually considered in static loading suggested by most Classification Societies. A specific form of partial coefficients inclusion in the fatigue damage equation as given by Almar-Næss (1985) is given as :

$$\sum_{i=1}^{b} (s_i \gamma_L)^m n_i \leq (S_i / \gamma_{SN})^m N_i \qquad (6.13)$$

where γ_L is the partial (safety) coefficient on loading and γ_{SN} is the partial coefficient on S-N data. These partial safety coefficients are suggested to be attained by advanced

probabilistic analysis, thus the uncertainty of the different parameters may be reasonably accounted for. Inspite of the urgent need in introducing such safety coefficients on fatigue assessment this has not so far been carried out. In this respect the concept of damage index would remain the only appropriate alternative in fatigue safety for a few years ahead.

As mentioned earlier one of the factors that influences the accuracy in fatigue prediction is the precision of the Weibull-shape parameter adopted in representing the stress distribution (see eq. 10). In order to gain a clear insight on the importance of the parameter a sensitivity evaluation is performed on SWATH-FV as shown in Table 6.3. In this particular case the Class-D weld joint S-N data is selected, and calculation is made with a constant stress range of 200 N/mm^2 and a total stress cycle n_o in a lifetime of 8.4 x 10^7. The Weibul-parameters evaluated are set between 0.85 and 1.05, in which the parameter ξ=0.94 is taken as the standard that will give a 20 year fatigue life. It can be readily seen from the corresponding table as to how fatigue life differ due to the small change in ξ. As shown, with only a relatively small changes in the parameter ($\pm$ 10% from the standard) a difference in fatigue life between 40% up to 70% is obtained. Fig. 6.7 is provided to supplement this evaluation, where five parameters are selected and the fatigue lifes are calculated for different stress values.

Considering the above evaluation one can easily judge the difference in fatigue life would be much too large when comparing between the all heading (ξ=0.94) and beam sea dominated (ξ=1.224) operations. As presented in Table 6.4 the difference of the fatigue lifes for the two conditions can be as much as 260%. It is clear fatigue analysis will not be valid if developed based only on a limited sea condition, although if it is considered to be the most critical (beam seas in case of SWATHs). Chen (1989) observe a further aspect which might arise from this sensitivity is that a seaway may produce a larger extreme stress range but less fatigue damage, and vice versa (see comparison of SWATH-FV and SWATH-3 in Fig. 6.2). This kind of observation brings out two interesting phenomena, namely, the severity of a given wave environment can be measured in at least two ways, i.e. the stress range severity and fatigue vulnerability. The latter is most closely related to the Weibull shape parameter of the stress range long term probability of exceedance

A sensitivity evaluation is further made on the effects of weld classes toward the fatigue life of SWATH-FV, as shown in Table 6.5. There is nothing so special about this evaluation as it is easily guessed that the higher the weld class (quality) the longer life they will endure. The main intention here, however, is to further emphasis the significance in maintaining proper workmanships as strongly suggested in Section 6.3, so that fatigue damage could be reasonably minimised. As can be seen, for instance, a degradation of weld quality from class-D down into class-E would lessen the fatigue life of about 30%, and so forth.

6.3.4. Effects of Stress Concentration Factor (SCF)

So far the fatigue analysis on the two SWATHs are presented on the basis of the nominal stress, that is on the structure where experiences stress fluctuation proportional to the load excitation. Nonetheless it should be accepted that fatigue damage on a structure persists initially on members where stress flow is somewhat blocked (concentrated). Such a circumstance may be brought about the discontinuity of details, the presence of openings, and change of geometry. In the assessment of fatigue life to any particular member in which stress concentration present a correction to the selected S-N data should then be implemented, because these data are mostly developed based on the nominal stress. A correction coefficient referred to as the stress concentration factor (SCF) usually are adopted in this case. This SCF is defined as the ratio of the hot spot stress S_{max} and the nominal stress S_n :

$$SCF = S_{max} / S_n \tag{6.14}$$

For any particular detail an SCF value can be determined both theoretically or experimentally. The former usually are now established by employing the finite element analysis. Experimental method generally are carried out to provide the data for the validation of theoretical approach, usually when a complex structural detail or geometry are concerned.

Recognising the fact on the importance in defining stress concentration, Sikora (1988) has carried a parametric study on this aspect specifically for SWATH ships. The governing factor observed in that observation is the effect of variation in transverse bulkhead spacing for SWATHs with a 45 degree haunch angle. The results of this study were extracted into design algorithms for predicting the peak stresses in several locations on the transverse bulkhead. These algorithms can be used to determine the relative SCF as functions of ship geometry as follows.

Haunch-wet deck intersection (knuckle) :

$$SCF = 1.83 + 6.11\ S_B/B_d \tag{6.15a}$$

Haunch-Inner Strut intersection :

$$SCF = 4.21 - 0.18\ S_B/S_h \tag{6.15b}$$

Main Deck-Long. Bulkhead intersection :

$$SCF = 0.83 + 2.80\ S_B/B_d \tag{6.15c}$$

Platform-Outer Shell intersection :

$$SCF = 1.20 + 1.78\ S_B/H \qquad \cdot \quad (6.15d)$$

where S_B is the longitudinal spacing between transverse bulkheads, B_d is the total span of the upper box structure, S_h is the height of the strut above the lower hull, and H is the height of main deck above the lower hull (see Fig. 6.8). The range of validity of those algorithms are, $0.31<S_B/B_d<0.61$, $1.38<S_B/S_h<3.12$, and $0.54<S_B/H<1.08$. Using the above algorithms the SCFs for SWATH-FV on those locations are found to be 3.0, 4.0, 1.4, and 2.0, respectively.

Using the nominal allowable stress range value S_{ca}=292 N/mm^2, the other allowable stresses for those critical parts on SWATH-FV are obtained by imposing the SCFs as 97 N/mm^2, 73 N/mm^2, 208 N/mm^2, and 146 N/mm^2, respectively. These allowable stress ranges are considerably lower than for the nominal structures, hence certain actions to enhance fatigue endurance of those critical members are necessary to be performed. Otherwise more regular inspections ought to be made so that fatigue damages can be detected as early as possible hence the risk of extensive failure can be minimised.

6.4. RELIABILITY AGAINST FATIGUE FAILURES

The method of fatigue analysis described in the foregoing sections can be viewed as the deterministic approach. In that way any variable involved in the formulation are assumed to be constant (unbiased). In actual situations this assumption may not valid as there are discrepancies between the design values so applied and the statistical properties of those variables, usually referred to as the uncertainties. These particular facts imply that those results derived deterministically can not be absolute justified for their accuracies. This issue then should be sought as a crucial consideration into the problem of safety.

In general structural design the uncertainties can be brought about the randomness of loadings, simplifying assumptions in the strength analysis, material properties, etc. The randomness of loadings on marine structures is obvious because the wave which acts as the primary source of external loads is naturally random. The simplification in prediction method usually is due to the limitation in modelling the physical phenomena generic to complexity of the problem concerned. The uncertainties regarding material properties mostly are related to the bias in data collection, such as the measurements of

yield stress, fatigue strength, notch toughness, and corrosion rates. In addition uncertainties due to fabrications and constructions have a strong influence on the strength of a structure.

To tackle the problem which arises due to uncertainties then a probabilistic analysis ought to be called for. The major benefit of the probabilistic design, or widely known as the reliability-based design, approach is that a designer will be able to generate an engineering system which is both efficient and reliable to the level specified. Faulkner (1987) quotes that in deterministic analysis it is common to make conservative assumptions with respect to modelling. This apparently includes the assumption in safety factors, which are mostly developed from past experiences without thorough examination on the effects of various uncertainties. Although the majority of safety factors would assure the strength of a structure will not be exceeded by the applied loads, but they are not necessarily give the best approximate of optimum structure. In reliability assessment the aim should be for a model which on average will be unbiased. This way would enable a designer to anticipate proper allowances for each of important design, fabrication and service variables.

In the concept of reliability design a problem can be contemplated as one of supply and demand correlation. Failure can then be defined to occur when the supply (the resistance or strength of the system) is less than the demand (the loading imposed onto the system). Hence, the risk of failure is the probability of a load (L) reaching or exceeding the resistance (R), which can be written as :

$$\text{Probability of Failure} = P_f = P\,(R < L) \tag{6.16}$$

It follows that the safety (reliability) of a structure is the converse of the probability of failure or

$$\text{Safety} = P\,(R > L) = 1 - P_f \tag{6.17}$$

which can be represented diagrammatically as shown in Fig. 6.9. Faulkner (1981) expresses the probability of failure, provided R and L are uncorrelated random variables and both are time invariant, in the the following equation :

$$P_f = \int_0^\infty \{P_R(x)\}\, p_L(x)\, dx, \quad \text{or}$$
$$P_f = 1 - \int_0^\infty \{P_L(x)\}\, p_R(x)\, dx \tag{6.18}$$

where P(x) and p(x) are probability distribution and density functions respectively for

the R and L curves. The above formulation is referred to as the 'fully probabilistic approach' (or level 3 approach) in which complete probability distributions of all relevant quantities (load, resistance, and limit values) are included in calculating the probability of failure. However, those quantities required for the calculation are not widely known, especially due to the lack of data available. Another alternative is therefore to use a simpler safety concept which combines conventional determinism statistics. This latter approach is hence known as the 'semi probabilistic', or the level 2 approach, which can further be classified into the partial safety factor method and second moment method. The former is as briefly mentioned in Section 6.3.3.2 (see eq. 6.13). The latter which is widely used at present is as described below.

In the second moment method the degree of structural safety is directly related to the margin (Z) between the actual magnitude of the resistance and load :

$$Z = R - L \tag{6.19}$$

and failure takes place when the margin Z becomes negative or

$$P_f = \text{prob}\,[Z < 0] \tag{6.20}$$

Since both resistance and load variables are random, likewise the margin Z which has a probability density function $p_z(Z)$ as shown in Fig. 6.9b. It follows, therefore, that safety is not only dependent to the mean value of the margin ($\overline{Z}$), i.e. the distance between mean values of resistance ($\overline{R}$) and load ($\overline{L}$), but also on the inverse of the spread between the two curves as measured by their coefficient of variations (COV). If the coefficient of variation of Z (denoted as COV_Z) is large then the degree of safety will be correspondingly less, and vise versa. Substracting $\overline{Z}$ from both sides of the inequality and normalise this using the standard deviation σ_z, eq (20) becomes :

$$P_f = \text{prob}\left[\frac{Z-\overline{Z}}{\sigma_z} < -\frac{\overline{Z}}{\sigma_z}\right] \tag{6.21}$$

or by using the COV eq. (6.21) converts to :

$$P_f = \text{prob}\left[\frac{Z-\overline{Z}}{\sigma_z} < -\frac{1}{COV_z}\right] \tag{6.21a}$$

The left-hand term within the bracket is the normalised margin, for which the distribution has zero mean and unit variance. It is clear from eq. (6.21a) that the safety is governed by the inverse value of the COV_z. Lets denotes the probability distribution

of the normalised margin as Φ and the inverse of COV_Z, i.e. the reliability index, as β, then the probability of failure may be rewritten as :

$$P_f = \Phi(-\beta) \qquad (6.22)$$

6.4.1. Analysis by AFOSM Method

For the present fatigue safety analysis an enhanced approach so called the Advanced First Order Second Moment (AFOSM) is employed in determining the safety index. In this approach the the margin of safety is considered to be the function of independent variables involved in the design. Lets n variables $x_1, x_2, ..., x_n$ are accounted for in the calculation then the limit static equation for the structure is :

$$Z = g(x_1, x_2, ..., x_n) > 0 \qquad (6.23)$$

where the nature of g depends on the structural type and limit state under consideration. At this point the failure surface is due for Z = 0. The linear approximation to this can be derived by applying the Taylor series expansion :

$$Z \cong g(x_1^*, x_2^*, ..., x_n^*) + \sum_1^n (x_i - x_i^*) g'_i(x^*) \qquad (6.24)$$

where

$$g'_i(x^*) = \frac{\partial g}{\partial x_i}$$

evaluated at the unknown design point $x^* = (x_1^*, x_2^*, ..., x_n^*)$.

If $\bar{x}_i$ and σ_i represent the means and standard deviations of the basic variables x_i, the mean value of Z is :

$$\bar{Z} \cong \sum_1^n (\bar{x}_i - x_i^*)\, g'_i(x^*) \qquad (6.25)$$

and its standard deviation :

$$\sigma_z \cong \left[\sum_1^n \left\{ g'_i(x^*)\, \sigma_i \right\}^2 \right]^{1/2} \qquad (6.26)$$

σ_z may be expressed as a linear combination of σ_is as follows :

$$\sigma_z = \sum_1^n \alpha_i g'_i(x^*)\sigma_i \tag{6.26a}$$

where

$$\alpha_i = \frac{g'_i(x^*)\sigma_i}{\left[\sum_1^n \left\{g'_i(x^*)\sigma_i\right\}^2\right]^{1/2}} \tag{6.27}$$

which are referred to as the sensitivity factors since they reflect the relative influence each of the design variables has on the strength model.

If the reliability index β of the design is defined as $\overline{Z}/\sigma_z$, then from eqs. (6.25) and (6.26a) we find :

$$\beta = \frac{\sum_1^n (\overline{x}_i - x_i^*)\, g'_i(x^*)}{\sum_1^n \alpha_i g'_i(x^*)\sigma_i} \tag{6.28}$$

from which it follows

$$\sum_1^n g'_i(x^*)(\overline{x}_i - x_i^* - \alpha_i \beta \sigma_i) = 0 \tag{6.29}$$

The solution of this equation is :

$$x_i^* = \overline{x}_i - \alpha_i \beta \sigma_i \quad \text{for all } i \tag{6.30}$$

in which x_i^* is referred to as the 'design point'. This design point corresponds to the point of maximum probability density of failure when all the variables are normally distributed.

A computer code has been developed by Pu (1992) to accommodate the above AFOSM formulations. More on the features of this code, such as the treatment of non-normal distributed variables, are fully described in that report. The generalised approach adopted in the developed program makes it suitable to be used in most engineering design, such as for fatigue analysis described below.

As given in eq. (6.10) fatigue damage is governed by the variables in S-N equation, the number of cycle experienced by the structure and the extreme stress. In

the reliability analysis those variables on the right-hand side of eq. (6.10) are treated as random variables. Lets Δ denotes the fatigue strength (damage index at failure) then the failure occurs when $\Delta < D$. Hence the safety margin for fatigue can be written as :

$$Z_F = \Delta - D \quad , \text{ or}$$
$$Z_F = \Delta - \frac{n_o}{A} \frac{S_e^m}{(\ln n_o)^{m/\xi}} \Gamma\left(\frac{m}{\xi} + 1\right) \tag{6.31}$$

The uncertainties on the variables involved in the above equation are taken from various sources. The S-N data considered herein is for the Class-D weld type, where from the listed data given by Gurney (1976) the COVs of A and m can be calculated and found on average to be 31% and 3%, respectively. The other COVs for Se, n_0 and ξ are taken from the paper by Guedes-Soares (1991) as 20%, 5% and 5%, respectively. The statistical values of these variables are relisted in Table 6.6. Some of the type of distributions pertinent to those variables are given by referring to Yang and Lee (1991).

The reliability analysis on SWATH-FV has been performed by varying the nominal stress ranges between 160 N/mm^2 and 320 N/mm^2. By imposing this variation it is expected to allow for the effect of different stress levels on fatigue safety to be observed. Two particular stress ranges of 290 N/mm^2 and 250 N/mm^2 are noteworthy here since those two values are deterministically derived as the allowable stress ranges for a 20 year and 30 year lifetime. As a reminder the latter has been compared to the allowable 30-year lifetime stress of the T-AGOS. Hence it would be very interesting to observe whether or not the reliability approach justify these deterministically derived stress values.

The results from the reliability analysis are presented as in Figs. 6.10 and 6.11, for the change of safety index and probability of fatigue damage as functions of operating year, respectively. From various investigations Lee and Faulkner (1989) suggest that the safety of marine structures can be assured if the safety index β for ultimate strength of components can be kept within the ranges of 3.0 and 4.0. The values for fatigue initiation could, however, be accepted between 2.0 and 3.0. Referring to Fig. 6.10 the lowest stress range (160 N/mm^2) would assure the safe life of SWATH-FV approximately up to 25 years. Nonetheless, it would be unreasonable to expect that a vessel such as SWATH-FV which is designed to operate in the North Atlantic will not be excited by waves much larger than that.

Regarding the the allowable stress for a 20-year lifetime (290 N/mm^2) the fatigue safety of the vessel may be preserved up to three years, although the probability of failure in 20 years is very high (see Fig. 6.11). This information would necessitate a

thorough inspection to be performed at least in the first 3 years of the vessel's operation. Excessive stress range (320 N/mm^2) would definitely unfavourable to the vessel because of the likelihood of fatigue damage. Focusing onto the stress range of 250 N/mm^2 a slightly longer period (5 years) before the first inspection ought to be carried is attained. Overall it seems that a lifetime stress range of 200 N/mm^2 is the most reasonable as the criterion for SWATH-FV. Considering this, the first extensive fatigue check may be performed within a period of 10 years without too much risk. This stress range apparently confirms that allowable stress imposed in the fatigue design of the T-AGOS. Further checks, however, still need to be carried out before design values can be firmly proposed.

6.4.2. Analysis by Wirsching's Method

As for deterministic analysis reliability against fatigue failure will be more convenient to be evaluated by a simplified formulation. Using such a formulation safety checks can be performed fairly quickly, especially when a large number of structural component ought to be dealt with. An expression of fatigue reliability for offshore structure has been derived by Wirsching (1984). The use of this fatigue reliability format has been made for various type of structural member of offshore structure, e.g. as presented by Wirsching (1986), and Wirsching and Chen (1987,1988). Eventually the various evaluations using this reliability format has been fairly successful, and a report by Wirsching (1985) was then accepted by the American Petroleum Institute (API) in effect to be recommended in the code for design practice.

The derivation of the fatigue reliability expression by Wirsching (1983) was performed using the simple lognormal format for multiplicative limit state functions. Accordingly, lognormal distribution is adopted for the number of cycle to failure N as in eq. (6.1), rather than Weibull distribution. In this respect fatigue strength coefficient A is defined as random variable describing the inherent variability of the fatigue strength. The median $\tilde{A}$ defines the median S-N curve, and the coefficient of variation (COV), C_A, is the COV of N given S. Bias and uncertainty in Miner's rule are defined by Δ, i.e. the damage index at failure; the event of failure is $D \geq \Delta$. B is defined as the parameter which describe the stress modelling error. Δ, B and A are assumed to have lognormal distribution with median ($\tilde{\Delta}$, $\tilde{B}$, $\tilde{A}$) and COVs (C_Δ, C_B, C_A), respectively.

In order to calculate the probability of failure as in eq. (6.22), the reliability index has been formulated by Wirsching (1983) which is :

$$\beta = \frac{\ln(\tilde{T}/T_S)}{\sigma_{\ln T}} \tag{6.32}$$

where T_S is service life in seconds and $\tilde{T}$ is the median time to failure, that is :

$$\tilde{T} = \frac{\tilde{\Delta}\,\tilde{A}}{(\tilde{B}^m\,\Omega)} \tag{6.33}$$

and

$$\sigma^2_{\ln T} = \ln\left\{(1+C^2_\Delta)(1+C^2_\Delta)(1+C^2_\Delta)^{m^2}\right\} \tag{6.34}$$

The stress parameter Ω in eq. (6.33) is defined to be the product of lifetime average zero crossing period f_0 times the expected 'once in a lifetime' stress range, and may be written as :

$$\Omega = f_0\,E(S^m) \tag{6.35}$$

where f_0 = n_0/T
T = the time of exposure (seconds)

A computation has been performed to evaluate the fatigue reliability of class-D weld joints as assumed for SWATH-FV using the above formulation. The same uncertainty values for Δ and A as adopted in AFOSM analysis (see Table 6.6) are used. The stress modelling uncertainties which was accounted for directly to the stress range value in AFOSM analysis, is now given by $\tilde{B}$= 0.90 and the corresponding coefficient variation, C_B = 0.25. The results of this analysis are plotted together with that from AFOSM fatigue reliability format as presented in Fig. 6.12.

As seen in that figure a fairly good correlation between the two results is evident, especially for lower stress ranges. The discrepancy in the predictions for larger stress range values probably is brought about the difference in the uncertainties of stress modelling parameter. Nonetheless, this discrepancy is witnessed to take place below the safety index value β of less than 2.0, that is the zone of unacceptable for fatigue criteria as forwarded in the previous section.

It might be interesting also to explore the effect of applying different median values of fatigue strength coefficient $\tilde{A}$. As shown in Table 6.6 the value of $\tilde{A}$ adopted in the above analysis is taken as the mean minus two standard deviations ($\tilde{A}=1.52\cdot10^{12}$), i.e. as suggested by most design codes. If it is allowed to adopt median value $\tilde{A}=3.99\cdot10^{12}$, that is the mean value for S-N curve of class-D weld

joints, then the reliability curves are as presented in Fig. 6.13. A substantial difference with the former results is obvious. According to the latter results a once in life stress range of 290 N/mm^2 can be accepted for minimum criteria of safety index equal to 2.0, and under the condition thorough inspection after 10 years operation have to be performed. Interestingly, this value is the same as the allowable stress range S_{ea} as derived from the deterministic evaluation, even though the mean minus two standard deviations value for A was used in this case. A remark to be made with the use of Wirsching's fatigue reliability format is simply that this particular model is adaptable and is recommended for a quick check in fatigue design for SWATHs.

The reliability analysis adopted herein may be checked against other approaches which are becoming available in recent years. Those reliability codes which are developed specifically to tackle the fatigue problem on ships are by, among others, Munse et al (1981), and White and Ayyub (1987).

6.5. DISCUSSION

Various important aspects in fatigue analysis for SWATH type vessels have been studied. The specific aim of this study is to contribute further information regarding fatigue design and performance of SWATH ships. Of special consideration in SWATH design is to attain a sufficiently safe structure but with a reasonably light weight. Fatigue considerations would not only affect the initial design but should also be beneficial during the operational life of a vessel. Hence proper fatigue analysis and design are not only beneficial in creating initial confidences but also as important in reducing the service cost. In repaired ships most damages, as inspected by Jordan and Cochran (1978), are found in the form of structural cracks. This type of damage is likely caused by fatigue. A thorough fatigue evaluation will be important for SWATHs to enhance their commercial competitiveness.

The study was performed by first identifying several structural areas where fatigue damage would likely to develop. Following this an evaluation of fatigue damage is carried out by adopting the Miner's approach. In the next stages evaluations were made by firstly deriving the Weibull-shape parameter pertinent to the SWATHs so studied. Those parameters are further incorporated in a simplified fatigue damage formulation, which would allow different sensitivity studies to be made rapidly. A first approximation to the allowable stress range has also been derived by employing the simplified formulation. Design check was treated by means of the probabilistic approach using two different formats, namely AFOSM and Wirsching's reliability methods. A more reasonable value of stress range which should be adopted in the design has been obtained by the later analysis.

The study remains inconclusive because certain information needed is not yet available. This is the S-N data for the structural parts of SWATHs where fatigue damage is expected to be severe. Furthermore, fatigue damages concerned within the study are only limited to the level where initial crack on any particular part of the structure takes place. In practice, however, fatigue analysis should also be concerned with the problems of crack propagation as addressed belows.

6.5.1. Fracture Mechanics for Crack Propagation Analysis

Structural designers should realise that failure on a structural member hardly occur instantly after an initial crack. Hence it may be of concerned in the evaluation of the required operational time before any repair ought to be performed. Such an analysis requires the information on crack growth rate,which is characterised by the stress strain fields at the vicinity of the crack tip and the range of the stress intensity factor. The appropriate approach in solving this problem is by employing the fracture mechanics analysis. This aspect is actually beyond the scope of the present study, but a brief remark for future investigation should be made.

Consider a single member under axial tension fatigue as shown in Fig. 6.14. The total fatigue life N_t can be considered as :

$$N_t = N_i + N_p \tag{6.36}$$

where N_i = cycles to initiate a crack, e.g. from fatigue S-N tests where $N_i = A/S^m$

N_p = further cycles to propagate a crack to a critical failure crack depth a_f which may be determined from fracture mechanics (FM) or from ductile UTS failure of remaining material, or some other criteria (depending on the nature of the structure and the load).

Upon the utilisation of FM analysis, the crack growth is normally defined by the Paris and Erdogan (1963) law as illustrated in Fig. 6.15, which is :

$$\frac{da}{dN} = C(\Delta K)^m \tag{6.37}$$

where C = crack growth rate parameter

ΔK = the stress intensity range which is given by :

$$\Delta K = Y(a)\, S_{eq} \sqrt{\pi a} \tag{6.38}$$

Y(a) = the geometry correction factor which can usually be assumed constant (and Y=1.12 often assumed)

a = current crack depth

S_{eq} = equivalent constant fatigue stress range, and is written as :

$$S_{eq} = \frac{S_e}{(\ln n_0)^{1/\xi}} (\Gamma(m/\xi + 1)^{1/m} \qquad (6.39a)$$

or

$$S_{eq} = \left(\frac{A\,D}{n_0}\right)^{1/m} \qquad (6.39b)$$

If one apply the Paris-Erdogan crack growth law as in eq. (6.37) with further assumptions :

-. no sequence effects

-. $K_{th} = 0$, i.e. no threshold level

-. a_0 is the initial crack size

it then follows that integrating eq. (6.37) gives :

$$N_p = \int_{a_0}^{a_f} \frac{dA}{C\left[Y(a) S_{eq} \sqrt{\pi a}\right]^m}$$

$$= \frac{1}{C\left[Y S_{eq} \sqrt{\pi}\right]^m} \int_{a_0}^{a_f} \frac{da}{a^{m/2}} = \frac{A_0}{S_{eq}^m}$$

where $$A_0 = \frac{a_0^{1-\frac{m}{2}} - a_f^{1-\frac{m}{2}}}{(\frac{m}{2} - 1) C Y \pi^{m/2}} \qquad (6.40)$$

which, as we would expect (within the assumptions made) is of similar form to the crack initiation law $NS^m=A$.

Taking the Class-D weld connection for the wet deck plate of SWATH-FV as an example (see Fig. 6.16), the crack propagation at position X can be analysed as in the following. Considers the lifetime stress cycle and so on as given in the previous sections, the allowable stress range for 20 year operation is found to be 290 N/mm^2. For this, the equivalent constant stress for $n_0=8.7\cdot10^7$ is :

$$S_{eq} = \left(\frac{A\,D}{n_0}\right)^{1/m} = \left(\frac{1 \times 1.52 \cdot 10^{12}}{8.7 \cdot 10^{7}}\right)^{1/3}$$

$$S_{eq} = 25.95\ N/mm^2$$

Taking C = $3.3 \cdot 10^{-13}$ in metric units, i.e. mean value plus two standard deviation as given by Almar-Næss (1985)

a_0 = 0.2 mm, which is a typical value taken in the UKOSRP (UK Offshore Steels Research Programme) as presented by Thorpe (1987)

a_f = 12 mm for through-the-thickness cracking

Y = 1.12, then from eq. (6.40)

$$A_0 = \frac{0.2^{-0.5} - 12^{-0.5}}{(0.5) \times 3.3 \cdot 10^{-13} \times 1.12 \times \pi^{1.5}} = 1.93 \cdot 10^{12}$$

Hence $$N_p = \frac{A_0}{S_{eq}^m} = 1.102 \times 10^8 \text{ cycles}$$

in which the total number of cycle to failure is

$$N_t = N_i + N_p = (0.87 + 1.102)10^8$$

From this figure it is found that the number of cycle for crack initiation is only some 45% of the through-the-thickness cracking.

However, taking this example still further, this N_t itself (which is around 2.25 times the design life n_0=$8.7 \cdot 10^7$) only takes the crack at X from the surface through the thickness t=12 mm. It still has to propagate laterally along the weld joint, say from one stiffener to another stiffener and beyond before total severance of the member is achieved. Thus the true total life so far as that single member is concerned is several times more again than the N_t estimated above.

Moreover, even after member severance (complete break of weld connection) the remaining three-dimensional structure adjusts with different load paths to take further load. In pursuing analysis still further it is sometimes convenient to think of 'series' and 'parallel' systems as forwarded by, e.g. Thoft-Christensen (1987).

A series system, as exemplified by Faulkner (1983), is like a link chain or a series of drill pipes screwed together to form a single tether or tendon in the *Hutton* TLP. A through crack and severance represents the total failure of the chain or of that tether. But, if as with the TLP, there are several structural system, then a failure in one tether does not itself represents the total loss of capacity. For example, the remaining three tethers in one corner (leg) of the *Hutton* TLP, would take further load, together with some being transferred to the 12 intact tethers in the other three legs.

The same sort of arguments apply to stiffened 'continuous' plated structures, such as the flat grillages and stiffened cylinders that make up ships and offshore structures. Any crack which initiates has to propagate until a large section of the whole structures is cracked. In many structures this may not happen as the crack may lie 'dormant' - stop propagating.

In view of these remarks it will be clear that there will generally be a significant 'reserve strength' beyond initiation of a fatigue crack (D>1). In summary this comes from

-. further propagation of a crack through the plate surface, i.e. $N_t=N_i+N_p$
-. further propagation along or around (in case of cylinders) the plate
-. the stopping of the crack in redundant structures because other load paths develop.

Hence the safety index β_i for initiation of fatigue can and should be much lower than the ultimate strength.

Considering further, if lower bound values A (mean minus two standard deviation) are used with $NS^m=A$, as most design rules require, then an 'annual' value for safety index β_i of about 2.0 should be acceptable for most structures where the reserve strength potential is significant. Nonetheless, a higher lifetime safety index, say $\beta_i=3.0$, is more appropriate for a critical member. Although this is still less than the safety index $\beta=3.7$ (10^{-4} probability of failure) per year as required by Norwegian Petroleum Directorate (NPD), but with careful monitoring the safety can be adequately maintained as will be described later in Section 6.5.3. This account is in favour with the fatigue criteria as proposed by Wirsching and Chen (1988) for TLP structure as listed in Table 6.7.

6.5.2. Aspects of Fatigue Design on Light Weight Material (GRP)

As is forwarded in the previous chapters the need to explore further the use of light weight material for SWATH constructions is obvious. Composite material is one of the promising choice for such applications. As is described by Spaulding (1966) the

use of glass-reinforced plastics (GRP) in marine structures was pioneered by the US Navy for boat constructions. The significant growth of GRP boat constructions between 1955 to 1972 is notably from 4% to 80%. At that time the application of FRP was mainly intended to replace the use of woods as the traditional boat building material. Smith (1990) clarifies the attributes of GRP in preference to woods in boat constructions as :

a. competitive first cost, particularly where many hulls are built to the same design, enhanced by the increasing cost of wood and scarcity of skilled woodworkers;
b. trouble-free performance and low maintenance costs resulting from the leak proof, rot-proof qualities of GRP hulls, their resistance to marine boring organisms and low cost of repair;
c. the ease with which complex shapes, which may be required for hydrodynamic and structural purposes or for aesthetic reasons, can be fabricated.

Larger ship constructions using GRP in recent years are mainly for mine counter measure (MCM) vessels. In this respect low magnetic signature of such material is the main attraction. More on the prospective applications of GRP in marine activities are discussed by Smith (1990) and Gullberg et al (1991).

With respect to the ship structural design with the use of composite materials Gullberg et al (1991) suggest that the designer must establish what tangible factors that interact to influence the behaviour of such materials. These factors ranging widely from the chemical compositions of the material, reinforcement method, etc right to the possible mode of failure of the constructed structures. Chalmers et al (1988) considers that for general marine applications the use of simple isotropic theory for structural design is acceptable. Even though, it is also emphasised that the material is essentially anisotropic, and for design of details and for an understanding of modes of failure more sophisticated design methods ought to be employed. In the following discussion is focused on the failure mode of GRP as associated to fatigue loadings.

Unlike steel structures where vast fatigue data is now available, fatigue information on GRP is much scarce. Within limited information on fatigue of GRP some findings on the mode of failure following cyclic load persistence has been established. Fatigue failure on FRP is different from metallic material where a crack, as it extends, carries with it a severe stress concentration at its tip and is therefore likely to propagate until it reaches a low stress region. Smith (1990) reveals fatigue failure in GRP laminates containing bidirectional and multidirectional fibres is less highly focused : fibres parallel to the direction of tensile load provide a crack-arresting action and fatigue damage takes the form of a diffuse patch of resin cracking and fibre debonding, possibly including some fibre fractures. Local moduli in the damage zone is likely to attenuate the stress concentration thereby inhibiting damage propagation.

Typical S-N curves for marine-type GRP laminates as compiled by Smith (1990) are shown in Fig. 6.17. Two types of laminates, namely woven rovings (WR) and chopped strand mats (CSM), are depicted in this figure. The full lines refer to complete failure under fully-reversed loading with zero mean stress, whereas the dotted lines indicate the onset of initial damage, that is fibre-debonding and resin cracking. Appropriate S-N data of GRP laminates such as this can be incorporated in fatigue analysis employing the Miner's cumulative damage law together with histograms of irregular cyclic loading as described in the previous sections. An alternative, quadratic version of this cumulative damage criterion has been found to give improved results for CSM GRP laminates. This quadratic version was introduced by Howe and Owen (1972) which is expressed as :

$$\sum_i \left[A\frac{n_i}{N_i} + B\left(\frac{n_i}{N_i}\right)^2 \right] = 1.0 \qquad (6.41)$$

where A and B are empirical constants. Cumulative damage expressions of this type may be related by either to initial fibre-debonding or to final laminate failure.

6.5.3. Fatigue Inspection and Repair Strategy

Up to this point the study has concerned mainly on the development of understandings necessity in ship design level without considering the lifetime process of ship operation. In this case the term of lifetime process may be narrowed to the maintenance of the ship. This might sound reasonable, since the current practice regards the two matters as a separate issue which ought to be dealt with by different specialists. Moreover, the hindrance of dealing with the two subjects as an integrated problem chiefly due to the difficulties in formulating the maintenance strategy as a scientific discipline. However, Skaar et al (1991) pointed out the growing research in the field of scientific maintenance method designated the 'terotechnology'.

It is not the intention of this section to discuss that immature technology, but the recent research development may indicate the way towards the future trend of ship maintenance strategy. Thoft-Christensen (1987) has recently shown the necessity of transferring reliability method into the scope of ocean structure inspections, which in turn could be of use to formulate the repair/maintenance planning. The adoption of probabilistic method in repair and maintenance activities should not be interpreted as to increase the reliability of structures, but to guarantee that the predefined safety level is maintained. Moreover, maintenance may be related to preventive actions necessary to

keep up the safety level, while repair is the same as corrective maintenance, which means actions to restore the safety level when lost for some reason.

Maintenance of ocean systems generally, as required by classification societies, is preceded by regular inspections throughout the life of the systems. Madsen et al (1987) has presented the methodology to incorporate probabilistic method in fatigue inspection of an offshore platform. Information from regular survey and inspection has been used in this matter. The inspection of fatigue cracks in this case was performed by Magnetic Particle Inspection (MPI) which is far more accurate than visual inspections. The probability of detecting a crack is a function of its surface crack length. Accounting for uncertainties in fatigue life predictions and reliability of the inspection method in the mathematical model, the fatigue reliability can be then updated according to Bayesian theory.

The above implies that if no failure has been identified the current probability of element failure may be reduced (current reliability increased), with a factor reflecting the quality of inspection method. This factor is the ratio between conditional probability of not detecting a failure with the present inspection technique given that a failure is present, and the current reliability of the member. The updated fatigue reliability for a fixed inspection interval is shown in Fig. 6.18. Inspection interval can actually be optimised while maintaining a prescribed minimum reliability level. If no cracks are detected during inspection interval is increased as function of service life, as illustrated in Fig. 6.19.

In the case where fatigue cracks have been detected, the decision is then to be made as wether or not a repair should be performed. This particular decision concerns especially if difficulties and costs to underway the works are of stubborn, in addition to the consideration of the importance of such member on the integrity of overall structure. In case the decision should call upon repair works, then remedial actions may be performed by selecting one or more of the five choices belows :

-. local repair of cracks
-. replacement of part of the structure
-. reinforcement of the structure
-. repair of protective coating
-. repair of cathodic protection.

For small fatigue defects normally the first choice will be considered. Skaar et al (1991) indicates that direct weld repair of a structure which has cracked because of fatigue loading is never very satisfactory because the weld quality will, almost invariably, be worse than the original. The repaired weld will thus fail even earlier than the original one unless certain treatments are made to reduce stress concentration at that

repaired member. The most significant method to fulfil this need is by as much as possible reducing the primary load that governs fatigue performance of the structural member. It is suggested then to avoid dominant waves, and other extreme load such as slamming, during ship operation. Nevertheless, such a method is hardly practical for actual operation.

The most practical way in an attempt to reduce local stress concentration probably is by certain reinforcements, e.g. using insert plate or additional support. In recent years the application of metal adhesives for crack repair has spread out significantly. The advantages of using adhesives are, for examples, that lagging, cables and pipes etc at ambient of the repaired member do not have to be removed as they do for weld repairs, as well as possibly much reduced residual stress. Allan et al (1986) describes in detail the aspects of metal adhesives utilisation in ship repair. The Department has in recent years involves with the research on metal adhesives for use in ocean structures, e.g. as presented by Winkle et al (1990). The study of metal adhesive for SWATH fabrication may be of interest for future research.

6.6. CONCLUSIONS

A preliminary analysis of fatigue behaviours on SWATH type vessels is put forward. Design procedures, involving a full spectral analysis followed by the simplified approach, commonly practised by conventional ship and offshore structure designers are adopted. Some aspects of SWATH fatigue performance has been addressed, although much more remains to do. Case studies on two hypothetical SWATHs, size of approximately 2500-tonne, operating in the North Atlantic region have been performed to illustrate the implementation of the design procedures.

One of an interesting results drawn from the analysis is the newly introduced Weibull shape parameters ξ pertinent to those SWATHs. Parameter values of 0.94 and 0.945 were derived for SWATH-FV and SWATH-3, respectively. These figures fall in the range of those normally applicable to monohull ships, i.e. between 0.7 and 1.3. Although Munse et al (1983) suggest that lifetime stress distributions for most monohulls of this size (2500 tonnes) are typically represented by the parameter values in the order of 1.0 to 1.3. Further, Clarke (1991) indicates an exponential cyclic load distribution, in which $\xi = 1.0$, has been widely practised in the Royal Navy warship designs. Such values, however, remain open to further refinement, especially if a wider range of wave scatter data representing the operational areas has been examined.

The allowable stress range as one of the most important measure in fatigue design has been evaluated. Stress ranges of approximately 290 N/mm^2 and 250 N/mm^2 have been deterministically derived for a 20-year and 30-year lifetime, respectively. The

latter was compared with the design stress for the T-AGOS, in which a design stress range of some 190 N/mm^2 is adopted for 30 years operation. The difference of the two values eventually is quite large, hence necessitated design check by way of probabilistic approach to be performed.

Two different reliability methods have been implemented for the analysis. The first method is a general advanced first order second moment (AFOSM) code which was developed in the Department by Pu (1992), and the second is fatigue reliability format by Wirsching (1984). The results from both analysis correlate fairly well for most stress ranges that have been investigated. These results suggest that a design stress range value of some 200 N/mm^2, which is close to that adopted for T-AGOS, should be acceptable and would give an adequate fatigue safety for SWATH-FV for a 30-year operation provided thorough inspection can be performed every 10-year interval.

The corresponding safety index after 10 years operation for the above stress range is approximately 2.0. It is initially from the rule of thumb that safety index of 2.0 to 3.0 is acquired for fatigue failure, that is based on the recognition that crack initiation on a structural members would not bring a catastrophic failure of SWATH structure. Later on a calculation regarding fatigue crack propagation was performed which conclude that much larger cyclic number (in the order of 2.25 times that for crack initiation) is required to bring a through the thickness cracking. This finding thus confirm the safety index so adopted. Another confirmation on the above target safety index is provided by Wirsching and Chen (1988) as shown in Table 6.7.

Full analysis on SWATH has yet not been able to be performed because of the limited information which is currently available, especially for the S-N data pertinent to the critical members of SWATH structure. Nonetheless, future direction to the research on SWATH fatigue performance, which involve fracture mechanics for crack propagation analysis and maintenance strategy, has been adequately pointed out.

Table 6.1. Fatigue life of the 2500-tonne SWATH-FV computed by Miner's rule (for Class-D weld)

BM (MNm)	ni	Stress (MPa)	Ni	ni/Ni
5.00	48082523.80	2.74	73602016400.00	0.000653
15.00	15556294.60	8.22	2726000607.41	0.005707
25.00	8117786.20	13.70	588816131.20	0.013787
35.00	4772118.40	19.18	214583138.19	0.022239
45.00	2860000.00	24.66	100962985.46	0.028327
55.00	1739176.60	30.14	55298284.30	0.031451
65.00	1072957.20	35.62	33501145.38	0.032027
75.00	668399.80	41.10	21808004.86	0.030649
85.00	419379.80	46.58	14981073.97	0.027994
95.00	264852.00	52.05	10730721.15	0.024682
105.00	168182.80	57.53	7947523.64	0.021162
115.00	107227.20	63.01	6049315.07	0.017726
125.00	68534.00	68.49	4710529.05	0.014549
135.00	43852.60	73.97	3739369.83	0.011727
145.00	28060.60	79.45	3017836.58	0.009298
155.00	17940.80	84.93	2470612.48	0.007262
165.00	11453.40	90.41	2048084.60	0.005592
175.00	7298.80	95.89	1716665.11	0.004252
185.00	4640.60	101.37	1453063.32	0.003194
195.00	2944.40	106.85	1240783.16	0.002373
205.00	1863.20	112.33	1067918.58	0.001745
215.00	1175.80	117.81	925730.02	0.001270
225.00	740.40	123.29	807703.88	0.000917
235.00	464.60	128.77	708918.22	0.000655
245.00	291.20	134.25	625606.82	0.000465
255.00	182.00	139.73	554854.59	0.000328
265.00	113.00	145.21	494381.38	0.000229
275.00	70.00	150.68	442386.27	0.000158
285.00	43.00	156.16	397434.12	0.000108
295.00	26.40	161.64	358371.68	0.000074
305.00	16.20	167.12	324265.10	0.000050
315.00	10.00	172.60	294352.73	0.000034
325.00	5.80	178.08	268009.16	0.000022
335.00	3.80	183.56	244717.66	0.000016
345.00	2.20	189.04	224048.71	0.000010
355.00	1.20	194.52	205643.35	0.000006
365.00	1.00	200.00	189200.00	0.000005
375.00	0.20	205.48	174464.04	0.000001
385.00	0.00	210.96	161219.49	0.000000
395.00	0.00	216.44	149282.34	0.000000
405.00	0.00	221.92	138495.18	0.000000
			D =	0.320742
			Fatigue Life (yrs) =	62.355347

Table 6.2. Iterative computation of Weibull-shape parameter (ξ) for SWATH-FV

$D = 0.3207$ {from $D=\Sigma(n_i/N_i)$ calc.}

$S_e = 200\ N/mm^2$ $A = 1.5136 \cdot 10^{12}$

$n_o = 8.4019 \cdot 10^7$ $m = 3.0$

ξ	$m/\xi + 1$	$\Gamma(m/\xi + 1)$	D (damage)
0.9000	4.3333	9.2605	0.2571
0.9100	4.2967	8.8166	0.2722
0.9200	4.2608	8.4032	0.2879
0.9300	4.2258	8.0179	0.3042
0.9350	4.2085	7.8447	0.3129
0.9360	4.2051	7.8093	0.3146
0.9370	4.2017	7.7764	0.3164
0.9380	4.1982	7.7391	0.3180
0.9390	4.1948	7.7070	0.3198
0.9400	**4.1914**	**7.6667**	**0.3213**
0.9500	4.1578	7.3380	0.3391
0.9600	4.1250	7.0354	0.3577
0.9700	4.0927	6.7477	0.3767
0.9800	4.0612	6.4785	0.3964
0.9900	4.0303	6.2345	0.4173
1.0000	4.0000	6.0000	0.4385

Table 6.4. Comparison of the fatigue lives of SWATH-FV for all heading weighted (A) and beam sea dominated (B)

S_e (N/mm^2)	D (All heading)	Life-A (years)	D (Beam)	Life-B(years)
100.00	0.04017	497.95	0.14564	137.32
120.00	0.06941	288.16	0.25167	79.47
140.00	0.11021	181.47	0.39964	50.05
160.00	0.16452	121.57	0.59655	33.53
180.00	0.23424	85.38	0.84938	23.55
200.00	0.32132	62.24	1.16513	17.17
220.00	0.42768	46.76	1.55079	12.89
240.00	0.55524	36.02	2.01335	9.93
260.00	0.70594	28.33	2.55980	7.81
280.00	0.88170	22.68	3.19713	6.26
300.00	1.08446	18.44	3.93233	5.09
320.00	1.31613	15.19	4.77239	4.19
340.00	1.57865	12.67	5.72430	3.49
360.00	1.87394	10.67	6.79506	2.94
380.00	2.20393	9.08	7.99165	2.50
400.00	2.57056	7.78	9.32107	2.15

Table 6.3. Dependance of the SWATH-FV's fatigue life on the Weibull-shape parameter

Class-D Weld S-N data $S_e = 200$ N/mm^2 ; $n_o = 8.4 \cdot 10^7$		
ξ	Fatigue Life (years)	Sensitivity (%)
0.850	33.7604	+ 68.8018
0.860	31.7270	+ 58.6349
0.870	29.8472	+ 49.2362
0.880	28.1070	+ 40.5348
0.890	26.4922	+ 32.4610
0.900	24.9975	+ 24.9873
0.910	23.6065	+ 18.0327
0.920	22.3200	+ 11.5999
0.930	21.1278	+ 5.6390
0.940	**20.0000**	**0.0000**
0.950	18.9536	- 5.2320
0.960	17.9677	- 10.1617
0.970	17.0607	- 14.6963
0.980	16.2134	- 18.9330
0.990	15.4011	- 22.9946
1.000	14.6550	- 26.7249
1.010	13.9549	- 30.2255
1.020	13.2957	- 33.5217
1.030	12.6788	- 36.6059
1.040	12.0928	- 39.5361
1.050	11.5478	- 42.2612

Table 6.5. Effect of different weld classes to the fatigue life of SWATH-FV (Allowable extreme stress range, S_{ca}=290 N/mm^2)

Weld Class	A	m	Damage (D)	Fatigue Life (years)	Sensitivity (%)
B	1.01E+15	4.0	0.000069	291869.86	1459249.3
C	4.23E+13	3.5	0.007668	2608.36	12941.8
D	**1.52E+12**	**3.0**	**1.000000**	**20.00**	**0.0**
E	1.04E+12	3.0	1.461539	13.68	-31.6
F	6.32E+11	3.0	2.405064	8.32	-58.4
F2	4.31E+11	3.0	3.526683	5.67	-71.6
G	2.48E+11	3.0	6.129035	3.26	-83.7
W	1.57E+11	3.0	9.681532	2.07	-89.7

Table 6.6. Data for fatigue reliability analysis

Variable	Mean	COV	Dist. type
Δ	1.0	0.50	Log-Normal
n_o	8.40 x 10^7	0.05	Log-Normal
A	1.51 x 10^{12}	0.31	Log-Normal
m	3.0	0.03	Normal
S	Varying	0.20	Log-Normal
ξ	0.94	0.05	Log-Normal

Table 6.7. Fatigue design criteria for TLP deck and hull structure

Target Safety Index, β_o	Application	Target Damage Level, Δ_o
2.0	The structure is redundant and cracks are easily inspected and repaired; used for deck structure, mating joints, main body of cylinders and pontoons, and production risers	0.55
2.5	For redundant and non-critical structure which is non-inspectable, i.e., non-inspectable deck structure	0.35
3.0	The structure is critical and, while inspection is possible, repairs are expensive; used for pontoon/cylinder interface, main braces, and for tension pile pullout	0.22

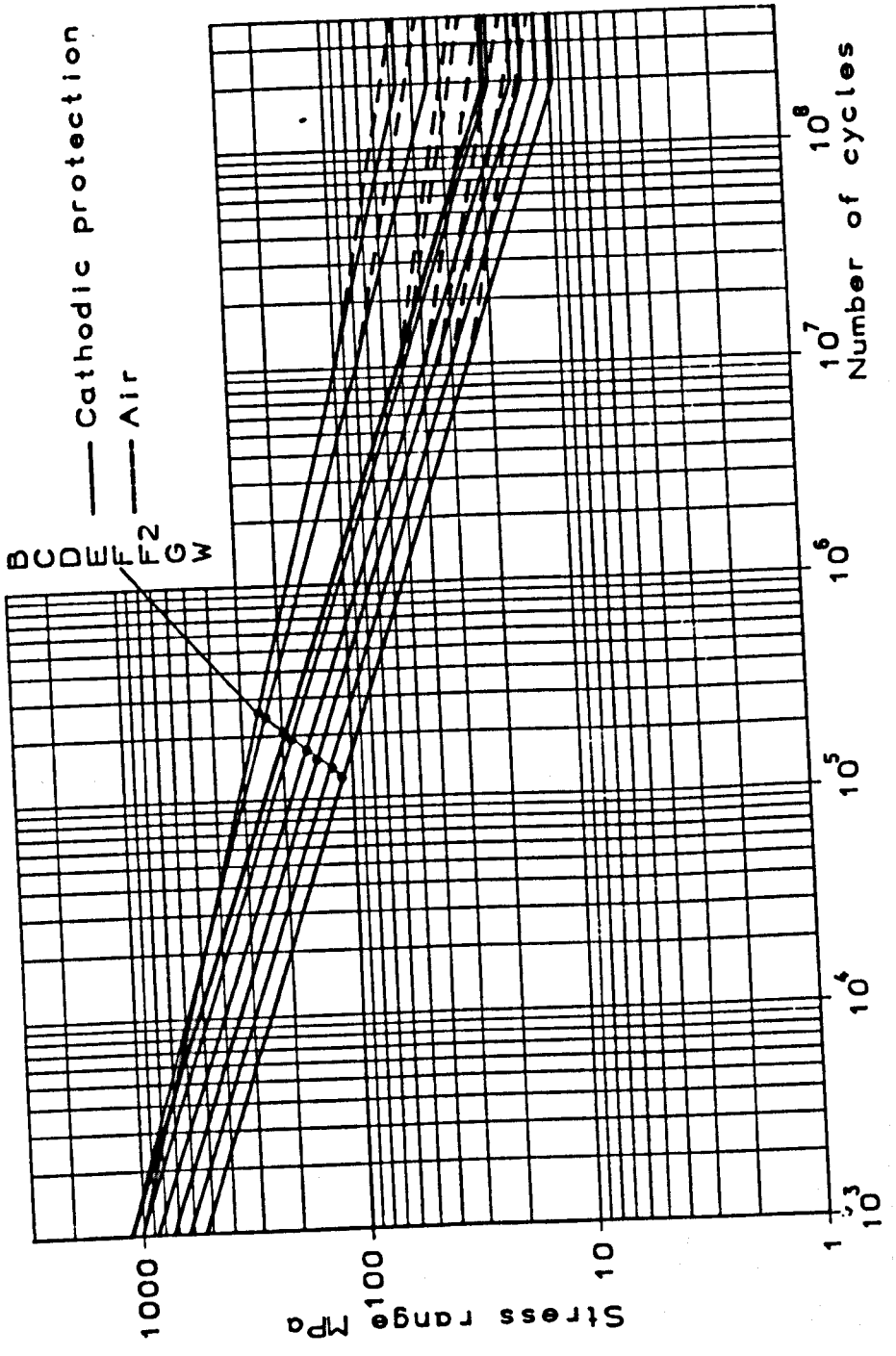

Figure 6.1. S-N design curves for non-tubular members and connections [Gurney (1976)]

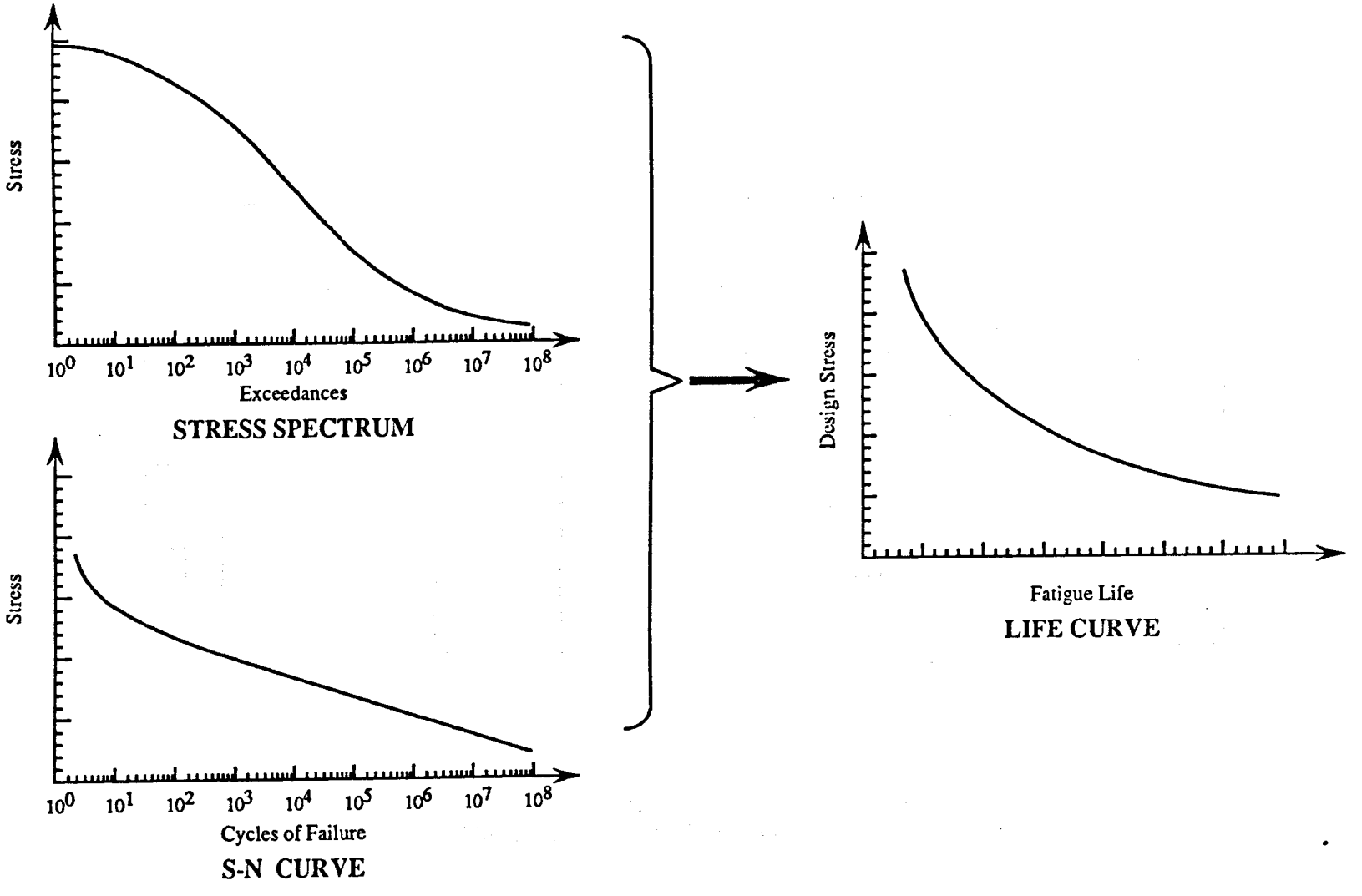

Figure 6.2. Schematic of fatigue prediction method

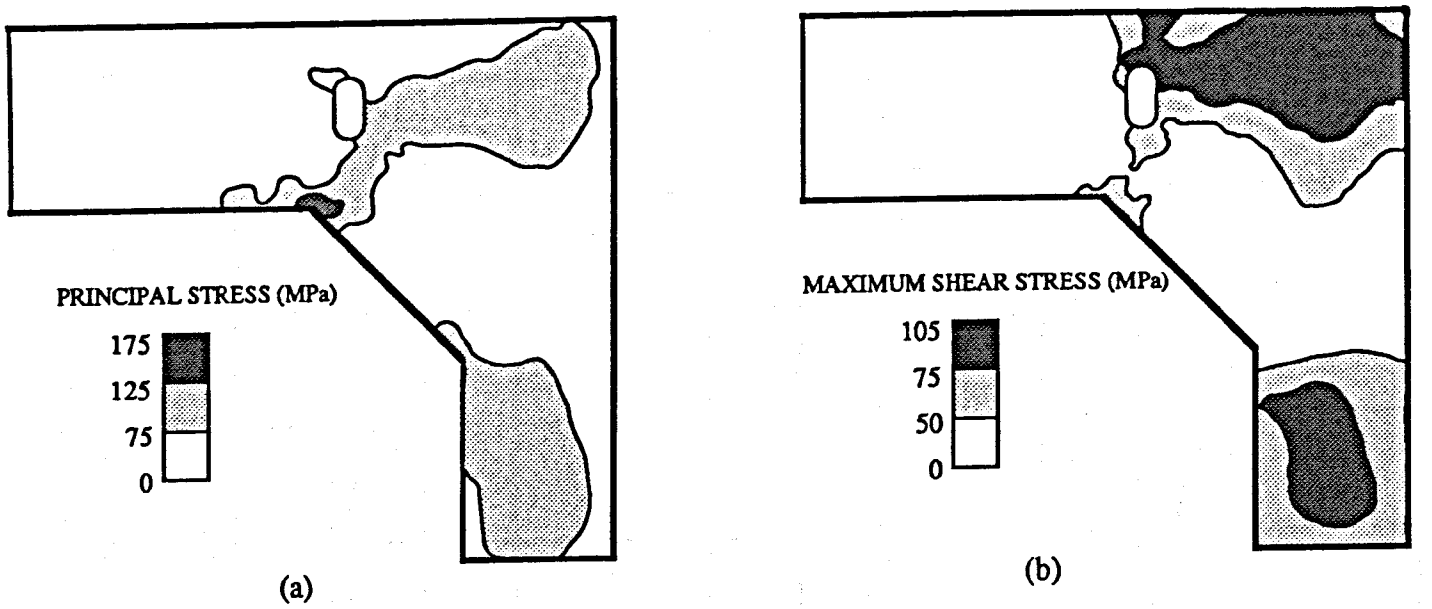

Figure 6.3. a) Principal stress contours and b) Shear stress contours on SWATH's bulkhead [Sikora (1988)]

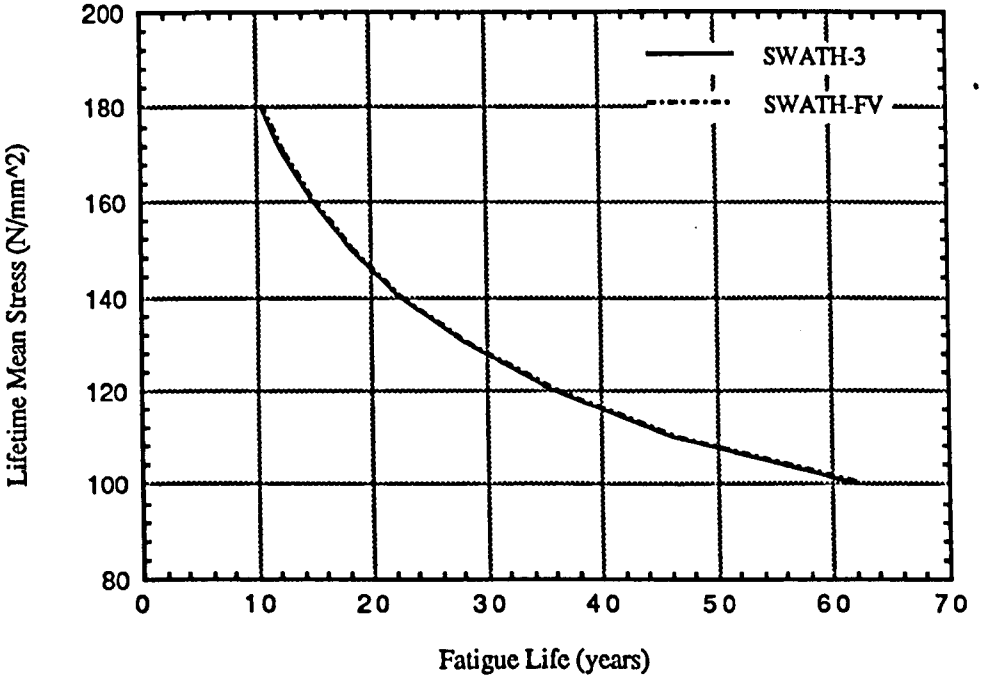

Figure 6.4. Fatigue life of two SWATH vessels in the North Atlantic based on the mean lifetime stress and Class-D weld joints

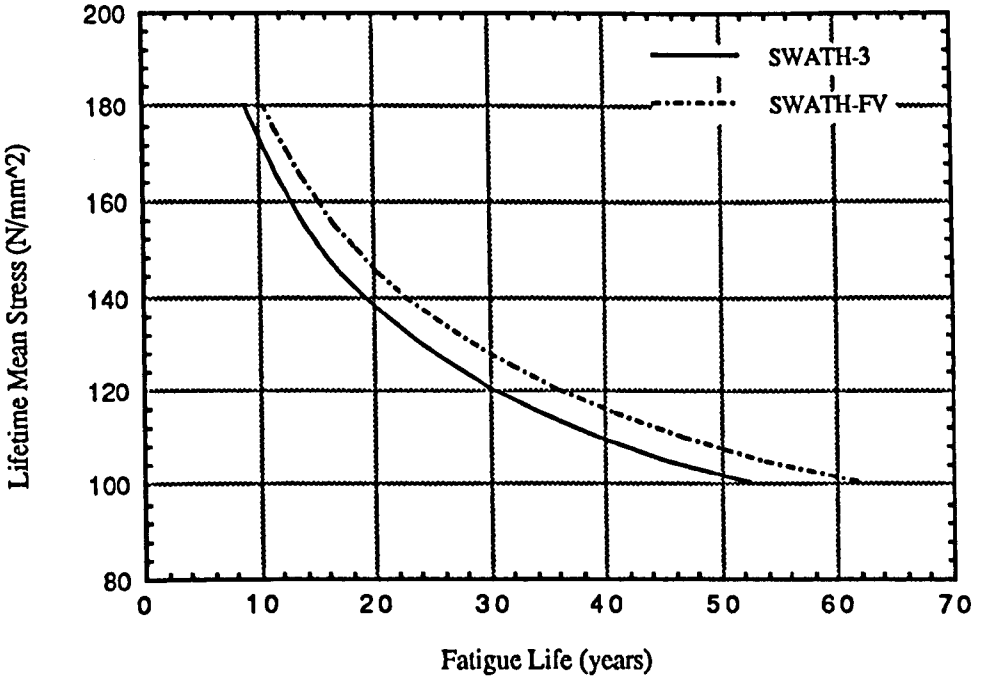

Figure 6.5. Fatigue life of two SWATH vessels in the North Atlantic (equal stress range proportion for the two vessels)

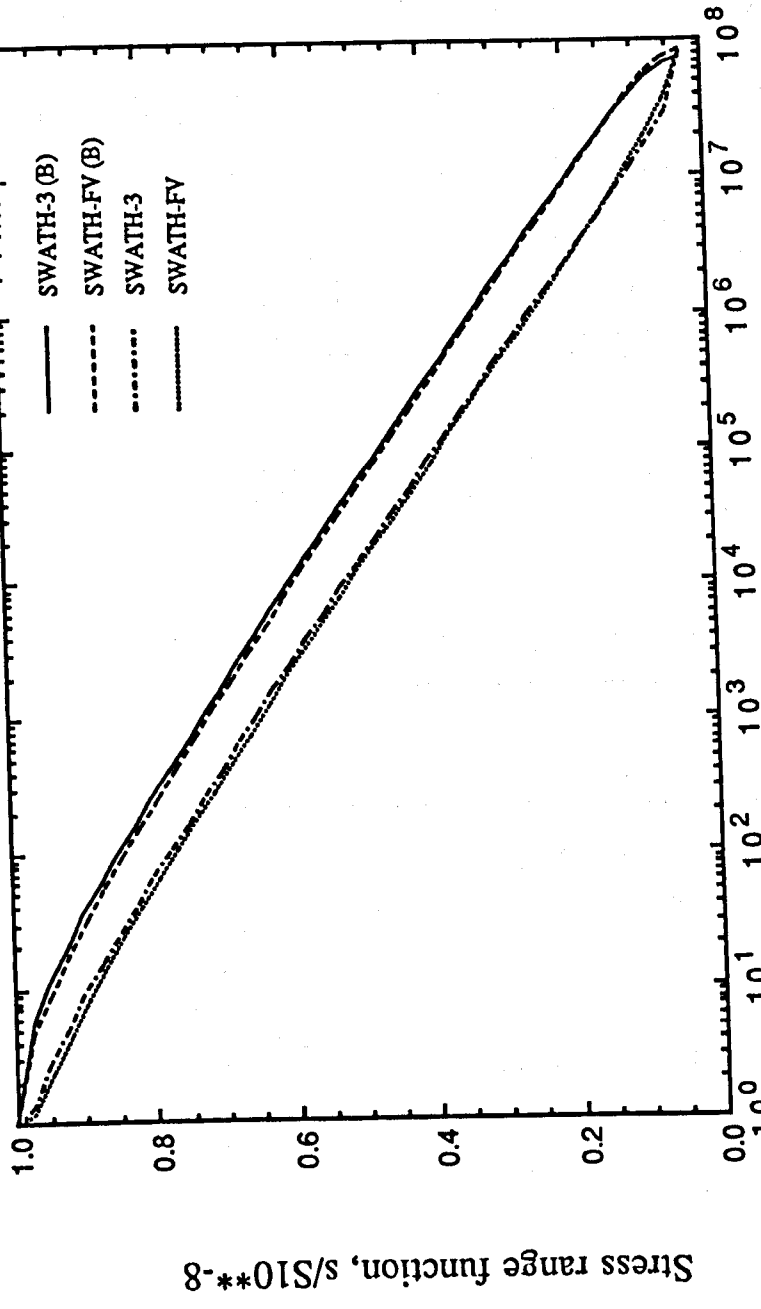

Figure 6.6. Loading histories of SWATH-3 and SWATH-FV
(B denotes the beam sea dominated operation)

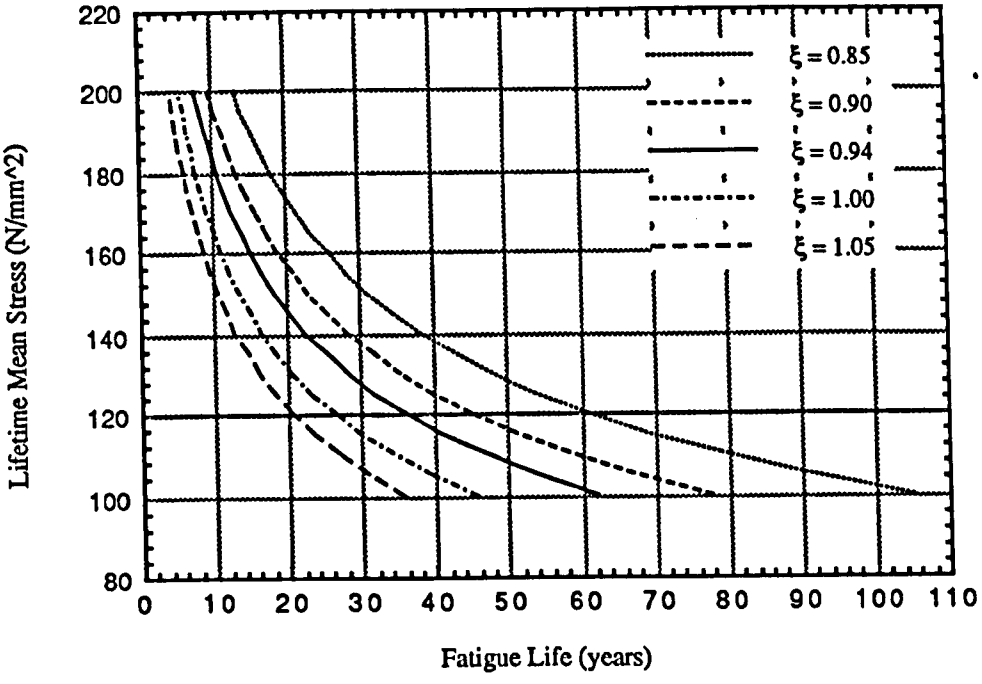

Figure 6.7. Fatigue life of SWATH-FV in the North Atlantic (for different Weibull shape parameters)

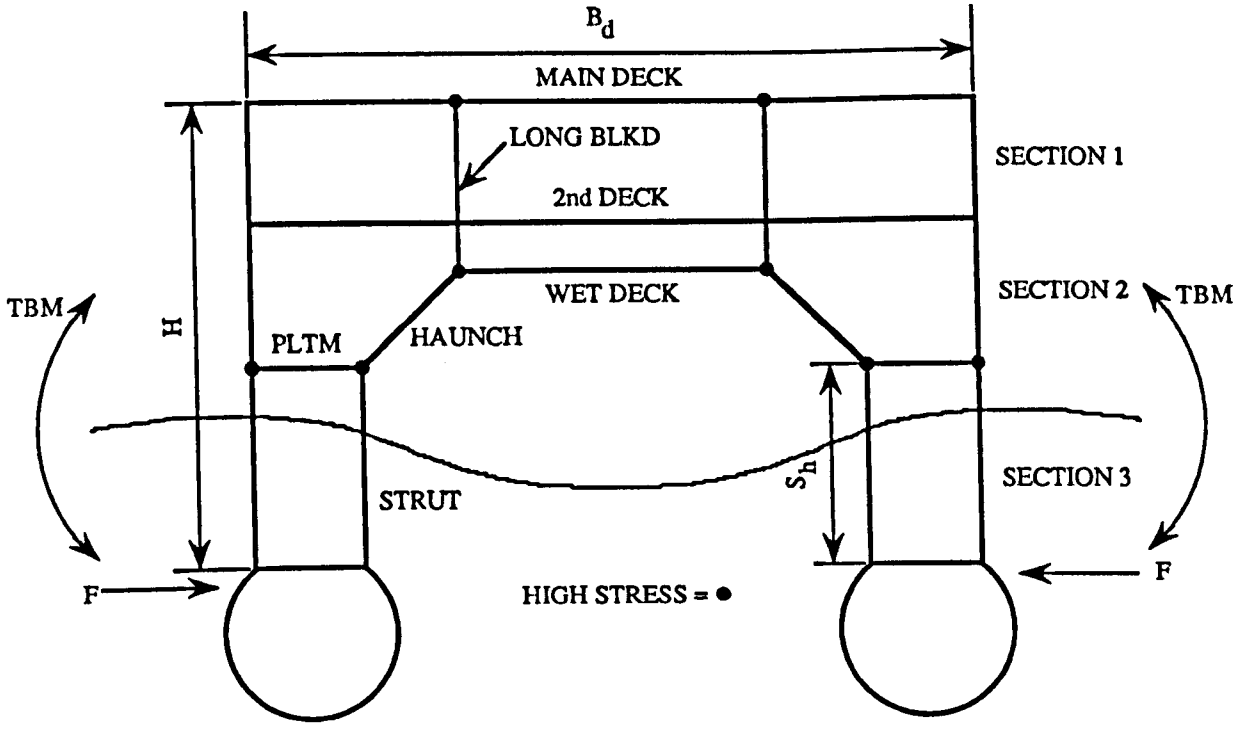

Figure 6.8. SWATH notation for the determination of SCFs [Sikora (1988)]

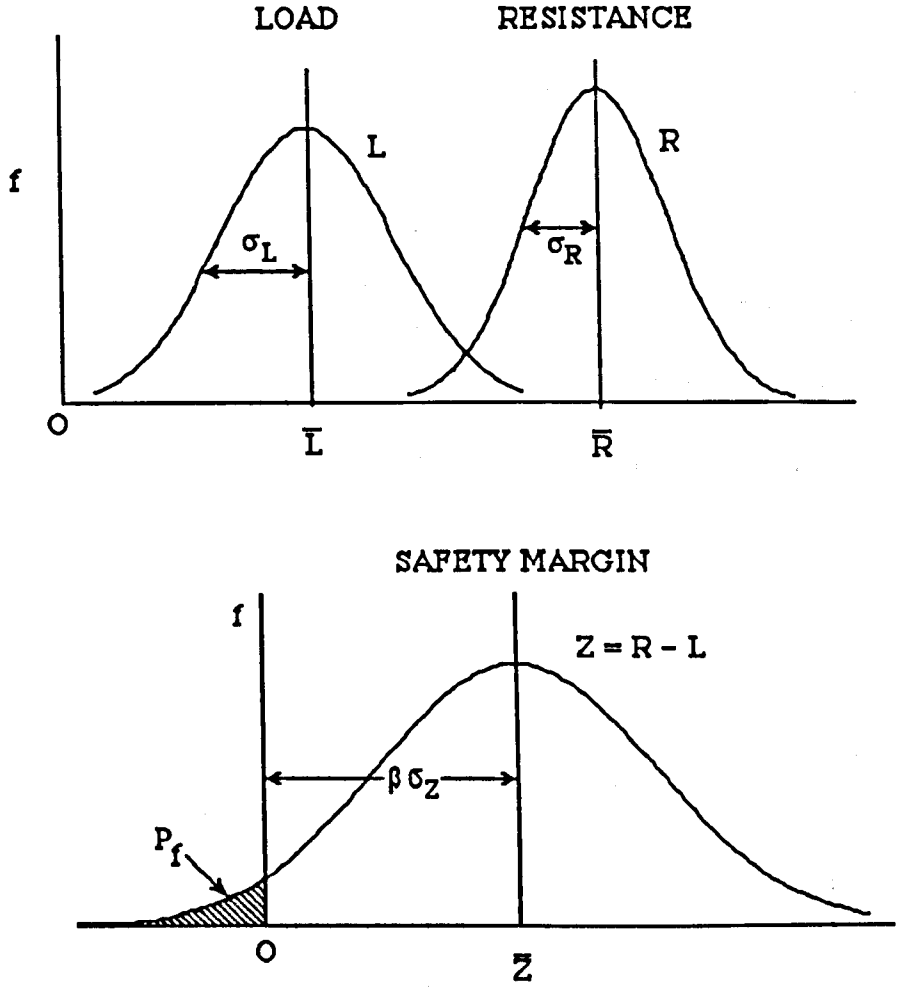

Figure 6.9. Probability distributions of load (L) and resistance (R)

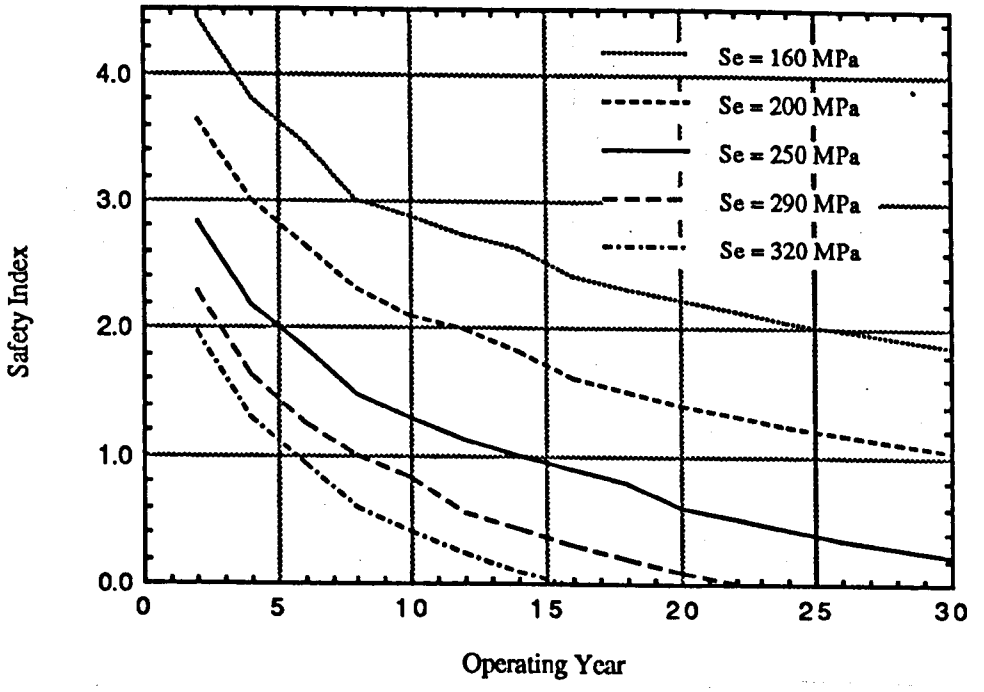

Figure 6.10. Change of fatigue reliability with operating time for SWATH-FV

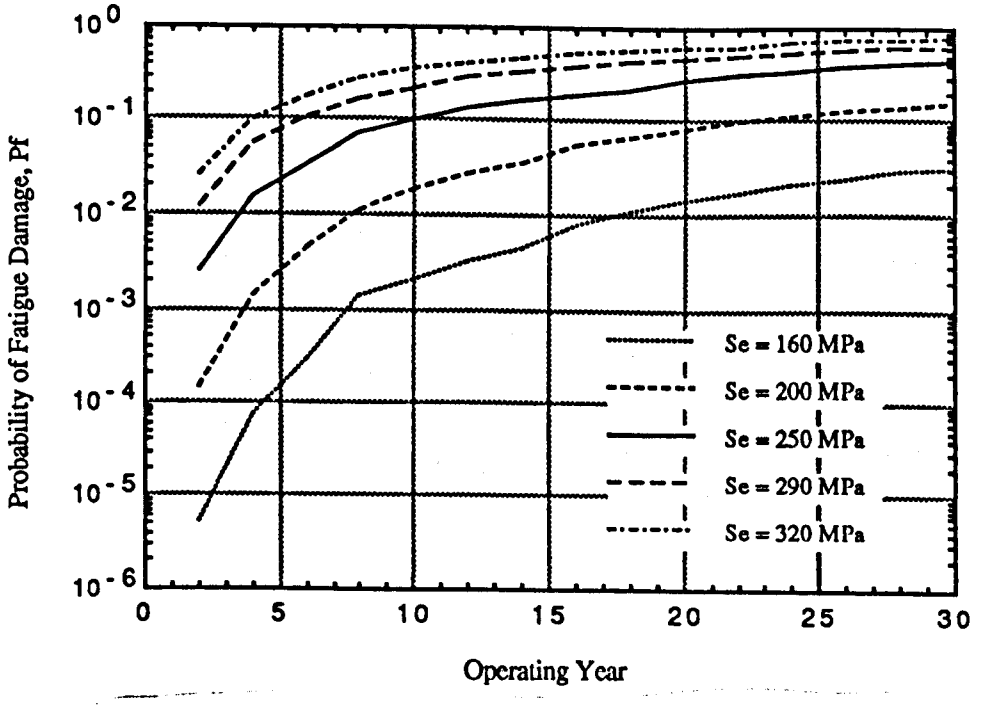

Figure 6.11. Probability of fatigue damage on SWATH-FV (Class-D weld joints)

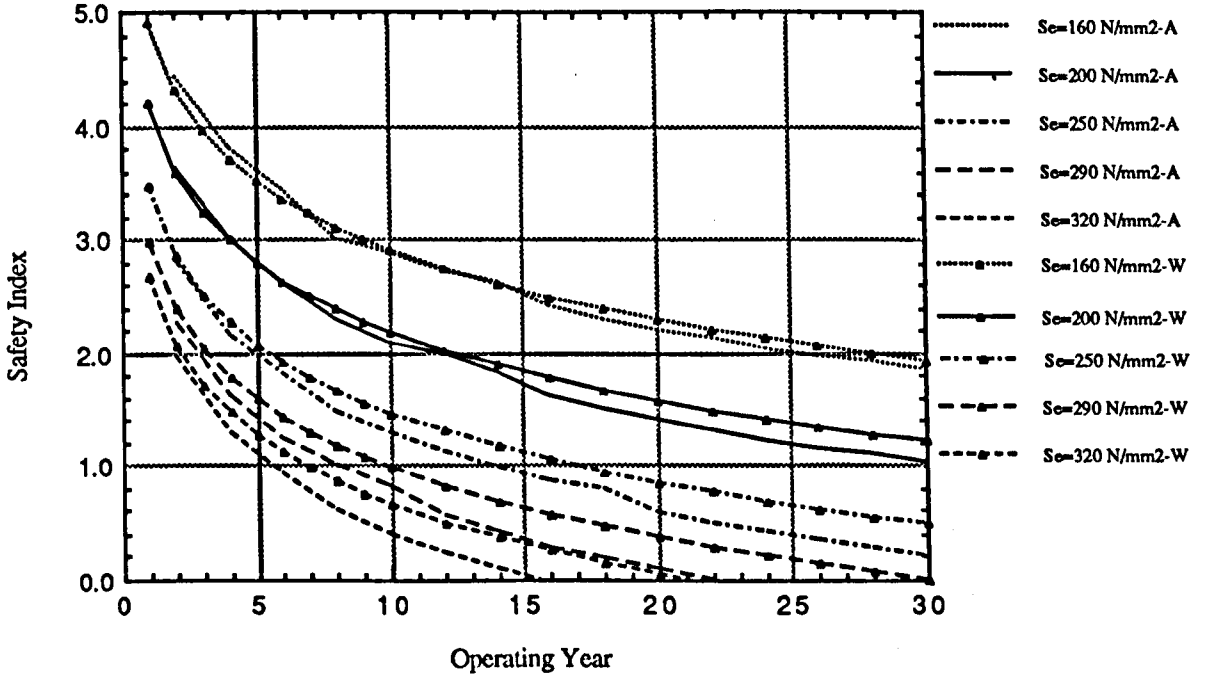

Figure 6.12. Change of fatigue reliability with operating time for SWATH-FV as predicted by AFOSM (A) and Wirsching (W) methods

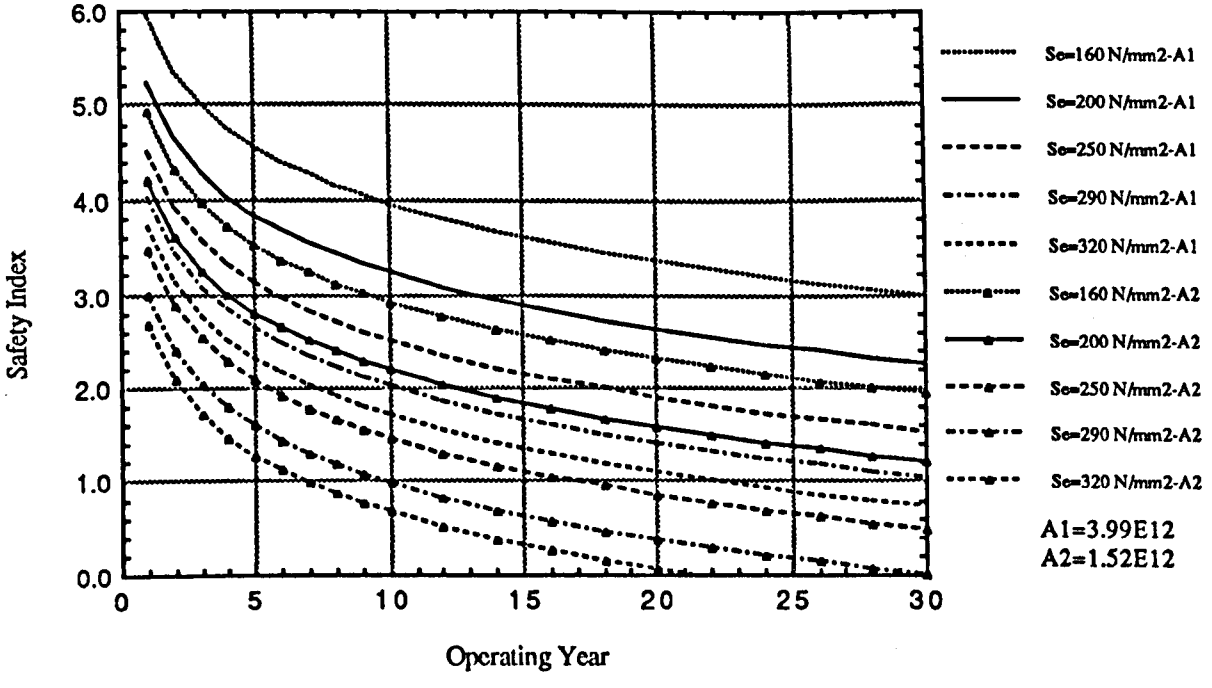

Figure 6.13. Change of fatigue reliability with operating time for SWATH-FV as predicted by Wirsching's method

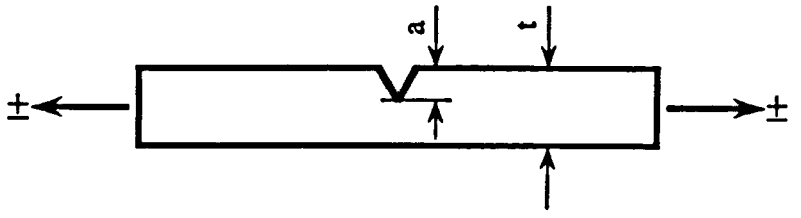

Figure 6.14. Specimen for crack growth observation

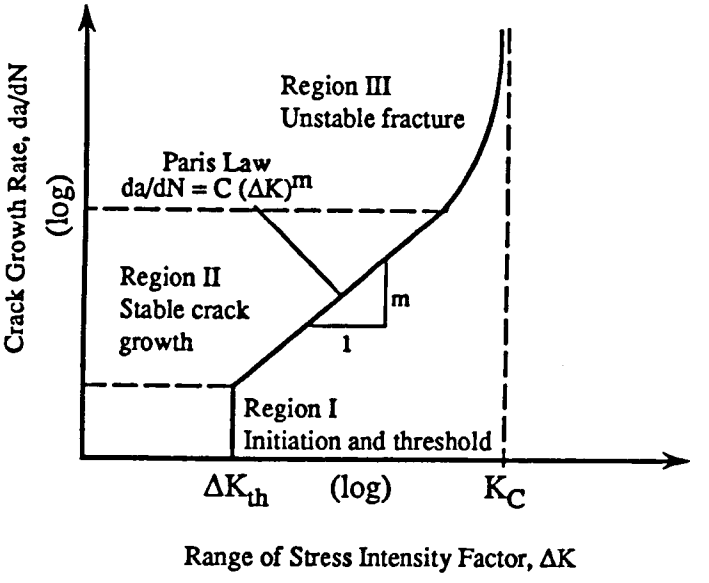

Figure 6.15. A model for fatigue crack growth according to Paris-Erdogan Law

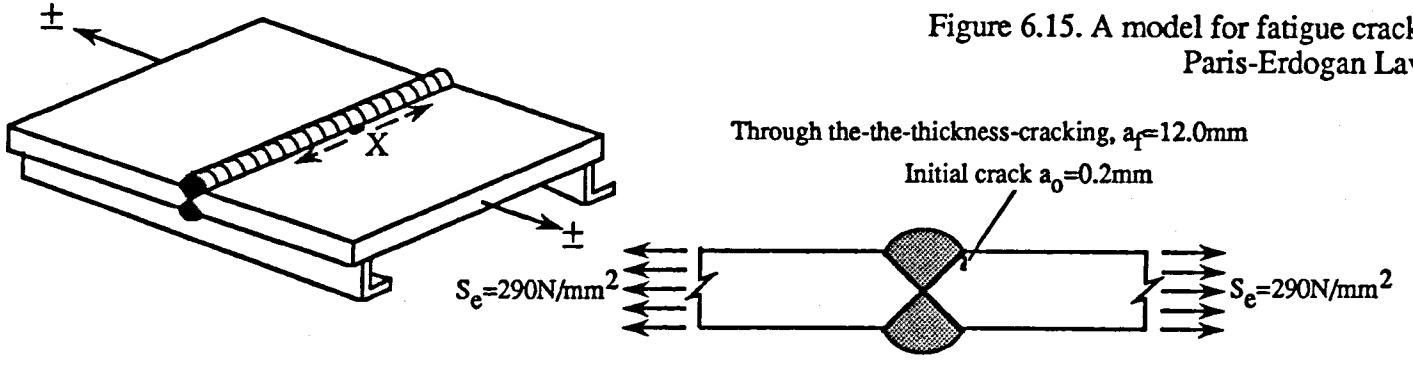

Figure 6.16. Crack growth in a simple butt weld on SWATH deck plating

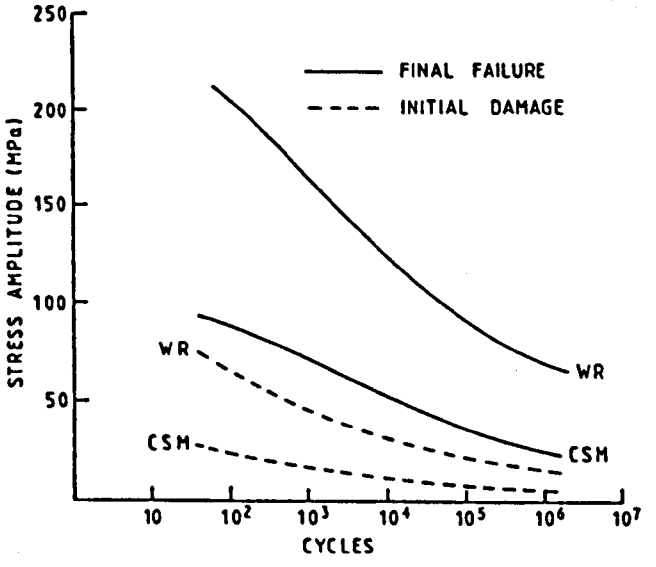

Figure 6.17. Typical S-N curves for marine-type GRP laminates [Smith (1990)]

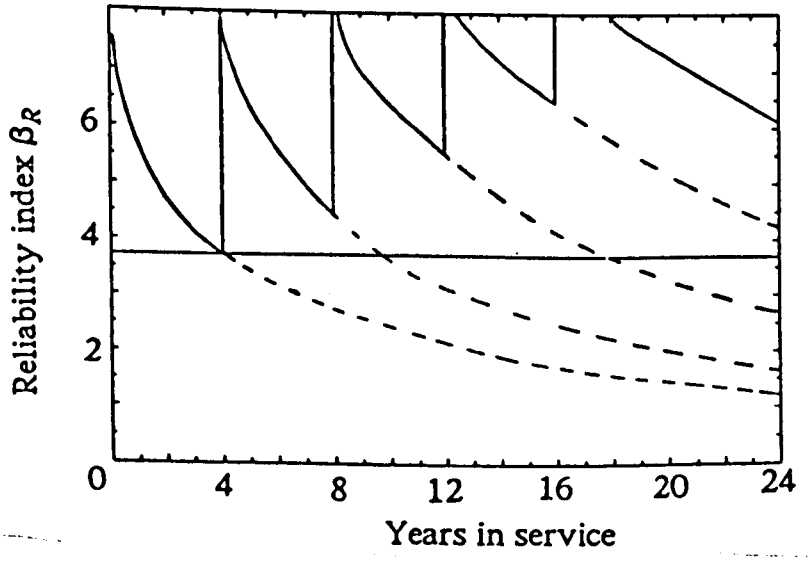

Figure 6.18. Updated fatigue reliability for fracture mechanics based analysis with MPI at regular intervals [Madsen et al (1987)]

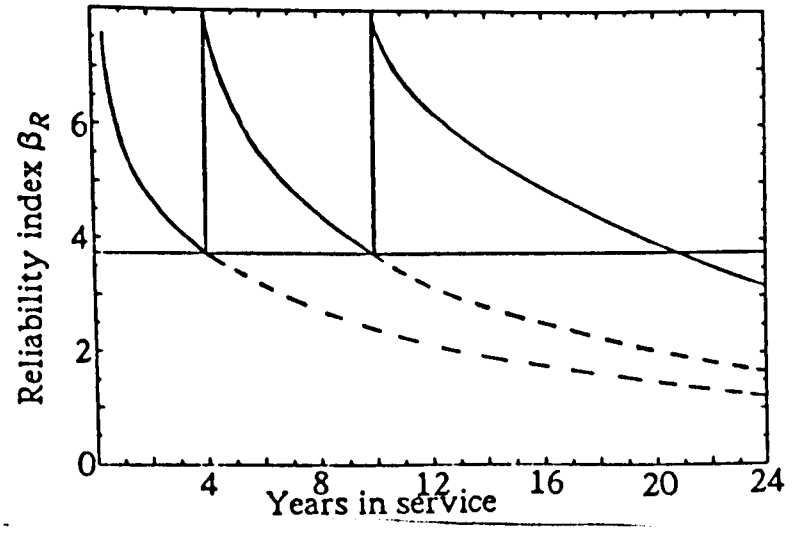

Figure 6.19. Updated fatigue reliability for fracture mechanics based analysis with MPI at optimised intervals [Madsen et al (1987)]

CHAPTER 7

CONCLUDING REMARKS

CHAPTER 7

CONCLUDING REMARKS

7.1. GENERAL

The primary objective of the current research presented in this thesis was to generate experimental data on hydrodynamic behaviour and wave-induced dynamic loadings of SWATH ships. Such experimental data was used to validate the mathematical model which has been developed in the Department recently. Evaluation of SWATH performance in actual seaways is subsequently made based on the acquired experimental data and the analytical predictions. Procedures for such an evaluation to identify the seakeeping quality of a given SWATH vessel, as well as the derivation of its primary and secondary design loads are fully described. The statistical approach is an important aspect which has been adopted throughout the evaluation.

A further stage of this study was chiefly concerned with the application of the dynamic load information in structural design of SWATH ships. Preliminary structural design is the first topic that has been dealt with. It is then followed by an observation of SWATH fatigue performance where a characteristic lifetime load distribution is the main element required in the analysis. To this extent, the study extensively demonstrates the implementation of theoretical and experimental data in practical design. Moreover, the study presented has served in bridging the gap between hydrodynamicists and structural engineers.

7.2. HYDRODYNAMIC PERFORMANCE

The nature of SWATH low motion characteristics was first advanced to give an insight in the need of pursuing research in this particular aspect. The underlying theoretical formulation of SWATH ship motions was presented. The limitation of two-dimensional strip theory led to the need to develop a more reliable three-dimensional analytical model. Descriptions of the motion programs evolved within the Department in recent years are given. The most recent motion program MARCHS by Chan (1990a) has been established based on the pulsating-translating source technique which has a capability to tackle forward speed and finite water depth effects more accurately.

Extensive experimental data on SWATH motions has been presented. The data was derived from the seakeeping tests of three SWATH models conducted at the Department's Hydrodynamics Laboratory. Some problems associated with the experimental arrangement, which in turn affect on the quality of the measured data, are indicated. Alternative arrangements, with the use of different measurement devices, to overcome such problems are described.

Efficiency in conducting seakeeping tests is of primary concern in both saving the tank time and experiment cost. Well planned model tests should be capable of simultaneously collecting the data for several types of measurements. These are now possible with the availability of more sophisticated data acquisition system using computers. Subsequently, test data analysis can be performed much more rapidly, and accurately, than reading from record papers as was done in the past.

Comparison of experimental data with theoretical predictions from MARCHS computer program was then performed. Test data measured at several important wave headings, which includes head, beam, bow quartering and following seas, has been collected. In general correlation between theoretical prediction and the measured data is excellent, hence validation to the newly developed analytical model is adequately achieved. The tool developed is reliable for a wider range of motion studies which need to be pursued in future.

A seakeeping performance analysis was made on three 2500-tonne SWATHs scaled up from the models. The results of motion predictions were integrated into a spectral analysis to assess the motion characteristics of the vessels operating in the North Atlantic. A seakeeping criteria was incorporated to weigh the operability rate of such vessels and rates between 82% and 89% are achievable by the present design. The rate of operability can be substantially improved when the SWATHs are fitted with stabilising fins. This particular aspect has been comprehensively investigated by Wu (1985).

Identification of SWATH motion characteristics necessary in the earlier design stage was discussed. Vertical modes of motion, namely, heave, roll and pitch, are the primary concern in achieving better seakeeping quality. Initial sizing and selection of underwater geometry have to be properly analysed. Basic parameters which govern motion performance of SWATH vessels should be determined so that low natural frequency of motions is obtained in order not to resonate with most sea waves.

SWATH resistance data derived from the simultaneous seakeeping test on a Fishing SWATH model have also been presented and compared with analytical predictions. An especially interesting observation is the finding of negative added resistance that arises when a certain frequency of wave is encountered. This confirms

the earlier observations made on the other models available at the Laboratory. However, further investigation is required, preferably from actual experience, before the issue can be considered to be conclusive.

7.3. PRIMARY DYNAMIC LOADS

The basic aspects of dynamic loads acting on SWATH structure have been thoroughly studied. A review is given of the efforts undertaken by a number of research institutions worldwide in the development of wave load peculiar to SWATH ships. In parallel theoretical backgrounds to this problems are briefly outlined. The enhancement to the motion program MARCHS to tackle the primary load on SWATHs is described.

A procedure for generating wave load data by a seakeeping experimental technique on SWATH models was fully described. Devices and instrumentation set up specifically were applied to measure structural responses. The most important element to achieve reliable experimental data stems from the accuracy and sensitivity of measuring devices which are used during the test.

The measured data from three SWATH models, comprising side force, vertical force and prying moment on the bridging structure of the models, are further compared with predictions from the analytical model. Very good correlation between the two is observed, hence, validation of the developed analytical model is attained. Further validation requires measured data of other load responses, namely, longitudinal shear, pitch torsional and yaw splitting moment. In addition, experimental data of load response for SWATH with increasing speeds should also be pursued.

Evaluation of design loads for SWATHs was conducted by applying the short- and long-term stochastic wave approaches. The former is primarily used in deriving the extreme loads as required in the ultimate strength design of SWATH structure. Adopting the long-term analysis, on the other hand, the designer are then able to generate information on the distribution of structural load over the lifetime of the vessel so designed. This type of load distribution which can represent the number of cyclic loads in specified ranges is then used in fatigue analysis and design of SWATH vessels. From the present analysis it was found that in terms of the number of cycles for fatigue damage, the lower amplitude wave loads contribute the largest portion. It is undisputable therefore that, as with monohull ships, the low magnitude wave loads govern fatigue life of SWATH structure, rather than the higher loads.

Although the main application of long-term analysis is to derive the lifetime cyclic load distribution it also of course gives directly the extreme lifetime load. By using

statistics of extreme values this can also be determined from the short-term distribution. Present evaluation shows that the two approaches were found to be in good agreement. For instance, the transverse moment with 99% confidence for SWATH-FV of 459 MNm was obtained from the long-term analysis compared to 470 MNm from the short term analysis. When only beam sea heading is considered in the long-term analysis then a value of 495 MNm is derived, which is some 4% larger than that predicted by the short-term analysis.

The design side loads for SWATH ships determined by the short- and long-term analysis was also compared with the values predicted by simple algorithms available in the open literature. The former generally overpredict the design load by as much as 50%, and sometimes even larger. These large values were derived by imposing a design significant wave height of 17 metres (corresponds to a sea state 9), which is cited by Lloyd (1989) as 'hypothetical' in its occurrence. A reasonable agreement is obtained, however, by restricting the evaluated SWATHs to operate in sea state 6.

7.4. SLAMMING INVESTIGATIONS

A review on the theoretical and experimental methods to predict slamming on marine vehicles has been reported in order to study this phenomenon on SWATH type ships. An analytical approach was then formulated which suggests the preference for time-domain simulation in view of its greater accuracy in slamming prediction. A detailed study of SWATH slamming by the seakeeping technique was also conducted.

A small SWATH model was used in the present study. SWATH slamming characteristics were investigated by measurement of relative motions and impact pressures. The measurement of impact pressure was first made by using pressure transducers located at discrete locations over the fore part of the wet deck. Further measurement was made by a load cell equipped panel attached on the wet deck. Slamming form factors were then extracted from the accumulated data. A large difference of form factor value was obtained from the point pressure and from panel pressure measurements, that is in the order of about 4 : 1. This is of course will vary with panel size, which should be chosen to represent plate panels.

Slamming characteristics were also evaluated for a hypothetical SWATH using the measured relative motion and slamming pressure data. SWATH operability related to slamming occurrence and weighted by certain criteria was identified by a probabilistic analysis. Using the form factors developed from the test, design slamming pressure of this particular SWATH was then derived. A design pressure value of some 1800 kPa was obtained, when the form factor from point pressure data is adopted,

compared to 518 kPa from the panel pressure measurement. The latter seems to be a reasonable value as compared to the design values derived using other simplified formulations. In addition, such a design value is within the range of 200 to 620 kPa as suggested by Sikora and Dinsenbacher (1988) for typical 2000 to 6000 tonne SWATHs.

Comparative evaluation was then performed on the existing design pressure data compiled so far. The trend in the increase of design slamming pressure with the increase in SWATH displacement is uncertain due to the substantial scatter of the data. Nevertheless, a regression analysis has been made and yields a simple pressure-displacement correlation pertinent to SWATHs. The expression developed is acceptable for first estimation of design pressure for SWATH ship displacements up to 6000 tonnes. A proper pressure correlation, however, should include the effect of ship speed because of the significance of this parameter. It is also preferable to incorporate characteristic wave height function in the expression of design slamming pressure of SWATH ships.

7.5. PRELIMINARY STRUCTURAL DESIGN

A preliminary SWATH structural design study has been presented by firstly indicating generic attributes of this type of vessel. Design procedures for such vessels should not differ from those traditionally practised for monohull ships. Some design criteria may also be adapted from monohull, but further evaluation is necessary. The difference in structural design approaches between the Royal Navy and the US Navy is highlighted. The former essentially adopts the ultimate limit state design (ULS) concept, which is based on the criteria of ultimate collapse a ship structure. The US Navy, on the other hand, regards yield stress of material as the governing criteria known as the working stress design (WSD).

A computer program was written to facilitate structural calculation which is iterative in nature. Some of the early findings have been presented. The primary comparison was to identify the differences between the shear lag stress magnification factor and effective width approaches on the resulting design values. A relatively large difference in structural weight (around 17%) is found from the two computations. Nevertheless, the effective width approach yields a better estimate of structural weight fraction when compared with other SWATH designs developed elsewhere. A value of 0.45 structural weight fraction is obtained in the present design on the SWATH-FV compared to a 0.42 for the SSV. Note that both vessels are 2500 tonnes in displacement. The corresponding value derived by the magnification factor approach is of the order 0.38.

A parametric study has been conducted in which the primary load is altered by ±30% from a given standard maximum value. In this way an average change of 12.5% in structural weight results. The discrepancy is quite large if compared with the observation by Aronne et al (1974). From their study it was found that altering the primary bending moment by ±50% only resulted in approximately 5% change of structural weight. This is obviously an area which needs to be pursued further. The parametric study follows with an investigation of the use of lightweight materials in SWATH construction. Aluminium-steel hybrid structure seems to be the best choice for the designer. By adopting such a combination some 37% weight saving is achievable, while the increase in structural cost is acceptable. An attempt to attain a respectable weight saving by changes in the primary configuration (maximum breadth or deck clearance) would not be beneficial. Additional transverse bulkheads would gain some weight reduction, in parallel with the improved shear lag characteristics.

7.6. FATIGUE PERFORMANCE

Analysis of fatigue behaviour of SWATH type vessels has been put forward. Design procedures, involving a full spectral analysis followed by the simplified approach, commonly practised by conventional ship and offshore structure designers are adopted. Case studies on two hypothetical SWATHs, size of approximately 2500-tonnes, operating in the North Atlantic region have been performed to illustrate these design procedures.

One of the interesting results drawn from the analysis is the importance of the Weibull shape parameters ξ pertinent to those SWATHs. Parameter values of 0.94 and 0.945 were derived for SWATH-FV and SWATH-3, respectively. These figures fall in the range of those normally applicable to monohull ships, i.e. between 0.7 and 1.3; although Munse et al (1983) suggest that lifetime stress distributions for most monohulls of this size (2500 tonnes) are typically represented by the parameter values in the order of 1.0 to 1.3. Further, Clarke (1991) indicates an exponential cyclic load distribution, in which $\xi = 1.0$, has been widely practised in the Royal Navy warship designs.

The allowable stress range as one of the most important measures in fatigue design has been evaluated. Extreme stress ranges of approximately 290 N/mm^2 and 250 N/mm^2 have been deterministically derived for a 20-year and 30-year lifetime, respectively. The latter was compared with the design stress for the T-AGOS, in which a design stress range of some 190 N/mm^2 is adopted for 30 years operation. The difference of the two values is evidently quite large, hence necessitating design check by way of the probabilistic approach to be performed.

Two different reliability methods have been implemented for the analysis. The first method is a general advanced first order second moment (AFOSM) code which was developed in the Department by Pu (1992), and the second is fatigue reliability format by Wirsching (1984). The results from both analysis correlate fairly well for most stress ranges that have been investigated. These results suggest that a design extreme stress range value of some 200 N/mm^2, which is close to that adopted for T-AGOS, should be acceptable and would give an adequate fatigue safety for SWATH-FV for a 30-year operation provided a thorough inspection can be performed at 10-year intervals.

The corresponding safety index after 10 years operation for the above stress range is approximately 2.0. From initial rule of thumb a safety index of 2.0 to 3.0 is acceptable for fatigue initiation failure. This is based on the recognition that crack initiation on a structural member would not constitute a catastrophic failure of SWATH structure. A later calculation based on fatigue crack propagation was performed which shows that a much larger cyclic number (in the order of 2.25 times that for crack initiation) is required to cause a through the thickness cracking. This finding supports the safety index adopted.

7.7. FUTURE WORK

More experimental investigations on SWATH motions and dynamic loads with increasing forward speed remains necessary. Collaboration is preferred with other research institutions where facilities to perform forward speed seakeeping tests in oblique waves are available. Yaw splitting and pitch torsional moments load data in oblique waves are further information that need to be accumulated. Construction of new SWATH models with elliptical section and contoured hull configuration seems to be necessary to enhance the experimental data base on both hydrodynamic and structural responses. All these experimental data are required to further validate the developed analytical model MARCHS.

The existing sophisticated motion and wave load prediction program MARCHS, supported with present experimental data, has undoubtedly broadened the opportunity to explore hydrodynamic design optimisation. Parametric studies of SWATH hydrodynamic performance can now be initiated. The seakeeping index method which has emerged in recent years might be adopted in such an exploration study.

The results of the present study will be useful in the development of a further study on SWATH ship slamming. Areas which need to be pursued in future are first of all, the development of a mathematical model for SWATH slamming assessment,

preferably a time-domain simulation. Secondly, the development of structural design procedure for SWATH deck bottom scantlings based on slamming impact. The accumulation of slamming data from model tests remains necessary to validate any analytical predictions that may be available in the future.

Full fatigue analysis on SWATH is not yet possible because of the limited information which is currently available. Explicit fatigue characterisation of SWATH structure should be developed in the near future. Suitable finite element programs are now available in the Department, and some experience has already been gained. SWATH structural stresses under various loadings have been evaluated and, in due course, these will provide accurate information required in fatigue design. Further fatigue S-N data pertinent to the critical members of SWATH structure, e.g. haunch-deck and strut-haunch details, should be explored. To a certain extent structural tests may be necessary for such a study. Moreover, future research on SWATH fatigue performance should also include fracture mechanics for crack propagation analysis and for maintenance strategy. Reliability aspects are to be fully incorporated in future developments.

7.8. CLOSURE

The study presented in this thesis constitutes the first stage in the development of the Integrated SWATH Structural Design Study programmed in the NA&OE Department. The programme is aimed at the development of rationally-based structural design method for SWATH type vessels. It is hoped that the work presented within this thesis will be useful, at least to the SWATH Research Group in the Department, in pursuing further research and in the development of SWATH technology.

REFERENCES

REFERENCES

Aertssen, G. (1968), "Laboring of Ships in Rough Seas with Special Emphasis on the Fast Ship", *Proc. Diamond Jubilee Int. Meeting*, SNAME, Paper No. 10, New York, USA, June

Aertssen, G. (1969), "Service Performance and Trials at Sea", *Proc. 12th Int. Towing Tank Conf.*, ITTC

Aertssen, G. (1972), "Service Performance and Seakeeping Trials on a Large Container Ship", *Trans. RINA*, Vol. 114, pp. 429-447

Aertssen, G. (1975), "The Effect of Weather on Two Classes of Container Ships in the North Atlantic", *Journal of the Royal Institution of Naval Architects*

Allan, R.C., Bird, J. and Clarke, J.D. (1986), "The Use of Adhesives in the Repair of Cracks in Ships", *Proc. Structural Adhesives in Engineering*, IMechE, Bristol

Allen, R.G. and Holcomb, R.S. (1982), "The Application of Small SWATH Ship to Coastal and Offshore Patrol Missions", *Proc. Symp. on Small Fast Warships and Security Vessels*, RINA, London

Allen, R.G. and Jones, R.R. (1978), "A Simplified Method for Determining Structural Design-Limit Pressure on High-Performance Marine Vehicles", *Proc. AIAA/SNAME Advanced Marine Vehicles Conf.*, Paper No. 78-754, San Diego, USA, April

Almar-Næss, A. (1985), "Fatigue Handbook : Offshore Steel Structures", *Tapir Publishers*, Trondheim, Norway

American Bureau of Shipping (1990), "Preliminary Guide for Building and Classing Small Waterplane Area Twin Hull (SWATH) Vessels", USA, Sep.

Ando, S. (1989), "Cushioning of Slamming Impact by Elastomeric Layers", *Journal of Ship Research*, SNAME, Vol. 33, No. 3, pp. 276-283, Sept.

Aronne, E.L., Lev, F.M. and Nappi, N.S. (1974), "Structural Weight Determination for SWATH Ships", *Proc. AIAA/SNAME Advanced Marine Vehicles Conf.*, Paper No. AIAA 74-326, San Diego, Ca, USA, Feb.

Arthur, E.K. (1988), "Time Domain Simulation of SWATH Ship Motions", *MSc Thesis*, Dept. of NA&OE, University of Glasgow, UK, May

Atlar, M. (1986a), "Method of Solution for 5 Degrees of Freedom Coupled Equations of Motions of a SWATH Ship", *Department Report*, No. NAOE-86-36, Dept. of NA&OE, University of Glasgow, Nov.

Atlar, M. (1986b), "The SWATH Wave Load Program - Some Aspects of Computer Program SWATHL", *Department Report*, No. NAOE-86-55, Dept. of NA&OE, University of Glasgow, Dec.

Atlar, M., Lai, P.S.K. and McGregor, R.C. (1987) "On Hydrodynamic Aspects of a Two-Dimensional Prediction of Loads and Motions of a Twin-Hull Semi Submersible", *IMAEM 4th Int. Congress*, Paper No. 25, Varna-Bulgaria, May

Atlar, M., Seren, D.B. and Validakis, J. (1985), "The Effect of Tilt and Interference on the Hydrodynamic Coefficients of SWATH-Type Sections", *Proc. Int. Conf. on SWATH Ships and Advanced Multi-Hulled Vessels*, RINA, London, April

Beghin, D., Huther, M. and Parmentier, G. (1992), "The probabilistic Approach : A Tool for Ship Rules Improvement" *Proc. Int. Conf. on Practical Design of Ships and Mobile Units*, PRADS 92, Vol. 2, pp. 2.847-2.859, Univ. of Newcastle upon Tyne, May

Berge, S. (1984), "Effect of Plate Thickness in Fatigue Design of Welded Structures", *Proc. Offshore Technology Conf.*, OTC-4829, Houston, TX, USA

Betts, C.V. (1988a), "Some UK Developments in SWATH Design Research", *Proc. Int. High-Performance Vehicle Conf.*, CSNAME, Paper VI-1, Shanghai, China, Nov.

Betts, C.V. (1988b), "A Review of Developments in SWATH Technology", *Proc. Int. Conf. on SWATH Ships and Advanced Multi-Hulled Vessels II*, RINA, Paper No. 1, London, Nov.

Bhattacharyya, R. (1980), "Dynamics of Marine Vehicles", John Wiley & Sons Inc., New York

Bishop, R.E.D., Price, W.G. and Temarel, P. (1986), "On the Hydroelastic Response of a SWATH to Regular Oblique Waves", *Proc. Advances in Marine Structures*, ARE, Paper No. 5, Dunfermline, Scotland, May

Boericke, H. Jr. (1959), "Unusual Displacement Hull Forms for Higher Speeds", *Int. Shipbuilding Progress*, Vol. 6, No. 58, pp 249-264, June

Bose, N. (1980), "A Computer Program to Obtain Preliminary Structural Scantlings and Steel Weights for Circular Hulled Semi-Submersibles with Bracing", *Department Report*, No. NAOE-HL-80-22, Dept. of NA&OE, University of Glasgow

Bretschneider, C.L. (1959), "Wave Variability and Wave Spectra for Wind-Generated Gravity Waves", Beach Erosion Board, US Army Corps of Engineers, Technical Memo No. 118, USA

Burke, R.J. (1982), "The Consequences of Extreme Loadings on Ship Structures", *Proc. Extreme Loads Response Symp.*, SSC/SNAME, pp. 5-14, Arlington, VA, USA, Oct.

Buxton, I.L. (1987), "Engineering Economics and Ship Design", *British Maritime Technology Ltd.*, UK

Caldwell, J.B. (1965), "Ultimate Longitudinal Strength", *Trans. RINA*, Vol. 107, pp. 411-430

Carreyette, J. (1977), "Preliminary Ship Cost Estimation", *Trans. RINA*, Vol. 119, pp. 235-258

Chalmers, D.W. (1989), "Structural Design Aspects of SWATH Ships", *10th WEGEMT on High-Speed and Pleasure Craft*, University of Genoa, Italy, Oct.

Chalmers, D., et al (1988), "Composite Structures", *Proc. 10th Int. Ship & Offshore Structures Congress*, ISSC, Report of Committee V.8, Vol. 2, pp. 291-327, Lyngby, Denmark, Aug.

Chalmers, D.W. and Smith, C.S. (1977), "The Ultimate Longitudinal Strength of a Ship's Hull", *Proc. Int. Conf. on Practical Design of Ships and Mobile Units*, PRADS 92, Vol. 2, pp. 2.745-2.763, Univ. of Newcastle upon Tyne, May

Chan, H.S. (1989), "Green Function in the Theory of Unsteady Forward Motion", *Department Report*, No. NAOE-89-22, Dept. of NA&OE University of Glasgow

Chan, H.S. (1990a), "A Three-Dimensional Technique for Predicting First- and Second-Order Hydrodynamic Forces on a Marine Vehicles Advancing in Waves", *PhD Thesis*, Dept. of NA&OE, University of Glasgow, Aug.

Chan, H.S. (1990b), "User Manual for MARCHS", *Department Report*, No. NAOE 90-28, Dept. of NA&OE, University of Glasgow, Oct.

Chan, H.S. (1991), "Prediction of Motion and Structural Responses of Mono- and Twin-Hull Ships Advancing in Waves", *Department Report*, No. NAOE-91-16, Dept. of NA&OE, University of Glasgow, July

Chan, H.S., Djatmiko, E.B., Miller, A.F. and Caldwell, L.B. (1992), "Structural Loading Aspects in the Design of SWATH Ships", *Proc. 5th Int. Symp. on the Practical Design of Ships and Mobile Units*, PRADS'92, Vol. 1, pp. 1.346 1.359, Newcastle on Tyne, UK, May

Chapman, R.B. (1972), "Spray Drag of Surface Piercing Struts", *Proc. AIAA/SNAME Advanced Marine Vehicles Meeting*, AIAA Paper No. 72-605, Annapolis, Maryland, USA, July

Chapman, R.B. (1977), "Wave Resistance and Kelvin Wake of Generalised Semi Submersible", SAI, Report No. 77-980-LJ, Lajolla, USA.

Chen, Y.N. (1989), "Fatigue Analysis and Assessment of Ship Structures", *TAPS Meeting*, ABS, May

Chen, Y.N. and Mavrakis, S.A. (1988), "Closed-Form Spectral Fatigue Analysis for Compliant Offshore Structures", *Journal of Ship Research*, SNAME, Vol. 32, No. 4, pp. 297-304, Dec.

Chilò, B. and Santos, R.T.C. (1983), "Seakeeping Assessment and Criteria of Naval Combatant SWATH Vehicles", *Proc. Int. Conf. on High Speed Surface Craft*, London, May

Chilò, B. and Sartori, G. (1979), "Seakeeping Merit Rating Criteria Applied to Ship Design", *Int. Shipbuilding Progress*, Vol. 26, No. 304, pp. 299-313, Dec.

Chuang, S-L. (1966), "Experiments on Flat-Bottom Slamming", *Journal of Ship Research*, SNAME, Vol. 10, No. 1, pp. 10-17, March

Chuang, S-L. (1969), "Theoretical Investigations on Slamming of Cone-Shaped Bodies", *Journal of Ship Research*, SNAME, Vol. 13, No. 4, pp. 276-283, Dec.

Chuang, S-L (1974), discussion of Hadler, J.B. et al, "Ocean Catamaran Seakeeping Design, Based on the Experience of USNS *Hayes*", *Trans. SNAME*, Vol. 82, pp. 151-152

Chun, H.H. (1988), "Theoretical and Experimental Studies on the Resistance of SWATH Ships", *PhD Thesis*, Dept. of NA&OE, University of Glasgow

Chun, H.H., Djatmiko, E.B., McGregor, R.C. and Ferguson, A.M. (1989), "SWATH Resistance in Waves with Associated Steady and Dynamic Responses", *Proc. 22nd American Towing Tank Conf.*, ATTC, St-John's, Newfoundland, Canada, Aug.

Chun, H.H., Djatmiko, E.B.and McGregor, R.C. (1990), "A Wide Ranging Study on the Motions of SWATH Ships with and without Forward Speeds", *Proc. 9th Int. Conf. on OMAE*, ASME, Houston, Texas, USA, Feb.

Chun, H.H., Grygorowicz, M. and Kobylinski, L. (1988), "Small Model Experiments of SWATH Concept", *Proc. of Int. Conf. on SWATH Ships and Advanced Multi-Hulled Vessels II*, RINA, Paper No. 8, London, Nov.

Chun, H.H. and McGregor, R.C. (1989), "Added Resistance of SWATH Models in Uniform Waves", *Proc. Intersociety Advanced Marine Vehicles Conf.*, Paper No. 89-1474-CP, Arlington, VA, USA, June

Clarke, J.D. (1991), "Fatigue Crack Initiation and Propagation in Warship Hulls", *Proc. of the Int. Conf. on Advances in Marine Structures-2*, ARE, Dunfermline, Scotland, May

Clayton, B.R. and Bishop, R.E.D. (1982), "Mechanics of Marine Vehicles", E.&F.N. Spon Ltd., London

Combat Craft (1985a)"RMI's Prototype SWATH on Sea Trials at San Diego", May/June

Combat Craft (1985b)"The Viability of Naval SWATH Ships", Sep./Oct.

Comstock, J.P. (1977), "Principles of Naval Architecture", *SNAME*, New York, USA

Conolly, J.E. (1974), "Standards of Good Seakeeping for Destroyers and Frigates in Head Seas", *Proc. Int. Symp. on the Dynamics of Marine Vehicles and Structures in Waves*, Office of Naval Research/RINA/IMechE, London, April

Covich, P.M. (1986), "SWATH T-AGOS : A Producible Design", *Proc. AIAA 8th Advanced Marine Systems Conf.*, Paper No. AIAA 86-2384, San Diego, USA, Sept.

Covich, P.M. (1987), "T-AGOS 19 : An Innovative Program for an Innovative Design", *Naval Engineers Journal*, ASNE, Vol. 99, No. 3, pp. 99-106, May

Creed, F.G. (1946), "Floating Structure", *U.S. Patent*, No. 2,405,115

Curphey, R.M. and Lee, C.M. (1974), "Analytical Determination of Structural Loading on ASR Catamaran in Beam Waves", *DTNSRDC*, Ship Performance Dept. R&D, Report No. 4267, Bethesda, Maryland, USA, April

Curphey, R.M. and Lee, C.M. (1977), "Theoretical Prediction of Dynamic Wave Loads on Small Waterplane Area, Twin Hull Ships", DTNSRDC, Report No. 77-0027, Bethesda, Maryland, USA

Dallinga, R.P. (1981), "Seakeeping Tests for a Small Waterplane Area Twinhull Ship", *NSMB*, Report No. 43755-2-2T, The Netherlands, Nov.

Dallinga, R.P. (1992), "Operability Characteristics of Monohulls and SWATH Vessels", *Proc. of MARIN Jubilee Meeting*, Workshop A - Advanced Vessels, MARIN, Wageningen, the Netherlands, May

Dally, J.M. and Riley, W.F. (1978), "Experimental Stress Analysis", McGraw Hill Book Co., New York

Det norske Veritas (1991), "Rules for Classification of High Speed and Light Craft", Høvik, Norway, Jan.

DeVries, R.L. (1991), "Producibility Benefits of the SWATH Configuration", *Marine Technology*, SNAME, Vol. 28, No. 1, pp. 23-29, Jan.

Djatmiko, E.B. (1987), "Experimental Investigations into SWATH Ship Motions and Loadings", *MSc thesis*, Dept. of NA&OE, University of Glasgow, Nov.

Djatmiko, E.B., Chun, H.H., McGregor, R.C. and MacGregor, J.R. (1990), "Hydrodynamic Behaviour of a SWATH Fishing Vessel", *Proc. CSME Mechanical Engineering Forum*, Paper No. SOD-1, University of Toronto Campus, Canada, June

Dow, R.S., Hugill, R.C., Clark, J.D. and Smith, C.S. (1981), "Evaluation of Ultimate Ship Hull Strength", *Proc. Extreme Loads Response Symp.*, SSC/SNAME, pp. 133-148, Arlington, VA, USA, Oct.

Drummond, T.G., Mackay, M. and Schmitke, R.T. (1976), "Wave Impacts on Hydrofoil Ships and Structural Implications", *Proc. 11th Symp. on Naval Hydrodynamics*, University College London, UK, April

Drysdale, L.H. (1986a), "Solution of Linear Motion Equation for Coupled Heave and Pitch for a SWATH Ship (including programming manual)", *Department Report*, No. NAOE-86-53, Dept of NA&OE, University of Glasgow

Drysdale, L.H. (1986b), "Effect of Active Control Fins on the Vertical Plane Response of SWATH Ships", *Department Report*, No. NAOE-86-61, Dept. of NA&OE University of Glasgow, Dec.

Drysdale, L.H. (1987), "Structural Loads Acting on a SWATH Ship", *Department Report*, No. NAOE-HL-87-45, Dept. of NA&OE, University of Glasgow, Dec.

Eames, M.C.and Drummond, T.G. (1977), "Concept Exploration - an Approach to Small Warships Design", *Trans. RINA*, Vol. 119, pp. 29-54

Evans, J.H. (1982), "Preliminary Design Estimation of Hull Girder Response to Slamming", *Trans. SNAME*, Vol. 90, pp. 55-83

Faltinsen, O., Hoff, J.R., Kvålsvold, J. and Zhao, R. (1992), "Global Loads on High-Speed Catamarans", *Proc. 5th Int. Symp. on the Practical Design of Ships and Mobile Units*, PRADS'92, Vol. 1, pp. 1.360-1.373, Newcastle on Tyne, UK, May

Faltinsen, O. and Svensen, T. (1992), "Behaviour of Catamarans, Foilcatamarans and SES in Waves", *Proc. MARIN Jubilee Meeting*, Workshop A : Advanced Vessels, Wageningen, The Netherlands, May

Fang, M-C (1988), "The Motions of SWATH Ships in Waves", *Journal of Ship Research*, SNAME, Vol. 32, No. 4, pp. 238-245, Dec.

Faulkner, D. (1965) discussion to Caldwell, J.B. (1965), ""Ultimate Longitudinal Strength", *Trans. RINA*, Vol. 107, pp. 411-430

Faulkner, D. (1975a), "Compression Strength of Welded Grillages" in Ship Structural Design Concepts, Evans, J.H. (ed), Cornell Maritime Press

Faulkner, D. (1975b), "A Review of Effective Plating for Use in the Analysis of Stiffened plating in Bending and Compression", *Journal of Ship Research*, SNAME, Vol. 19, No. 1, pp. 1-17, March

Faulkner, D (1981), "Semi-Probabilistic Approach to the Design of Marine Structures", *Proc. Extreme Loads Response Symp.*, SSC/SNAME, pp. 213-230, Arlington, VA, USA, Oct.

Faulkner, D. (1983), "On Selecting a Target Reliability for Deep Water Tension Leg Platforms", *Proc. 11th IFIP Conf. on System Modelling and Optimization*, pp. 490-513, Copenhagen, Denmark, July

Faulkner, D. (1987), "A Brief Introduction to Structural Reliability", *Proc. Seminar on Reliability Methods in Fatigue, Fracture and NDT*, the Welding Institute, Opening Lecture, Newcastle, UK, May

Faulkner, D. (1991a) discussion to Djatmiko, E.B., "Estimation of Long-Term Dynamic Load Characteristics of SWATH Ships", *Research Student Colloquium*, Dept. of NA&OE, Univ. of Glasgow, Jan.

Faulkner, D. (1991b), "What is Wrong with Offshore Design Codes ?", *Extraordinary Meeting*, IESIS, Paper No. 1512, Glasgow, Feb.

Faulkner, D. (1991c), "New Technologies for Ship and Offshore Structural Analysis and Design", *Proc. Int. Symp. on Marine Structures*, ISMS'91, Shanghai, China, Sep.

Faulkner, D. (1992), "Structural Design Philosophy for Small and Large High Speed Multi-Hull Ferries", *Proc. Int. Conf. on Safety for High-Speed Craft - The Way Ahead*, RINA, London, May

Faulkner, D. and Sadden, J.A. (1979), "Toward Unified Approach to Ship Safety", *Trans. RINA*, Vol. 121

Faulkner, D., Incecik, A. and Prince-Wright, R. (1989), "Toward Improved Loading Model for Design of Offshore Platforms", *Proc. ICOSSAR'89*, San Fransisco, USA, Aug.

Faulkner, D., Warwick, D.M. and Incecik, A. (1986), "Integrated Structural Design of SWATH Ships", *SERC Proposal*, Dept. of NA&OE, University of Glasgow

Faust, J.G. (1932), "Marine Vessel", *U.S. Patent*, No. 1,861,338

Frank, W. (1976), "On the Oscillations of Cylinders In or Below the Free Surface of Deep Fluids", *DTNSRDC*, Report No. 2375, Bethesda, Maryland, USA, Oct.

Gallagher, P. (1985), "Slam Simulations : An Application of Computational Fluid Dynamics", *PhD Thesis*, Dept. of NA&OE, University of Glasgow, May

Geers, T.L. (1982), "A Boundary-Element Method for Slamming Analysis", *Journal of Ship Research*, SNAME, Vol. 26, No. 2, pp. 117-124, June

Geritsma, J. and Beukelman, W. (1972), "Analysis of the Resistance Increase in Waves of a Fast Cargo Ship", *Int. Shipbuilding Progress*, Vol. 19, No. 217

Giannotti, J.G. (1975), "Prediction of Slamming Loads for Catamarans", *Proc. 7th Offshore Technology Conf.*, Paper No. OTC 2281, Houston, Texas, USA, May

Gore, J.L. (1985), "SWATH Ships", *Naval Engineers Journal*, ASNE, Special Edition, Vol. 97, No. 2, pp. 83-112, Feb.

Graham, R. (1988), "Slamming Experiments with a Radio-Controlled SWATH Model", *Proc. Int. Conf. on SWATH Ships and Advanced Multi-Hulled Vessels II*, RINA, Paper No. 9, London, UK, Nov.

Graham, R. (1990), "Motion-Induced Interruptions as Operability Criteria", *Naval Engineers Journal*, ASNE, Vol. 102, No. 2, pp. 65-71, March

Guedes Soares, C. (1991), "Model Uncertainty in the Long-term Distribution of Wave-Induced Bending Moments for Fatigue Design of Ship Structures", *Marine Structures*, Vol. 4, pp. 295-315

Gullberg, O., et al (1991), "Composite Structures", *Proc. 11th Int. Ship & Offshore Structures Congress*, ISSC, Report of Committee V.8, Vol. 2, pp. 317-360, Wuxi, China, Sept.

Gupta, S.K. and Schmidt, T.W. (1986), "Developments in SWATH Technology", *Naval Engineers Journal*, ASNE, Vol. 98, No.3, pp. 171-188, May

Gurney, T.R. (1976), "Fatigue Design Rules for Welded Steel Joints", *The Welding Institute Research Bulletin*, Vol. 17, No. 5, May

Hadler, J.B., Lee, C.M., Birmingham, J.T. and Jones, H.D. (1974), "Ocean Catamaran Seakeeping Design, Based on the Experience of USNS *Hayes*", *Trans. SNAME*, Vol. 82, pp. 151-152

Hadler, J.B., Hubble, E.N., Allen, R.G.and Blount, D.L. (1978), "Planing Hull Feasibility Model - Its Role in Improving patrol Craft Design", *Proc. of Symp. on Small Fast Warships and Security Vessels*, RINA, London, March

Hasselman, K., et al (1973), "Measurement of Wind-Wave Growth and Swell Decay During the Joint North Sea Wave Project (JONSWAP)", *Deutschen Hydrographischen Zeitschrift*, Vol. 13, No. A

Heller, S.R. and Jasper, N.H. (1961), "On the Structural Design of Planing Craft", *Trans. RINA*, Vol. 103, pp. 49-65

Henrickson, W.A. and Spencer, J.S. (1982), "A Synthesis of Aluminium Crewboat Design", *Marine Technology*, SNAME, Vol. 19, No. 1, pp. 52-72, Jan.

Hightower, J.D. and Seiple, R.L. (1978), "Operational Experiences with the SWATH Ship SSP *Kaimalino*", *Proc. AIAA/SNAME Advanced Marine Vehicles Conf.*, Paper 78-741, San Diego, USA, April

Hightower, J.D., Parnell, L.A., Strickland, A.T. and Warnshuis, P.L. (1985), "SWATH Technology Development at the Naval Ocean System Center", *Proc. Int. Conf. on SWATH Ships and Advanced Multi-Hulled Vessels*, RINA, Paper No.14, London, April

Hoffman, D. (1976), "The Impact of Seakeeping on Ship Operations", *Marine Technology*, SNAME, Vol. 13, No. 2, pp. 241-262, July

Holcomb, R.S. and Allen, R.G. (1983), "Investigation of the Characteristics of Small SWATH Ship Configured for United States Coast Guard Missions", *DTNSRDC*, Report No. DTNSRDC/SSD-83-3, USA, June

Hong, Y.S. (1986), "Heave and Pitch Motions of SWATH Ships", *Journal of Ship Research*, SNAME, Vol. 30, No. 1, pp. 12-25, March

Hosada, R., Kunitake, Y, Koyama, H. and Nakamura, H. (1983), "A Method for Evaluation of Seakeeping Performance in Ship Design Based on Mission Effectiveness Concept", *Proc. 2nd Int. Symp. on Practical Design of Ships and Mobile Units*, PRADS'83, Tokyo & Seoul, Oct.

Howe, R.J. and Owen, M.J. (1972), "Cumulative Damage in Chopped Strand Mat/Polyester Resin Laminates", *Proc. 8th Int. Reinforced Plastics Congress*, British Plastics Federation, London

Hugill, P.N. and Sumpter, J.D.G. (1990), "Fatigue Crack Prediction at a Ship Deck/Superstructure Intersection", *The BSSM Journal 'Strain'*, Vol. 26, No.3, Aug

Hutchison, B.L. (1990), "Seakeeping Studies : A Status Report", *Trans. SNAME*, Vol. 98, pp. 263-317

Incecik, A. (1982), "Design Aspects of the Hydrodynamic and Structural Loading on Floating Offshore Platforms Under Wave Excitation", *PhD Thesis*, Dept. of NA&OE, University of Glasgow

ISSC Committee II.3 (1979), "Impact on Novel-Type Vessels", *Proc. 7th Int. Ship Structures Congress*, ISSC, Vol. 2, Paris, France, Aug.

Jones, A.H., Chun, H.H. and McGregor, R.C. (1990), "SWATH Ship Motion Simulation in the Time Domain", *Proc. CSME Mechanical Engineering Forum 1990*, Paper No. SOD-2, University of Toronto Campus, Toronto, Canada, June

Joosen, W.P.A. (1966), "Added Resistance of Ships in Waves", *Proc. 6th Symp. on Naval Hydrodynamics*, ACR 136, Office of Naval Research, Washington, D.C., USA

Jordan, C.R. and Cochran, C.S. (1978), "In-Service Performance of Structural Detail", *Ship Structure Committee*, Report No. SSC-272, Washington D.C., USA

Kallio, J.A. and Ricci, J.J. (1976), "Seaworthiness Characteristics of a Small Waterplane Area Twin Hull (SWATH IV) Part II", *DTNSRDC*, Ship Performance Department, Report No. SPD 620-02, Bethesda, Maryland, USA, May

Kaplan, P. (1987), "Analysis Prediction of Flat Bottom Slamming Impact of Advanced Marine Vehicles in Waves", *International Shipbuilding Progress*, Vol. 34, No. 391, pp. 44-53, March

Keane, A.J., Price, W.G., Temarel, P., Wu, X-J and Wu, Y. (1988), "Seakeeping and Structural Responses of SWATH Ships in Waves", *Proc. Int. Conf. on SWATH Ships and Advanced Multi-Hulled Vessels II*, RINA, Paper No. 13, London, Nov. 1988

Kennell, C. (1985), "SWATH Ship Design Trends", *Proc. Int. Conf. on SWATH Ships and Advanced Multi-Hulled Vessels*, London, April

Kerr, G.D., Anderson, T.A. and Kennell, C.G. (1978), "SWATH Ship Design State of the Art", *Proc. AIAA/SNAME Advanced Marine Vehicles Conf.*, Paper AIAA 78-737, San Diego, Ca, USA, April

Kim, C.H. and Chou, F. (1973), "Motions of a Semi-Submersible Drilling Platform in Head Seas", *Marine Technology*, SNAME, pp 112-123, April

Kobayashi, M. and Shimada, K. (1990), "Wave Loads on Small-Waterplane-Area Twin-Hull (SWATH) Ship with Forward Speed", *Proc. 19th Int. Towing Tank Conf.*, ITTC, Vol. 2, pp. 330-334, Madrid, Spain, Sep.

Kobayashi, M., Shimada, K., and Nishimura, K. (1990), "Wave Loads on a Semi Submerged Catamaran (SSC) with Forward Speed", *Journal of the Soc. of Naval Architect Japan*, SNAJ, Vol. 168, pp. 159-170

Koehler, B.R. and Kettleborough,C.F. (1977), "Hydrodynamic Impact of a Falling Body upon a Viscous Incompressible Fluid", *Journal of Ship Research*, SNAME, Vol. 21, No. 3, pp. 165-181, Sept.

Koops, A. and Nethercote, W.C.E. (1988), "An Extended SWATH Concept Exploration Model", *Proc. Int. Conf. on SWATH Ships and Advanced Multi Hulled Vessels II*, RINA, Paper No. 4, London, Nov.

Lamb, G.R. (1988), "Some Guidance for Hull Form Selection for SWATH Ships", *Marine Technology*, SNAME, Vol. 25, No. 4, pp. 239-252, Oct.

Lang, T.G. (1971), "High-Speed Ship with Submerged Hulls", *U.S. Patent*, No.3,623,444, Nov.

Lang, T.G. (1989), "SWATH Evolution : From Ideas to Ships", *Proc. Intersociety Advanced Marine Vehicles Conf.*, Paper No. 89-1520-CP, Arlington, VA, USA, June

Lang, T.G. et al (1971), "Naval Feasibility of the NUC Semi-Submerged Ship Concept", Naval Under Sea Research and Development Center, TP 235

Lang, T.G. et al (1973), "Design and Development of the 190-ton Stable Semisubmersible Platform (SSP)", ASME, Winter Annual Meeting, Paper No. 73-WA/Oct.-2, Nov.

Lang, T.G. and Higdon, D.T. (1974), "Hydrodynamics of the 190-ton Stable Semisubmerged Platform (SSP)", *Proc. AIAA/SNAME Advanced Marine Vehicles Conf.*, Paper No. AIAA 74-328, San Diego, CA, USA, Feb.

Lee, C.M. (1976)"Theoretical Predictions of Motion of Small-Waterplane Area, Twin Hull (SWATH) Ships in Waves", *DTNSRDC*, Report No. 76-0046, Dec.

Lee, C.M. and Curphey, R.M. (1977), "Prediction of Motion, Stability, and Wave Load of Small-Waterplane-Area, Twin-Hull Ships", *Trans. SNAME*, Vol. 85, pp. 94-130

Lee, C.M., Jones, H.D. and Curphey, R.M. (1973), "Prediction of Motion and Hydrodynamic Loads of Catamarans", *Marine Technology*, SNAME, Vol. 10, No. 4, Oct.

Lee, K.Y. et al (1988), "On the Design Technology of SWATH High Speed Passenger Ship", *Proc. Int. Conf. on SWATH Ships and Advanced Multi-Hulled Vessels II*, RINA, Paper No. 17, London, Nov.

Lee, J-S (1992), "Reliability Based Limit State Design Format of Ship Structures", *Proc. Int. Conf. on Practical Design of Ships and Mobile Units*, PRADS 92, Vol. 2, pp. 2.820-2.833, Univ. of Newcastle upon Tyne, May

Lee, J.S. and Faulkner, D. (1989), "Reliability Analysis of TLP Structural Systems", *Proc. 8th OMAE Conf.*, The Hague, March

Lee, J-S and Faulkner, D. (1989), "System Design of Floating Offshore Structures", Paper No. 8, RINA Spring Meeting, London, April

Leopold, R. (1969a), "Marine Vessel", *U.S. Patent*, No. 3,447,502

Leopold, R. (1969b), "A New Hull Form for High Speed Volume Limited Displacement Type Ships", *Spring Meeting*, SNAME, Paper No. 8, Beverly Hills, May

Lewis, E.V. and Zubaly, R.B. (1981), "Predicting Hull Bending Moments for Design", *Proc. Extreme Loads Response Symp.*, SSC/SNAME, pp. 31-62, Arlington, VA, USA, Oct.

Lewison, G. and Maclean, W.M. (1968), "On the Cushioning of Water Impact by Entrapped Air", *Journal of Ship Research*, SNAME, Vol. 12, No. 2, pp. 116 130, June

Liu, D. (1989), "Development and Analysis of SWATH Ships", A Paper presented at the Hellenic Institute of Marine Technology, Pireaus, Greece, Oct.

Lloyd, A.R.J.M. (1989), "Seakeeping : Ship Behaviour in Rough Weather", Ellis Horwood Ltd., Chichester, West Sussex, UK

Lloyd, A.R.J.M. (1991), "The Seakeeping Design Package (SDP) - a Technique for Designing Hull Forms for a Specific Seakeeping Performance", *RINA Spring Meetings*, London, April

Lloyd's Register of Shipping (1990), "Provisional Rules for the Classification of High Speed Catamarans", London, Aug.

Lloyd's Ship Manager (1992), "*Radisson Diamond* - A Revolutionary Cruiser Development", Vol. 13, No. 2, Supplement, pp. S5-S7, May

Loscombe, R. (1987), "An Exploratory Study of Alternative Structural Materials for Small SWATH Craft", *Ship Science Report*, No. 34, Dept. of Ship Science, University of Southampton, May

Loscombe, R. (1988), "An Exploratory Study of Alternative Structural Materials for Small SWATH Ships", *Int. Shipbuilding Progress*, Vol. 35, No. 404, pp. 331-347, Dec.

Loscombe, R. (1989), "Key Aspects of the Structural Design of Small SWATH Ships", *PhD Thesis*, Dept. of Ship Science, University of Southampton, Dec.

Loscombe, R. (1990), "Initial Design Stage Slam Pressure Prediction for Small SWATH Ships", *Ship & Boat International*, RINA, Issue 10/08, Oct.

Luedeke, G. Jr. and Montague, J. (1984), "RMI's Small Waterplane-Area-Twin-Hull (SWATH) Boat Project", *Branch Meeting*, SNAME, San Diego Section, USA, Nov.

Luedeke, G.Jr., Montague, J., Posnansky, H. and Lewis, Q. (1985), "The RMI SD 60 SWATH Demonstration Project", *Proc. Int. Conf. on SWATH Ships and Advanced Multi Hulled Vessels*, RINA, Paper No. 10, London, April

Lundborg, C.G. (1880), "Construction of Ships", *U.S. Patent*, No. 234,794

Mabuchi, T., Kunitake, Y. and Nakamura, H. (1985), "A Status Report on Design and Operational Experiences with the Semi-Submerged Catamaran (SSC) Vessels", *Proc. Int. Conf. on SWATH Ships and Advanced Multi-Hulled Vessels*, RINA, Paper No. 5, London, April

MacGregor, J.R. (1986), "An Analysis of SWATH Design and Performance Data", *Department Report*, No. NAOE-86-30, Dept. of NA&OE, University of Glasgow, Nov.

MacGregor, J.R. (1989), "A Computer Aided Method for Preliminary Design of SWATH Ships", *PhD Thesis*, Dept. of NA&OE, University of Glasgow, May

MacGregor, J.R., Bose, N. and Small, G. (1988), "Design and Construction of a Small Waterplane Area Twin Hull (SWATH) Fishing Vessel", *Proc. World Symp. on Fishing Gear and Fishing Vessel Design*, St John's, Newfoundland, Canada, Nov.

Maddox, S.J. (1991), "Fatigue Strength of Welded Structures", *Abington Publishing*, Cambridge, UK

Madsen, H.O., Skjong, R. and Kikermo, F. (1987), "Probabilistic Fatigue Analysis of Offshore Structures - Reliability Updating Through Inspection Results", *Proc. 3rd Int. Symp. on Integrity of Offshore Structures*, pp. 361-374, University of Glasgow, Sept.

Malakhoff, A., Thomas Packard, W., Engle, A.H. and Sielski, R.A. (1991), "Towards Rational Surface Ship Structural Design Criteria", *Proc. of the Int. Conf. on Advances in Marine Structures-2*, ARE, Dunfermline, Scotland, May

Mansour, A.E. (1981), "Combining Extreme Environmental Loads for Reliability Based Designs", *Proc. Extreme Loads Response Symp.*, SSC/SNAME, pp. 63-74, Arlington, VA, USA, Oct.

Mansour, A. and d'Oliveira, J.M. (1975), "Hull Bending Moment Due to Ship Bottom Slamming in Regular Waves", *Journal of Ship Research*, SNAME, Vol. 19, No. 2, pp. 80-92, June

Mansour, A. and Faulkner, D. (1973), "On Applying the Statistical Approach to Extreme Sea Loads and Ship Hull Strength", *Trans. RINA*, Vol. 115, pp. 277-314

Mantle, P.J. (1980), "A Technical Summary of Air Cushion Craft Development", *DTNSRDC*, Report No. 80/012 (4727 revised), Jan.

Marine Report (1990), "Model Tests for a SWATH Cruise Liner", Maritime Research Institute Netherlands, No. 41, Nov.

Maruo, H. (1957), "The Excess Resistance of a Ship in Rough Seas", *Int. Shipbuilding Progress*, Vol. 4, No. 35

Mathisen, J. and Carlsen, C.A. (1980), "A Comparison of Calculation Methods for Wave Loads on Twin Pontoon Semi-Submersibles", *Proc. Int. Symp. on Ocean Engineering and Ship Handling*, Gothenburg, Sweden.

McCreight, K.K. (1987), "Assessing Seaworthiness of SWATH Ships", *Trans. SNAME*, Vol. 95, pp. 189-214

McGregor, R.C. (1983), "An Illustration of Some SWATH Vessel Characteristics", *Proc.High-Speed Surface Craft Conf.*, London, May

McGregor, R.C., et al (1988), "Comparative Study of SWATH Seakeeping", *Proc. Int. High-Performance Vehicle Conf.*, CSNAME, Paper No. VI-4, Shanghai, China, Nov.

McGregor, R.C., Chun, H.H., Djatmiko, E.B. and Jones, A.H. (1990), "On Modelling the Hydrodynamic Behaviour of SWATH Vessels", *Proc. Int. Conf. on Modelling and Control of Marine Craft*, Paper No. 21, pp. 336-357, Exeter, UK, April

McPherson, J.L. and Voight, B.D. (1983), "An Experimental Comparison of Zero Speed Seakeeping Characteristics of Single and Double Strut SWATHs", US Naval Academy, Div. of Engg. and Weapons, Report No. EW-15-83, Annapolis, Maryland, USA, April

Meyerhoff, W.K. et al. (1988) "Novel Design Concepts - SWATH", *Proc. 10th Int. Ship & Offshore Structures Congress*, ISSC, Vol. 2, Report of Committee V.4, Lyngby, Denmark, Aug.

Milgram, J.H. (1976), "Waves and Wave Forces", *Proc. Int. Conf. on Behaviour of Offshore Structures*, BOSS'76, Norwegian Institute of Technology, Trondheim, Norway, Aug.

Miller, A.F. (1991a), "A Review of Techniques Employed to Predict Wave Induced Global Loadings on SWATH Ships", *Department Report*, No. NAOE-91-29, Dept. of NA&OE, University of Glasgow, July

Miller, A.F. (1991b), "Aspects of SWATH Design and Evaluation", *MSc Thesis*, Dept. of NA&OE, University of Glasgow, Sept.

Milner, R. (1990), "The World's First 30-knot Fast Displacement Catamaran (SWATH) Ferry", *Proc. 7th Int. High Speed Surface Craft Conf.*, London, Jan.

Miner, M.A. (1945), "Cumulative Damage in Fatigue", *Journal of Applied Mechanics*, ASME, Vol. 12, p. A-159

Moan, T. et al (1991), "Design Philosophy", *Proc. 11th International Ship & Offshore Structures Congress*, ISSC, Report of Committee IV.1, Wuxi, China, Sep.

Moskowitz, L., Pierson, W.J. and Mehr, E. (1965), "Wave Spectra Estimated from Wave Record Obtained by OWS *Weather Reporter* ", New York University, College of Engineering (I) 1962, (II) 1963, (III) 1965, USA

Mulligan, R.D. and Edkins, J.N. (1985), "ASSET/SWATH - A Computer Based Model for SWATH Ships", *Proc. Int. Conf. on SWATH Ships and Advanced Multi Hulled Vessels*, RINA, London, April

Munk, M.M. (1924), "The Aerodynamic Forces on Airship Hulls", *National Advisory Committee on Aeronautics*, NACA, Report No. 184, USA

Munse, W.H. (1981), "Fatigue Criteria for Ship Structure Detail", *Proc. of the Extreme Loads Response Symp.*, SNAME, Arlington, VA, USA, Oct.

Munse, W.H. et al (1983), "Fatigue Characterization of Fabricated Ship Details for Design", *Ship Structure Committee*, Report No. SSC-318, Washington D.C., USA

Nagai, T. and Chuang, S-L (1977), "Review of Structural Response Aspects of Slamming", *Journal of Ship Research*, SNAME, Vol. 21, No. 3, pp. 182-190, Sept.

Nelson, A. (1905), "Vessel", *U.S. Patent*, No.795,002, July

Nethercote, W.C.E. and Schmitke, R.T. (1982), "A Concept Exploration Model for SWATH Ships", *Trans. RINA*, Vol. 124, pp. 113-130

Newland, D.E. (1986), "An Introduction to Random Vibrations and Spectral Analysis", Longman Inc., New York

Nordenström, N.(1973), "A Method to Predict Long-term Distributions of Waves and Wave-Induced Motions and Loads on Ships and Other Floating Structures", *Det norske Veritas*, Publ. 81, April

Nordenström, N., Faltinsen, O. and Pedersen, B. (1971), "Prediction of Wave Induced Motions and Loads for Catamarans", *Proc. Offshore Technology Conf.*, Paper No. OTC-1418, Houston, Texas, USA

Ochi, M.K. (1958), "Model Experiment on Ship Strength and Slamming in Regular Waves", *Trans. SNAME*, Vol. 66

Ochi, M.K. (1964), "Extreme Behaviour of a Ship in Rough Seas - Slamming and Shipping of Green Water", *Trans. SNAME*, Vol. 72

Ochi, M.K. (1973), "On Prediction of Extreme values", *Journal of Ship Research*, SNAME, Vol. 17, No. 1, pp. 29-37, March

Ochi, M.K. (1978), "Wave Statistics for the Design of Ships and Ocean Structures", *Trans. SNAME*, Vol. 86, pp. 47-76

Ochi, M.K. and Bales, S.L. (1977), "Effect of Various Spectral Formulations in Predicting Responses of Marine Vehicles and Ocean Structures", *Proc. 9th Annual Offshore Technology Conference*, OTC, Paper No. OTC-2743, Houston, Texas, USA, May

Ochi, M.K. and Hubble, E.N. (1976), "On Six-Parameter Wave Spectra", *Proc. 15th Coastal Engineers Conf.*, ASCE, USA

Ochi, M.K. and Motter, L.E. (1969), "Prediction of Extreme Values of Impact Pressure Associated with Ship Slamming", *Journal of Ship Research*, SNAME, Vol. 13, No. 2, pp. 85-91, June

Ochi, M.K. and Motter, L.E. (1971), "A Method to Estimate Slamming Characteristics for Ship Design", *Marine Technology*, SNAME, Vol. 8, No. 2, pp. 219-232, April

Ochi, M.K. and Motter, L.E. (1973), "Prediction of Slamming Characteristics and Hull Responses for Ship Design", *Trans. SNAME*, Vol. 81, pp. 144-176

Ochi, M.K. and Motter, L.E. (1974), "Prediction of Extreme Ship Responses in Rough Seas of the North Atlantic", *Proc. Int. Symp. on Dynamics of Marine Vehicles and Structures in Waves*, IMechE/RINA, pp. 187-197, London, April

Ochi, M.K. and Wang, S. (1976), "Prediction of Extreme Wave-Induced Loads on Ocean Structures", *Proc., Int. Conf. on Behaviour of Offshore Structures (BOSS'76)*, Norwegian Institute of Technology, Trondheim, Norway, Aug.

Olson, S.R. (1978), "An Evaluation of the Seakeeping Qualities of Naval Combatants", *Naval Engineers Journal*, ASNE, Vol. 90, No. 1, pp. 23-40, Feb.

Oshima, M., Narita, H. and Kunitake, Y. (1979), "Experiences with 12 Meter Long Semi-Submerged Catamaran (SSC) *Marine Ace* and Building of SSC Ferry for 446 Passengers", *Proc. AIAA/SNAME Advanced Marine Vehicles Conf.*, Paper No. 79-2019, Baltimore, Maryland, USA

Papanikolaou, A,.Schellin, T.E. and Zaraphonitis, G (1990), "A 3 D-Method to Evaluate Motions and Loads of Ships with Forward Speeds in Waves", *Proc. 5th Int. Congress of Marine Technology*, HIMT, pp. 452-457, Athens, Greece

Paris, P. and Erdogan, F. (1963), "A Critical Analysis of Crack Propagation Laws", *Journal of Basic Engineering*, ASME, Vol. 85, pp. 528-534

Pattison, D.R., Rose, P.H.A. and Harris, S.A. (1988), "SWATH-The UK MOD Design and Assessed Programme", *Proc. Int. Conf. on SWATH Ships and Advanced Multi Hulled Vessels II*, RINA, Paper No. 6, London, Nov.

Paulling, J.R. and Hong, Y.S. (1977), "Analysis of Semi-Submersible Catamaran Type Platforms", *Proc. Offshore Technology Conf.*, Paper No. OTC-2977, Houston, Texas, USA

Pegg, N.G., Gilroy, L.E. and Cumming, D.W. (1990), "Load, Motion and Structural Response Trials of the SWATH Vessel 'Frederick G. Creed' ", *Proc. Symp. on the Dynamics of Marine Vehicles and Structures in Waves*, IUTAM (Int. Union of Theoretical and Applied Mechanics), Brunel University, U.K., June 1990

Penney, P.W. and Riiser, R.M. (1984), "Preliminary Design of Semisubmersibles", *Trans. NECIES*, Vol. 101

Petershagen, H.G., et al (1982), "Ferrous Materials", *Proc. of the 8h Int. Ship & Offshore Structures Congress*, Report of Committee III.1, Gdansk, Poland

Petershagen, H.G., et al (1986), "Fatigue Problems in Ship Structures", *Proc. of the Int. Conf. on Advances in Marine Structures*, ARE, Dunfermline, Scotland, May

Petty, W. (1660), Manuscripts concerning "Ye Double Bodyed Shippe", National Maritime Museum SPB/16

Pieroth, C.G. and Lamb, G.R. (1983), "The SWATH Option as V/STOL Aircraft Carrier", *Proc. 7th Intersociety Marine System Conf.*, AIAA/SNAME/ASNE, New Orleans, USA, Feb.

Pieroth, C.G. and Lamb, G.R. (1985), "The SWATH Option as a V/STOL Aircraft Carrier", *Branch Meeting*,SNAME, Hampton Road Sect., March

Pierson, W.J.Jr. and Moskowitz, L. (1964), "A Proposed Spectral Form for Fully Developed Wind Seas, Based on the Similarity Theory of S.A. Kataigorodsky", *Journal of Geophysical Research*, Vol. 69, No. 24, pp. 5181-5190, Dec.

Pierson, W.J. Jr. and St. Denis, M. (1953), "On the Motions of Ships in Confused Seas", *Trans. SNAME*, Vol. 61, pp. 280-357

Price, W.G., Temarel, P. and Wu, Y. (1985), "Structural Responses of a SWATH or Multi-Hull Vessel Travelling in Waves", *Proc. Int. Conf. on SWATH Ships and Advanced Multi-Hulled Vessels*, RINA, Paper No. 15, London, April

Price, W.G., Temarel, P. and Wu, Y. (1987), "Responses of a SWATH Travelling in Unidirectional Irregular Seas", *Underwater Technology*, SUT, Vol. 13, No. 4, pp. 2-10

Price, W.G. and Wu, Y. (1987), "The Influence of Non-Linear Fluid Forces in the Time Responses of Flexible SWATH Ships Excited by a Seaway", *Proc.8th Int. Conf. on OMAE*, pp. 125-135, the Hague, the Netherlands, March

Pu, Y. (1992), "Reliability Analysis of Stiffened Plates", *Annual Report*, Dept. of NA&OE, University of Glasgow, (in preparation)

Reilly, E.T., Ingram, T.J. and Arntson, S.G. (1990), "SWATH Vessels for Naval Applications Design and Analysis", *A Paper*, ABS, USA

Reilly, E.T., Shin, Y.S. and Kotte, E.H. (1988), "A Prediction of Structural Load and Response of a SWATH Ship in Waves", *Naval Engineers Journal*, ASNE, Vol. 99, No. 3, pp. 251-264, May

Routa, T. (1985), "Application of the SWATH Principle to Passenger Vessels", *Proc. Int. Conf. on SWATH Ships and Advanced Multi-Hulled Vessels*, RINA, Paper No. 3, London, April

Rutherford, S.E. and Caldwell, J.B. (1990), "Ultimate Longitudinal Strength of Ships : A Case Study", *Trans. SNAME*, Vol. 98, pp. 441-471

Salvensen, N., et al (1985), "Hydro-Numeric Design of SWATH Ships", *Trans. SNAME*, Vol. 93, pp. 325-346.

Sariöz, K., Hearn, G.E. and Hills, W. (1992), "Practical Seakeeping for Design : An Optimised Approach", *Proc. of 5th Int. Symp. on Practical Designof Ships and Mobile Units*, PRADS'92, Newcastle upon Tyne, UK, May

Schellin, T.E. and Papanikolaou, A (1991), "Prediction of Seakeeping Performance of a SWATH Ship and Comparison with Measurements", *Proc. 1st Int. Conf. on Fast Sea Transportation*, FAST'91, pp. 811-827, Trondheim, Norway, June

Seascape (1987), "Many Hulls Make Light Work", *Seascape*, Int. Maritime Magazine, No. 2, p. 21, June

Seidl, L. (1992) discussion to Band, E.G.U. et al, "Novel Design Concepts - High Performance Vehicles", *Proc. 11th Int. Ship & Offshore Structures Congress*, ISSC, Vol. 3, pp. 233-241, Wuxi, China, Sep.

Sellars, F.H. (1976), "Water Impact Loads", *Marine Technology*, SNAME, Vol. 13, No. 1, pp. 46-58, Jan.

Seren, D.B. (1983), "SWATH - the Shape of Ships to Come", *High-Speed Surface Craft*, Dec.

Seren, D.B. and Atlar, M. (1984a), "The SWATH Wave-Load Program, Progress Report No 6; An Overview of the Concepts Employed to Predict the Hydrodynamic Forces Imposed on an Unappended SWATH-ship Proceeding in a Seaway ", *Department Report*, No. NAOE-84-63, Dept. of NA&OE, University of Glasgow

Seren, D.B. and Atlar, M. (1984b), "An Overview of the Concepts Employed to Predict the Hydrodynamic Forces Imposed on An Unappended SWATH Ship Proceeding in a Seaway", *Department Report*, No. NAOE-84-63, Dept. of NA&OE, University of Glasgow, Dec.

Seren, D.B. and Leitch, E. (1982), "The SWATH Wave-Load Program, Progress Report No 1; The Wave Input", *Department Report*, No. NAOE-82-30, Dept. of NA&OE, University of Glasgow,

Seren, D.B., Leitch, E. and Miller, N.S. (1983a), "The SWATH Wave-Load Program, Progress Report No 3; Manual for Structure Geometry Description", *Department Report*, No. NAOE-83-38, Dept. of NA&OE, University of Glasgow

Seren, D.B., Leitch, E. and Miller, N.S. (1983b), "The SWATH Wave-Load Program, Progress Report No 4; Program for Offshore Structures Hydrostatics (POSH)", *Department Report*, No. NAOE-83-35, Dept. of NA&OE, University of Glasgow

Seren, D.B., Leitch, E. and Miller, N.S. (1984), "The SWATH Wave-Load Program, Progress Report No 5; A Package to Compute and Control the Weight Distribution, Dynamic Properties and Static Loads of Floating Offshore Configurations (MAD)", *Department Report*, No. NAOE-84-32, Dept. of NA&OE, University of Glasgow,

Seren, D.B. and Miller, N.S. (1982), "The SWATH Wave-Load Program, Progress Report No 2; The Tentative Outline of the Treatment of the Geometry", *Department Report*, No. NAOE-82-31, Dept. of NA&OE, University of Glasgow

Seren, D.B., Miller, N.S., Ferguson, A.M. and McGregor, R.C. (1985), "Some Motion and Resistance Aspects of SWATH Ship Design", *Proc. Int. Conf. on SWATH Ships and Advanced Multi-Hulled Vessels*, RINA, Paper No. 10, London, April

Sheridan, D., Clark, D.J., Jones, R. and Fein, J. (1984), "The ASSET Program - A Current Navy Initiative", *Proc. SNAME STAR Symp.*, Los Angeles, USA, April

Shin, Y, Kotte, E., Thayamballi, A. and Unger, D. (1989), "Analysis Procedure of Hydrodynamic Load and Fatigue Life Prediction for SWATH Ships in Waves", *Proc. Intersociety Advanced Marine Vehicles Conf.*, Paper No. 89-1477-CP, Arlington, VA, USA, June

Sikora, J.P. (1988a), "Some Design Approaches for Reducing the Structural Weight of SWATH Ships", *Proc. Int. Conf. on SWATH Ships and Advanced Multi Hulled Vessels II*, RINA, Paper No. 18, London, Nov.

Sikora, J.P. (1988b), discussion to Lee, K-Y, et al (1988), "On the Design Technology of SWATH High Speed Passenger Ship", *Proc. Int. Conf. on SWATH Ships and Advanced Multi-Hulled Vessels II*, RINA, Paper No. 17, London, Nov.

Sikora, J.P. and Beach, J.E. (1986), "Automated Method for Predicting Maximum Lifetime Loads and Fatigue Lives of Ships", *Proc. of the 9th Annual Energy-Sources Technology Conf. & Exhibition : Current Practices and New Technology in Ocean Engineering*, ASME, New Orleans, USA, Feb.

Sikora, J.P. and Dinsenbacher, A.L. (1988), "SWATH Structure : Navy R & D Design Applications", *Branch Meeting*, SNAME, Chesapeake Section, Oct.

Sikora, J.P. and Dinsenbacher, A.L. (1990), "SWATH Structure : Navy Research and Development Applications", *Marine Technology*, SNAME, Vol. 27, No. 4, pp. 211-220, July

Sikora, J.P., Dinsenbacher, A. and Beach, J.E. (1983), "A Method for Estimating Lifetime Loads and Fatigue Lives for SWATH and Conventional Monohull Ships", *Naval Engineers Journal*, ASNE, Vol. 95, No.3, pp. 63-85, May

Sikora, J.P. and Swanek, A.D. (1982), "SWATH Preliminary Structure ; Design Considerations and Stress Calculation Method", Enclosure to DTNSRDC letter 173 ADS, 5605,82-173-55, April

Skaar, K.T., Valsgård, S., Köhler, P.E. and Mürer, C. (1987), "How Low Can Steel Weight Go with Safety and Economy ?", *Proc. of the 3rd Symp. on Practical Design of Ships and Mobile Units*, PRADS'87, Trondheim, Norway, June

Skaar, K.T., et al (1991), "Inspection, Monitoring, Maintenance/Repair", *Proc. 11th Int. Ship & Offshore Structures Congress*, ISSC, Report of Committee V.2, Vol. 2, pp. 41-86, Wuxi, China, Sept.

Smith, C.S. (1977), "Influence of Local Compressive Failure on Ultimate Longitudinal Strength of a Ship's Hull", *Proc. Int. Conf. on Practical Design in Shipbuilding*, PRADS 77, Tokyo & Seoul

Smith, C.S. (1990), "Design of Marine Structures in Composite Materials", Elsevier Science Publishers Ltd., London and New York

Smith, C.S. and Monks, E.H. (1982), "Design of High Performance Hulls in FRP", *Proc. of 2nd Symp. on Small Fast Warships*, RINA, London, May

Smith, D.L., Cuthbertson, W., MacGregor, J.R. and McGregor, R.C. (1987), "SWATH Sonar Support Vessel (SSV)", Contract NSS 41A/1800, Concept Study Report, Yarrow Shipbuilder Ltd., July

Smith, S.N. (1982a), "Design and Hydrodynamic Assessment of a Small Semi Submersible SWATH-Type Vessel", *PhD Thesis*, Dept. of NA&OE, University of Glasgow

Smith, S.N. (1983), "Design and Hydrodynamic Performance of a Small Semi Submersible (SWATH) Research Vessel", *Trans. RINA*, Vol. 125, pp. 69-91

Spaulding, K.B. (1966), "A History of the Construction of Fibreglass Boats for the Navy", *Naval Engineers Journal*, ASNE, Vol. 78, April

Spencer, J.S. (1975), "Structural Design of Aluminium Crewboats", *Marine Technology*, SNAME, Vol. 12, No. 3, pp. 267-274, July

Stavovy, A.B. and Chuang, S-L (1976), "Analytical Determination of Slamming Pressures for High-Speed Vehicles in Waves", *Journal of Ship Research*, SNAME, Vol. 20, No. 4, pp. 190-198, Dec.

Stenson, R.J. (1976), "Full Scale Powering Trials of the Stable Semi-Submerged Platform, SSP *Kaimalino*", DTNSRDC, Report SPD-650-01, April

Stevens, R.M. (1972), "New Dimensions for Naval Catamarans", *NSRDC*, Report No. 3830, Bethesda, Maryland, USA, May

Stirling, A.G., Jones,G.L. and Clark, J.D. (1988), "Development of a SWATH Structural Design Procedure for Royal Navy Vessels", *Proc. Int. Conf. on SWATH Ships and Advanced Multi Hulled Vessels II*, RINA, Paper No. 19, London, Nov.

Strom-Tejsen, J., Yeh, H.Y.H. and Moran, D.D. (1973), "Added Resistance in Waves", *Trans. SNAME*, Vol. 81

Suhrbier, K.R. et al. (1990), "Report of the High-Speed Marine Vehicles Committee", *Proc. 19th Int. Towing Tank Conference*, ITTC, Vol. 1, pp. 289-378, Madrid, Spain, Sept.

Takeuchi, M., Takagawa, S., Miyanabe, R. and Watanabe, T. (1985), "Structural Design of the Semi-Submerged Catamaran-Type Underwater Work Test Vessel", *JAMSTEC*, Technical Report No. 15

Thoft-Christensen, P. (1987), "Application of Structural Systems Reliability Theory in Offshore Engineering, State-of-the-Art", *Proc. 3rd Int. Symp. on Integrity of Offshore Structures*, pp. 1-23, University of Glasgow, Sept.

Thorpe, T.W. (1987), "A Simple Model for Fatigue Prediction and In-Service Defect Assessment of Tubular Joints", *Proc. 3rd Int. Symp. on Integrity of Offshore Structures*, pp. 285-326, University of Glasgow, Sept.

Thwaites, B. (1960), "Incompressible Aerodynamics", Oxford University Press, pp. 405-421

Tolikas, C, et al (1992), "Integrated SWATH Structural Design", *Department Report*, No. NAOE-14-92, Dept. of NA&OE, University of Glasgow, April

van Sluijs, M.F. (1974), "Ship Relative Motions and Related Phenomena", *Proc. Int. Symp. on the Dynamics of Marine Vehicles and Structures in Waves*, Office of Naval Research/RINA/IMechE, London, April

Verhagen, J.H.G. (1967), "The Impact of a Flat Plate on a Water Surface", *Journal of Ship Research*, SNAME, Vol. 11, No. 4, pp. 211-223, Dec.

Wahab, R., Pritchett, C. and Ruth, L.C. (1971), "On the Behavior of the ASR Catamaran in Waves", *Marine Technology*, Vol. 8, No. 3, pp. 334-360, July

Walker, M.A. (1984), "SWATH vs Monohull Initial Design", *MSc Dissertation*, University College London, Oct.

Watanabe, I. (1987), "Effects of the Three Dimensionality of Ship Hull on the Wave Impact Pressure", *Journal of Society of Naval Architect Japan*, SNAJ, Vol. 162, pp. 33-47, Dec.

White, G.J. and Ayyub, B.M. (1987), "Reliability-Based Fatigue Design for Ship Structures", *Naval Engineers Journal*, ASNE, Vol. 99, No. 3, pp. 135-149, May

Whitman, A.M. and Pancione, M.C. (1973), "A Similitude Relation for Flat-Plate Hydrodynamic Impact", *Journal of Ship Research*, SNAME, Vol. 17, No. 1, pp. 38-42, March

Wiernicki, C.J., Gooding, T.G. and Nappi, N.S. (1983), "The Structural Synthesis Design Program - Its Impact on the Fleet", *Naval Engineers Journal*, ASNE, Vol. 95, No. 3, pp. 87-99, May

Winkle, I.E., Cowling, M.J. Hashim, S.A. and Smith, E.M. (1990), "What Can Adhesives Offer to Shipbuilding", *Proc. Ship Production Symp.*, NSRP 1990, SNAME, Milwaukee, USA, Aug.

Wirsching, P.H. (1983), "Fatigue Reliability for Offshore Structures", *Journal of Structural Engineering*, ASCE, Vol. 110, No. 10, pp. 113-120, Oct.

Wirsching, P.H. (1985), "Probability Based Fatigue Design Criteria for Offshore Structures", *Final Report API-PRAC-15*, American Petroleum Institute, Dallas, TX, USA, Jan.

Wirsching, P.H. (1986), "Probability Based Fatigue Criteria for TLP Tendons", *Proc. 5th Int. Symp. on OMAE*, ASME, New York,

Wirsching, P.H. and Chen, Y-N. (1987), "Fatigue Design Criteria for TLP Tendons", *Journal of Structural Division*, ASCE, Vol. 113, No. 7, pp. 1398-1414, July

Wirsching, P.H. and Chen, Y-N. (1988), "Considerations of Probability-Based Fatigue Design for Marine Structures", *Marine Structures*, Vol. 1, No. 1, pp. 23-45

Woolaver, D.A. and Peters, J.B. (1980), "Comparative Ship Performance Sea Trials for the U.S. Coast Guard Cutters 'Mellon' and 'Cape Corwin' and the U.S. Navy Small Waterplane Area Twin Hull Ship *Kaimalino*", *DTNSRDC*, Report 80/037, Bethesda, Maryland, USA, March

Wu, J.Y. (1984) "A Study of Effects of Fin Size on the Pitching and Heaving of a SWATH Ship", *Department Report*, No. NAOE-84-55, Dept. of NA&OE, University of Glasgow, June

Wu, J.Y. (1985a), "Experimental Investigation of Vertical-Plane Response of a SWATH Ship with and without Aft Fins in Head Seas", *Department Report*, No. NAOE-85-31, Dept. of NA&OE, University of Glasgow, Jan.

Wu, J.Y. (1985b), "SWATH Vertical Motions with Emphasis on Fixed Fins Control", *PhD Thesis*, Dept. of NA&OE, University of Glasgow,

Wu, J.Y. and McGregor, R.C. (1986), "SWATH Seakeeping in the Presence of Control Fins", *Proc. 5th Int. High-speed Surface Craft Conf.*, Southampton, UK, May

Yamamoto, Y., et al (1985), "Structural Damage Analysis of a Fast Ship Due to Bow Flare Slamming", *Int. Shipbuilding Progress*, Vol. 32, No. 369, pp. 124-136, May

Yang, P.D.C. and Lee, J-S. (1991), "Safety Assessment of Double Skinned Hull Structure Against Ultimate Bending and Fatigue Strength", *Proc. of SNAK'91 Spring Meeting*, Soc. of Naval Architect Korea, University of Ulsan, Korea, April

Zheng, X. (1985), "Calculation of Potential Flow about Arbitrary Three-Dimensional Bodies, Part I - Free Surface Flow", *Department Report*, No. NAOE-85-54, Dept. of NA&OE, University of Glasgow,

Zheng, X. (1986) "Calculation of Potential Flow about Arbitrary Three-Dimensional Bodies, Part II - Flow about Submerged Bodies", *Department Report*, No. NAOE-86-52, Dept. of NA&OE, University of Glasgow

Zheng, X. (1988), "Prediction of Motion and Wave Load of Mono and Twin Hull Ships in Waves", *PhD Thesis*, Dept. of NA&OE, University of Glasgow, June

Zheng, X. (1989), "User's Guide of Program 'SHIPM1.0' - For Twin Hull", *A Manual Report*, Dept. of NA&OE, University of Glasgow

Zheng, X. and McGregor, R.C. (1987), "Prediction of Force and Motion Response in Crane Vessels", *Proc. of Marintec China 87 Conf.*, Shanghai, Dec.

APPENDIX A

FURTHER SWATH MOTION DATA

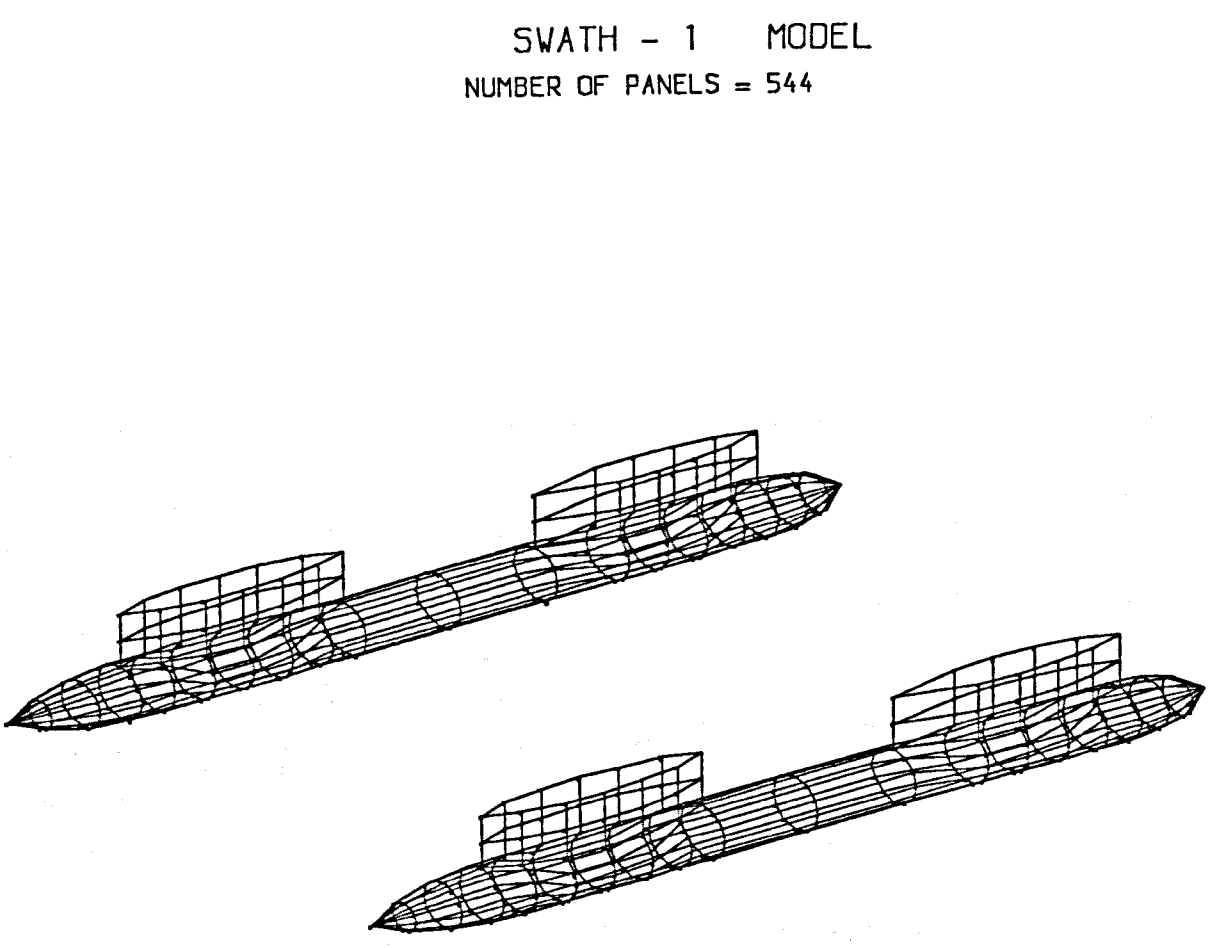

Figure A1. Discretisation of SWATH-1 model
(Number of panels = 544)

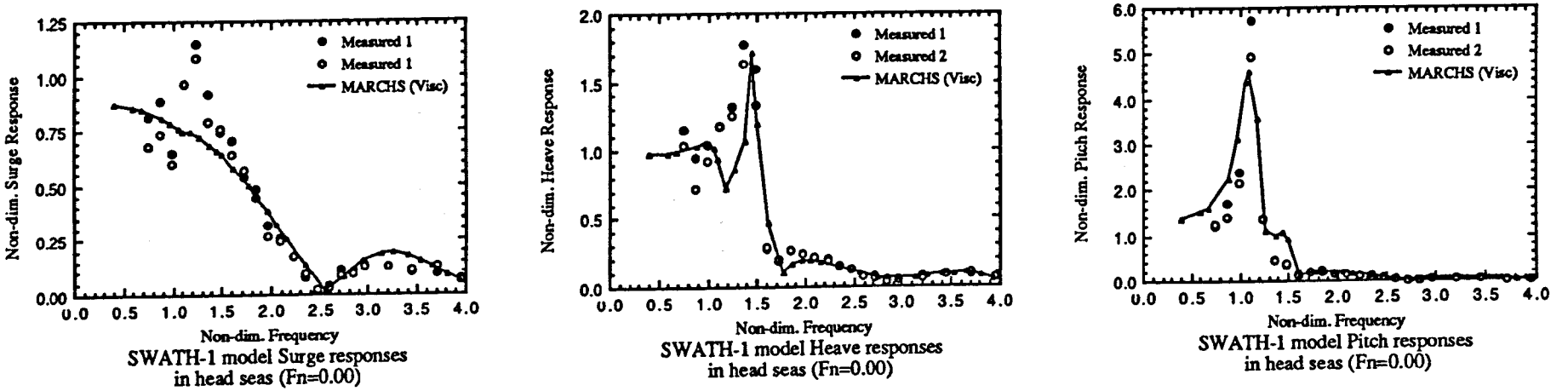

Figure A2. SWATH-1 model motions in head seas (Fn=0.00)

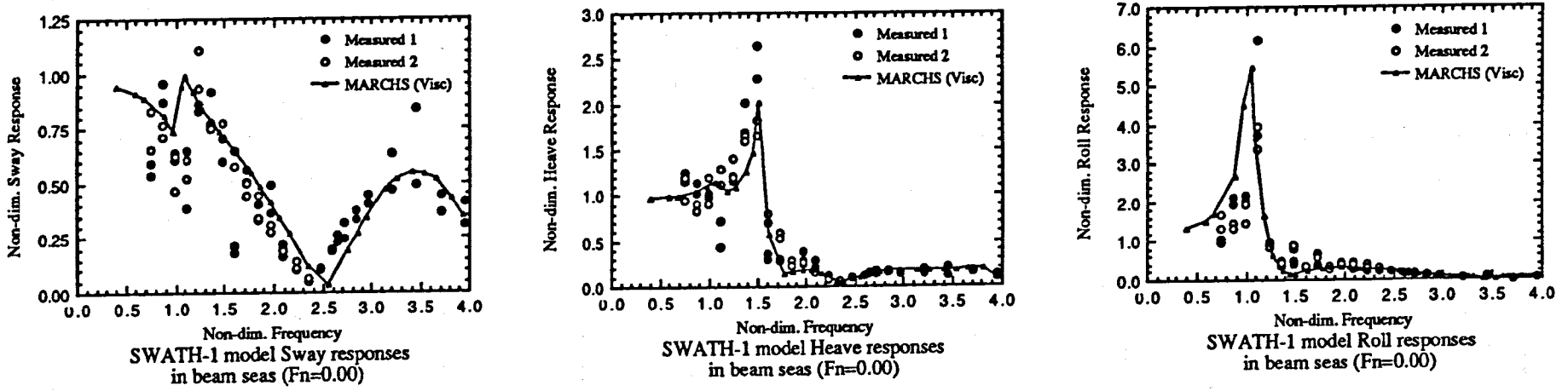

Figure A3. SWATH-1 model motions in beam seas (Fn=0.00)

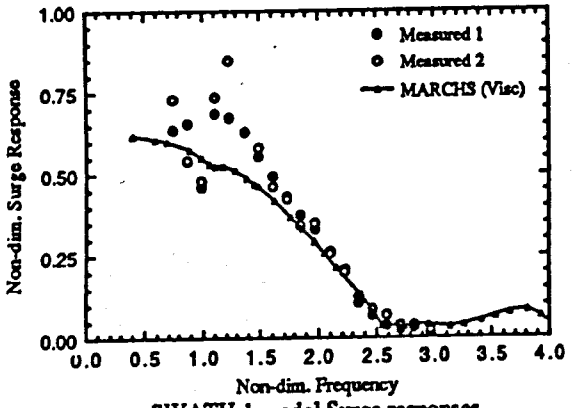

SWATH-1 model Surge responses
in quartering seas (Fn=0.00)

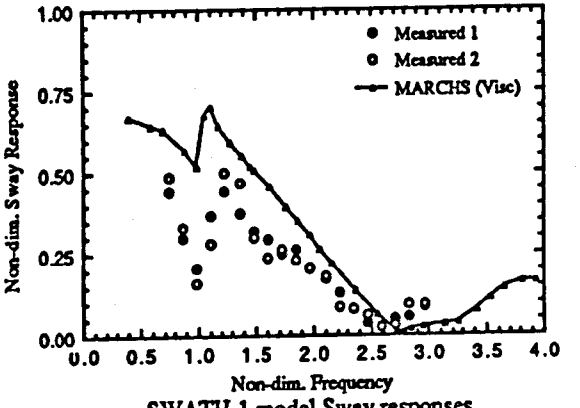

SWATH-1 model Sway responses
in quartering seas (Fn=0.00)

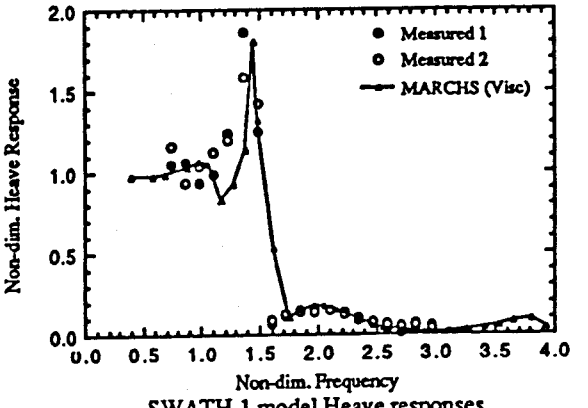

SWATH-1 model Heave responses
in quartering seas (Fn=0.00)

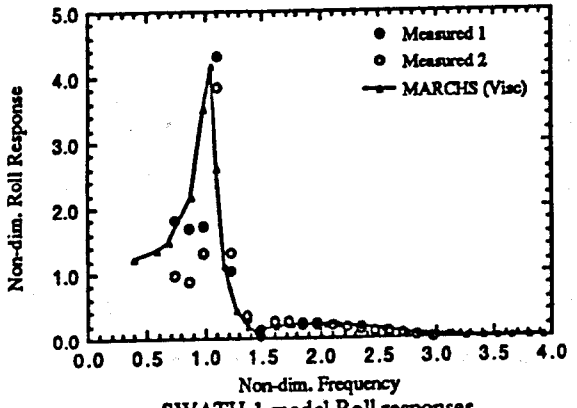

SWATH-1 model Roll responses
in quartering seas (Fn=0.00)

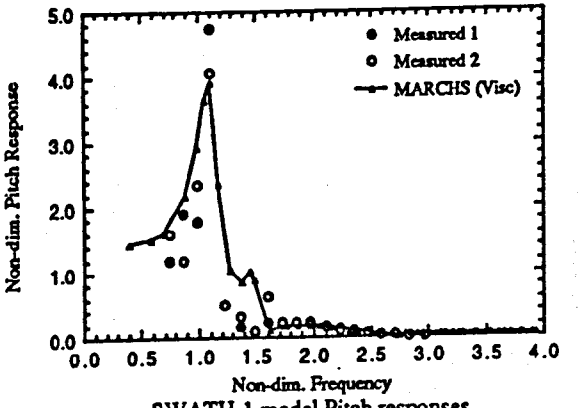

SWATH-1 model Pitch responses
in quartering seas (Fn=0.00)

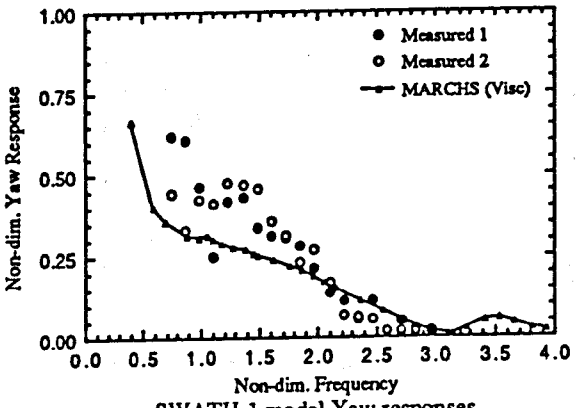

SWATH-1 model Yaw responses
in quartering seas (Fn=0.00)

Figure A4. SWATH-1 model motions in bow-quartering seas
(Fn=0.00)

PAGE MISSING IN ORIGINAL

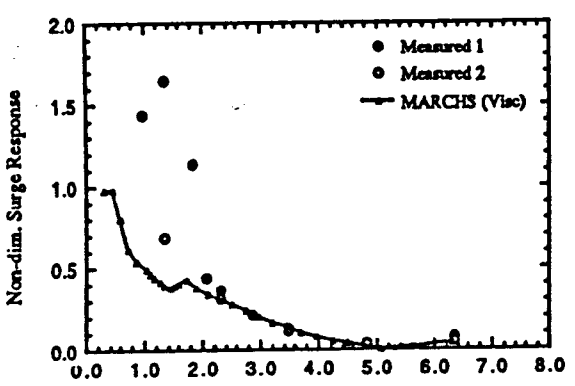

SWATH-1 model Surge responses in head seas (Fn=0.39)

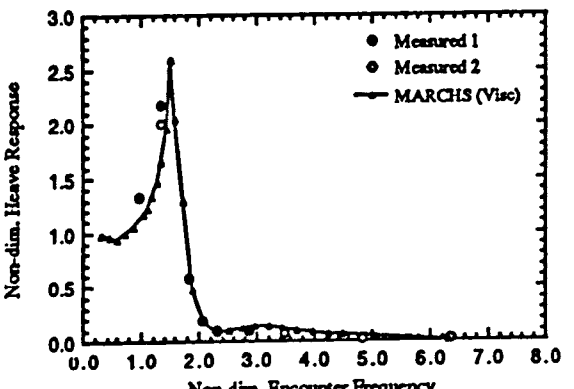

SWATH-1 model Heave responses in head seas (Fn=0.39)

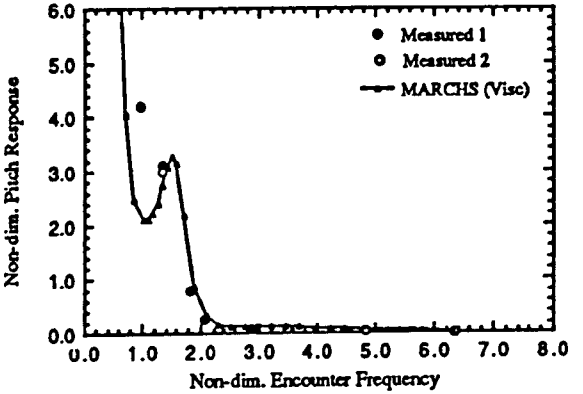

SWATH-1 model Pitch responses in head seas (Fn=0.39)

Figure A7. SWATH-1 model motions in head seas (Fn=0.39)

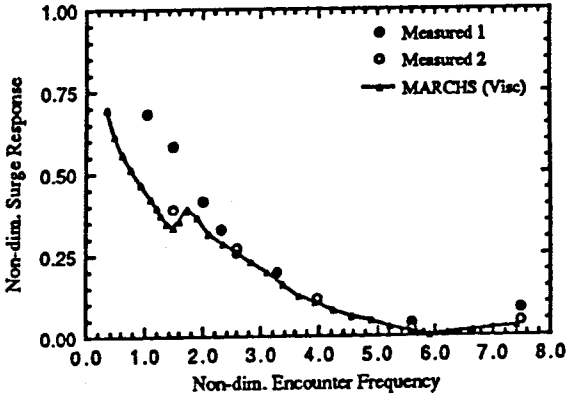

SWATH-1 model Surge responses in head seas (Fn=0.52)

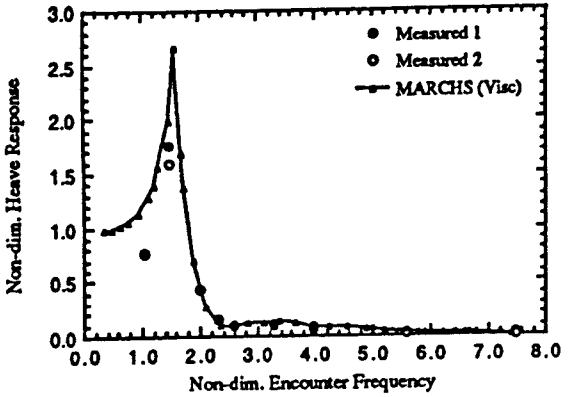

SWATH-1 model Heave responses in head seas (Fn=0.52)

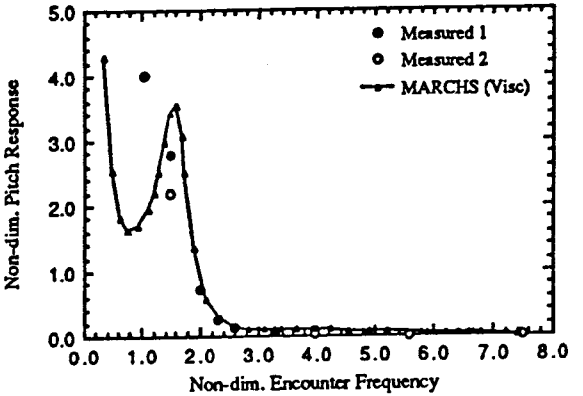

SWATH-1 model Pitch responses in head seas (Fn=0.52)

Figure A8. SWATH-1 model motions in head seas (Fn=0.52)

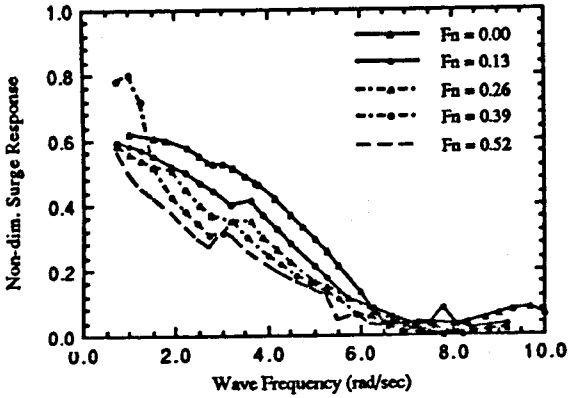

SWATH-1 model Surge responses in quartering seas

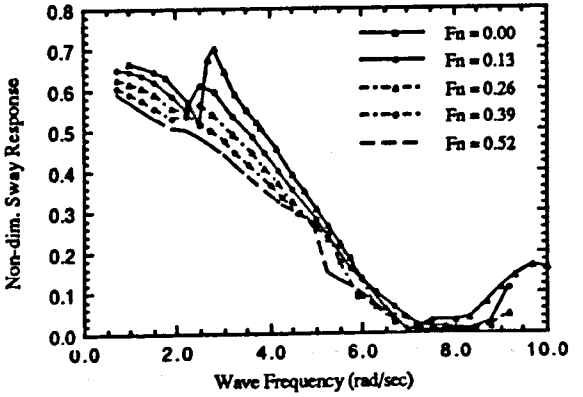

SWATH-1 model Sway responses in quartering seas

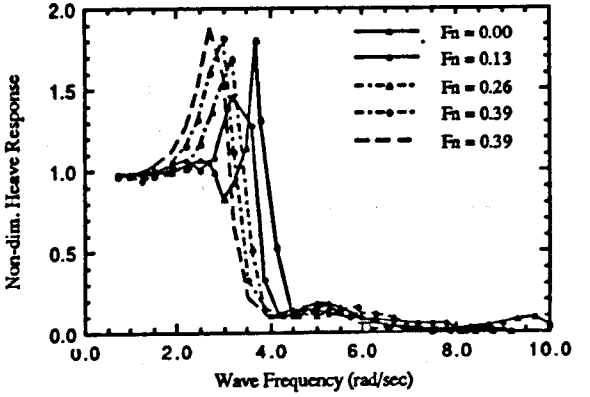

SWATH-1 model Heave responses in quartering seas

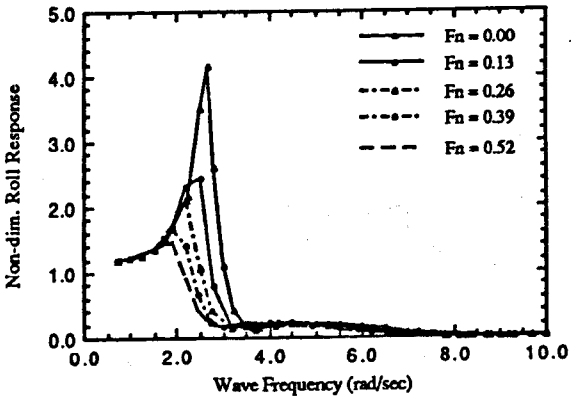

SWATH-1 model Roll responses in quartering seas

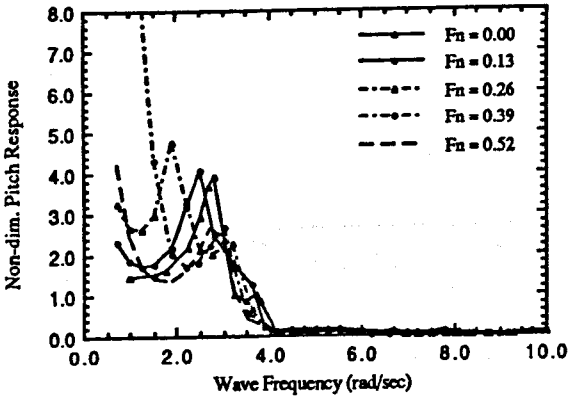

SWATH-1 model Pitch responses in quartering seas

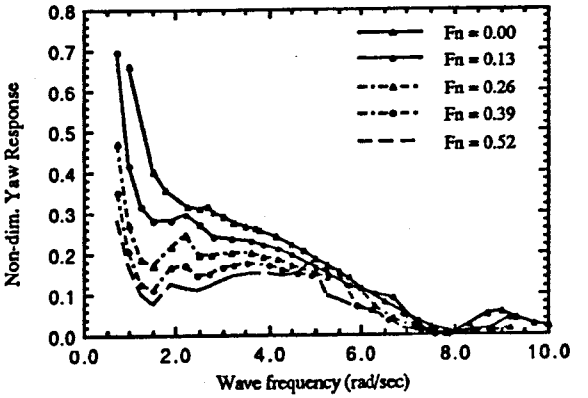

SWATH-1 model Yaw responses in quartering seas

Figure A9. SWATH-1 model motions in bow-quartering seas at various Froude numbers

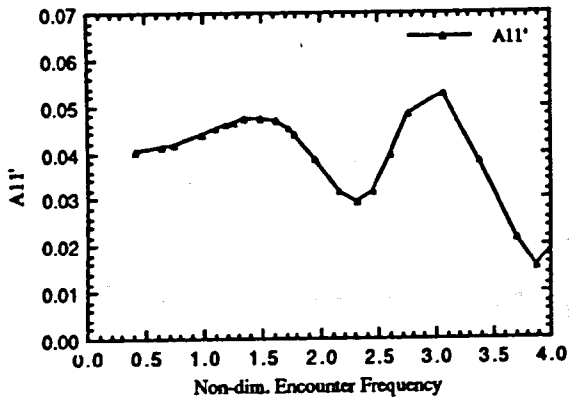

Surge added mass coefficient of SWATH-1 (Fn=0.13)

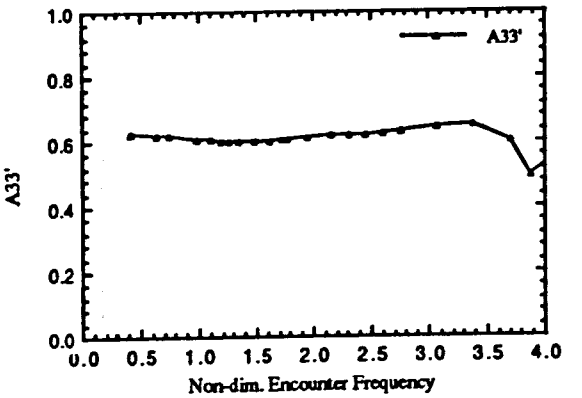

Heave added mass coefficient of SWATH-1 (Fn=0.13)

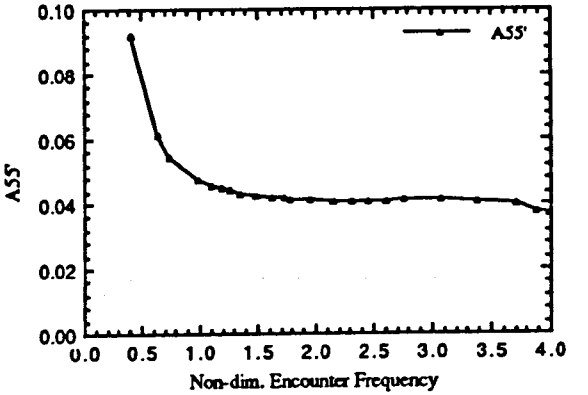

Pitch added inertia coefficient of SWATH-1 (Fn=0.13)

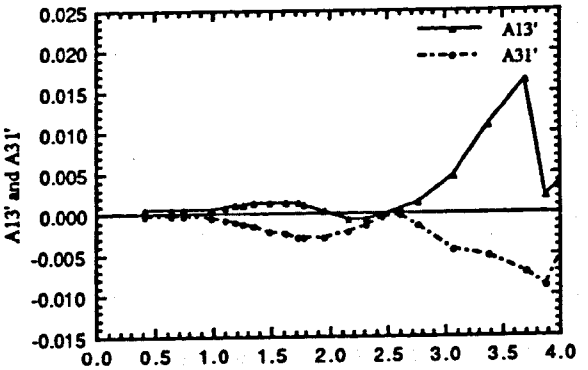

Surge-heave coupled added mass coefficients of SWATH-1 (Fn=0.13)

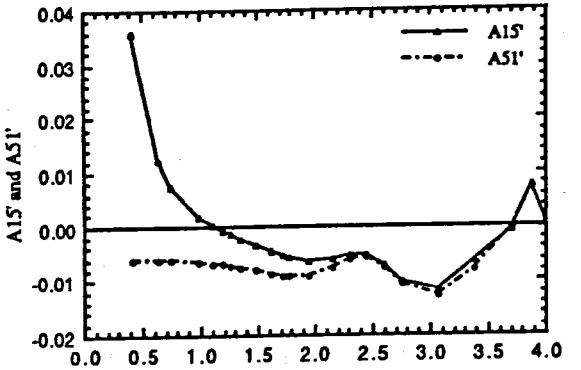

Surge-pitch coupled added mass coefficients of SWATH-1 (Fn=0.13)

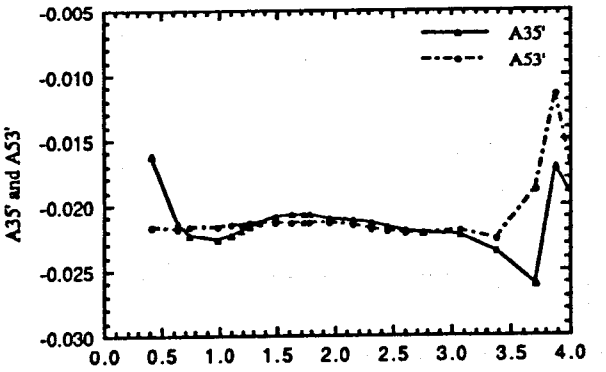

Heave-pitch coupled added mass coefficients of SWATH-1 (Fn=0.13)

Figure A10. Added mass and inertia coefficients for vertical motions of SWATH-1 model (Fn=0.13)

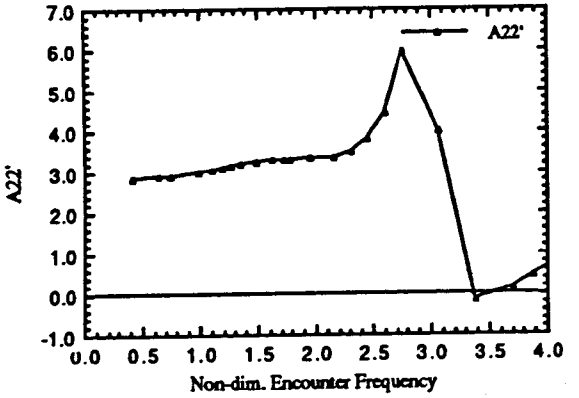

Sway added mass coefficient of SWATH-1 (Fn=0.13)

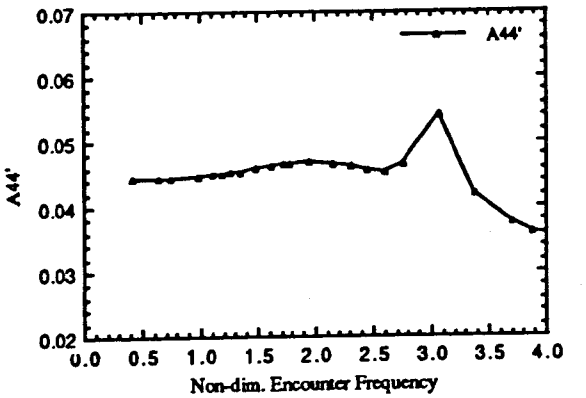

Roll added inertia coefficient of SWATH-1 (Fn=0.13)

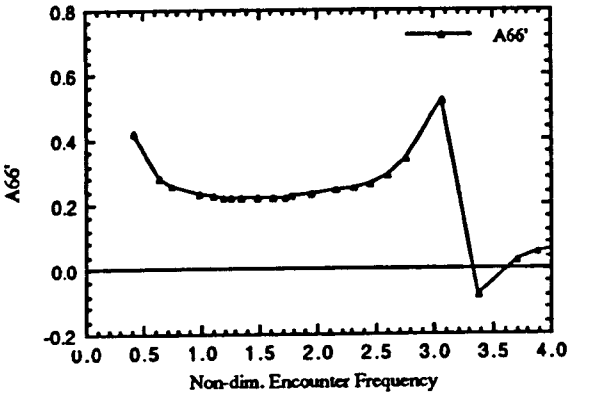

Yaw added inertia coefficient of SWATH-1 (Fn=0.13)

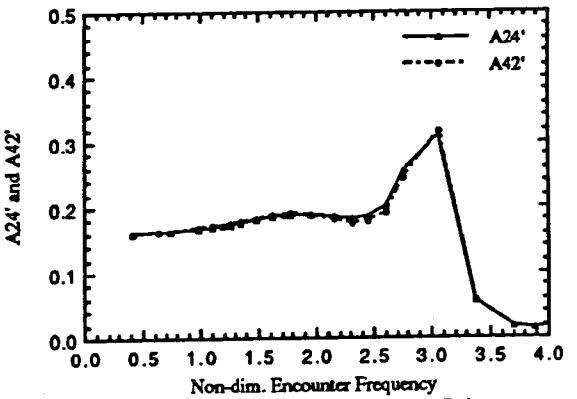

Sway-roll coupled added mass coeficients of SWATH-1 (Fn=0.13)

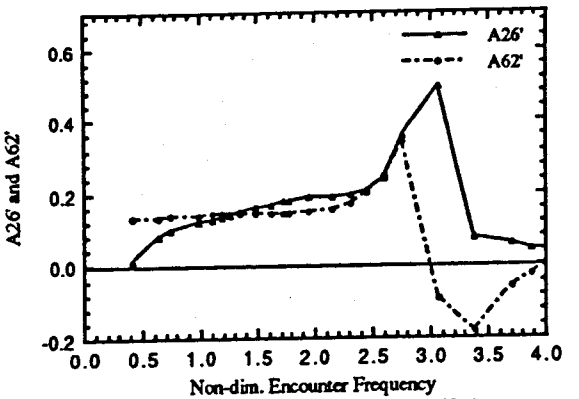

Sway-yaw coupled added mass coefficients of SWATH-1 (Fn=0.13)

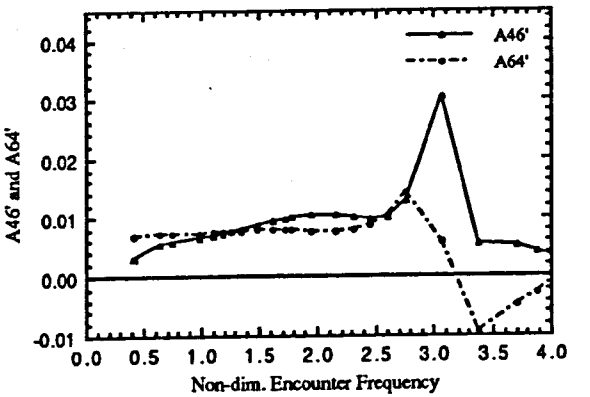

Roll-yaw coupled added inertia coefficients of SWATH-1 (Fn=0.13)

Figure A11. Added mass and inertia coefficients for horizontal motions of SWATH-1 model (Fn=0.13)

Figure A12. Discretisation of SWATH-3 model
(Number of panels = 496)

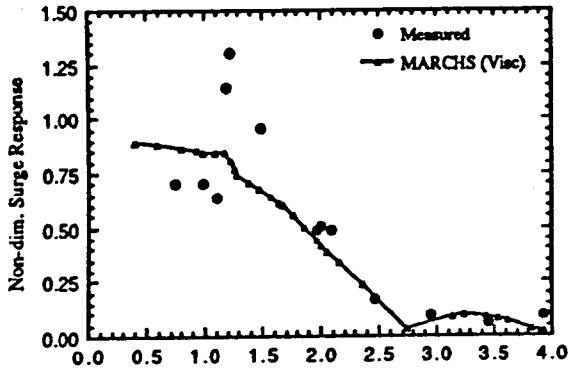

SWATH-3 model Surge responses
in head seas (Fn=0.00)

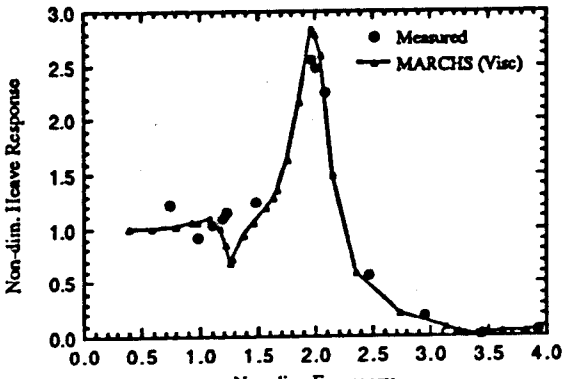

SWATH-3 model Heave responses
in head seas (Fn=0.00)

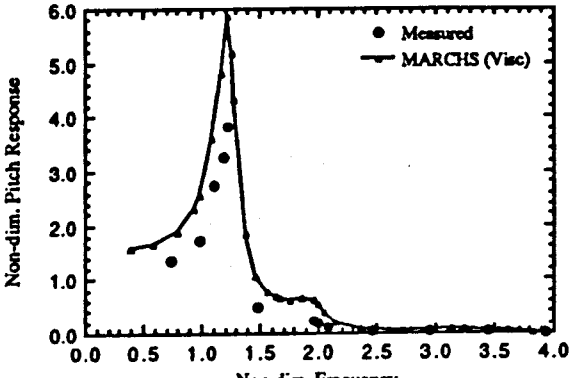

SWATH-3 model Pitch responses
in head seas (Fn=.00)

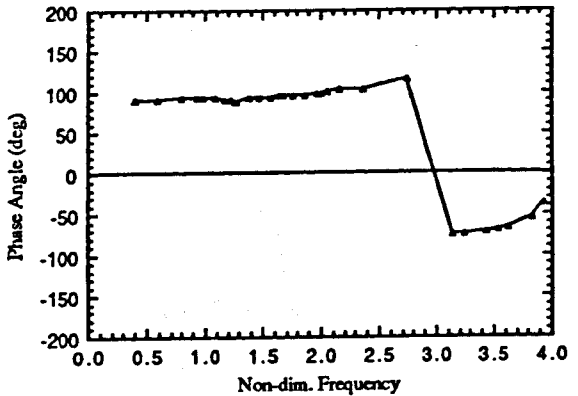

Phase angle of the Surge motion of the SWATH-3 model
in head seas (Fn=0.00)

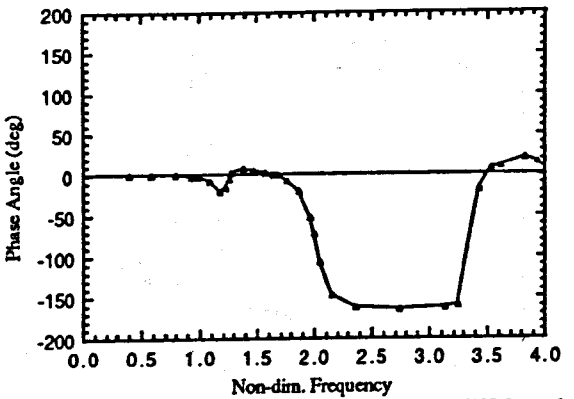

Phase angle of the Heave motion of the SWATH-3 model
in head seas (Fn=0.00)

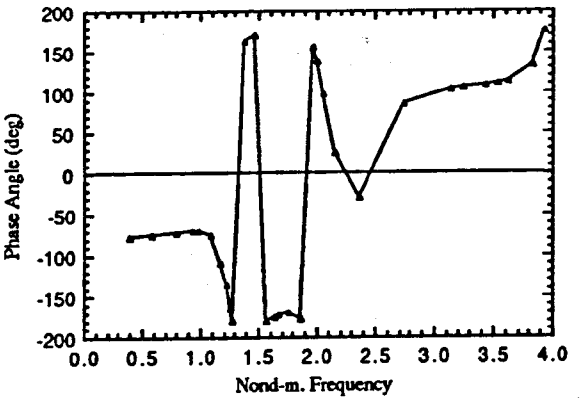

Phase angle of the Pitch motion of the SWATH-3 model
in head seas (Fn=0.00)

Figure A13. SWATH-3 model motions and phase angles
in head seas (Fn=0.00)

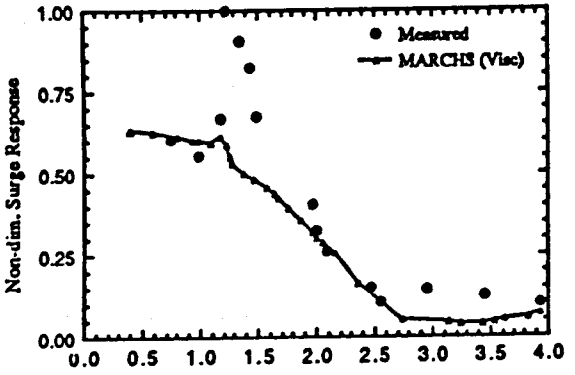

SWATH-3 model Surge responses
in quartering seas (Fn=0.00)

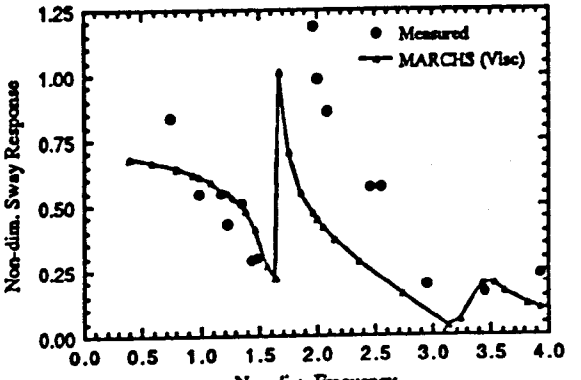

SWATH-3 model Sway responses
in quartering seas (Fn=0.00)

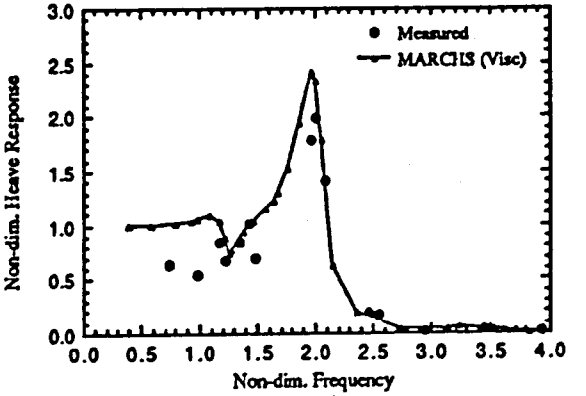

SWATH-3 model Heave responses
in quartering seas (Fn=0.00)

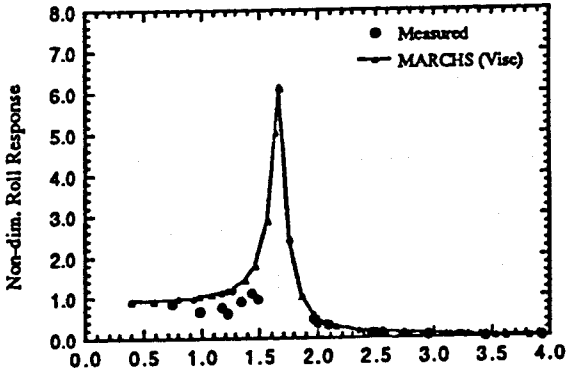

SWATH-3 model Roll responses
in quartering seas (Fn=0.00)

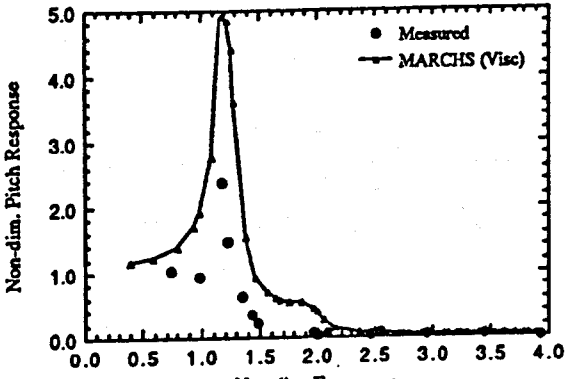

SWATH-3 model Pitch responses
in quartering seas (Fn=0.00)

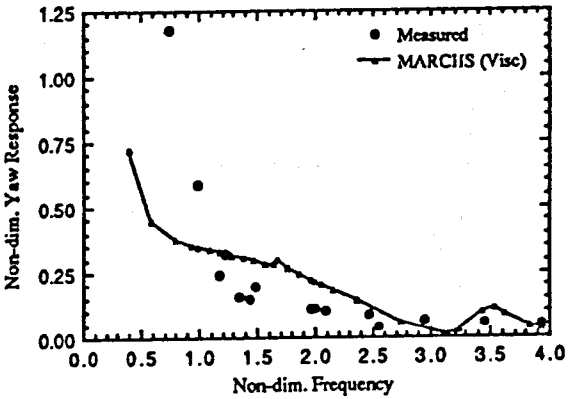

SWATH-3 model Yaw responses
in quartering seas (Fn=0.00)

Figure A14. SWATH-3 model motions in bow-quartering seas
(Fn=0.00)

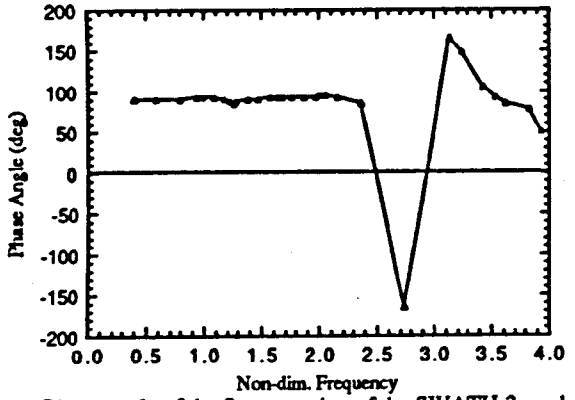

Phase angle of the Surge motion of the SWATH-3 model in quartering seas (Fn=0.00)

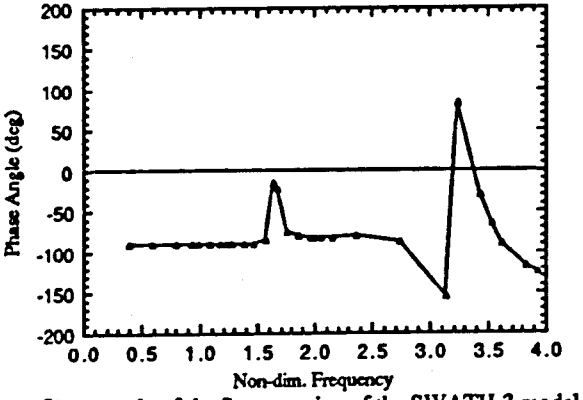

Phase angle of the Sway motion of the SWATH-3 model in quartering seas (Fn=0.00)

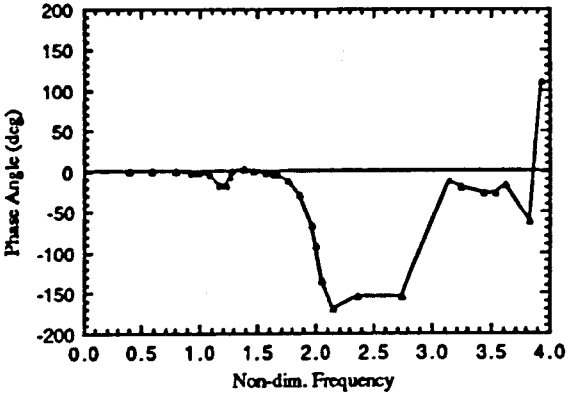

Phase angle of the Heave motion of the SWATH-3 model in quartering seas (Fn=0.00)

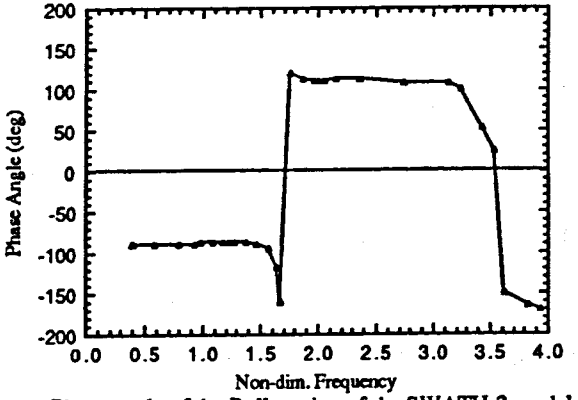

Phase angle of the Roll motion of the SWATH-3 model in quartering seas (Fn=0.00)

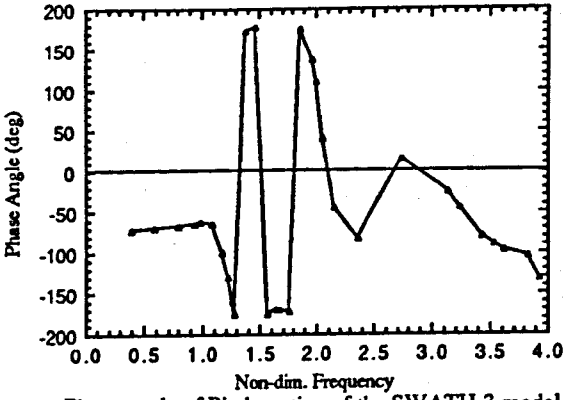

Phase angle of Pitch motion of the SWATH-3 model in quartering seas (Fn=0.00)

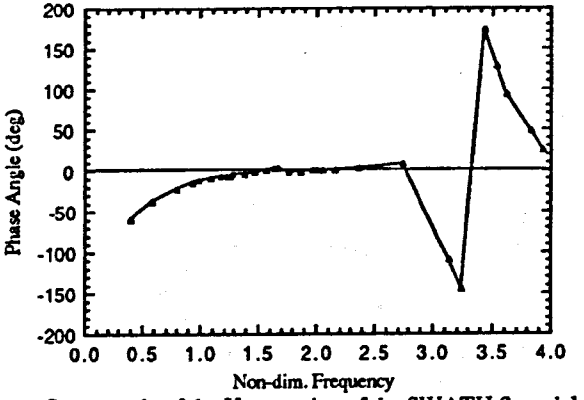

Phase angle of the Yaw motion of the SWATH-3 model in quartering seas (Fn=0.00)

Figure A15. SWATH-3 phase angle of motions in bow-quartering seass (Fn=0.00)

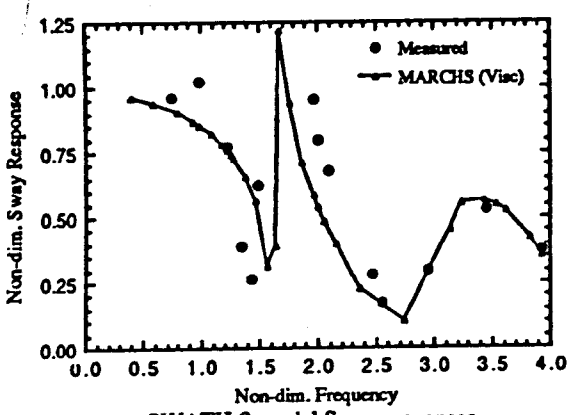

SWATH-3 model Sway responses
in beam seas (Fn=0.00)

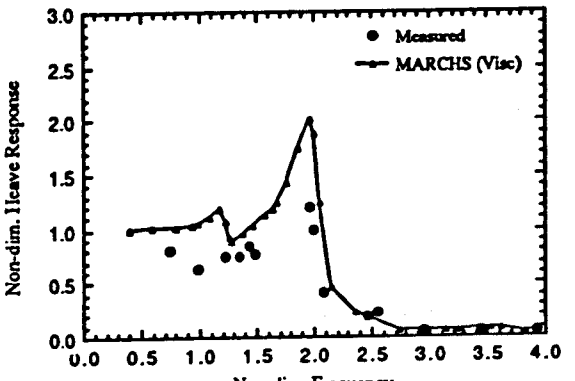

SWATH-3 model Heave responses
in beam seas (Fn=0.00)

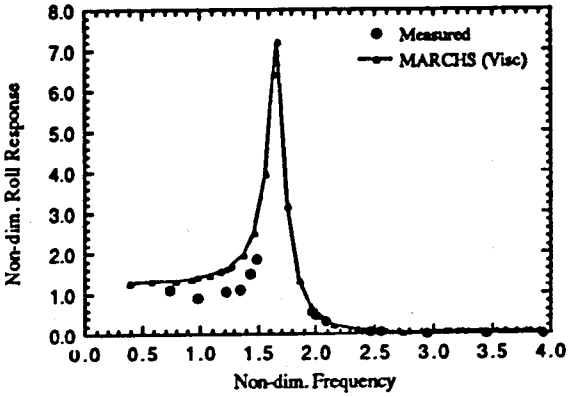

SWATH-3 model Roll responses
in beam seas (Fn=0.00)

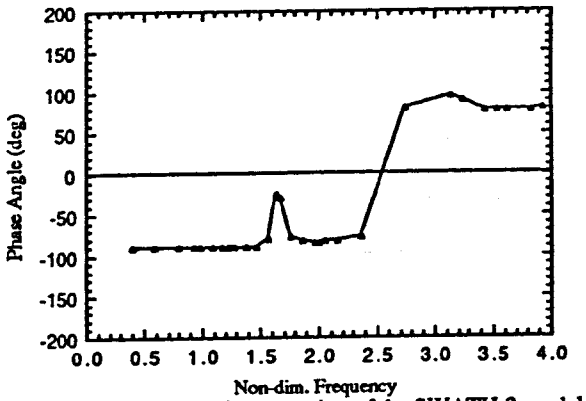

Phase angle of the Sway motion of the SWATH-3 model
in beam seas (Fn=0.00)

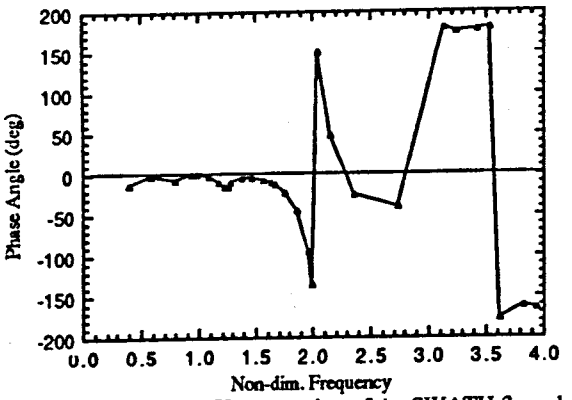

Phase angle of the Heave motion of the SWATH-3 model
in beam seas (Fn=0.00)

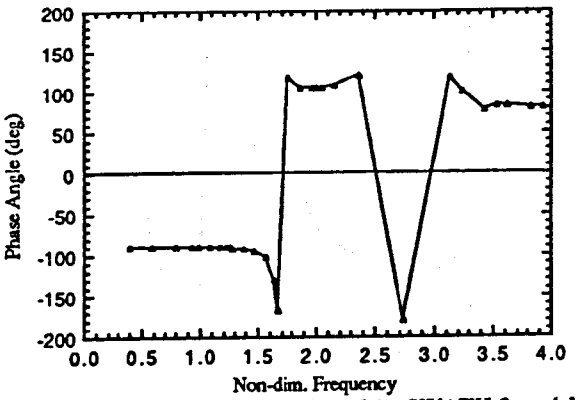

Phase angle of the Roll motion of the SWATH-3 model
in beam seas (Fn=0.00)

Figure A16. SWATH-3 model motions and phase angles
in beam seas (Fn=0.00)

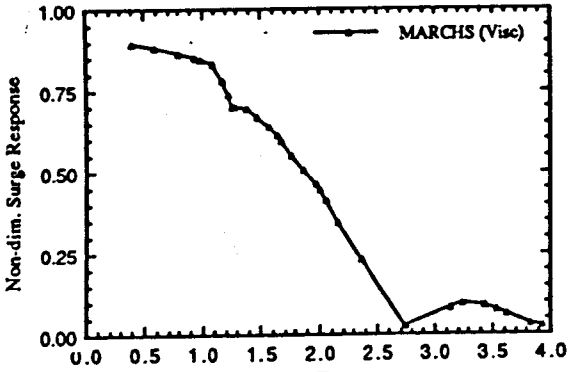

SWATH-3 model Surge responses
in following seas (Fn=0.00)

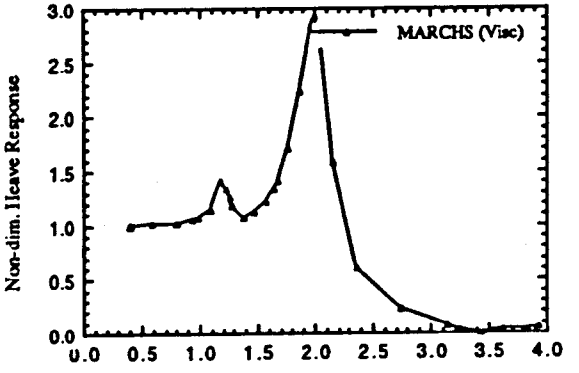

SWATH-3 model Heave responses
in following seas (Fn=0.00)

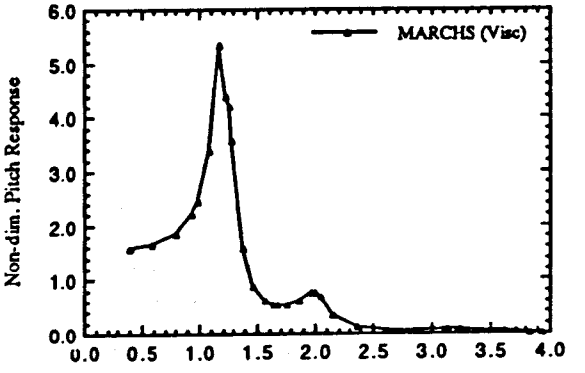

SWATH-3 model Pitch responses
in following seas (Fn=0.00)

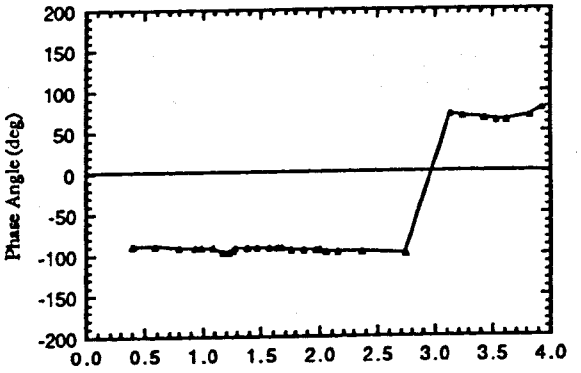

Phase angle of the Surge motion of the SWATH-3 model
in following seas (Fn=0.00)

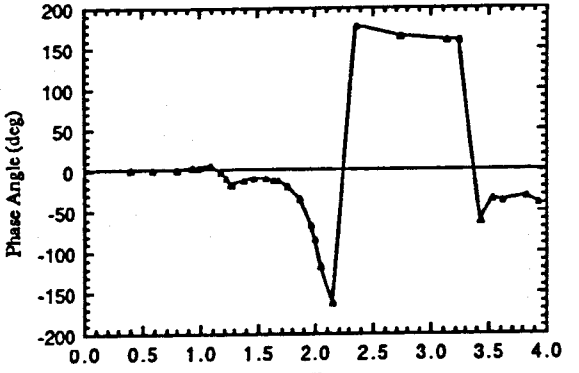

Phase angle of the Heave motion of the SWATH-3 model
in following seas (Fn=0.00)

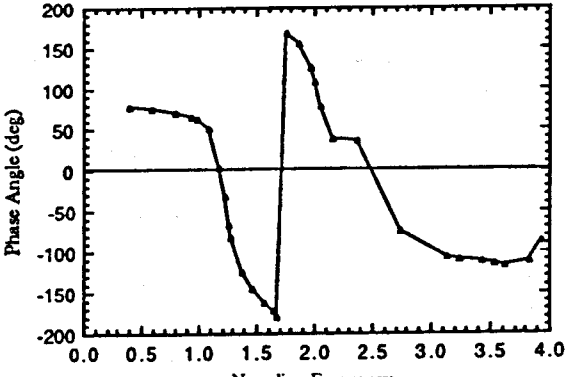

Phase angle of the Pitch motion of the SWATH-3 model
in following seas (Fn=0.00)

Figure A17. SWATH-3 model motions and phase angles
in following seas (Fn=0.00)

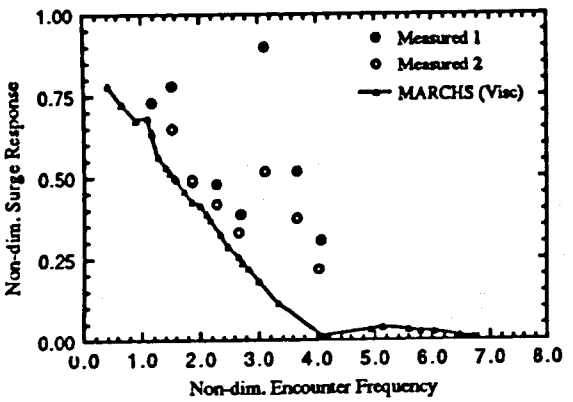

SWATH-3 model Surge responses in head seas (Fn=0.18)

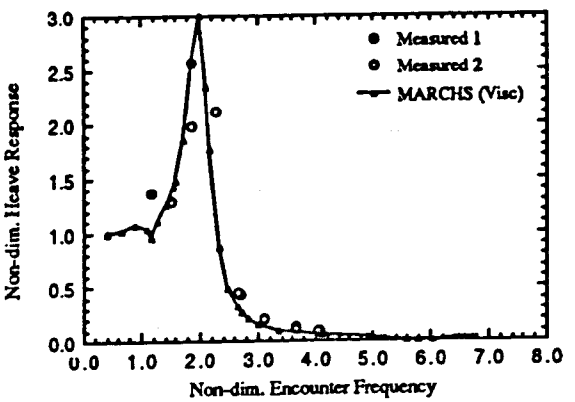

SWATH-3 model Heave responses in head seas (Fn=0.18)

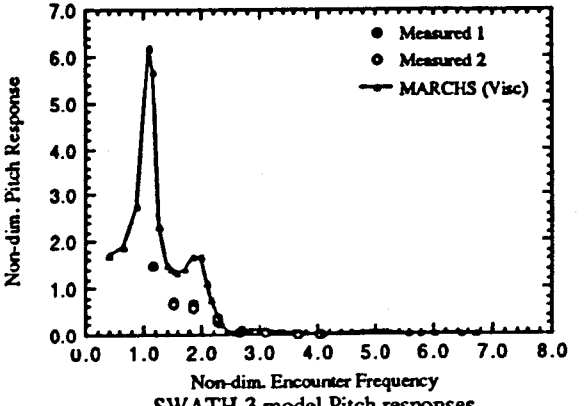

SWATH-3 model Pitch responses in head seas (Fn=0.18)

Figure A18. SWATH-3 model motions in head seas (Fn=0.18)

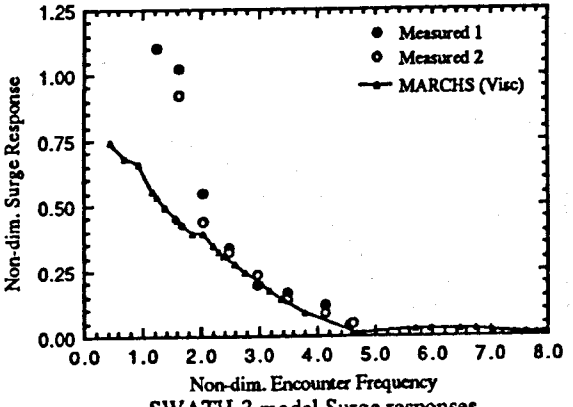

SWATH-3 model Surge responses in head seas (Fn=0.26)

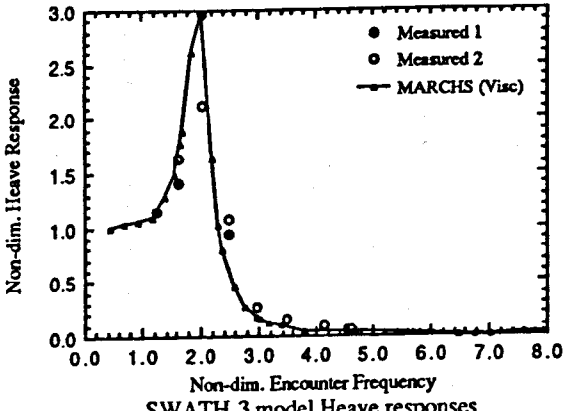

SWATH-3 model Heave responses in head seas (Fn=0.26)

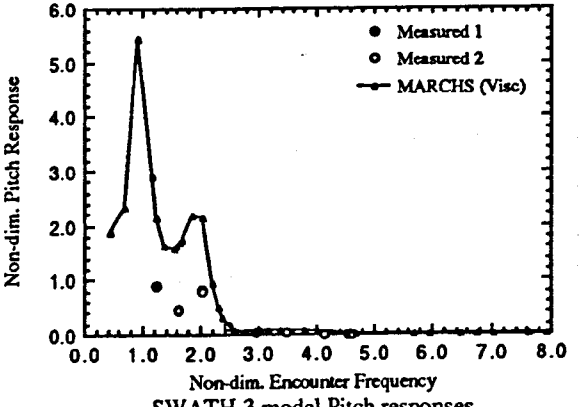

SWATH-3 model Pitch responses in head seas (Fn=0.26)

Figure A19. SWATH-3 model motions in head seas (Fn=0.26)

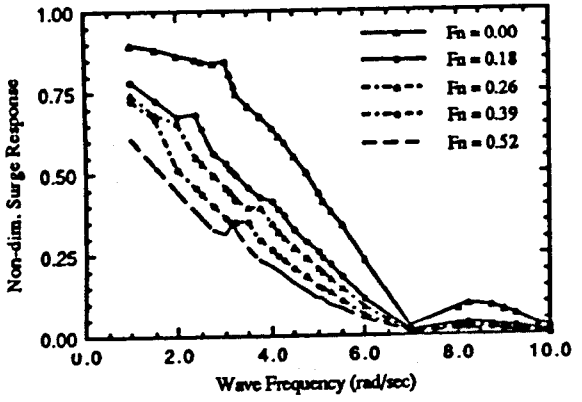

SWATH-3 model Surge responses in head seas

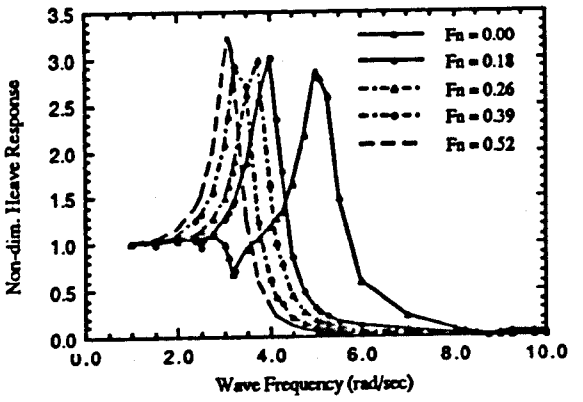

SWATH-3 model Heave responses in head seas

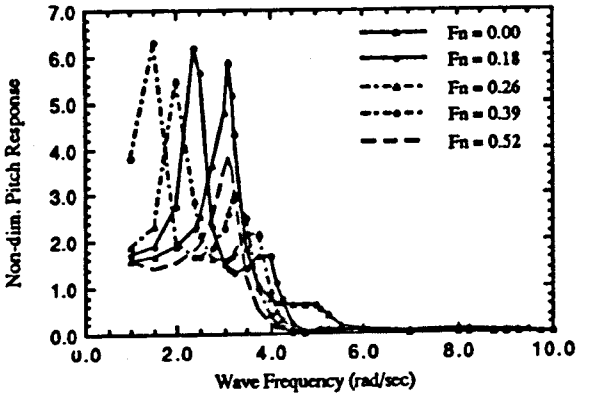

SWATH-3 model Pitch responses in head seas

Figure A20. SWATH-3 model motions in head seas at various Froude numbers

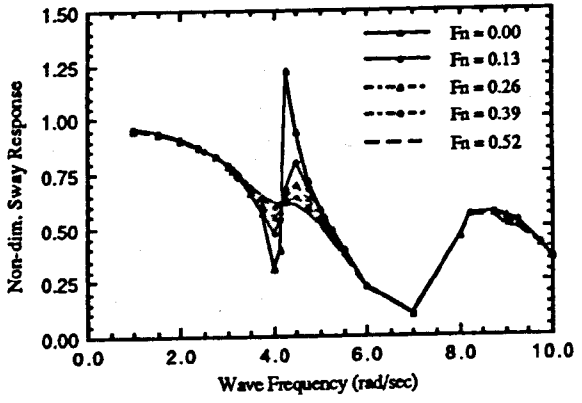

SWATH-3 model Sway responses in beam seas

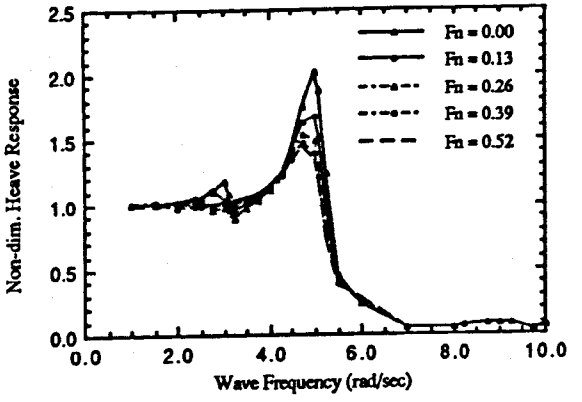

SWATH-3 model Heave responses in beam seas

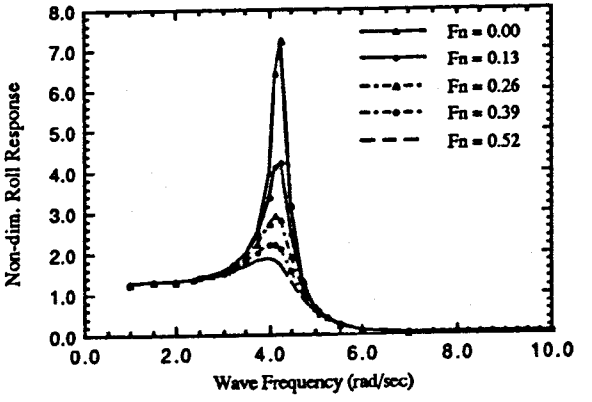

SWATH-3 model Roll responses in beam seas

Figure A21. SWATH-3 model motions in beams seas at various Froude numbers

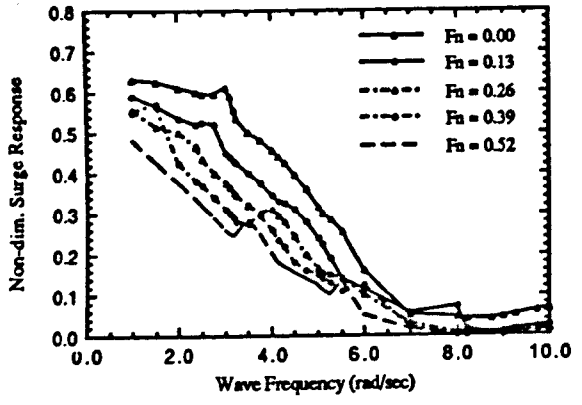

SWATH-3 model Surge reponses in quartering seas

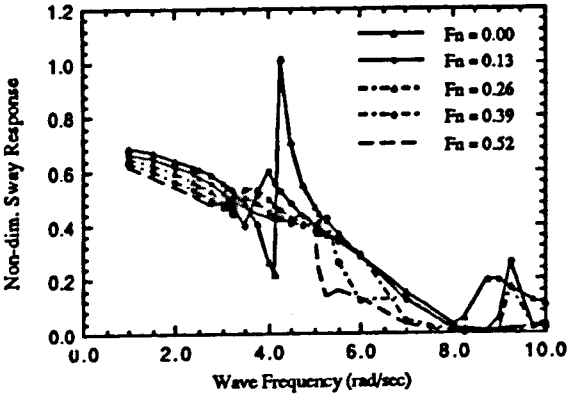

SWATH-3 model Sway responses in quartering seas

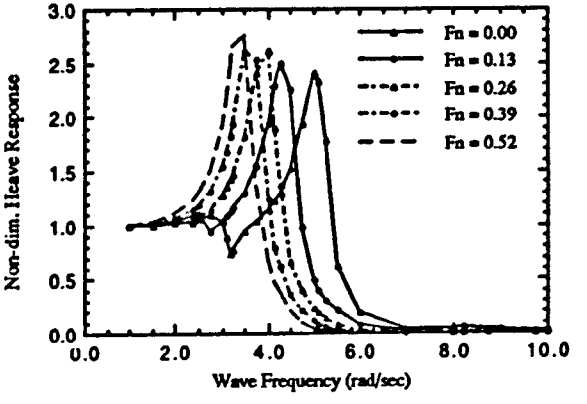

SWATH-3 model Heave responses in quartering seas

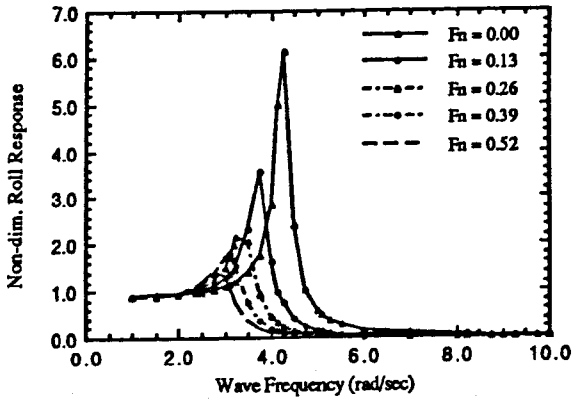

SWATH-3 model Roll responses in quartering seas

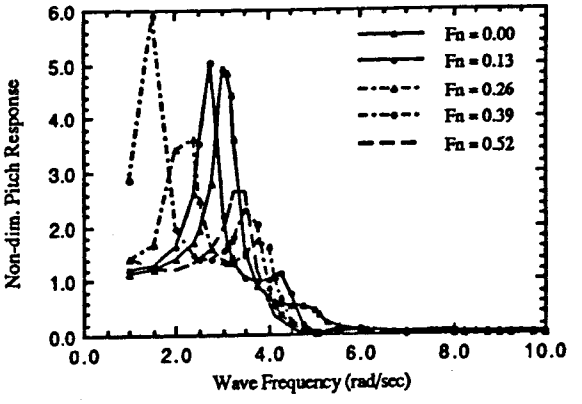

SWATH-3 model Pitch responses in quartering seas

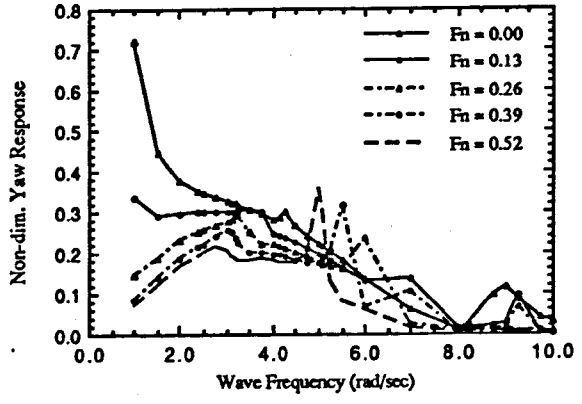

SWATH-3 model Yaw responses in quartering seas

Figure A22. SWATH-3 model motions in bow-quartering seas at various Froude numbers

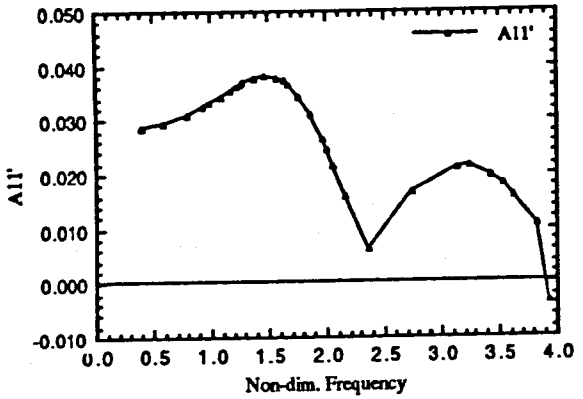

Surge added mass coefficient of SWATH-3

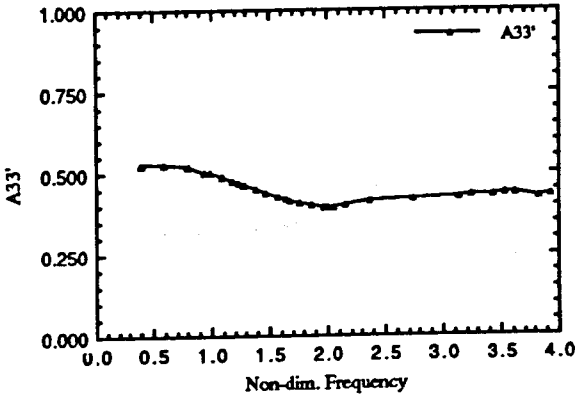

Heave added mass coefficient of SWATH-3

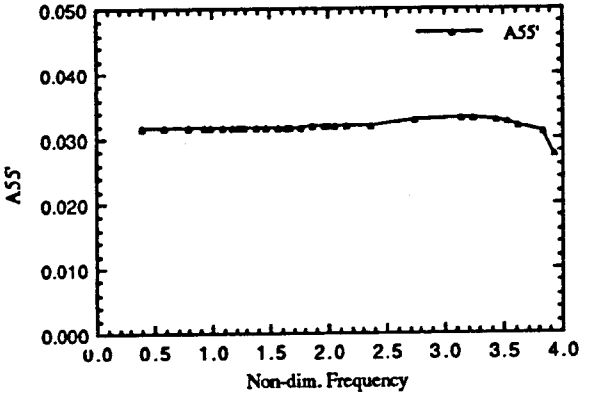

Pitch added inertia coefficient of SWATH-3

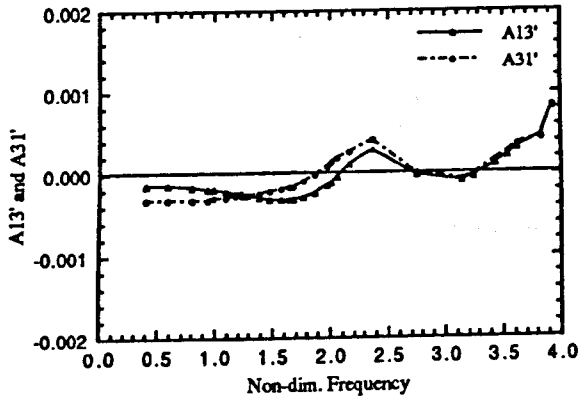

Surge-heave coupled added mass coefficients of SWATH-3

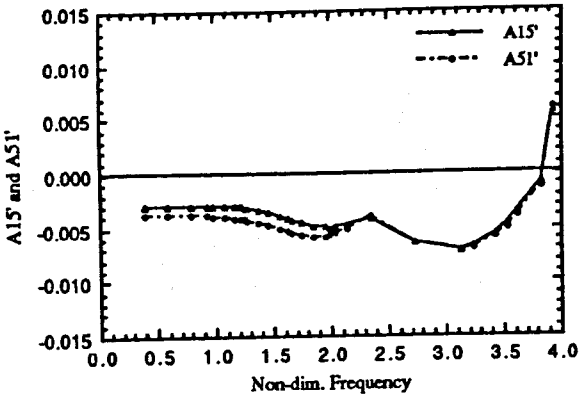

Surge-pitch coupled added mass coefficients of SWATH-3

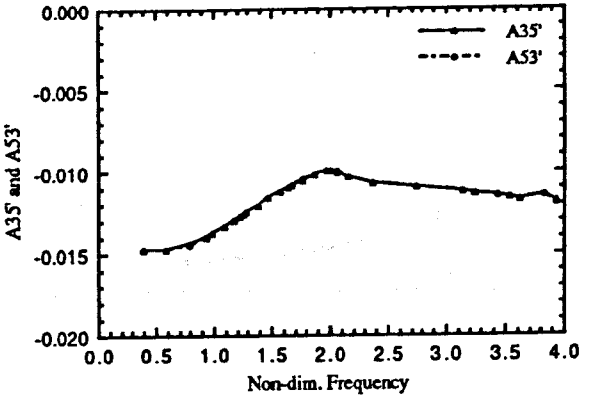

Heave-pitch coupled added mass coefficients of SWATH-3

Figure A23. Added mass and inertia coefficients for vertical motions of SWATH-3 model (Fn=0.00)

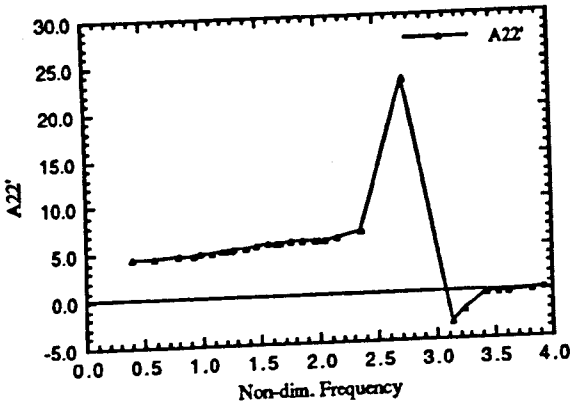

Sway added mass coefficient of SWATH-3

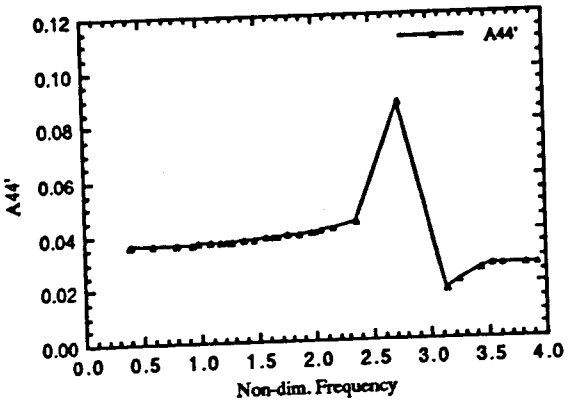

Roll added inertia coefficient of SWATH-3

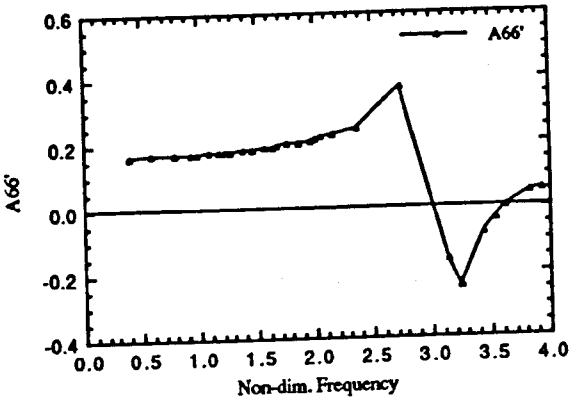

Yaw added inertia coefficient of SWATH-3

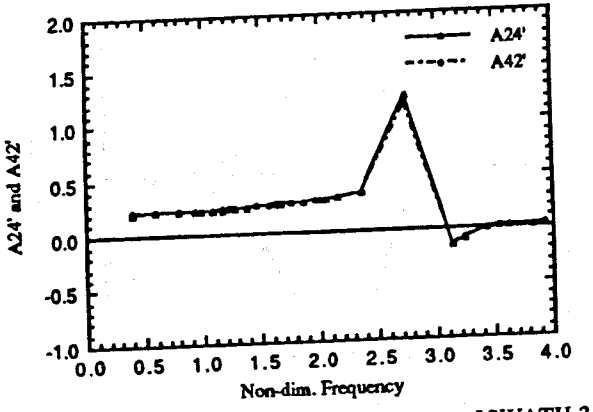

Sway-roll coupled added mass coefficients of SWATH-3

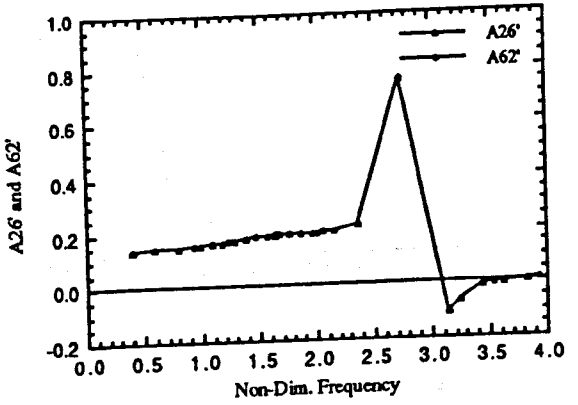

Sway-yaw added mass coefficients of SWATH-3

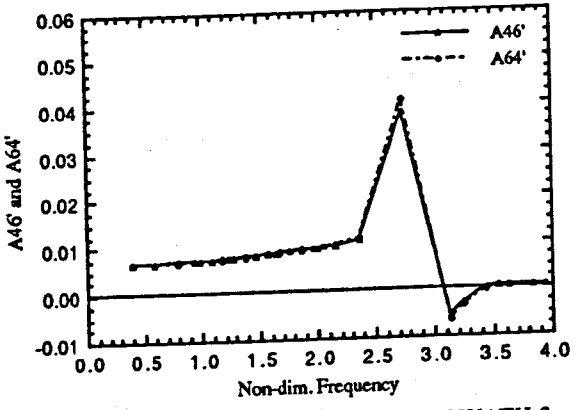

Roll-yaw added inertia coefficients of SWATH-3

Figure A24. Added mass and inertia coefficients for horizontal motions of SWATH-3 model (Fn=0.00)

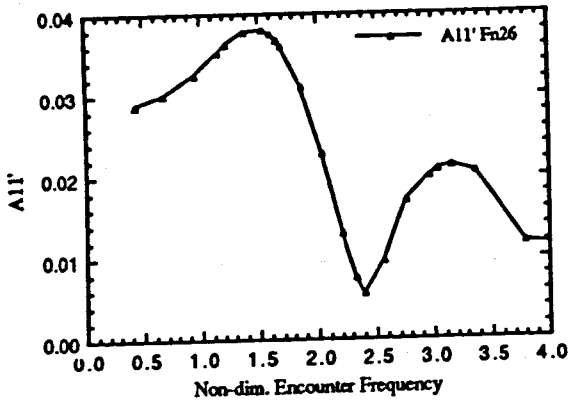

Surge added mass coefficient of SWATH-3 (Fn=0.26)

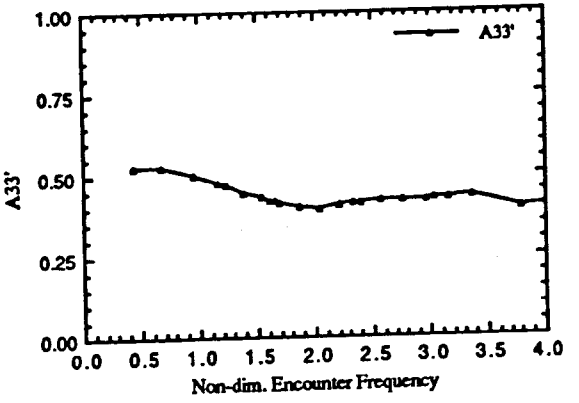

Heave added mass coefficient of SWATH3 (Fn=0.26)

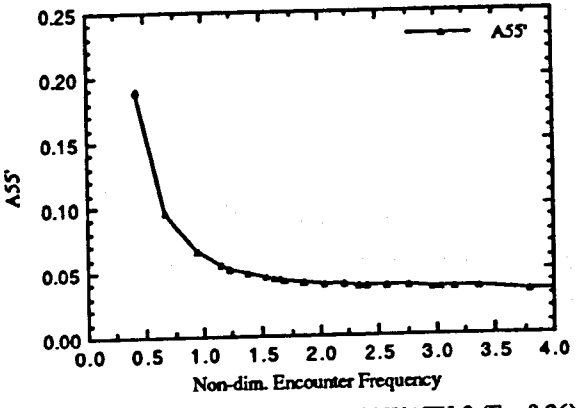

Pitch added inertia coefficient of SWATH-3 (Fn=0.26)

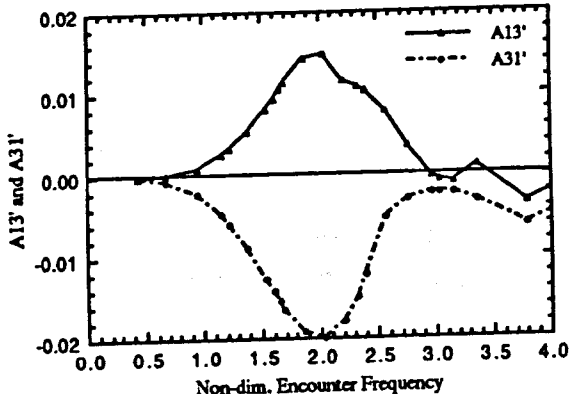

Surge-heave coupled added mass coefficients of SWATH-3 (Fn=0.26)

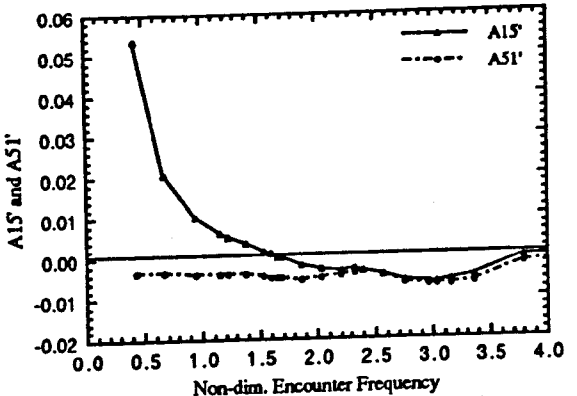

Surge-pitch coupled added mass coefficients of SWATH-3 (Fn=0.26)

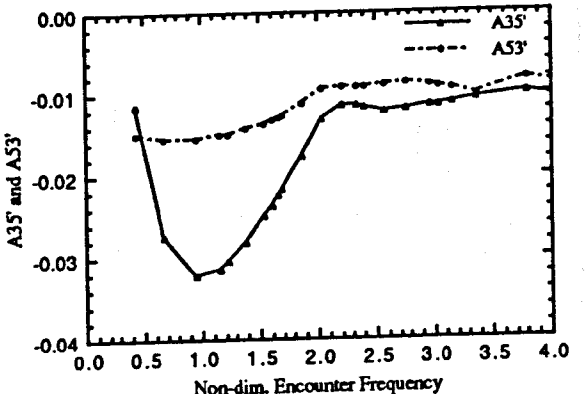

Heave-pitch coupled added mass coefficients of SWATH-3 (Fn=0.26)

Figure A25. Added mass and inertia coefficients for vertical motions of SWATH-3 model (Fn=0.26)

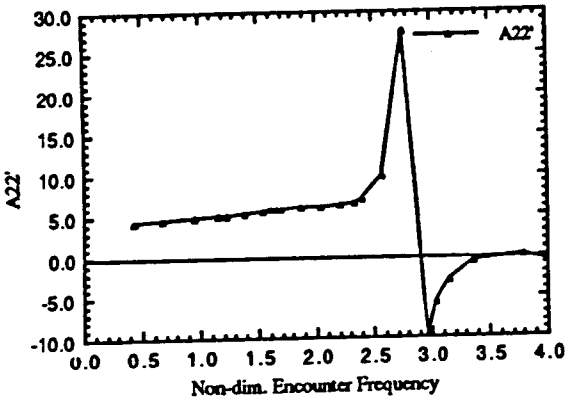

Sway added mass coefficient of SWATH-3 (Fn=0.26)

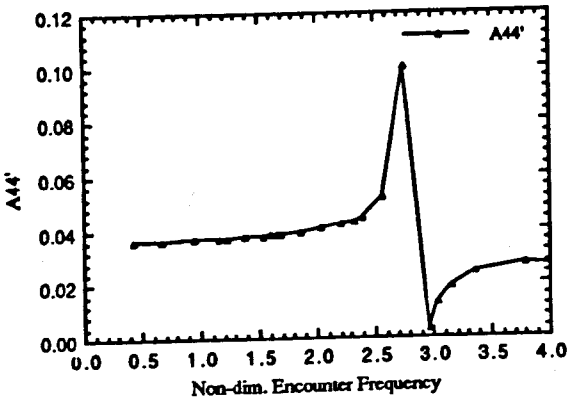

Roll added inertia coefficient of SWATH-3 (Fn=0.26)

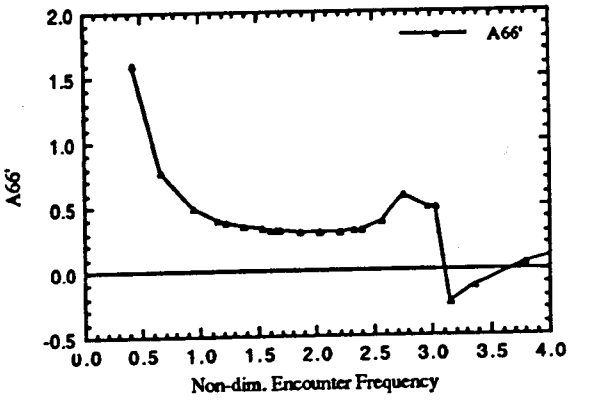

Yaw added inertia coefficient of SWATH-3 (Fn=0.26)

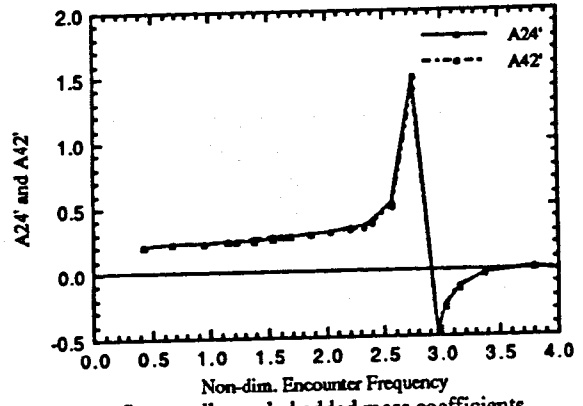

Sway-roll coupled added mass coefficients of SWATH-3 (FN=0.26)

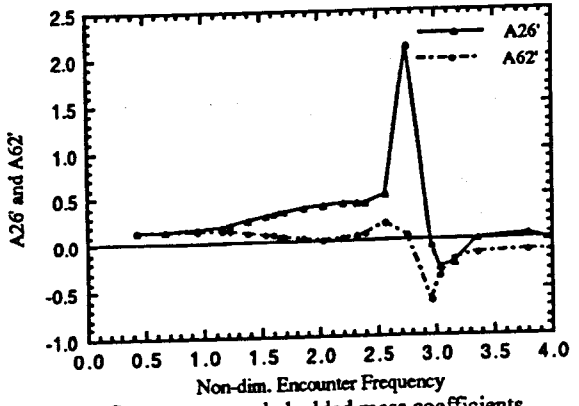

Sway-yaw coupled added mass coefficients of SWATH-3 (Fn=0.26)

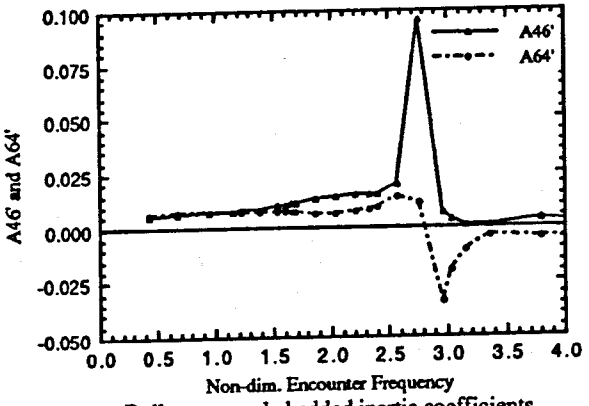

Roll-yaw coupled added inertia coefficients of SWATH-3 (Fn=0.26)

Figure A26. Added mass and inertia coefficients for horizontal motions of SWATH-3 model (Fn=0.26)

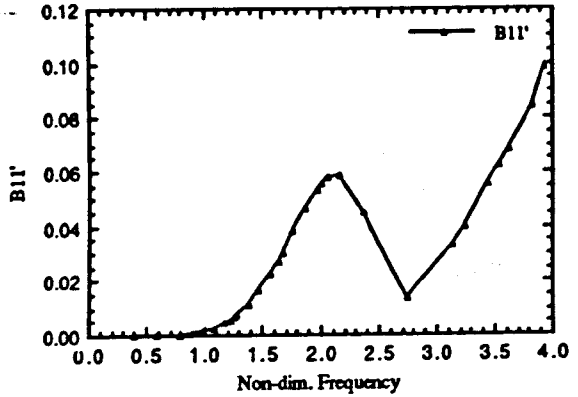

Surge damping coefficient of SWATH-3

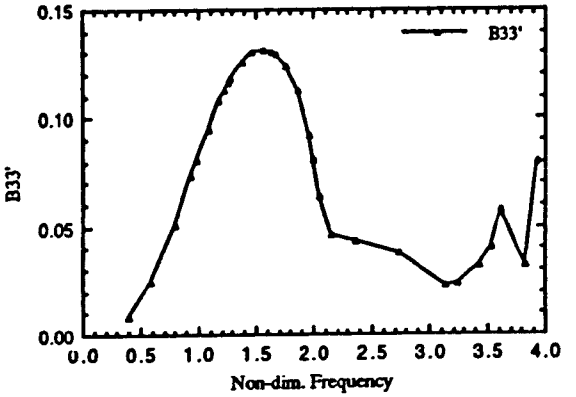

Heave damping coefficient of SWATH-3

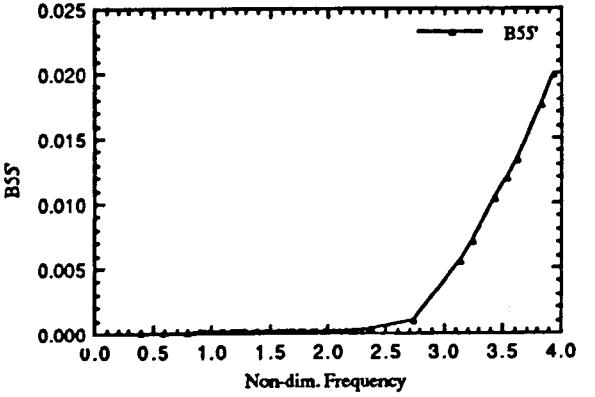

Pitch damping coefficient of SWATH-3

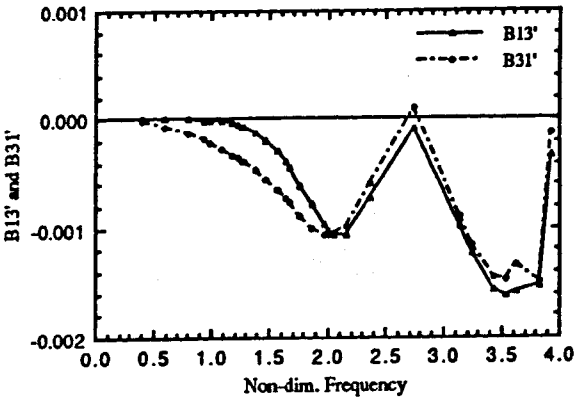

Surge-heave coupled damping coefficients of SWATH-3

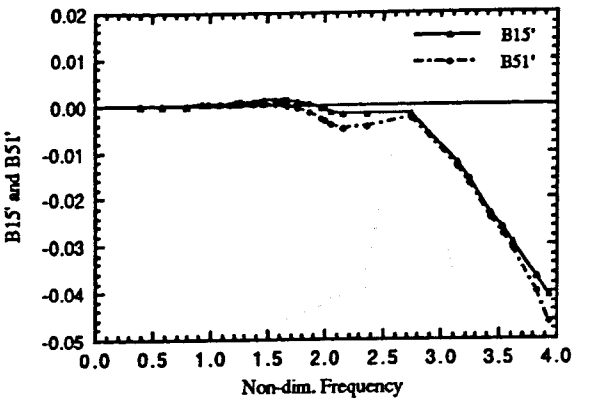

Surge-pitch coupled damping coefficients of SWATH-3

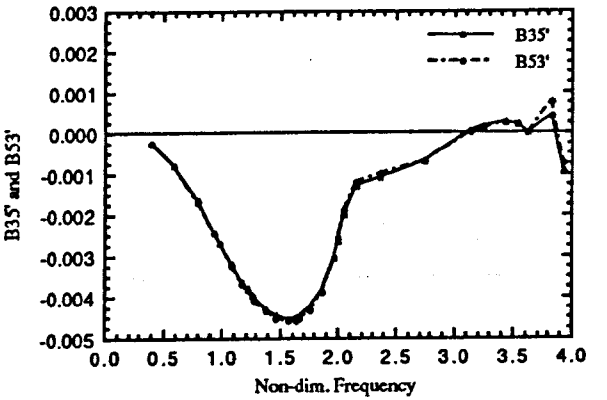

Heave-pitch coupled damping coefficients of SWATH-3

Figure A27. Damping coefficients for vertical motions of SWATH-3 model (Fn=0.00)

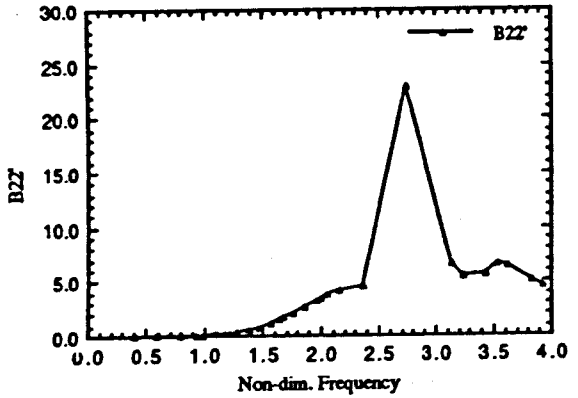

Sway damping coefficient of SWATH-3

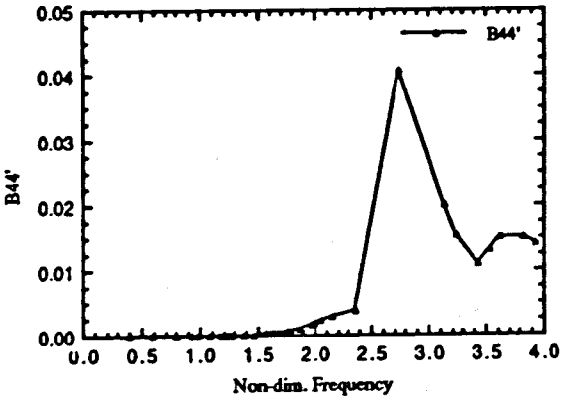

Roll damping coefficient of SWATH-3

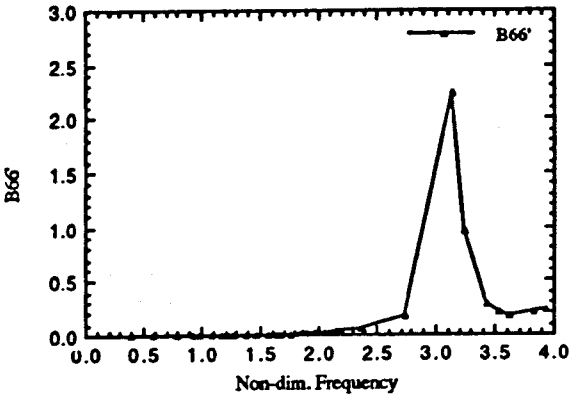

Yaw damping coefficient of SWATH-3

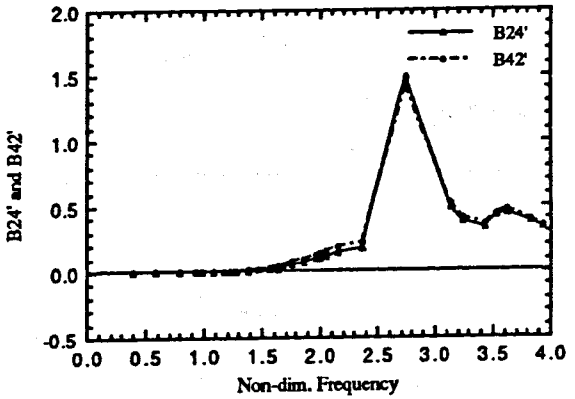

Sway-roll coupled damping coefficients of SWATH-3

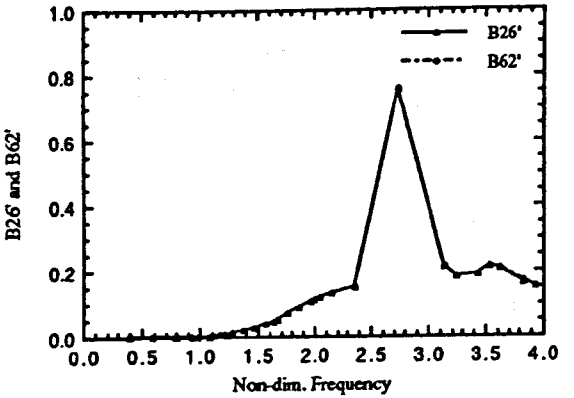

Surge-yaw coupled damping coefficients of SWATH-3

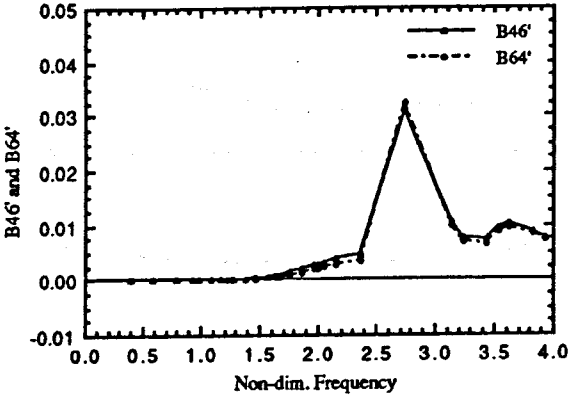

Roll-yaw coupled damping coefficients of SWATH-3

Figure A28. Damping coefficients for horizontal motions of SWATH-3 model (Fn=0.00)

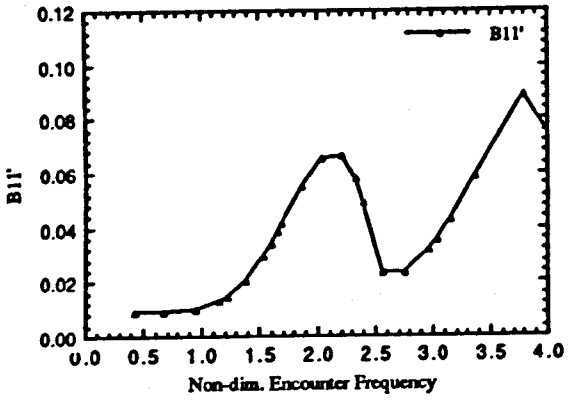

Surge damping coefficient of SWATH-3 (Fn=0.26)

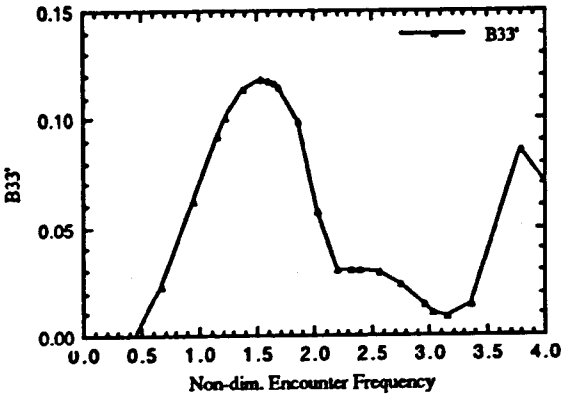

Heave damping coefficient of SWATH-3 (Fn=0.26)

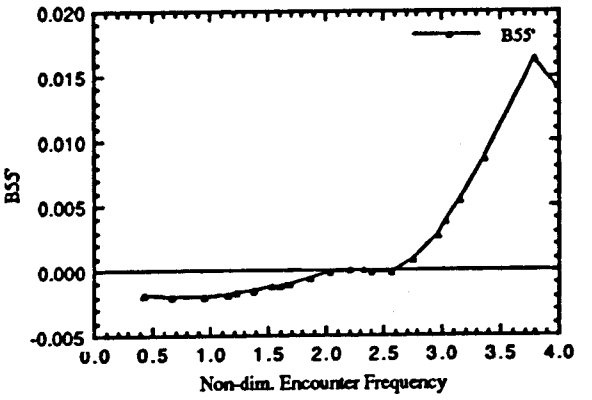

Pitch damping coefficient of SWATH-3 (Fn=0.26)

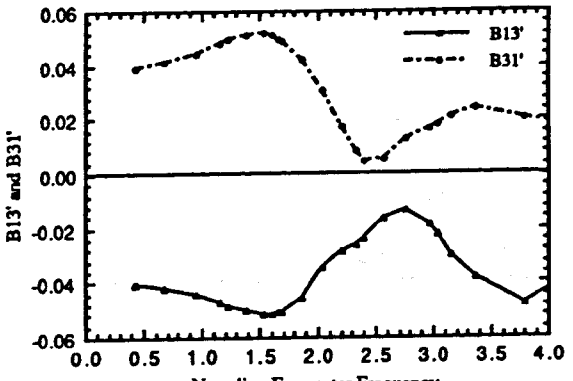

Surge-heave coupled damping coefficients of SWATH-3 (Fn=0.26)

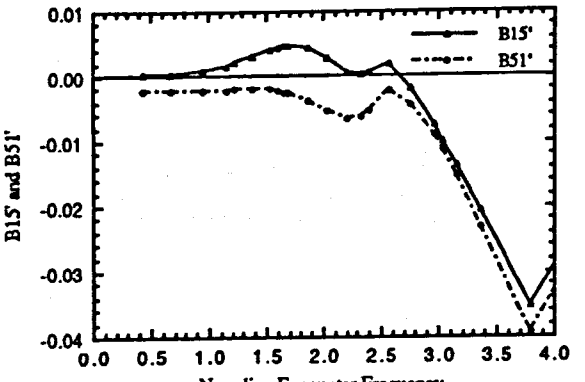

Surge-pitch coupled damping coefficients of SWATH-3 (Fn=0.26)

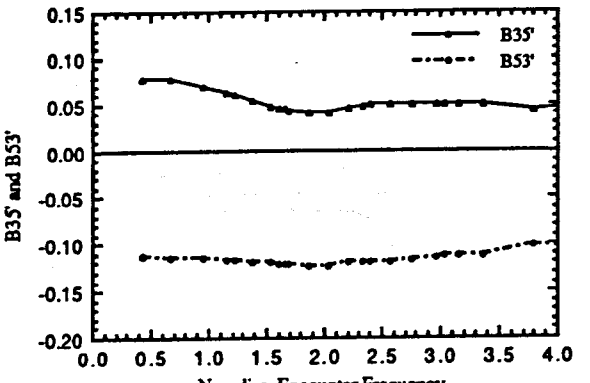

Heave-pitch coupled damping coefficients of SWATH-3 (Fn=0.26)

Figure A29. Damping coefficients for vertical motions of SWATH-3 model (Fn=0.26)

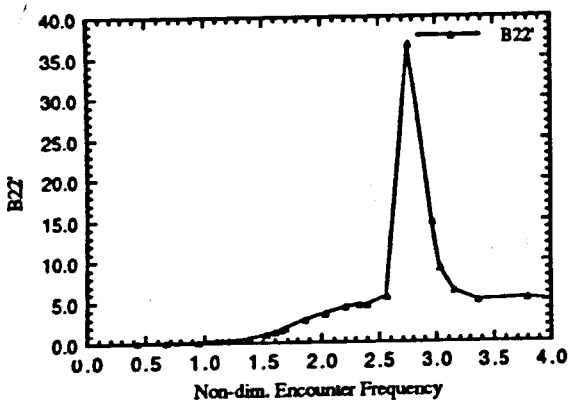

Sway damping coefficient of SWATH-3 (Fn=0.26)

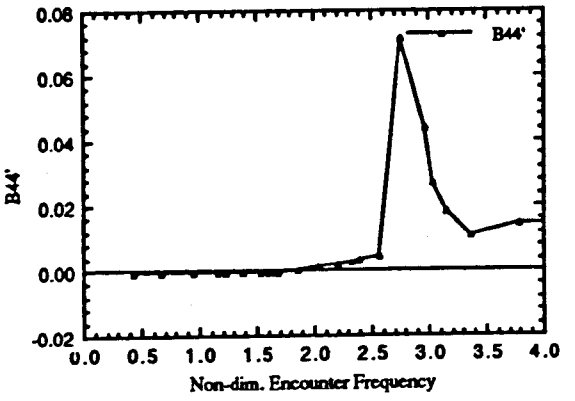

Roll damping coefficient of SWATH-3 (Fn=0.26)

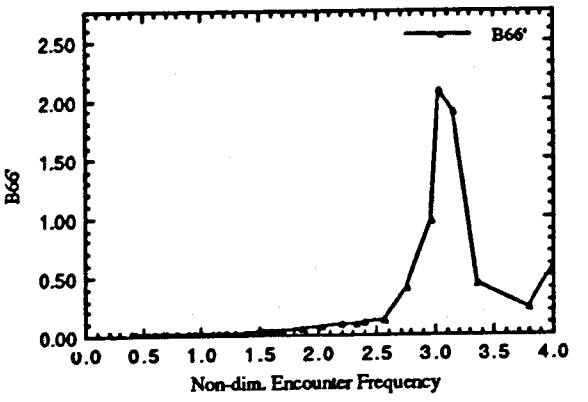

Yaw damping coefficient of SWATH-3 (Fn=0.26)

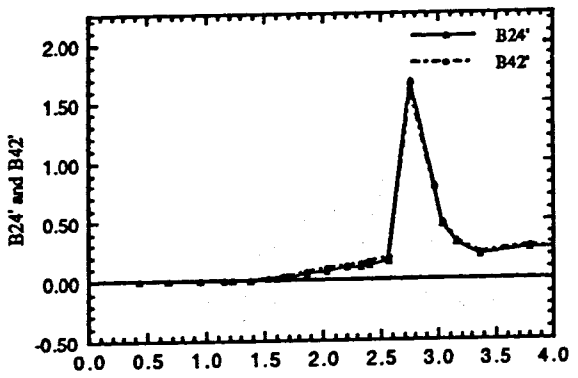

Sway-roll coupled damping coefficients of SWATH-3 (Fn=0.26)

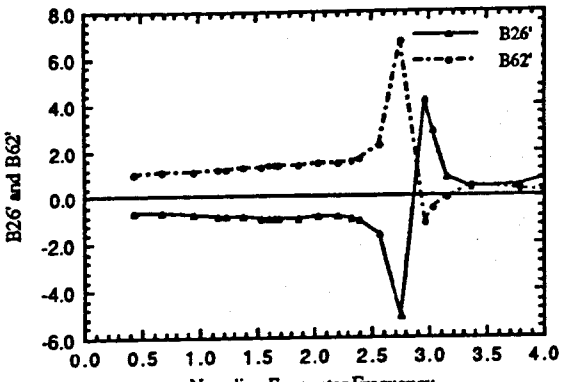

Sway-yaw coupled damping coefficients of SWATH-3 (Fn=0.26)

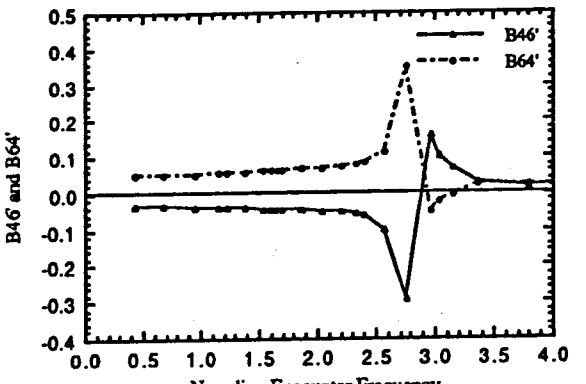

Roll-yaw coupled damping coefficients of SWATH-3 (Fn=0.26)

Figure A30. Damping coefficients for horizontal motions of SWATH-3 model (Fn=0.26)

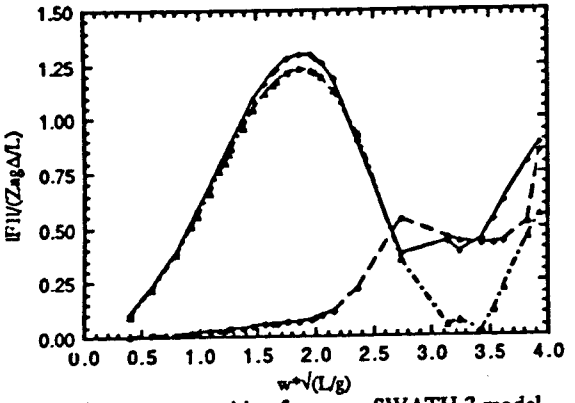

Surge wave exciting forces on SWATH-3 model in quartering seas (Fn=0.00)

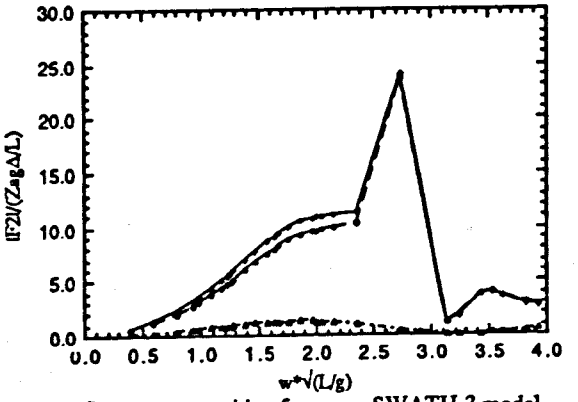

Sway wave exciting forces on SWATH-3 model in quartering seas (Fn=0.00)

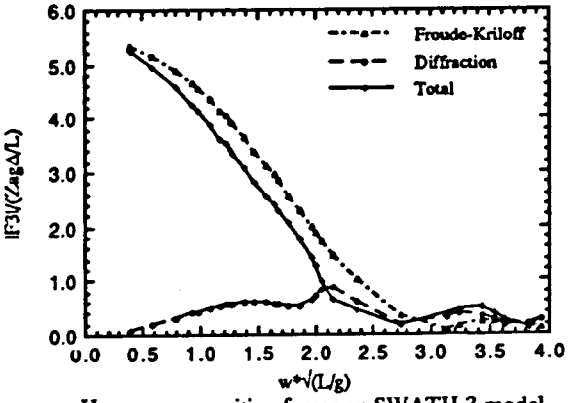

Heave wave exciting forces on SWATH-3 model in quartering seas (Fn=0.00)

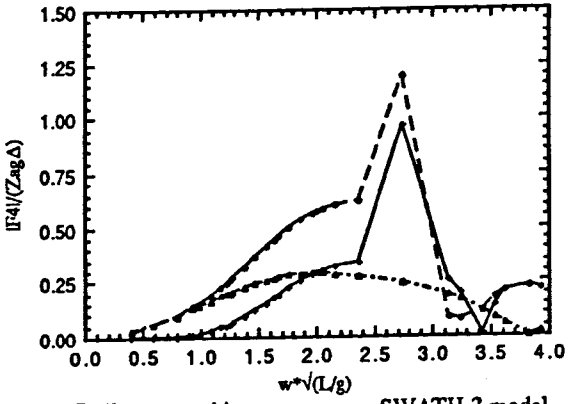

Roll wave exciting moments on SWATH-3 model in quartering seas (Fn=0.00)

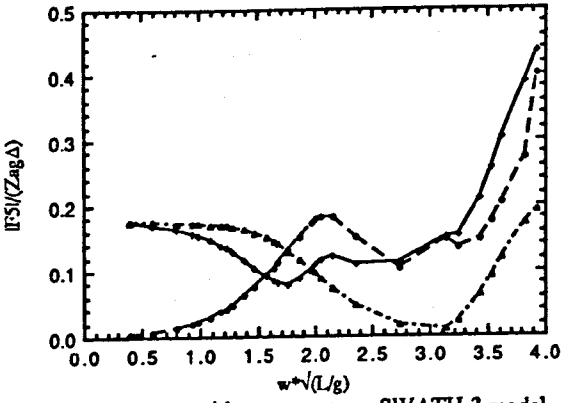

Pitch wave exciting moments on SWATH-3 model in quartering seas (Fn=0.00)

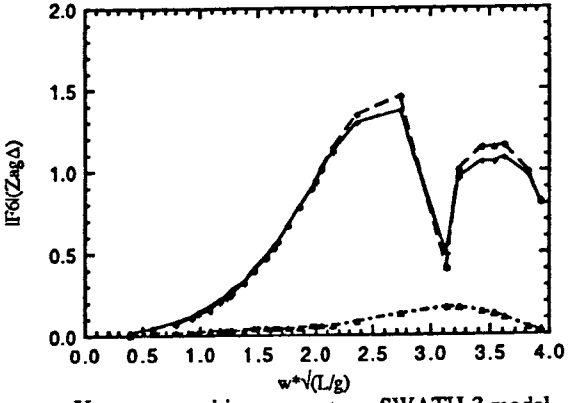

Yaw wave exciting moments on SWATH-3 model in quartering seas (Fn=0.00)

Figure A31. Wave exciting forces and moments on SWATH-3 model in bow-quartering seas (Fn=0.00)

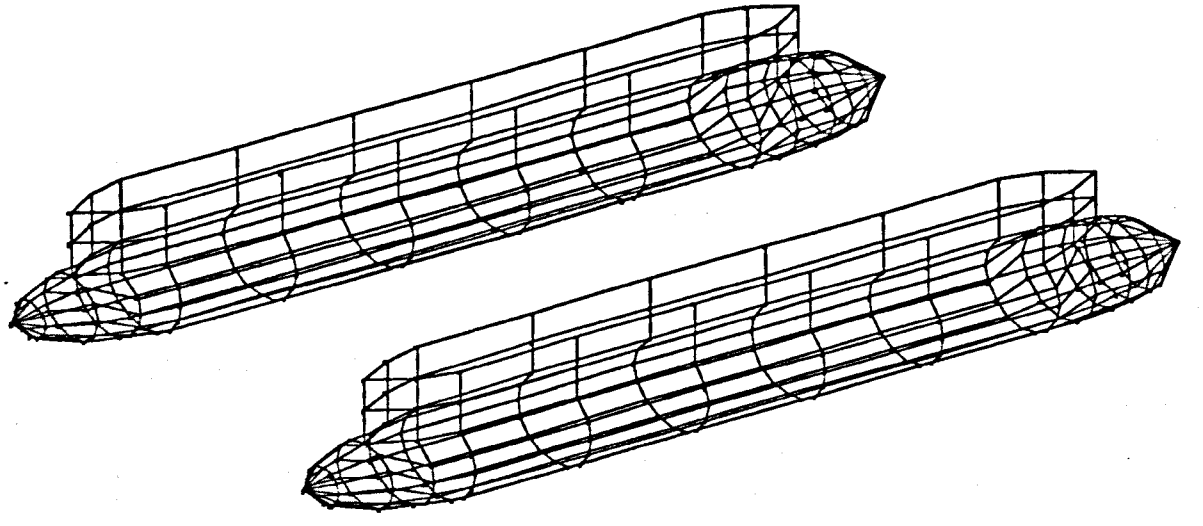

Figure A32. Discretisation of SWATH-FV model
(Number of panels = 408)

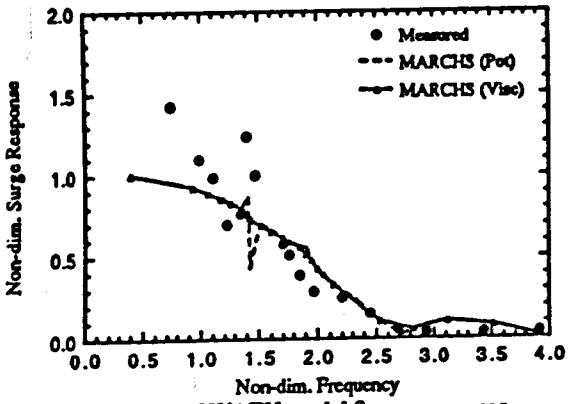

Fishing SWATH model Surge responses in head seas (Fn=0.00)

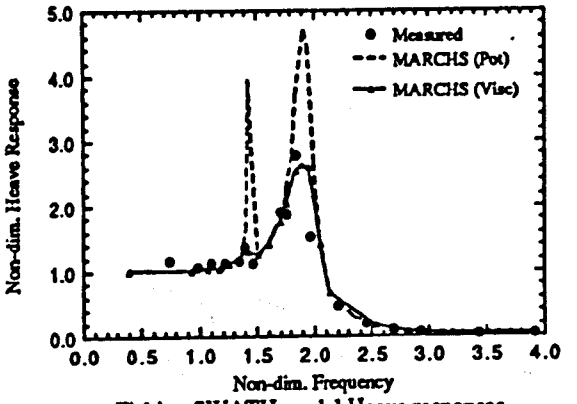

Fishing SWATH model Heave responses in head seas (Fn=0.00)

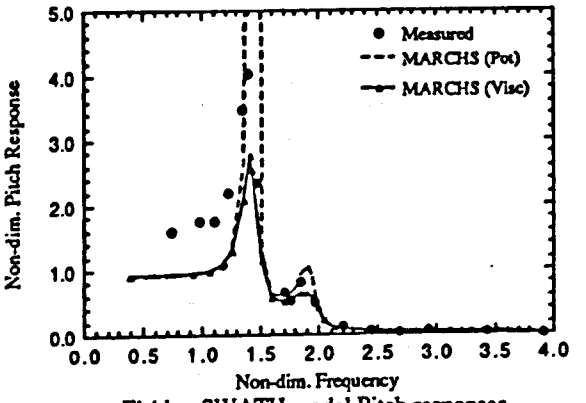

Fishing SWATH model Pitch responses in head seas (Fn=0.00)

Figure A33. SWATH-FV model motions in head seas (Fn=0.00)

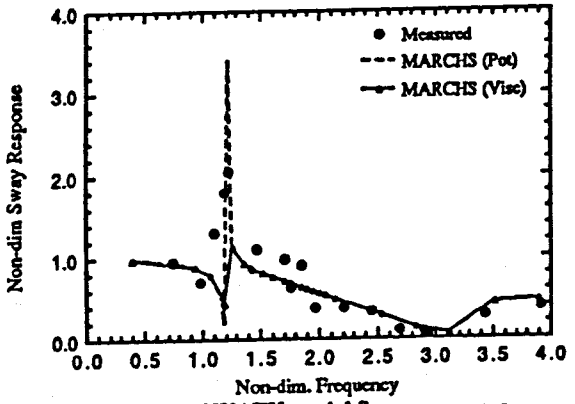

Fishing SWATH model Sway responses in beam seas (Fn=0.00)

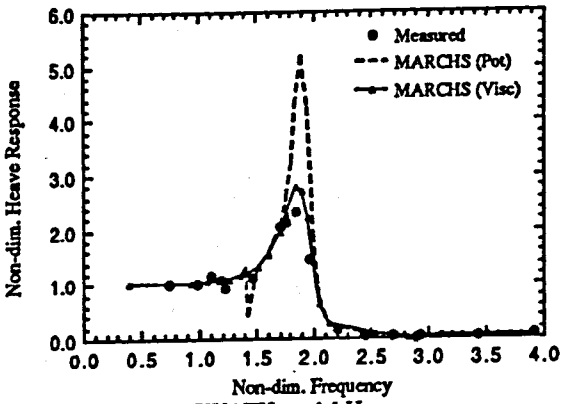

Fishing SWATH model Heave responses in beam seas (Fn=0.00)

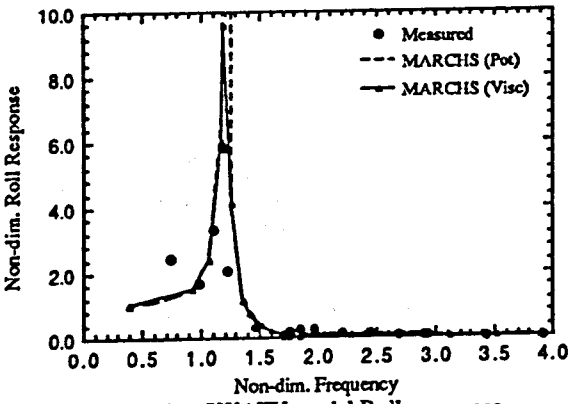

Fishing SWATH model Roll responses in beam seas (Fn=0.00)

Figure A34. SWATH-FV model motions in beam seas (Fn=0.00)

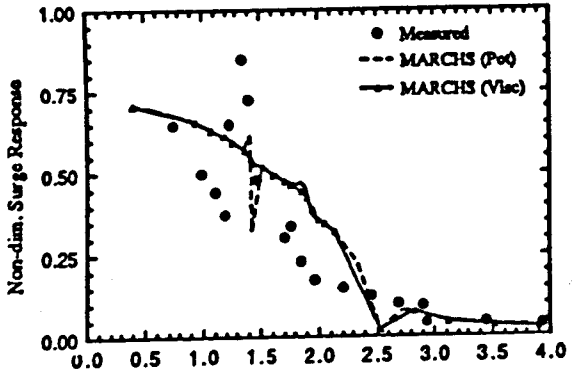

Fishing SWATH model Surge responses in quartering seas (Fn=0.00)

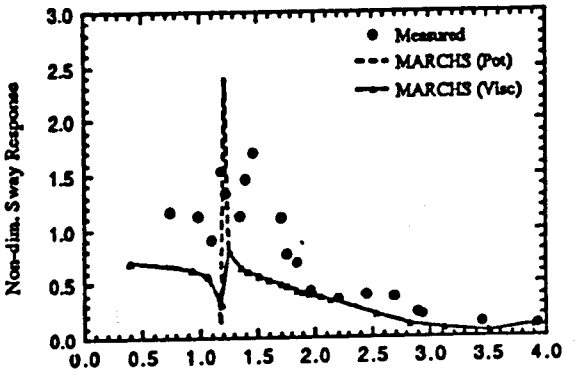

Fishing SWATH model Sway responses in quartering seas (Fn=0.00)

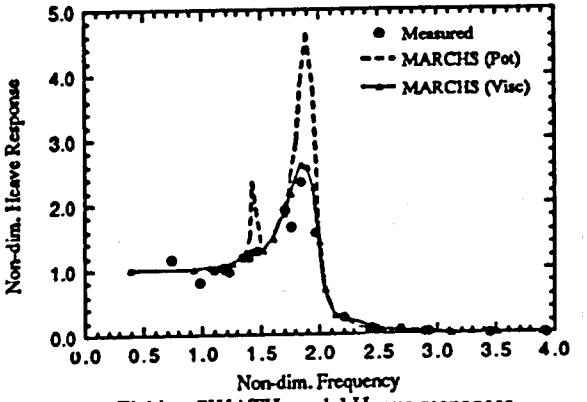

Fishing SWATH model Heave responses in quartering seas (Fn=0.00)

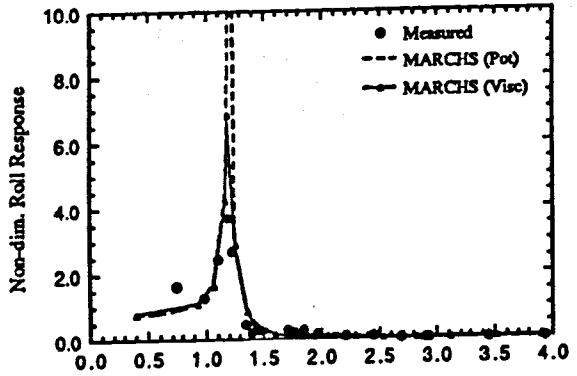

Fishing SWATH model Roll responses in quartering seas (Fn=0.00)

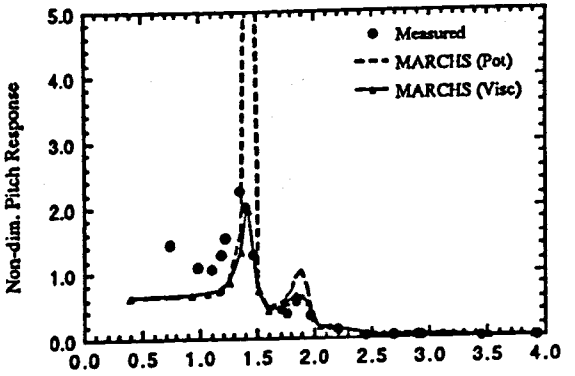

Fishing SWATH model Pitch responses in quartering seas (Fn=0.00)

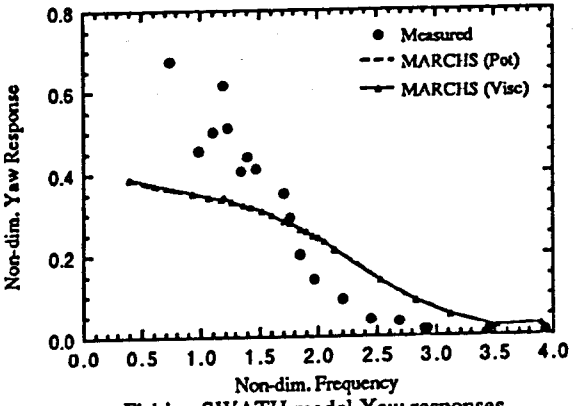

Fishing SWATH model Yaw responses in quartering seas (Fn=0.00)

Figure A35. SWATH-FV model motions in bow-quartering seas (Fn=0.00)

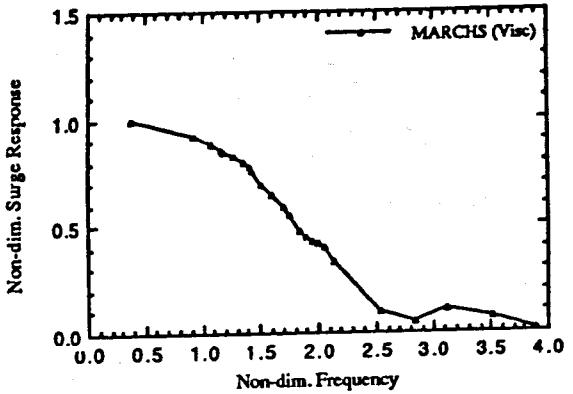

Fishing SWATH model Surge responses in following seas (Fn=0.00)

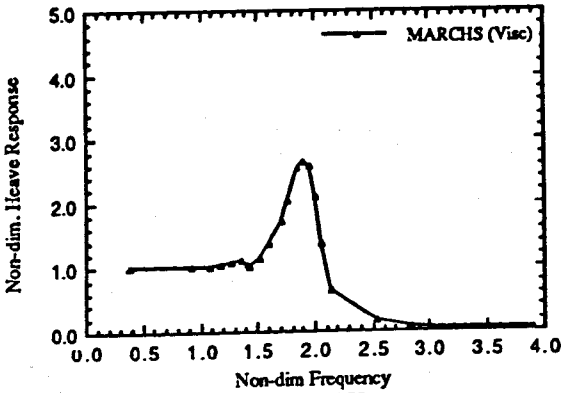

Fishing SWATH model Heave responses in following seas (Fn=0.00)

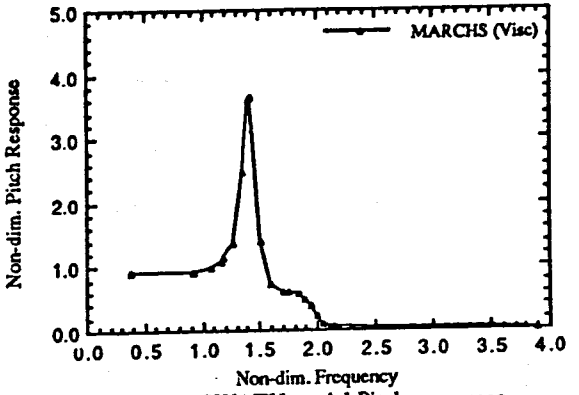

Fishing SWATH model Pitch responses in following seas (Fn=0.00)

Figure A36. SWATH-FV model motions in following seas (Fn=0.00)

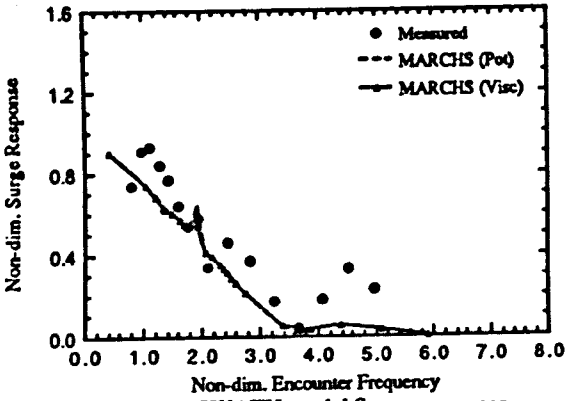

Fishing SWATH model Surge responses in head seas (Fn=0.13)

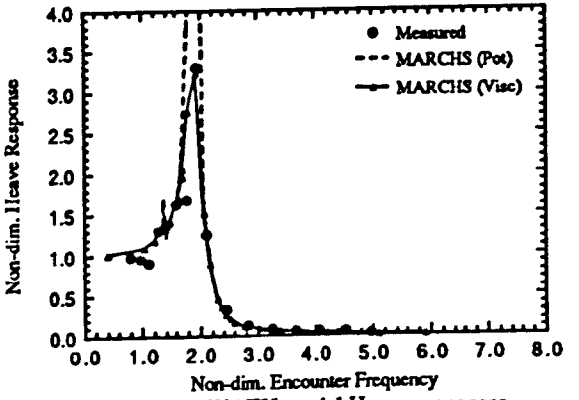

Fishing SWATH model Heave responses in head seas (Fn=0.13)

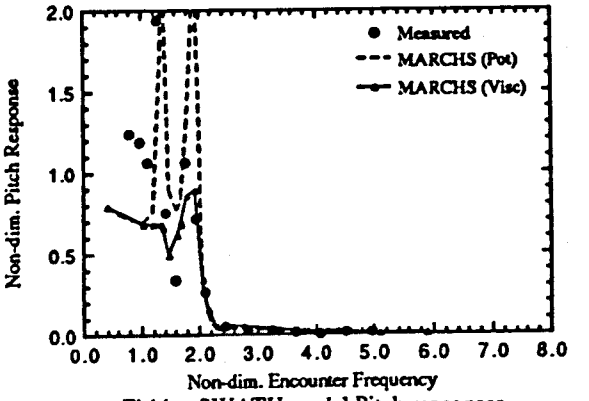

Fishing SWATH model Pitch responses in head seas (Fn=0.13)

Figure A37. SWATH-FV model motions in head seas (Fn=0.13)

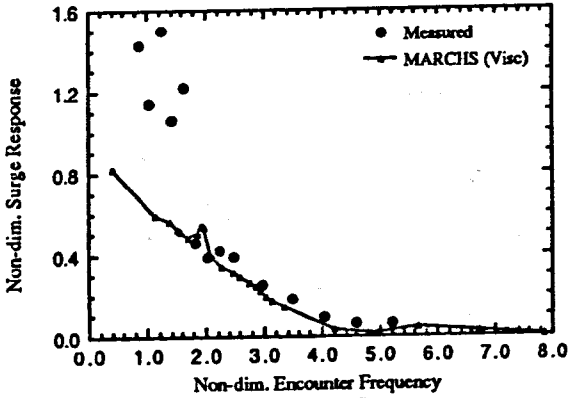

Fishing SWATH model Surge responses in head seas (Fn=0.26)

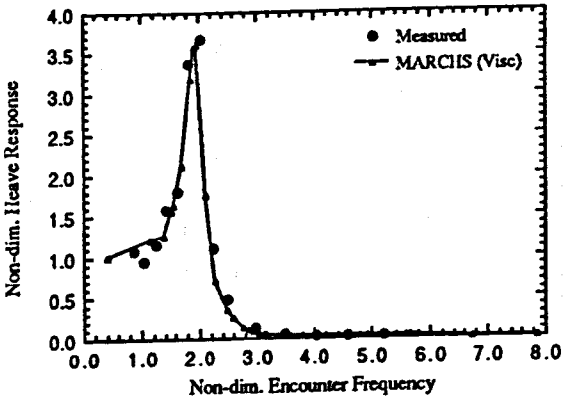

Fishing SWATH model Heave responses in head seas (Fn=0.26)

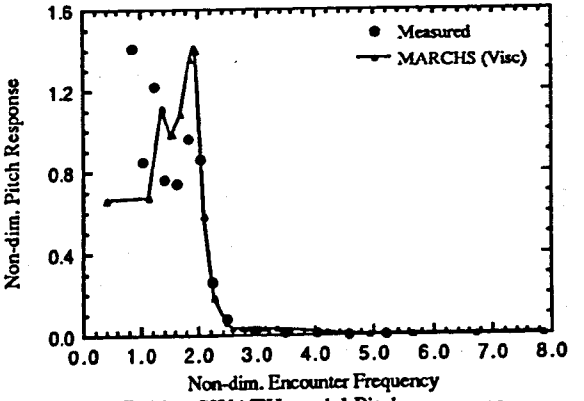

Fishing SWATH model Pitch responses in head seas (Fn=0.26)

Figure A38. SWATH-FV model motions in head seas (Fn=0.26)

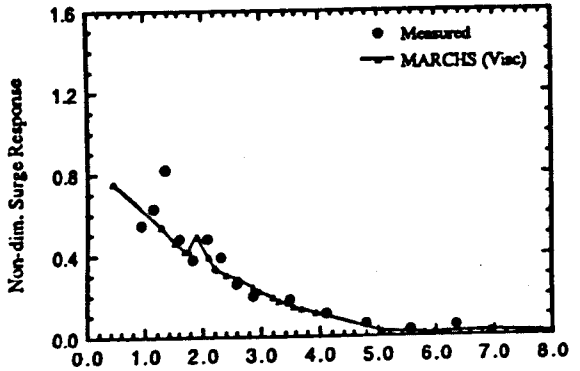

Fishing SWATH model Surge responses in head seas (Fn=0.39)

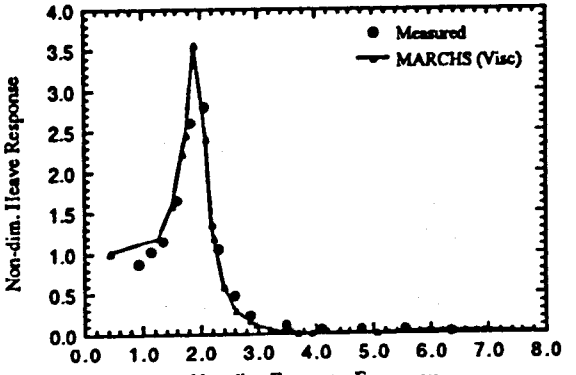

Fishing SWATH model Heave response in head seas (Fn=0.39)

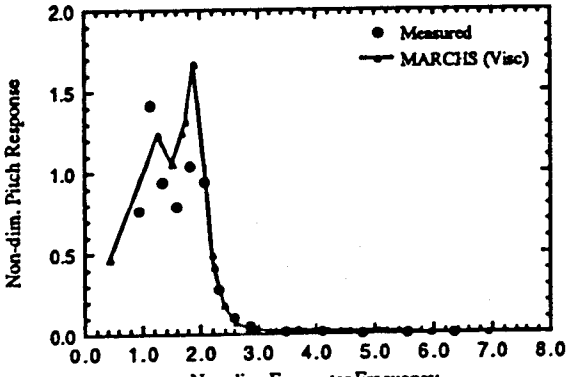

Fishing SWATH model Pitch responses in head seas (Fn=0.39)

Figure A39. SWATH-FV model motions in head seas (Fn=0.39)

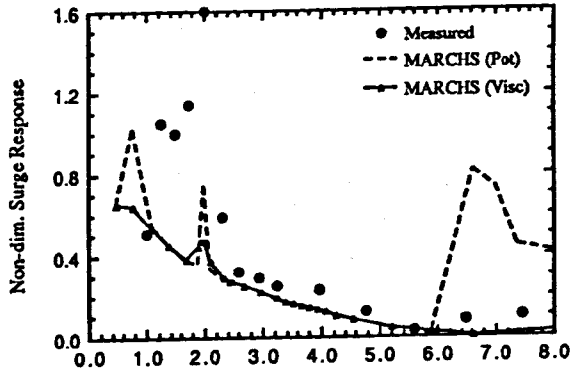

Fishing SWATH model Surge responses in head seas (Fn=0.52)

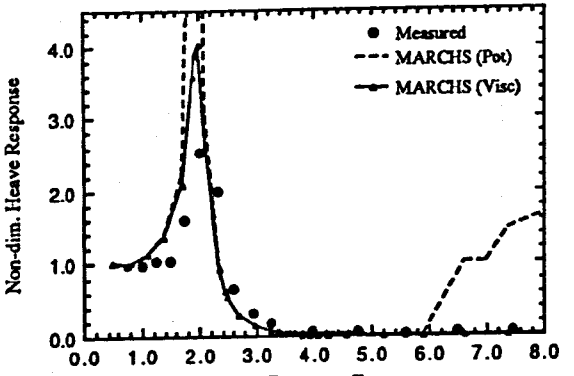

Fishing SWATH model Heave reponses in head seas (Fn=0.52)

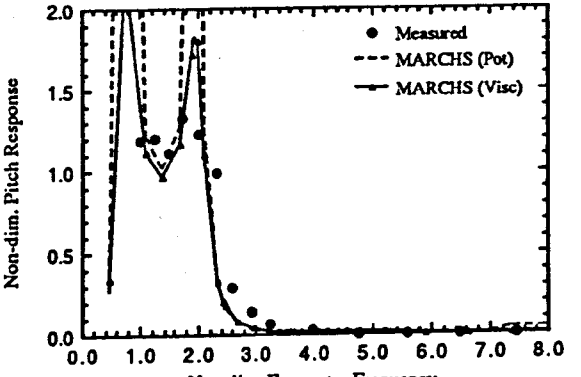

Fishing SWATH model Pitch responses in head seas (Fn=0.52)

Figure A40. SWATH-FV model motions in head seas (Fn=0.52)

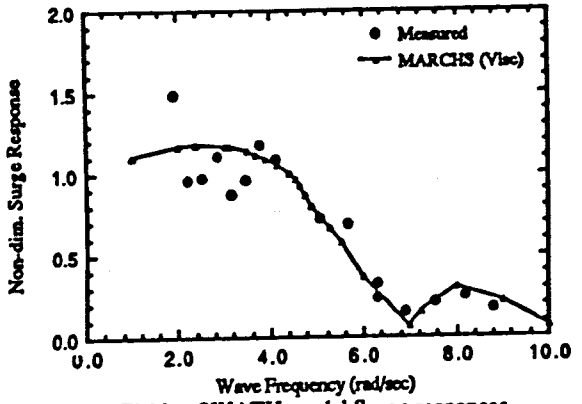

Fishing SWATH model Surge responses in following seas (Fn=0.13)

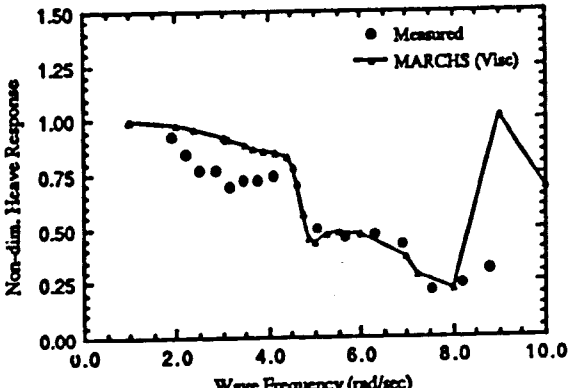

Fishing SWATH model Heave responses in following seas (Fn=0.13)

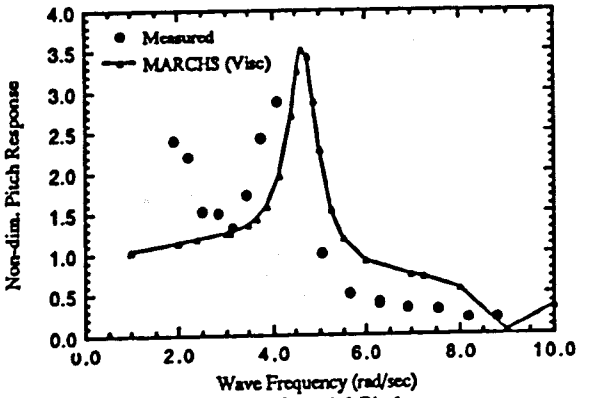

Fishing SWATH model Pitch responses in following seas (Fn=0.13)

Figure A41. SWATH-FV model motions in following seas (Fn=0.13)

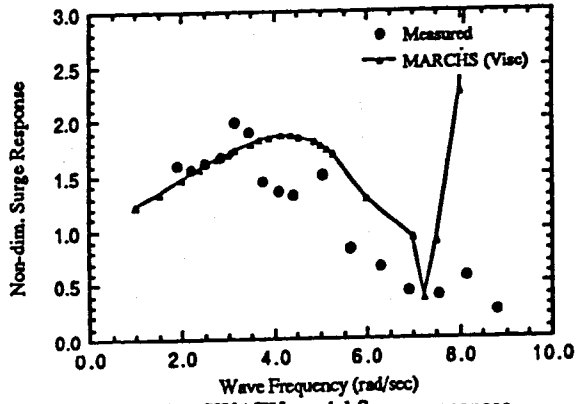

Fishing SWATH model Surge responses in following seas (Fn=0.26)

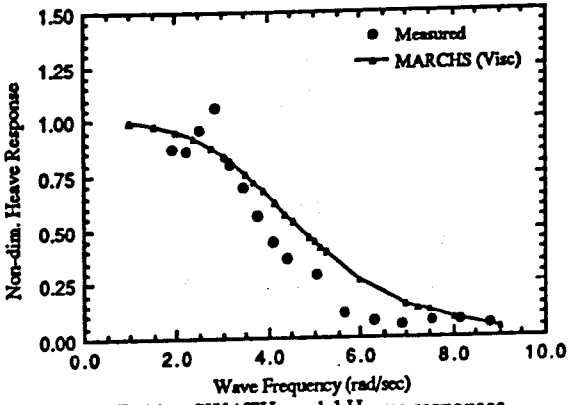

Fishing SWATH model Heave responses in following seas (Fn=0.26)

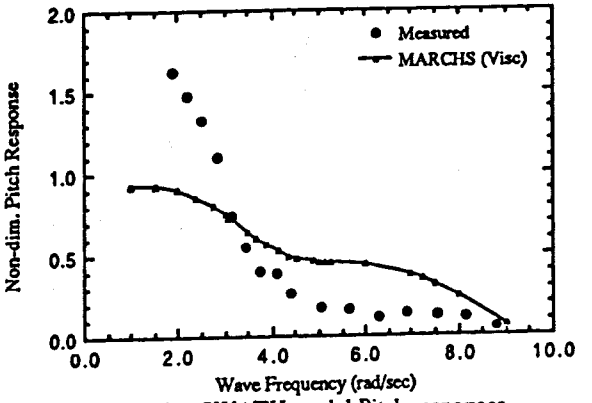

Fishing SWATH model Pitch responses in following seas (Fn=0.26)

Figure A42. SWATH-FV model motions in following seas (Fn=0.26)

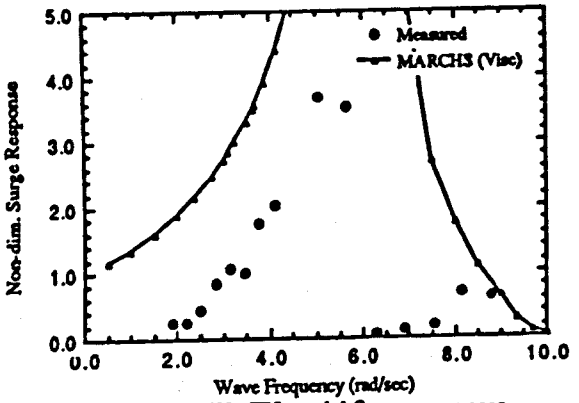

Fishing SWATH model Surge responses in following seas (Fn=0.39)

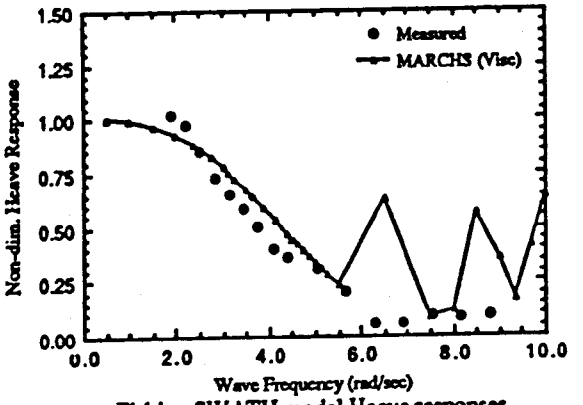

Fishing SWATH model Heave responses in following seas (Fn=0.39)

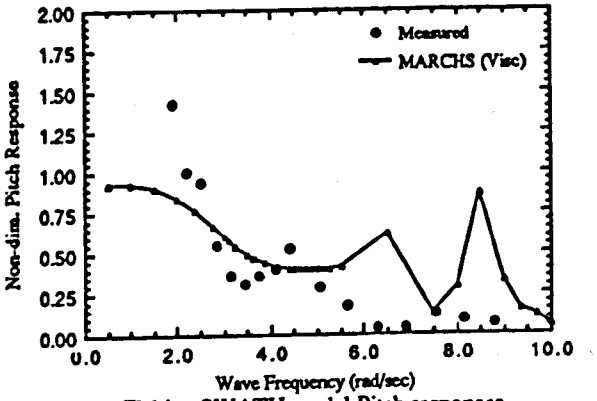

Fishing SWATH model Pitch responses in following seas (Fn=0.39)

Figure A43. SWATH-FV model motions in following seas (Fn=0.39)

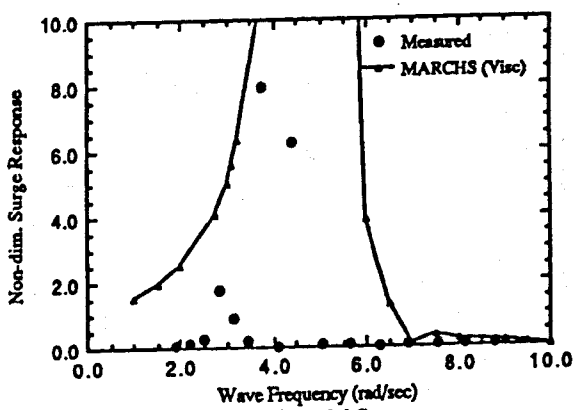

Fishing SWATH model Surge responses in following seas (Fn=0.52)

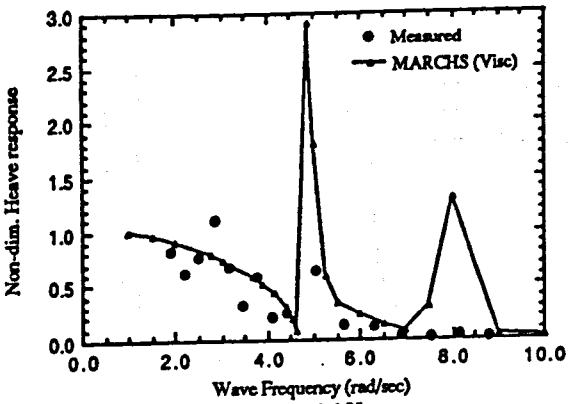

Fishing SWATH model Heave responses in following seas (Fn=0.52)

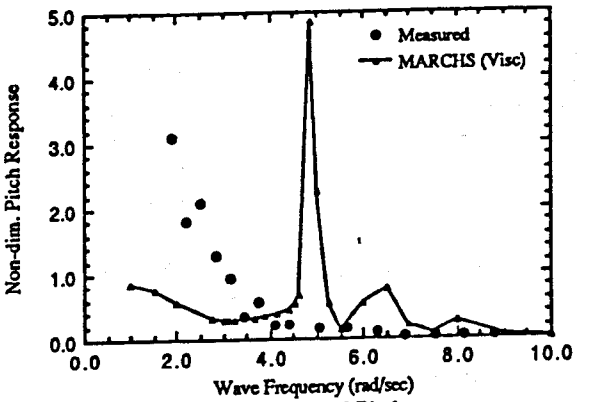

Fishing SWATH model Pitch responses in following seas (Fn=0.52)

Figure A44. SWATH-FV model motions in following seas (Fn=0.52)

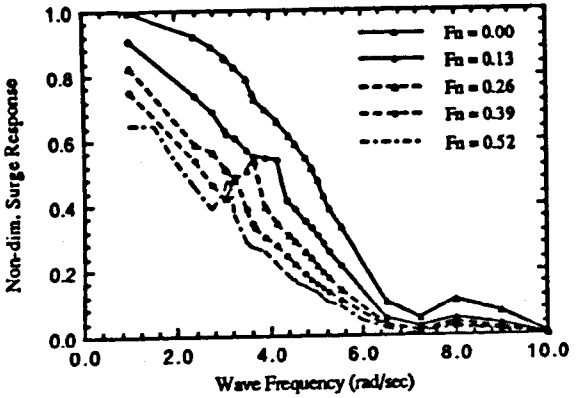

Fishing SWATH model Surge responses in head seas

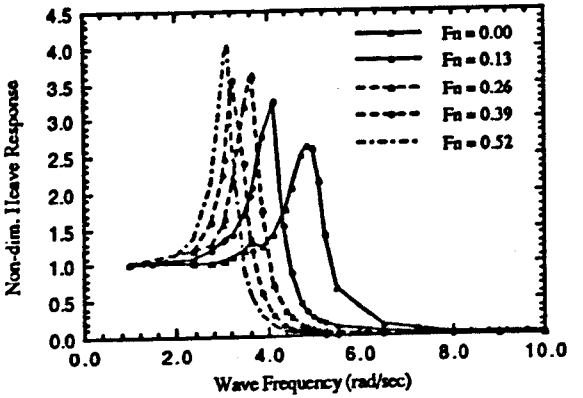

Fishing SWATH model Heave responses in head seas

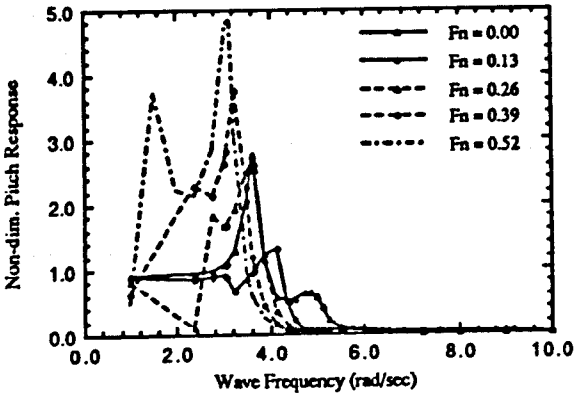

Fishing SWATH model Pitch responses in head seas

Figure A45. SWATH-FV model motions in head seas at various Froude numbers

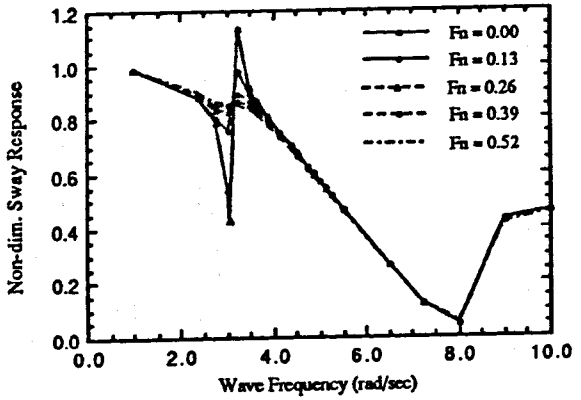

Fishing SWATH model Sway responses in beam seas

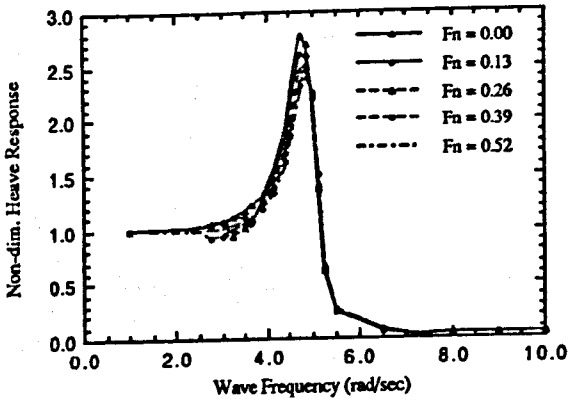

Fishing SWATH model Heave responses in beam seas

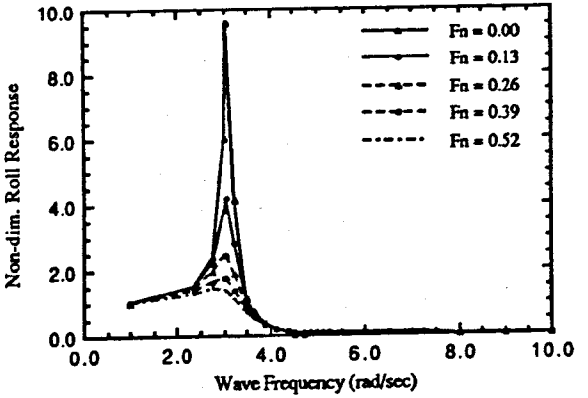

Fishing SWATH model Roll responses in beam seas

Figure A46. SWATH-FV model motions in beam seas at various Froude numbers

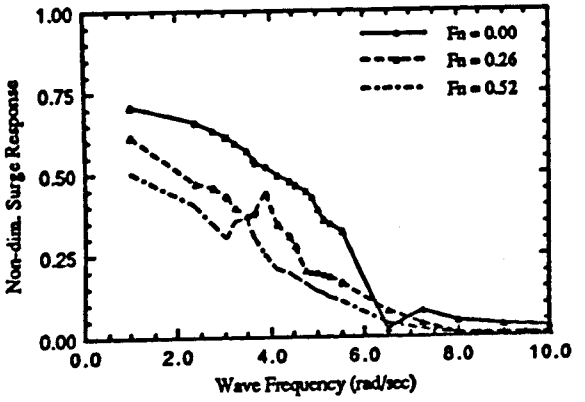

Fishing SWATH model Surge responses in quartering seas

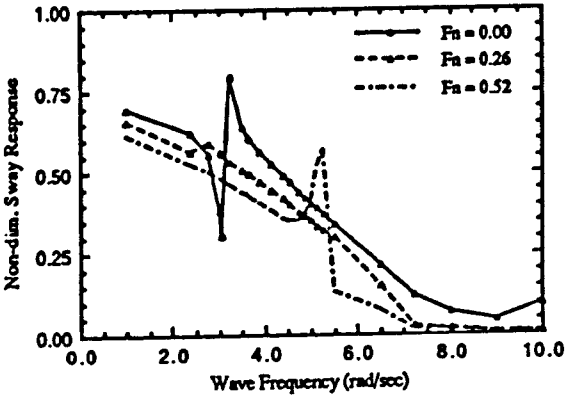

Fishing SWATH model Sway responses in quartering seas

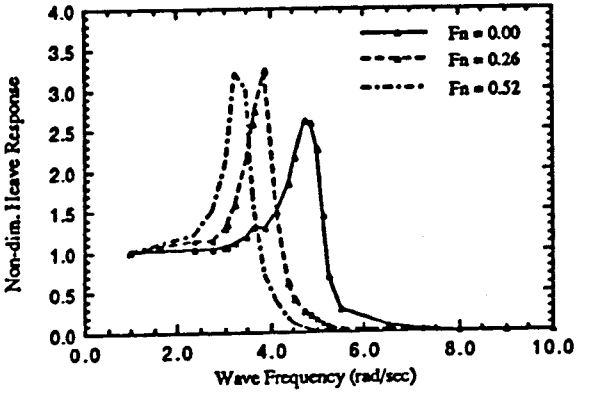

Fishing SWATH model Heave responses in quartering seas

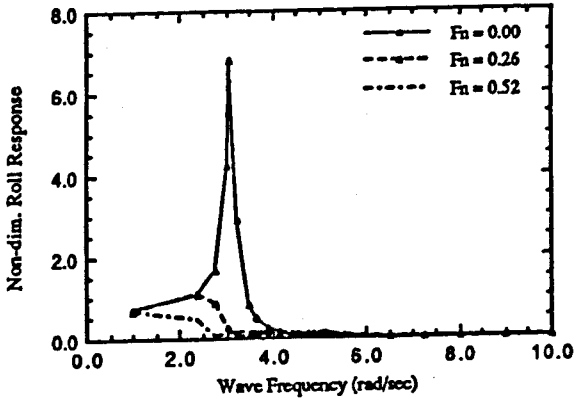

Fishing SWATH model Roll responses in quartering seas

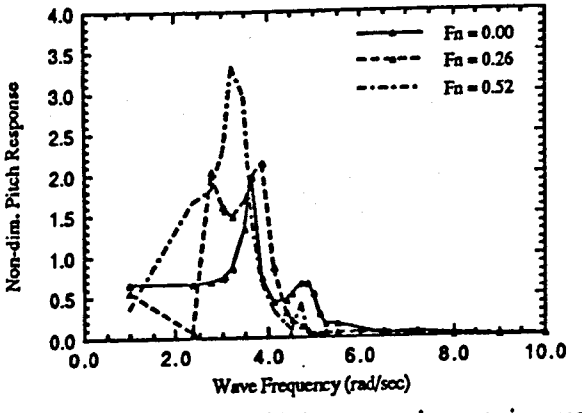

Fishing SWATH model Pitch responses in quartering seas

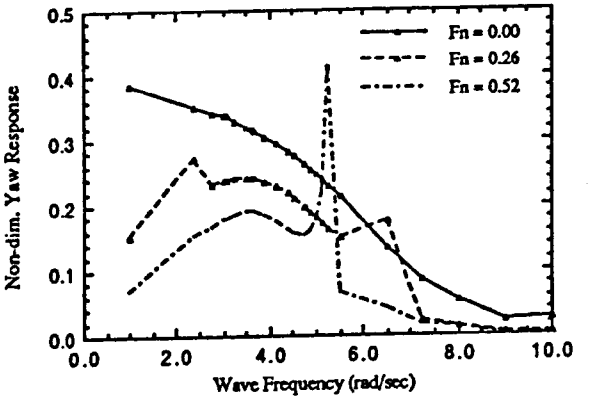

Fishing SWATH model Yaw responses in quartering seas

Figure A47. SWATH-FV model motions in bow-quartering seas at various Froude numbers

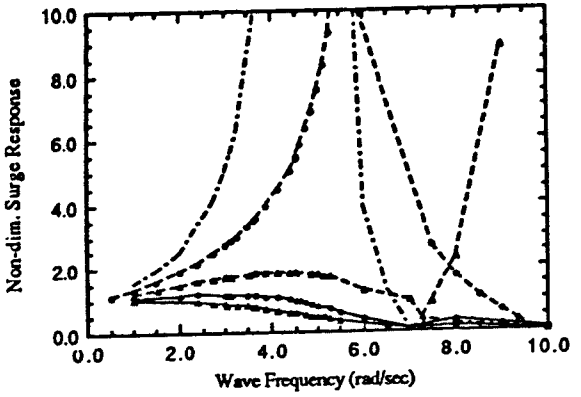

Fishing SWATH model Surge responses in following seas

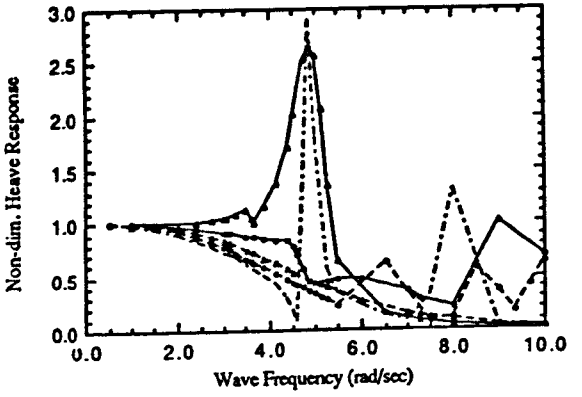

Fishing SWATH model Heave responses in following seas

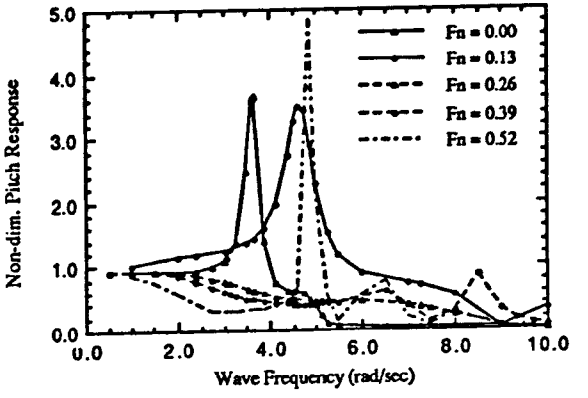

Fishing SWATH model Pitch responses in following seas

Figure A48. SWATH-FV model motions in following seas at various Froude numbers

APPENDIX B

FURTHER SWATH WAVE LOAD DATA

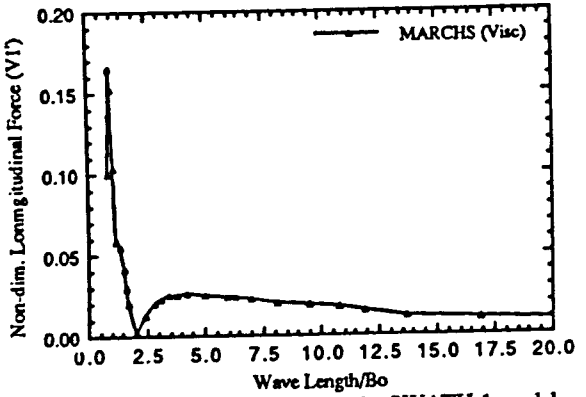

Longitudinal shear forces on the SWATH-1 model in beam seas (Fn=0.00)

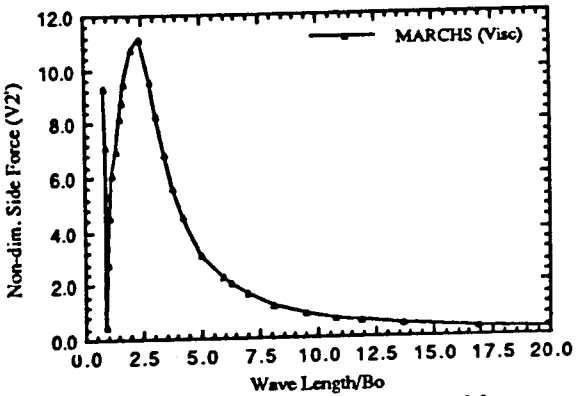

Side forces on the SWATH-1 model in beam seas (Fn=0.0)

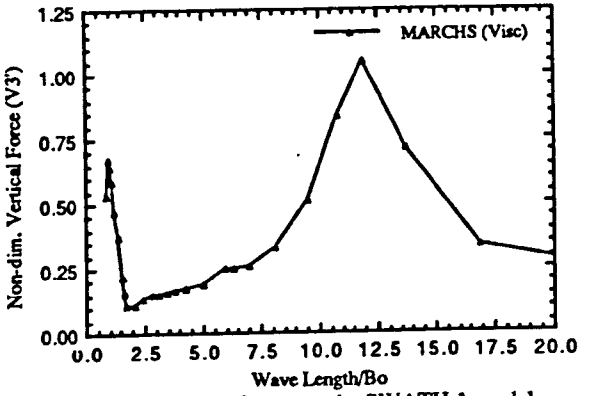

Vertical shear forces on the SWATH-1 model in beam seas (Fn=0.00)

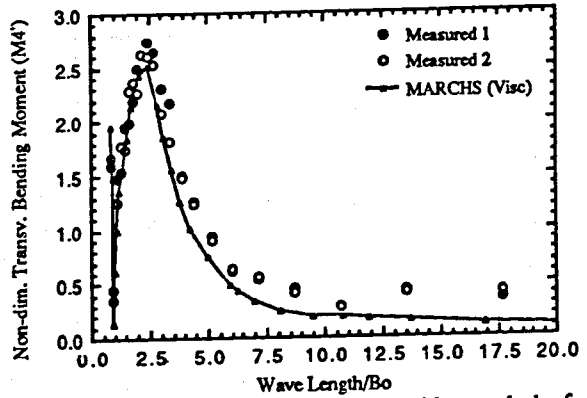

Transverse bending moment at the mid cross-deck of the SWATH-1 model in beam seas (Fn=0.00)

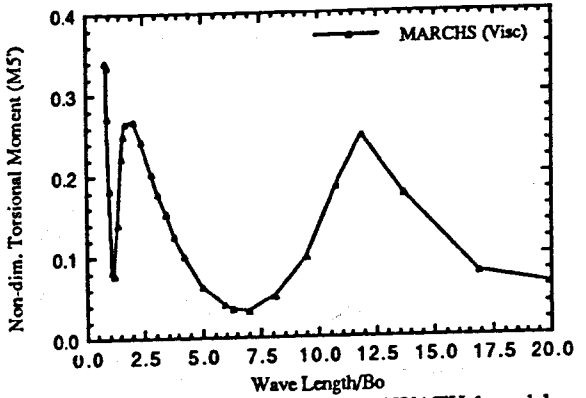

Pitch torsional moments on the SWATH-1 model in beam seas (Fn=0.00)

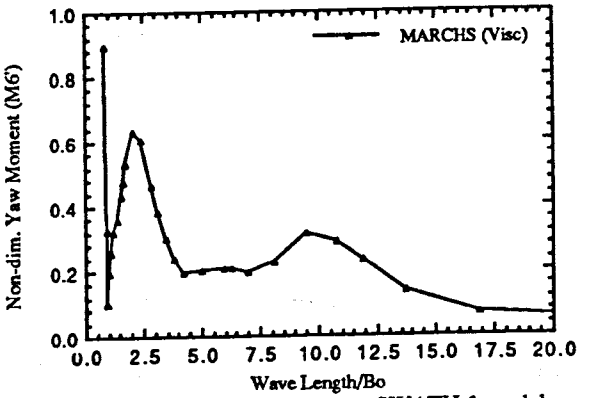

Yaw splitting moments on the SWATH-1 model in beam seas (Fn=0.00)

Figure B1. Wave load responses of SWATH-1 model in beam seas (Fn=0.00)

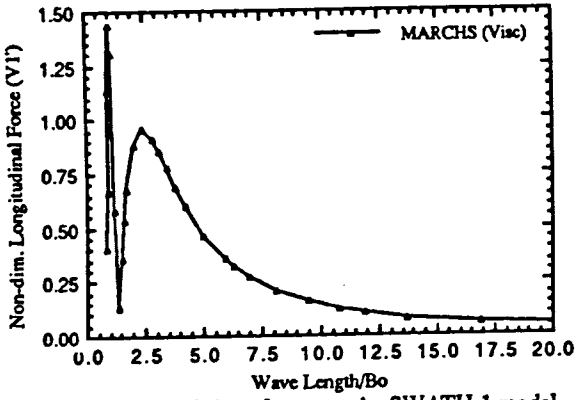

Longitudinal shear forces on the SWATH-1 model in quartering seas (Fn=0.00)

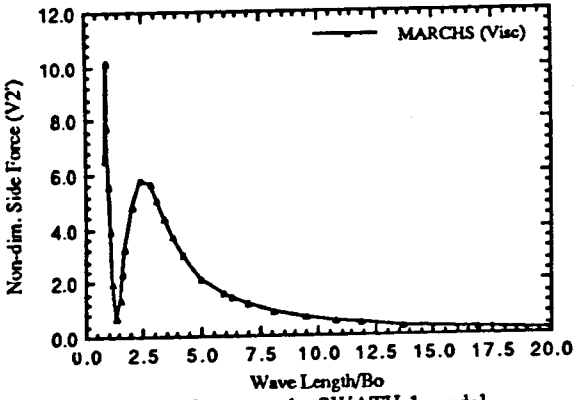

Side forces on the SWATH-1 model in quartering seas (Fn=0.00)

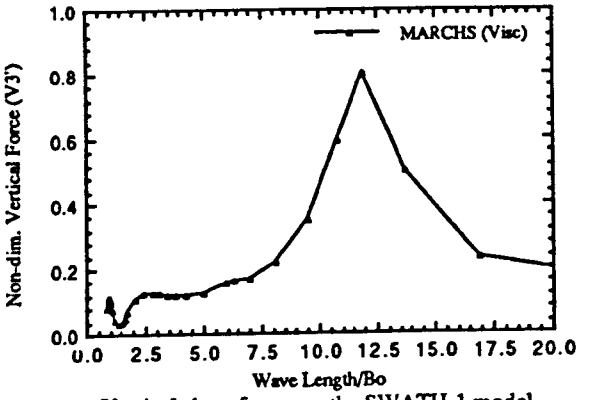

Vertical shear forces on the SWATH-1 model in quartering seas (Fn=0.00)

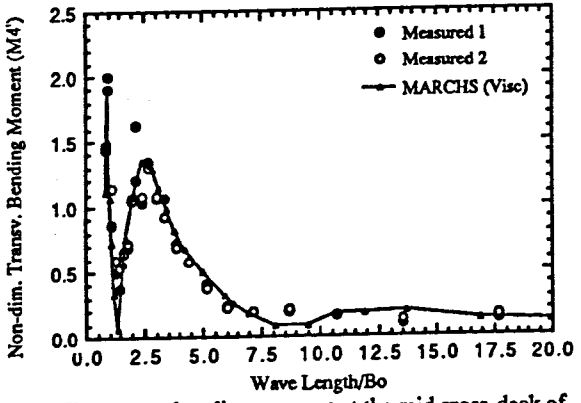

Transverse bending moment at the mid cross-deck of the SWATH-1 model in quartering seas (Fn=0.00)

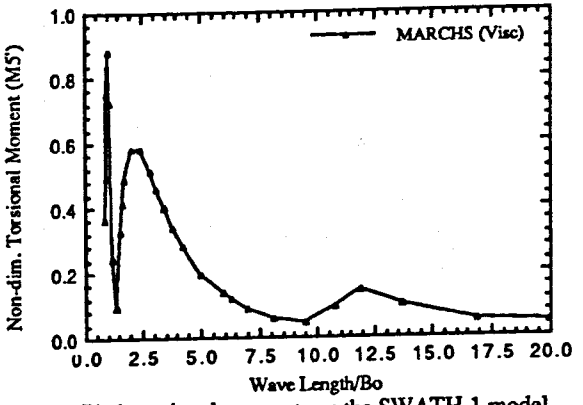

Pitch torsional moments on the SWATH-1 model in quartering seas (Fn=0.00)

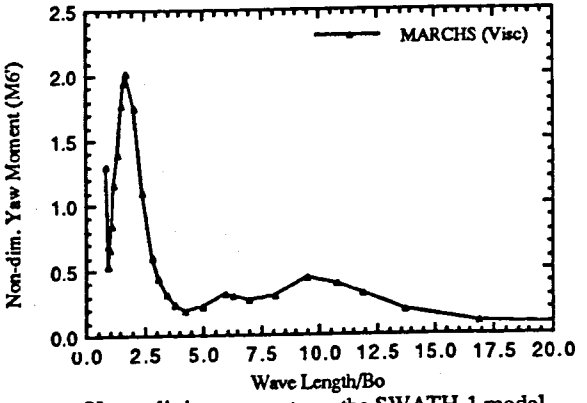

Yaw splitting moments on the SWATH-1 model in quartering seas (Fn=0.00)

Figure B2. Wave load responses of SWATH-1 model in bow-quartering seas (Fn=0.00)

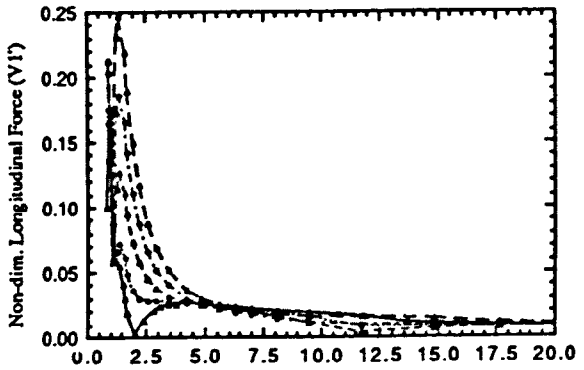

Longitudinal shear forces on SWATH-1 model in beam seas for various Fn

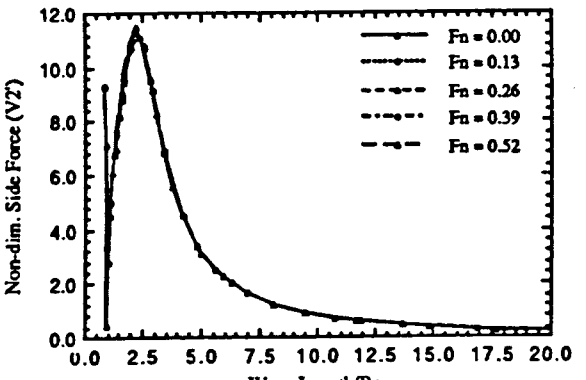

Side forces on SWATH-1 model in beam seas for various Fn

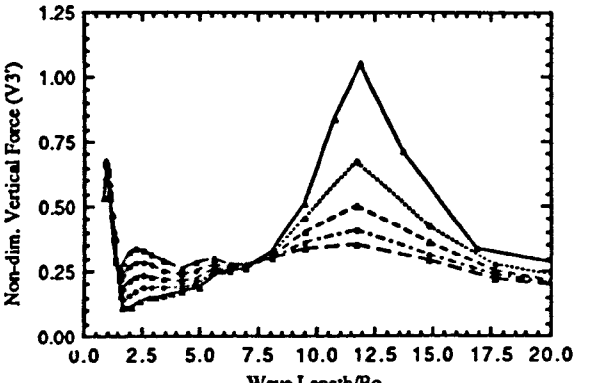

Vertical shear forces on SWATH-1 model in beam seas for various Fn

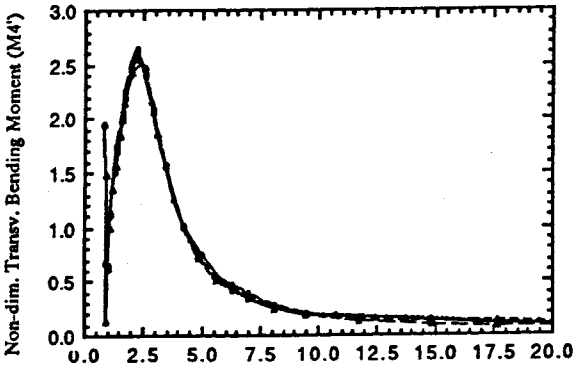

Transverse bending moment on SWATH-1 model in beam seas for various Fn

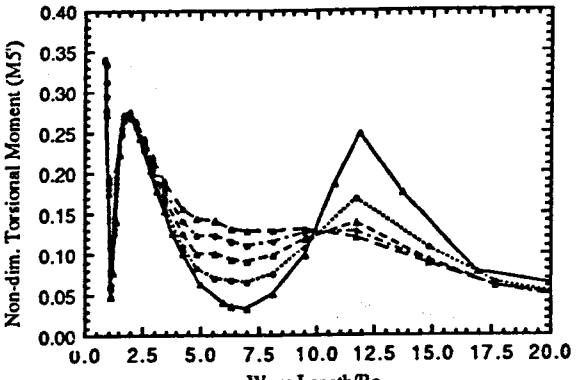

Pitch torsional moments on SWATH-1 Model in beam seas for various Fn

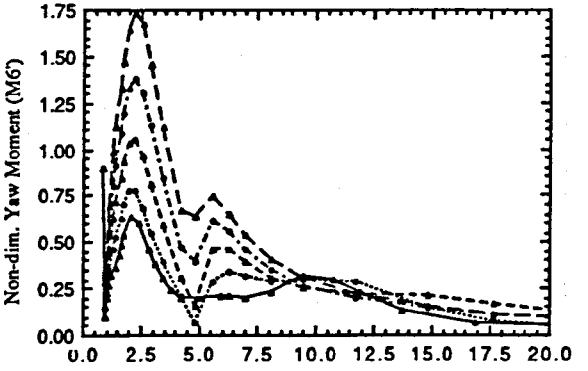

Yaw splitting moment on SWATH-1 model in beam seas for various Fn

Figure B3. Wave load responses of SWATH-1 model in beam seas for various Froude numbers

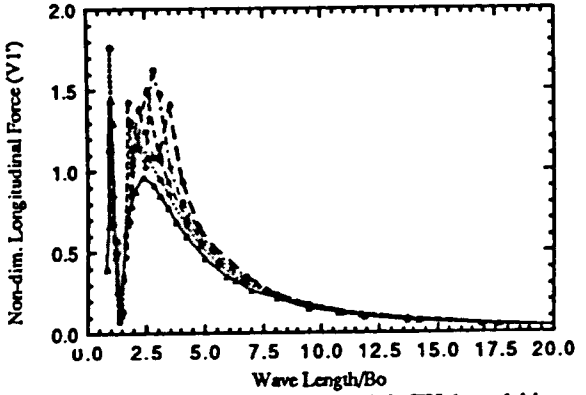

Longitudinal shear forces on SWATH-1 model in quartering seas for various Fn

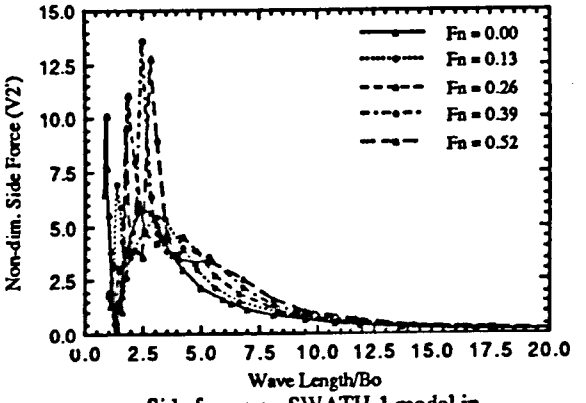

Side forces on SWATH-1 model in quartering seas for various Fn

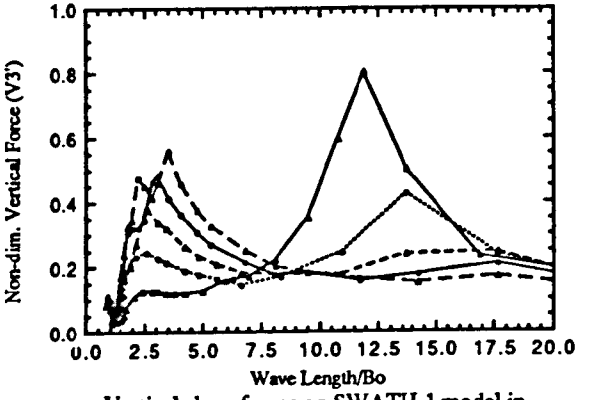

Vertical shear forces on SWATH-1 model in quartering seas for various Fn

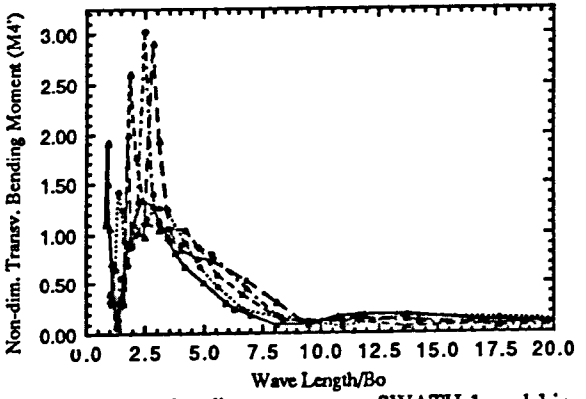

Transverse bending moments on SWATH-1 model in quartering seas for various Fn

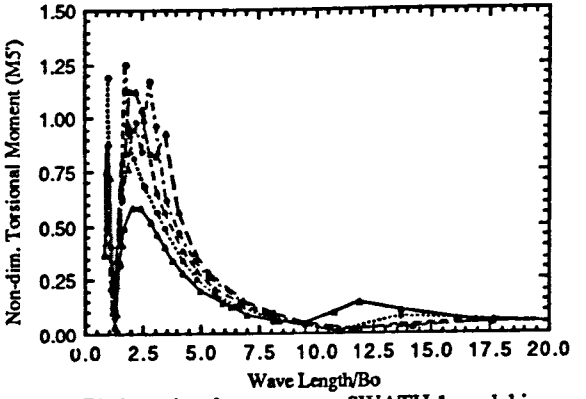

Pitch torsional moments on SWATH-1 model in quartering seas for various Fn

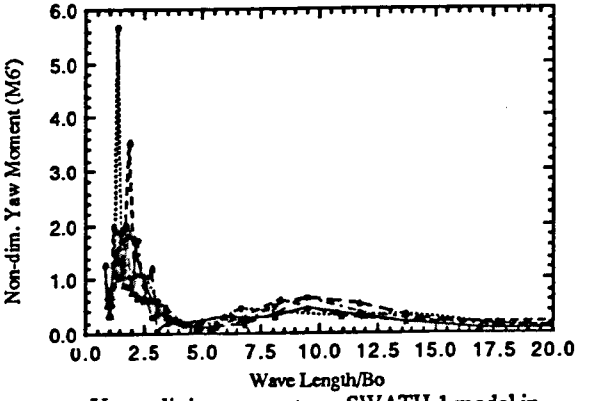

Yaw splitting moments on SWATH-1 model in quartering seas for various Fn

Figure B4. Wave load responses of SWATH-1 model in bow-quartering seas for various Froude numbers

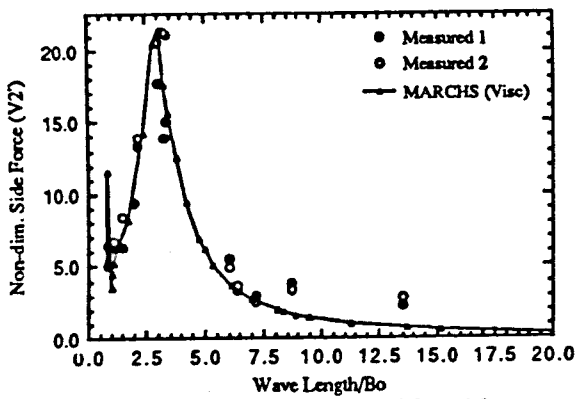

Side forces on the SWATH-3 model in beam seas (Fn=0.00)

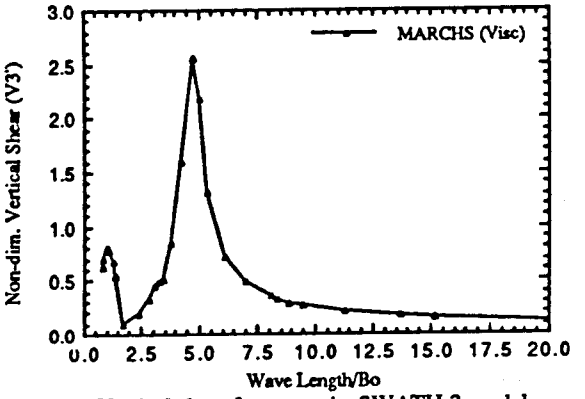

Vertical shear forces on the SWATH-3 model in beam seas (Fn=0.00)

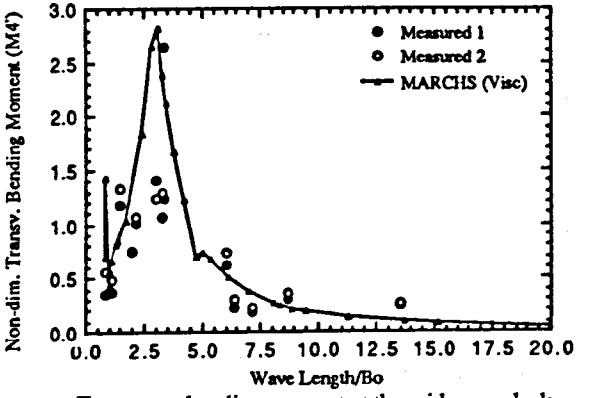

Transverse bending moment at the mid cross-deck of the SWATH-3 model in beam seas (Fn=0.00)

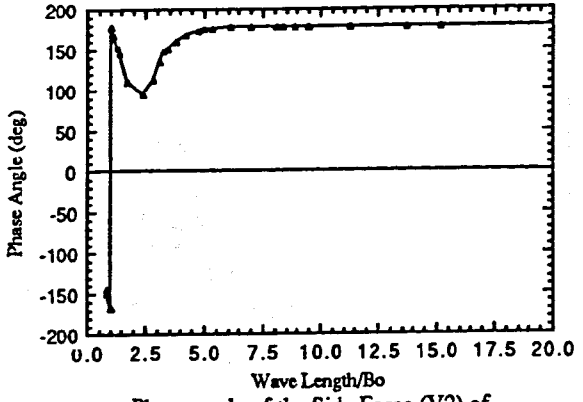

Phase angle of the Side Force (V2) of the SWATH-3 model in beam seas (Fn=0.00)

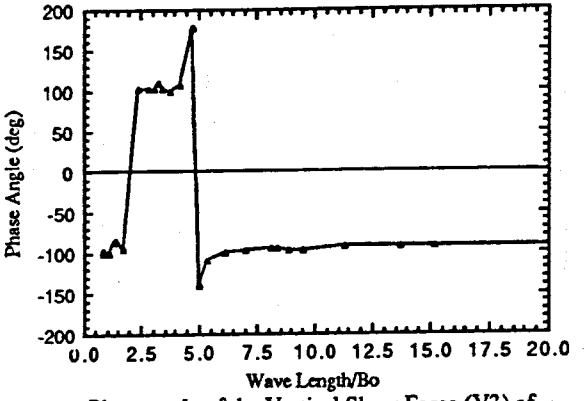

Phase angle of the Vertical Shear Force (V3) of the SWATH-3 model in beam seas (Fn=0.00)

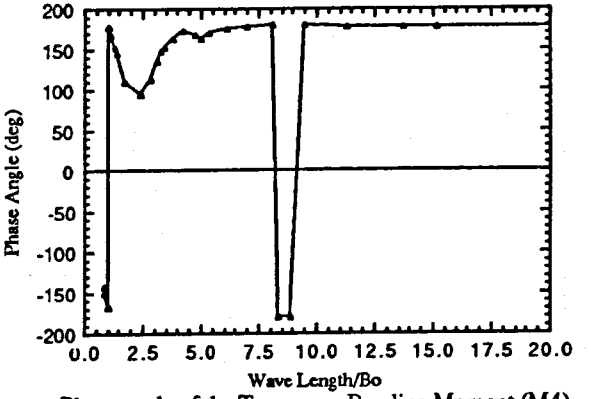

Phase angle of the Transverse Bending Moment (M4) of the SWATH-3 model in beam seas (Fn=0.00)

Figure B5. Wave load responses and phase angles of SWATH-3 model in beam seas (Fn=0.00)

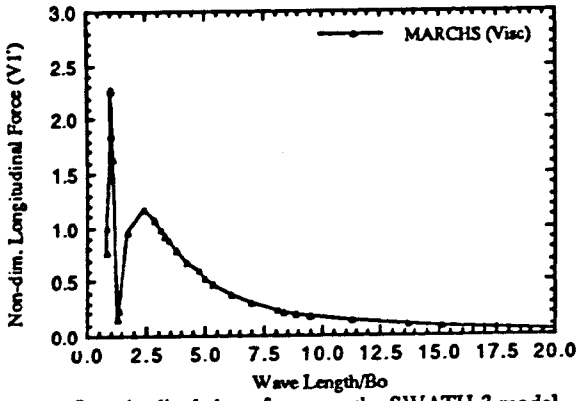

Longitudinal shear forces on the SWATH-3 model in quartering seas (Fn=0.00)

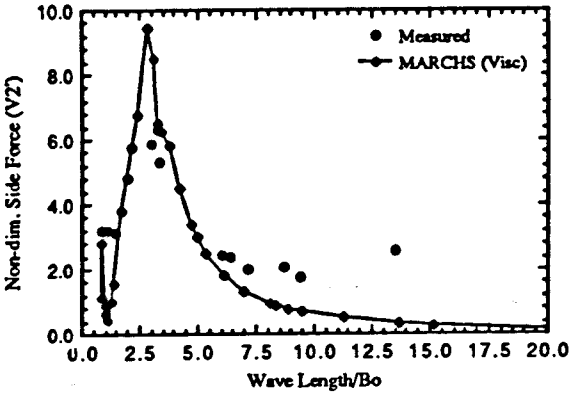

Side forces o the SWATH-3 model in quartering seas (Fn=0.00)

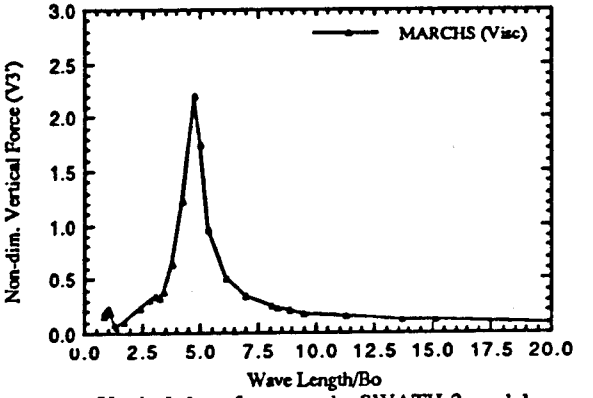

Vertical shear forces on the SWATH-3 model in quartering seas (Fn=0.00)

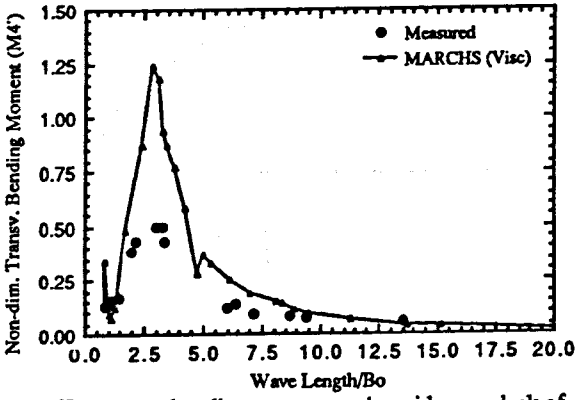

Transverse bending moment at the mid cross-deck of the SWATH-3 model in quartering seas (Fn=0.00)

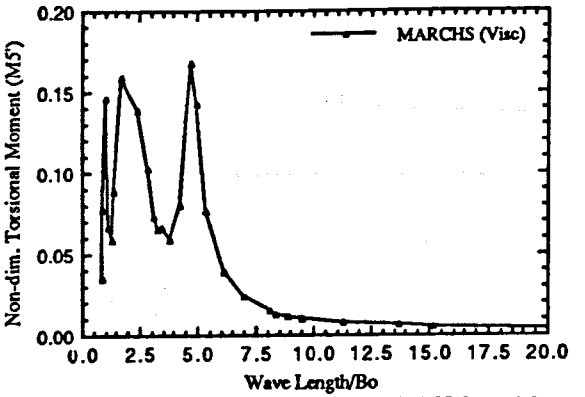

Pitch torsional moment on the SWATH-3 model in quartering seas (Fn=0.00)

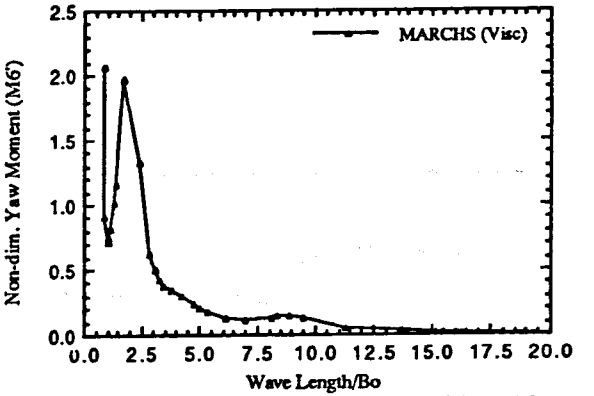

Yaw splitting moment on the SWATH-3 model in quartering seas (Fn=0.00)

Figure B6. Wave load responses of SWATH-3 model in bow-quartering seas (Fn=0.00)

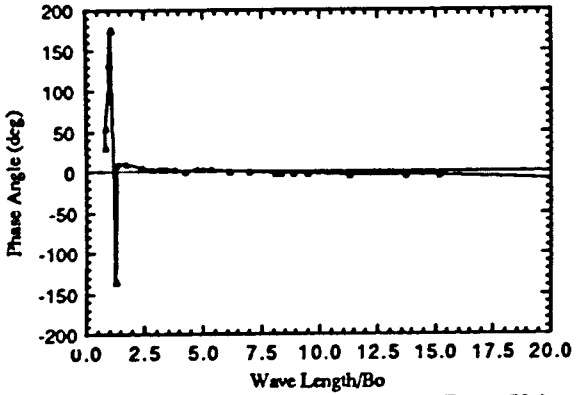

Phase angle of the Longitudinal Shear Force (V1) of the SWATH-3 model in quartering seas (Fn=0.00)

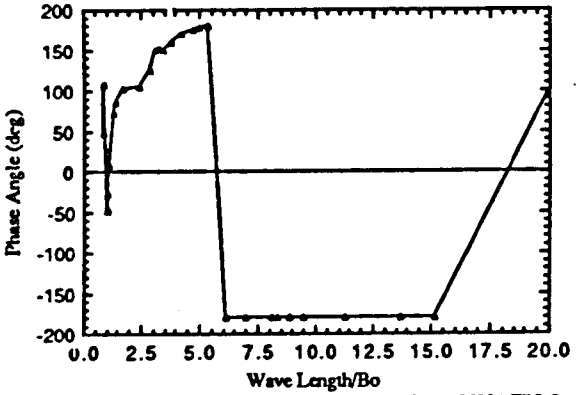

Phase angle of the Side Force (V2) of the SWATH-3 model in quartering seas (Fn=0.00)

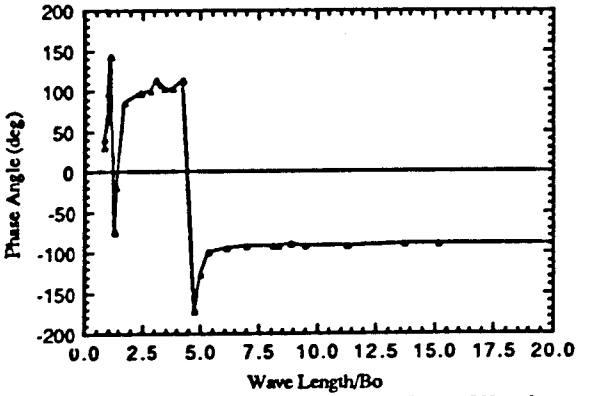

Phase angle of the Vertical Shear Force (V3) of the SWATH-3 model in quartering seas (Fn=0.00)

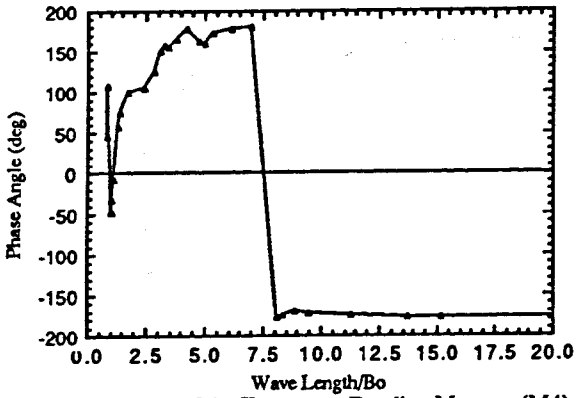

Phase angle of the Transverse Bending Moment (M4) of the SWATH-3 model in quartering seas (Fn=0.00)

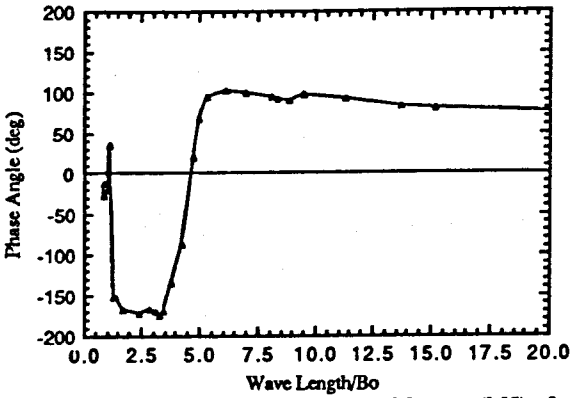

Phase angle of the Pitch Torsional Moment (M5) of the SWATH-3 model in quartering seas (Fn=0.00)

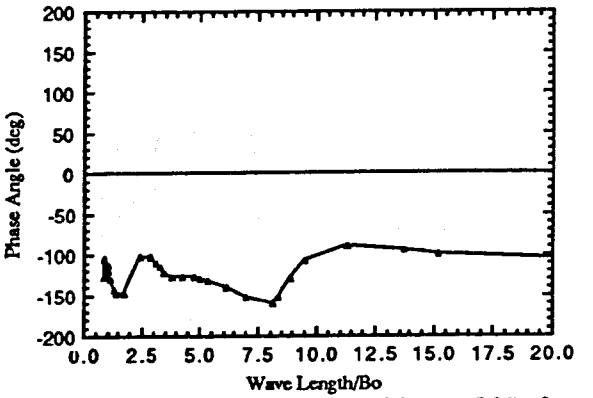

Phase angle of the Yaw Splitting Moment (M6) of the SWATH-3 model in quartering seas (Fn=0.00)

Figure B7. Wave load phase angles of SWATH-3 model in bow-quartering seas (Fn=0.00)

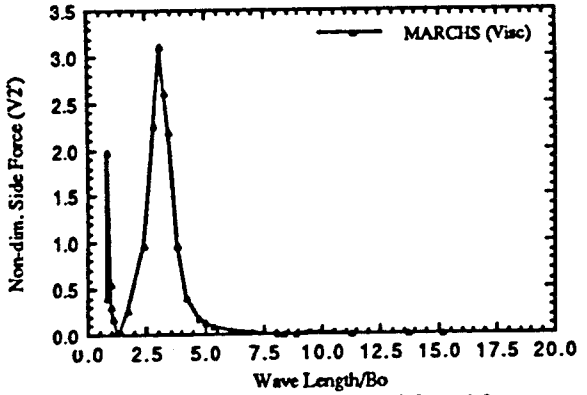

Side forces on the SWATH-3 model in head seas (Fn=0.00)

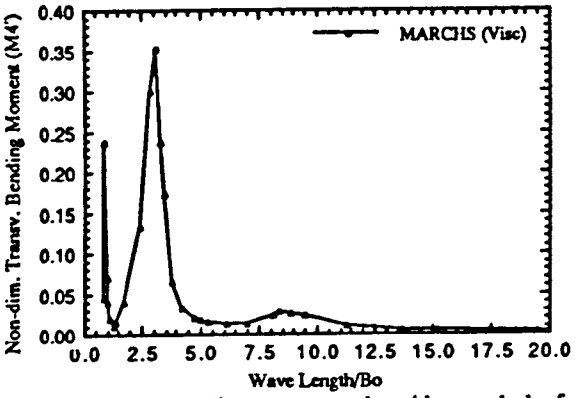

Transverse bending moment at the mid cross-deck of the SWATH-3 model in head seas (Fn=0.00)

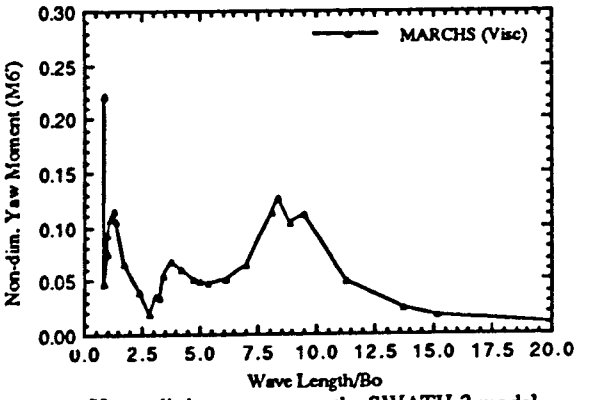

Yaw splitting moment on the SWATH-3 model in head seas (Fn=0.00)

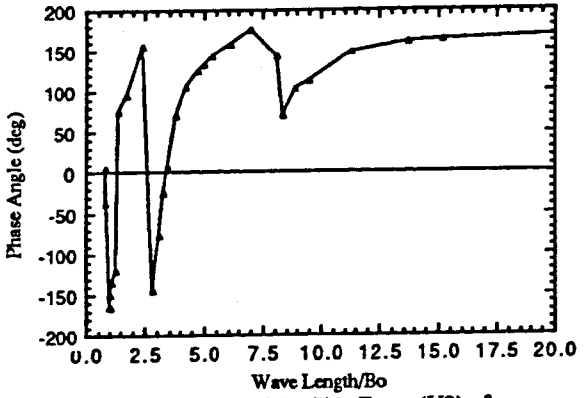

Phase angle of the Side Force (V2) of the SWATH-3 model in head seas (Fn=0.00)

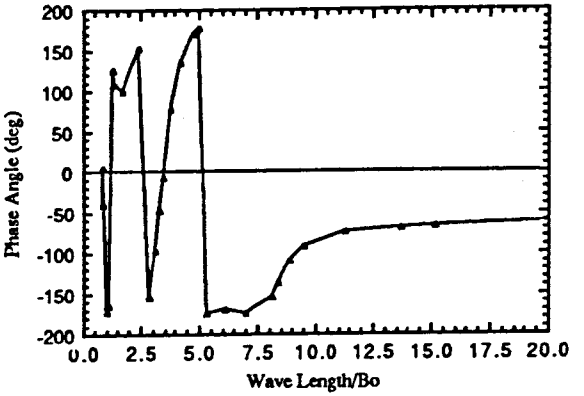

Phase angle of the Transverse Bending Moment (M4) of the SWATH-3 model in head seas (Fn=0.00)

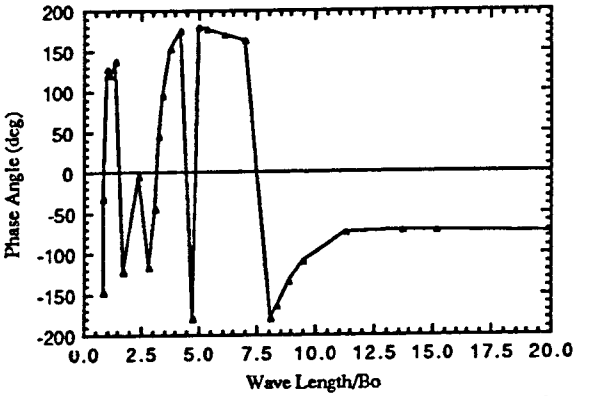

Phase angle of the Yaw Splitting Moment (M6) of the SWATH-3 model in head seas (Fn=0.00)

Figure B8. Wave load responses and phase angles of SWATH-3 model in head seas (Fn=0.00)

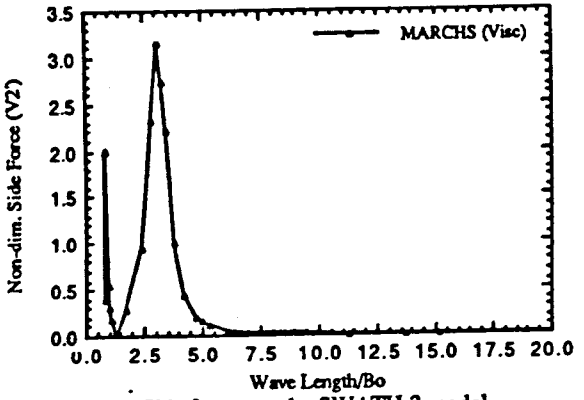

Side forces on the SWATH-3 model in following seas (Fn=0.00)

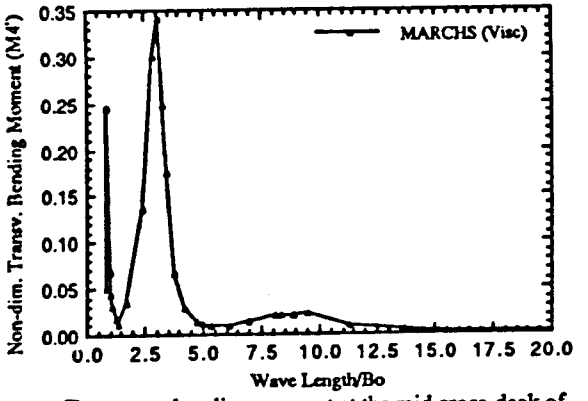

Transverse bending moment at the mid cross-deck of the SWATH-3 model in following seas (Fn=0.00)

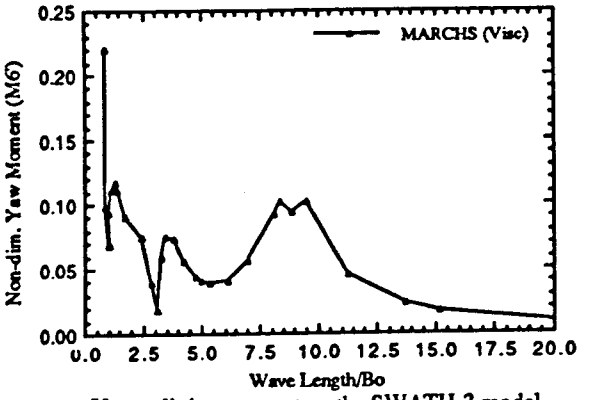

Yaw splitting moment on the SWATH-3 model in following seas (Fn=0.00)

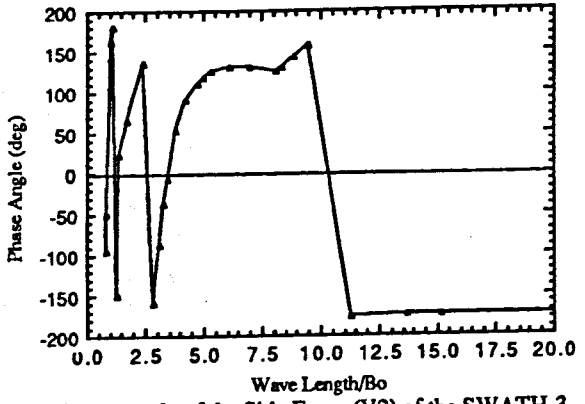

Phase angle of the Side Force (V2) of the SWATH-3 model in following seas (Fn=0.00)

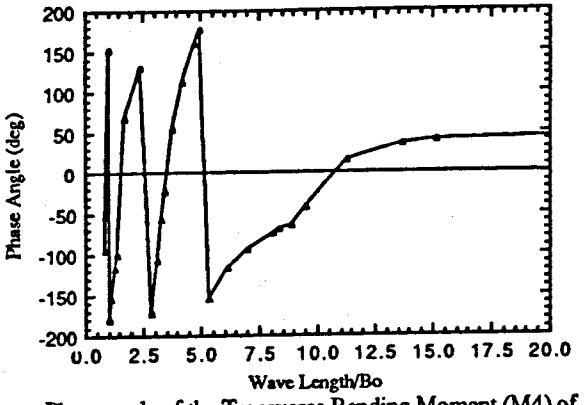

Phase angle of the Transverse Bending Moment (M4) of the SWATH-3 model in following seas (Fn=0.00)

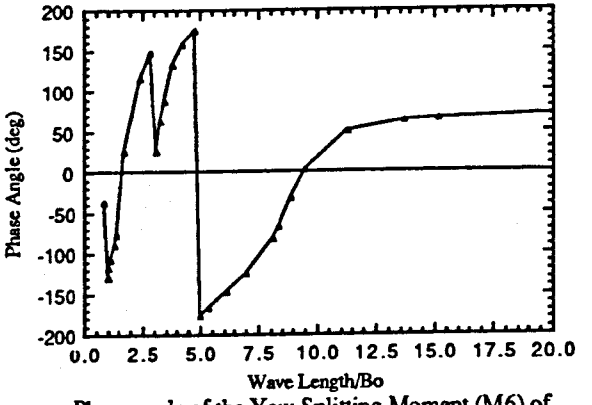

Phase angle of the Yaw Splitting Moment (M6) of the SWATH-3 model in following seas (Fn=0.00)

Figure B9. Wave load responses and phase angles of SWATH-3 model in following seas (Fn=0.00)

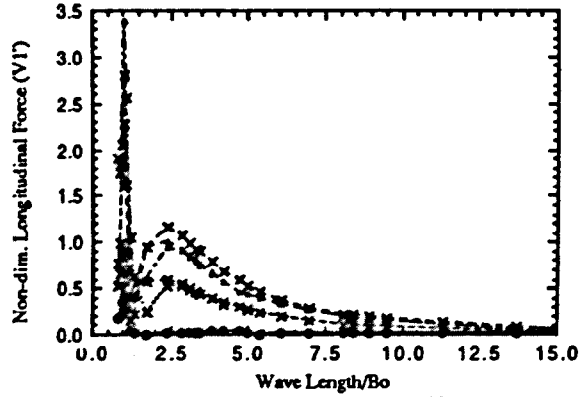

Longitudinal shear forces on SWATH-3 model in various wave headings (Fn=0.00)

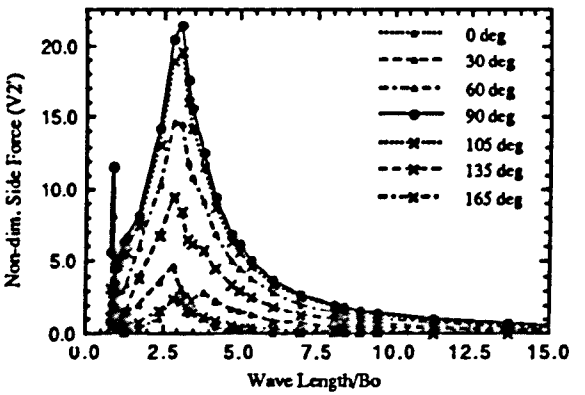

Side forces on SWATH-3 model in various wave headings (Fn=0.00)

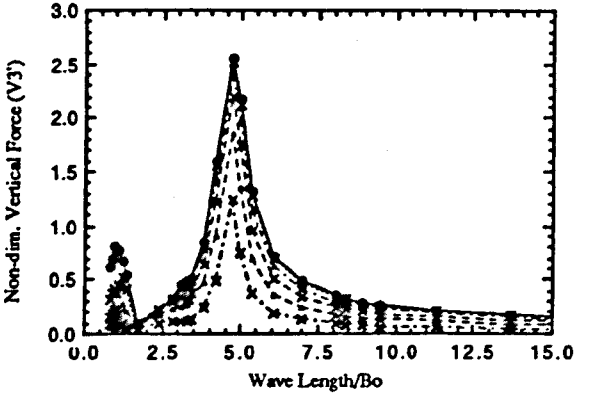

Vertical shear forces on SWATH-3 model in various wave headings (Fn=0.00)

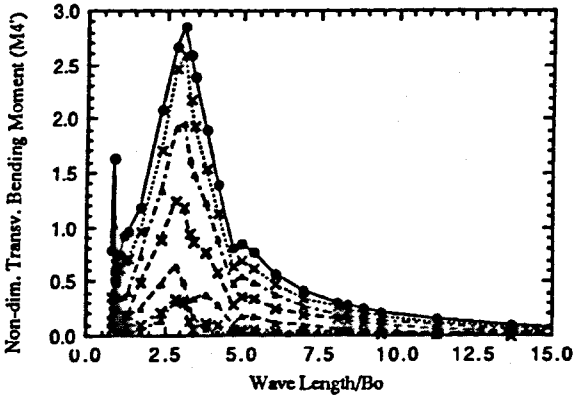

Transverse bending moments on SWATH-3 model in various wave headings (Fn=0.00)

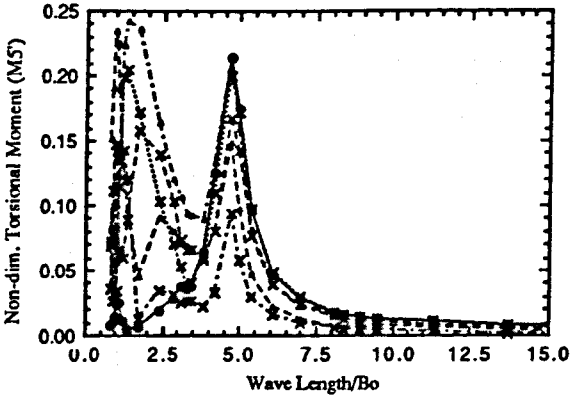

Pitch torsional moments on SWATH-3 model in various wave headings (Fn=0.00)

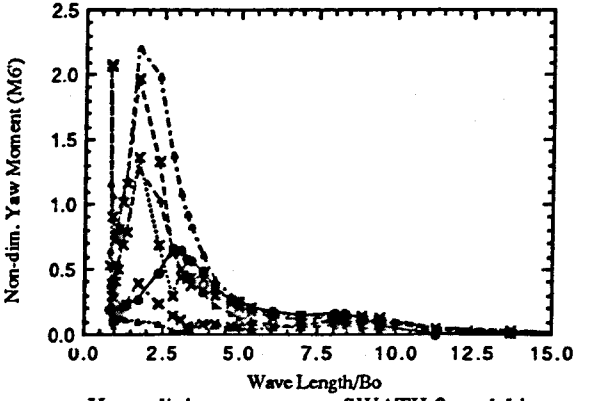

Yaw splitting moments on SWATH-3 model in various wave headings (Fn=0.00)

Figure B10. Wave load responses of SWATH-3 model in various wave headings (Fn=0.00)

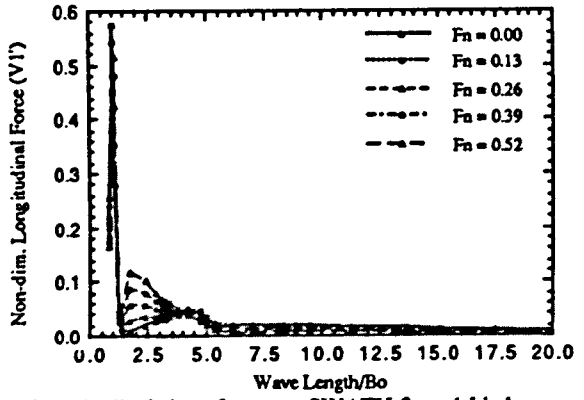

Longitudinal shear forces on SWATH-3 model in beam seas for various Fn

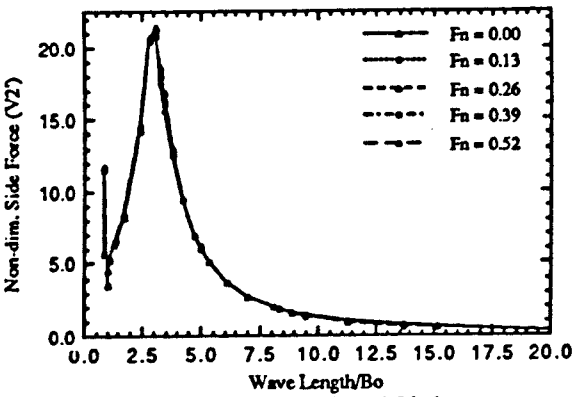

Side forces on SWATH-3 model in beam seas for various Fn

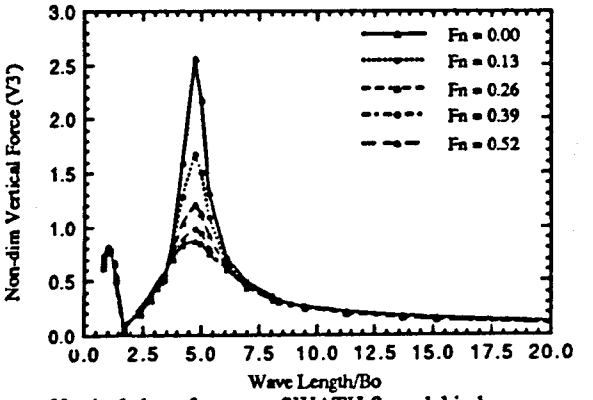

Vertical shear forces on SWATH-3 model in beam seas for various Fn

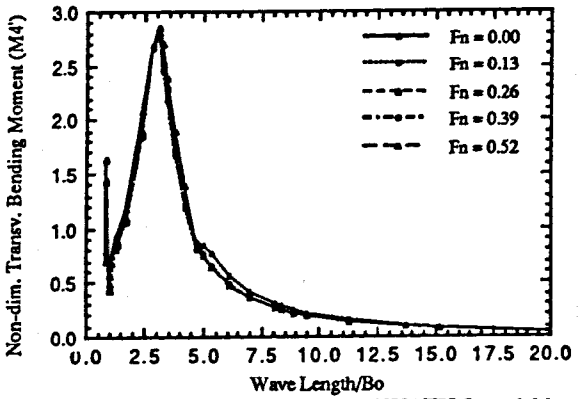

Transverse bending moments on SWATH-3 model in beam seas for various Fn

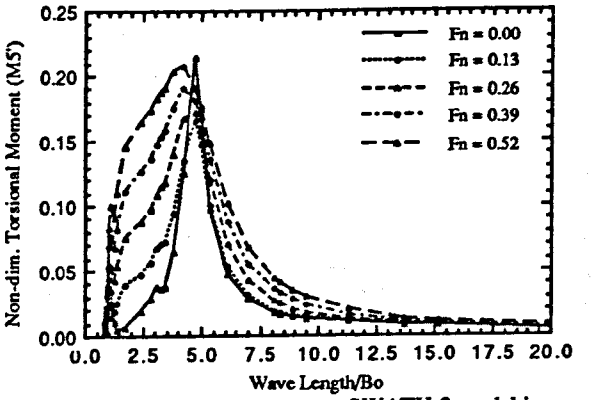

Pitch torsional moments on SWATH-3 model in beam seas for various Fn

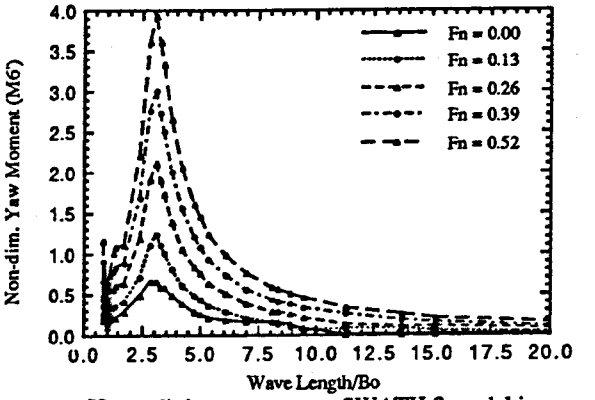

Yaw splitting moments on SWATH-3 model in beam seas for various Fn

Figure B11. Wave load responses of SWATH-3 model in beam seas for various Froude numbers

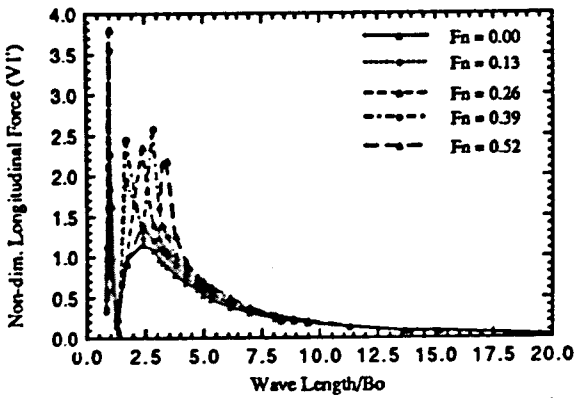

Longitudinal shear forces on SWATH-3 model in quartering seas for various Fn

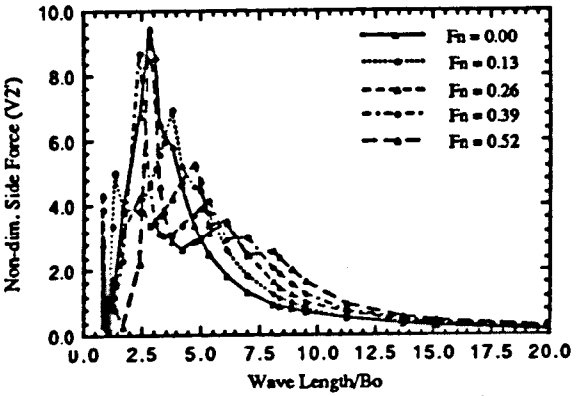

Side forces on SWATH-3 model in quartering seas for various Fn

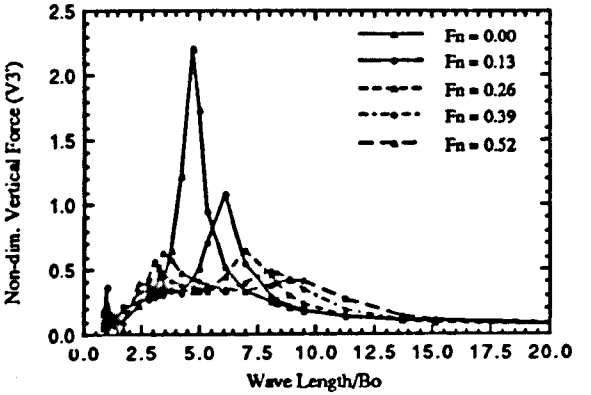

Vertical shear forces on SWATH-3 model in quartering seas for various Fn

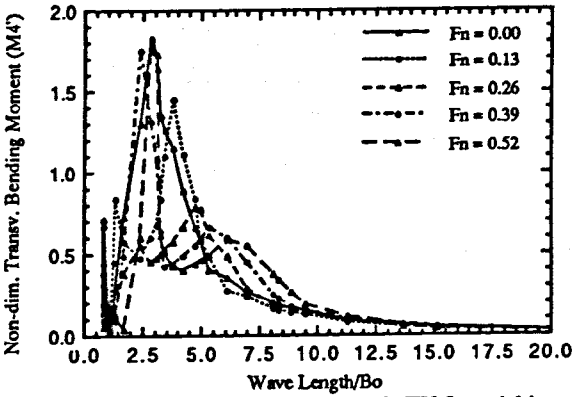

Transv. bending moment on SWATH-3 model in quartering seas for various Fn

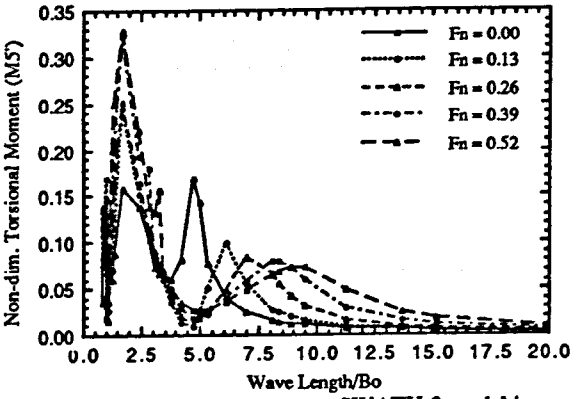

Pitch torsional moment on SWATH-3 model in quartering seas for various Fn

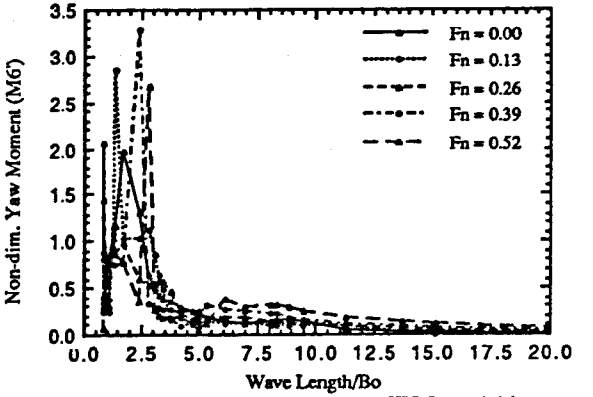

Yaw splitting moment on SWATH-3 model in quartering seas for various Fn

Figure B12. Wave load responses of SWATH-3 model in bow-quartering seas for various Froude numbers

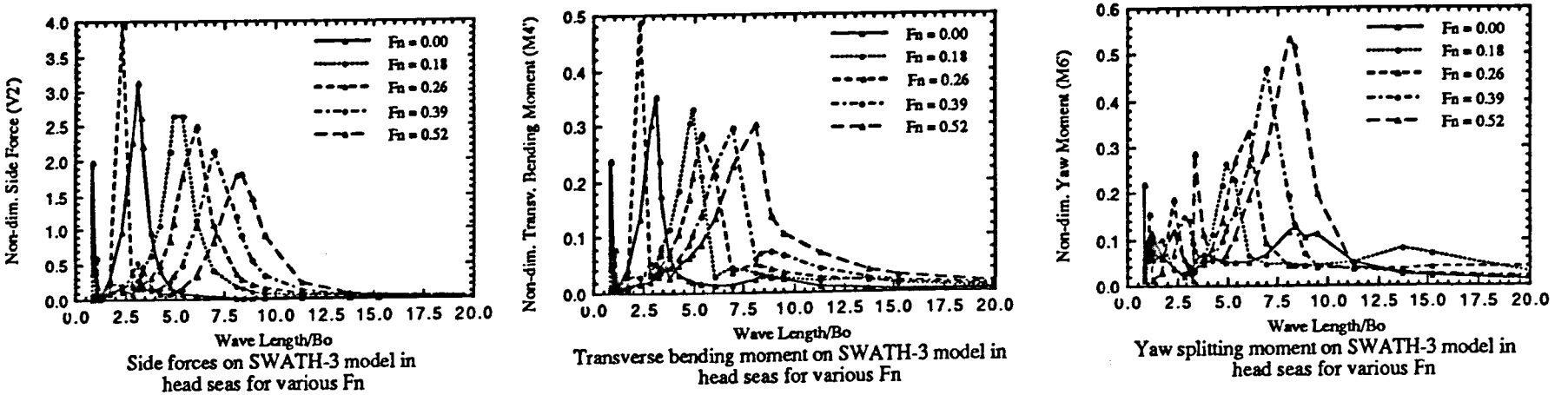

Figure B13. Wave load responses of SWATH-3 model in head seas for various Froude numbers

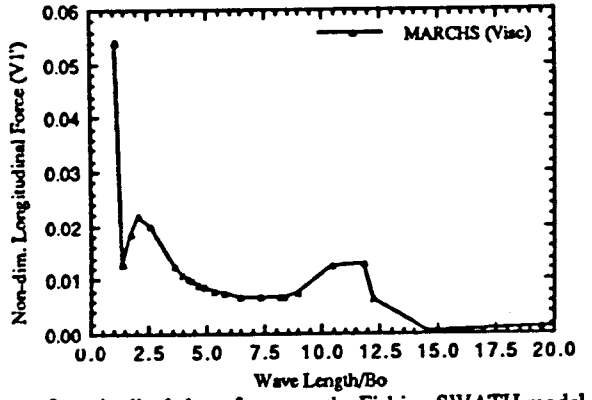

Longitudinal shear forces on the Fishing SWATH model in beam seas (Fn=0.00)

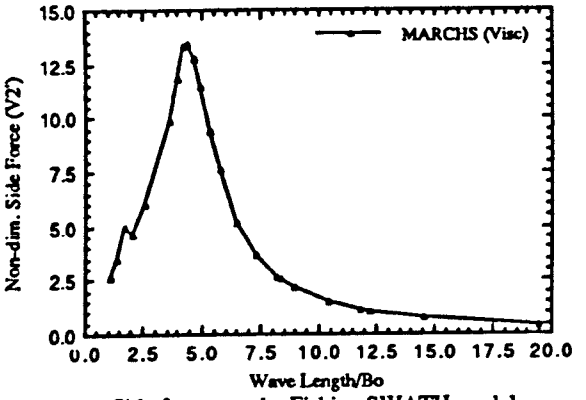

Side forces on the Fishing SWATH model in beam seas (Fn=0.00)

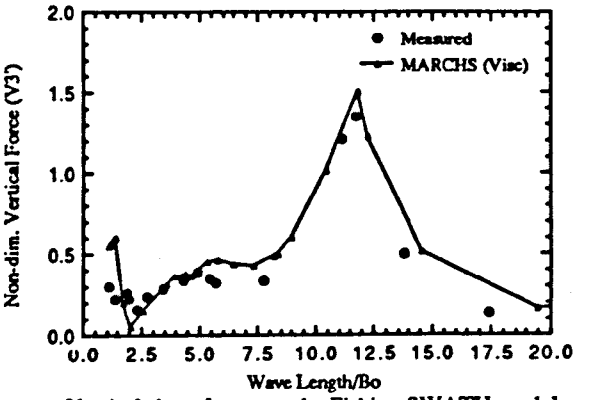

Vertical shear forces on the Fishing SWATH model in beam seas (Fn=0.00)

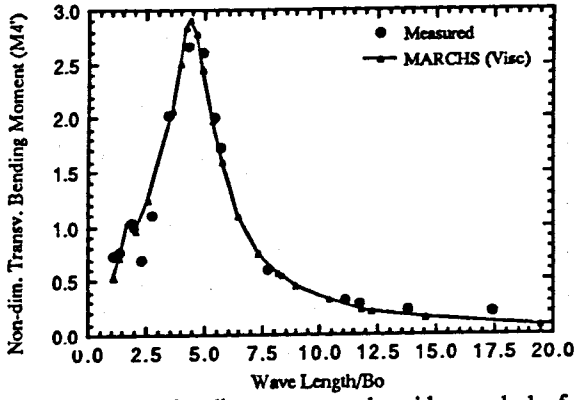

Transverse bending moment at the mid cross-deck of the Fishing SWATH model in beam seas (Fn=0.00)

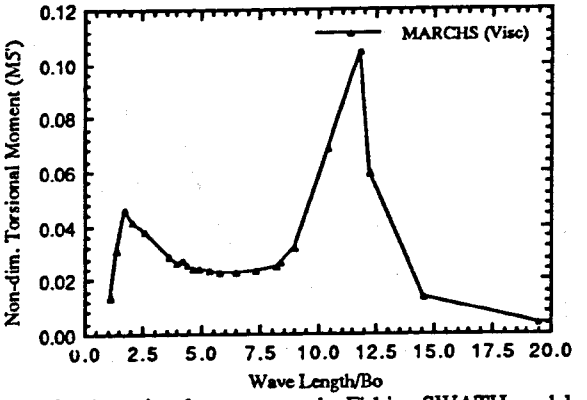

Pitch torsional moment on the Fishing SWATH model in beam seas (Fn=0.00)

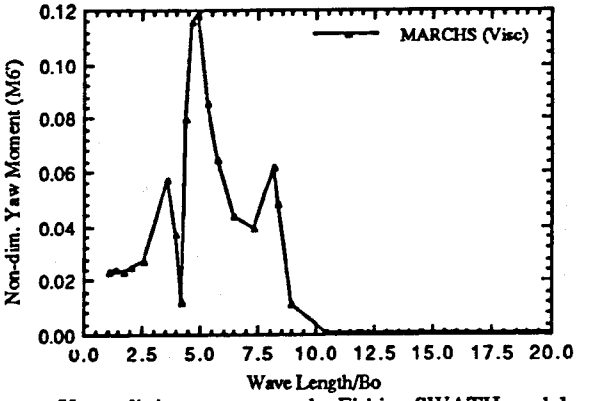

Yaw splitting moment on the Fishing SWATH model in beam seas (Fn=0.00)

Figure B14. Wave load responses of SWATH-FV model in beam seas (Fn=0.00)

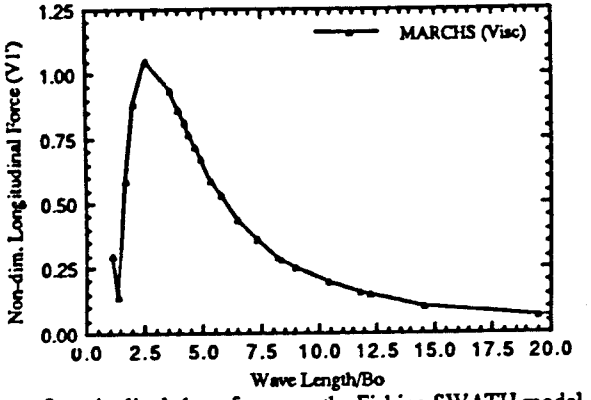

Longitudinal shear forces on the Fishing SWATH model in quartering seas (Fn=0.00)

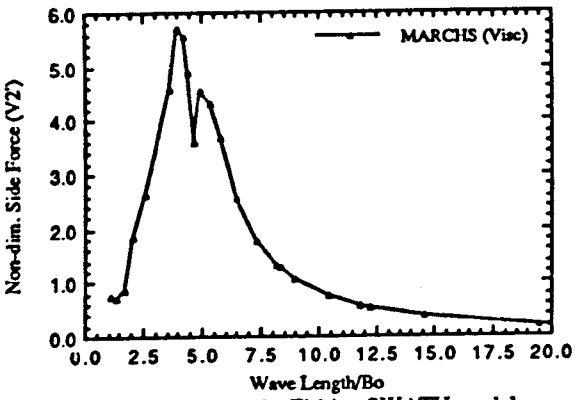

Side forces on the Fishing SWATH model in quartering seas (Fn=0.00)

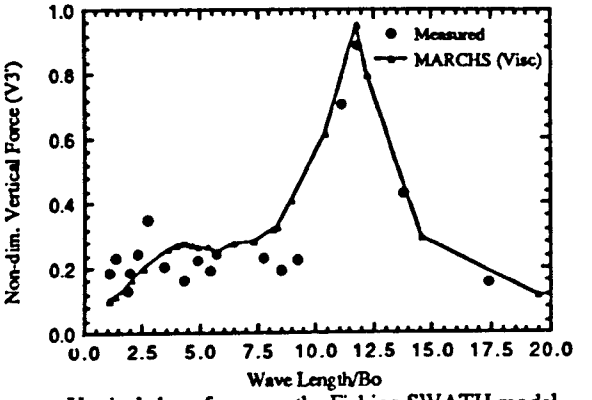

Vertical shear forces on the Fishing SWATH model in quartering seas (Fn=0.00)

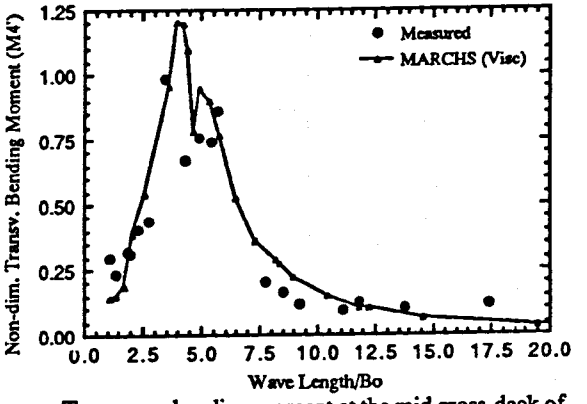

Transverse bending moment at the mid cross-deck of the fishing SWATH model in quartering seas (Fn=0.00)

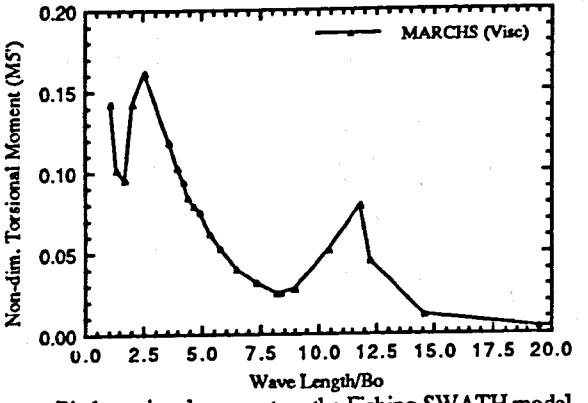

Pitch torsional moment on the Fishing SWATH model in quartering seas (Fn=0.00)

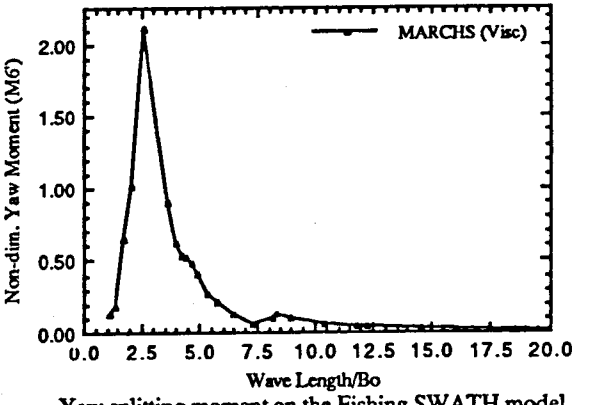

Yaw splitting moment on the Fishing SWATH model in quartering seas (Fn=0.00)

Figure B15. Wave load responses of SWATH-FV model in bow-quartering seas (Fn=0.00)

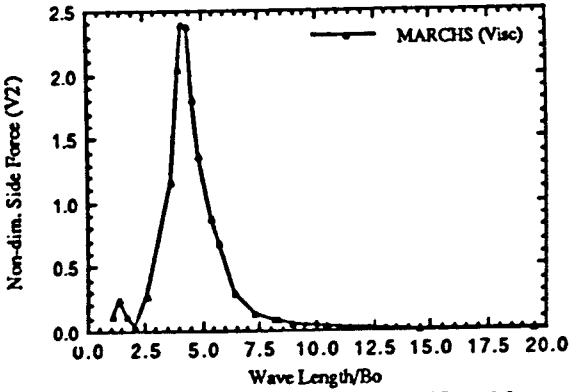

Side forces on the Fishing SWATH model in head seas (Fn=0.00)

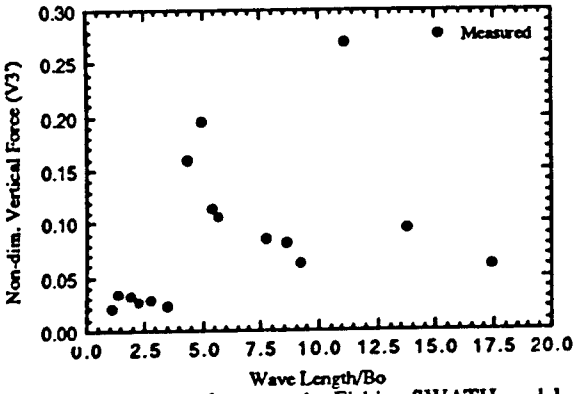

Vertical shear forces on the Fishing SWATH model in head seas (Fn=0.00)

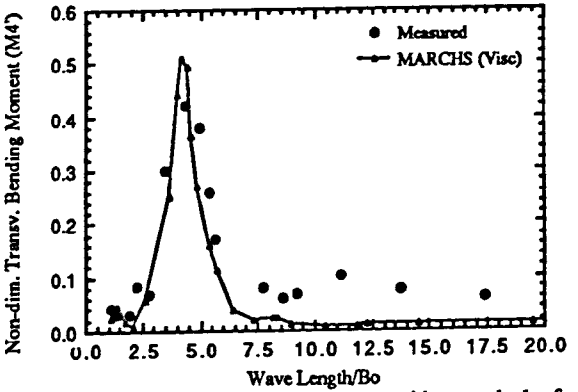

Transverse bending moment at the mid cross-deck of the Fishing SWATH model in head seas (Fn=0.00)

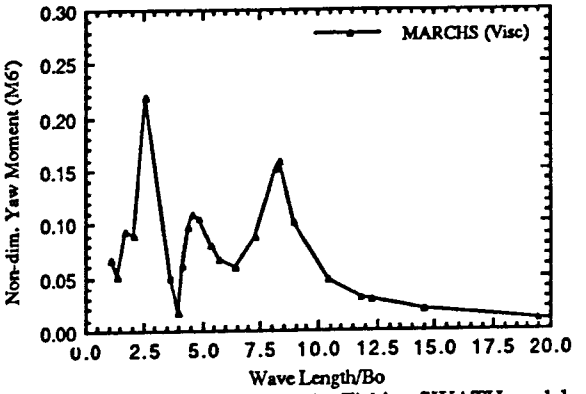

Yaw splitting moment on the Fishing SWATH model in head seas (Fn=0.00)

Figure B16. Wave load responses of SWATH-FV model in head seas (Fn=0.00)

APPENDIX C

ON THE STUDY OF SHIP SLAMMING BY DROP TEST MODELS

APPENDIX C

ON THE STUDY OF SHIP SLAMMING BY DROP TEST MODELS

Abstract

The significance of drop tests in the development of ship slamming studies during the last three decades is reviewed within this report. Three types of drop test models, namely flat-bottomed, wedge-shaped, and ship form, are discussed. Theoretical studies based on the results of some experimental investigations are also highlighted. Examples of implementing drop test data in ship structural design are given to demonstrate the applicability of such data.

C1. INTRODUCTION

Slamming impact has long been recognised as one of the major sources of ship structural damage resulting from operation in rough seas [C1,C2]. Slamming damage may develop in a small local area where the impact pressure persists, but it could also extend to a larger area which, up to a certain level, brings about global structural failures due to the so-called hull whipping. To explore the main pressure that affects a local area, not considering the global response, remains a complex task despite extensive investigations which have been performed in the past. It is not surprising, therefore, that such a study on ship slamming is now pursued and continuously updated.

A further aspect which, in most cases is over-shadowed by much concern for ship safety (structural failure) and sometimes not so well realised by ship designers is the degradation of economical operation of the ship caused by slamming. This particular aspect is related to the speed loss by virtue of voluntary slowing down ordered by the ship master. If, in moderate seas, the speed loss is mainly induced by the increase in added resistance of the ship, then in more severe waves this predominancy is replaced by the insistence of slamming that which to some level forces the ship to divert its course headings [C3]. Such an effect is even pronounced in the case of advanced marine crafts where high speed operation is much more susceptible to surface wave slamming.

The study of ship slamming, like in any other branch of ship science, is commonly performed both theoretically, by adopting hydrodynamic principles, and

experimentally, i.e. by carrying out small scale model tests. Slamming measurements on full scale ships are also made sometimes but, in view of the longer time as well as the appreciable expenses incurred on such an investigation, it is less frequently organised. Experimental study of ship slamming may be arranged in different ways, namely, drop tests on a 2-dimensional model, a 3-dimensional model and a 3-dimensional model seakeeping test. Drop test on a 2-dimensional model may be regarded as the simplest method, yet it is the most appropriate in the first place to gain insight of the ship slamming in general regardless of the peculiar performance of the ship being investigated (e.g. slow and high speed ships), unless it is specifically designed for a given ship form.

This report presents a review of ship slamming studies based on the drop test approach. The review attempts to collect as much information as is available in the open literature for such a study and to summarise the state-of-art of the work in this particular ship research area. Theoretical studies that were developed in conjunction with some of the experimental work are an important topic for discussion. The experimental investigations dealt with in this report are these three main types, namely, the drop tests on flat-bottomed structures, wedge-shaped structures, and ship form models. The main features of the tests put forward are those of the instrumentation and experimental set up, impact parameters being explored, and discussion of the test results. The significance of the drop test data for further development in ship structural design will be indicated.

C2. DROP TESTS ON FLAT-BOTTOMED MODELS

C2.1. Chuang

During the mid 1960s Chuang performed an extensive experimental investigation on ship slamming by way of a flat bottom drop test at the DTMB [C4]. The test was carried out on a flat-bottomed steel model, size 20x26.5x0.5 in. (LxBxt) attached to a steel box, which accumulated a total weight of 255 lbs. The flat bottom was stiffened with four 0.5 in. x 3 in. therefore the model can be considered to be a rigid body. The drop heights were 3 up to 7.5 in. with increment of 1.5 in. Flat plates were mounted vertically on the platform to provide two rigid sidewalls on the model box to ensure that two-dimensional flow is maintained.

The instrumentation system used for this experiment consisted of quartz-crystal pressure transducers, charge amplifiers, a dual-beam oscilloscope, and a high-speed streak camera. Two transducers were installed, one at the the centre of the model and the other near the edge at the middle of the longer side of the plate. The transducers

were rated to have a natural frequency of 200 kc and a rise time of 1 microsec. There is no mention about the maximum pressure capacity of the transducers, even though, from an existing ref. [C5], a maximum pressure of 70 psi was anticipated to excite the model.

The main aim of this drop test was to generate a slamming parameter that correlates between the impact pressure and the vertical drop velocity. Further, the investigation was also directed to prove the presence of a certain factor, called the acoustic pressure, which was believed at that time to contribute significantly to the build up of the flat bottom pressure magnitude. The existence of acoustic pressure in conjunction with the development of flat bottom impact can be explained as follows. When a flat body strikes the surface of a fluid at an impact velocity V_0, the propagation of the momentary increase of pressure in the fluid takes place at the speed of sound in the fluid, designated by c_1 [C6]. The mass of fluid accelerated in the time Δt is

$$m_f = \rho A c_1 \Delta t \tag{C2.1}$$

where ρ is the mass density of the fluid and A is the striking area of the flat body upon the fluid surface.

Since the velocity of the mass of fluid is increased from zero to V_0 in the time Δt, the force F acting upon the falling body is therefore

$$\begin{aligned} F &= m_f\left[\frac{V_0 - 0}{\Delta t}\right] \\ &= \rho A c_1 V_0 \end{aligned} \tag{C2.2}$$

The pressure p (the approximate maximum value), which is the force per unit area, is

$$p = \rho c_1 V_0 \tag{C2.3}$$

Although such an acoustic pressure is believed to exist during flat bottom impacts, the experiment, however, has not been successfully generated to prove this. So far it can only be explained, firstly, that the instrument was not sufficient to record the event which takes place at only a fraction of instant Δt. Secondly, it was also thought that the elastic deformation of the plate relieved the acoustic pressure. Thus, it was finally presumed that the ship hull will response largely to the impact which develops upon the formation of hydrodynamic pressures. Furthermore, the effect of entrapped air should also be taken into consideration.

From the test data analysis it was found that the maximum magnitude of impact pressure at the edges of the model was very much the same as at the centreline. This evaluation implied the peak pressure was generally evenly distributed over the flat surface at the initial impact. It was further observed from the high-speed photographs taken during the experiment that the air cushion did exist. The maximum pressure recorded for the model dropped on calm water surface has been compared to those on rippled water. However, no substantial difference was found in the two cases. The scaling law has not been thoroughly observed in the experiment. Overall only a few peak pressure data was presented (see Fig. C2.1), but this seems to adequately represent the trend for a wider range of peak pressure-velocity correlation.

Following this experiment, a theoretical study of flat bottom slamming phenomenon was performed. Based on the pressure record, a mathematical approximation of the pressure time history has been derived. This mathematical formulation is written as

$$p(t) = 2p_{max} e^{-1.4t/T} \sin \pi \frac{t}{T} \qquad \text{(C2.4)}$$

where T is the duration of the first positive pulse and equal to $4L/c_a$, where L is the half-width of an infinitely long plate and c_a is the speed of sound in air. The maximum impact pressure p_{max} was derived on the assumption that a layer of air is trapped between the falling body and the fluid. It follows that the time required for pressure waves to travel in air from zero to maximum is $2L/c_a$, and the same amount is required to decay. Mathematical manipulation was further developed by the fact that total impulse produced during impact is the same whether it is or is not present. The resulting maximum impact pressure formulation is finally given by

$$p_{max} = \frac{1}{32(144)} \left[\frac{1.4^2 + \pi^2}{e^{-1.4} + 1} \right] \rho c_a V_0 \quad \text{(psi)} \qquad \text{(C2.5)}$$

Implementing $\rho = 1.94$ lb-sec^2/ft^4 for fresh water and $c_a = 1125$ fps, eq. (C2.5) reduces to

$$p_{max} = 4.5\, V_0 \quad \text{(psi)} \qquad \text{(C2.6)}$$

The maximum pressure predicted by the foregoing mathematical formulation has been compared with the experimental data of the corresponding study and those from other sources. The conclusion is that the theory agrees well with the test data (see Fig. C2.2), although additional testing still needs to be performed for examination.

Another flat bottom test has been conducted by Chuang [C7] on a larger scale model, that is, a one-quarter scale representation of the bottom structure of a U.S. Coast Guard ship (see Fig. C2.3). The model scantlings are arranged as on the actual ship (with an overall size of 80 in. x 90 in.), and hence it can be regarded as a flexible structure. The model was extensively instrumented with pressure transducers, strain gauges, deflection gauges, velocity meters and an accelerometer which are located at various positions over the bottom area. Although this large scale test was performed near an exposed bay where the water surface is subjected to small waves, the condition was regarded to be advantageous. From an impact characterisation point of view such a test on rippled water closely resembled that on full-scale ships in which slamming normally occurs on water surfaces which are highly irregular. Observation during the test was made for the model dropped from three different heights, namely, 2, 4 and 6 feet above the water surface. No testing beyond a 6 feet drop height was performed because the bottom of the model had been dished-in approximately 0.8 in so that it was no longer representative of a flat-bottom hull construction.

A typical test result on this large flat-bottom model is as seen in Fig. C2.4. An evaluation of structural response of the flat-bottomed model reveals that the peak strain for the 2 ft drop is larger than for the 4 and 6 ft drop, although the former has suffered approximately the same magnitude of impact pressure. It was found that the larger strain for the 2 ft drop was induced by the pressure which has more persistent dynamical characteristic than the other. The structural deformation of the model, however, may be considered to linearly correlate to the drop height, that is, the deformation will increase as the drop height is increased.

C2.2. Verhagen

The study by Verhagen was carried out to investigate the importance of the air cushion in reducing the impact pressure intensity [C8]. Both theoretical and experimental methods were adopted in this study on a drop test model.

The whole tests were carried out in a moderate aquarium 1000 mm x 405 mm x 400 mm with glass walls and bottom. The flat-bottomed model used in the experiment was sized 400 mm x 400 mm x 20 mm, made of a cast of aluminium plate with a total weight of approximately 8 kg. Perspex vertical strips were attached at the two parallel edges of the model so that a two-dimensional flow condition could be simulated. The model was restrained from rotation by a vertical shaft which slid down on a steel frame support fixed over the aquarium.

One pressure transducer of barium-titanat crystal type was used in the test to measure the impact pressure at the centre of the flat bottom of the model. Observations were made of the model which was dropped from various heights up to 50 cm on a smooth water. A photo-electric cell was used to detect the plate which had fallen to a few mm above the water, which at the same time would activate an oscilloscope. The pressure-time history for each drop was recorded on a high-speed photograph. Several phenomena were able to be identified during the test, as follows. The water elevation was at first noticeable at the plate edges just before the plate touches the water surface, that is, the water touched annularly from its circumference and progressed to the centre. In this instant the air cushion was rapidly formed and induced to an increase in pressure. After the two surfaces touched the air layer broke up into bubbles, beginning at the edges and extending to the centre of the plate with the speed approximately equal to the velocity of sound in air.

The theoretical analysis within this study was developed to calculate the pressure as a function of time during impact. The underlying assumption and the lay out of the procedure in developing the mathematical model can be described as follows. Considering the flow in the air layer under the falling body to be a one dimensional compressible flow of a perfect gas, the flow conditions are then calculated by the method of characteristics. The disturbance of the water surface owing to the imposed air pressure is solved by adopting the potential theory. Compressibility of water is neglected, as the characteristic time interval for the impulsive pressure appears to be large compared to l/c_1, where l is the half-width of the bottom plate. At the moment the edges of the plate touches the elevated water surface an air cushion is trapped. This volume of air is calculated. Assuming that the escape of air after that moment can be neglected and that the downward velocity of the mean water surface under the plate is independent of the place co-ordinate, the adiabatic compression of air layer is calculated. The full mathematical derivation to predict the impact pressure time history is given in ref. [C8], which results in the following expression

$$\frac{d(p/p_1)}{d(c_0 t/l)} = \pm\left(\frac{p}{p_1}\right)^{\frac{1+\gamma}{\gamma}} x \left[\frac{\frac{\pi}{2}l^2\rho_1 + M}{M}\frac{8\gamma l\rho_a}{\pi h_1\rho_1}\left[\frac{p_1}{p_0(\gamma-1)} x \left\{1-\left(\frac{p}{p_1}\right)^{\frac{\gamma-1}{\gamma}}\right\}+1-\left(\frac{p}{p_1}\right)^{\frac{1}{\gamma}}\right]+\frac{\gamma^2 l^2}{h_1^2}\left(\frac{w_1 - V_1}{c_0}\right)^2\right]^{1/2} \qquad \text{(C2.7)}$$

With the initial condition $p=p_1$ for $t=t_1$ the relation between pressure and time can be solved numerically. The impulsive pressure becomes maximum when $dp/dt=0$. The magnitude of $p=p_{max}$ follows from

$$\frac{1}{\gamma-1}\frac{p_1}{p_0}\left\{1-\left(\frac{p_{max}}{p_1}\right)^{\frac{\gamma-1}{\gamma}}\right\}+1-\left(\frac{p_{max}}{p_1}\right)^{-\frac{1}{\gamma}}$$

$$=-\frac{\pi}{8}\frac{\rho_1}{\rho_a}\frac{\gamma l}{h_1}\frac{M}{\frac{\pi}{2}l^2\rho_1+M}\left(\frac{w_1-V_1}{c_0}\right)^2 \qquad \text{(C2.8)}$$

The initial condition of the trapped air layer h_1/l, p_1/p_0, w_1/c_0, and V_1/c_0 can be obtained from [C8].

A numerical evaluation has been made using the above expression for the different values of drop height h, half width l and mass of the free falling body M, by considering the normal atmospheric conditions. The results from the numerical evaluation and the drop test are as shown in Fig. C2.5, in which the maximum impact pressure is plotted against the drop height. The analysis on the effects of different plate widths on the maximum impact pressure is as presented in Fig. C2.6. Comparison of the pressure time history generated using the analytical formulation and from the experiment is depicted in Fig. C2.7 where a fairly good agreement of the two results is evident.

From those evaluations Verhagen has drawn the conclusion related to flat bottom impact as follows. The air cushioning effect does exist under the bottom at the limit of impact and the most significant pressure rise under the body occurs after the moment the escape velocity of the air reaches the velocity of sound. The maximum impact pressure p_{max} exerted on a flat bottom dropped on to a water surface is approximately directly proportional to the drop height or to the square of the downward body speed for a small value of $M/\rho l^2$. With the increase of mass, there is a more or less linear correlation between p_{max} and impact velocity V. Nonetheless, the maximum impact pressure seems to be independent of the plate size (see Fig. C2.6). Hence, to develop the same impact pressure of two bodies falling from an equal distance above the water surface, the mass of the body per unit bottom surface must be directly proportional to the two-dimensional body width. In other words, the larger body must be relatively heavier than the smaller one.

The pressure time history in Fig. C2.7 reveals that with the increasing value of the maximum pressure the gradient of the pressure-time curve becomes steeper. The theory of air entrapment is in good agreement with experimental data, even though, in general the theory is valid only to relatively light models. Further, an important pressure variation can occur in a small time interval compared to $c_a t/l$, such that the

time-dependent term in the wave equation can no longer be neglected. That is, the compressibility effects of the water cannot be neglected when the maximum pressure increases. Also, the elasticity of the structure in that case must be accounted for (the more rigid the structure the higher the impact pressure induced on to it).

C2.3. Lewison and Maclean

The drop test on probably the largest flat bottom model reported so far has been carried out by Lewison and Maclean at the University of California, Berkeley [C9]. The nominal size of the flat bottom is 10 ft wide and 8ft long constructed out of a 1/2 in thick steel plate, that is a quarter-scale model representing a ship bottom structure which had suffered large deformations in service. In the absence of any well proven flat bottom impact theory, the model was designed based on the knowledge of the largest ship slamming pressure recorded at the time, i.e. about 300 psi. By comparing the results of slamming measurements on the Unimak it was assumed that the duration of such an impact load is about 4 msec and related to an impact velocity of 20 fps. The test machine was then designed to achieve a model impact velocity of up to 25 fps. To ensure the model did not suffer too many deformations under the maximum impact force it was fabricated with 9 in. spaced transverse stiffeners and 30 in. spaced longitudinal beams, hence, it was a substantially robust structure.

The weight of the flat bottom model was about 6100 lb and, bolted to the water ballasted drop test car (steel box), formed an ultimate total weight of 39,300 lb. A winch was used to hoist the car after each drop, and it was retained in place by a vacuum. This was maintained between the top of the car and a holding plate suspended below a top platform by lead screws. The car was fitted with guidance arms that slid between vertical guide tracks. The car was also equipped with eight arrest pistons which mated with cylinders in the box girders at the side, forcing water through small side holes and simultaneously compressing coil springs to bring the model to rest after it had penetrated some distance into the water.

During the initial tests the instrumentation used comprised only one pressure transducer and an accelerometer attached to the car. Despite this limitation, extensive tests have been made on the model, that is, by placing the transducer in different locations to record the pressure distribution over the model. The tests were carried out up to a drop height of 5 ft with a thorough observation at certain drop conditions. A typical test result of the pressure distribution along the centreline of the model is as shown in Fig. C2.8. As is expected for the two-dimensional flow, the variation of the peak pressure in this plane is sufficiently small. On the other hand, the peak pressure distribution along the transverse mid-section of the model is considerably large (see

Fig. C2.9). The peak pressure distribution in this case reaches its maximum at the centre and decreasing towards the edges, even though the peak pressure occurred earlier at the edges and moved towards the centre. In view of the variation in impact pressures for different drop heights it was observed that the peak pressure increased linearly with the increasing of drop height and therefore with the square of impact velocity.

Based on the test results, a theoretical study was then performed to develop new analytical approaches designated as one-dimensional theory and two-dimensional theory. The study adopts the assumption that the falling body has an under surface flat and parallel to the undisturbed water surface, that the model is rigid, and that the water is compressible. For the one-dimensional theory further assumptions was made, i.e. the model is so large compared with the air gap between it and the water surface so as the sideways movement of the air can be ignored and the entrapped air is enduring an adiabatic compression. Working out the relationship between the model surface and water surface movements to the standard atmospheric conditions of air the following second-order differential equation for the pressure is obtained.

$$\ddot{p} - \frac{1.715\dot{p}^2}{p} + \frac{1.4p^{1.715}\dot{p}}{p_A^{0.715}bdC} + \frac{1.4p^{1.715}}{p_A^{0.715}bm} x\,(p - p_A - mg) = 0 \qquad \text{(C2.9)}$$

where b is the height of initial air-gap, C is the velocity of sound in water, d is the density of water and m is the mass loading of the model. The numerical solution of eq. (C2.9) is made by adopting the experimental values of m and V, with b as a parameter, and setting out the initial conditions of t=0, $p=p_A$, and x=V, hence $p=1.4p_AV/b$. Figure C2.10 shows the comparison of the theoretical and experimental results with the values of b chosen from experimental observation. The conformity of the two results is rather poor even though the peak pressure and the duration of pressure derived by the theory seems to be in the right order. These are still much better than that given by Ogilvie [C10].

An improvement to the one-dimensional theory was then synthesised by taking into account that the sideways movement of the air takes place during the flat bottom impact. Another assumption adopted to this phenomenon is that the average pressure, causing deceleration of the model, is essentially a constant fraction of the pressure on the centreline. Allowing this effect, the modified differential equation for p can be written as

$$\ddot{p} = \frac{1.715p^2}{p} + \frac{0.4V\dot{p} - \frac{1.4p^{1.715}}{p_A^{0.715}}\left\{\frac{f(p_\alpha - p_A)}{m} - g + \frac{\dot{p}}{dC}\right\}}{b - 0.2tV} \qquad \text{(C2.10)}$$

with the initial conditions of t=0, $p=p_A$, and $\dot{p}=1.12p_AV/b$. In Fig. C2.11 some typical results are shown, compared to the same experimental curve. The improvement over the earlier formulation is marked, but the agreement between theory and experiment is still only moderate.

In the two-dimensional theory the hydrodynamic movement of the water (which is not dependent on its compressibility) is considered at the same time as the motion and properties of the air which are thoroughly treated. The solution to the problem was overcome by first contemplating the continuity of mass, conservation of momentum and energy equations which yield to the differential equations in four variables, p, ρ, w and U, i.e. the pressure, density, model's bottom-water surface distance and the outward air velocity, respectively. Each of these variables can be further approximated as a polynomial in z (see Fig. C2.12) and is written :

$$\begin{aligned} p &= p_0 - p_2 z^2 - p_3 z^2|z| \ldots\ldots \\ \rho &= \rho_0 - \rho_2 z^2 \ldots\ldots \\ U &= U_1 z + U_3 z^3 \ldots\ldots \\ w &= w_0 + w_2 z^2 \ldots\ldots \end{aligned} \qquad \text{(C2.11)}$$

The coefficients in the above equations are assumed to vary with time, t. Moreover, it is assumed that this expansion is valid for the area of the integration of interest and that the polynomials are convergent.

The polynomial coefficients in eq. (C2.11) are computed from the following set of five equations which are differentiated from the continuity, momentum and energy equations as follows :

$$\rho_0 \dot{w}_0 + w_0 \dot{\rho}_0 + w_0 \rho_0 U_1 = 0 \qquad \text{(C2.12)}$$

$$w_0 \rho_0 (\dot{U}_1 + U_1^2) + 1.784_{10}6(p_0 w_2 - p_2 w_0) = 0 \qquad \text{(C2.13)}$$

$$-w_0 p_3 + 3.74_{10} - 9\rho U_1 |U_1| = 0 \qquad \text{(C2.14)}$$

$$p_0 \dot{w}_0 + 0.7143 w_0 p_{0,6} + U_1 p_0 w_0 = 0 \qquad \text{(C2.15)}$$

$$\begin{aligned} p_0 \dot{w}_2 - \dot{w}_0 p_2 + 0.7143(w_2 \dot{p}_0 - w_0 \dot{p}_2) + 3 w_0 p_0 U_3 \\ - 2.4286 U_1 (w_0 p_2 - w_2 p_0) = 0 \end{aligned} \qquad \text{(C2.16)}$$

The calculation is procured by setting up an initial value of the w terms which are then revised after the p terms are obtained by imposing the boundary condition accounting for the constant ratio of pressure at the edge and that on the centreline of the model. The

latter is executed with an iteration procedure on those equations, namely, if p_0 and $\dot{p}_0$ are estimated, eq. (C2.15) gives U_1; then eq. (C2.12) gives ρ_0, eq. (C2.13) gives p_2, eq. (C2.16) gives U_3 and finally, eq. (C2.14) gives p_3. A rigorous mathematical manipulation to derive the above numerical formulations is fully described in ref. [C9]. A typical example of the theoretical result is as shown in Fig. C2.13 and is plotted together with the experimental result. The agreement between theoretical and experimental pressure curves is very good, both in terms of the pressure duration and the peak pressure value.

In the second experimental programme Lewison has conducted a further study on slamming to explore the mechanism in reducing slamming impact on seagoing ships [C11]. One way in which slamming pressure reduction may be attained is by the aid of a control mechanism in the form of two parallel external side keels that would activate the air entrapment effect underneath the impacting surface. For this investigation the drop test model was fitted with outside keels (flanges) of two different sizes, namely, 1.5 and 3.0 in. in height, positioned near the edges of the flat bottom. Experimental results show the effectiveness of the flange attachment in the reduction of maximum impact pressure, as shown in Fig. C2.14.

This encouraged Lewison to carry out a further slamming experiment at NPL on the Mariner type ship model by seakeeping techniques. The Mariner form was chosen for this investigation because it has already been extensively studied at NSRDC, notably by Ochi [C12], so that the slamming data is widely available for comparison. In this particular test the model (1/55 scale of the real ship) was fitted with two forefoot outside keels parallel to the centreline at a sufficiently concave bottom area which was subjected to severe damage. Pressure transducers of range 0-10 psig (0-550 psig for ship) were installed on the forefoot centreline. The first experiment was done in calm water to scrutinise the flow lines over the forefoot so that the keels would not unduly disturb the local flow pattern. The actual slamming observation was then conducted in irregular head seas, with and without keels in position, in respectably severe conditions. The results of this test suggests that the reduction in numbers of most severe impacts is achievable on the model with fitted keels. The maximum impact pressure recorded also showed a substantial reduction, that is, about 124-137 psig compared to 55-69 psig for the bare hull and keels in position, respectively.

In conjunction with the above investigation a detailed study of flat bottom impact was also explored, especially regarding the phenomenon of air entrapment and the development of impact pressure, as follows. Until the model is within a few inches of the water surface, no noticeable increase of pressure occurs on the underside, and it accelerates downward under gravity. As the volume of air underneath the model continuously diminishes, there is an outward airflow across the vertical planes into the

direction of the open edges. The flow velocity would be expected to vary across the height of air gap but, if this is quite small, say 0.1 x the half-breadth of the model, then the flow may be treated as uniform across the air gap. (The analysis is only valid when the model is already close to the water surface, therefore when to start the analysis must be chosen, along with some means of estimating the conditions at that instant). As the model continues to descend the outward air velocity at the edges increases rapidly and consequently a pressure difference occurs between the edges of the model and its centre. Provided the velocity at the edges is subsonic, the pressure there will be atmospheric and therefore there will be an increased air pressure towards the centre of the model. A pressure gradient is also needed to oppose friction between the fast moving air and the underside of the model and the water surface; this makes an additional contribution to the pressure on the centreline of the model. At this stage, the pressure time history is termed as progressing in the regime I.

While the above process is taking place in regime I, the water surface under the model has been experiencing the same rise of pressure and has started to move downwards. This downward movement arises from two sources, namely, the compressible movement in which the velocity of the water surface is proportional to the pressure, and the hydrodynamic movement which would take place equally in the absence of compressibility. The effects of both of these movements means the depression of the water is greater under the centre of the model than at the edges; consequently the height of the air gap decreases steadily towards the edge forming a throat.

At some time the air velocity in the throat at the edge of the model will reach the local speed of sound. As the air under the model continues to be compressed the throat velocity must remain sonic, but the pressure will rise above the atmospheric pressure and wave expansion will occur beyond the edge of the model. The process continues where pressure rises rapidly, being greatest on the centreline and will fall off smoothly towards the edge of the model. This stage of process is called regime II; as opposed to the subsonic regime I.

The height of the air gap at the throat will continually diminish and at some time the gap will close, although the air jet will delay its closure by blowing the surface away to form spray. (This process cannot easily be represented analytically which is one of the difficulties of the theory). As the closure takes place and the outward airflow at the edges stops, a pressure wave travels inward in the direction of the centre of the model. There are air bubbles trapped under the model and further compressed. This process is called regime III.

As the air continues to be compressed the downward velocity of the water surface will increase and will eventually equal the downward velocity of the model. When the

velocity of the model and the water surface are equal, the local air pressure will be at a maximum and, thereafter, as the water surface moves downwards more quickly than the model, the pressure will decrease. The water velocity will accordingly diminish and for the second time it will be equal to the model velocity, and the air pressure will be at a minimum which, from experimental observation, is normally below atmospheric pressure.

Based on this new admission Lewison attempted to modify the previous theory by adopting boundary conditions which apply pressure to the edges instead of considering a constant fraction of centreline-edge pressure ratio. In regime I the edge pressure is essentially unity, i.e.

$$p(z = a) = 1 \tag{C2.17}$$

In regime II the edge velocity is sonic and so

$$U(x = a) = C_a\sqrt{\frac{p(z = a)}{\rho(z = a)}} \tag{C2.18}$$

In regime III there is no outward flow and simply

$$U(z = a) = 0 \tag{C2.19}$$

These boundary conditions are used to solve the enhanced governing equations to derive the coefficients in the polynomial equations of p, ρ, U and w as below.

$$\rho_0\dot{w}_0 + w_0\dot{\rho}_0 + w_0\rho_0 U_1 = 0 \tag{C2.20}$$

$$\rho_0\dot{w}_2 - \rho_2\dot{w}_0 + w_2\dot{\rho}_0 - w_0\dot{\rho}_2 + 3U_1(\rho_0 w_2 - w_0\rho_2) + 3U_3\rho_0 w_0 = 0 \tag{C2.21}$$

$$\rho_0(\dot{U}_1 + U_1^2) - 1.784_{10}6p_2 = 0 \tag{C2.22}$$

$$-w_0 p_3 + 3.74_{10} - 9\rho_0 U_1^2 = 0 \tag{C2.23}$$

$$(\dot{U}_1 + U_1^2)(w_2\rho_0 - w_0\rho_2) + w_0\rho_0(\dot{U}_3 + 4U_1U_3) - 1.784_{10}6(p_2 w_2 + 2p_4 w_0 = 0 \tag{C2.24}$$

$$w_0\dot{p}_0 + 1.4p_0\dot{w}_0 + 1.4U_1 p_0 w_0 = 0 \tag{C2.25}$$

$$1.4(p_0\dot{w}_2 - p_2\dot{w}_0) + (w_2\dot{p}_0 - w_0\dot{p}_2) + 4.2p_0(U_1 w_2 + U_3 w_0) - 3.4U_1 w_0 p_2 = 0 \tag{C2.26}$$

$$p_3\left(1.4\dot{w}_0 - 4.4w_0U_1\right) + \dot{p}_3w_0 + 5.6U_4p_0w_0U_1$$
$$= 4.48_{10} - 9\rho_0U_1^3 \qquad \text{(C2.27)}$$

whereas the polynomial equations with some additional coefficients are rewritten as follows :

$$\begin{aligned} p &= p_0 - p_2z^2 - p_3z^2|z| - p_4z^4 ..... \\ \rho &= \rho_0 - \rho_2z^2 - \rho_3z^2|z| ..... \\ U &= U_1z + U_3z^3 + U_4z^3|z| ..... \\ w &= w_0 + w_2z^2 ..... \end{aligned} \qquad \text{(C2.28)}$$

The comparison of pressure histories from experimental and modified theory is shown in Fig. C2.15. It is apparent that the theoretically predicted pressures are higher than those measured and that the curves are more sharply peaked. Moreover, for the centreline pressure, the estimation of the modified theory is not as good as that predicted by the previous theory (see Fig. C2.13). The new theory, however, gives a much better description of the underlying physical mechanism of two-dimensional flat impact. As can be seen in Fig. C2.15, the theory predicts the correct ratios of the pressures at the centreline and at the edge of the model, as regards with the maximum values and also that before the peak pressure at the edge; the pressure is greater on the centreline. Furthermore, the peak pressure at the edge is shown to occur before that at the centreline, and the time differences are in the right order of magnitude, i.e. about 1-2 msec.

C2.4. Ando

Many attempts to reduce structural damage due to ship slamming have been made in the past, and one of the most recent studies was made by Ando [C13].He suggests that slamming force can be reduced by covering a certain area of ship bottom, which is felt to be susceptible to such a load, with a kind of elastomeric material. To verify his suggestion Ando has carried out experimental and analytical studies to evaluate the effectiveness of elastomeric layers on a flat bottom model.

The model which was used in the drop test was 26.5 in. x 20 in. x 0.5 in. (LxBxt) and was made of steel plate and attached to a steel box. Including the lead ballast, guide rods, and other attachments, the total weight of the dropped structure was about 275 lb. To ensure two-dimensional flow condition consistent with the analysis

two parallel rigid walls were erected from the bottom of the tank to a certain distance above the water level. The only measuring instrument mounted on the model was a piezo-electric type accelerometer, which was located on the bottom plate near the centre inside the steel box. The signals from the accelerometer were fed into a spectrum analyser and the display was plotted on a printer.

Three conditions of test were observed, namely, one rigid bottom and two layered bottom conditions. The layer material used was a closed cellular rubber in two thicknesses, 1 and 0.5 in. In this context the steel bottom is considered infinitely rigid compared to the elastomeric layered bottoms, since Young's modulus of steel is 210 kN/mm^2 while Young's moduli of the layer material was well below 1 N/mm^2. The model was observed for the drop height of 3, 4.5, 6, 7 and 7.5 in. Several drops were made at each combination of drop height and bottom plate configuration, and the measured maximum impact accelerations were averaged to give the final results.

The pressure-strain relations for the closed cellular rubber sheets under static loading were measured for the two thicknesses using test pieces whose surface areas, 10 x 13.2 in., were equal to a quarter of the bottom area of the model. The strain of a test piece is the absolute ratio of the deflection (the change of thickness) to the undeformed thickness. An analytical approximation derived from the measurement was found as

$$p = \exp\left(0.713\varepsilon + \varepsilon^5\right)\frac{2E_0}{\pi}\tan\frac{\pi\varepsilon}{2} \qquad \text{(C2.29)}$$

where p is pressure, ε is strain, and $E_0 = 124\ kN/m^2$ is the initial Young's modulus of the layer material.

The analytical model for flat bottom impact was developed by assuming that the same mechanism for the formation of the air layer was in effect regardless whether or not an elastomeric layer was applied to the under surface. Away from the immediate vicinities of the bottom edges, the deformation of the free surface was considered negligible, so that entrapped air was seen to form a layer of uniform thickness and of width equal to that of the bottom [C4,C8]. The differential equation governing the total height Δ of the air and elastomeric layers (see Fig. C2.16) may be derived by taking into account the difference in descending velocities of the flat bottom (V) and the water surface (v) as follows

$$\begin{aligned}\ddot{\Delta} = \dot{v} - \dot{V} &= \frac{2b}{m}(p - p_0) + \frac{2b}{M}(p - p_0) - g \\ &= \left(\frac{m+M}{mM}\right)2b(p - p_0) - g \end{aligned} \qquad \text{(C2.30)}$$

where b is the half-width of the bottom, g the acceleration of gravity, M and m the drop mass and added mass per unit length, respectively, and p_0 the initial pressure of the entrapped air. The added mass is given by assuming an irrotational flow condition at the impact surface as [C6]

$$m = \frac{\rho}{2}\pi b^2$$

The above differential equation is valid from immediately the edges of the model contact the piled up water (t = 0) to at least the instant when p achieves its maximum.

By assuming that at t = 0 the deviation of the pressure of the entrapped air from the atmospheric pressure was negligible, and that the initial downward motion v of the free surface beneath the bottom was consequently negligible compared with the descending velocity of the bottom, then the initial conditions are set out as

$$\Delta(0) = \Delta_0 = h_0 + d_0 \quad \text{and}$$
$$\dot{\Delta}(0) = V_0 = -\sqrt{2g(H_0 - h_0)} \qquad \text{(C2.31)}$$

where h_0 and d_0 are the initial heights of the air layer and the elastomeric layer, respectively, and H_0 is the drop height. It follows that h_0 is equal to the height of the elevated water measured from the calm surface level at t = 0.

Let $\delta_a = f_a(p)$ and $\delta_e = f_e(p)$ denote the pressure-deflection relations for individual layers of air and elastomeric, respectively, hence the total deflection δ of the two layers for given pressure p is found as

$$\delta = \delta_a + \delta_e = f_a(p) + f_e(p) = f(p) \qquad \text{(C2.32)}$$

Considering l as denoting the function relating δ to Δ; that is, $\delta = l(\Delta) = \Delta_0 - \Delta$, then pressure p can be expressed in terms of Δ via

$$p = f^{-1}(\delta) = f^{-1}[l(\Delta)] = F(\Delta) \qquad \text{(C2.33)}$$

where f^{-1} denotes the inverse function of f defined in eq (C2.32) and F the composite function of f^{-1} and l. The solution to eq. (C2.30) is achieved by substituting eq. (C2.33), and gives Δ as a function of time t. The temporal variation of the acceleration of the bottom in units of gravity, G=V/g can be obtained through

$$G = 1 - \frac{2b}{Mg}(p - p_0) = 1 - \frac{2b}{Mg}[F(\Delta) - p_0]$$

If G_{max} is designated maximum impact acceleration of the bottom in units of gravity then, by solving the initial-value problem it is possible to derive the following functional relationship

$$G_{max} = G(E_0, H_0, M, b, d_0, h_0) \qquad \text{(C2.34)}$$

Ultimately the variation of G_{max} as a function of E_0 can be evaluated to demonstrate the effectiveness of the elastomeric layer and to determine the optimal E_0 for given drop conditions.

Typical test results of flat bottom slamming for three different configurations are as shown in Fig. C2.17. The graphs exhibit a substantial decrease in the maximum acceleration when elastomeric layers are attached to the model. However, the peak period of the layered model tends to be larger than that of the rigid bottom. The test data for all drop heights are presented, together with the predicted value using the above semi-empirical formulation, as shown in Fig. C2.18. The agreement between the experimental data and theoretical approximation is essentially good. The correlation of the maximum impact acceleration and Young's modulus of the elastomeric layer was then deduced from the experimental data and pressure-strain equation, as presented in Fig. C2.19. As can be seen, the curves reflect the fact that in the limit as $E_0 \to 0$ or $E_0 \to \infty$, the cushioning effect of the elastomeric layer becomes negligible and the maximum impact acceleration of the body approaches a value corresponding to that of the rigid bottom.

C3. DROP TESTS ON WEDGE-SHAPED MODELS

C3.1. Chuang

As the sequence to his initial investigation on the impact pressure of flat-bottom slamming Chuang carried out a further set of drop tests on the same flat-bottomed model, as well as on wedge-shaped bodies [C14]. The primary reason for conducting another flat-bottom test was to observe more closely whether the previously measured impact pressures were generated by the compression of the trapped air or by the actual contact between the bottom and the water surfaces. Such information is important to clarify the assumption made in deriving the empirical estimations of flat bottom slamming as given in eqs. (C2.4) and (C2.5), that is, the first positive pulse of the

impact pressure occurred during the split second when the air was trapped momentarily between the falling body and the water surface. In the case of wedge-shaped bodies, the study was aimed at evaluation of the semi-empirical formulations in predicting impact pressure as proposed by Wagner [C15] and von Kármán [C6] below.

The formulation of impact pressure distribution p(x) due to unsteady hydrodynamic pressure exerted on a rigid wedge-shaped body penetrating a water surface is written as

$$p(x) = \frac{1}{2}\rho V^2 \left[\frac{\pi}{\beta\left(1-\frac{x^2}{L^2}\right)^{1/2}} - \frac{\frac{x^2}{L^2}}{1-\frac{x^2}{L^2}} + \frac{2\ddot{z}}{V^2}\left(L^2-x^2\right)^{1/2} \right] \qquad \text{(C3.1)}$$

The notations used within eq. (C3.1) are in Fig. C3.1. The maximum impact pressure p_{max} is obtained by setting dp/dx=0 and by assuming the acceleration of the falling body $\ddot{z}$ to be negligibly small. This gives :

$$p_{max} = \frac{1}{2}\rho V^2 \left[1 + \frac{\pi^2}{4\beta^2} \right] \qquad \text{(C3.2)}$$

which takes place at the point where :

$$x = L\left(1 - \frac{4\beta^2}{\pi^2}\right)^{1/2} \qquad \text{(C3.3)}$$

The velocity V adopted to compute the maximum pressure is not necessarily the initial impact velocity V_0, because such a pressure generally occurs some time t after the instant of impact t_0. The magnitude of pressure at the keel of the wedge is calculated by substituting x = 0 into eq. (C3.1), thus :

$$p_{keel} = \frac{1}{2}\rho V^2 \left[\frac{\pi}{\beta} + \frac{2\ddot{z}}{V^2} L \right] \qquad \text{(C3.4)}$$

or, if $\ddot{z}$ can be neglected this equation reduces to :

$$p_{keel} = \frac{1}{2}\rho V^2 \frac{\pi}{\beta} \qquad \text{(C3.5)}$$

The above equation eventually resembles the formulation given earlier by von

Kármán [C6] for the maximum pressure at the moment t_0 when the keel makes first contact with the water surface, i.e.

$$p_{keel} = \frac{1}{2}\rho V_0^2 \frac{\pi}{\tan\beta} \tag{C3.6}$$

The test facilities used in these later tests at DTMB were the same as those for the flat-bottomed model [C4]. The tests were carried out for five different wedge-shaped models with the deadrise angles β of 1, 3, 6, 10 and 15 deg. Modification to the flat-bottomed model was made to construct the wedge-shaped models by cutting a 20-in. side into two equal widths and then welding two pieces of plates to form a V-shaped bottom with an intended deadrise angle. Three pressure transducers were positioned transversely at three different locations, namely, at the keel, mid-span of the slope, and near the upper edge of the wedge. The investigations were then performed on the wedge models at four variations of drop heights, that is, 3 to 7.5 in. at 1.5 in. increments.

Additional instruments, i.e. two very thin copper probes, were used in the second set of flat-bottom tests in order to observe the effects of air trapped on impact pressure. The two probes were located at a certain distance from one another at the flat-bottom so that they were electrically isolated. If both probes are electrically in contact because of the mass of water, a certain level of electrical resistance will develop between them, otherwise the resistance will be infinite. The result of this particular test shows that the first positive pulse (maximum pressure) occurs about 13 msec before the water comes into contact with the bottom surface of the model. It is therefore concluded that the maximum pressure developed is when the air is momentarily trapped between the falling body and the water surface. Observation of the effects of deadrise angle on the trapped air was also made in the study. From the underwater photographs taken during the tests it is revealed that only the flat-bottom and the 1-deg wedge models trapped a substantial amount of air, whereas for larger deadrise models most of the air had escaped at the instant of impact. Hence, in the later cases, the effect of trapped air on the the magnitude of impact pressure may be insignificant, but it does exist.

The test results can further explain the effect of deadrise angle on slamming pressure. Several sample records show that the impact pressure histories at the keel were quite different from those away from the keel. For the 3-deg deadrise angle or higher, the pressure at the keel began with an impulse of short duration (less than 0.05 msec) and was followed by the so-called hydrodynamic pressure. On the other hand, the maximum pressures persisted away from the keel were purely due to hydrodynamic movement and generally take a longer period to decay. Another fact which could be learned from the results is that the peak pressures measured away from the keel are

larger (approximately twice) than those at the keel, except for the 1-deg deadrise where the magnitude is on average the same (see Fig. C3.2). The theoretical predictions by Wagner and von Kármán are also plotted on those graphs. In general the two theories agree well with the experimental data for the case of maximum pressure at the keel. With respect to the pressures away from the keel, Wagner's prediction shows much too high values for low deadrise angles, especially on 1-deg deadrise, but become closer to the experimental data by increase of the deadrise angles. An explanation for this may be that the theory was developed without considering the air trapped which may affect the magnitude of slamming pressure of small deadrise wedges. On the basis of the experimental data Chuang proposes, a new general form of pressure equation may be written as

$$p = BV^n \qquad \text{(C3.7)}$$

where B and n are arbitrary constant and n has a limit of $1 \leq n \leq 2$. Figure C3.3 is plotted from eq. (C3.7) for a wider range of impact velocity values and deadrise angles.

It is further claimed that the slamming pressure on the wedge-shaped ship bottom might be closely approximated to the model results. This is because a one-to-one scaling factor can be suitably applied as the deadrise angle of the model should equal the deadrise angle of the full-scale ship. Nevertheless, tests with large scale models over a much wider range of drop heights are needed before the results can be considered conclusive.

In subsequent ship slamming research Chuang performed a larger scale test of a wedge body represented by the ship bottom with 10 deg deadrise angle [C16,C17]. The model (size 80 in. by 90 in.) was designed for standard construction rules and in a sense may be considered as a flexible structure. The model was tested for drop heights of 6, 8 and 25 feet on an irregular water surface. A typical test result is as that depicted in Fig. C3.4, which shows the time histories of impact pressures, structural strains, plate deformation, velocities and model accelerations. Analysis of the test results provides some useful information as summarised in the following.

When comparing a rigid and flexible bottom structure it is found that the pressure time pulses of the flexible bottom are more highly irregular. Measurements on the magnitude of peak impact pressures show that in lower drop heights (6 and 8 ft) the flexible model may experience local pressure of approximately 25% larger than that of a rigid model, whereas, for 25 ft drop height the pressure is lower, i.e. only about 70% of that measured on the rigid model. A similar situation is observed on the widths of the pressure pulses. Comparison of a flat-bottomed model and a 10 deg deadrise angle model of similar size shows that the latter produces substantially lower overall bottom loadings but higher local plating pressures and stresses when dropped from the same height.

C3.2. Ando

In the second set of his experiments, Ando tested three wedge-shaped model configurations with the deadrise angles of 6, 10 and 15 deg [C13]. The wedge bottom plates were made by welding together a pair of 10 x 26.5 x 0.5 in. steel plates along the long-edge for each deadrise angle. The elastomeric layers, instrumentation and the testing procedure for the wedge models were the same as those applied to the flat bottom model. However, no theoretical study has been developed in conjunction with the wedge-shaped model test.

According to Wagner [C15] impact of a flexible wedge-shaped bottom is comparable to that of a rigid cambered bottom. That is, the force of impact on an elastic bottom is somewhat less than that for a comparable rigid prismatic bottom at the beginning of immersion but becomes greater towards the end of the immersion, or the instant when water reaches the edges of the bottom. This suggestion apparently is qualitatively justified by the test data from Ando, shown in Fig. C3.4 [C13]. It is obvious from this Figure that the smaller the deadrise angle the greater the effect of elasticity of the bottom, even though it is interesting also to observe the larger maximum load imposed on the bottom when the layer is applied compared to the rigid plate. However, the maximum impact load imposed on the layered wedge-shaped bottom remains respectably lower than that of the flat bottom.

In conclusion of his study Ando suggests that an elastomeric layer will be effective as a means of reducing slamming impact force, and hence minimising the local and structural damage, if it is applied to the flat areas of the ship bottom. A potential application of elastomeric layer is also suggested for the prevention of slamming damage to the under surface of cross-structures of SWATH ships.

C3.3. Hayman et al

The increase in demand of high-speed marine craft for passenger ferry operation worldwide in recent years has led to a new trend of ship research. For instance, to keep up with the latest requirements for high-speed structural safety. Being the leading producer and operator of high-speed crafts, especially advanced catamarans, Norway has undoubtedly acquired the latest technology for their development. Apart from the capability of any individual shipyard or marine consultant company to adapt the new developments, full support from the Norwegian classification society (DnV) in the form of enhanced structural design guidance (rules) based on their extensive research has eventually fostered the competitiveness of Norwegian marine companies. One of the latest research programme set out by DnV was the investigation of structural response

of fast craft due to slamming loads [C18]. During the earliest stage of this programme a series of drop tests on stiffened aluminium and GRP models were performed.

The size of each model was 2000 mm wide and 1000 mm long with flat bottom panels having a deadrise angle of about 30 deg, and ballasted to a total weight of 1350 kg giving a draught of approximately 0.73 m in sea water. The bottom panels of both models were designed according to the 1985 DnV rules for High Speed Light Craft with the following parameters :

Reference area	$A_R = 60\ m^2$
Vertical acceleration at LCG	$a_v = 3.0\ g$
Longitudinal distribution factor	$k_1 = 1.0$
Draught	$T = 1.0\ m$

In order to maintain a 2-dimensional flow, the model was fitted with two large aluminium end plates. In addition, the model was fitted with a deck plate, lifting frame and trolley, which was bolted to one of the end plates and engaged to the vertical test rig. The model was raised to a certain distance above the water level (drop height) by a mobile crane fitted with a quick-release hook which held the lifting crane. The unique feature of the model is that it can be rotated on a support axis so that the angle of impact between the model bottom and the water surface can be set up prior to any test run. Generally tilt angles from 0 deg to 25 deg have been used during the test to give impact angles from 30 deg down to 5 deg. A more detailed description of the model and test rig design and arrangement can be found in ref. [C19].

The measuring devices mounted on the model consisted of 4 accelerometers to investigate global accelerations of the model in the vertical and transverse directions, and one accelerometer at the centre of the bottom panel. A row of 6 pressure transducers positioned transversely at the mid-length of the model, plus two additional transducers off-centre, were used to measure the impact pressure distribution on the model's bottom. Several strain gauges were also fitted to observe the bottom plate responses due to slamming impacts. Signals from those electronic devices were fed into a personal computer endowed with data acquisition software. 32 channels in all can be stored in the computer with 2000 samples on each channel. Sampling intervals were mostly made to give a total record of 30-100 ms. The primary test data which can be readily plotted from the computer were pressure and plating strain time histories (eg. Fig. C3.5). A preliminary data analysis of the pressure data for the aluminium model has been made and compared with theoretical predictions.

There were two theoretical approaches. The one which was developed by Wagner [C15] (see section C3.1) and the one by Payne [C20], have been evaluated by DnV to be used in the comparison with the experimental data. Payne suggests that the maximum pressure of impacting wedge body can be calculated by

$$p_{max} = \frac{1}{2}\rho V_s^2 \qquad \text{(C3.8)}$$

where V_s is the absolute stagnation line velocity, in which the stagnation line is located somewhere in the splash-up water region probably at some fixed ratio η of the splash-up distance Δl (see Fig. C3.6). The stagnation line velocity for an impact angle β is given by

$$V_s^2 = \left(\frac{\dot{z}}{\tan\beta}\right)^2 + \left[\frac{4\pi\eta\,\dot{z}\,f(\beta)}{\cos\beta}\right]^2 + 2\,\frac{\dot{z}}{\tan\beta}\,\frac{4\pi\eta\,\dot{z}\,f(\beta)}{\cos\beta} \qquad \text{(C3.9a)}$$

or simply

$$V_s = \dot{z}\left[\cot\beta + 4\pi\eta f(\beta)\sec\beta\right]^2 \qquad \text{(C3.9b)}$$

where the deadrise angle dependent correction factor $f(\beta)$ can be approximated by $1-\beta/\pi$ and η is approximately 0.05.

As is shown in Fig. C3.7, the maximum pressures measured on the aluminium model dropped symmetrically (28.8 deg effective slamming angle) are plotted against the drop height, H, which corresponds to the impact velocity of $V=\sqrt{2gH}$. Theoretical values derived by the formulation of Wagner and Payne are also shown, in which the latter gives much better agreement than the former. The results of pressure analysis of the GRP model are not presented in ref. [C18], nonetheless it is mentioned that a comparison of the two models has been made. The initial objective of comparing the test data of the two models was to investigate the effects of the model flexibility onto the maximum impact pressure, where it is in general presumed that the more flexible structure will excite less impact pressure. Nevertheless, it was found that this difference is rather scarce, and hence the comparison is inconclusive. It is further claimed that it would be preferable to compare values of pressure integrated over a given area, as is presented in [C21], or a given period of time.

A more extensive analysis has been performed on the test data of a GRP model, especially on the values of the strain of the GRP sandwich (core, inner laminate and outer laminates). The results indicate that in the symmetric position (30 deg effective impact angle) the greatest strains occur at the keel, while in the lower effective impact angle (10-deg) the maximum shear strain is experienced at the chine. From the strain data it was then able to deduce the shear stress at failure, i.e. about 2.6 and 3.1 N/mm^2, which agrees well with the shear ultimate strength of 2.9 - 3.2 N/mm^2.

The use of drop test data in the structural analysis using the finite element method is also demonstrated in ref. [C18]. Both dynamic and quasi-static analysis were performed to develop a comparison of deformations and stresses induced by uniformly

distributed static pressure loadings. The finding reveals that the quasi-static analysis reproduce the measured behaviour quite well, whereas the dynamic one gives spurious oscillations due to lack of explicit damping on the model.

The tests described above prove to be very useful in giving insight into the way in which slamming propagates over the hull surface, and into the structural deformations that are generated. Investigations on the hull flexibility on the pressure distributions and histories could also be performed, although a better evaluation method remains to be established. In view of the development of simplified calculation methods, such as those used in classification rules, combination of measured data with theoretical predictions is of importance for validation.

C4. DROP TESTS ON SHIPFORM MODELS

C4.1. Ochi and Bledsoe

The drop tests conducted by Ochi and Bledsoe at the DTMB [C22] was directed toward establishing the exact impact pressure velocity relationship as a function of ship form. The model used in the experiment was a 1/20 scale of the Mariner section at 17.5% of the length aft of the forward perpendicular, which has been modified to a V-form. The size of this two-dimensional model was 26.5 in. x 42 in. x 30 in. (L x B x D) and was made of pine with a hull thickness of 2.5 in. normal to the hull surface, which was covered with 3/4 in. plates. The ballasted weight of the model was 190 lb, which corresponds to approximately 45% loading condition for the Mariner. The drop tests were performed at five different drop heights covering the impact velocity up to 10 fps. This upper limit corresponds to an impact velocity of about 50 fps for a 520-ft ship.

The test facility for this experiment was the same as that used by Chuang [C4]. The main instrumentation utilised for the test comprised of diaphragm type pressure transducers with the capacity range from 15 to 50 psi, and their natural frequencies were about 7000 cps. The transducers were mounted at seven positions around the girth from the keel of the model at its mid-section. Two accelerometers, which were used to measure the acceleration and velocity, were attached to the inside of the model's base. The immersion of the model in the water was detected matching pinion which travelled on the vertical track and at the same time activated a potentiometer. The output of all measuring instruments was fed through carrier amplifiers and recorded on a consolidated string oscillograph. In addition, a high-speed movie camera was used to observe the piled-up water.

The test data analysis of this particular experiment were performed to receive information peculiar to ship-form slamming, which covered the primary impact pressure-velocity relationship right to impact force and impulse behaviours. With respect to the maximum impact velocity of 10 fps, i.e. corresponds to a 6 in. drop height, only four out of seven transducers were found to have registered any impact pressure, with the most outboard location of transducer at 6 in. and 4 in. abreast and above the keel, respectively (see Fig. C4.1). The pressure-velocity relation obtained from the test is shown in Fig. C4.2. Since the data for each transducer falls on a straight line when plotted on logarithmic scale the pressures may be simply expressed in the form of

$$p = CV_0^n \qquad \text{(C4.1)}$$

where C is a constant and n is the power velocity factor.

The time history of downward velocity from the instant of model release as well as the time history of the model immersion into the water have also been extracted from the test data. An interesting phenomenon was therefore learned as follows. Even though the uppermost position of the transducer which has registered maximum impact pressures is about 4 in. above the keel, observation indicated maximum impact pressure persisted at those four transducers when the model was only immersed 2 in. into the water for the maximum drop height of 6 in. This circumstance was explainable later on having evaluated the manner in which calm water surface instigate after an initial contact with model bottom. In only a few milliseconds after this contact water pile-up began to develop and in effect the wetted breadth of the body increased. The wetted half-breadth is defined as the distance of a spray root, that is, the point at which the (piled up) water surface meets the model section from the centreline of the model. From the experiment the rate of wetted breadth was measured, and it was found to be constant after a sharp increase about 1.45 larger than the actual breadth. It seems obvious that impact pressure was induced by the piled-up water and its location happens to be at the vicinity of the spray root.

The pressure distribution at the bottom of the model was traced from the pressure records at those four locations. For a 6 in. drop height the first peak pressure in the order of 27 psi was detected on the transducer attached to the keel at t = 0.4 msec after impact. The next maximum pressure was measured at the transducer located $2^1/4$ in. outboard at t = 5.7 msec with the magnitude of around 3 psi, whilst at the same time the pressure at the keel attenuated to as low as 1.2 psi. By 30 msec the peak pressure was completed for all four transducers, and a pressure envelope was established around the bottom at a magnitude of less than 1.0 psi. For any instant of time elapsed the average pressure acting on the section can be derived by integration of the pressure and dividing by the wetted breadth.

C4.2. Yamamoto et al

One of the real cases on fierce ship structural damage due to slamming when operating in adverse seas has been reported by Yamamoto et al [C23]. The ill-fated ship in question was a high-speed container ship with a loading capacity of 819 TEU, which was on a west bound voyage in a fully laden condition on the North Pacific Ocean on January 28, 1978. This ship suffered severe damage on its bow structure, that is, a long crack and corrugations in the shell plating on the starboard side, as well as buckling deformations due to shearing forces on the port side shell plating, when it was struck by slamming impact on the flare part on the starboard side. More than that, the individual decks, flats, bulkheads, ship side members, and rib frames inside the long forecastle showed plastic deformations, as well as deformations due to buckling or breakdown, in many different locations.

A reconstruction of the slamming load that caused the damage to the ship has been made following a thorough enquiry into the nature of the accident. Upon the study of the damaging pressure loads the primary information required as the relative speed of the hull and the wave surface at the fore body of the ship, as these two parameters determine the relative velocity and hence the slamming pressure. This information was further transformed into an input data for running a program [C24] to compute the motion characteristics of the ship and ultimately estimating the impact load. For the sake of simplicity the analysis was made by selecting a train of regular waves in which the ship is advancing with a predetermined speed at a certain variation of heading angles. The estimation of impact pressure itself was then made using von Kármán's formulation having determined the impact velocity and the impact angle from previous analysis. This investigation has in the end resulted in enhanced guidelines of the design and operation of high-speed container ships.

In conjunction with the investigation of the slamming load, especially to validate the result as predicted using von Kármán's formulation, a series of drop tests have been carried out on a 2-dimensional small scale model of the bow-flare section of the ship [C23]. The model, whose geometrical dimensions are 1/26 of those of the actual ship, was equipped with 10 pressure transducers (capacity : 10 kgf/cm^2) positioned at various points along the girth of the mid-span of the model (see Fig. C4.3). The aggregate weight of the dropped body, which comprised the model and the track, was 381 kgf. The attachment of the model to the track was designed in such a way that the model could be tilted to ensure any practical impact angle between the model and the water surfaces. Slamming impacts imposed on the model were observed in five variations of tilting angles of the model at its centreline, namely, 15, 22.5, 30, 40 and 45-deg. It is not explicitly mentioned in ref. [C23], however, as to what extent of drop height or impact velocity ranges the drop test was conducted.

A typical plot of the recorded data which is as depicted in Fig. C4.4, shows the time-series of the impact pressures on any individual location of the transducers. The values of impact pressures derived by Wagner's formulation are also plotted on the same graphs for comparison. The discrepancy is thought to be brought about by the assumption adopted in the formulation, where the peak impact pressure is considered to persist for a relatively short period, while the test shows otherwise. The overall test data is as plotted in Fig. C4.5, together with the theoretical results from Wagner and von Kármán as well as with the analytical formulation by Stavovy and Chuang [C25]. On this Figure the pressure coefficient k is plotted against the corresponding impact angle β on the flare part at which severe damage on the ship structure has been found. The impact pressure, which is proportional to the drop velocity V, can be computed by counting the pressure coefficient as

$$p = \frac{1}{2} \rho k V^2 \qquad \text{(C4.2)}$$

The test data are in good conformity with von Kármán's formula, which represents the mean value of dynamic water pressure on a 2-dimensional wedge. Nevertheless, this conformity remains questionable to some extent because the impact angle β of the test data presented within the Figure is not actually the angle formed between the model surface with the piled up water at a particular position where a transducer is located, but is the angle between the model surface with the initial water surface.

C5. DISCUSSION

A general review on the study of ship slamming by drop test models is presented in this report. Much has been revealed by previous investigators in this area of research, yet some aspects of the phenomena remain uncertain, especially when dealing with a specifically designed model. Understanding of the rigid model's drop over a calm water surface, both of flat-bottomed and wedge types, is now quite well defined. One of the most notable achievements is in the conclusion of the presence of air cushioning effect in the case of flat bottom impact. Such an effect is in large believed to cause a significant reduction in the peak impact pressure in which it is previously predicted to be infinite. Furthermore, it is realised that the pressure developed during flat impact would not be evenly distributed over the flat surface as observation shows pressure rise will begin at the edges of the model and travel inward to the centreline of the model. On the evaluation of the effect of model weight variation it is generally agreed that the heavier model (with the same geometrical size) will result in a larger impact pressure. This observation also reveals that the maximum pressure-drop height

correlation resulted from models having a characteristic weight within a normal range is essentially linear, hence the pressure is directly proportional to the square of the drop velocity [C8,C11]. At very high mass loading the peak impact pressure tends to fall below the line of proportionality, and may bring about a linear relationship between maximum pressure and drop velocity.

In contrast to the flat bottom impact, the pressure behaviour of wedge shaped bodies is characterised by the larger peak pressure which occurs at a distance away from the keel than along the keel. This larger peak pressure is explained as being caused by the splashed up water after the instant of impact which carries a certain amount of mass of spray sheet at a given velocity which is opposed by the downward movement of the plate surface. The maximum pressure itself is believed to build up along the so-called stagnation line (see Fig. C3.6). Experimental evidence [C14] shows the largest impact pressure away from the keel would be experienced on wedge shape bodies with a deadrise angle of about 3 deg. The expectation of larger impact pressure occurring at lower deadrise angles than 3 deg. is not satisfied due to the fact that at such angles the cushioning effect of the entrapped air still exists although not as intense as in the case of flat bottom impact.

In most theoretical treatments of the ship slamming problem the water is considered to be incompressible and non-viscous. In the mathematical idealisation of the problem it is assumed, moreover, that the velocity of the specified part of the free water surface is increased instantaneously from zero to the downward speed of the falling body. The slamming pressures resulting from such analyses are in good agreement with experimental results as long as the deadrise angle of the ship's bottom is not too small (e.g. as is presented in [C15]). In the extreme case of a flat bottom, however, the theory predicts infinitely high pressures at the instant of impact. The high pressure predicted by these theories could not be verified experimentally.

The drop test of ship form models apparently shows similar behaviour as for wedge shaped models in the way that the peak pressure occurs to be in the bottom area covered by the splashed up water. In this case, however, the largest peak pressure is notably developed along the keel rather than away from it. This situation is quite understandable if one considers that the keel area of the ship form where the largest impact persists normally has a flat shape, so the phenomenon will resemble that of flat-bottomed impact. Slamming severity is further explained [C26] to be influenced by the bottom portion of a section only rather than by the section shape up to LWL. A drop test on ship form model could also be very useful to clarify specific cases such as the one conducted in Japan in the investigation of bow flare slamming[C24].

Other investigations regarding ship slamming which may be made by performing a drop test is the study of mechanisms for slamming pressure reduction. Two reports, by Lewison [C11] and Ando [C13], address this particular subject for monohull ships and advanced crafts, respectively. Their findings are principally promising although further confirmation still needs to be pursued if it is to be implemented for full scale ships. On the use of external keels, for instance, argument did arise regarding the more practical way of enforcing the bottom structure to ease slamming damages, such as by using thicker plate or by reducing the panel size [C27].

The ultimate objective of a slamming study by drop test model is of course the implementation of the experimental data for ship bottom design. The usefulness of drop test data in this study is obvious, for instance as is demonstrated in the design study of hydrofoil crafts by Drummond et al [C28]. For this study the drop test data on wedge-shaped bodies accumulated by Chuang [C14] was combined with the statistical approach by Ochi and Motter [C29] to estimate the design pressure for such crafts. From the initial values of slamming impact pressures it allowed further to perform a parametric study in order to quantify the influence of geometrical as well as operational parameters. As a result of this sort of study Drummond was then proposing a simple algorithm to calculate the design pressure as a function of those parameters specifically for hydrofoils. Another example of the implementation of drop test data (of ship form models) in predicting design pressure for monohull is fully reported in [C26].

In spite of the confidence in implementing drop test data as above, some may consider that further refinements are still necessary to be explored so that more realistic predictions can be made. There are some areas that have not been sufficiently incorporated in the slamming investigation by a drop test model which, to some extent, would improve the utility of such data, for instance, the effects of structural flexibility, disturbed (irregular) water surface, and horizontal (forward) speed. Furthermore, verification of drop test data should be made against the information from seakeeping tests and/or full scale tests. Characterisation of impact pressure due to effects of the structural flexibility and the disturbed water surface has been initiated in order to clarify the viability of replacing equivalent static load criteria as widely adopted at present with more realistic dynamic load criteria [C30,C31]. It is also suggested to estimate the time and space distribution of impact pressure over the ship bottom [C32]. The concern over forward speed effects arises primarily in the study of high speed craft behaviour. Experimental data of high speed craft (see Fig. C5.1) shows that forward speed effects are dependent on the magnitude of slamming pressure as the speed is increased outside the range of conventional ship normal operations. In this respect, correction factors, probably derived from seakeeping tests or full scale measurements, need to be introduced into the pressure data from drop tests.

C6. CONCLUSIONS

The importance of conducting drop tests in ship slamming studies is obvious. Various information could be drawn by such an investigation ranging from impact pressure to structural responses. To some extent drop test data of rigid bodies could be directly applicable in ship structural design. Nevertheless, further observations accounting for structural flexibility and disturbed water surface need to be pursued in the interest of enhancing the accuracy of drop test data for practical uses. Some remarks to the various predictions of impact pressure may be clarified as follows.

1. Maximum impact pressure on flat bottom plate would not be appropriate to be predicted by classical theories such as those given by Wagner or von Kármán. In this particular case peak pressures is definitely reduced by the presence of air cushioning effects which develop when the closing gap between flat bottom surface and the water surface come to a certain limit.

2. The worst impact pressure for any impact velocity on the model bottom plate would be expected to occur the wedge-shaped body with deadrise angle around 3-deg. Drop tests have given a better insight towards slamming phenomenon on seagoing ships which can be adopted in a further development of slamming study.

3. The measured pressures from drop tests may be regarded as the raw information that would not directly applicable in ship structural design. A further analysis to process such data by incorporating the rectifications, such as that due to the effect of surface waves and so on must be taken into account to generate the correct values for design. Further, it should be able to estimate the time and space distribution of impact pressure over the ship bottom [C1].

REFERENCES TO APPENDIX C

C1. Townsend, H.S., "Some Observations on the Shape of Ship Forebodies with Relation to Heavy Weather Damage", SNAME, New York Metropolitan Section, USA, Apr. 1960

C2. Townsend, H.S., "Observations of Ship Damage Over the Past Century", *Proc., SNAME Ship Structures Symp.*, Washington D.C., USA, Oct. 1975

C3. Fukuda, J. and Shinkai, A., "Speed Loss of Container Ship on the Different Routes in the North Pacific Ocean in Winter", *Proc., Int. Symp. on Ship Hydrodynamics and Energy Saving (ISSHES-83)*, Madrid, Spain, Sept. 1983

C4. Chuang, S.L., "Experiments on Flat-Bottom Slamming", *Journal of Ship Research*, SNAME, Vol. 10, No. 1, pp. 11-17, Mar. 1966

C5. Keil, A.H., "The Response of Ships to Underwater Explosions", *Trans. SNAME*, Vol. 69, pp. 366 - 410, 1961
C6. Th. von Kármán, "The Impact on Seaplane Floats During Landing", *National Advisory Committee for Aeronautics (NACA)*, Technical Note 321, USA, 1929
C7. Chuang, S.L., "Experiments on Slamming of Ship Flat-Bottom Structural Models", NSRDC, Report No. 2528, Feb. 1968
C8. Verhagen, J.H.G., "The Impact of a Flat Plate on a Water Surface", *Journal of Ship Research*, SNAME, Vol. 11, No. 4, pp. 211-223, Dec. 1967
C9. Lewison, G. and Maclean, W.M., "On the Cushioning of Water Impact by Entrapped Air", *Journal of Ship Research*, SNAME, Vol. 12, No. 2, pp. 116 130, June 1968
C10. Ogilvie, T.F., "Compressibility Effects in Ship Slamming", *Schiffstechnik*, Vol. 10, pp. 147-154, 1963
C11. Lewison, G.R.G., "On the Reduction of Slamming Pressures", *Trans. RINA*, Vol. 112, pp. 285-306, 1970
C12. Ochi, M.K., "Extreme Behaviour of a Ship in Rough Seas - Slamming and Shipping of Green Water", *Trans. SNAME*, Vol. 72, pp. 143-202, 1964
C13. Ando, S., "Cushioning of Slamming Impact by Elastomeric Layers", *Journal of Ship Research*, SNAME, Vol. 33, No. 3, pp. 169-175, Sept. 1989
C14. Chuang, S.L., "Experiments on Slamming of Wedge-Shaped Bodies", *Journal of Ship Research*, SNAME, Vol. 11, No. 3, pp. 190-198, Sept. 1967
C15. Wagner, H., "Uber die Landung von Seeflugzeugen", *Zeitschrift fur Flugtechnik und Motorluftschiffahrt*, Vol. 22, No. 1, pp. 1-8, 1931
C16. Chuang, S.L., "Slamming Tests of Structural Model Representing a Ship Bottom with 10-Degree Deadrise Angle - General Outline of Tests and Test Results", NSRDC, Report No. 3007, Aug. 1969
C17. Chuang, S.L., "Slamming Tests of Structural Model Representing a Ship Bottom with 10-Degree Deadrise Angle - Analysis and Discussion of Test Results", NSRDC, Report No. 3008, Aug. 1969
C18. Hayman, B., Haug, T. and Valsgård, S., "Response of Fast Craft Hull Structures to Slamming Loads", *Proc., Ist Int. Conf. on Fast Sea Transportation (FAST'91)*, Trondheim, Norway, June 1991
C19. Bøe, Å, Haug, T. and Hayman, B., "Slamming Drop Test Arrangement", *Det norske Veritas*, DnVC report No. 90-0051, Norway, Sept. 1990
C20. Payne, P.R., "The Vertical Impact of a Wedge on a Fluid", *Ocean Engineering*, TN, Vol. 8, No. 4, pp. 421-436
C21 Allen, R.G. and Jones, R.R., "A Simplified Method for Determining Structural Design-Limit Pressures on High Performance Marine Vehicles", *Proc., Advanced Marine Vehicles Conf.*, AIAA/SNAME, Paper No. 78-754, San Diego, USA, Apr. 1978
C22. Ochi, M.K. and Bledsoe, M.D., "Hydrodynamic Impact with Application to Ship Slamming", *Proc., 4th Symp. on Naval Hydrodynamics*, Ship Propulsion and Hydroelasticity, Vol. 3, Washington, D.C., Aug. 1962
C23. Yamamoto, Y et.al., "Structural Damage Analysis of a Fast Ship Due to Bow Flare Slamming", *Int. Shipbuilding Progress*, Vol. 32, No. 369, pp. 124-136, May 1985

C24. Yamamoto, Y., Fujino, M. and Fukosawa, T., "Motion and Longitudinal Strength of a Ship in Head Seas and the Effects of Non-Linearities", *Journal of the Soc. of Naval Architects of Japan*, Vols. 143-144, 1978
C25. Stavovy, A.B. and Chuang, S.L., "Analytical Determination of Slamming Pressures for High-Speed Vehicles in Waves", *Journal of Ship Research*, SNAME, Vol. 20, No. 4, pp. 190-198, Dec. 1976
C26. Ochi, M.K. and Motter, L.E., "A Method to Estimate Slamming Characteristic for Ship Design", *Marine Technology*, SNAME, Vol. 8, No. 2, pp. 219-232, Apr. 1971
C27. Kendrick, S. discussion to Lewison, G.R.G., "On the Reduction of Slamming Pressures", *Trans. RINA*, Vol. 112, pp. 285-306, 1970
C28. Drummond, T.G., Mackay, M. and Schmitke, R.T., "Wave Impacts on Hydrofoil Ships and Structural Implications", *Proc., 11th Symp. on Naval Hydrodynamics*, Univ. College London, UK, Apr. 1976
C29. Ochi, M.K. and Motter, L.E., "Prediction of Slamming Characteristics and Hull Responses for Ship Design", *Trans. SNAME*, Vol. 81, pp. 144-176, 1973
C30. Sharov, Y.F., "Slamming Stresses in Ship Bottom Plates", *Sundostroenie*, Vol. 24, No. 4, pp. 5-9, 1958
C31. Buckley, W.H. and Stavovy, A.B., "Progress in the Development of Structural Load Criteria for Extreme Waves", *Extreme Load Response Symp.*, SNAME, Arlington, VA, USA, Oct. 1981
C32. Lewis, E.V., "Structural Dynamics of Ships", *Proc., Int. Symp. on the Dynamics of Marine Vehicles and Structures in Waves*, IMECHE, London, UK, Apr. 1975

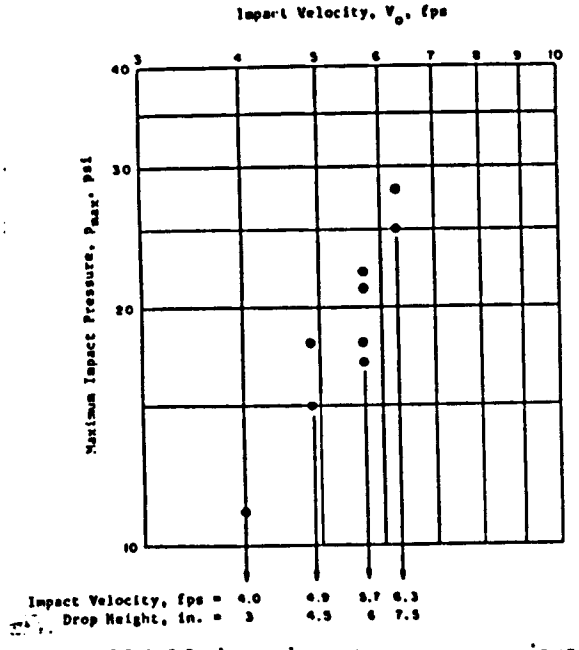

Figure C2.1. Maximum impact pressure vs various impact velocities [C4]

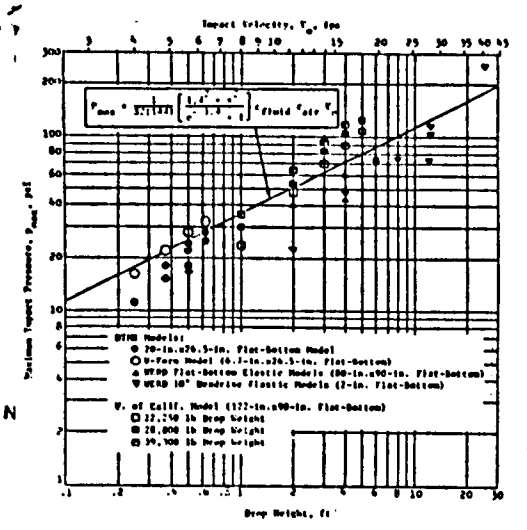

Figure C2.2. Comparison of theoretical and experimental flat-bottom impact pressures [C4]

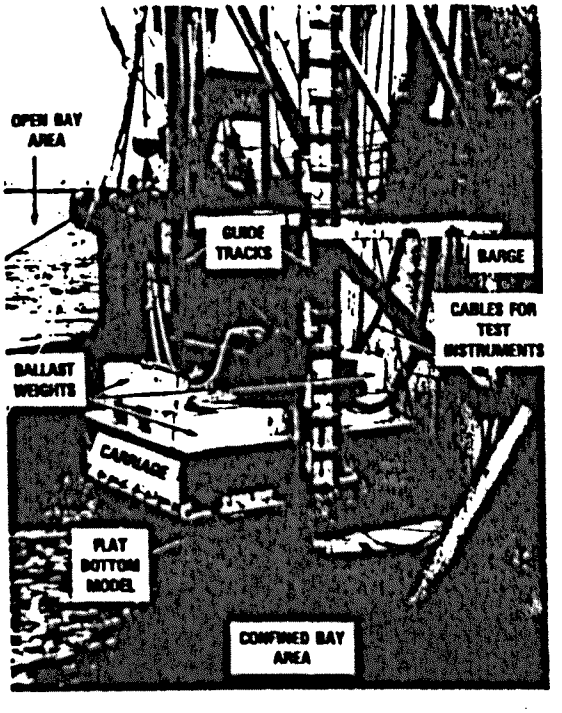

Figure C2.3. Facility for a 1/4-scale model droptest [C7]

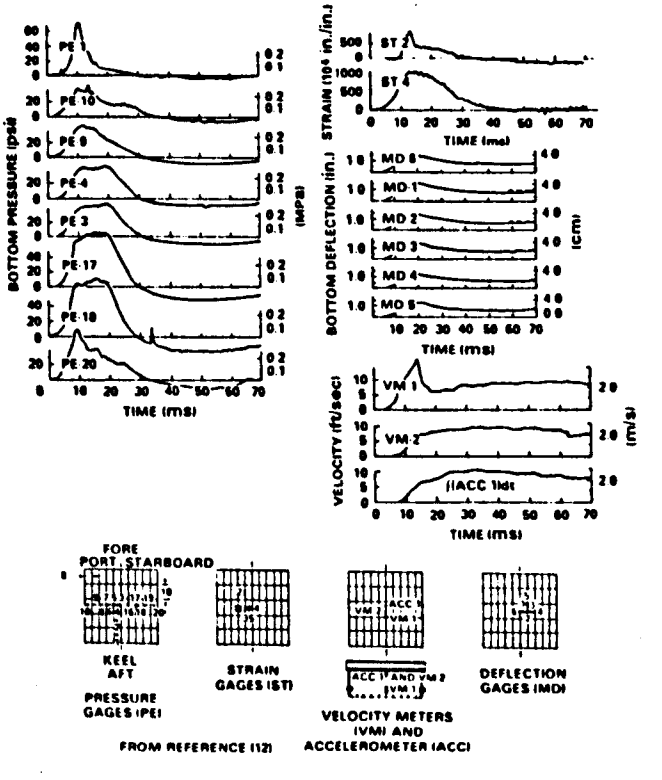

Figure C2.4. Test result for 6-foot drop test of flat-bottomed model [C7]

PAGE MISSING IN ORIGINAL

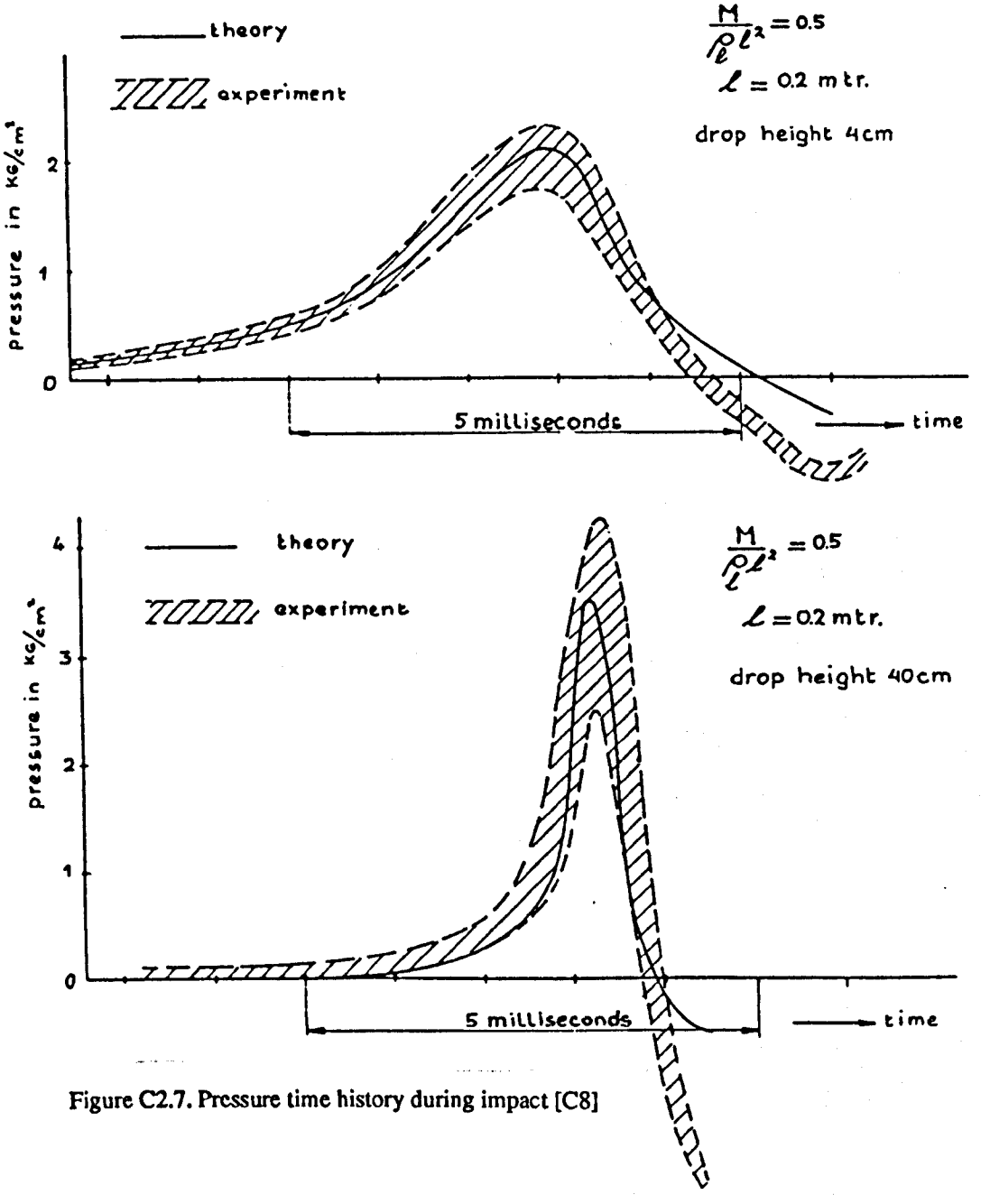

Figure C2.7. Pressure time history during impact [C8]

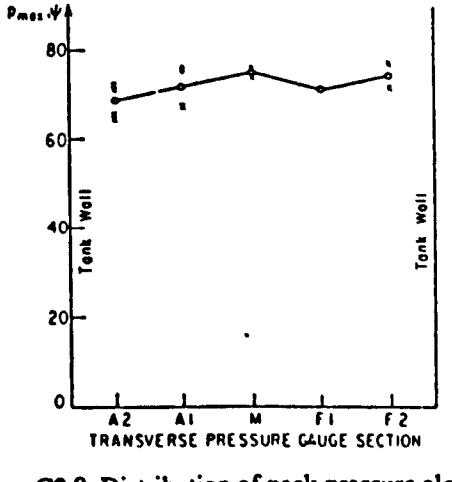

Figure C2.8. Distribution of peak pressure along model centreline [C9]

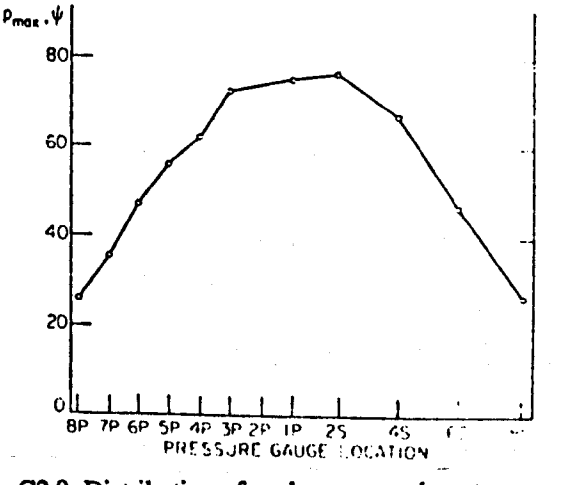

Figure C2.9. Distribution of peak pressure along transverse mod-plane of the model [C9]

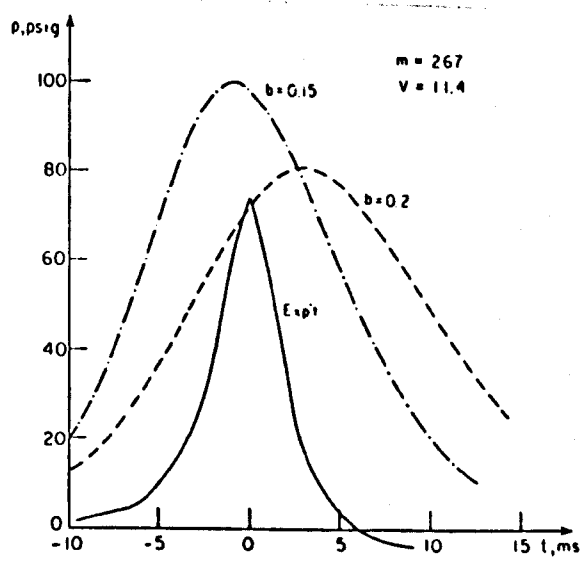

ure C2.10. Pressure-time curves on centreline as measured and predicted by the simple one-dimensional theory [C9]

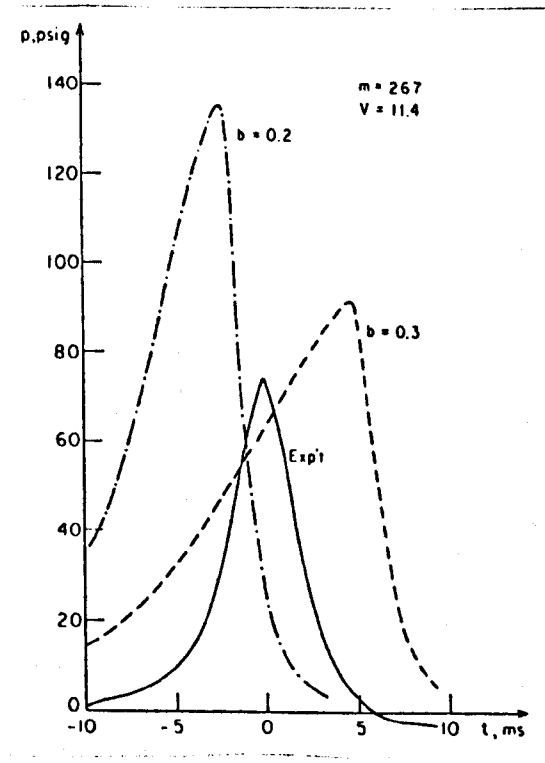

Figure C2.11. Pressure-time curves on centreline as measured and predicted by the modified one-dimensional theory [C9]

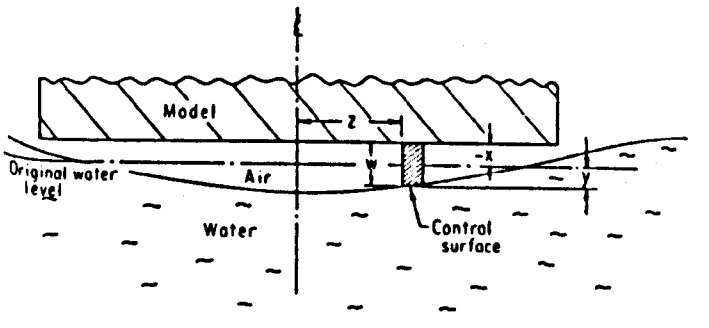

Figure C2.12. Diagram of falling body and control surface enclosing air [C9]

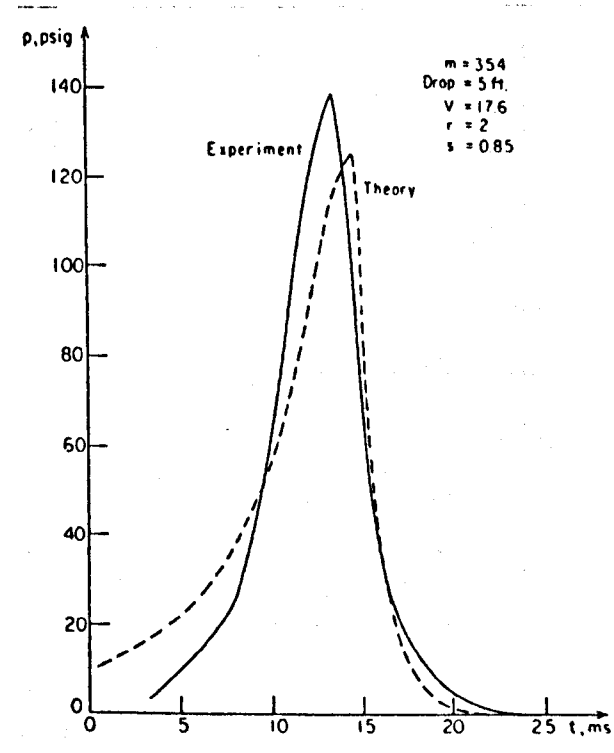

Figure C2.13. Pressure-time curves on centreline as measured and predicted by the two-dimensional theory [C9]

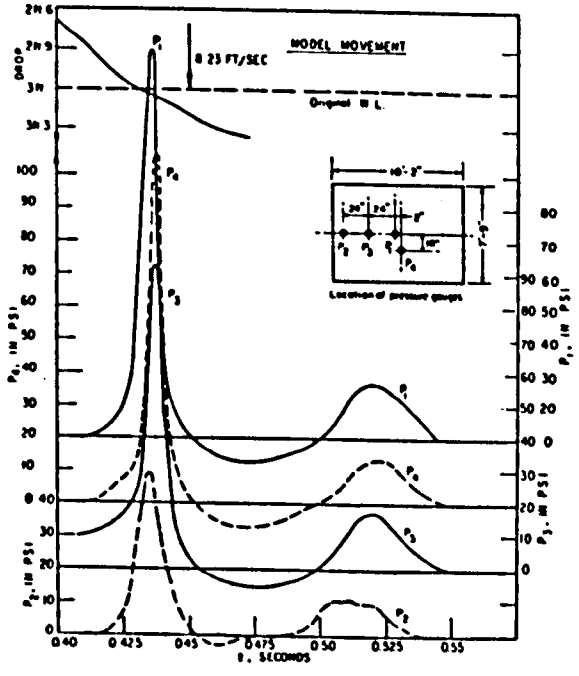

Fig. 14. Pressure curves: m = 481, no flanges

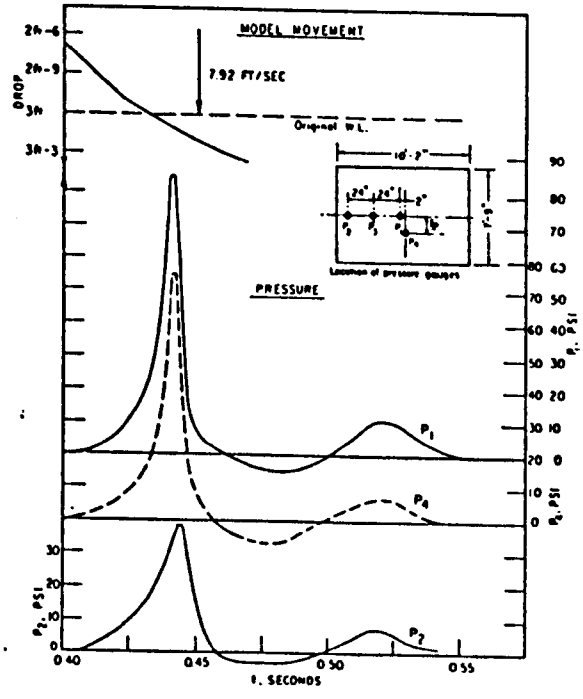

Fig. 16. Pressure curves: m = 481, 1½ in. flanges

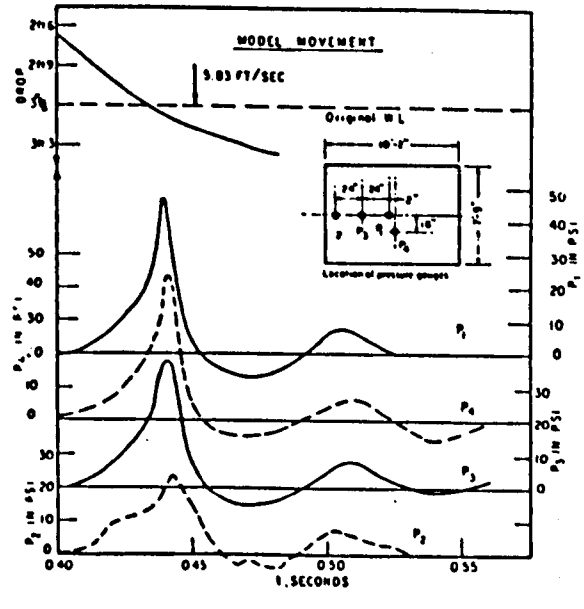

Fig. 15. Pressure curves: m = 287, 1½ in. flanges

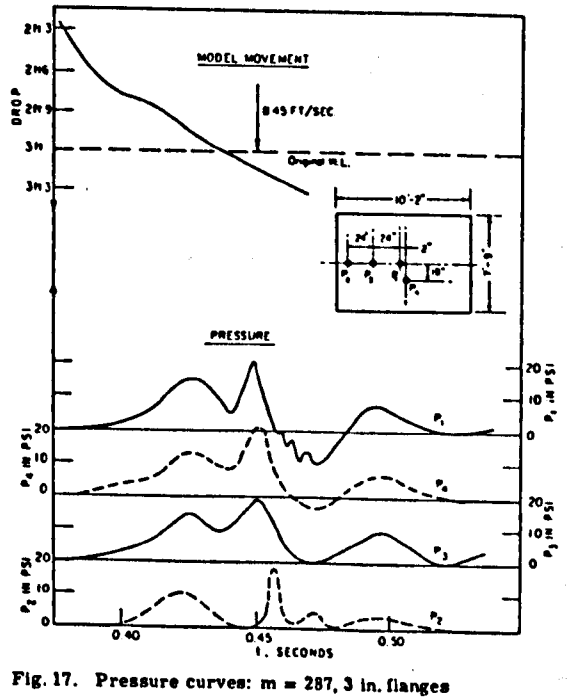

Fig. 17. Pressure curves: m = 287, 3 in. flanges

Figure C2.14. Various pressure curves with and without flanges attached on the flat-bottomed model [C11]

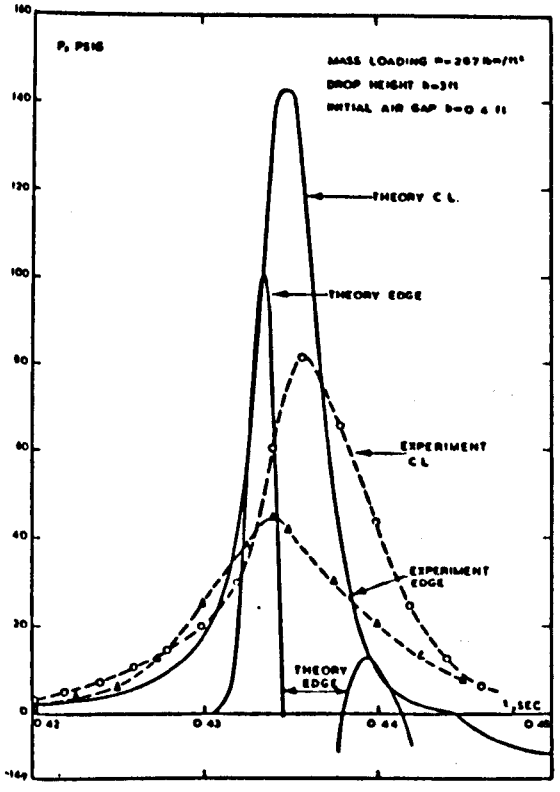

Figure C2.15. Pressure-time curves as measured and predicted by the enhanced two-dimensional theory [C11]

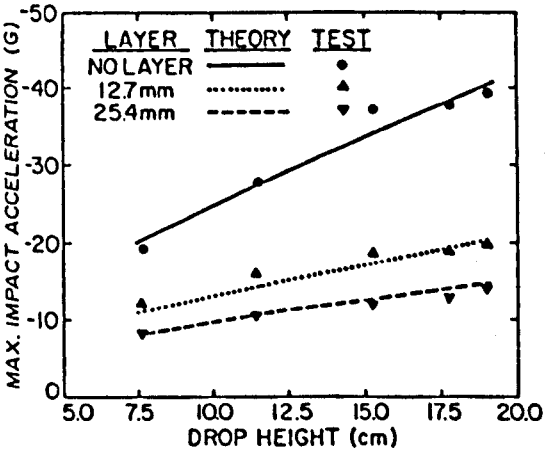

Figure C2.18. Comparison of predicted and measured maximum impact acceleration of flat plate [C13]

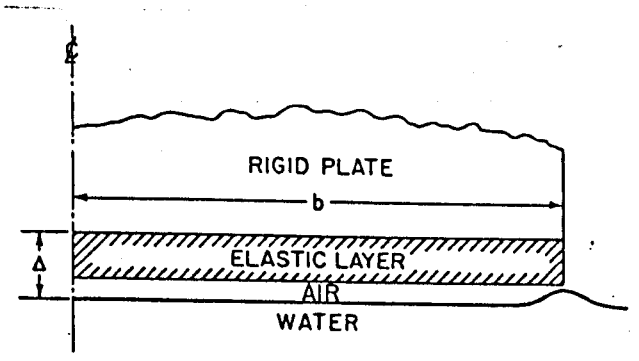

Figure C2.16. Diagram of descending flat plate and water surface [C13]

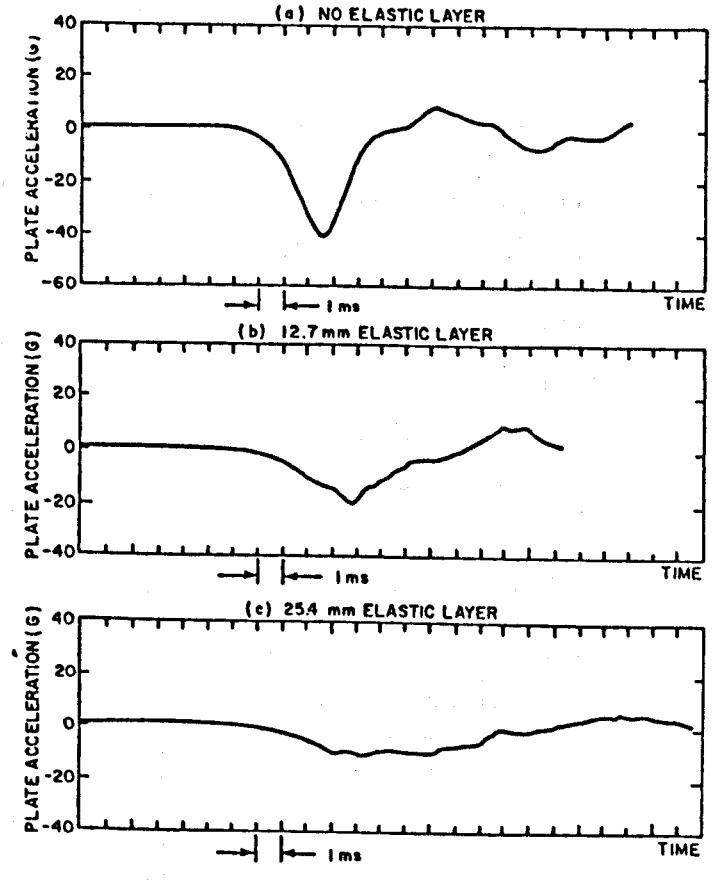

Figure C2.17. Typical plots of impact acceleration for flat plate (drop height = 7.5 in.) [C13]

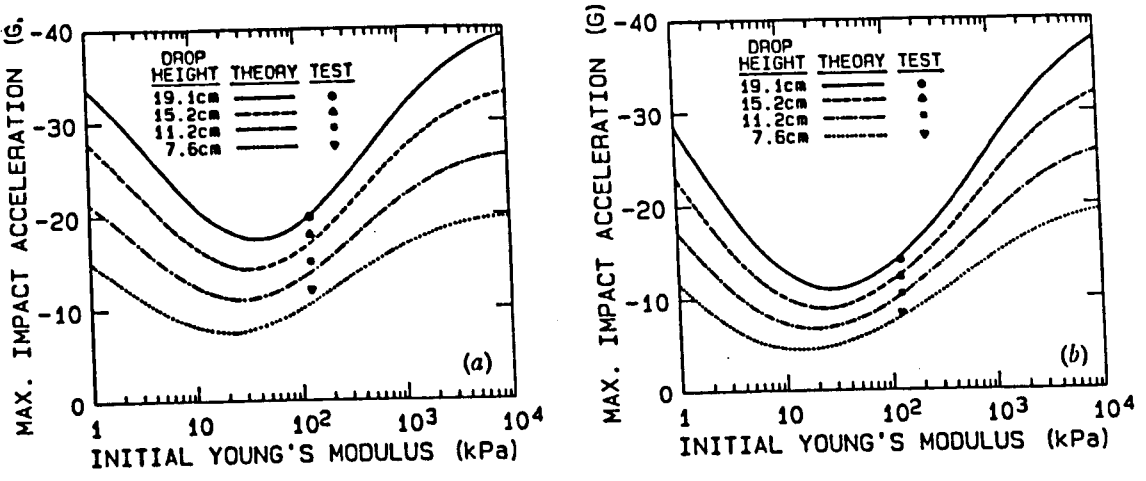

Figure C2.19. Initial Young's modulus of elastomeric layers vs maximum impact acceleration of flat plate [C13]
(a) layer thickness = 12.7 mm; (b) layer thickness = 25.4 mm

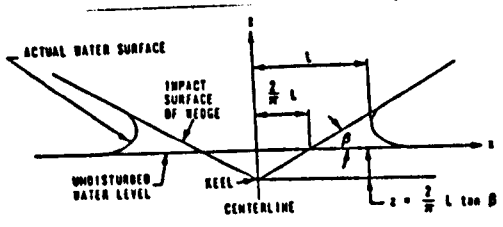

Figure C3.1. Representation of wedge penetration [C14]

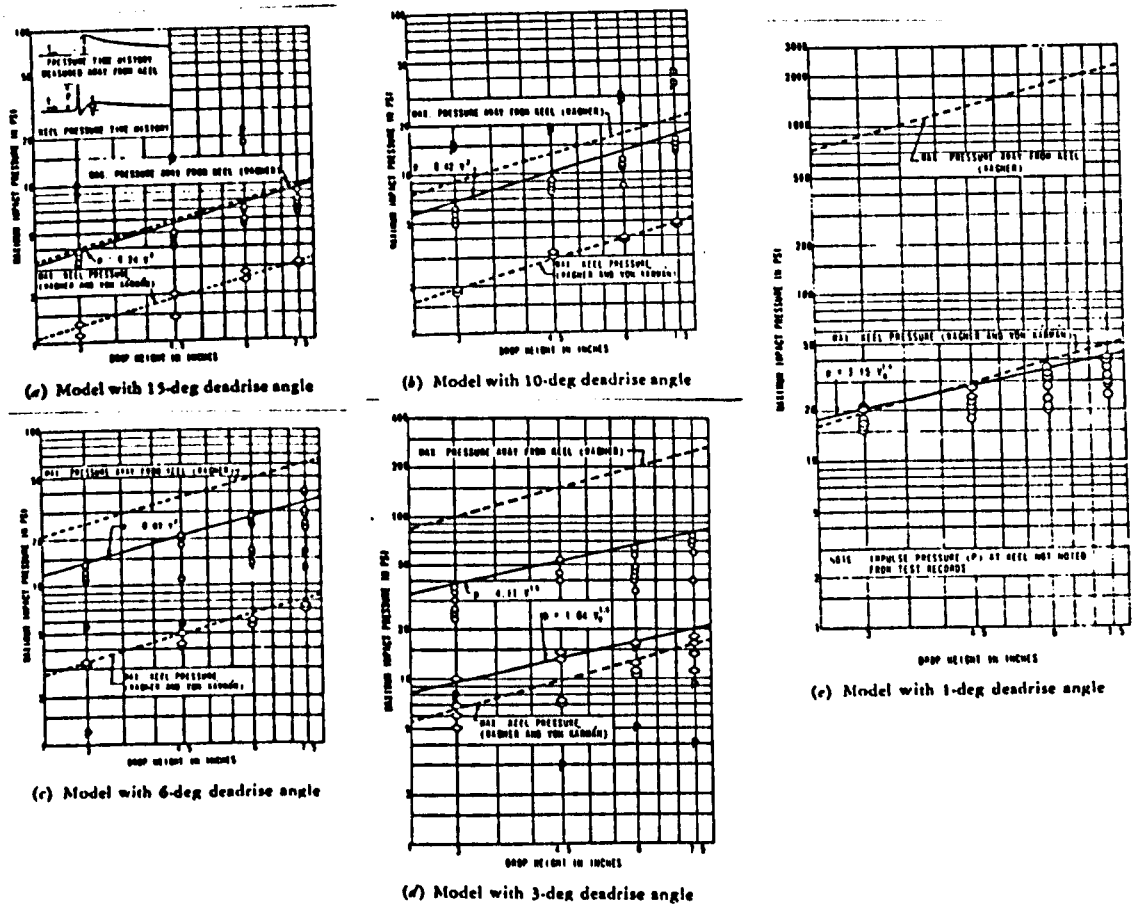

Figure C3.2. Experimental results of maximum impact pressure due to slamming of rigid wedge-shaped models [C14]

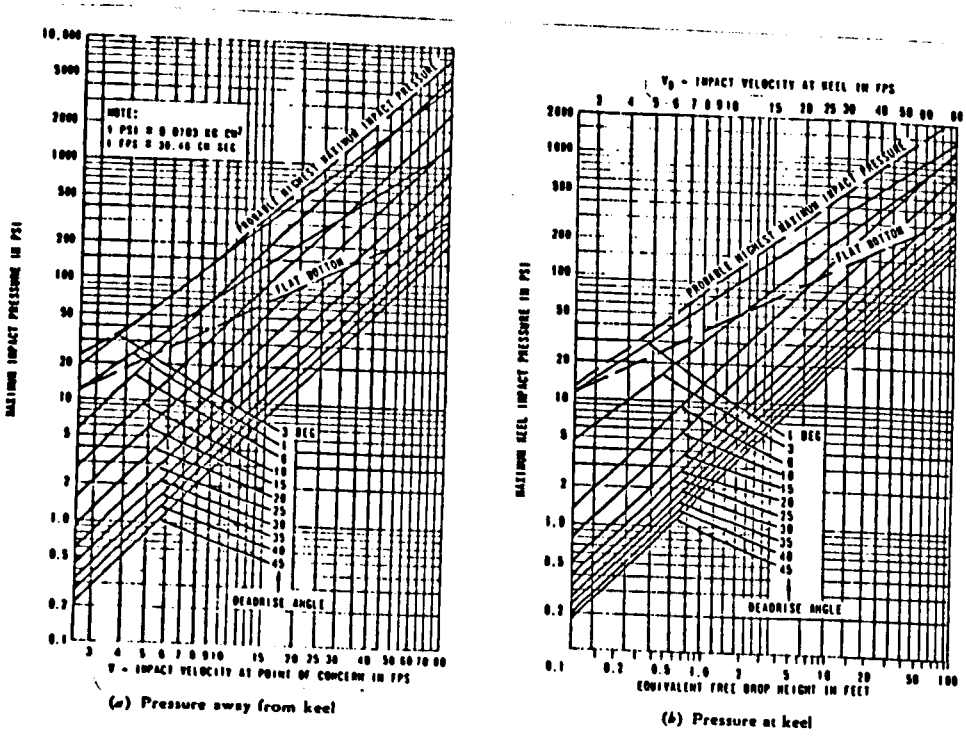

Figure C3.3. Maximum impact pressure due to rigid-body slamming of wedges vs impact velocity [C14]

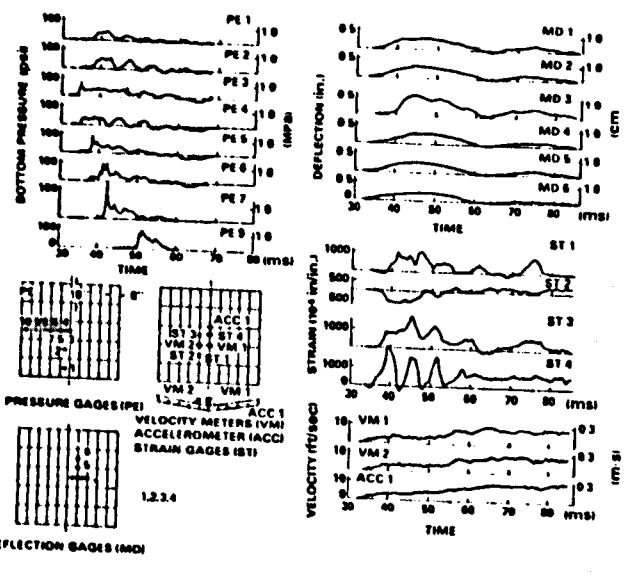

Figure C3.4. Test results for 6-foot drop test of 10-degree deadrise model [C16]

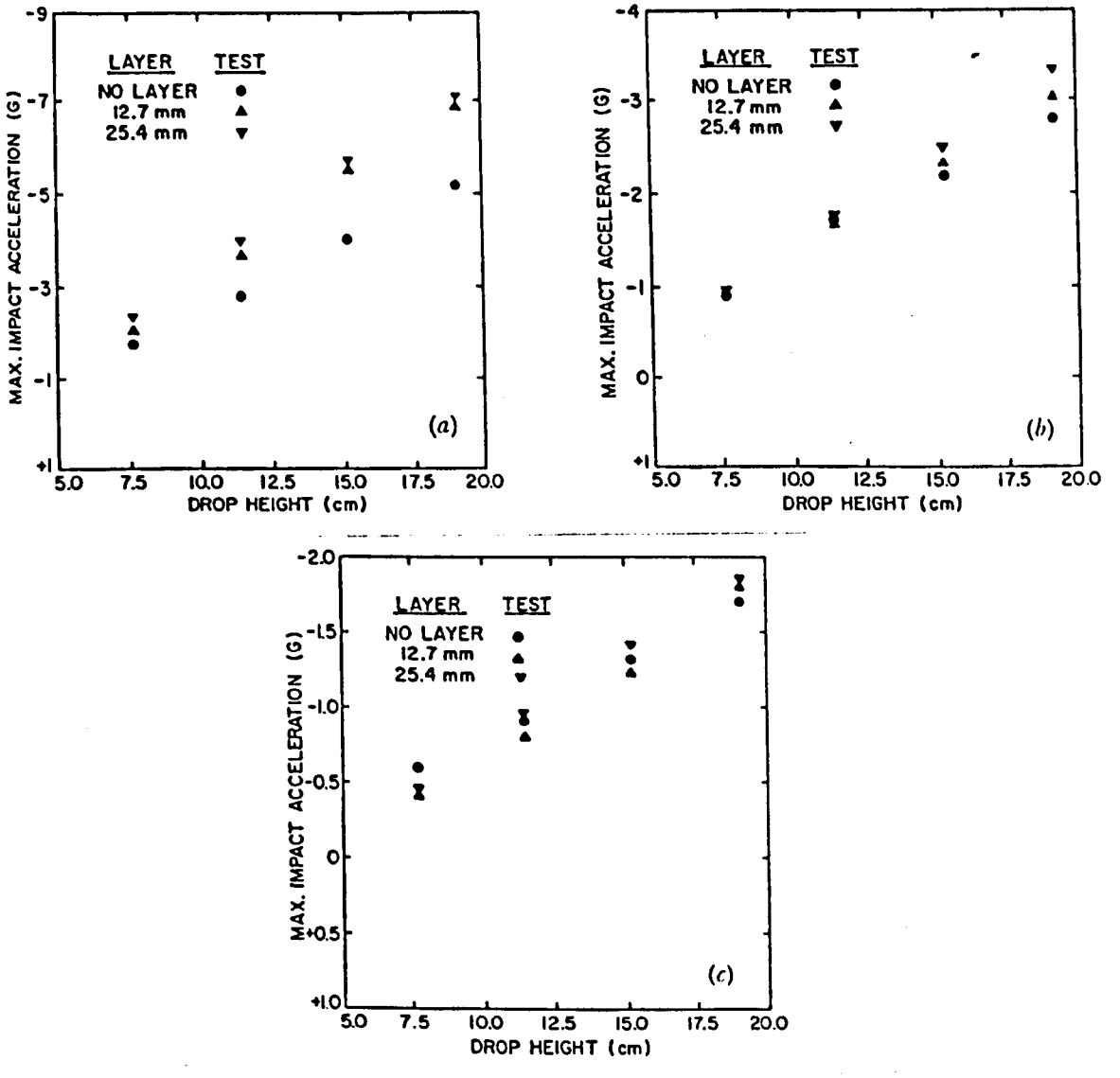

Figure C3.5. Measured maximum impact accelerations of wedge-shaped bottoms [C13]
(a) deadrise = 6 deg.; (b) deadrise = 10 deg.; (c) deadrise = 15 deg.

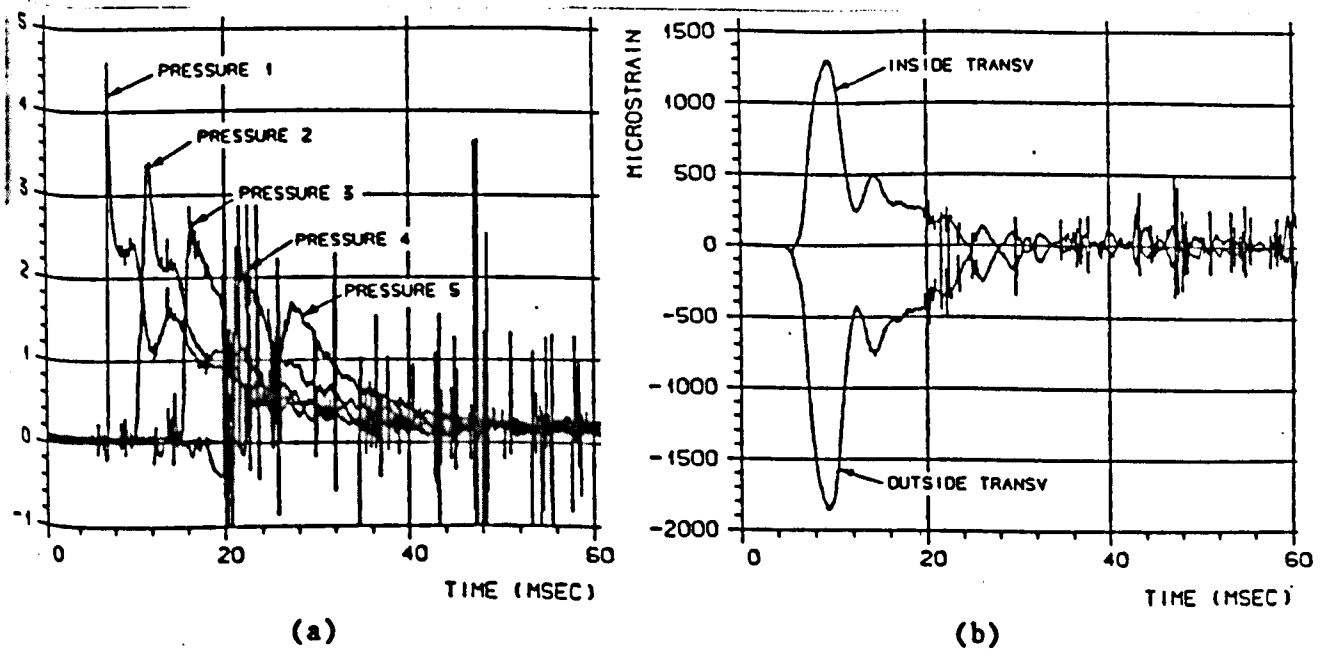

Figure C3.6. Slamming drop test on stiffened aluminium model; H=8.0m, symmetrical position, (a) Pressure signal, (b) plating strain [C18]

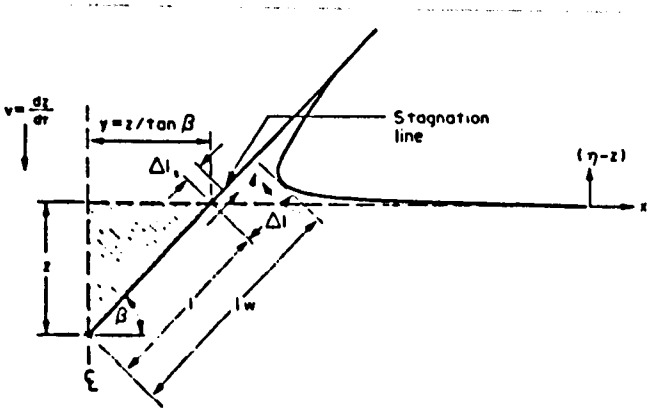

Figure C3.7. An impacting wedge [C20]

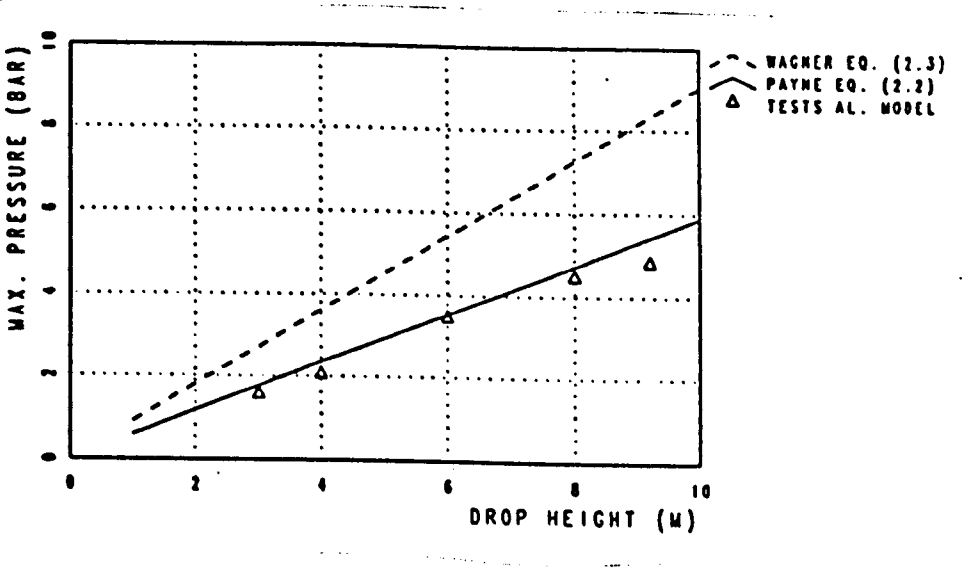

Figure C3.8. Maximum recorded pressures plotted against drop height [C18]

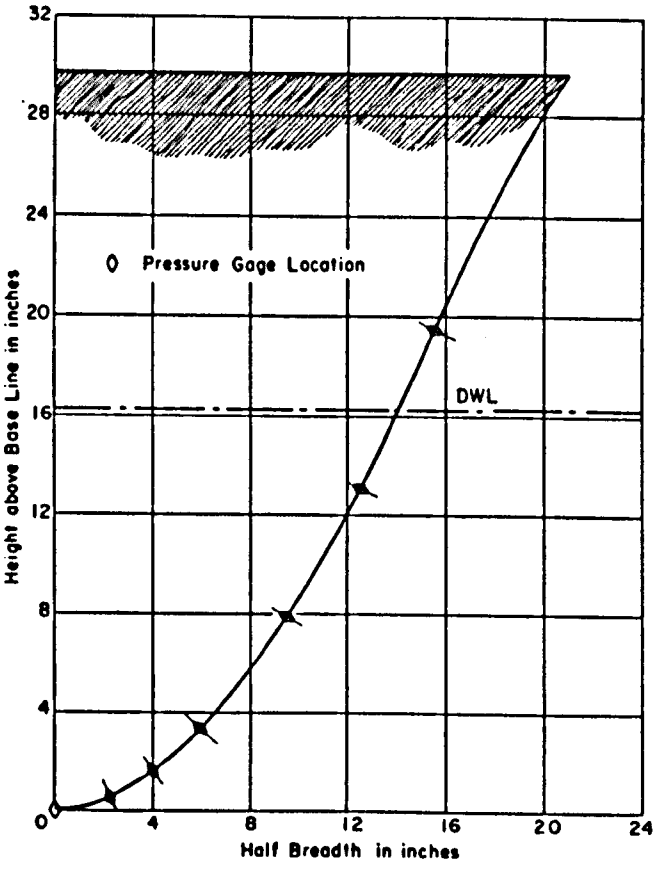

Figure C4.1. Offsets of V-form model and pressure transducer locations [C22]

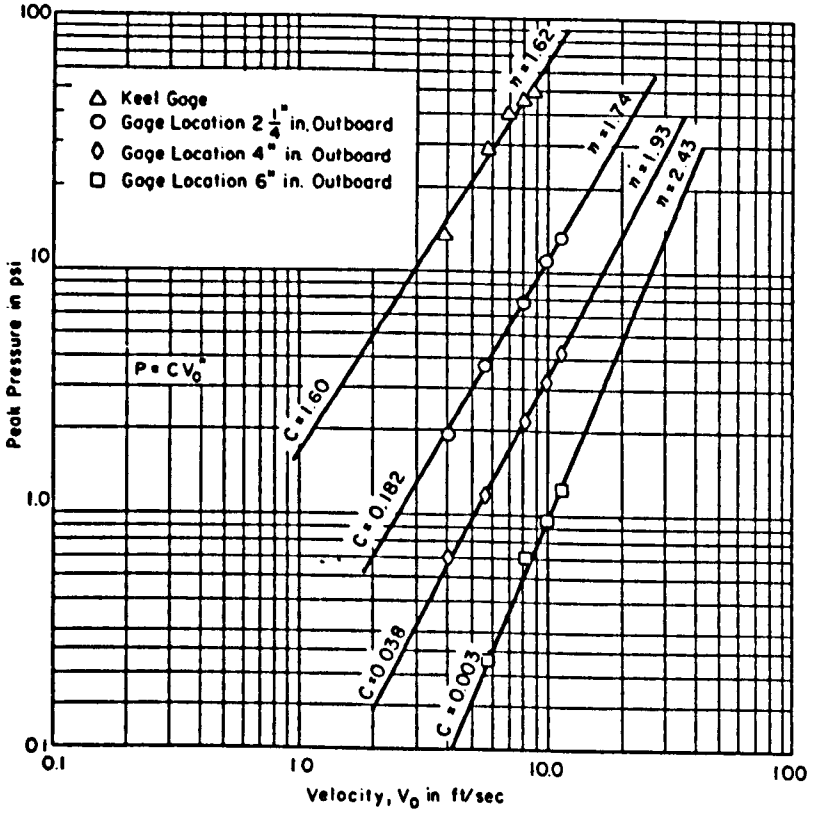

Figure C4.2. Peak pressure as a function of impact velocity for a V-form model [C22]

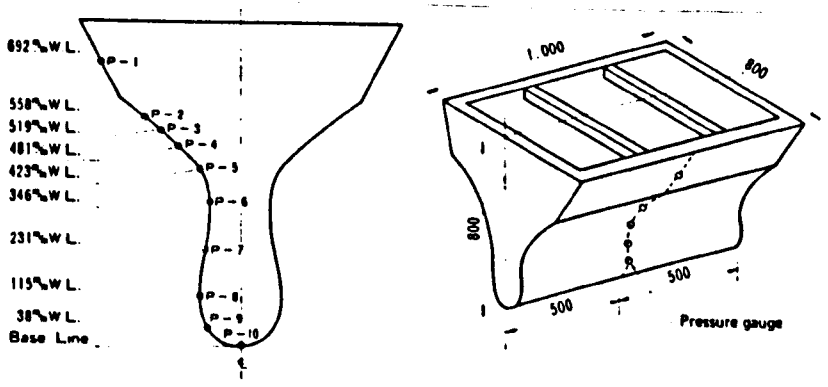

Figure C4.3. Drop test model and pressure gauge locations [C23]

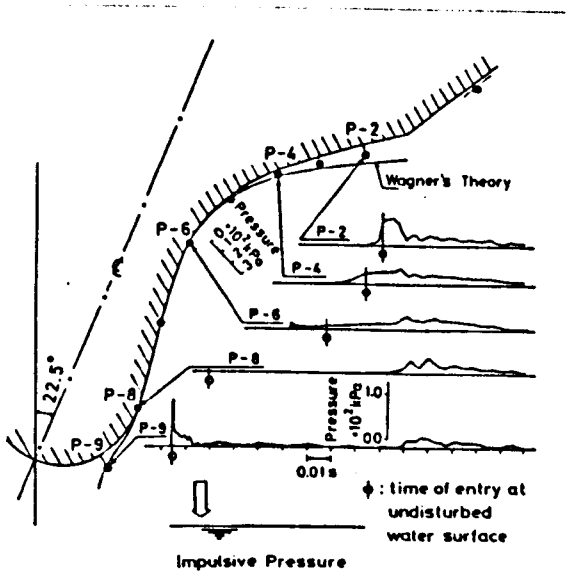

Figure C4.4. Drop test result of inclined section model and comparison with peak pressures by Wagner's theory [C23]

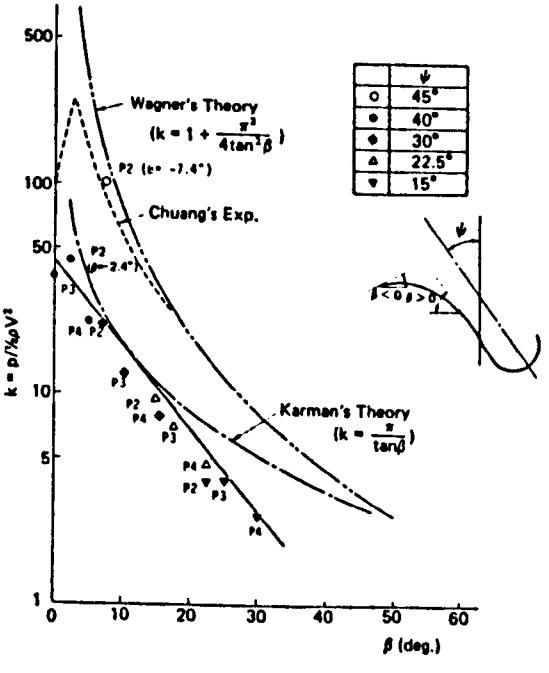

Figure C4.5. Maximum pressure on the flare part vs impact angle [C23]

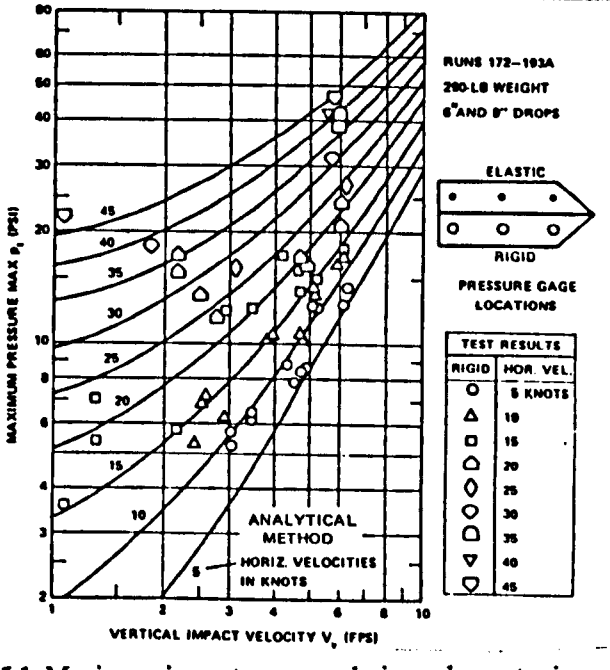

Figure C5.1. Maximum impact pressure during calm-water impact of 3-D, 10 deg model with 6 deg trim and various horizontal velocities [C25]

APPENDIX D

ON THE DESIGN OF A MULTIPLE-ANGLE SWATH DROP TEST MODEL

APPENDIX D

ON THE DESIGN OF A MULTIPLE-ANGLE SWATH DROP TEST MODEL

Abstract

The preliminary design of a drop test model of a typical basic configuration of SWATH ship forward structure is described in this report. Structural design of the model which includes the determination of bottom plate thickness and stiffener sizing is explained. Structural check against vibrational effect due to slamming is made. Specific features of the model pertinent to SWATH's wet deck configuration are described along with the instrumentation to be applied.

D1. INTRODUCTION

It is reported from practical experiences with at least two full-scale SWATH ships, i.e. the SSP Kaimalino and the *Frederick G. Creed* [D1,D2], that wet deck slamming which occured during their sea trials could seriously damage the bottom structure. Further, slamming load is believed by some to be one of the most important governing factors in the SWATH structural design, especially for smaller vessels, as highlighted in ref. [D3]. In order to gain more information for efficient design well calibrated SWATH slamming pressure data is, therefore, required. Despite this urgent need it appears only four institutions [D4-D7] have so far attempted to generate slamming data based on SWATH model tests. The accumulated data from these sources, however, remains inadequate to formulate an acceptable approach to predict slamming pressures which can be readily adopted for design. Further slamming data is therefore sought from drop tests in the near future.

This brief report contains the description on the preliminary design of a drop test model of a typical basic configuration of SWATH ship forward structure. This test is organised in a collaboration between the University of Glasgow and Yarrow Shipbuilders Ltd. (YSL) [D8]. The former will be responsible for constructing the model and for data analysis, while YSL will provide the test rig and site facilities.

Initially three small models, i.e. the model of the *Victorious* (T-AGOS 19), *Patria* and the Fishing SWATH MV *Ali*, were proposed to be fabricated for the test programme. It was later to construct only one slightly larger model which would allow different impact angles to be tested and observed. This idea was based on experience

gained from drop tests recently conducted at DnV [D7]. During these tests the maximum impact pressure was not found to occur on flat bottom models but rather at a small tilt angle of approximately 5 deg [D7]. This finding apparently confirms that reported in ref. [D9].

The drop test to be carried out at YSL will of course be similar to those conducted previously by others (for instance ref. [D9,D10]). However, peculiar features inherent to the SWATH configuration such as the presence of haunches will be introduced at a later stage of the tests. The overall arrangement will be attempted in such a way so that slamming characteristics of SWATH can be reasonably accurately simulated.

D2. DESIGN IMPACT PRESSURE

The maximum impact pressure expected to be imposed on the model is derived based on the maximum impact velocity of approximately 3.0 m/s which corresponds to the drop height of about 2.0 feet. From various data of drop tests available elsewhere [D9-D12] the maximum impact pressure generated under that magnitude of velocity could reach as high as 275 kPa (40 psi).This pressure value is adopted throughout the design of the drop test model now described.

D3. BOTTOM PLATE DESIGN

D3.1. Determination of Plate Thickness

The bottom of the model will be assembled by welding two pieces of steel plate (size of 1000x750mm each) with 160 deg inclining angle one to another. A stiffener will be attached transversely at the midspan of each panel to provide reinforcement on the bottom structure as shown in the technical drawing in the back pages. The bottom plating of the model (a=1000mm, b=375mm and α=2.67) is designed to avoid yielding and checked against Clarkson's various plate design criteria. The design pressure p_d is as given above (275 kPa), the safety factor required is 1.5 and the panel is designed using plastic collapse criteria, which further should satisfy the plate slenderness parameter $\beta \leq 2.5$. This plate slenderness parameter is given by the following equation.

$$\beta = \frac{b}{t}\sqrt{\frac{\sigma_y}{E}} \qquad \text{(D1)}$$

By assuming that the edges of the panel are rigidly clamped, the ultimate pressure

$p_{3h}(=1.5p_d)$ to cause a 3-hinge collapse on the long panel can then be written as

$$p_{3h} = 4.5\sigma_y\left[\frac{t}{b}\right]^2 \qquad \text{(D2)}$$

Substituting the panel width b=375 mm, the typical yield stress of material σ_y=245 N/mm^2 and the modulus elasticity of material E=207 kN/mm^2 into eq. (D2) plate thickness of 7.25 mm is obtained. A value t=10mm was finally chosen for unsupported panel which should then provide a reasonably rigid structure so that any vibrational effect due to slamming is eliminated.

A further evaluation is then made towards the selected plate thickness as follows. Substituting the plate thickness t=10mm into eq. (D1) the slenderness parameter β is found to be 1.29, which is less than the maximum allowed as above (=2.5). Using this value and assuming that there will be some initial deflection given by

$$\frac{\delta}{b}\sqrt{\frac{E}{\sigma_y}} = 0.2 \qquad \text{(D3)}$$

(which is about 55% greater than expected than mean value $0.1\beta^2 t$) then the pressure parameter to cause further yield P_y of approximately 2.0 is obtained from the data sheet. Where

$$P_y = \frac{p_y E}{\sigma_y^2} \qquad \text{(D4)}$$

From this equation p_y=580 kN/m^2 (=2.10p_d) is obtained, which is a satisfactory margin for a safe panel design.

D3.2. Natural Frequency Calculation

On the evaluation of vibrational characteristics the natural frequency of the model rectangular bottom plate, with assumption of all edges being clamped, is determined by [D13]

$$f_{ij} = \frac{\lambda_{ij}}{2\pi a^2}\left[\frac{Et^3}{12\gamma(1-\upsilon^2)}\right]^{1/2} \qquad \text{(D5)}$$

in which f_{ij} is the frequency at ij^{th} mode, i is the number of half waves in mode shape along the horizontal axis, j is the number of half waves in mode shape along the vertical axis, γ is mass per unit area of plate and ν is Poisson's ratio.

λ_{ij} is a dimensionless frequency parameter and is generally a function of the boundary conditions applied at the edges of the plate panel, aspect ratio α and in some cases Poisson's ratio ν.

For a rectangular plate of aspect ratio 2.67 in this case, the constant λ_{ij} values may apply that for general plate with aspect ratio of 2.5, as given belows.

	Mode Sequence					
	1	2	3	4	5	6
λ_{ij}^2	147.80	173.90	221.50	291.90	384.70	394.40

Substituting the values of λ_{ij} and other parameters into eq.(D5) the following natural frequencies for different modes are obtained.

	Natural Frequency Modes					
	f_{11}	f_{21}	f_{31}	f_{41}	f_{51}	f_{12}
Nat. freq. (cps) :	363.0	427.0	544.0	717.0	945.0	969.0

Hence the resonance vibration on the plate could safely be avoided as those natural frequencies for various mode of plate vibrations are much larger than the frequency of exciting force due to slamming impact, which ranges between 20 upto 50 cps.

D3.3. Stiffener Sizing

On the design of the siffeners a symmetric trapezoidal pressure loads as shown in Fig. D1a is applied. The magnitude of the total load (P_t) can then be approximated by

$$P_t = pb(a - \frac{b}{2}) \qquad \text{(D6)}$$

The equivalent uniform load distribution (w) acting on the beam, as shown in Fig. D1b, is then written as

$$w = \frac{P_t}{a} = \frac{pb(a - \frac{b}{2})}{a}$$

or

$$w = pb\left(1 - \frac{b}{2a}\right) = 0.275x375\left(1 - \frac{375}{2x1000}\right) \quad \text{(D7)}$$
$$= 83.79 \text{ N/mm}$$

By assuming that the beam is simply supported at both ends, the maximum bending moment at the midlength of the beam, as shown in Fig. D1c, is calculated by

$$M = \frac{wa^2}{8} = \frac{83.79x1000^2}{8} \quad \text{(D8)}$$
$$= 10473750\text{Nmm}$$

Using a safety factor of 2.0 against yield, the allowable stress is derived as

$$\sigma_{allow} = 245/2 \text{ N/mm}^2 = 122.5 \text{ N/mm}^2.$$

Hence the required section modulus can be calculated by

$$Z_{req} = \frac{M}{\sigma_{allow}} = \frac{10473750}{122.5} \quad \text{(D9)}$$
$$= 85.5 \text{ cm}^3$$

A tee steel profile provided from a mid-depth cut of a standard universal beam size of 203mm x 102mm, with an effective panel width of 375mm gives a section modulus of 103 cm^3 is selected. The calculation to this section modulus is given in Table D1. Having determined the size, the actual allowable stress of the stiffener is found to be

$$\sigma_{actual} = \frac{10473750}{103696} N / mm^2 = 101.0 N / mm^2$$

which provides a safety factor against yield of

$$SF = \frac{245}{101} = 2.42$$

D4. DESCRIPTION OF THE MODEL

The drop test model will be constructed out of three major components, namely, the steel box, the supporting web frame and the sliding frame, as shown in the technical drawings. Most of the components will be fabricated using 10 mm thick steel plate which yields to an overall model weight of approximately 775 kgs. The dimension of the steel box will be 1500x1000x1000 mm with 20 deg ramp angle at midlength of the bottom. A top lid (steel cover) will be added to ensure no water spray can spill into the box which may damage to the electronic instruments mounted inside. Another stiffener made of a prefabricated steel profile (size of T 102mm x 153mm) will be welded transversely at the midlength of the bottom plate to give an adequate rigidity on the connection of the two bottom plate sections. The sliding frame, as can be seen in the drawings, will simply be fabricated by welding 10 mm thick steel plate to form a rectangular column of size 1400x200x100 mm mounted onto the top flange of the web frame. The two ends of the frame will be attached to the vertical steel column of the test rig available at the drop test tank.

As is mentioned in the introduction the model is designed to allow different impact angles to be investigated. For it to work the arrangement is made in such a way so that one end (in this arrangement the aft end) of the model is fixed and the other end (fore end) is free to move up and down. The aft end of the model which will function as a hinge is fixed to the web frame by two aft pins at both sides of the model through the aft pin supports (see drawings). The fore end of the model is connected to the web frame by the detachable pins at both sides through the pin supports. To change the tilting angle of the model, the fore pins are detached followed by positioning the model in a desired impact angle and then replace the pins in the prescribed slot as depicted in the drawing of detail 1. There are seven pin slots are provided which corresponds to the tilt angles of 0, 2, 4, 5, 6, 8 and 10 deg. While the two pieces of the bottom plates having 160 inclining angle one to another, hence there will be 14 variations of impact angles between 0 and 20 deg can be investigated. Further, such an arrangement allows two impact angles to be measured simultaneously by pressure transducers located on the two faces of the bottom plate at each run of the test. For example when the model is tilted down by 2 deg this means the fore portion of the bottom plate will decline into 18 deg towards the horizontal plane (water surface) whereas the aft bottom plate will rise up by 2 deg, and so on.

The design of the fore and aft pins is done by using the force-area correlation. As is seen in those drawings the pins are subjected to forces acting perpendicular to the pins axis, hence the pins need to be designed to resist shear forces. The force-area relation in this condition is written as

$$\tau_{allow} = \frac{F_s}{2A} \qquad \text{(D10)}$$

where τ_{allow} is the allowable shear stress of the material, F_s is the shear load and A is the sectional area of the pin. The factor 2 on the right hand side of eq. (D10) is introduced due to the fact that the pin supports and the web frame resist the load in opposite direction thus creating two shearing surfaces on the pin. The average shear stress properties of a material (τ_{ave}) is related to the yield stress in tension (σ_y) by factor of 0.5 upto 0.6 [D14]. The allowable shear stress in turn is derived by applying a design safety factor to the average shear stress. In the present pin design a safety factor of 2.0 and the worst possible average shear stress ($0.5\sigma_y$) are selected to produce an allowable shear stress value of approximately 61.3 N/mm^2. The design load for the pins is taken as the maximum force generated by the maximum slamming pressure acting on the flat bottom plate. It is assumed that the maximum force is evenly distributed among the four pins and hence the load on each pin is found to be 51.6 kN. The diameter of the pin is then obtained using eq. (D10) and is approximately 23.2 mm. Rounded up the value the final pin is selected as having a diameter of 1 inch (25.4 mm).

D5. SPECIFIC FEATURES OF THE SWATH DROP TEST MODEL

The proposed drop test is chiefly aimed at generating slamming pressure data pertinent to SWATH ships. It is, therefore, necessary to formulate the model geometry which represents specific features of SWATH underdeck configuration. Among other geometries which characterised a typical SWATH underdeck structure are the presence of ramp angle, haunches and the struts. Ramp angle, as is applied to other twin hull crafts like catamaran or SES, is widely believed to be one of the mechanisms which could induce a reduction in the severity of wet deck slamming. Nonetheless, optimum ramp angle for a particular vessel remains uncertain to the designer. Probably relative impact velocity, which obviously should have taken into account the forward speed effects, is the best parameter to be associated in the selection of ramp angle for wet deck design. Observation of different angle of impacts on the model as is clarified in the previous section can be directed towards the exploration of effective ramp angle to be implemented for SWATHs.

The application of haunches on SWATHs is primarily designed to increase the strength at the intersections of the struts and the cross deck which are vulnerable to the side force. To a certain degree haunches are also expected to render beneficial effects to the problem of wet deck slamming. The potential of haunches in reducing maximum

slamming pressure may be sought from the aspect of the increase in vertical damping due to the surface water disturbance before actual slamming is imposed on the flat wet deck. The deflected water surface and the water swell up could further compress the air into the middle of impact space thus creating an additional cushioning effect to the flat bottom. The drop test on the model with haunches attached will follow after the plain bottom test is carried out. Comparison will then be made between slamming on plain flat bottom and bottom with haunches. The assembly of the prefabricated haunches onto the model flat bottom will be arranged as shown in Fig. D2.

The possibility of impact pressure reduction with the presence of struts is quite obvious. In case of SWATH bottom slamming the struts will behave like two side walls which impede the transverse air flow beneath the wet deck thus providing an air cushioning effect to the bottom structure [D11,D15,D16]. The experimental set up incorporating the presence of haunches and the struts is as sketched in Fig. D3. When the model is tested without the haunches mounted the struts (side walls) will then function as a boundary which will induce the 2-dimensional flow simulation as required in item A of ref. [D8].

The main instrumentations to be employed in the drop test are as depicted in Fig. D4. Impact pressures will be measured by means of 16 pressure transducers located along the bottom plate. The positions of the transducers are arranged in such a way so that the pressure distribution at any mode, i.e. in flat bottom or in tilting angle modes, can be aptly recorded. In addition, the measurement of the pressure induced bending stresses on the mid-span stiffener will also be taken. Two locations will be investigated, that is, at the mid-length of the stiffener where maximum stress is expected and the other near the edge. For this purpose strain gauges will be mounted on the flange and the base of the stiffeners. In this way the average distributed load on the bottom panel can be estimated.

D6. CONCLUSION

The design of the SWATH drop test model has been described within this report. An attempt has been made to produce model that would reasonably simulate the slamming characteristics of SWATHs. Detail arrangements, however, remain to be fixed and alteration to the model will be made if necessary after a confirmation and further considerations are given by Yarrow Shipbuilders Ltd.

REFERENCES TO APPENDIX D

D1. Hightower, J.D. et al, "SWATH Technology Development at the Naval Ocean System Center", *Proc., Int. Conf. on SWATH Ships and Advanced Multi Hulled Vessels*, Paper No. 14, RINA, London, U.K., Apr. 1985

D2. Pegg, N.G., Gilroy, L.E. and Cumming, D.W., "Load, Motion and Structural Response Trials of the SWATH Vessel 'Frederick G. Creed' ", *Proc., Symp. on the Dynamics of Marine Vehicles and Structures in Waves*, IUTAM, Brunel University, U.K., June 1990

D3. Loscombe, P.R., "Key Aspects of the Structural Design of Small SWATH Ships", *PhD Thesis*, Univ. of Southampton, Dept. of Ship Science, U.K., 1989

D4. Graham, R., "Slamming Experiment with a Radio-Controlled SWATH Model", *Proc., Int. Conf. on SWATH Ships and Advanced Multi-Hulled Vessels II*, Paper No. 9, RINA, London, U.K., Nov. 1988

D5. Sikora, J.P. and Dinsenbacher, A.L., "SWATH Structure : Navy Research and Development Applications", *Marine Technology*, SNAME, Vol. 27, No. 4, pp. 211-220, July 1990

D6. Djatmiko, E.B., "Comparative Evaluation of Some Slamming Prediction Methods for SWATH Type Vessels", *Department Report*, No. NAOE-91-14, Dept. of NA&OE, University of Glasgow, June 1991

D7. Hayman, B., Haug, T. and Valsgård, S., "Response of Fast Craft Hull Structures to Slamming Loads", *Proc., Ist Int. Conf. on Fast Sea Transportation (FAST'91)*, Trondheim, Norway, June 1991

D8. Djatmiko, E.B., "Slamming Drop Test Programme", *Notes of a Meeting Held at YSL*, Oct. 1991

D9. Chuang, S.L., "Experiments on Slamming of Wedge-Shaped Bodies", *Journal of Ship Research*, SNAME, Vol. 11, No. 3, pp. 190-198, Sep. 1967

D10. Chuang, S.L., "Experiments on Flat-Bottom Slamming", *Journal of Ship Research*, SNAME, Vol. 10, No. 1, pp. 11-17, March 1966

D11. Lewison, G. and Maclean, W.M., "On the Cushioning of Water Impact by Entrapped Air", *Journal of Ship research*, SNAME, Vol. 12, No. 2, pp. 116 130, June 1968

D12. Sellars, F.H., "Water Impact Loads", *Marine Technology*, SNAME, Vol. 13, No. 1, pp. 46-58, Jan. 1976

D13. Blevins, R.D., "Formulas for Natural Frequency and Mode Shape", Van Nostrand Reinhold Co., 1979

D14. Gere, J.M. and Timoshenko, S.P., "Mechanics of Materials", Van Nostrand Reinhold (UK) Co. Ltd., UK, 1987

D15. Verhagen, J.H.G., "The Impact of a Flat Plate on a Water Surface", *Journal of Ship research*, SNAME, Vol. 11, No. 4, pp. 211-223, Dec. 1967

D16. Ando, S., "Cushioning of Slamming impact by Elastomeric Layers", *Journal of Ship research*, SNAME, Vol. 33, No. 3, pp. 169-175, Sept. 1989

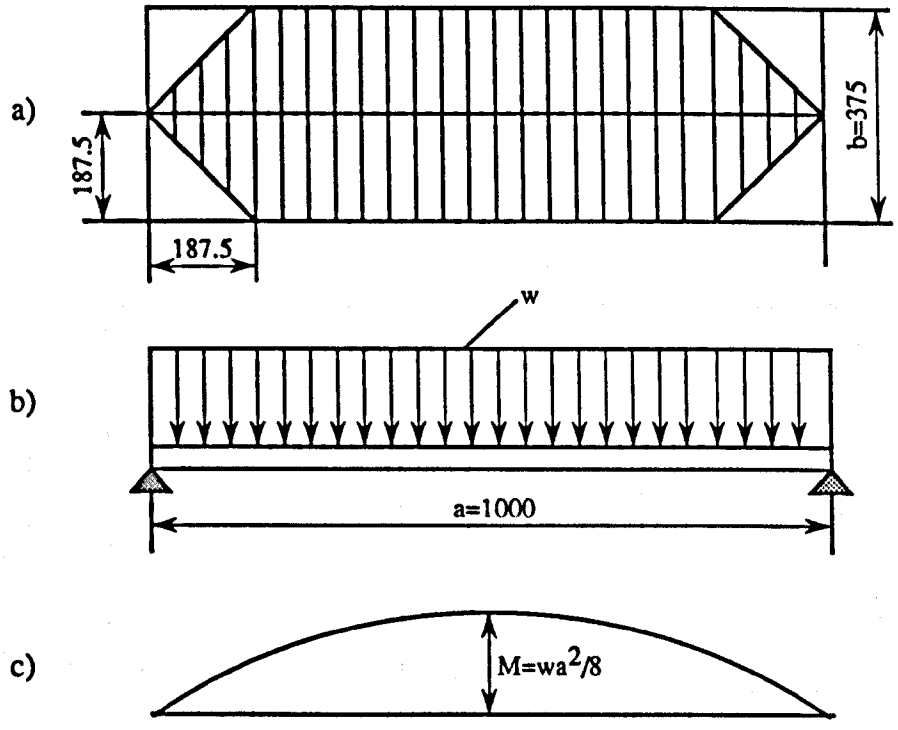

Figure D1. Panel stiffener design

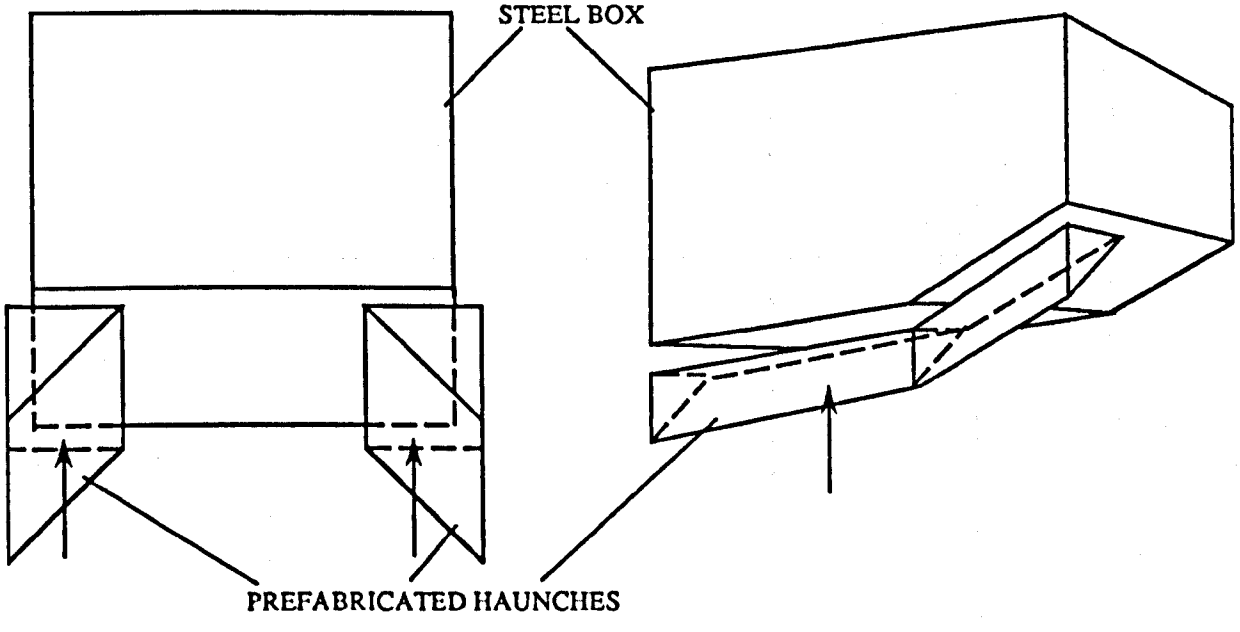

Figure D2. Haunches assembly

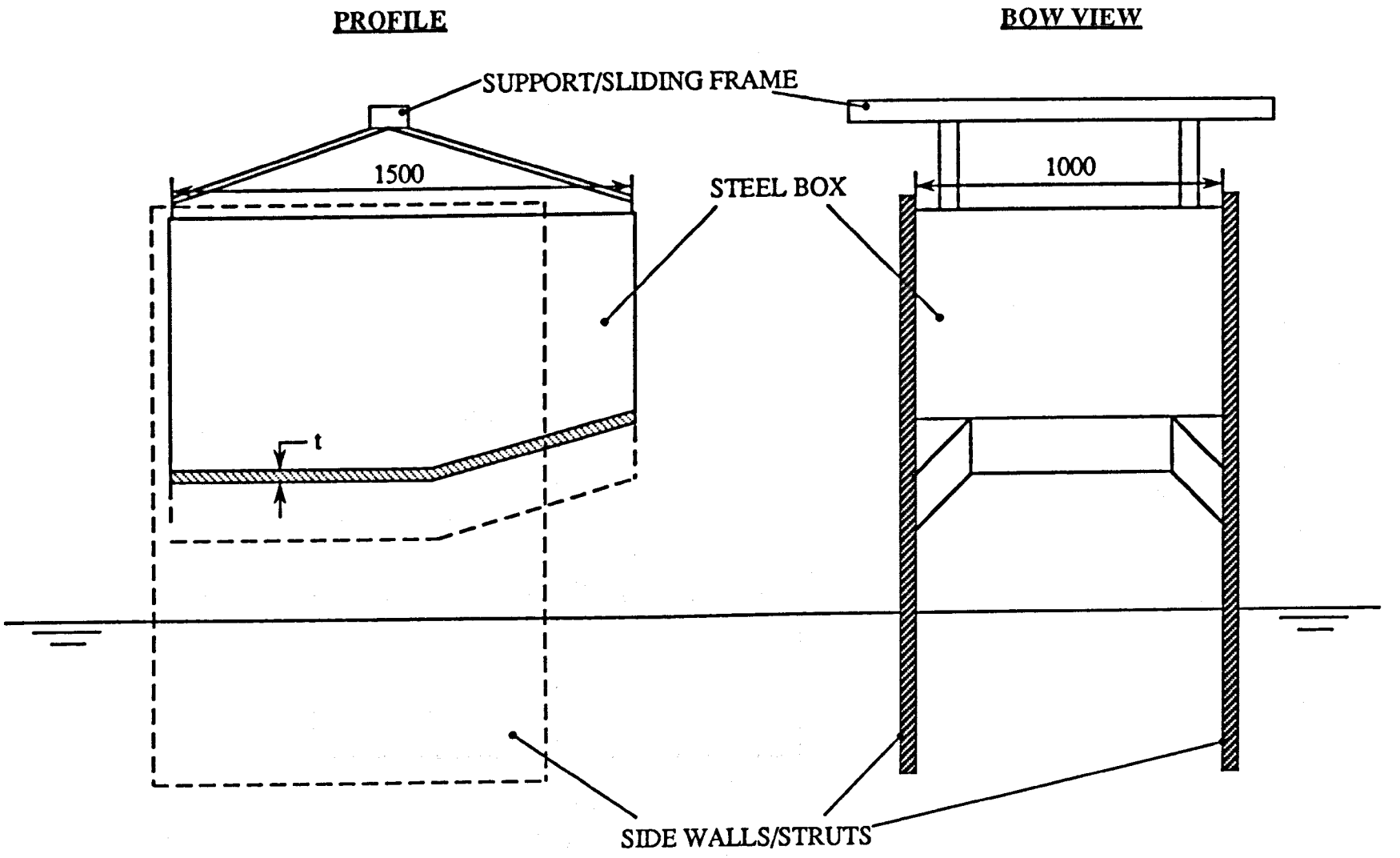

Figure D3. Drop test set up for bow section of a SWATH model

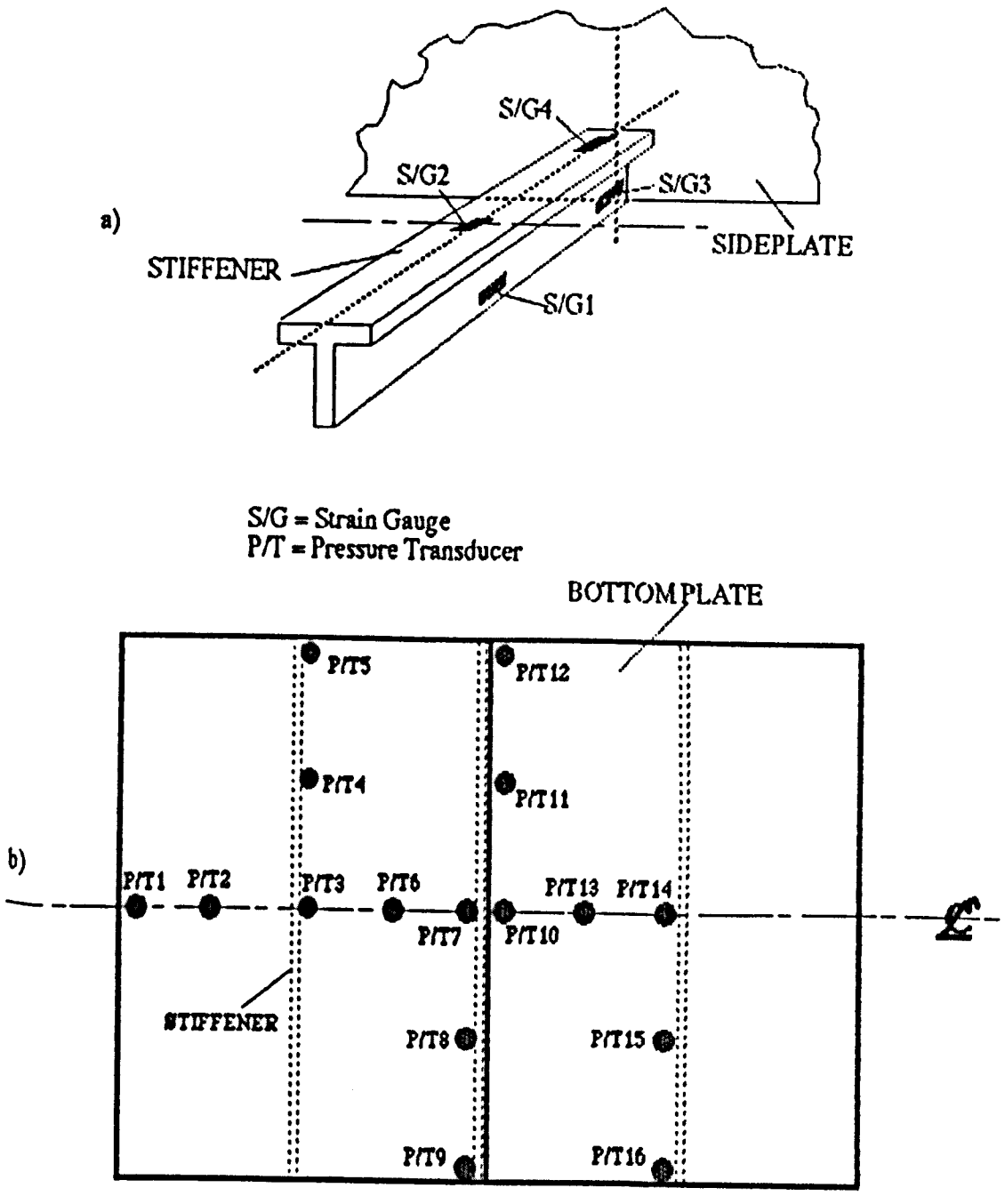

Figure D4. Basic instrumentation arrangement

Table D1. Calculation of section modulus for the stiffener
(Tee split of universal beam serial 203 x 102)

	a (mm)	b (mm)	A (mm^2)	y (fro botom)	y x A	Ixc	d=yNA-y	Ixna	Ixc+Ixna
Sect 1	375.00	10.00	3750.00	5.00	18750.0000	31250.0000	23.3593	2046213.3618	2077463.3618
Sect 2	5.20	92.30	479.96	56.15	26949.7540	340743.2024	27.7907	370684.1502	711427.3526
Sect 3	101.60	9.30	944.88	106.95	101054.9160	6810.2226	78.5907	5836049.5498	5842859.7724
	Σ=	111.60	5174.84		146754.6700			Ina (mm^4)=	8631750.4868
				yNAb (mm)=	28.3593			Zb(mm^3)=	304371.4227
				yNAt(mm)=	83.2407			Zt(mm^3)=	103696.2337

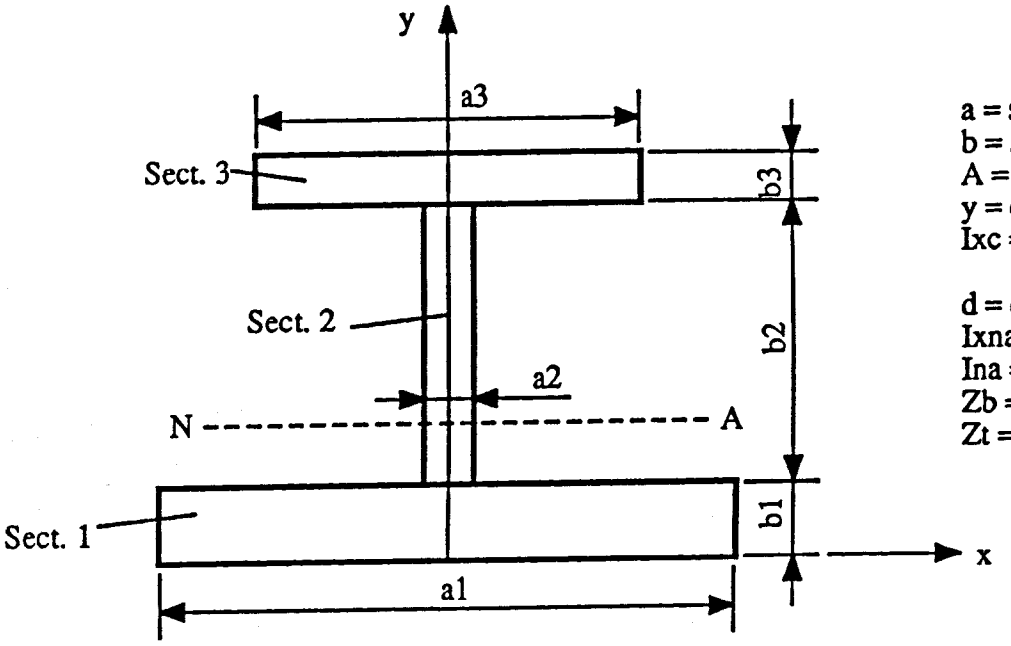

a = sectional dimension in x direction
b = sectional dimension in y direction
A = sectional area
y = distance of centre area to x axis
Ixc = moment of inertia about an axis through centre area parallel to x axis
d = distance from centre area to neutral axis (NA)
Ixna = Ad^2
Ina = moment inertia of the section about neutral axis
Zb = section modulus about the bottom line of the section
Zt = section modulus about the top line of the section

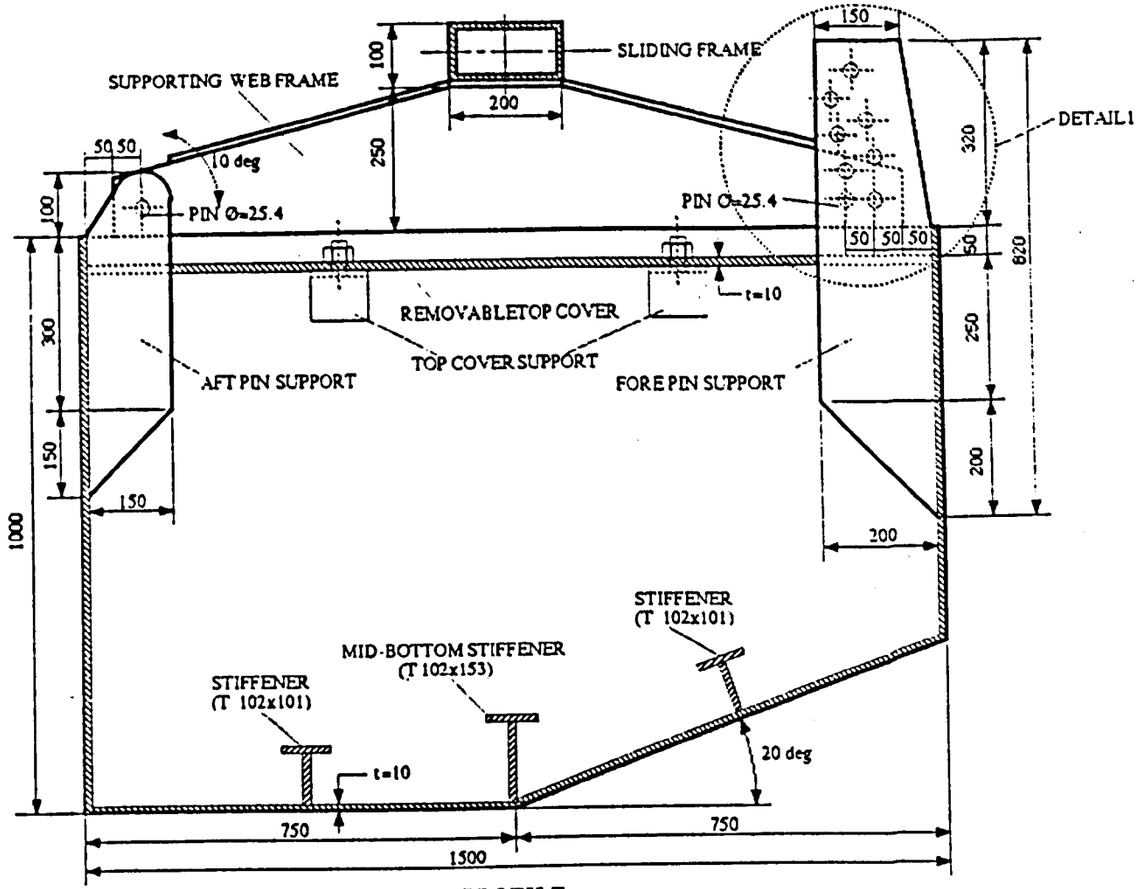

PROFILE

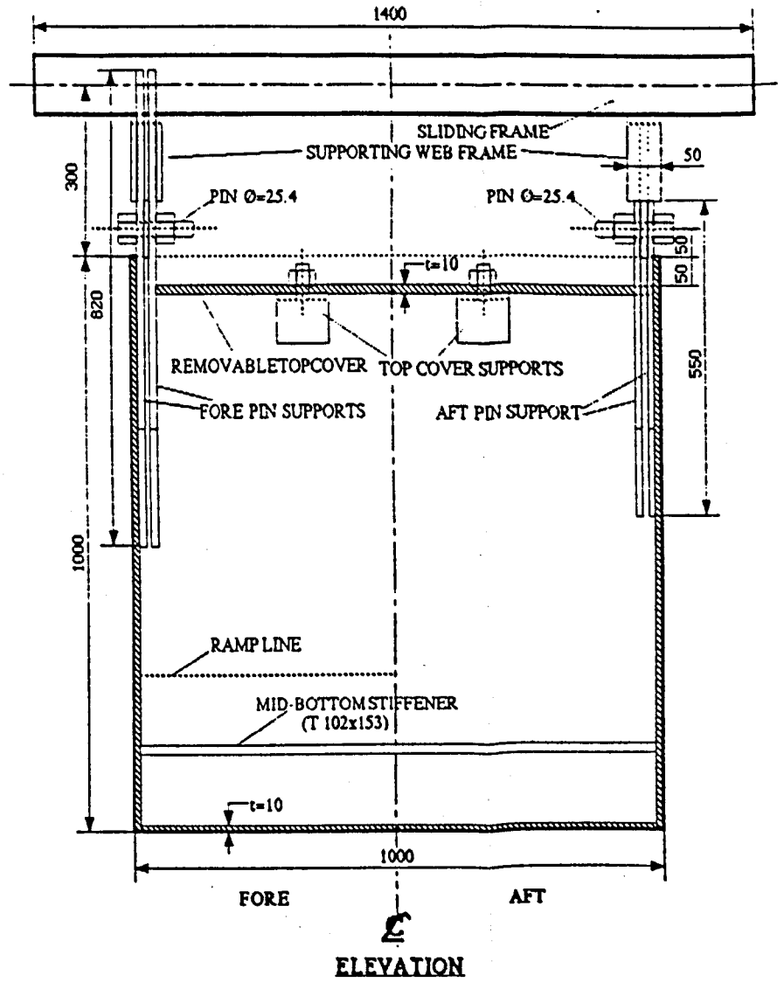

ELEVATION

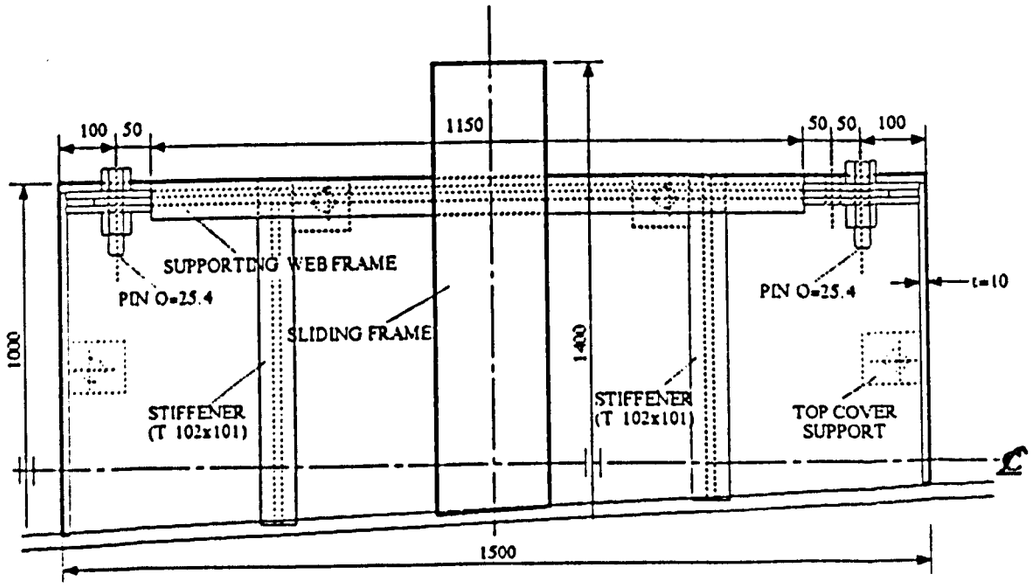

PLAN

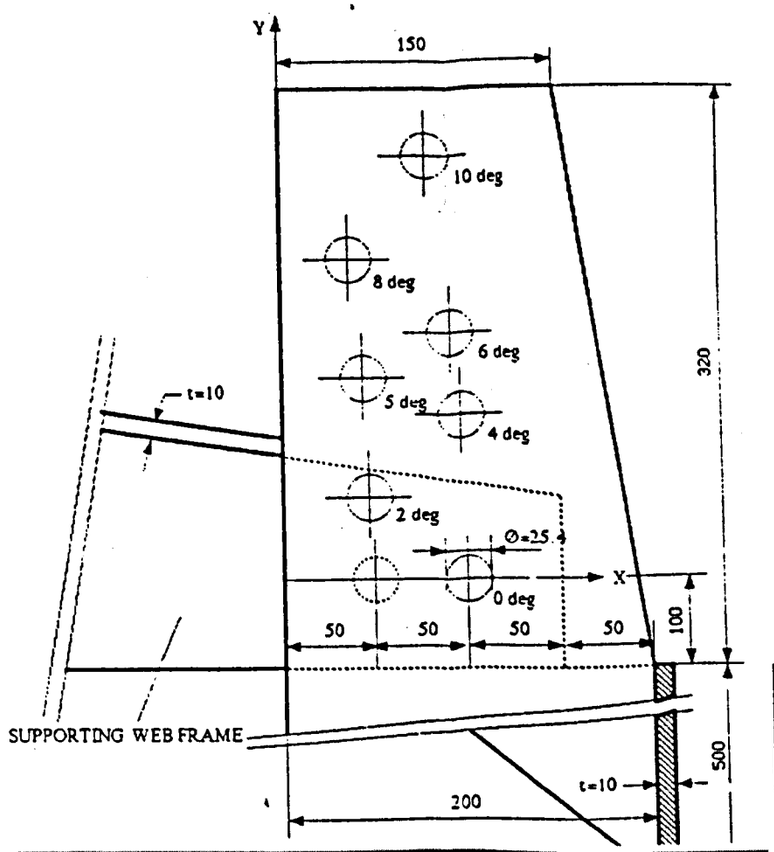

DETAIL 1 (Scale = 1 : 2.5)

POSITIONS OF PIN SLOT AXIS

Tilt Angle	X (mm)	Y (mm)
0 deg	100.00	0.00
2 deg	49.23	43.26
4 deg	96.83	90.68
5 deg	45.24	108.94
6 deg	92.88	135.88
8 deg	37.84	173.96
10 deg	80.25	225.74

D-14

MULTIPLE-ANGLE SWATH DROP TEST MODEL

by E.B.Djamiko
Dept. of NA&OE - Univ. of Glasgow

APPENDIX E

SWATH STRUCTURAL DESIGN AND ARRANGEMENTS

APPENDIX E

SWATH STRUCTURAL DESIGN AND ARRANGEMENTS

Abstract

A number of structural design and arrangement of SWATH vessels, ranging from below 100 tonnes upto 15000 tonnes, compiled from open literature are presented. Design approaches are to be highlighted along with the use of alternative materials to gain a reasonable weight saving. Technical drawing of the vessels are provided as much as it is available. The reviewed information should be useful for reference in the early design stage of SWATH ships.

E1. INTRODUCTION

This Appendix contains descriptions of SWATH structural arrangements extracted from those available in open literature. The descriptions attempt to be as thorough as possible depending on the comprehensiveness of the source of information. The structural configurations to be presented are not only those developed in the actual SWATH designs, but also cover those in the hypothetical studies. The wider range of information presented is viewed as being useful to aid SWATH designers in establishing a firm base in the initial stage of design. Hence, the infomation in this Appendix would be appropriate to be incorporated in the preliminary structural design study, as is in Chapter 5.

Basic approaches in the structural design of each SWATH vessel covered herein are addressed, with examples of their outcome primarily in the form of structural drawings. Nevertheless, most structural drawings that are available present only the configuration of SWATH mid-ship sections because complete drawings are rarely found at this stage. The use of construction material highlighted are there in which most small SWATHs are fabricated out of aluminium material, whereas larger SWATHs are mainly made of steel.

E2. STRUCTURAL DESIGN AND ARRANGEMENT OF THE *HALCYON*

The *Halcyon* (60-tonne SWATH boat) was built by RMI Inc., a small company with objectives of pursuing advanced marine vehicles (AMVs) development and

construction [E1,E2]. The construction of the *Halcyon* was iniatially aimed at providing a demonstrator to study the development of larger SWATHs within the company. In 1985 the vessel was hired by the US Coast Guard for a technical evaluation [E3]. Discussions on the design of the *Halcyon* (main particulars as listed in Table E1 and configuration shown in Fig. E1) are fully reported in refs. [E1,E2], and only the particular part in her structural design is extracted in following.

The design and construction of the *Halcyon* departed from the practice adopted in monohull ship development. The vessel was designed using aluminium alloy, with all primary hull structural elements continuously welded. The most significant loads were expected to impose when the vessel encounters beam waves in its operational route. Considering the study by the US Navy [E4], a maximum lifetime side load around 0.95 to 1.0 times the craft gross weight colud exist on a vessel of this size. A side load of 1.2 times craft gross weight was then selected in the design of the *Halcyon*.

Longtudinal hull bending loads for the vessel, given the unique operating characteristics of the SWATH concept, are relatively low even if simultaneous slam is experienced by the vessel. Hence, longitudinal load could be ruled out as a substantial source of global structural failures, unlike those on monohulls. On the other hand, slamming load governs crucially in the design of local under deck scantlings. Maximum plating pressure, given a wave impact forward of the knuckle, was estimated for a boat speed of 20 knots at 20 psi, while pressures on the wet deck aft of the knuckle and elsewhere were estimated at less than 5 psi for normal operation. Further, based on a combination of side loads and V-line loads (the load originated from flooding after the ship sustains underwater hull damage), sidehull and strut pressures were estimated to be approximately 7.8 psi. The compartment boundaries, including the watertight transverse subdivision bulkheds, watertight longitudinal bulkheads, side shell and vital space boundaries were also designed to V-line loads equal to hydrostatic head of water measured perpendicular to the most extreme flooded water line in the area of compartment. The flooding level was determined by the conditions considering several factors, such as the extension of hull damage, position of the damage, motion (roll angle) of the craft and the list angle resulting from hull damage.

The resulting hydrostatic pressures were applied to either side of the compartment boundaries as any individual compartment could be unflooded. In case of the shell plating, the pressure was applied from outside only.

Primary hull bending, shear, and torsion loads for dry docking and hoisting of the craft were also determined for lightship weight conditions. A load factor of 4 was applied to the lightship weight and was considered to be appropriate for both dry docking and hoisting operations. The *Halcyon* can be supported on keel blocks in dry dock and can be hoisted from four lifting points designed into the main deck structure.

In order to more fully explore the effects of transverse loads on the structure a NASTRAN finite element model was developed. The model was representative and limited to the hull structure between bulkheads at stations 37 ft. and 49 ft. This segment of the structure was selected for analysis because of the large opening in the main deck for machinery, and area likely to cause the most severe internal stress distributions and concentrations.

Given the *Halcyon*'s beam sea loading assumptions, the average stress for the NASTRAN section was calculated to be 3905 psi which was well within the material allowance for the alloys selected. This calculated stress provided a good basis for computing the total deck loads. Analysis indicated that relatively high stress peaking would exist at the transverse bulkhead adjacent to the deck cut out. It also showed that transverse loading resulted in compression in the wetdeck which would result in higher stresses at frames and bulkheads since they would be carrying higher loads to take up the slack. Table E2 lists the safety factors used for the Halcyon structural analysis.

Five interior transverse watertight bulkheads were provided that continued into the cylindrical lower sidehulls. Circular tee frames located at 36 in. centres stiffened the lower hulls and were joined to the non-tight frames of the struts. Inboard of the shell were three longitudinal watertight bulkheads located at the hull centreline and at 7.5 ft. off centreline (port and starboard) at the inboard joint of the sponson and wet deck. Longitudinal and transverse framing were of increased thickness in the areas of machinery openings and at hull lift points.

The midship section, shown in Fig. E2, illustrated many of the design features of the *Halcyon* structure. In particular, it shows the design approach taken at the cross structure-sponson and sponson-strut joints to provide continuity at joint interface. Continuous, double sided fillet welds were used throughout mitigate against fatigue failure and stress concentrations at weld bead terminations. Only the *Halcyon*'s lightly loaded superstructure and pilot house used conventional 'skip' welding construction. Longitudinal hull plating below the wet deck is primarily of 0.224 in. thick plating stiffened by 3 in. x 0.224 in. flatbars (welded continuously) at 10 and 15 in. centres. The wet deck is primarily 0.2 in plating inboard of 7 ft. 6 in. and 0.281 outboard. The deck is reinforced with 3/8 in. x 24 in. plate spanning the width of the ship at watertight bulkheads. The main deck is generally 0.35 in. plating inboard of 6ft. 3 in. and 0.313 in. plating outboard reinforced at machinery openings by 0.375 plate. The wet deck and main deck were also stiffened by continuous welded 3 in. x 0.224 flatbars 15 in. centres.

All plating and flatbars are marine grade 5456-H116 aluminium alloy. This alloy provides the highest welded strength of any of the marine grade aluminiums while

retaining good weldability and corrosion resistance. Extrusion materials are of 5456-H111 aluminum alloy (as available) with alternates of 5083-H111 or 5086-H111 alloys.

E3. STRUCTURAL DESIGN AND ARRANGEMENT OF THE *VICTORIOUS* (T-AGOS 19)

The *Victorious* is the first large SWATH appraised by the US Navy to replace its ageing monohull ocean surveilance (T-AGOS class) fleet. A SWATH of this size (3500 tonnes) is viewed to be amenable for an operation to tow long sonar arrays at very low speeds. Compared to its monohull counterparts, towing sonar arrays at, say, three knots, was not particularly comfortable [E5], especially in rough seas, thus more stable platforms such as SWATHs should be utilised.

The design of the *Victorious* was quite unique in which the development was carried out by a team of personnel from NAVSEA, DTNSRDC, local naval architectural firms and a large core of shipyard personnel selected from a list of prospective shipbuilders [E6]. So the programme was basically a joint effort which was envisaged to benefit the government as well as the industry. Because of the newness of the SWATH concept it was accepted that past Navy design practices were not generally directly applicable in this particular task. Further, the designer also recognised the major disadvantage of SWATHs because of their added cost and size over comparable monohull ship size for the same mission. To offset these size and cost differences, considerable effort was expended during the design to minimise the ship size differences and to reduce the construction cost through enhanced producibility and widespread use of commercial practice. The development of hull configuration, for instance, has evolved from initially elliptical cross-section to the final form, ie a combination of rectangular and circular section. The final configuration of the vessel (see Fig. E3) demonstrates the key features of a producible design with emphasis on reducing fabrication cost. The particular dimensions of the Victorious may be found in Table E3.

The structural design of the SWATH was another area where considerable work was done to arrive at the producibilty edge [E6,E7]. The initial design was based on standard Navy practice (see ref. [E8]). This baseline was iterated before the final commercial structural configuration was finally gained. Navy practice is distinguished from commercial practice in that it generally optimises structural weight at the expense of the uniformity of the structure or ease of construction. As an example, shapes or plating thicknesses are more apt to be different in a Navy strcutural design since each structural member is sized to develop its full strength. Commercial practice, on the other hand, tend to use more of the same size shapes or sizes in the interest of

uniformity of the construction. This results in many reduced stresses on many of the structural members.

To apprehend the above aspects more clearly it is best to refer to Fig. E4, ie details of the T-AGOS 19 structure amidships for the Navy point, and the commercial configuration for the same section at the end of contract design. The most apparent difference in comparing the two sections is the widespread use of angles in the final design versus the use of 'T' shapes in the earlier Navy point design. Upon closer examination, the structural differences are much more significant. The extensive use of insert plates on the main deck of the final design has been minimised. Originally, the main deck was fabricated with 12.75 # plate and 20.4 # inserts at the intersection of the transverse and longitudinal bulkheads. These were eliminated and 15.3 # plate was installed over the entire main deck. The inserts were kept in case of the wet deck as the weight penalty associated with their removal was considered to be significant. The transverses at the main deck were initially 5 x 4 x 6 # /ft 'T', which were replaced by 6.6 # /ft angles (10% heavier). Although the change seems small, it eliminates half the collars (clips or lugs) for all the stiffeners which penetrate members. This is approximately 600 collars for the main deck alone. Conversely, fitted joint connections were used extensively as opposed to the more common cost effective commercial practice of lap joints, by virtue of fatigue considerations.

The modification from Navy type to commercial type of strcutural arrangement was claimed to have not much effect on the increase in weight normally inherent in the different practices. A rough approximation is that a commercial structure is normally 10% heavier than an equivalent Navy structure. Finally, the structure, based on model test results confirmed by computer finite element analyses, has met the commercial requirements of the American Bureau of Shipping classification +A1 (E, Unrestricted Ocean Service, +AMS, +ACCU and Class E ice strengthtening) [E5].

E4. STRUCTURAL DESIGN AND ARRANGEMENT OF A SMALL SWATH FISHING VESSEL *ALI*

MV *Ali* (principal dimensions as given in Table E4) is a small SWATH fishing boat designed and built by a private bussiness enterprise in Glasgow [E9], and to be operated in the Scotland's North West coast and Islands. The vessel was designed to have an overall length less than 12 m. Multiples of standard plate lengths to form the mid body combined with adequate entrance and run to set the length of the lower hulls at 10.475 m. A circular hull (1 m in diameter) configuration was selected for ease of fabrication, although asymmetric sections would allow greater sectional area useful in providing sufficient buoyancy.

Single short strut per hull was used to minimise structural weight and construction time. Strut thickness of 0.6 m was dictated purely from considerations of access during fabrication and operation. Nevertheless the strut thickness/hull diameter ratio of 0.6 is still within the upper bound of the normal SWATH range [E10]. The design draught of the craft was governed by the desire to adequately submerge the lower hulls to provide satisfactory resistance and seakeeping performance. Whereas the separation of the demihulls was dictated principally by seakeeping considerations. A hull centrelines separation of 4 m was adopted to guarantee that coincidence of the natural periods of heave, pitch and roll was avoided.

The structural design of MV *Ali* was directed to meet the criteria of maximum side load in beam seas at zero speed. The first estimate of the design side force was taken from Fig. E5 [E4], combined with large factors of safety on allowable stress to ensure adequate fatigue life. Local wet deck panels were designed to sustain maximum slamming loads which were expected to impose in head seas at a certain forward speed by the method given in ref. [E11]. The uncertainty about the effect of shear lag and stress concentrations which are mostly critical for large SWATHs is not considered as a perplexity on the SWATHs of MV *Ali*'s size.

The main load carrying structure (see Fig. E6 and E7) is formed by five transverse bulkheads extending from the lower hulls through the struts to the cross structure. Plating is supported by flatbar framing carried round the inner and outer shell of the vessel with ring frames in each hull. In the cross structure the frames and bulkheads are supported by three longitudinal webs. All corners are radiused a minimum of 100 mm to mitigate stress concentration, especially in the inner haunch area between struts and deck structure. With hindsight, greater continuity of stiffening in this area could have been maintained in this small vessel by utilising a fully radiused haunch. The overall design of this small SWATH with the selection of the all mild steel structure shows a thorough effort in achieving simplicity in fabrication with minimal work force.

E5. STRUCTURAL DESIGN AND ARRANGEMENT OF THE *KAIYO*

Most existing SWATHs nowadays were built and operated in Japan, but publications addressing their sufficiently explicit structural design are rare. Among these Japanese SWATHs only the structural data of the *Kaiyo* is now available [E12-E14] even then it is only very limited. The *Kaiyo* WAS put into operation in 1985 for underwater support works, after an extensive sea trial proceeded the delivery from Mitsui Engineering and Shipbuilding (MES) Co Ltd. The design of the *Kaiyo* was commissioned by Japanese Marine Science and Technology Centre (JAMSTEC)

involving universities, ship operators and institutions possessing technical knowledge and experience in advanced marine vehicles, as well as industries. A full discussion on the design and trial of the *Kaiyo* can be found in ref. [E12]. The main particulars of the vessel are given in Table E5.

The *Kaiyo* is classified by the Nippon Kaiji Kyokai (NK) for steel ocean going vessels. Although the NK regulations are among the most extensive rules available, nonetheless they were not sufficient to assist in the structural design of the vessel. Hence, the structural design and the scantling selections had to be established from the first principles of structural design. The external forces due to wave were estimated by calculations after the most careful investigations approved by the classification society. A strength analysis was also carried out to decide the scantlings for the whole structure with the solid framework structure model (FEM). Calculations, such as the wave load analysis by strip method, structural analysis among the waves with solid framework model, and the long-term prediction of stress in the structural members, have been carried out consistently using the Offshore System Program developed jointly by MES and NK [E13,E15].

Evaluation of the strength is made with respect to allowable stress, buckling and fatigue to confirm the safety of the structure. As a SWATH has a uniquely shaped hull form, the strut to deck connecting section is subject to particularly intensive stress in beam seas. MES, therefore, assessed stress in the subject parts by FEM calculations and reinforced the parts as required. Special attention was called for during construction as well as at the design stage. The midship section of the Kaiyo with some scantling sizes is shown in Fig. E8.

As it is seen in Fig. E8, the *Kaiyo* has a higher characteristic of hull to draught ratio than normally adopted for most SWATHs. This diversion from the usual practice is primarily because of the need of shallow draught for harbouring. Other particular reasons for this design are, firstly, lower overall draught is favourable in view of reducing frictional drag as a result of the decrease in wetted area without much affecting the motion performance of the vessel [E14]. Secondly, lower draught is also beneficial to reduce the amount of structural material in fabrication. On top of that, lower draught will induce lower lever arms, hence reducing bending responses on a given transverse section of the vessel [E10].

All steel construction was selected because of building costs and hull maintainability. Because of the relatively low design speed the weight increase, by adopting steel as a hull material, does not vitally affect the ship's performance. High tensile steel (yield strength 32 kg/mm^2) was used for bottom and side shell plate as well as the longitudinal members of the lower hulls and the transverse webs below the upper

deck, while the deck house was constructed out of mild steel. The ship provides sufficient deadweight of about 860 tonnes at the ship's draught of 6.3 m. Additional information on other MES SWATH designs regarding the structural material is given below [E12].

In the case of the *Marine Ace* (22 tonnes) and the *Seagull* (343 tonnes), anti-corrosive aluminium alloy was used as hull material to reduce the structural weight and accordingly use of less power to attain the design speed. For the hull material of the *Kotozaki* (236 tonnes) three alternatives were considered, namely, Al-alloy, high-tensile steel and a hybrid structure. The choice of Al-alloy for the entire hull showed an unacceptably high building cost. High tensile steel necessitated bigger engines to attain the design speed of 20 knots due to the larger displacement to sustain the required payload. Consequently, a hybrid structure with high tensile steel hulls and anti-corrosive Al-alloy was selected to allow for a reasonable design. To compare the use of different structural material, however, Mitsui has provided data on the effect of structural material on the manufacturing cost of a 400 tonne SWATH, as shown in Table E6.

E6. STRUCTURAL DESIGN AND ARRANGEMENT OF THE *PATRIA*

The *Patria* is an FDC400-Seamaster class built by FBM Marine Limited at Cowes on the Isle of Wight. Although the class FDC stands for Fast Displacement Catamaran, *Patria* is principally a SWATH type vessel or, more accurately, MWATH (Medium Waterplane Area Twin Hull), since its waterplane area is relatively larger than most of the common SWATHs. This vessel, which is presently operating as a regular ferry between Madeira and Porto Santo, was claimed in 1989 to be the fastest (at maximum speed of 32 knots) amongst the existing SWATHs [E16].

The design of the FDC may be regarded as somewhat revolutionary by the SWATH community. It could be explained that, having recognised one of SWATH's drawbacks in which, due to its slender struts, the vessel is in a way rather vulnerable to the so-called Munk moment effect. The Munk effect in SWATHs is basically the tendency to plough in or nose dive caused by the inherent lack of natural pitch stability in submerged hull design with narrow struts. The most common way to overcome such an effect on SWATHs is by mounting canard fins forward of the underwater hulls. What FBM Marine has set out to achieve in the FDC is to purposely design out the use of 'active' fins which are required in order to maintain natural pitch stability at speed by increasing the waterplane area. A parameter used in measuring the range of waterplane area is designated as the waterplane area ratio ($WPA/\Delta^{2/3}$), where this ratio is about 0.5 to 1.5 and around 1.5 to 2.5 for ordinary SWATHs and for FDC respectively. Further,

such a concept is also beneficial to enhance the problem related to payload sensitivity, hence, it requires a less substantial ballast system. From structural and constuction viewpoints, larger waterplane area (wider struts) also means less stress in the strut-deck intersection, and easier internal access for welding and maintenance. The main particulars of the *Patria* are listed in Table E7.

What basic approach adopted in developing the structural design of the FDC is not particularly revealed. Even so, it is mentioned [E17] that the vessel was built according to the IMO Code of Safety for Dynamically Supported Craft A373(X) and classified DnV +1A1 R90 Light Craft EO. The vessel was constructed of salt water resistant aluminium alloy plates and specially designed extrusions welded by automatic Robot Metal Electrode Inert Gas method. The use of lightweight extruded aluminium planks with an integral T stiffener, as on the FDC, proves to be advantageous in enhancing producibilty, especially in view of minimum welding and distortion during construction [E18,E19]. Even though, it would not be appropriate to apply extruded planks on any curved section of the structure, such as the hulls and strut ends of SWATHs.

The FDC hulls were produced with a combination framing system of deep transverse web frames at 1250 mm centres and closely spaced longitudinal extrusions. Bottom plating is 6 mm, the deck plating is 4 mm and an aluminium channel rubbing strake is fitted. An expanded aluminum mesh is also located over the foredeck wells. Bolted panels in the decks over the main engines allow direct vertical removal of engines and generators. Removal plates are also fitted for the gear boxes, generators and other small machinery items. All tanks incorporate bolted inspection hatches, vent pipes and drain cocks. Typical structural arrangements for the FDC are as shown in Fig. E9 and E10.

E7. STRUCTURAL DESIGN STUDY OF A 3000-TON SWATH AT THE NUC

A design study of an earlier SWATH designated as the 3000 S^3 (see Fig. E11) was conducted at the Naval Undersea Reasearch and Development Center (NUC) in 1971 [E20]. The vessel was designed to reach a maximum speed of 35 knots, with an operational speed of 25 knots to traverse an endurance of 3000 to 5000 miles. Both theoretical and experimental investigations have been extensively carried out to accomplish the preliminary design of the vessel, which was to provide substantial improvements in operational capability with vertical/short takeoff and landing (V/STOL) aircraft, weapons, sonar, and personnel through sea state 6. Circular hulls with tandem strut configuration were selected for this particular SWATH (main dimensions as listed in Table E8).

Rigorous efforts were made in the structural design of the S^3 as it was firmly believed the conventional naval-ship-design methods and the use of standard marine structural steels were not applicable to the novel concept. As it was found, preliminary estimates for the hull fraction (structural weight/Δ) indicate a value of around 0.6 for bare hull structure if steel structure and conventional construction, technique, and philosophy were adopted [E21]. On the other hand, the weight fraction can be reduced to below 0.4 with light weight structural materials and advanced structural concepts, which would create a payload capacity comparable to that of conventional high-performance monohull ships. Extracts of this comparative study are presented in Table E9, in which aluminum structure is preferable. Further, apart from lightweight, a preference for aluminium can be seen to be come from considerations of formability, corrosion resistance, and flammability. Aluminum is available in a wide range of extrusions in the form of rib stiffened single- or double-wall panels, with outstanding stiffness. Use of integrally stiffened panels in structural design generally results in an additional 10% overall weight saving. Corrosion resistance aluminium eliminates the need for painting, which may result in an additional 1% overall weight saving. Moreover, although aluminium melts and ignites at a lower temperature than steel, the absence of paint and high thermal conductivity of the metal makes a bare aluminium structure more resistant to initiation of fires.

The structural concept and the underlying assumptions adopted within the S^3 structural design are outlined as follows. The platform (cross-deck), which acts as a box beam under simultaneous bending and twisting will be appropriately implemented by the structural concept of a skin-stressed sandwich panel with the deck room partitions acting as stressed cells of the sandwich. The vertical struts, which act as restrained cantilever beams, provide a connection between the buoyancy-producing hulls and the platform. These parts are best constructed as sandwich beams of lenticular cross-section. Whereas the most efficient structural concept for the submerged hulls, which act as shallow running submarines, will be a sandwich-constructed monocoque hull (see Fig. E12). Representative marine-alloy selections for ship construction are 5454-H117 and 6061 aluminiums. The 6061 alloy in a T651 temper would be used primarily in sandwich extrusions, while the 5454-H117 would be utilised in plate, angles, I-beams, and integrally stiffened panels.

Aluminium-extruded cellular sandwich plates and integrally stiffened panels can be used as structural building blocks. Use of extruded panels will significantly increase the buckling resistance of the structural members without an increase in weight. The structure should be of welded construction. Optimum use of extrusions will minimise the amount of welding required which, in turn will reduce on-site labour costs. The structure can be designed on a modular basis to allow parallel fabrication of sub-asemblies and the use of similar modules in many areas of the vessel (see Fig. E13).

A detailed analysis on the above structural arrangements was made by dividing the structure into 11 components and accounting for their interactions (as opposed to independent substructures). These components or frame members comprised 2 hulls, 4 struts, 1 stabiliser, 2 cross-deck members, and 2 axial deck members. The framework was then divided into several two-dimensional sections and loads were applied. The loads are related to individual component members (as shown in Table E10). The two-dimensional frames were then analysed by means of the moment distribution method. Internal moments were calculated and a superposition was used to combine these moment diagrams into a full three-dimensional framework. Once these moments were known and all local loading conditions were added, a required cross-sectional moment of inertia could be calculated from the flexure or combined stress formulae. To generate the necessary moment of inertia, the double-walled cellular extrusion was used in all beams, as shown in Fig. E12. Calculations were reduced by specifying that all platform members would be circular and symmetrical in cross-section; including the submerged hulls which are circular in any case (with elliptic extensions). The struts were considered as twin panels of cellular form, and moment of inertia was calculated for the flat sections rather than the actual slightly curved sections.

E8. STRUCTURAL DESIGN STUDY OF A 4300-TON SWATH AT THE NSRDC

A comparative study of an ASR catamaran with a comparable size SWATH, formerly referred to as LWP (Low Waterplane Area) catamaran, was performed at the NSRDC in 1972 [E22]. Identification of the potential application of SWATH in naval operation was recognised as an air support platform and, more specifically, as a new generation Sea Control Ship. Most design aspects of the LWP (Δ=4300 tons) ranging from hydrodynamic performances and powering selection have been observed to certain depths to built up a milestone for a further detailed study.

One major problem area associated with the LWP catamaran has to do with the development of efficient structures. Further, it was noted that, relative to its displacement, an LWP catamaran will have substantially more enclosed volume and deck area than monohuls. If the structural weight densities estimated and adjusted from monohull practice are applied to LWP, it is soon evident that hull weights will exceed acceptable values and that payload-carrying capability will be reduced (see Table E11). Hence, the designer is forced to reduced fixed weights wherever practicable and, subsequently, propulsion installations which use lightweight marine gas turbine engines become essential. Even then, such weight savings are not actually adequate and every effort must be made to further reduce weight by using light but reliable structures.

Based on the above consideration, it is apparent that if the LWP are to be competitive with monohulls in payload weight-carrying capability, structural weight must be reduced and held within closely controlled limits. As a consequence, this requires reliable prediction of applied loads and precise design in the area where prior knowledge is limited. Furthermore, selection of construction material has to be studied conscientiously, e.g. by comparing steels and aluminium as an alternative.

The principal structural design tool was a design computer program developed at NSRDC to optimise the weight of midship section structures according to accepted Navy criteria [E23]. The program uses an iterative procedure and selects spacings for supporting structure, panel sizes and all scantlings suitable for the applied loads. For purposes of the LWP study, the program was modified to design a catamaran transverse section and a longitudinal section through the bridging structure. Use of the program allowed assessment of many more design approaches and structural concepts than would have been possible through manual methods.

It was learned from the study that the bridging structure deserved prime consideration inasmuch as more than one-half of the structural weight was in the structure. Sea induced loads (which included transverse bending, vertical inertial effects of dead and live loads, axial/transverse load on the bridge, and slamming on the bottom panels) dominated the structural design in the transverse direction. In contrast, the longitudinal structure was dictated by local loads (dead loads, hydrostatic loads, etc.) with sea induced loads (i.e. longitudinal bending) contributing little to total stress. For this particular study, the ratio of primary stresses in the transverse structure at the centreline to those in the longitudinal structure were found to be approximately 10 : 1. The relative levels of primary stress will vary with different hull geometries; the relative importance of primary loads in these two directions will not.

Thus far, a number of structural arrangements have been examined and their corresponding structural weights and scantlings computed. It was not possible to know a priori which structural arrangement would yield the lightest structure. Since an adequate experience base was lacking, a large number of structural arrangements and assumptions had to be tested. Some insight has been gained on the effect of major variables (hull spacing, bulkhead, web and girder spacing, effective breadth of plating), and sub-optimal structural designs have been developed. Figure E14 is representative of the kinds of structure that were examined for the LWP. The design has an overall structural density of 7.2 lb/ft^3 with the distribution as shown in Table E12. It is further mentioned that structural density of 6 lb/ft^3 was targeted for future investigation.

E9. STRUCTURAL DESIGN STUDY OF A SWATH V/STOL AIRCRAFT CARRIER

By the early 1980s an escalating confidence was seen among naval ship operators towards the potential application of SWATHs. This was mainly brought about by promising evidence becoming available from operational experience of several SWATHs. It is not surprising, therefore, that some research bodies have projected their research on much larger size than those in existence. Such a development is on a large SWATH V/STOL aircraft carrier having displacement ranging up to 15,000 tonnes [E24].

The design of this V/STOL was based on the common requirements of ordinary naval aircraft carriers, as well as on specific requirements, hence a SWATH configuration is in great demand. Specific requirements include providing the ability to launch a single aircraft in the STO (short take-off) mode and launch/recover multiple aircraft in VTOL (Vertical take-off/landing) mode. V/STOL in turn defines the length of take-off run and ship areas peripheral to actual launch and recovery operations, as well as the maintenance and support areas (hangar, shops, elevators, etc.) and storage areas (ordinance, fuel, etc.). Further, the design was initiated with preliminary estimates of weight and deck areas to satisfy those functional requirements. The preliminary estimates assumed a structural density range of 5.5 to 6.0 lb/ft^3 of enclosed volume and main deck area of the order of 75,000 ft^2. The resulting displacement of the vessel, which was thence named as SWATH 83 (see Fig. E15), is in the range of 14,300 to 15,300 tons. The main dimensions of the SWATH 83 are listed in Table E13.

For structural design purposes various local loading and hull impact conditions are taken into account, as given in table E14. Overall ship longitudinal bending cases were also determined for hogging and sagging conditions, based on semi-uniform weight distributions. The hogging condition produces maximum bending moment amidships of 89,500 ft-tons. Based upon this moment and an average material allowance of 27 ksi a section modulus of approximately 89,100 in^3 is required. Actual modulus is at least twelve times that required resulting in calculated bending stresses at the flight deck of 1,512 psi and at the keel of 2,188 psi. Longitudinal strength is not a driving structural design criteria for SWATH 83. However, it is not clearly described to what extent the transverse load criteria has been considered in the design. Typical structural sections for SWATH 83 are shown in Fig. E16 for the forebody, Fig. E17 for midship sections, and Fig. E18 for the afterbody. Deck house structure is shown in Fig. E19.

It is noticed from the former three figures that SWATH 83 has a canted strut configuration. According to the designer [E24], it was found that inclining or canting

the basic strut plane inboard could provide required transverse stability. Moreover, this would also provide a substantial increase added mass and damping, and hence lengthening the natural period of motion and reducing the resonant peak. Another advantage of canted struts is in enhancing the pitch stability, i.e. to counteract the Munk moment inherent to slender body in forward speeds. From the structural point of view canted struts are inferior due to the increase in static bending moment. However, the dynamic moment by wave action is reduced dramatically with increasing cant angle. The net result is that the combined static and dynamic lifetime loads are about the same as those with vertical struts [E25].

E10. STRUCTURAL DESIGN STUDY OF SMALL SWATHS

It has been repeatedly mentioned in the foregoing sections that the problem to be overcome in SWATH structural design is the reduction in structural weight. The matter is so pronounced when a designer should deal with smaller crafts (displacement 250 tonne and below), where steel structure would be considered as the last choice. Accordingly, exploratory studies of alternative SWATH structural materials has evolved substantially, such as that reported in refs. [E26-E28].

Two alternative materials, namely, aluminIum alloy and glass reinforced plastic (GRP), has been studied and compared with steel structure for SWATH displacement range from 30 to 250 tonnes [E26,E27], with variation of structural arrangements as shown in Figs. E20 and E21. A simplified approach of the design loads was adopted in the preliminary design study in which the maximum side load (and hence transverse bending moment) is derived from a default data and the peak slam pressure is obtained by two methods given in [E29,E30]. The peak side force obtained was further used in designing of shear area of SWATH strut and haunch area. The transverse bending moment was adopted in the design of cross deck and strut structures. Whereas peak slamming pressure value governed the sizes of wet deck panels and haunch scantlings. In addition, hydrostatic pressure was included in the design of panels of plating and stiffeners where this is more appropriate than slam pressure.

Computer programs were developed to facilitate the above procedures and combined with an evaluation program to finally appraise an economic measure of merit of any given SWATH design. An example of the output of the structural design program on a 70-tonne SWATH (main dimensions as listed in Table E15) is given in Table E16. The structural weight of each material configuration for the scantlings shown in Table E16, is 42.4 tonnes, 26.9 tonnes, and 25.9 tonnes, respectively, for mild steel, aluminium alloy and GRP structures.

E11. STRUCTURAL DESIGN STUDY OF NAVAL SWATHS AT UCL

From many publications UCL is well known for its comprehensive studies in monohull naval vessels, and also on SWATHs (see Table 1 of [E31]). Two of those studies are on anti-submarine warfare (ASW) SWATH frigate [E32], and on a single role minehunter (SRMH) SWATH [E33]. A thorough identification of naval mission for such vessels in general has to be first developed to proceed in their design studies. The primary role of an ASW frigate, for instance, is to give assurance of sea control by providing support and escort to task forces or resupply and reinforcement (Re-Re) convoys. These missions will in turn govern the payload requirements for the vessel, such as weaponry and number of personnel on board, and further it is considered in the initial sizing of the vessel.

The ASW SWATH studied (see Fig. E22) having a displacement of 4678 tonnes with some other features, as given in Table E17, which has been established in part for the improvement of its hydrodynamic performance. In the structural design, the primary loading considered is the transverse bending moment in the box and haunch due to the strut acting as a cantilever under lateral load. A computer program has been developed at UCL and was used to assess the structural behaviour of the ASW, as well as determining the scantling of the vessel.

The resulting midship section obtained by that analysis can be seen in Fig. E23. Admiralty 'B' quality steel is used for the majority of the structure, while insert plates in the haunch and strut are HY80. Longitudinals are spaced 1.4 m apart and transverse framing 0.7 m to remain within the celularity philosophy and standards [E34]. the helicopter deck was considered as a special structural case and plating here is 17 mm thick. A detailed check on the structural loading and strength would be necessary for the next design stage, as the present design is based on a simplified approach [E32].

The structural design of of the SRMH SWATH (see Fig. E24 and Table E18 for the main particulars) was developed in a similar manner as that on ASW frigate, where transverse bending is recognised as the dominant load to result in structural stress. The stress level due to this load was analysed at high stress points on the amidships section. A safety factor of 4.0 was applied for fatigue consideration. The cross structure was analysed in bending, shear, plate/stiffener buckling, and plate buckling. Primary loading of the strut and shear analysis of the plate/stiffener combination in the strut were considered. The hulls were analysed for elastic buckling [E35].

Transverse framing arrangement (with intercoastal longitudinal bulkheads) was called for due to the consideration of dominant lateral loads. Structural material chosen was GRP based on the contemplations of low weight (0.43 times of steel structure),

ease of production, satisfactory shock performance, and non-existent magnetic signatures [E33]. Table E19 presents the structural scantlings as determined from the above analysis.

E12. STRUCTURAL DESIGN STUDY OF A KOREAN FERRY

Learning from the success of SWATH operations in some countries, Hyundai Heavy Industries Co., Ltd. (HHI) and Korea Institute of Machinery and Metals (KIMM) in Korea commenced an extensive research on SWATH vessels in 1986. The first design explored was on a high speed coastal passenger vessel [E36]. Parameteric studies which followed the joint research contract have been made on four SWATH variants. Each size of the SWATHs was developed on the basis of a techno-economic study regarding the operator requirements. As a sequel to the selection of the most amenable variant an observation was then conducted in determining the type of hullform aimed at optimising its hydrodynamic performance. Finally, the initial sizing drawn the principal particulars for the SWATH coastal ferry are given in Table E20. Figure E25 depicts the general arrangement of the ferry.

The primary load assessment adopted in designing the structural members of the SWATH ferry is the one developed by Sikora [E37], where the maximum side force is estimated from the principal characteristics of the SWATH. A prediction of wave loads based on the strip method was also made to confirm the approximation given by Sikora's algorithm. The secondary load (slam pressure), which is dominant to the determination of underdeck structure, was estimated by the formulation given in [E30] and a motion analysis as introduced in [E38].

The lightweight construction material selected for the design was alluminium alloy A 5083-H321, which was considered to have a minimum deterioration in strength after welding. Transverse framing system (at 0.5 m spacing) was chosen to sustain the prevailing side load from sea waves. Cross structure and struts which are long and slender type structure, were stiffened by solid floor instead of by angles, so that the hull weight is reduced while an increase in strength can be attained. Web frames were arranged in position at every third frame, and transverse bulkheads at every sixth frame considering the slenderness of the structure. Figure E26 shows the scantling arrangement amidships.

The analysis of the structural configuration was carried out by FEM model, primarily on the midship section of the SWATH ferry. In the analysis, transverse side force and still water bending moments were considered as primary load and the result indicated that the stress level of the outer shell is not too high (see Fig. E27). In a more detailed analysis for the transverse members of the web section showed highly

concentrated stresses in the vicinity of the openings (see Fig. E28). So a reduction in the size of the opening was called for, from 1020x170x130 mm to 900 x 170x130 mm, and also stiffened by flat bar of 80x8 mm on the opening circumference. After this modification the stress level was found to be significantly lower and much below the allowable stress.

E13. STRUCTURAL DESIGN STUDY OF EODSC SWATH

As part of its overall programme, the Combatant Craft/Service Craft/Amphibious Craft Acquisition Program Office of the US Navy (NAVSEA PMS300) authorised a study to determine if the SWATH concept could be used to satisfy requirements for an Explosive Ordnance Disposal Support Craft (EODSC) [E39]. The design was to be configured to accommodate an enlarged payload relative to the 65-ft EODSC then in design by the NAVSEA Combat System Engineering Station. Desirable attributes of the SWATH concept which seem promising for the EOD mission included excellent seakeeping, large deck area and good survivability.

The principal characteristics of the SWATH design which meet the operational and performance requirements by the Navy are given in Table. E21. The general arrangement of the EOD SWATH is shown in Fig. E29. The basic configuration chosen is conventional for a SWATH, in which the relative sizes of the major components, such as, box length and beam, etc., all fall within a range that is normal for this size of boat and payload. The structural design was made by first identifying the most critical loading source and condition, followed by determining the scantling arrangement to provide sufficient strength to the structure. Basic design criteria developed within the Navy was adopted in the study where a stress level of around 18,000 psi was permitted for plating and 14,000 psi for transverse webs.

The midship section drawing, Fig. E30, indicates the basic hull structural properties and illustrates the arrangement. It is emphasised that no effort has been made to optimise the use of shapes to minimise differences in scantlings. The structural design of the hull and strut exploit the use of 'T' sections to develop the requisite inertia and beam load carrying ability. For the cross structure, comprising the wet and dry decks, longitudinal girders, stiffeners, and transverse webs form an orthotropic grillage. The grillage supplies both upper and lower local panel strength and overall transverse load carrying capability. Longitudinals segregate the cross structure athwartship and render a support to prevent lateral transverse instability in lateral bending.

Superstructure design was established by consideration of the stiffened panels of bulkhead and 01 level plating. Stanchions and partial interior bulkheads form assemble

the main interior support for the arrangement. Exterior bulkheads were designed to resist wave slam loads, and 01 level deck scantlings were sized for 150 psf uniform loads. This design pressure allows the structure to sustain ice loads.

E14. CONCLUSIONS

From the review of some SWATH structural design and arrangements above it can be emphasised that the adoption of transvese load as being the primary design consideration has firmly developed among SWATH designers. In addition, secondary load due to slamming is recognised to govern local scantling designs, especially for small crafts. Having mentioned that, nevertheless, the structural design criteria adopted by different SWATH designers is very limited.

Most SWATH structural designs, as identified, are directed towards minimising structural weight with the expectation of increasing the effective payload capability. Correspondingly, alternative construction materials have been comprehensively explored in parallel to optimising structural arrangements and configurations. Further steps in SWATH structural design are required to establish a more producible configuration in the interest of reducing labour costs, but without violating the principal strength of the structure. Alternative SWATH configurations for pruducible design may be seen in Fig. E31 [E40] and Fig. E32 [E41].

REFERENCES TO APPENDIX E

E1. Luedeke, G. Jr. and Montague, J. "RMI's Small-Waterplane-Area-Twin-Hull (SWATH) Boat Project", *SNAME*, San Diego Section, Nov. 1984

E2. Luedeke, G. Jr, Montague, J., Posnansky, H. and Lewis, Q., "The RMI SD-60 SWATH Demonstration Project", *Proc. Int. Conf. on SWATH Ships and Advanced Multi-Hulled Vessels*, RINA, Paper No. 10, London, Apr. 1985

E3. Coe, T.J., "A Technical Evaluation of the 60-foot SWATH Ship Halcyon to Determine Utility in Coast Guard Operations", *Proc. Intersociety Advanced Marine Vehicles Conf.*, Paper No. 89-1443-CP, Arlington, VA, June 1989

E4. Allen, R.G. and Holcomb, R.S., "The Application of Small SWATH Ships to Coastal and Offshore Patrol Mission", *Proc.Symp. on Small Fast Warships and Security Vessels*, RINA, London, 1982

E5. MER (editor), "SWATH *Victorious* - a Firm Base for Towed Arrays", *Marine Engineering Reviews (MER)*, IMarE Magazine, Aug. 1990

E6 Covich, P.M., "T-AGOS 19 : An Innovative Program for an Innovative Design", *Naval Engineers Journal*, ASNE, May 1987

E7. Covich, P.M., "SWATH T-AGOS a Producible Design", *Proc. AIAA 8th Advanced Marine Systems Conf.*, Paper No. AIAA 86-2384, San Diego, USA, Sept. 1986

E8. Malakhoff, A., Packard, W.T., Engle, A.H. and Sielski, R.A., "Towards Rational Surface Ship Design Criteria", *Proc. Int. Conf. on Advances in Marine Structures-2*, TS-8, DREA, Dunfermline, Scotland, May 1991

E9. MacGregor, J.R., Bose, N. and Small, G., "Design and Construction of a Small Waterplane Area Twin Hull (SWATH) Fishing Vessel", *Proc.World Symp. on Fishing Gear and Fishing Vessel Design*, St. John's, Newfoundland, Canada, Nov. 1988

E10. Gore, J.L., "SWATH Ships", *Naval Engineers Journal*, ASNE, Special Edition, Feb. 1985

E11. Allen, R.G. and Jones, R.R., "A Simplified Method for Determining Structural Design Limit Pressures on High Performance Marine Vehicles", *Proc. Advanced Marine Vehicles Conf.*, AIAA/SNAME, Paper AIAA 78-754, San Diego, USA, Apr. 1978

E12. Mabuchi, T., Kunitake, Y. and Nakamura, H., "A Status Report on Design and Operational Experiences with the Semi-Submerged Catamaran (SSC) Vessels", *Proc. Int. Conf. on SWATH Ships and Advanced Multi-Hulled Vessels*, RINA, Paper No. 5, London, Apr. 1985

E13. Takeuchi, M., Takagawa, S., Miyanabe, R. and Watanabe, T., "Structural Design of the Semi-Submerged Catamaran-Type Underwater Work Test Vessel", *JAMSTEC*, Technical Report No. 15, 1985

E14. Ozawa, H., "The Design and Operation of Catamaran Vessels", *Trans. NECIES*, Vol. 103, 1986-1987

E15. Akita, Y. et al, "On the Program System for Design and Analysis of Offshore Structures", *Journal of SNAME of Japan*, Vol. 126, Dec. 1969

E16. Milner, R., "The World's First 30-knot Fast Displacement Catamaran (SWATH) Ferry", *Proc.*, The 7th Int. High Speed Surface Craft Conf., London, Jan. 1990

E17. Editor of FFI, "First FBM Marine FDC 400 on Trials", *Fast Ferry International*, Dec. 1989

E18. Milner, R. and Warren, N., "Presentation by FBF Marine Ltd.", *Proc. Int. Conf. on SWATH Ships and Advanced Multi-Hulled Vessels II*, RINA, Paper No. 20, London, Nov. 1988

E19. Blyth, A., "SWATH Passenger Ship Development", *Fast Ferry International*, March 1989

E20. Lang, T.G., et.al., "Preliminary Design Study of a 3000-Ton S^3 - A High Performance Semisubmerged Ship for Naval Operation", *Technical Report.*, NUC TN 574, San Diego, CA, USA, Sept. 1971.

E21. Lang, T.G., et.al., "Naval Feasibility Study of the S^3 - A New Semisubmerged Ship Concept", *Technical Paper*, NUC TP 235, Part IV, San Diego, CA, USA, Sept. 1970

E22. Stevens, R.M., "New Dimensions for Naval Catamarans", *NSRDC*, Report 3830, Bethesda, Maryland, USA, May 1972

E23. Nappi, N.S. and Lev, F.M., "Midship Section Design for Naval Ships", *NSRDC*, Report 3815, 1972

E24. Pieroth, C.G. and Lamb, G.R., "The SWATH Options as a V/STOL Aircraft Carrier", *SNAME*, Hampton Roads Section, March 1985
E25. Gupta, S.K. and Schmidt, T.W., "Developments in SWATH Technology", *Naval Engineers Journal*, ASNE, Vol. 98, No. 3, pp. 171-188, May 1986
E26. Loscombe, R., "An Exploratory Study of Alternative Structural Materials for Small SWATH Craft", *Ship Science Report*, No. 34, Dept. of Ship Science, Univ. of Southampton, May 1987
E27. Loscombe, R., "An Exploratory Study of Alternative Structural Materials for Small SWATH Ships", *Int. Shipbuilding Progress*, Vol. 35, No. 404, pp. 331-347, Dec. 1988
E28. Loscombe, R., "Key Aspects of the Structural Design of Small SWATH Ships", *PhD Thesis*, Dept. of Ship Science, Univ. of Southampton, Dec. 1989
E29. Sellars, F.H., "Water Impact Loads", *Marine Technology*, SNAME, Vol. 13, No. 1, pp. 45-68, July 1991
E30 Allen, R.G. and Jones, R.R., "A Simplified Method for Determining Structural Design-Limit Pressure on High Performance Marine Vehicles", *Proc. AIAA/SNAME Advanced Marine Vehicles Conf.*, Paper No. 78-754, April 1978
E31. Betts, C.V., "Some UK Development in SWATH Design Research", *Proc. Int. High-Performance Vehicle Conf.*, CSNAME, Paper VI-1, Shanghai, China, Nov. 1988
E32. Betts, C.V., et.al., "Design Study for an Anti-Submarine Warfare SWATH Frigate", *Proc. Int. Conf. on Anti-Submarine Warfare*, RINA, London, May 1987
E33. Henry, B.B., Figes, K.J. and Dunaud, P., "SWATH Single Role Minehunter", *Proc. WARSHIP'89*, RINA, Vol. 2, Paper No. 32, London, May 1989
E34. Gates, P.J., "Cellularity : An Advanced Weapon Electronics Integration Technique", *The Naval Architect*, RINA, May 1986
E35. Smith, C.S., "Buckling Problems in the Design of Fibreglass-Reinforced Plastic Ships", *Journal of Ship Research*, SNAME, Sept. 1972
E36. Lee, K-Y, Lee, D-K, Kim, E-S, Kim, J-G, and Kim, J-H, "On the Design Technology of SWATH High Speed Passenger Ship", *Proc. Int. Conf. on SWATH Ships and Advanced Multi-Hulled Vessels II*, RINA, Paper No. 17, London, Nov. 1988
E37. Sikora, J.P., Dinsenbacher, A. and Beach, J.E., "A Method of Estimating Lifetime Loads and Fatigue Lives for SWATH and Conventional Monohull Ships", *Naval Engineers Journal*, ASNE, Vol. 95, pp. 63-85, May 1983
E38. Hadler, J.B., et.al., "Ocean Catamaran Seakeeping Design Based on the Experiences of USNS 'Hayes' ", *Trans. SNAME*, Vol. 82, pp. 126-161, 1974
E39. Schaffer, R.L., Kupersmith, J.A. and Valsi, T.J., "Explosive Ordnance Disposal SWATH Ship Design", *Marine Technology*, SNAME, Vol. 28, No. 4, pp. 181 196, July 1991
E40. Kraine, G.L., "Producibility in Ship Design", *Journal of Ship Production*, SNAME, Vol. 6, No. 4, pp. 256-267, Nov. 1990
E41. De Vries, R.L., "Producibility Benefits of the SWATH Configuration", *Marine Technology*, SNAME, Vol. 28, No. 1, pp. 23-29, Jan. 1991

Table E1. Main Particulars of the Halcyon [E1]

Length overall (LOA)	60.00 ft
Maximum beam (B_{max})	30.00 ft
Nominal draught (T)	7.00 ft
Full load displacement (Δ)	57 longtons
Lightship displacement	43 longtons
Cargo deck area	589.00 ft^2
No. of passengers	20
Cargo load	5.25 longtons
Crew	3
Maximum speed (V_{max})	>20.0 knots
Cruise speed (V)	18.0 knots

Table E2. Structural design safety factors for the Halcyon [E1]

Condition	Operational	Emergency	V-Line
Yield strength	1.15	1.00*	No Req't
Ultimate strength	1.50	1.20	1.20

* local yielding is allowed

Table E3. T-AGOS 19 principal characteristics [E7]

Length overall (LOA)	234.00 feet
Beam on design waterline	80.00 feet
Beam maximum (B_{max})	93.00 feet
draught (T)	24.75 feet
Full load displacement (Δ)	3380 tonnes
Lightship displacement	2680 tonnes
Transit speed (V)	9.5 knots
Towing speed	3.0 knots
Propulsive power	2 x 800 SHP

Table E4. Principal dimensions of MV 'Ali' [E9]

Length overall (LOA)	10.475 m
Beam maximum (B_{max})	5.000 m
Draught (T)	1.600 m
Hull diameter (d_H)	1.000 m
Strut thickness (t_s)	0.600 m
WPA coefficient (C_w)	0.920
Prismatic coefficient (C_p)	0.820
Displacement (Δ)	21.00 tonnes
Maximum speed (V_{max})	8.0 knots

Table E5. Principal dimensions of the Kaiyo [E12]

Length overall (LOA)	61.55 m
Length between perpendiculars (L_{pp})	53.00 m
Beam moulded (B_{mld})	28.00 m
Depth moulded (D_{mld})	10.60 m
Maximum draught (T_{max})	6.30/5.00 m
Displacement (Δ)	3000 ~ 3500 tonnes
Deadweight (DWT)	1159 tonnes
Normal speed (V)	13.25 knots
Maximum speed (V_{max})	14.00 knots

Table E6 Comparison of weight and manufacturing costs [E12]

Hull material	Hul weight Index	Cost Index
All H-T Steel	1.00	1.00
All Aluminum Alloy	0.55	3.10
H-T Steel and Alum. Alloy	0.70	2.10

Table E7. Main particulars of the Patria [E17]

Length overall (LOA)	36.40 m
Length waterline (LWL)	21.70 m
Beam overall (B_{max})	13.00 m
Depth (D)	5.80 m
Full load draught (T_{max})	2.70 m
Displacement (Δ)	± 180 tonnes
Maximum speed (V_{max})	32.10 knots
Cruise speed (V)	30.00 knots

Table E8. General characteristics for a 3000-ton S^3 [E20]

Displacements (Δ)	3000 tons
Length (L)	315 feet
Beam (B)	137 feet
Maximum draught (T_{max})	28 feet
Underdeck clearance	14 feet
Hull diameter (d_{hull})	14 feet
Strut thickness (t_s)	5 feet
Maximum speed (V_{max})	35 knots
Endurance at 25 knots	3000 - 5000 nmiles
Endurance at 10 knots	15000 nmiles

Table E9. Hull fraction estimates for the 3000-ton S^3 [E20]

Substructure	Approach 1	Approach 2	Approach 3
Submerged hulls	0.1	0.076	0.071
Vertical struts	0.2	0.157	0.130
Above-water platform	0.3	0.251	0.199
Total	0.6	0.484	0.400

Note :
Approach 1 : Conventional approach, with plate and stringer comb. structure
Approach 2 : Conventional approach, with aluminum and cellular structure
Approach 3 : Frame analyis approach

Table E10. List of structural components and loads [E20]

Component	Load	Strength Criteria
Fwd-Stbd Strut	Spreading Force,	I-Flexure
and	Wave Slap, Armour	P/A Impact
Fwd-Port Strut	Column Load	I-Buckling
Fwd Deck Cross	Spreading Force	I-Flexure
Member	Out of phase $P_{s(hear)}$	I-Flexure
	Self Weight	I-Flexure
	Deck Load	I-Flexure
	Deck Housing	H-Torsion
Aft-Stbd Strut	Spreading Force,	I-Flexure
and	Wave Slap, Armour	P/A Impact
Aft-Port Strut	Column Load	I-Buckling
Aft Deck Cross	Spreading Force	I-Flexure
Member	Out of phase P_s	I-Flexure
	Self Weight	I-Flexure
	Deck Load	I-Flexure
Stbd Deck Member	Spreading Force	J-Torsion
and	Two-Point, Dry-Dock Load	J-Torsion
Port Deck Member	Self Weight	I-Flexure
	Deck Load	I-Flexure
	Deck Housing	I-Flexure
	Out of phase P_s	I-Flexure
Aft Stabiliser	Spreading Force	P/A Axial Tension,Compssn.
Port Hull	Hydrostatic Load	PR/t Membrane
and		P_{CR} - Buckling
Stbd Hull	Spreading Force	J-Torsion
	Buoyant Force	I-Flexure

Table E11. Densities of primary hull structure [E22]

Structure	Density (lb/ft^3)
Escort (monohull)	5.7
Helicopter Carrier (monohull)	4.9
ASR (catamaran)	7.5
Hydrofoil (aluminum)	2.3
Landing Ship Dock (monohull)	5.5

Table E12 Structural density for the 4300-Ton LWP [E22]

Structure	Density (lb/ft^3)	% of Total Hull Vol.
Bridging platform	6.5	58
Struts	8.2	24
Lower hulls	8.0	18

Table E13. Main dimensions of SWATH 83 [E24]

Length overall (LOA)	140.80 m
Length between perpendiculars (L_{pp})	128.00 m
Beam maximum (B_{max})	44.00 m
Depth (D)	26.33 m
Draught (T)	11.58 m
Displacement (Δ)	15,067 tonnes
Cruising speed (V)	20.00 knots
Maximum speed (V_{max})	28.00 knots
Endurance at 20 knots	7500 nmiles

Table E14. Hull applied loads for SWATH 83 [E24]

Circular hulls :	
External (crushing 38 ft head + 4.5 psi wave)	3,024 PSF
Internal (bursting) 88ft head (ballast in fuel tank less 10.9 psi external pressure	4,060 PSF
Shell plating :	
Bow (underside) cross structure	7,368 PSF
Flat (undderside) cross structure	2,105 PSF
Deadrise sections of cross structure	2,575 PSF
Strut inside vertical face	1,065 PSF
Sheer outside flare	1,368 PSF
Bulkheads :	
Head of salt water to main deck (68'.0")	4,350 PSF (max)
Fuel tank bulkheads head to flight deck (88'.0")	5,625 PSF (max)
Flight (02) and hangar (main) decks :	
02 level (flight deck) A/C area concentrated loads	27,750 lbs
Clear of A/C parking	1,000 PSF
Main (hangar) similar to 02 level	

Table E15. Main dimensions of a 70-tonne SWATH Ferry [E26]

Length overall (LOA)	19.50 m
Length of hull (L_{hull})	17.90 m
Diameter of hull (d_{hull})	1.50 m
Length of strut (L_s)	18.50 m
Beam (B)	9.20 m
Depth (D)	4.25 m
Draught (T)	2.20 m
Displacement (Δ)	70.00 tonnes
Maximum speed (V_{max})	24.00 knots
Cruising speed (V)	18.00 knots
Endurance	400 nmiles

Table E17. General characteristics of the ASW SWATH [E32]

Displacements (Δ)	4678 tonnes
Box length (L_{box})	102.00 m
Hull length (L_{hull})	107.00 m
Strut length (L_s)	92.00 m
Beam (B)	28.00 m
Maximum draught (T_{max})	10.00 m
Underdeck clearance	4.90 m
Hull diameter vertical ($d_{hull\text{-}v}$)	4.40 m
Hull diameter horiz. ($d_{hull\text{-}h}$)	6.60 m
Strut thickness (t_s)	3.30 m
Maximum speed (V_{max})	28.00 knots

Table E18. General characteristics of the SRMH SWATH [E33]

Displacements (Δ)	925 tonnes
Box length (L_{box})	41.90 m
Hull length (L_{hull})	52.30 m
Strut length (L_s)	41.90 m
Beam (B)	20.00 m
Maximum draught (T_{max})	4.60 m
Underdeck clearance	2.60 m
Hull diameter vertical ($d_{hull\text{-}v}$)	2.87 m
Hull diameter horiz. ($d_{hull\text{-}h}$)	4.59 m
Strut thickness (t_s)	1.60 m
Maximum speed (V_{max})	14.50 knots

Table E16. Preliminary scantlings of a 70-tonne SWATH Ferry [E26]

Structures	Mild Steel	Alum. Alloy	GRP
1. Bridging deck Scantlings			
Wet deck :			
Plating	5.00	8.25	10.00
Deck beams	120x6.75*	130x5.50*	110x6.00*
(depth or width x thickness)		60x5.50+	80x7.00□, 50x6.00~
Longitudinal girders	110x3.75*	140x5.75*	120x4.00*
	40x3.75+	60x5.75+	100x5.00□,50x4.00~
Dry deck :			
Plating	3.00	4.25	7.00
Deck beams	70x4.00*	80x3.50*	95x3.50*
		40x3.50+	80x4.50□,50x3.50~
Longitudinal girders	90x3.25*	80x3.50*	90x3.00*
	30x3.25+	40x3.50+	80x4.00□,50x3.00~
Plate frame thickness	3.00	4.25	7.00
2.Haunch Scantlings			
Shell plating	5.00	8.25	6.50^{s},30.00^{c}
Shell longitudinals	90x5.50*	120x8.25*	
Web frames	150x5.00*	180x7.50*	180x6.00*
	60x5.00+	90x7.50+	140x7.00□,50x6.00~
3. Strut scantlings			
Shell plating	3.50	5.75	5.50^{s},20.00^{c}
Shell longitudinals	80x4.50*	100x6.75*	
Web frames (spaced 325)	110x3.75*	140x5.75*	90x3.00*
	40x3.75+	60x5.75+	80x4.00□,50x3.00~
4. Lower hull			
Shell plating	4.25	7.00	6.00^{s},25.00^{c}
Hull stringers (spaced 337)	90x5.00*	110x7.50*	
Ring frame transverse	120x4.25*	190x6.50*	150x5.00*
	60x5.25+	90x7.50+	70x6.00□, 50x5.00~
Docking girder	240x5.50*	240x5.50*	120x4.00*
	80x6.50+	80x6.50+	100x5.00□,50x4.00~

Notes :
(*) web, (+) flange, (□) crown for GRP, (~) lap for GRP
(s) skin thickness for GRP, (c) core thickness for GRP
All dimension in mm

Table E19. Structural scantlings for SRMH SWATH [E33]

Structural	Details
Superstructure	Equivalent thickness : 8.0 mm
Cross Structure	Plate thickness : 20.0 mm Transverse frame spacing : 8.0 m Stiffener Specifications : 12 table reinforcement plies 16 stiffener plies Longitudinal spacing : in the double bottom 2.25 m in the haunch 1.25 m in the balance 2.20 m
Struts	Plate thickness : 31.0 mm Stiffener spacing : 0.80 m Stiffener Specifications : 10 table reinforcement plies 14 stiffener plies
Hulls	Plate thickness : 20.0 mm Stiffener spacing : 0.80 m Stiffener Specifications : 10 table reinforcement plies 12 stiffener plies

Table E20. Principal particulars of the HHI SWATH Ferry [E36]

Displacements (Δ)	132 tonnes
Length overall (LOA)	21.70 m
Length between perpendiculars (L_{pp})	23.60 m
Breadth moulded (B_{mld})	12.40 m
Depth moulded (D_{mld})	5.30 m
Designed draught (T)	2.60 m
Underdeck clearance	1.70 m
Crusing speed (V)	25.00 knots

Table E21. Principal particulars of the EODSC SWATH [E39]

Full displacement (Δ)	73.30 tons
Light displacement	59.90 tons
Length overall (LOA)	63-0 feet-in
Length between perpendiculars (L_{pp})	58-0 feet-in
Beam overall (B_{max})	30-0 feet-in
Beam at DWL	26-0 feet-in
Depth to superstructure (D_{max})	24-0 feet-in
Draught to DWL (T)	6-7 1/2 feet-in
Operational speed (V)	12.70 knots

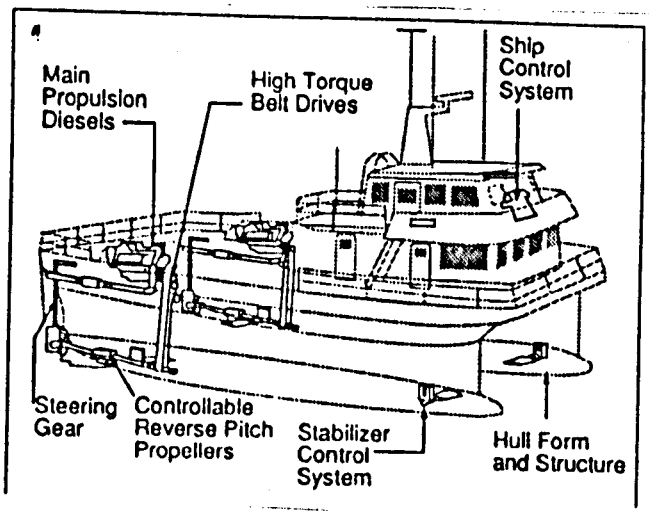

Figure E1. SWATH demonstrator *Halcyon* [E3]

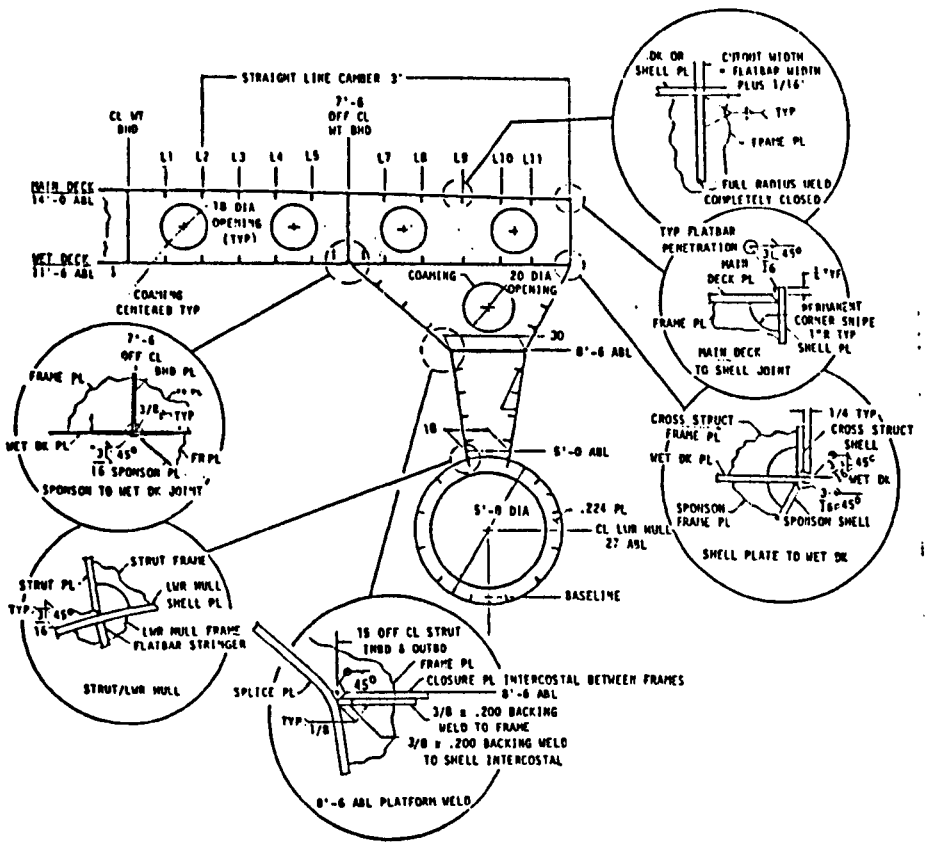

Figure E2. *Halcyon's* midship section [E1,E2]

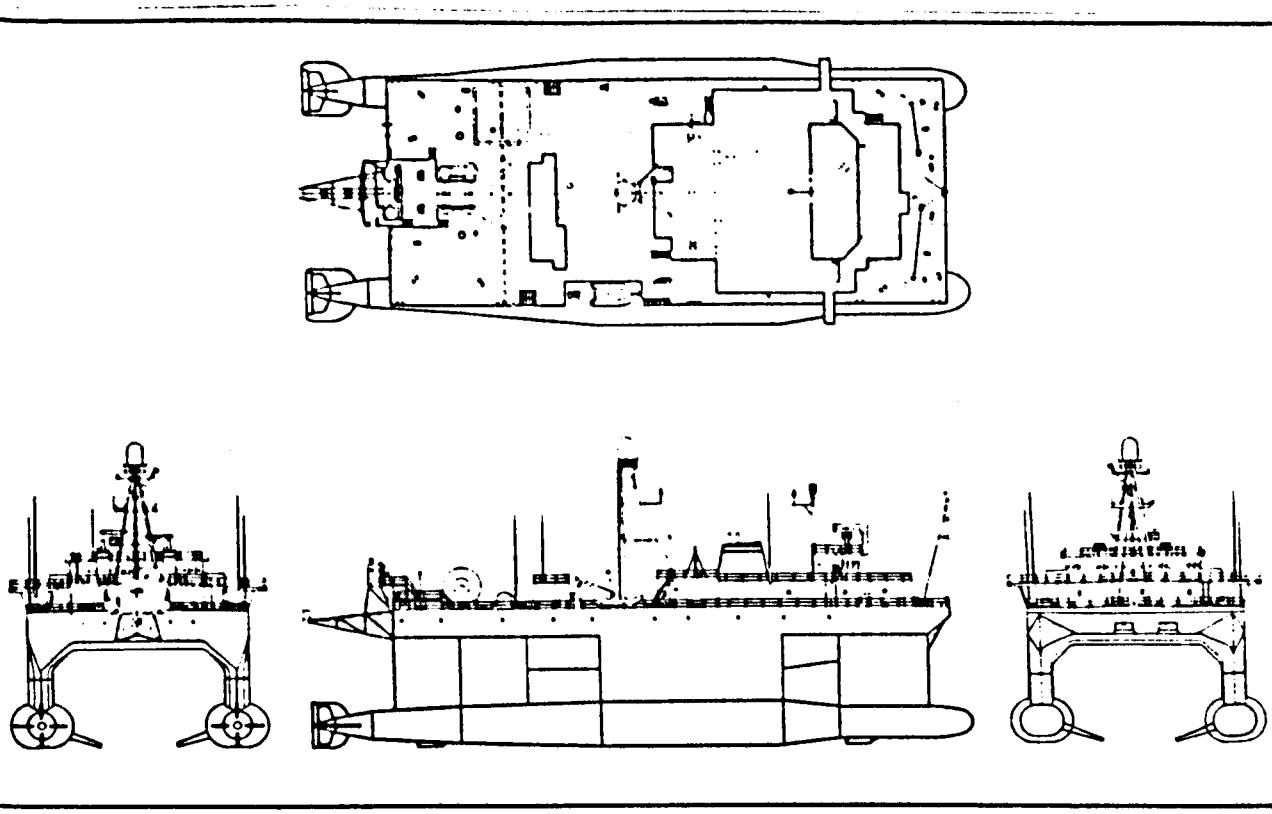

Figure E3. T-AGOS 19 profile, plan, bow and stern views [E6,E7]

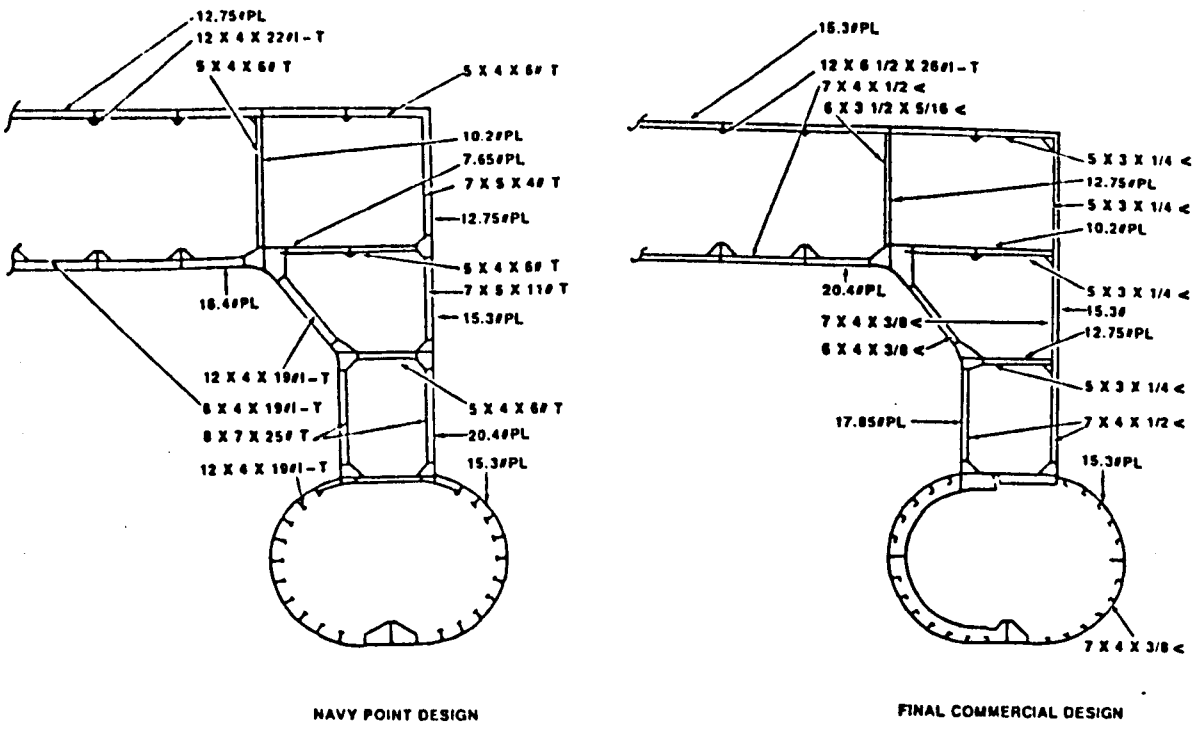

Figure E4. Midship sections for T-AGOS 19 [E6,E7]

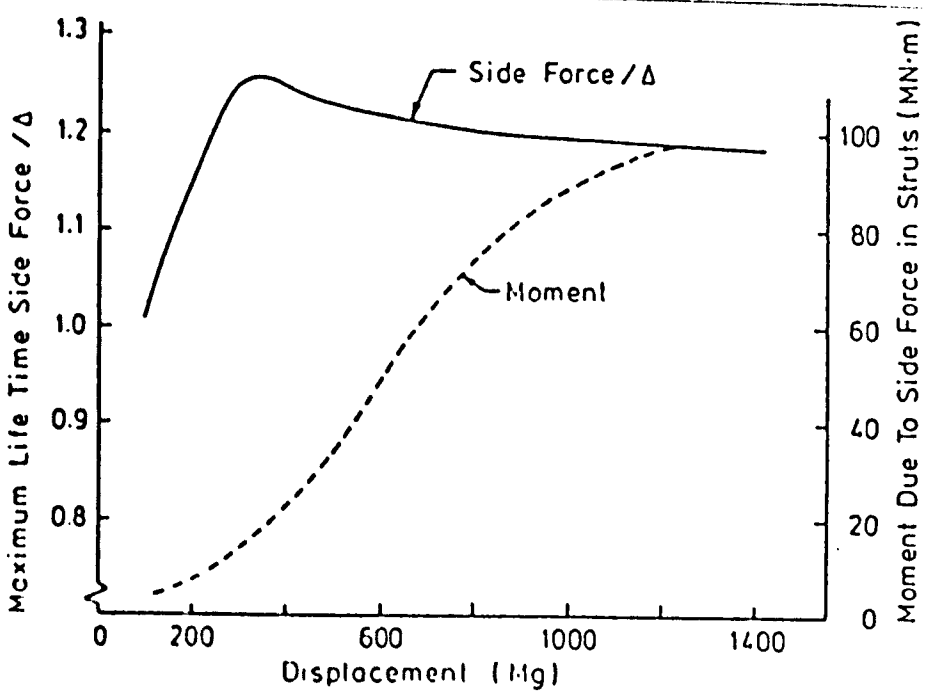

Figure E5. Design side load for small SWATHs [E4]

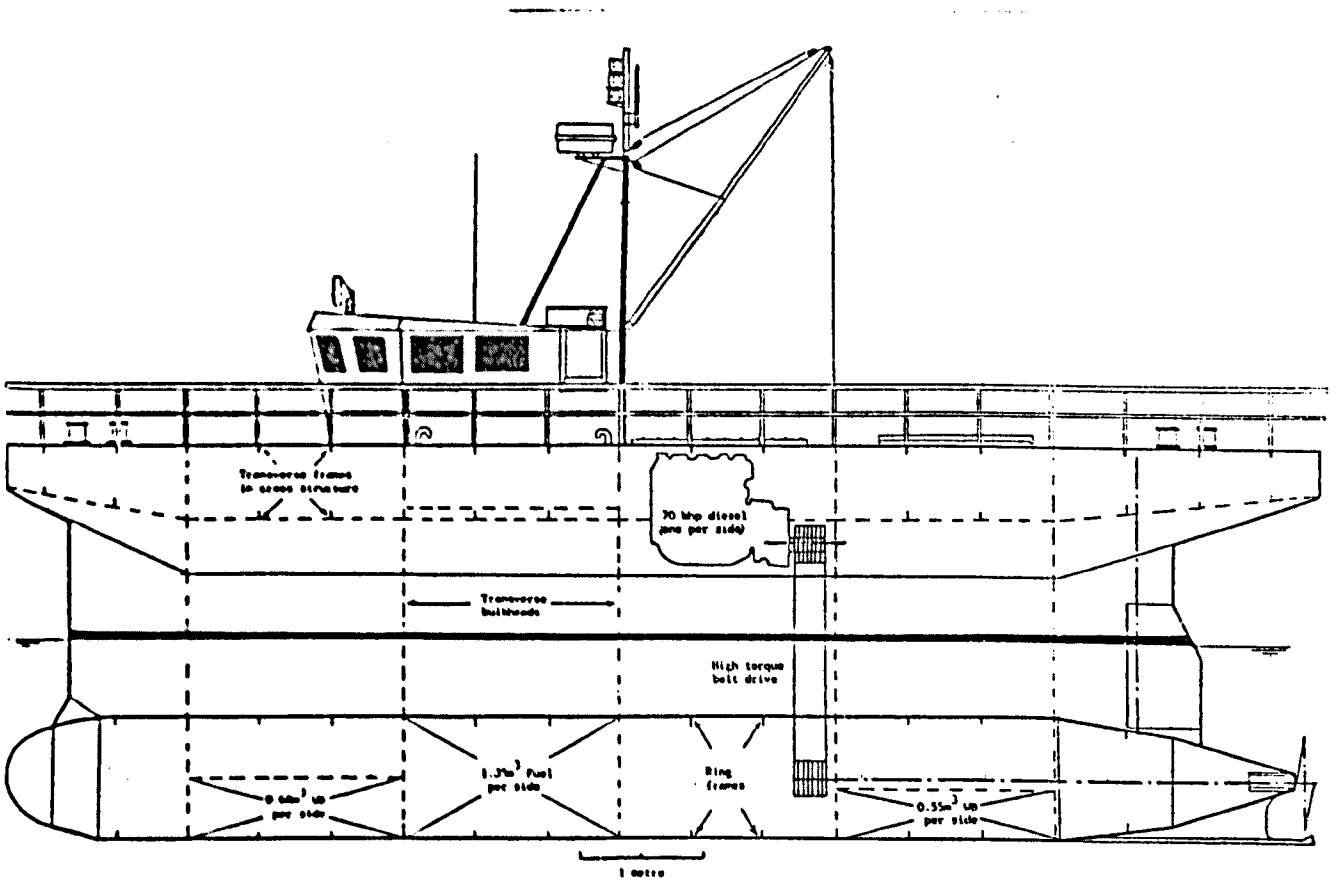

Figure E6. Fishing SWATH general arrangement [E9]

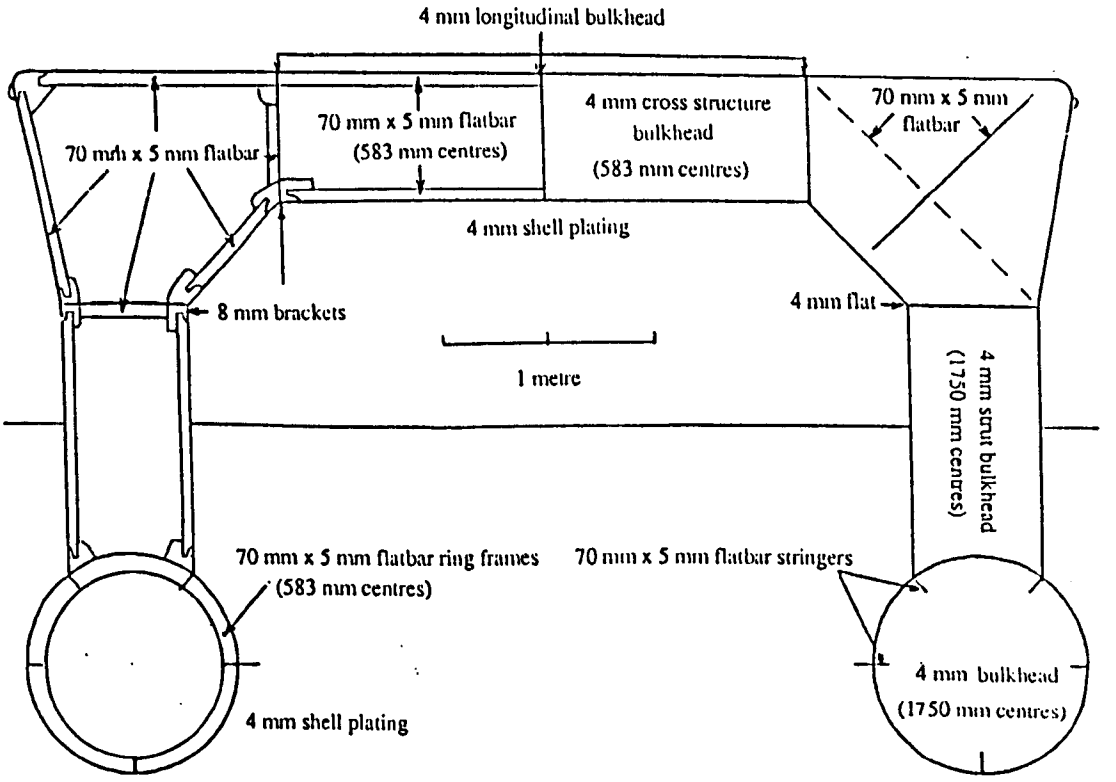

Figure E7. Fishing SWATH midship section [E9]

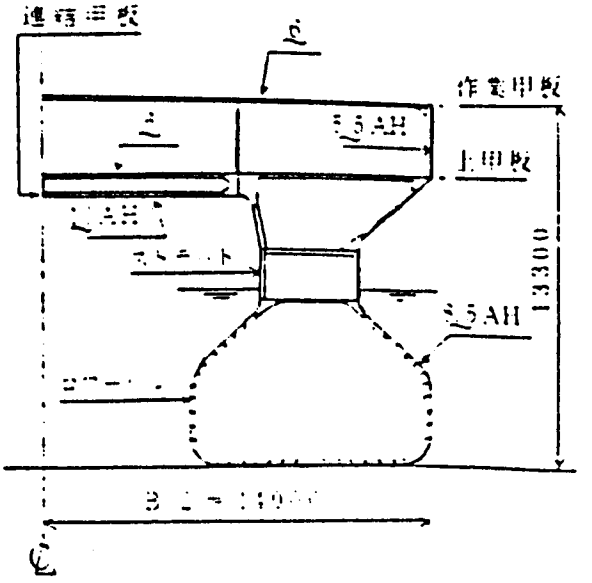

Figure E8. Midship section of the *Kaiyo* [E13]

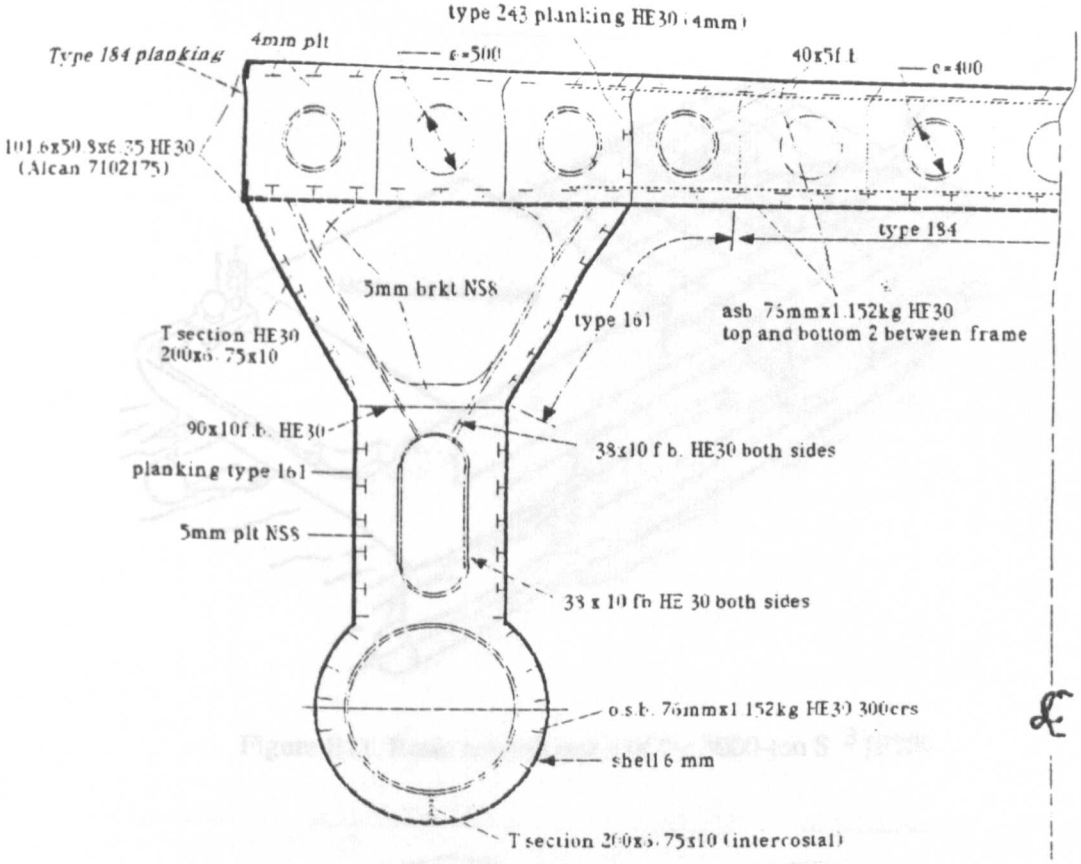

Figure E9. Typical framing section for the *Patria*

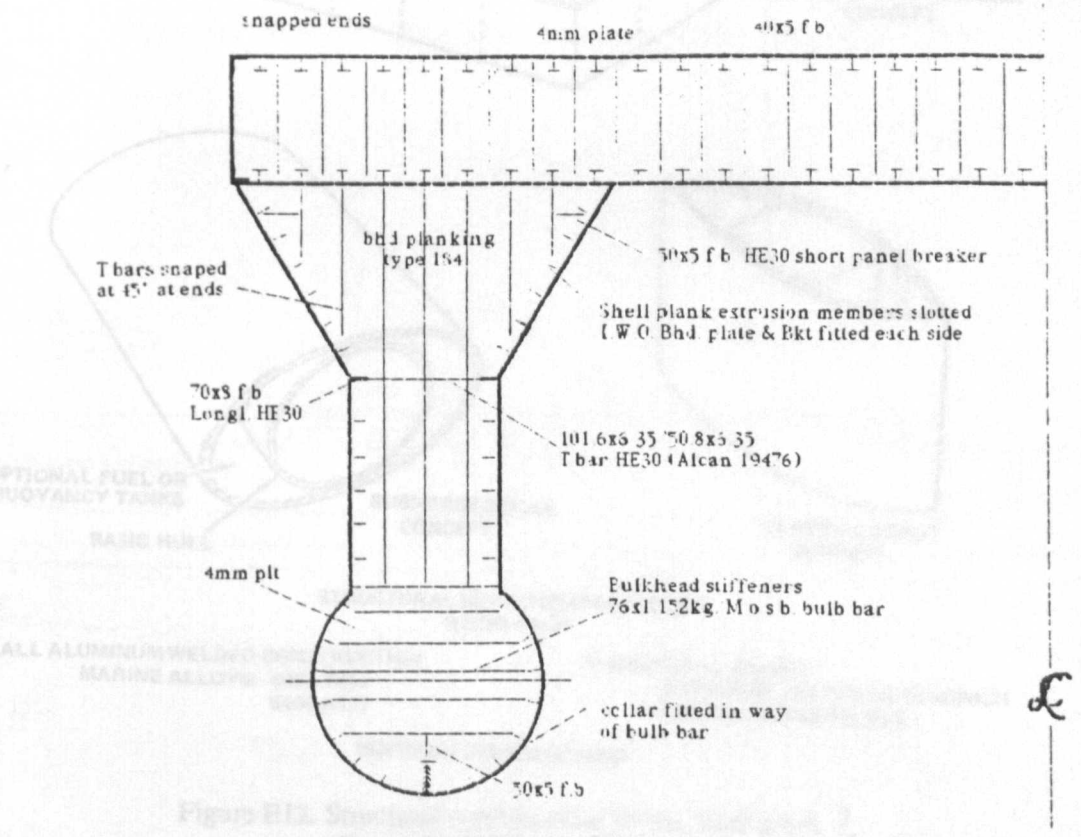

Figure E10. Bulkhead arrangement for the *Patria*

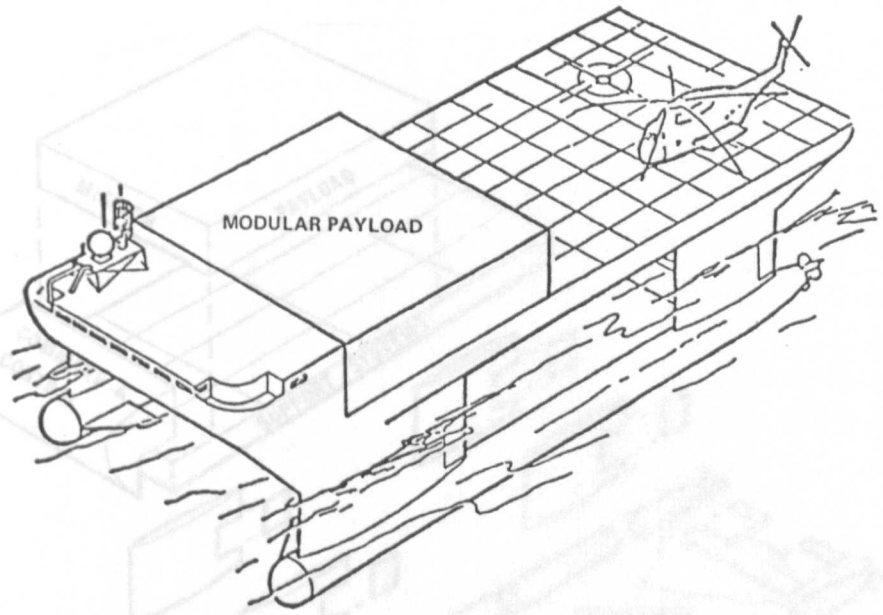

Figure E11. Basic configuration of the 3000-ton S ^{3} [E20]

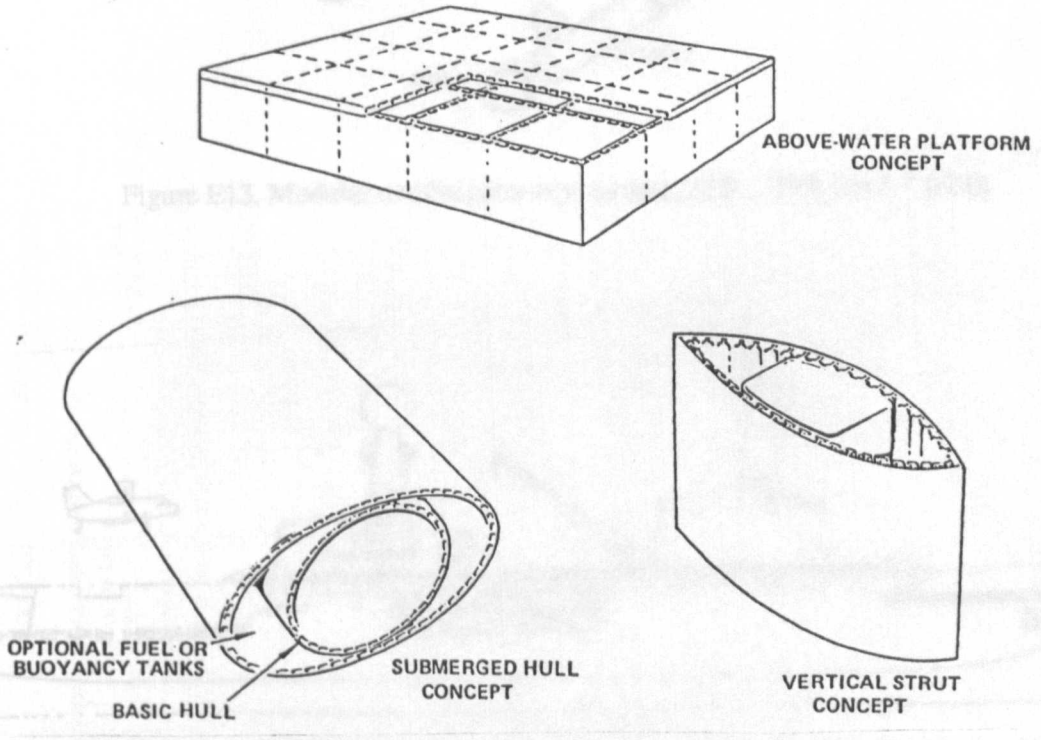

Figure E12. Structural configuration of the 3000-ton S ^{3}, Conceptual Subsystems [E20]

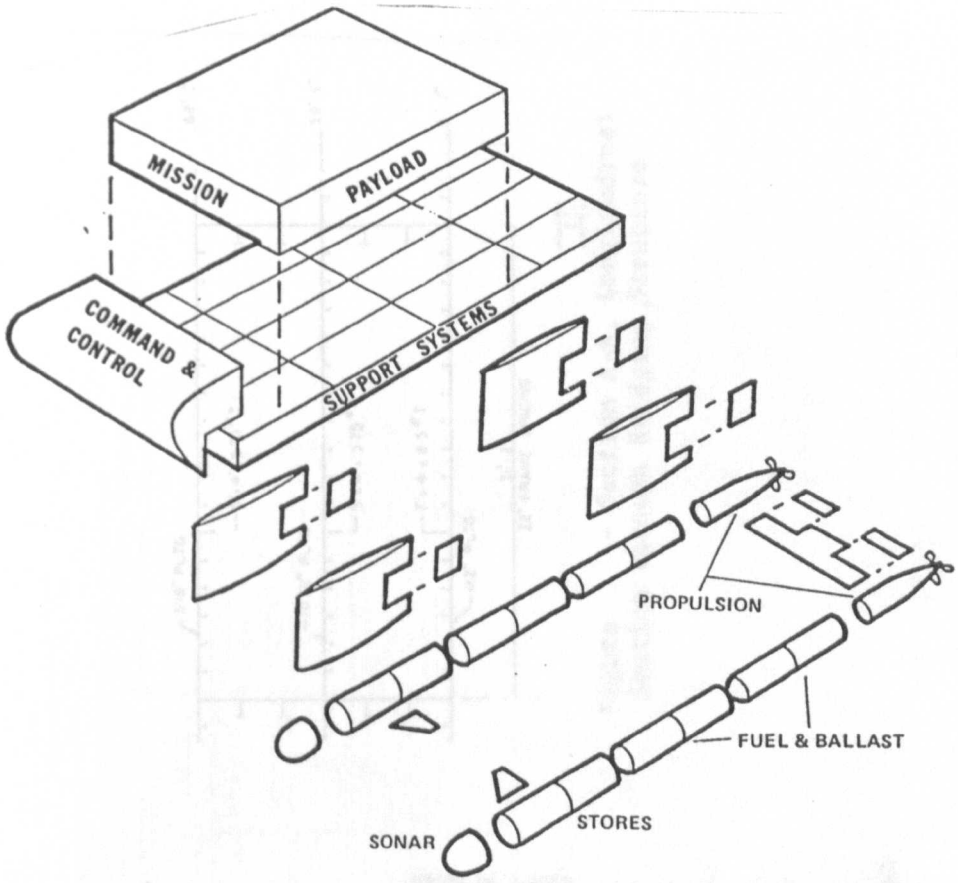

Figure E13. Modular construction as proposed for the 3000-ton S [3] [E20]

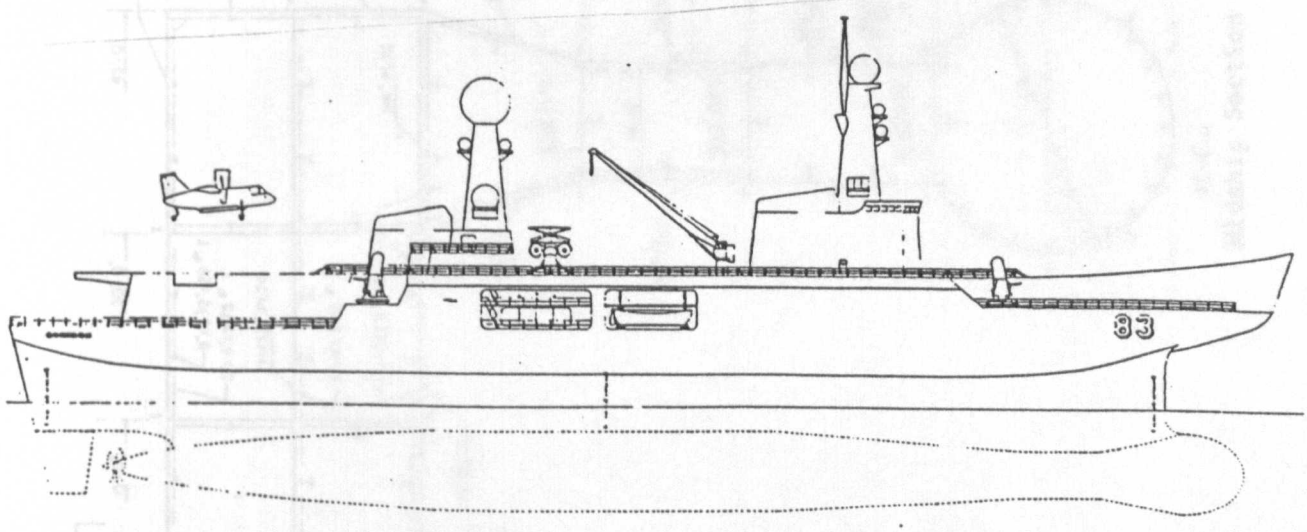

Figure E15. SWATH83, V/STOL Aircraft Carrier [E24]

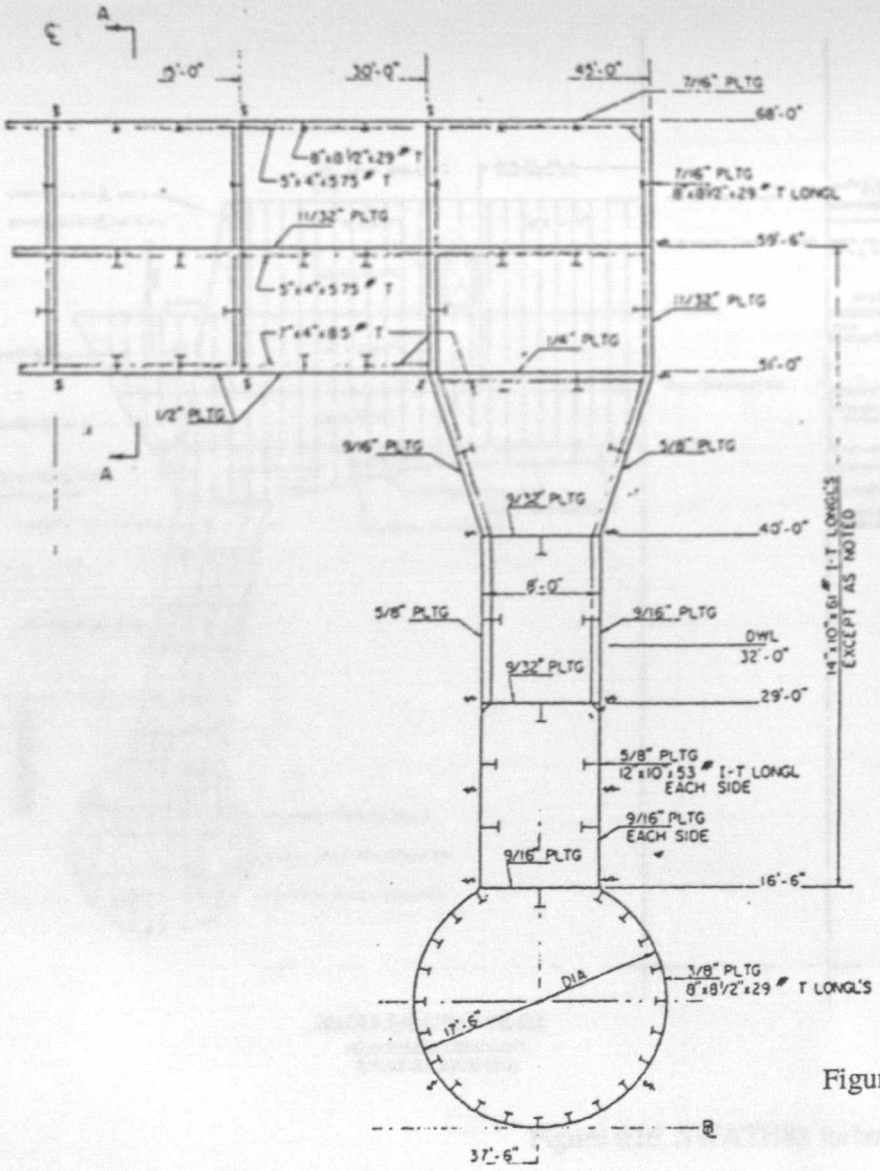

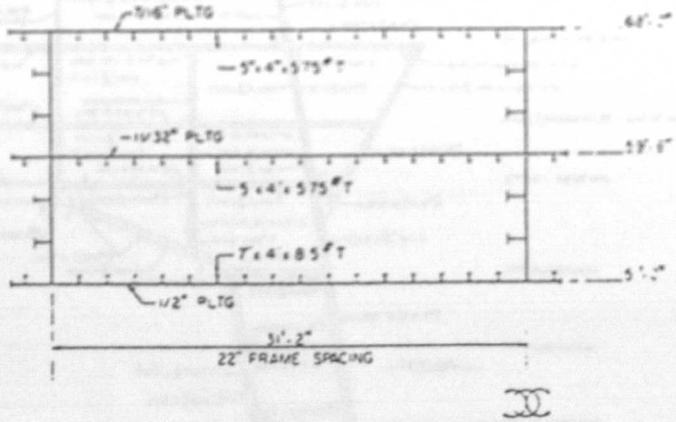

Figure - Section A-A, Longitudinal Section through Bridging Structure

Figure E14. Structural arrangement of a 4300-ton LWP [E22]

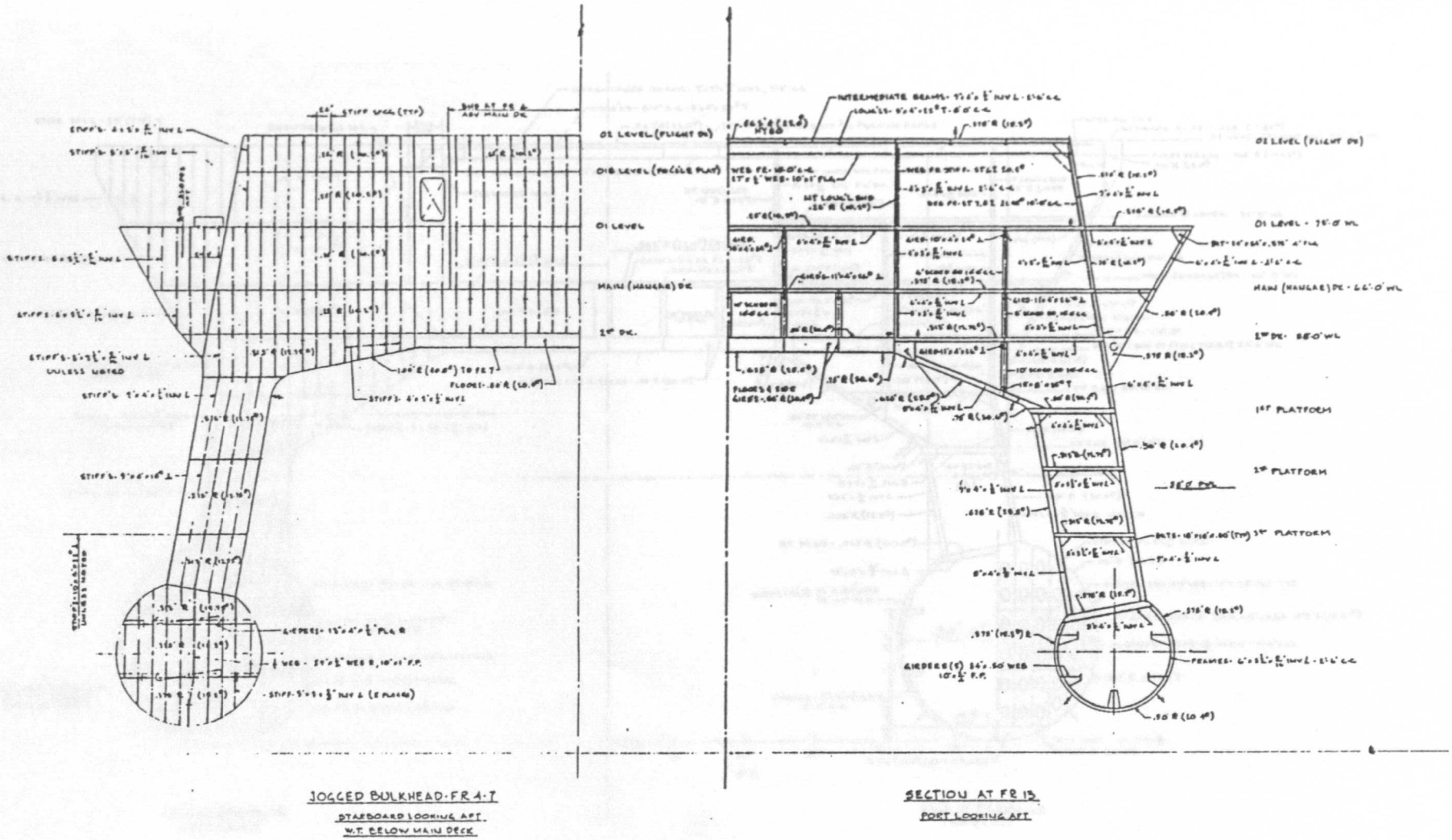

Figure E16. SWATH83 forbody sections [E24]

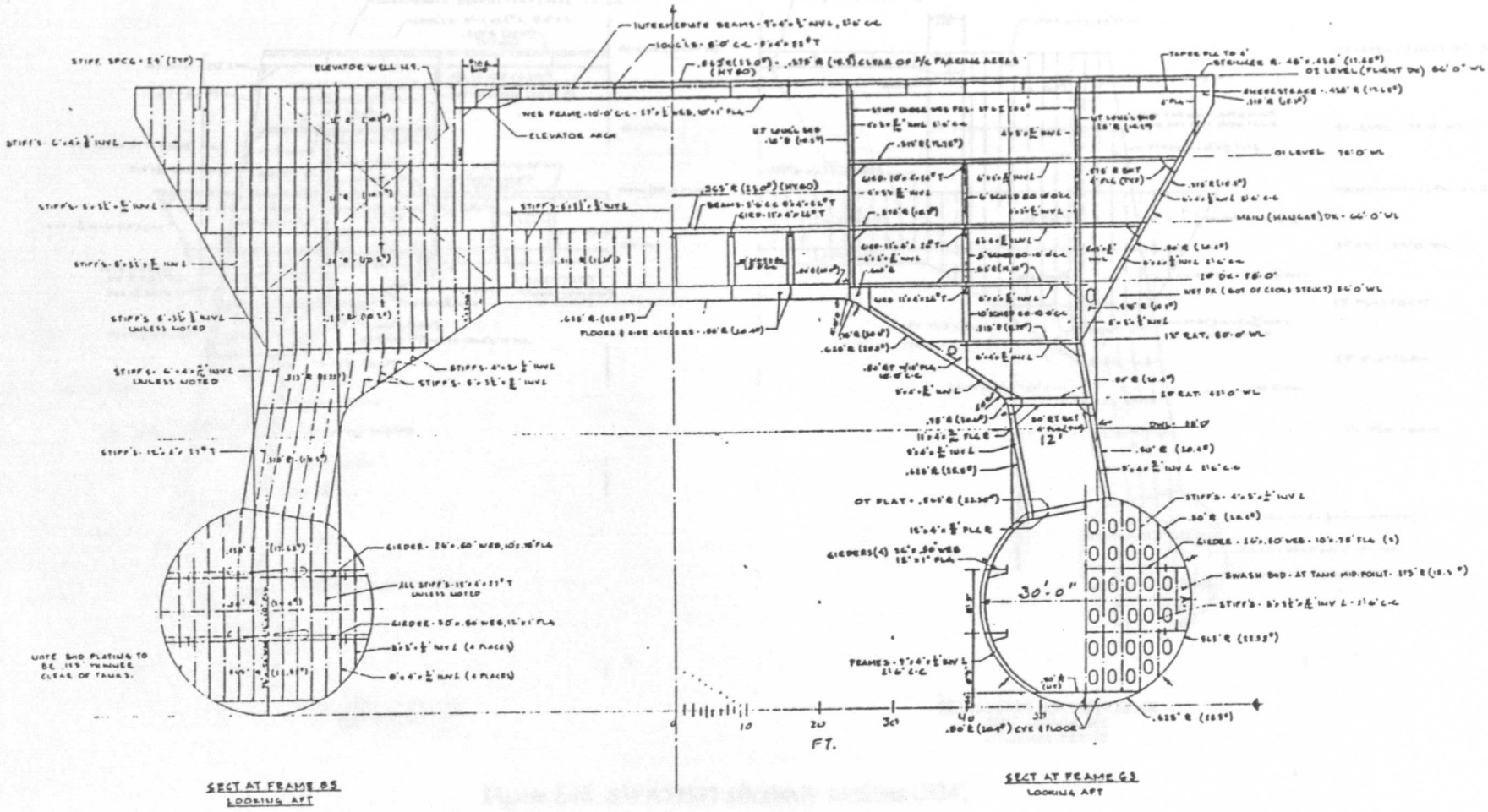

Figure E17. SWATH83 midship sections [E24]

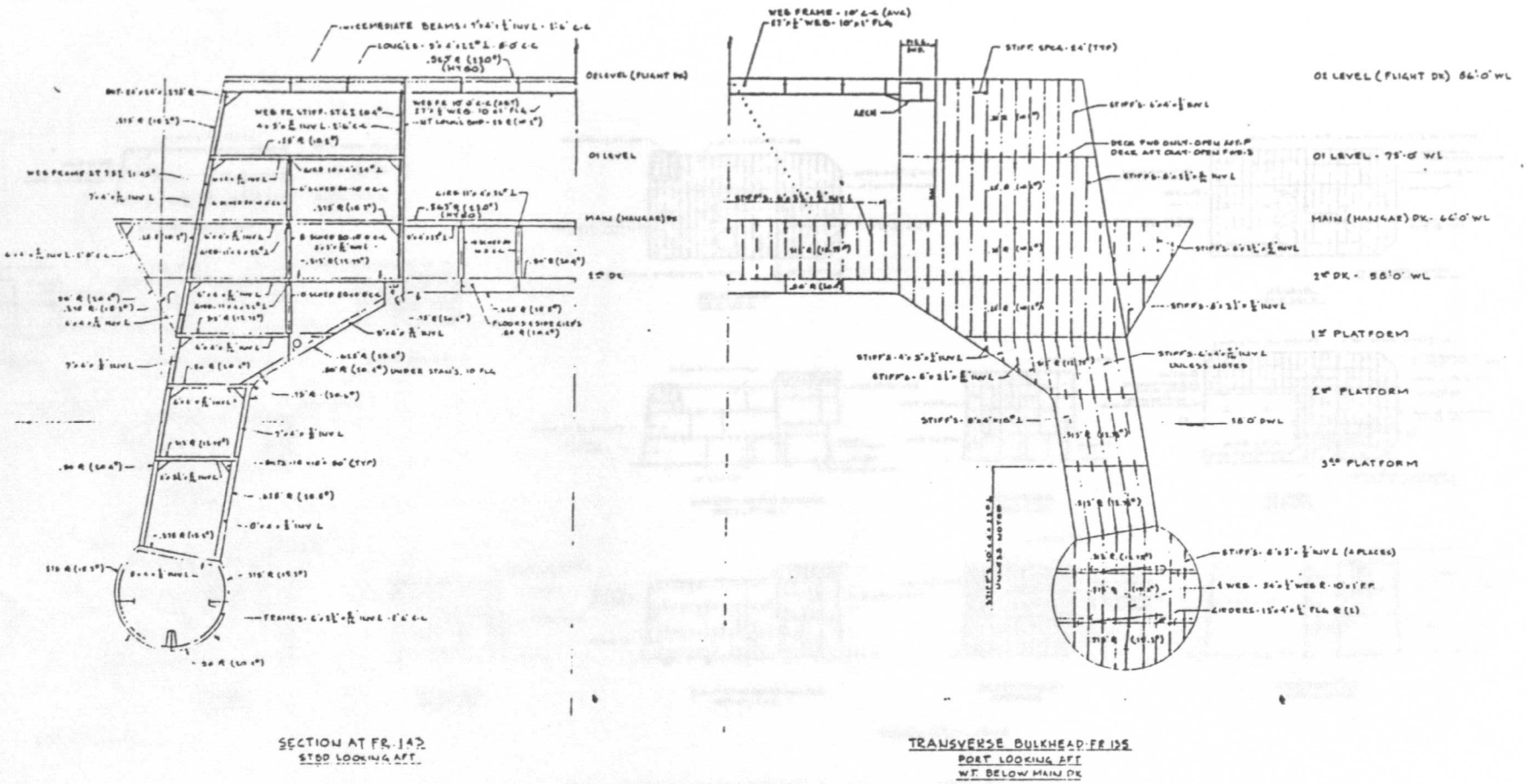

Figure E18. SWATH83 afterbody sections [E24]

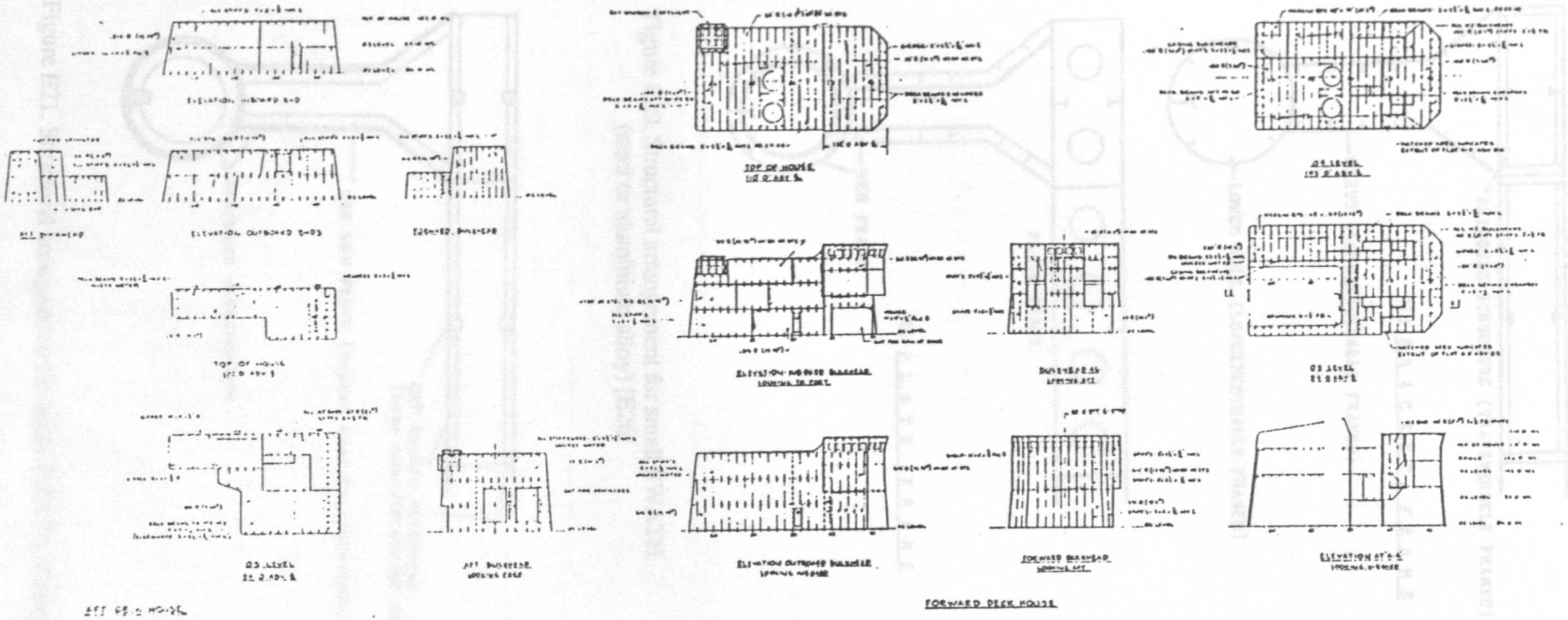

Figure E19. SWATH83 deckhouses [E24]

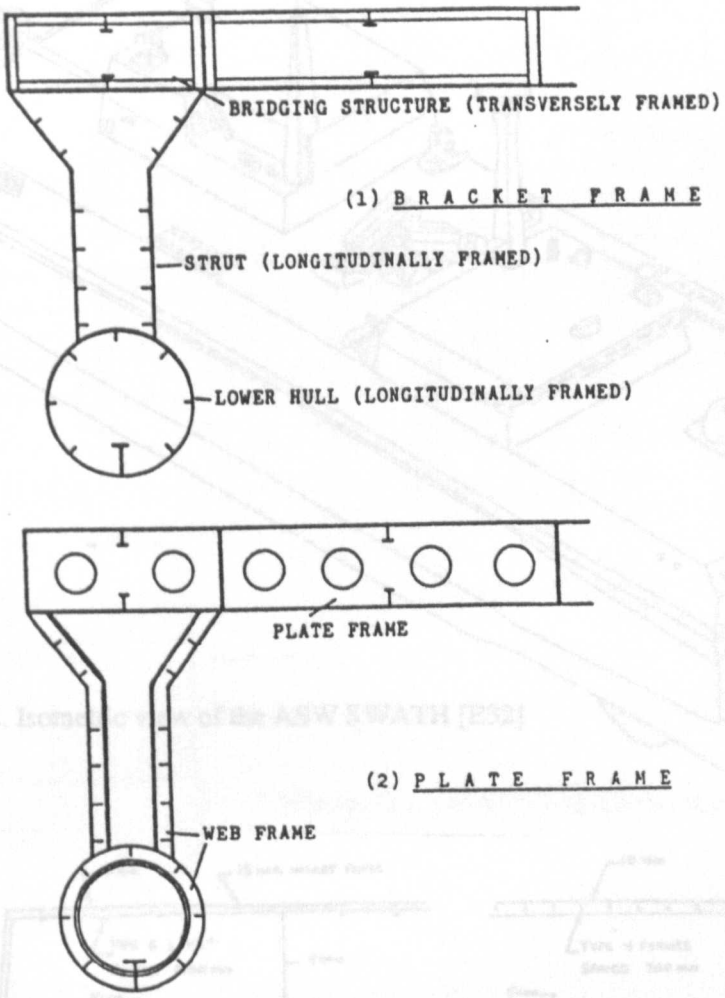

Figure E20. Structural arrangement for small SWATH (steel or aluminium alloy) [E26]

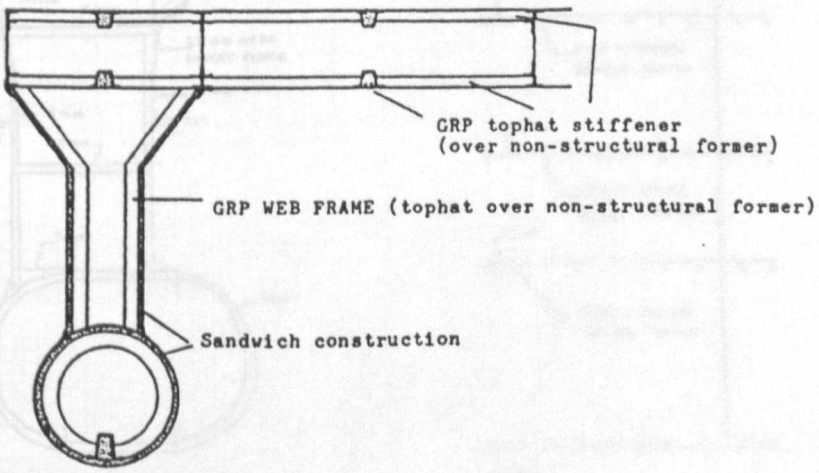

Figure E21. Structural arrangement for small SWATH (GRP) [E26]

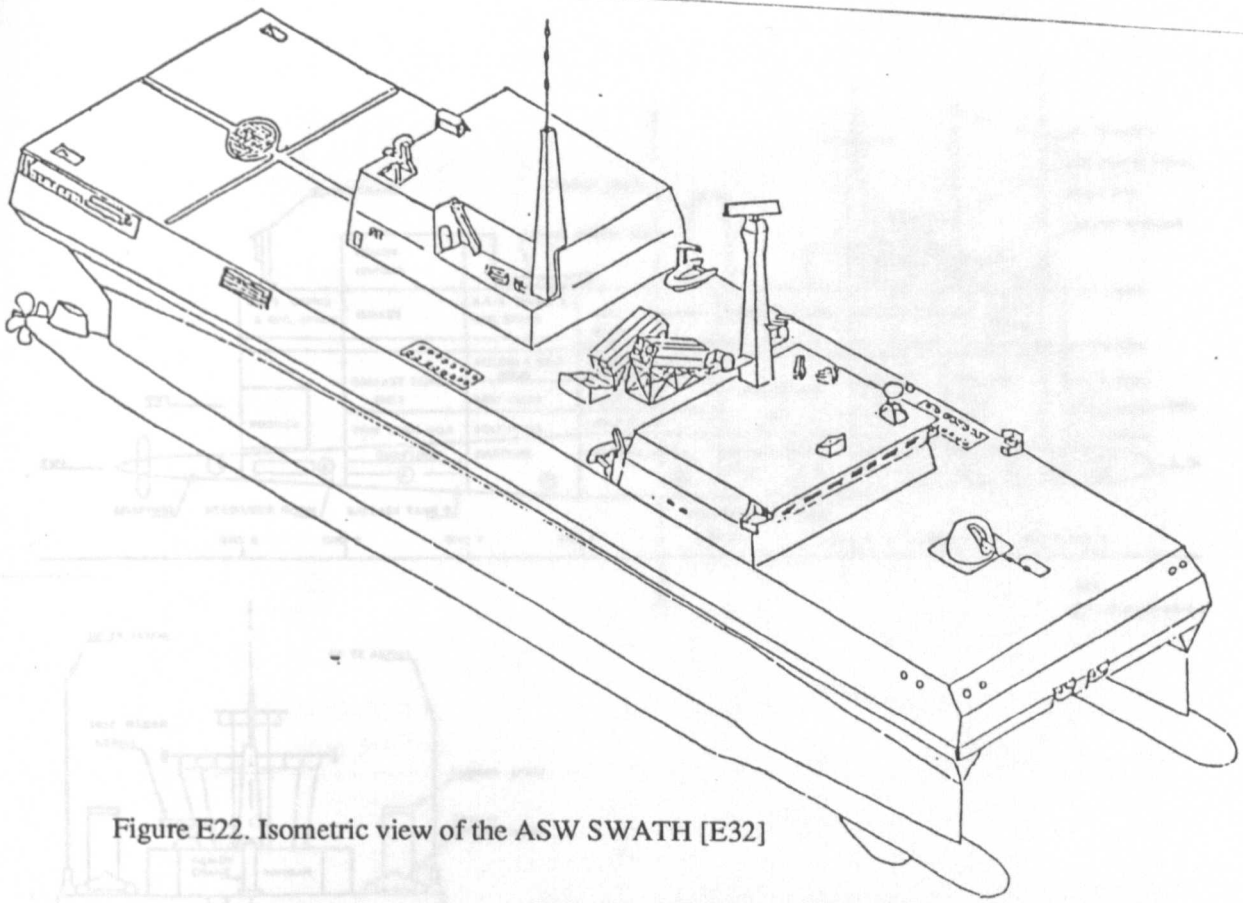

Figure E22. Isometric view of the ASW SWATH [E32]

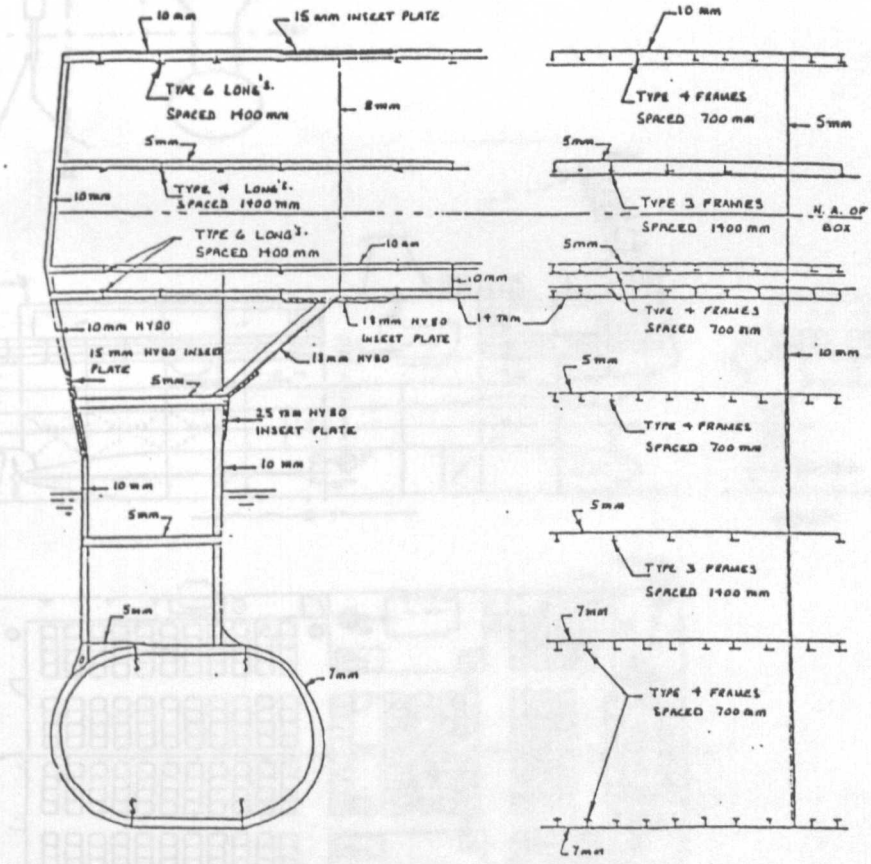

Figure E23. ASW SWATH structural midship section [E32]

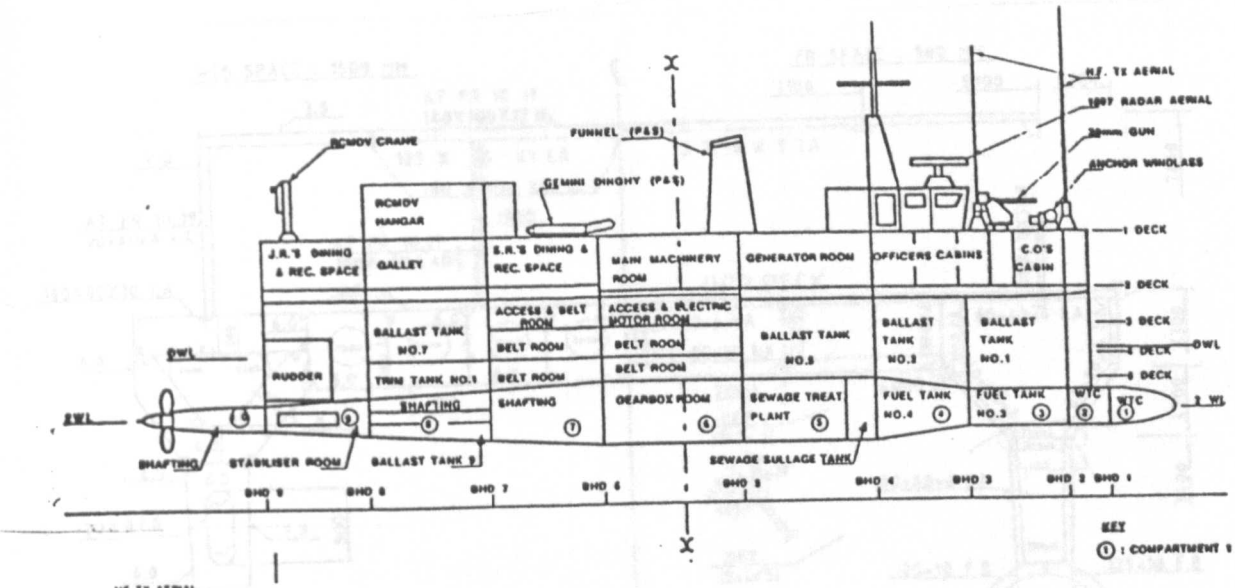

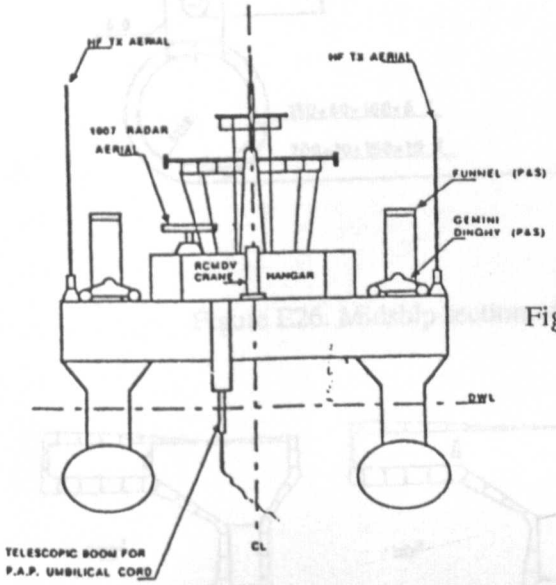

Figure E24. SWATH single role mine hunter (SRMH) [E33]

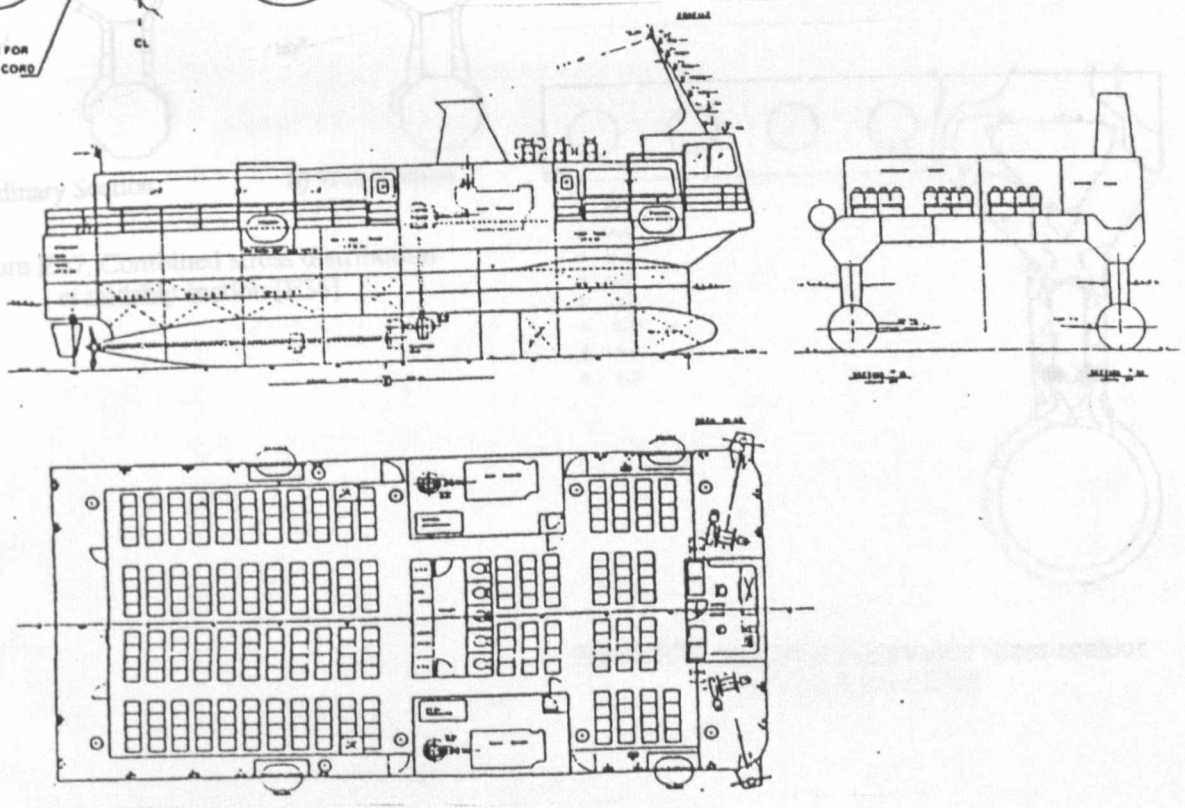

Figure E25. General arrangement of Korean SWATH Ferry [E36]

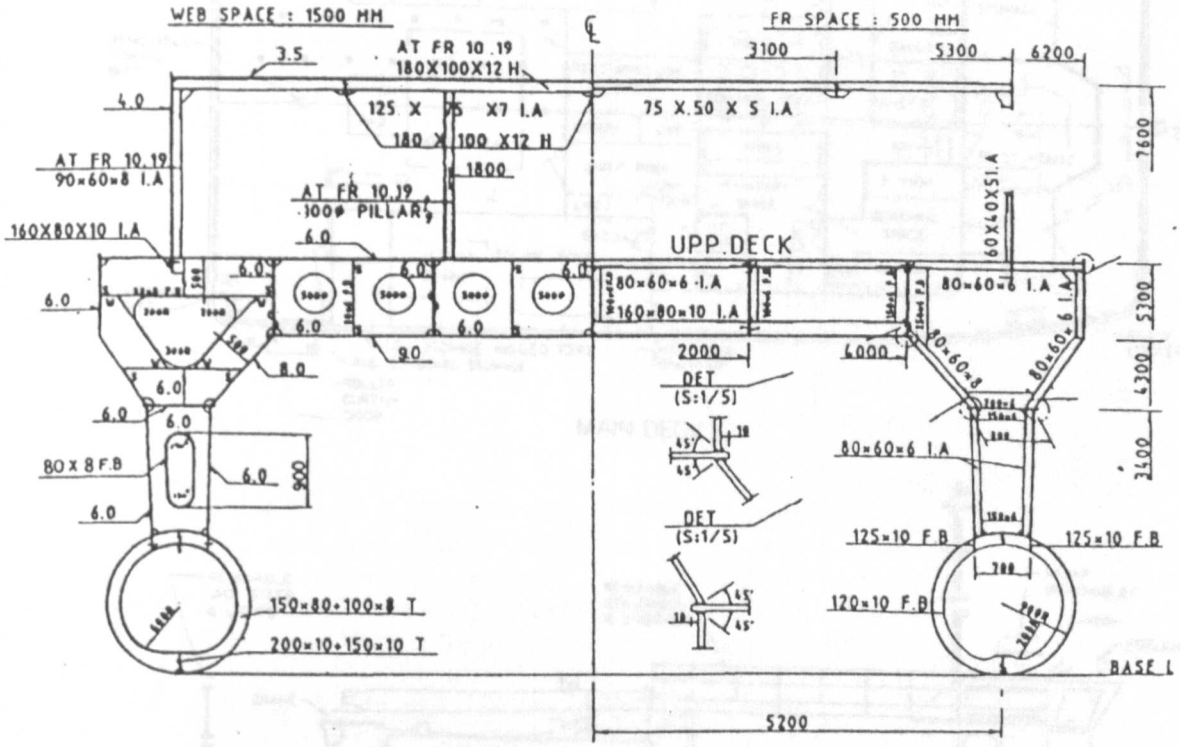

Figure E26. Midship section of Korean SWATH Ferry [E36]

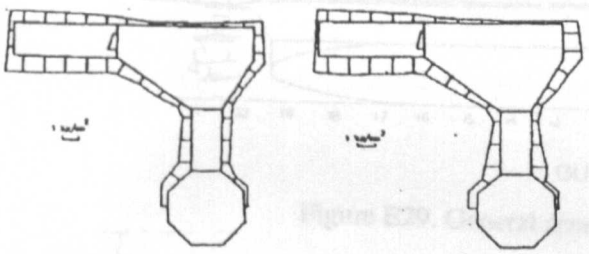

a) Ordinary Section b) Web Section

Figure E27. Combined stress distribution at midship section [E36]

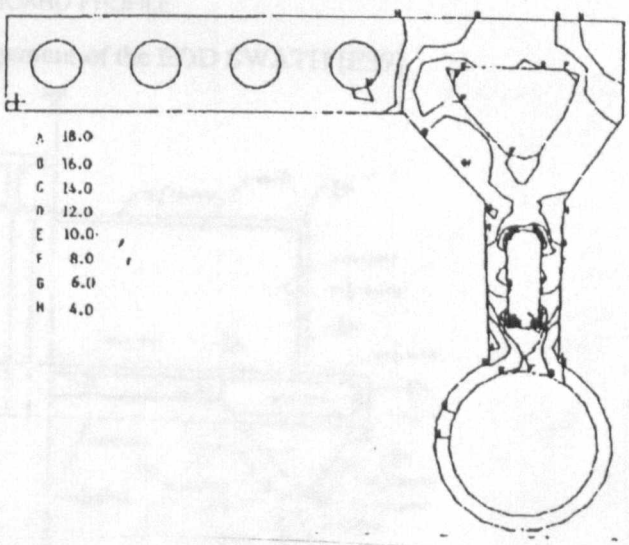

Figure E28. Von Mises equivalent stress contour of web frame [E36]

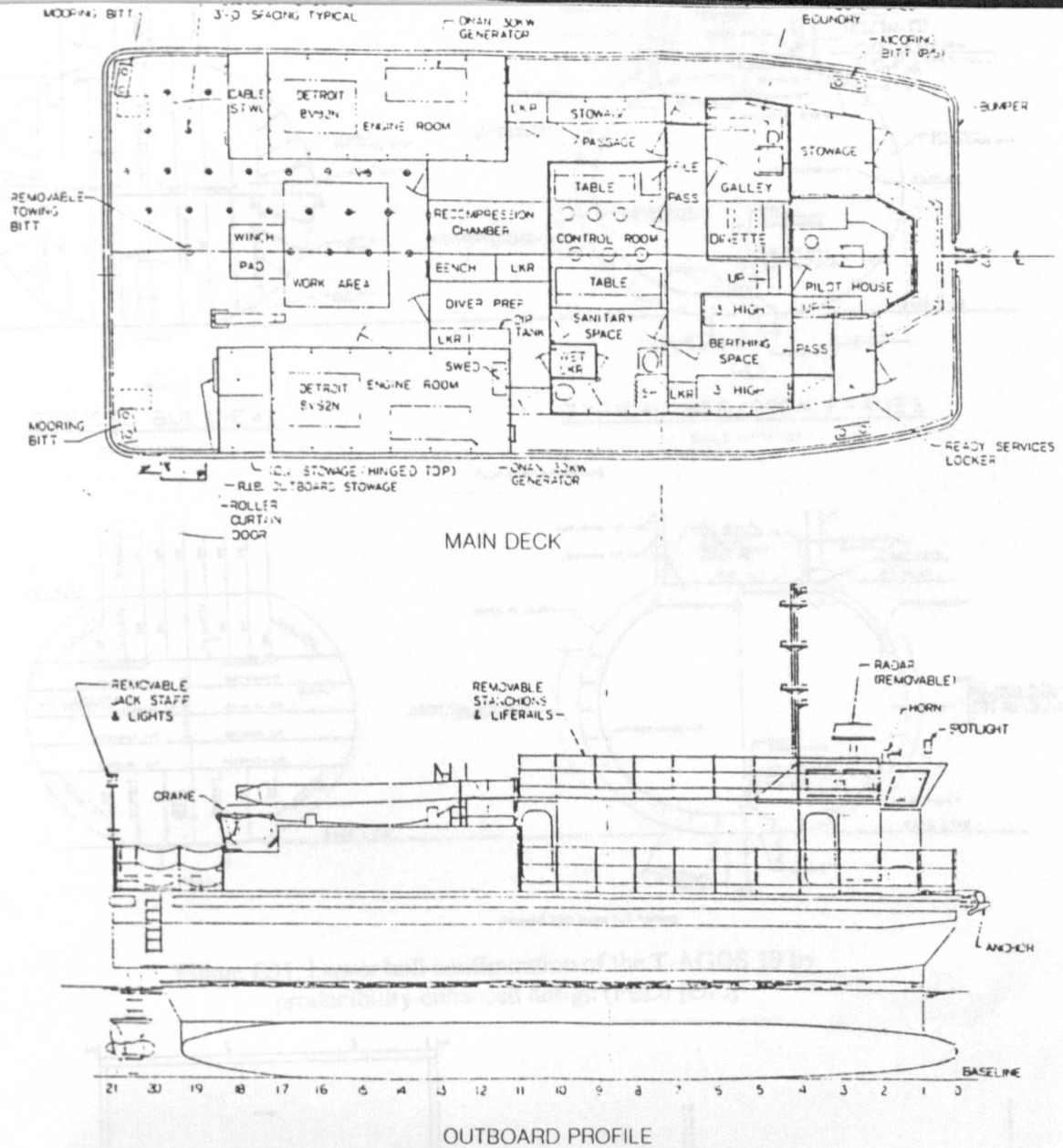

Figure E29. General arrangement of the EOD SWATH [E39]

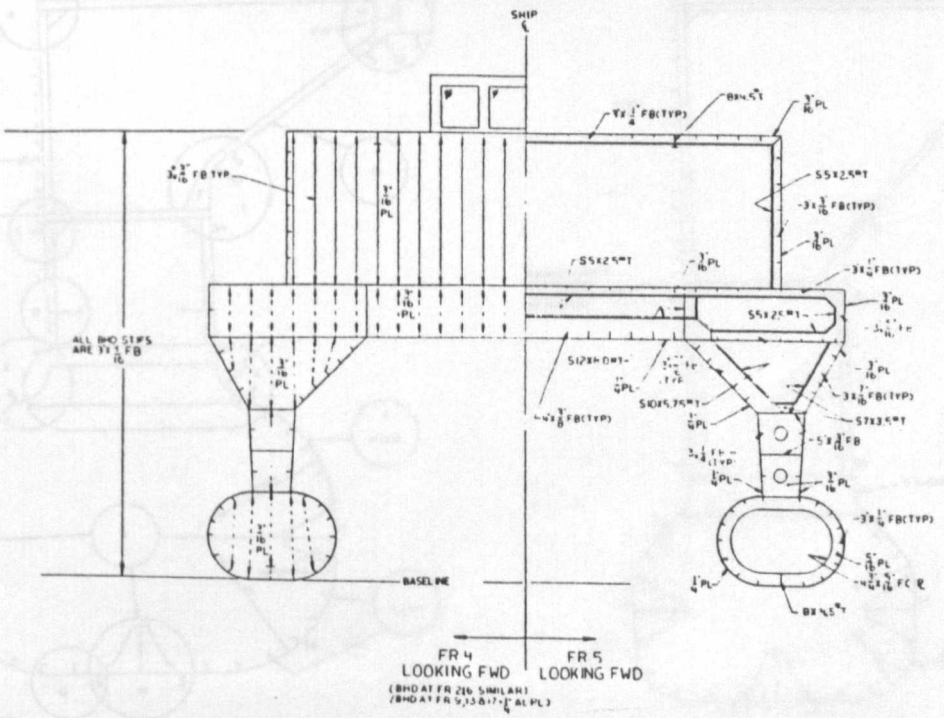

Figure E30. Midship section of the EOD SWATH [E39]

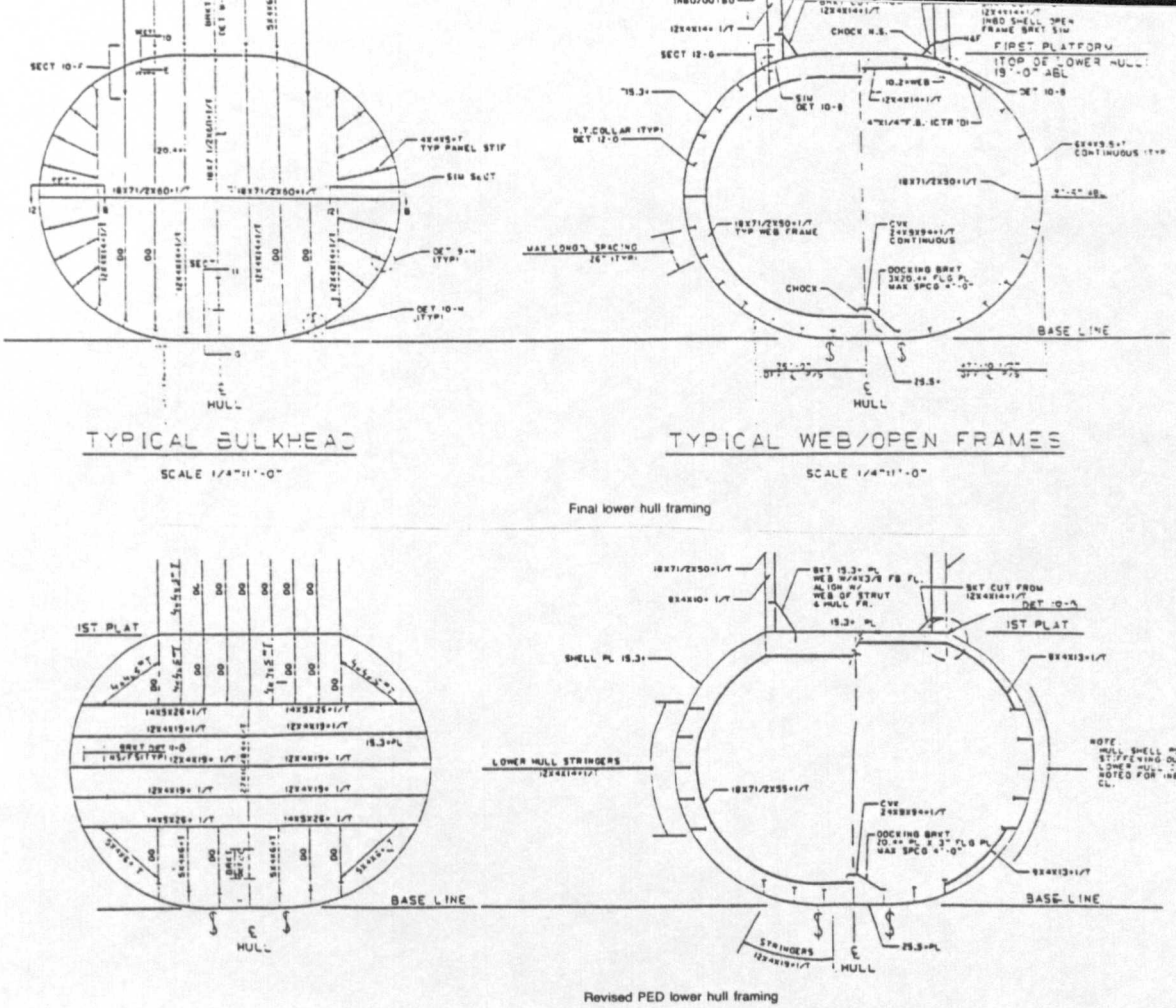

Figure E31. Lower hull configuration of the T-AGOS 19 by producibility-enhanced design (PED) [E40]

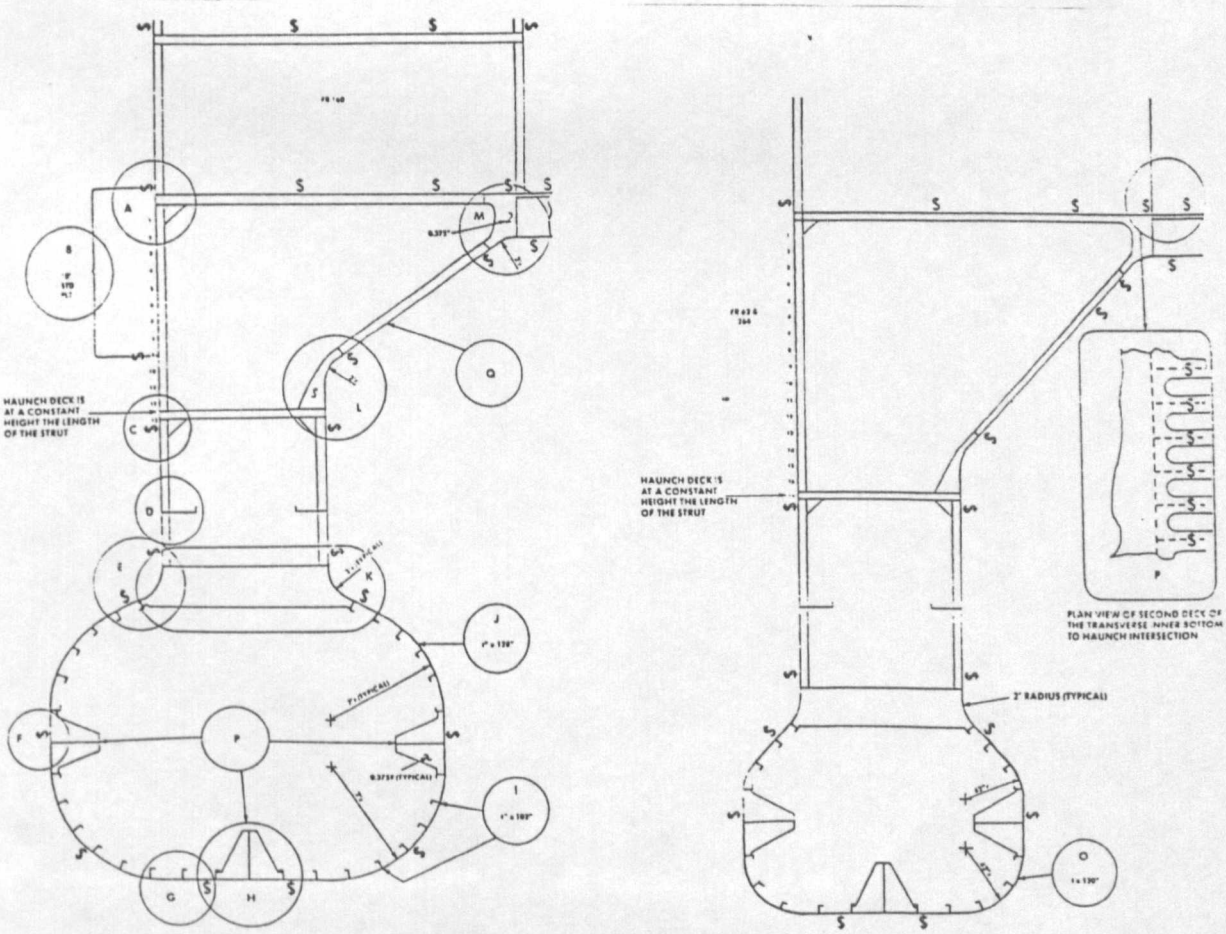

Figure E32. Enhanced haunch/strut/underwater hull for better producibility [E41]